FINAL REPORT TO
THE CALIFORNIA DEPARTMENT OF
TRANSPORTATION

SOCIO-ECONOMIC EFFECT OF SEISMIC RETROFIT IMPLEMENTED ON BRIDGES IN LOS ANGELES HIGHWAY NETWORK

RTA-59A0304

By

Masanobu Shinozuka[1], Professor

and

Youwei Zhou[1], Graduate Research Assistant

Sang-Hoon Kim[1], Post-Doctoral Researcher

Yuko Murachi[1], Visiting Researcher

Swagata Banerjee[1], Graduate Research Assistant

Sunbin Cho[2], Research Engineer

Howard Chung[2], Research Engineer

1 Department of Civil and Environmental Engineering
University of California, Irvine
2 ImageCat, Inc.

October 2005

STATE OF CALIFORNIA DEPARTMENT OF TRANSPORTATION

TECHNICAL REPORT DOCUMENTATION PAGE

TR0003 (REV. 10/98)

1. REPORT NUMBER	2. GOVERNMENT ASSOCIATION NUMBER	3. RECIPIENT'S CATALOG NUMBER
F/CA/SD-2005/03		

4. TITLE AND SUBTITLE	5. REPORT DATE
SOCIO-ECONOMIC EFFECT OF SEISMIC RETROFIT IMPLEMENTED ON BRIDGES IN THE LOS ANGELES HIGHWAY NETWORK	October 2005
	6. PERFORMING ORGANIZATION CODE
7. AUTHOR(S)	8. PERFORMING ORGANIZATION REPORT NO.
Masanobu Shinozuka, Youwei Zhou, Sanghoon Kim, Yuko Murachi, Swagata Banerjee, Sunbin Cho and Howard Chung	
9. PERFORMING ORGANIZATION NAME AND ADDRESS	10. WORK UNIT NUMBER
Department of Civil and Environmental Engineering The Henry Samueli School of Engineering University of California, Irvine Irvine, California 92697	11. CONTRACT OR GRANT NUMBER RTA-59A0304
12. SPONSORING AGENCY AND ADDRESS	13. TYPE OF REPORT AND PERIOD COVERED
California Department of Transportation Division of Research and Innovation, MS-83 1227 O Street Sacramento CA 95814	Final Report 14. SPONSORING AGENCY CODE

15. SUPPLEMENTAL NOTES

16.ABSTRACT

This research studied socio-economic effect of the seismic retrofit implemented on bridges in Los Angeles Area Freeway Network. Firstly, advanced FE (Finite Element) modeling and nonlinear time history analysis are carried out to evaluate the seismic performance in the form of fragility curve, of representative bridges before and after retrofit. This analysis resulted in the determination of retrofit effect in such a way that we can quantify, through the change in fragility parameters, the improvement of bridge seismic performance after retrofit. Secondly, an integrated traffic assignment model is introduced to consider change in the post-earthquake OD characteristics due to building damage, and is utilized to evaluate the post-earthquake network performance of the damaged freeway network in terms of daily travel delay (compared with the travel time associated with the freeway network not damaged) and attendant opportunity cost. Furthermore, the process of system restoration is simulated to estimate the total social cost based on bridge functionality restoration (repair / replacement) process. The benefit from the retrofit is defined as the combined social and bridge restoration cost avoided by comparing the total social and bridge restoration cost before and after bridge retrofit. The benefit resulting from combined social and bridge restoration cost avoided together with the bridge retrofit cost are used for a cost-benefit analysis. The result shows that the retrofit is cost-effective if both social and bridge restoration cost avoided are considered, and the bridge restoration cost avoided can only contribute a small portion of the initial bridge retrofit cost.

17. KEY WORDS	18. DISTRIBUTION STATEMENT	
Bridge Fragility, Retrofit, Seismic Risk Analysis, Traffic Assignment, Monte Carlo Simulation, Loss Estimation, Cost-Benefit Analysis	No restrictions. This document is available to the public through the National Technical Information Service, Springfield, VA 22161	
19. SECURITY CLASSIFICATION (of this report)	20. NUMBER OF PAGES	21. PRICE
Unclassified	314	

Reproduction of completed page authorized

DISCLAIMER: The Opinions, findings, and conclusions expressed in this publication are those of the authors and not necessarily those of the STATE OF CALIFORNIA

ABSTRACT

This research studied socio-economic effect of the seismic retrofit implemented on bridges in Los Angeles Area Freeway Network. Firstly, advanced FE (Finite Element) modeling and nonlinear time history analysis are carried out to evaluate the seismic performance in the form of fragility curve, of representative bridges before and after retrofit. This analysis resulted in the determination of retrofit effect in such a way that we can quantify, through the change in fragility parameters, the improvement of bridge seismic performance after retrofit. Secondly, an integrated traffic assignment model is introduced to consider change in the post-earthquake OD characteristics due to building damage, and is utilized to evaluate the post-earthquake network performance of the damaged freeway network in terms of daily travel delay (compared with the travel time associated with the freeway network not damaged) and attendant opportunity cost. Furthermore, the process of system restoration is simulated to estimate the total social cost based on bridge functionality restoration (repair / replacement) process. The benefit from the retrofit is defined as the combined social and bridge restoration cost avoided by comparing the total social and bridge restoration cost before and after bridge retrofit. The benefit resulting from combined social and bridge restoration cost avoided together with the bridge retrofit cost are used for a cost-benefit analysis. The result shows that the retrofit is cost-effective if both social and bridge restoration cost avoided are considered, and the bridge restoration cost avoided can only contribute a small portion of the initial bridge retrofit cost.

ACKNOWLEDGEMENT

The research presented in this report was sponsored by the California Department of Transportation (Caltrans) with Li-Hong Sheng as contract monitor. The authors are indebted to Caltrans for its support of this project and to Li-Hong Sheng for his most valuable advice.

TABLE OF CONTENTS

Abstract……..…….i
Acknowledgements……ii
Table of Contents……..…iii
List of Figures……...vi
List of Tables……xii
Chapter 1 Introduction……...1
Chapter 2 Development of Analytical Fragility Curves…….……...7
2.1 Introduction…… ….7
2.2 Column Retrofit with Steel Jacketing……..8
2.2.1 Background……...8
2.2.2 Steel Jacketing……..9
2.2.3 Stress-Strain Relationship for Confined Concrete……....9
2.3 Bridge Model…….…….11
2.3.1 Bridge Description……...11
2.3.2 Bridge Modeling……..12
2.4 Development of Moment-Curvature Relationship……..15
2.4.1 Moment-Curvature Relationship in Longitudinal Direction……....15
2.5 Bridge Response Analysis……...19
2.5.1 Input Ground Motions……..19
2.5.2 Response of Structures…….….22
2.6 Fragility Analysis of Bridges……...26
2.6.1 Fragility Analysis…….….26
2.6.2 Damage States……...27
2.7 Pounding, Soil, Jacketing, and Restrainer Effects on Fragility Curves……...28
2.7.1 Pounding at Expansion Joint…….…28
2.7.2 Numerical Simulation for Pounding…….31
2.7.3 Pounding Effects on Fragility Curves……...33
2.7.4 Pounding and Soil Effects on Fragility Curves…….38
2.7.5 Jacketing and Restrainer Effects on Fragility Curves……...43

2.8 Fragility Enhancement after Column Retrofit…….48
2.8.1 Fragility Curves after Retrofit by Column Jacketing for Longitudinal Direction…….48
2.8.1.1 Enhancement for Circular Column……55
2.8.1.2 Enhancement for Oblong Shape Column……..56
2.8.1.3 Enhancement for Rectangular Column……..56
2.8.1.4 Enhancement for All Types of Columns……...57
2.8.2 Enhancement after Calibrating the Analytical Fragility Curves.....58
2.8.3 Fragility Curves after Retrofit by Column Jacketing for Transverse Direction…….61
Chapter 3 Development of Empirical Fragility Curves…….……67
3.1 Empirical Bridge Damage Data……...67
3.2 Bridge Classification……70
3.3 Parameter Estimation……...71
3.4 Enhancement of Empirical Fragility Curves……98
Chapter 4 Seismic Hazard Modeling for Spatially Distributed Highway System……...101
4.1 Highway Network: Spatially Distributed System……..101
4.2 Deterministic Seismic Hazard……....102
4.3 Probabilistic Seismic Hazard…….103
Chapter 5 Methodology for System Performance Evaluation of Highway Network…..107
5.1 Overview……...….107
5.2 Site Ground Motion……..…108
5.3 Network Modeling……109
5.4 Bridge Damage State Simulation……..110
5.5 Assignment of Link Damage State and Residual Capacity……..……111
5.6 Traffic Demand: Origin-Destination Data……113
5.6.1 1996 SCAG Origin-Destination Data……..113
5.6.2 Origin-Destination Data Condensation……....117
5.6.3 Origin-Destination Data Change After Earthquake…….118
5.7 The Integrated Model……...…….121
5.8 Drivers' Delay……...……123

5.9 Opportunity Cost……..124
Chapter 6 Direct Economic Loss: Bridge Repair Cost……127
6.1 Number of Seismically Damaged Bridges ……127
6.2 Bridge Repair Cost Estimation in an Earthquake……..134
6.3 Expected Annual Repair Cost of a Site-Specific Bridge……..…….137
6.3.1 Annual Probability of Damage……...…137
6.3.2 Expected Annual Repair Cost before Retrofit……138
6.3.3 Expected Annual Repair Cost after Retrofit……...……138
6.3.4 System Annual Bridges Repair Cost…….……..139
Chapter 7 Social Cost Estimation……143
7.1 Daily Social Cost……...…143
7.1.1 Daily Social Cost under no Retrofit Condition……...…143
7.1.2 Retrofit Effect on Daily Social Cost…….…..147
7.2 System Restoration..……..……154
7.2.1 System Restoration Based on Bridge Repair Process……....154
7.2.2 System Restoration Based on Bridge Functionality Restoration...157
7.2.3 OD Recovery……..……158
7.2.4 System Restoration Curve and Total Social Cost……..…159
7.3 Economic Loss Estimation Related to System Social Cost……...……167
Chapter 8 Cost-effectiveness Analysis……....171
8.1 Introduction……171
8.2 Retrofit Cost ……..……...……...……..171
8.3 Benefit from Retrofit……..……...…168
8.4 Cost-Effectiveness Evaluation……...…179
Chapter 9 Conclusions ……189
Appendix A Moment-Rotation Curves of Bridge Columns……..…….…....193
Appendix B Integrated Traffic Assignment Model.……..……..257
Appendix C HighwaySRA Manual……..……..…293
Reference……...……..311

LIST OF FIGURES

Fig. 2.1	Stress-Strain Model for Concrete in Compression	10
Fig. 2.2	Elevation of Sample Bridges	13
Fig. 2.3	Nonlinearities in Bridge Model	15
Fig. 2.4	Column 2 of Bridge 1 before retrofit	16
Fig. 2.5	Column 2 of Bridge 1 after retrofit	18
Fig. 2.6	Acceleration Time Histories Generated for Los Angeles	21
Fig. 2.7	Responses at Column End of Bridge 1	23
Fig. 2.8	Displacement at Expansion Joints of Bridge 1	25
Fig. 2.9	Gap Element	31
Fig. 2.10	Ground Motion Time History for LA01	32
Fig. 2.11	Pounding Force at Expansion Joint	32
Fig. 2.12	Structural Responses without Pounding	32
Fig. 2.13	Structural Responses with Pounding	32
Fig. 2.14	Pounding Effect on Fragility Curves of Bridge 2	34
Fig. 2.15	Pounding Effect on Fragility Curves of Bridge 3	35
Fig. 2.16	Pounding Effect on Fragility Curves of Bridge 4	36
Fig. 2.17	Pounding Effect on Fragility Curves of Bridge 5	37
Fig. 2.18	Pounding and Soil Effects on Fragility Curves of Bridge 2	39
Fig. 2.19	Pounding and Soil Effects on Fragility Curves of Bridge 3	40
Fig. 2.20	Pounding and Soil Effects on Fragility Curves of Bridge 4	41
Fig. 2.21	Pounding and Soil Effects on Fragility Curves of Bridge 5	42
Fig. 2.22	Jacketing and Restrainer Effects on Fragility Curves of Bridge 2	44
Fig. 2.23	Jacketing and Restrainer Effects on Fragility Curves of Bridge 3	45
Fig. 2.24	Jacketing and Restrainer Effects on Fragility Curves of Bridge 4	46
Fig. 2.25	Jacketing and Restrainer Effects on Fragility Curves of Bridge 5	47
Fig. 2.26	Retrofit Effect on Fragility Curves of Bridge 1 (Longitudinal)	50
Fig. 2.27	Retrofit Effect on Fragility Curves of Bridge 2 (Longitudinal)	51
Fig. 2.28	Retrofit Effect on Fragility Curves of Bridge 3 (Longitudinal)	52
Fig. 2.29	Retrofit Effect on Fragility Curves of Bridge 4 (Longitudinal)	53

Fig. 2.30	Retrofit Effect on Fragility Curves of Bridge 5 (Longitudinal)	54
Fig. 2.31	Enhancement Curve for Circular Columns with Steel Jacketing	55
Fig. 2.32	Enhancement Curve for Oblong Columns with Steel Jacketing	56
Fig. 2.33	Enhancement Curve for Rectangular Columns with Steel Jacketing	57
Fig. 2.34	Enhancement Curve for Five Sample Bridges with Steel Jacketing	58
Fig. 2.35	Empirical Fragility Curves and Calibrated Analytical Fragility Curves of Bridge 2	60
Fig. 2.36	Retrofit Effect on Fragility Curves of Bridge 5 (Transverse)	62
Fig. 2.37	Retrofit Effect on Fragility Curves of Bridge 5 (Transverse)	63
Fig. 2.38	Retrofit Effect on Fragility Curves of Bridge 5 (Transverse)	64
Fig. 2.39	Retrofit Effect on Fragility Curves of Bridge 5 (Transverse)	65
Fig. 2.40	Retrofit Effect on Fragility Curves of Bridge 5 (Transverse)	66
Fig. 3.1	1994 Northridge Earthquake: PGA Distribution	68
Fig. 3.2	1994 Northridge Earthquake: PGV Distribution	68
Fig. 3.3	Fragility Curve on the basis of PGA (Composite)	77
Fig. 3.4	Fragility Curve on the basis of PGV (Composite)	77
Fig. 3.5	Fragility Curve in PGA (Single Span)	78
Fig. 3.6	Fragility Curve in PGA (Multiple Span)	78
Fig. 3.7	Fragility Curve in PGA (Skew 0^0-20^0)	79
Fig. 3.8	Fragility Curve in PGA (Skew 20^0-60^0)	79
Fig. 3.9	Fragility Curve in PGA (Skew $>60^0$)	80
Fig. 3.10	Fragility Curve in PGA (Soil A)	80
Fig. 3.11	Fragility Curve in PGA (Soil B)	81
Fig. 3.12	Fragility Curve in PGA (Soil C)	81
Fig. 3.13	Fragility Curve in PGA (Single Span /Skew 0^0-20^0)	82
Fig. 3.14	Fragility Curve in PGA (Single Span/Skew 20^0-60^0)	82
Fig. 3.15	Fragility Curve in PGA (Single Span/Skew $>60^0$)	83
Fig. 3.16	Fragility Curve in PGA (Multiple Span /Skew 0^0-20^0)	83
Fig. 3.17	Fragility Curve in PGA (Multiple Span/Skew 20^0-60^0)	84
Fig. 3.18	Fragility Curve in PGA (Multiple Span/Skew $>60^0$)	84
Fig. 3.19	Fragility Curve in PGA (Skew 0^0-20^0/Soil A)	85

Fig. 3.20	Fragility Curve in PGA (Skew 0^0-20^0/Soil B)	85
Fig. 3.21	Fragility Curve in PGA (Skew 0^0-20^0/Soil C)	86
Fig. 3.22	Fragility Curve in PGA (Skew 20^0-60^0/Soil A)	86
Fig. 3.23	Fragility Curve in PGA (Skew 20^0-60^0/Soil B)	87
Fig. 3.24	Fragility Curve in PGA (Skew 20^0-60^0/Soil C)	87
Fig. 3.25	Fragility Curve in PGA (Skew >60^0/Soil A)	88
Fig. 3.26	Fragility Curve in PGA (Skew >60^0/Soil C)	88
Fig. 3.27	Fragility Curve in PGA (Single Span / Soil A)	89
Fig. 3.28	Fragility Curve in PGA (Single Span / Soil B)	89
Fig. 3.29	Fragility Curve in PGA (Single Span / Soil C)	90
Fig. 3.30	Fragility Curve in PGA (Multiple Span / Soil A)	90
Fig. 3.31	Fragility Curve in PGA (Multiple Span / Soil B)	91
Fig. 3.32	Fragility Curve in PGA (Multiple Span / Soil C)	91
Fig. 3.33	Fragility Curve in PGA (Single Span /Skew 0^0-20^0 / Soil A)	92
Fig. 3.34	Fragility Curve in PGA (Single Span /Skew 0^0-20^0 / Soil B)	92
Fig. 3.35	Fragility Curve in PGA (Single Span /Skew 0^0-20^0 / Soil C)	93
Fig. 3.36	Fragility Curve in PGA (Single Span /Skew 20^0-60^0 / Soil C)	93
Fig. 3.37	Fragility Curve in PGA (Single Span /Skew >60^0 / Soil C)	94
Fig. 3.38	Fragility Curve in PGA (Multiple Span /Skew 0^0-20^0 / Soil A)	94
Fig. 3.39	Fragility Curve in PGA (Multiple Span /Skew 0^0-20^0 / Soil C)	95
Fig. 3.40	Fragility Curve in PGA (Multiple Span /Skew 20^0-60^0 / Soil A)	95
Fig. 3.41	Fragility Curve in PGA (Multiple Span /Skew 20^0-60^0 / Soil B)	96
Fig. 3.42	Fragility Curve in PGA (Multiple Span /Skew 20^0-60^0 / Soil C)	96
Fig. 3.43	Fragility Curve in PGA (Multiple Span /Skew >60^0 / Soil A)	97
Fig. 3.44	Fragility Curve in PGA (Multiple Span /Skew >60^0 / Soil C)	97
Fig. 3.45	Enhanced Fragility Curve (Minor)	99
Fig. 3.46	Enhanced Fragility Curve (Moderate)	99
Fig. 3.47	Enhanced Fragility Curve (Major)	100
Fig. 3.48	Enhanced Fragility Curve (Collapse)	100
Fig. 5.1	Flow Chart for System Performance Evaluation	107
Fig. 5.2	Highway Network: Link, Node and Bridge Component	109

Fig. 5.3	Network Model: Los Angeles and Orange County	109
Fig. 5.4	Detour after Northridge Earthquake (January 20th 1994)	113
Fig. 5.5	1996 Southern California Origin-Destination Data	115
Fig. 5.6	OD Data Condensation: Thiessen Polygon	117
Fig. 5.7	Integrated Trip Reduction And Network Models	120
Fig. 6.1	Bridge Damage in Elysian Park 7.1 (Without Retrofit)	128
Fig. 6.2	Link Damage in Elysian Park 7.1 (Without Retrofit)	129
Fig. 6.3	Bridge Damage in Elysian Park 7.1 (23% Retrofit)	129
Fig. 6.4	Link Damage in Elysian Park 7.1 (23% Retrofit)	130
Fig. 6.5	Bridge Damage in Elysian Park 7.1 (100% Retrofit)	130
Fig. 6.6	Link Damage in Elysian Park 7.1 (100% Retrofit)	131
Fig. 7.1	System Risk Curve in terms of Daily Drivers' Delay Under different Link Residual Capacity Assumptions (without retrofit)	145
Fig. 7.2	System Risk Curve in terms of Daily Opportunity Cost Under different Link Residual Capacity Assumptions (without retrofit)	146
Fig. 7.3	System Risk Curve in terms of Daily Social Cost Under different Link Residual Capacity Assumptions (without retrofit)	146
Fig. 7.4	Effect of Retrofit on System Risk Curve (Assumption 1)	150
Fig. 7.5	Effect of Retrofit on System Risk Curve (Assumption 2)	151
Fig. 7.6	Effect of Retrofit on System Risk Curve (Assumption 3)	154
Fig. 7.7	Probability Distribution of Functions used to Model Repair Processes	156
Fig. 7.8	Restoration Curves for Highway Bridges (after ATC-13, 1985)	158
Fig. 7.9	System Recovery Curves After Elysian Park M7.1 (No Retrofit)	159
Fig. 7.10	System Recovery Curves After Elysian Park M7.1 (23% Retrofit)	160
Fig. 7.11	System Recovery Curves After Elysian Park M7.1 (100% Retrofit)	160
Fig. 7.12	Retrofit Effect on System Recovery Curve(Elysian Park 7.1, Assumption 1)	162
Fig. 7.13	Retrofit Effect on System Recovery Curve(Elysian Park 7.1, Assumption 2)	162
Fig. 7.14	Retrofit Effect on System Recovery Curve(Elysian Park 7.1, Assumption 3)	163

Fig. 7.15	Fig. 7.15 Retrofit Effect on System Recovery Curve (Elysian Park 7.1, HAZUS)	163
Fig. A.1	Moment-Curvature Analysis of Bridge 1(Longitudinal)	195
Fig. A.2	Moment-Curvature Analysis of Bridge 2(Longitudinal)	196
Fig. A.3	Moment-Curvature Analysis of Bridge 3(Longitudinal)	200
Fig. A.4	Moment-Curvature Analysis of Bridge 4(Longitudinal)	201
Fig. A.5	Moment-Curvature Analysis of Bridge 5(Longitudinal)	220
Fig. A.6	Moment-Curvature Analysis of Bridge 3(Transverse)	225
Fig. A.7	Moment-Curvature Analysis of Bridge 4(Transverse)	234
Fig. A.8	Moment-Curvature Analysis of Bridge 5(Transverse)	245
Fig. B.1	Framework of Trip Reduction Estimation	258
Fig. B.2	Integrated Analysis of Trip Reduction and Network Models	262
Fig. B.3	Personal Trip Reductions caused by Regional Building Damage	263
Fig. B.4	Comparison of EPEDAT Fragility and the Study Estimated Fragility for Selected Building Occupancy Types	272
Fig. B.5	Trip Reduction Rate	279
Fig. B.6	Estimation Procedure of Truck Trip Reduction	279
Fig. B.7	Truck Trip Reduction Ratio	286
Fig. B.8	Conceptual OD Recovery Model	292
Fig. C.1	Main Interface	295
Fig. C.2	Menu “Map”	296
Fig. C.3	Map of Study Region	297
Fig. C.4	Map of Faults	297
Fig. C.5	Map of Freeway Network	298
Fig. C.6	Map of Bridges	298
Fig. C.7	Menu “Inventory”	299
Fig. C.8	Inventory: Bridges	299
Fig. C.9	Inventory: Network Links	300
Fig. C.10	Menu “Hazard”	300
Fig. C.11	Predefined Events	301
Fig. C.12	Importing PGA and MMI Shape Map	301

Fig. C.13 User Defined Event 302
Fig. C.14 Current Event Information 302
Fig. C.15 Analysis: Setting 303
Fig. C.16 Bridge Fragility Setting 303
Fig. C.17 Residual Link Performance Setting 304
Fig. C.18 Economic Loss Estimation Parameter Setting 304
Fig. C.19 Risk Analysis Option 305
Fig. C.20 Menu "Results" 306
Fig. C.21 PGA distribution 306
Fig. C.22 Display Bridge Damage States 307
Fig. C.23 Display Link Damage States 308
Fig. C.24 System Performance 309
Fig. C.25 Economic Loss 310

LIST OF TABLES

Table 2.1	Description of Five (5) Sample Bridges	12
Table 2.2	Description of Los Angeles Ground Motions	20
Table 2.3	Description of Damaged States	28
Table 2.4	Peak Ductility Demand of First Left Column of Sample Bridges	28
Table 2.5	Number of Damaged Bridges: Pounding Effect in Bridge 2	34
Table 2.6	Number of Damaged Bridges: Pounding Effect in Bridge 3	35
Table 2.7	Number of Damaged Bridges: Pounding Effect in Bridge 4	36
Table 2.8	Number of Damaged Bridges: Pounding Effect in Bridge 5	37
Table 2.9	Number of Damaged Bridges: Pounding and Soil Effects in Bridge 2	39
Table 2.10	Number of Damaged Bridges: Pounding and Soil Effects in Bridge 3	40
Table 2.11	Number of Damaged Bridges: Pounding and Soil Effects in Bridge 4	41
Table 2.12	Number of Damaged Bridges: Pounding and Soil Effects in Bridge 5	42
Table 2.13	Number of Damaged Bridges: Jacketing and Restrainer Effects on Bridge 2	44
Table 2.14	Number of Damaged Bridges: Jacketing and Restrainer Effects on Bridge 2	45
Table 2.15	Number of Damaged Bridges: Jacketing and Restrainer Effects on Bridge 2	46
Table 2.16	Number of Damaged Bridges: Jacketing and Restrainer Effects on Bridge 2	47
Table 2.17	Number of Damaged Bridges: Retrofit Effect in Bridge 1 (longitudinal)	50
Table 2.18	Number of Damaged Bridges: Retrofit Effect in Bridge 2 (longitudinal)	51
Table 2.19	Number of Damaged Bridges: Retrofit Effect in Bridge 3 (longitudinal)	52
Table 2.20	Number of Damaged Bridges: Retrofit Effect in Bridge 4 (longitudinal)	53

Table 2.21	Number of Damaged Bridges: Retrofit Effect in Bridge 5 (longitudinal)	54
Table 2.22	Simulated Ductility Capacities of Sample Bridges	59
Table 2.23	Fragility Curves based on Adjusted Damage States Definitions	61
Table 2.24	Enhancement Ratios Comparison	61
Table 2.25	Number of Damaged Bridges: Retrofit Effect in Bridge 1(Transverse)	62
Table 2.26	Number of Damaged Bridges: Retrofit Effect in Bridge 2 (Transverse)	63
Table 2.27	Number of Damaged Bridges: Retrofit Effect in Bridge 3 (Transverse)	64
Table 2.28	Number of Damaged Bridges: Retrofit Effect in Bridge 4 (Transverse)	65
Table 2.29	Number of Damaged Bridges: Retrofit Effect in Bridge 5 (Transverse)	66
Table 3.1	Summary of Bridge Damage Status in 1994 Northridge Earthquake	67
Table 3.2	Bridge Seismic Damage Table in the 1994 Northridge Earthquake	69
Table 3.3	Empirical Fragility Curve: First Level (Composite)	71
Table 3.4	Empirical Fragility Curve: Second Level	71
Table 3.5	Empirical Fragility Curve: Third Level	72
Table 3.6	Empirical Fragility Curve: Fourth Level	74
Table 4.1	Probabilistic Scenario Earthquake Set	105
Table 5.1	Assumption for Residual Link Capacity	113
Table 5.2	Trip ratios of each directional trip for 4 time span	115
Table 5.3	3 hours average of am peak and midday applied peak ratio and car occupancy rates	115
Table 6.1	Damaged Bridges in Elysian Park M7.1(Total 3133 bridges)	131
Table 6.2	Comparison: Number of Damaged Bridges	132
Table 6.3	Reduction in Number of Damaged Bridges	133
Table 6.4	Damage Ratios for Highway Bridge Components (from HAZUS 99)	136
Table 6.5	Expected Bridge Repair Cost (in $ thousand)	136

Table 6.6	Annual Probability of Sustaining Damage for a Bridge before and after Retrofit	140
Table 6.7	Annual Bridge Repair Cost in the System	141
Table 7.1	Daily Travel Delay and Opportunity Cost (without retrofit)	144
Table 7.2	Daily Travel Delay and Opportunity Cost (23% retrofit)	147
Table 7.3	Daily Travel Delay and Opportunity Cost (100% Retrofit)	148
Table 7.4	Restoration Function for Highway Bridges (after ATC-13, 1985)	158
Table 7.5	Total Travel Delay and Opportunity Cost (no retrofit)	164
Table 7.6	Total Travel Delay and Opportunity Cost (23% retrofit)	165
Table 7.7	Total Travel Delay and Opportunity Cost (100% retrofit)	166
Table 7.8	Economic Loss due to System Dysfunction (No Retrofit)	168
Table 7.9	Economic Loss due to System Dysfunction (23% Retrofit)	169
Table 7.10	Economic Loss due to System Dysfunction (100% Retrofit)	170
Table 8.1	Annual Avoided Social Loss (Assumption 1)	174
Table 8.2	Annual Avoided Social Loss (Assumption 2)	175
Table 8.3	Annual Avoided Social Loss (Assumption 3)	176
Table 8.4	Annual Avoided Social Loss (HAZUS Model)	177
Table 8.5	Discount Factor	179
Table 8.6	Cost-Effectiveness Analysis (Discount Rate 3%)	182
Table 8.7	Cost-Effectiveness Analysis (Discount Rate 5%)	184
Table 8.8	Cost-Effectiveness Analysis (Discount Rate 7%)	186
Table 8.9	Cost-Benefit Analysis Summary	188
Table B.1	Building fragility by structure types	265
Table B.2	Southern California Building Stock by Structure Types	267
Table B.3	Southern California Building Stock by Occupancy Types	268
Table B.4	Summary of Southern California Buildings by structure and occupancy Types	269
Table B.5	Vulnerability of Building Occupancy	271
Table B.6	Activity Population by Building Occupancy Types	275
Table B.7	Trip Types and Building Occupancy types	276
Table B.8	Person Trip Reduction Rates	277

Table B.9 Truck Generation Rate 281
Table B.10 Building Usage and Truck-trip Generating Industries 282
Table B.11 Estimated PCE by Industries 283
Table B.12 Calibration of Decay Function Parameter 290

Chapter 1 Introduction

Past experience showed too often that earthquake damage to highway components (e.g., bridges, roadways, tunnels, retaining walls, etc.) can severely disrupt traffic flows and thus negatively impacting on the economy of the region as well as post-earthquake emergency response and recovery. Furthermore, the extent of these impacts will depend not only on the nature and magnitude of the seismic damage sustained by the individual components, but also on the mode of functional impairment of the highway system as a network resulting from physical damage of its components. In order to estimate the effects of the earthquake on the performance of the transportation network, an analytical framework must be developed to integrate bridge and other structural performance model and transportation network model in the context of seismic risk assessment.

Highway transportation networks are complex with many engineered components placed in equally complex hazardous environments, natural or manmade. Among the engineered components, bridges represent potentially the most vulnerable components under earthquake conditions as demonstrated as vividly in the San Fernando, Loma Prieta, Northridge and Kobe Earthquakes. Recognizing this, the Caltrans' seismic retrofit program has been underway since the 1971 San Fernando Earthquake, and accelerated since the 1989 Loma Prieta event. At this time (June, 2005), 23% of Caltrans freeway bridges in Los Angeles and Orange Counties have been retrofitted by the steel and composite jacketing of the columns as well as rebuilding and upgrading of the restraining devises at expansion joints for which the seismic retrofit was deemed necessary. It is therefore most timely at this time to assess not only the engineering significance of such retrofit but also the socio-economic benefit arising therefrom.

The purpose of this research therefore is to assess the socio-economic impact of seismic retrofit implemented on the Caltrans' bridges on the freeway network in the Los Angeles and Orange Counties. The research concentrates on the evaluation of the socio-economic benefit resulting from the retrofit performed on the Caltrans' bridges primarily by means of column jacketing with steel. The three major tasks of this research are (1) development of fragility curves of the bridge, (2) assessment of the seismic performance of the freeway and (3) related socio-economic analysis.

In order to perform a seismic risk analysis of a highway network, it is imperative to identify seismic vulnerability of bridges associated with various states of damage. As a widely practiced approach, the vulnerability information is expressed in the form of fragility curve to account for a multitude of uncertain sources involved (Shinozuka et al, 2003a). In Chapter 2, a manageable number of representative bridges are selected for the fragility analysis. Finite Element Model for each of the representative bridges, without or with retrofit (column jacketing with steel) is developed and used to perform nonlinear dynamic time history analysis. Based on the result of this dynamic analysis, a family of fragility curves associated with various states of damage are estimated with a statistical procedure. The seismic performance improvement of the retrofitted bridges is evident in that the median value of fragility curve of these bridges is significantly increased. The median value is one of the two fragility parameters with the other being the log-standard deviation. The enhancement ratios for median values of analytical fragility curves are then applied to empirical fragility curves based on bridge damage data obtained from the 1994 Northridge Earthquake to consider the effect of the bridge retrofit (Chapter 3). The

enhancement ratio is defined as (median value for retrofitted bridges) / (median value for bridges not retrofitted).

After the introduction of major features of seismic risk analysis for spatially distributed system, both deterministic and probabilistic seismic modeling methods are described in Chapter 4. Particularly, a set of 47 probabilistic scenario earthquakes is provided for the probabilistic seismic risk analysis for the highway transportation network in Los Angles and Orange Counties. In chapter 5, a methodology is developed to evaluate the seismic performance of highway transportation network in terms of related social cost. Based on fragility curves developed above and the site ground motion originating from scenarios, the damage states of bridges are simulated, which determine the reduced link traffic capacity. A comprehensive traffic assignment analysis, which features realistic consideration of trip reduction and recovery after a damaging earthquake, is then performed in the degraded highway network with variable OD input. The daily social cost, including the traffic delay time and opportunity cost, is used to measure the post-event performance of the damaged highway network. The enhancement of the network performance is then studied by comparing the social cost in using fragility curves of bridges with and without retrofit in the network performance simulation under the same scenario earthquake.

Chapter 6 describes the method for estimation of bridge restoration (repair/replacement) cost. For the given scenarios, the expected bridge repair cost is calculated for each of the 3 cases of bridge retrofit status: No retrofit, 23% retrofit (current status) and 100% retrofit, assuming that no freeway bridges (in Los Angeles and Orange County), 23% of them (actual % at the time of writing this report) and 100% of them have been retrofitted. To estimate the total social cost resulting from an earthquake, the network

restoration curves are developed in Chapter 7. Using a probabilistic time-dependent bridge repair model, the new set of bridge damage states are determined based on Monte Carlo simulation at any given time point after an earthquake. The traffic assignment analysis is performed again to obtain the corresponding daily social cost for the partially restored network. The integration of the daily social cost over the restoration period gives the total social cost in time for a particular earthquake event. The economic loss due to the time cost is estimated by considering the local unit time value.

Whether a retrofit strategy is cost effective is evaluated by a cost-benefit analysis introduced in Chapter 8. The restoration cost for the damaged bridges, the retrofit cost and economic loss due to social cost are estimated. The difference between the economic loss without and with retrofit represents the cost avoided. The economic benefit is then measured by the cost avoided minus the cost of retrofit. The economic analysis is performed for each of the probabilistic scenario earthquakes and expected annual benefit of the retrofit measure obtained by considering the annual probabilities of these scenarios. The results show that the bridge restoration cost avoided alone cannot compensate for the retrofit cost. However, when the social cost avoided is considered, the cost-effectiveness ratios in both retrofit cases are much larger than 1, indicating very high benefit for the public obtained from the Caltrans bridge retrofit measures. Chapter 9 summarizes the conclusions obtained from this research.

At the end of the report, three documents are appended. Appendix A provides the cross-sections and moment-rotation relationship of 5 sample bridges' columns before and after retrofit. Appendix B describes the background of the traffic assignment model integrating the OD change due to earthquake damage. In Appendix C, A GIS-based

Program for Highway Seismic Risk Analysis (HighwaySRA) developed at UCI is introduced and its usage and functionality are demonstrated in a manual which is part of the Appendix C.

Chapter 2 Development of Analytical Fragility Curve for Bridges

2.1 Introduction

Several recent destructive earthquakes, particularly the 1989 Loma Prieta and 1994 Northridge earthquakes in California, and the 1995 Hanshin-Awaji (Kobe) earthquake in Japan, caused significant damage to a large number of highway structures that were seismically deficient (Basoz and Kiremidjian 1998, Buckle 1994). The investigation of these negative consequences gave rise to serious discussions about seismic design philosophy and extensive research activity on the retrofit of existing bridges as well as the seismic design of new bridges. In this respect, this study presents an approach for the seismic assessment of older bridges retrofitted by steel jacketing of the columns having substandard seismic characteristics and by restrainers at expansion joints to prevent bridge decks from unseating. The main objective of the study is focused to evaluate the effects of column retrofit with steel jacketing on the ductility capacity of bridge columns.

The Caltrans' seismic retrofit program was underway prior to the 1994 Northridge earthquake and was accelerated after the 1989 Loma Prieta event. This resulted in implementation of steel and composite jacketing of the columns, and of installing and upgrading of the restraining devices at expansion joints for many bridges for which the seismic retrofit was deemed necessary. Therefore, it is most timely to assess the engineering significance and benefit from such retrofit.

This study first develops moment-curvature curves of bridge columns and then performs nonlinear dynamic time history analyses producing fragility curves for five (5) sample bridges before and after retrofitting their columns with steel jacketing. The effect of retrofit is demonstrated by means of the ratio of the median value of the fragility curve for retrofitted column to that of the column before retrofit. This ratio is referred to as fragility enhancement. The fragility enhancement is found to be more significant for more severe state of damage. It is then assumed that the same fragility enhancement is applicable to the empirical fragility curves developed from the Northridge damage data (Chapter 3). The fragility curves for four (4) of sample bridges are also developed before and after retrofitting its expansion joints with restrainers.

This physical improvement of the seismic vulnerability due to steel jacketing becomes evident in terms of enhanced fragility curves shifting those associated with the bridges before retrofit to the right when plotted as functions of PGA (Peak Ground Acceleration). Thus, this study makes it possible to evaluate the improvement of the highway network performance resulting from such retrofit by providing basic information for fragility enhancement.

2.2 Column Retrofit with Steel Jacketing

2.2.1 Background

Concrete columns of earlier design often lack flexural strength, flexural ductility and shear strength. One of the main causes for these structural inadequacies is lap splices in critical regions and/or premature termination of longitudinal reinforcement. A number of column retrofit techniques, such as steel jacketing, wire pre-stressing and composite material jacketing, have been developed and tested. Although advanced composite

materials and other methods have been recently studied, the steel jacketing has been widely applied to bridge retrofit as the most common retrofit technique.

Chai *et al*. (1991) observed that confinement of the concrete columns can be improved if transverse reinforcement layers are placed relatively close together along the longitudinal axis by restraining the lateral expansion of the concrete. It makes it possible for the compression zone to sustain higher compression stresses and much higher compression strains before failure occurs. Obviously, however, this is for original design and construction, but not applicable to existing bridges, to enhance the performance of columns by adding transverse reinforcement layers. In this respect, this study focuses on the steel jacketing technique for retrofitting existing bridge columns to improve their seismic performance.

2.2.2 Steel Jacketing

An experiment was performed by Chai *et al*. (1991) to investigate the retrofit of circular columns with steel jacketing. In this experiment, for circular columns, two half shells of steel plate rolled to a radius slightly larger than that of the column are positioned over the area to be retrofitted and are site-welded up the vertical seams to provide a continuous tube with a small annular gap around the column. This gap is grouted with pure cement. It is typical that the jacket is cut to provide a space of about 50 mm (2 in) between the jacket and any supporting member. It is for the jacket to avoid the possibility to act as compressing reinforcement by bearing against the supporting member at large drift angles. It is noted that the jacket is effective only in passive confinement and the level of confinement depends on the hoop strength and stiffness of the steel jacket.

The thickness of steel jacket is calculated from the following equation (Priestley *et al*., 1996).

$$t_j = \frac{0.18(\varepsilon_{cm} - 0.004)Df_{cc}^{'}}{f_{yj}\varepsilon_{sm}} \tag{2.1}$$

where ε_{cm} is the strain at maximum stress in concrete, ε_{sm} the strain at maximum stress in steel jacket, D the diameter of circular column, $f_{cc}^{'}$ the compressive strength of confined concrete and f_{yj} the yield stress of steel jacket.

2.2.3 Compression Stress-Strain Relationships for Confined Concrete

The effect of confinement is to increase the compression strength and ultimate strain of concrete as illustrated in Fig 2.1 (after Priestley *et al*., 1996). Many different stress-strain relationships have been developed for confined concrete. Most of these are applicable under certain specific conditions. A recent model applicable to all cross-sectional shapes and at all levels of confinement is used for the analysis defined by the key equations that also appears in Priestley *et al*. (1996).

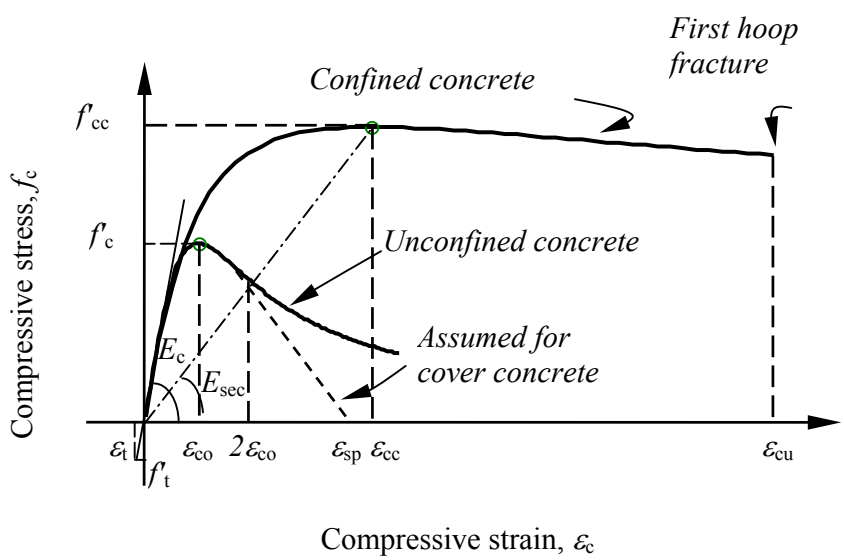

Fig 2.1 Stress-Strain Model for Concrete in Compression

2.3 Bridge Model

Not all but a manageable number of bridges, representing typical bridges in California and covering many types of bridge structures, have been selected for the fragility analysis.

2.3.1 Bridge Description

Five (5) sample bridges used for example analysis are listed in Table 2.1 and shown in Fig 2.2. Bridge 1 has the overall length of 34 m (112 ft) with three spans. The superstructure consists of a longitudinally reinforced concrete deck slab 10 m (32.8 ft) wide and it is supported by two sets of columns (and by an abutment at each end). Each set has three columns of circular cross section with 0.8 m (31.5 in) diameter.

Bridge 2 has an overall length of 242 m (794 ft) with five spans and an expansion joint in the center span. This bridge is supported by four columns of equal height of 21 m (69 ft) between the abutments at the ends. Each column has a circular cross section with 2.4 m diameter. The deck has a 3-cell concrete box type girder section 13 m (42.6 ft) wide and 2 m (6.6 ft) deep.

Bridge 3 has an overall length of 226 m (741 ft) with five spans, consisting of three frames separated by two expansion joints. The columns have varying lengths with longer ones in the center span and shorter ones near the abutments. The superstructure consists of a RC box girder to the left of the left expansion joint and to the right of the right expansion joint, and a prestressed box girder in the central span. The deck has a 6-cell box girder section 20 m (65.6 ft) wide and 2.6 m (8.5 ft) deep, and the column section is octagonal.

Bridge 4 has an overall length of 483 m (1584 ft) with ten spans and four expansion joints. This bridge is supported by nine columns having different heights. Each column has a rectangular cross section which is 1.2 m (3.9 ft) by 3.7 m (12.1 ft) in dimension. The deck has a 5-cell concrete box type girder section 17 m (56 ft) wide and 2 m (6.6 ft) deep.

Bridge 5 has an overall length of 500 m (1640 ft) with twelve spans and an expansion joint. This bridge is supported by eleven columns of equal height of 12.8 m (42.0 ft) between the abutments at the ends. Each column section is oblong in shape. The deck has a 4-cell concrete box type girder section 15 m (49.2 ft) wide and 2 m (6.6 ft) deep.

Table 2.1 Description of Five (5) Sample Bridges

Bridges	Overall Length meter (foot)	Number of Spans	Number of Hinges	Column Height meter (foot)
1	34(112)	3	0	4.7 (15.4)
2	242(794)	5	1	21.0 (68.9)
3	226(741)	5	2	9.5 - 24.7(31.2-81.0)
4	483 (1584)	10	4	9.5 - 34.4 (31.2-112.83)
5	500 (1640)	12	1	12.8 (42.0)

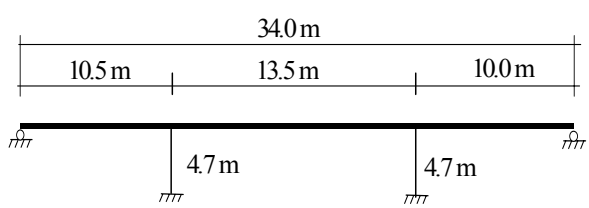

(a) Bridge 1

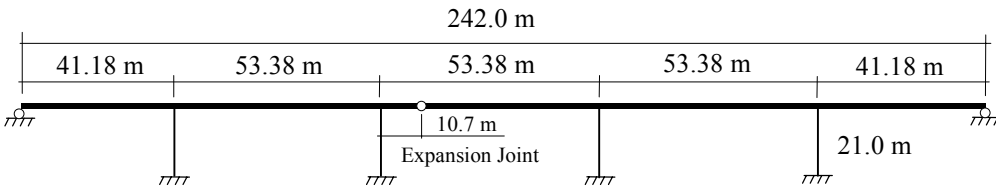

(b) Bridge 2

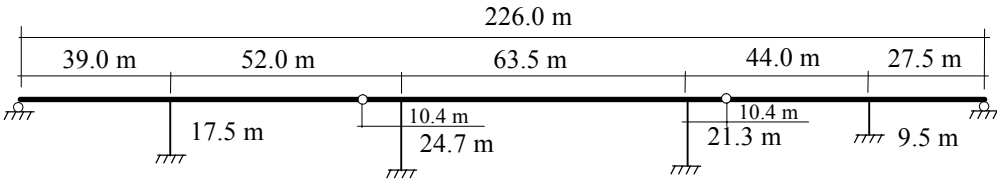

(c) Bridge 3

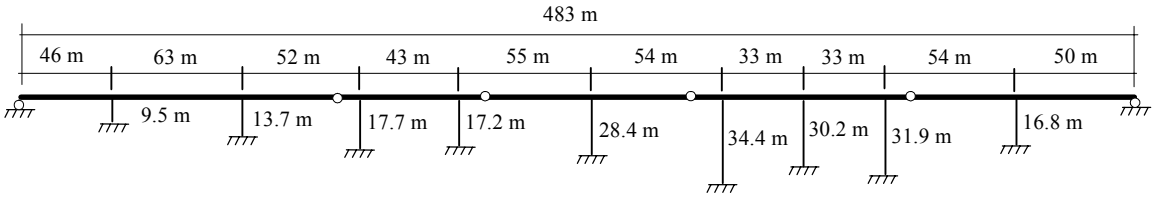

(d) Bridge 4

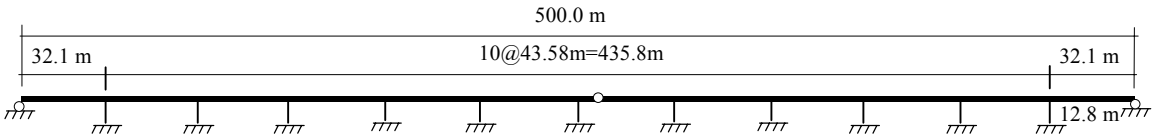

(e) Bridge 5

Fig 2.2 Elevation of Sample Bridges

2.3.2 Bridge Modeling

The bridges are modeled to exhibit the nonlinear behavior of the columns. A column is modeled as an elastic zone with a pair of plastic zones at each end of the column. Each plastic zone is then modeled to consist of a nonlinear rotational spring and

a rigid element depicted in Fig 2.3. The plastic hinge formed in the bridge column is assumed to have bilinear hysteretic characteristics. Furthermore, pounding effect at the expansion joint of the bridges is reflected in the structural response analysis, so that the fragility information of the structure becomes more realistic. In this respect, the expansion joint is constrained in the relative vertical movement, while freely allowing horizontal opening movement and rotation. The closure at the joint, however, is restricted by a gap element when the relative motion of adjacent decks exhausts the initial gap width of 2.54 cm (1 in) leading to deck pounding. A hoop element sustaining tension only is used for the bridge retrofitted by restrainers at expansion joints and the opening is restricted by the element when the relative motion exhausts the initial slack of 1.27 cm (0.5 in). Springs are also attached to the bases of the columns to account for soil effects, while two abutments are modeled as roller supports. To reflect the cracked state of a concrete bridge column for the seismic response analysis, an effective moment of inertia is employed, making the period of the bridge longer.

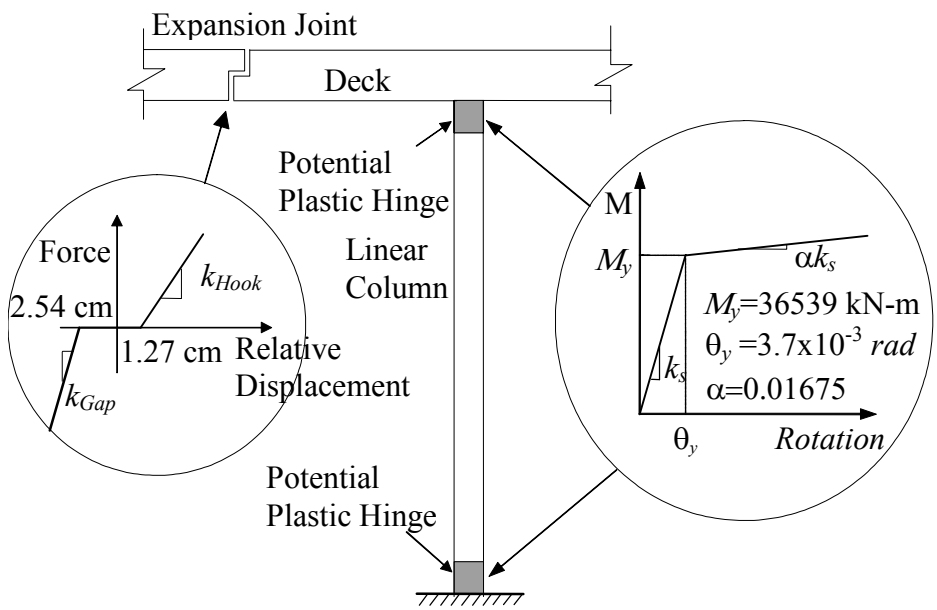

Fig 2.3 Nonlinearities in Bridge Model

2.4 Development of Moment-Curvature Relationship

The column ductility program developed by Kushiyama (2002) (the code is attached in Appendix A) is used to model the moment-curvature relationship of plastic hinges for columns. The critical parameter used to describe the nonlinear structural response in this study is the ductility demand. The ductility demand is defined as θ / θ_y, where θ is the rotation of a bridge column in its plastic hinge and θ_y is the corresponding rotation at the yield point.

Nonlinear response characteristics associated with the bridges are based on moment-curvature curve analysis taking axial loads as well as confinement effects into account. The moment-curvature relationship used in this study for the nonlinear spring is bilinear without any stiffness degradation. Its parameters are established according to the equations in Priestley et al. (1996).

2.4.1 Moment-Curvature Curves for Longitudinal Direction of Bridges

In Fig 2.4 and 2.5, Section of the column, stress-strain relationship, distribution of axial force, P-M interaction diagram, moment-curvature curve and moment-rotation curve for column 2 of Bridge 1 before and after retrofit are plotted. The cross sections and the moment- rotation curves of all the other columns of Bridge 1-5 are provided in Appendix A.

One of results, for example, shows that the moment-curvature curve after retrofit gives a much better performance than that before retrofit by 4 times based on curvature at the ultimate compressive strain and by 1.6 times at the ultimate moment.

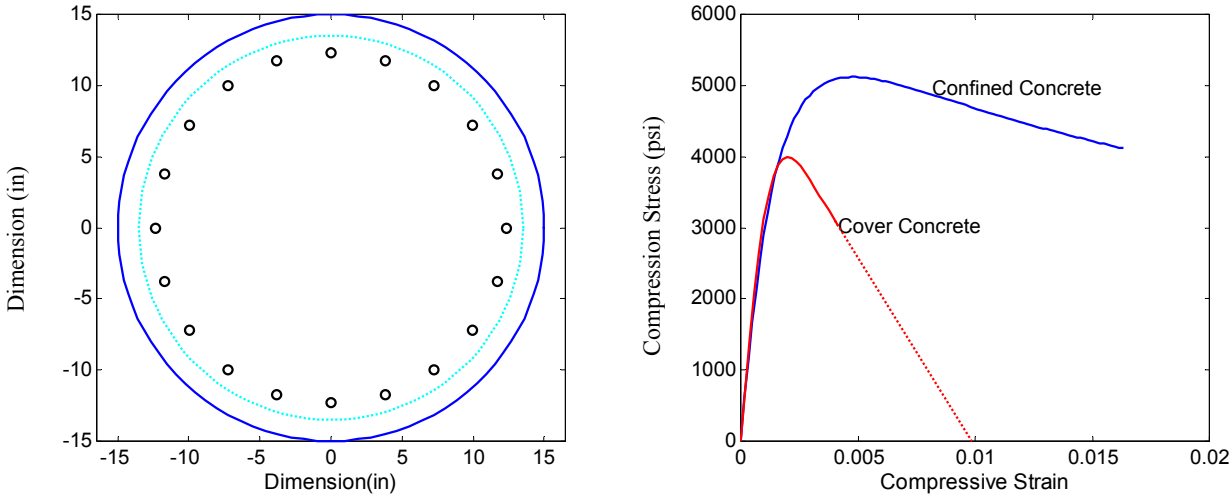

(a) Section of Column (b) Stress-Strain Relationship

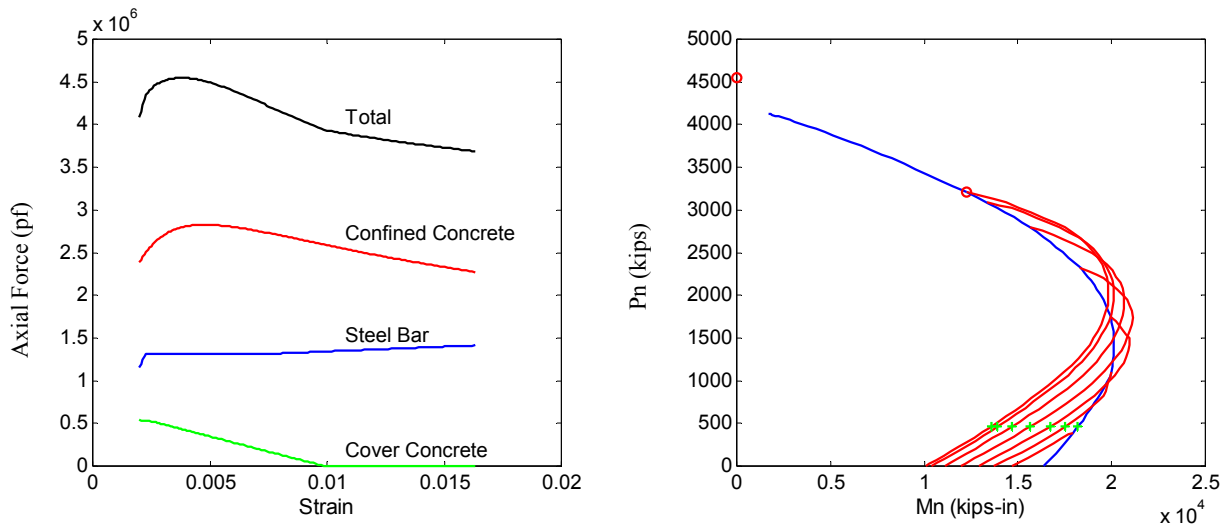

(c) Distribution of Axial Force (d) P-M Interaction Diagram

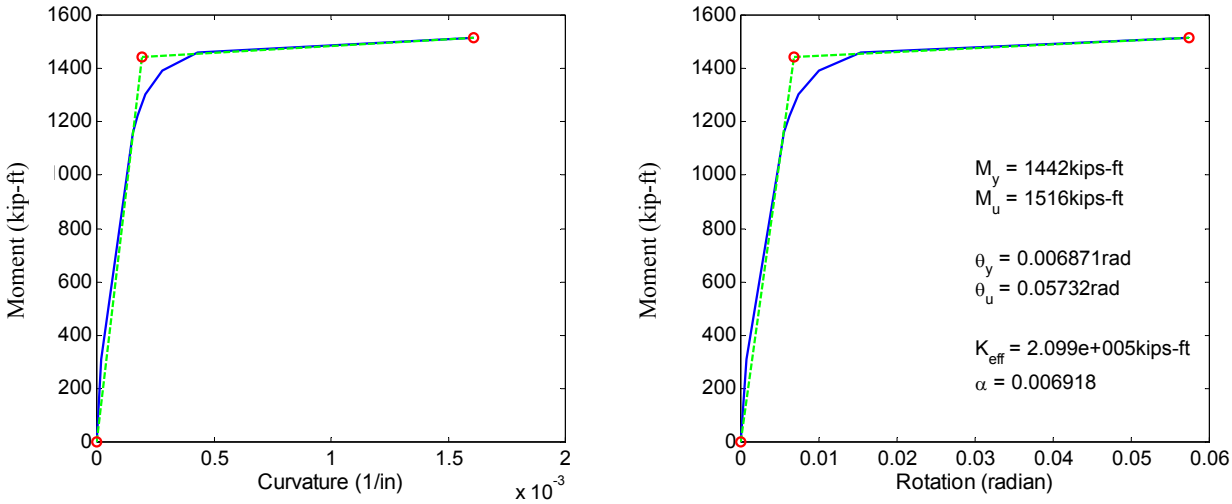

(e) Moment-Curvature Curve (f) Moment-Rotation Curve

Fig 2.4 Column 2 of Bridge 1 Before Retrofit

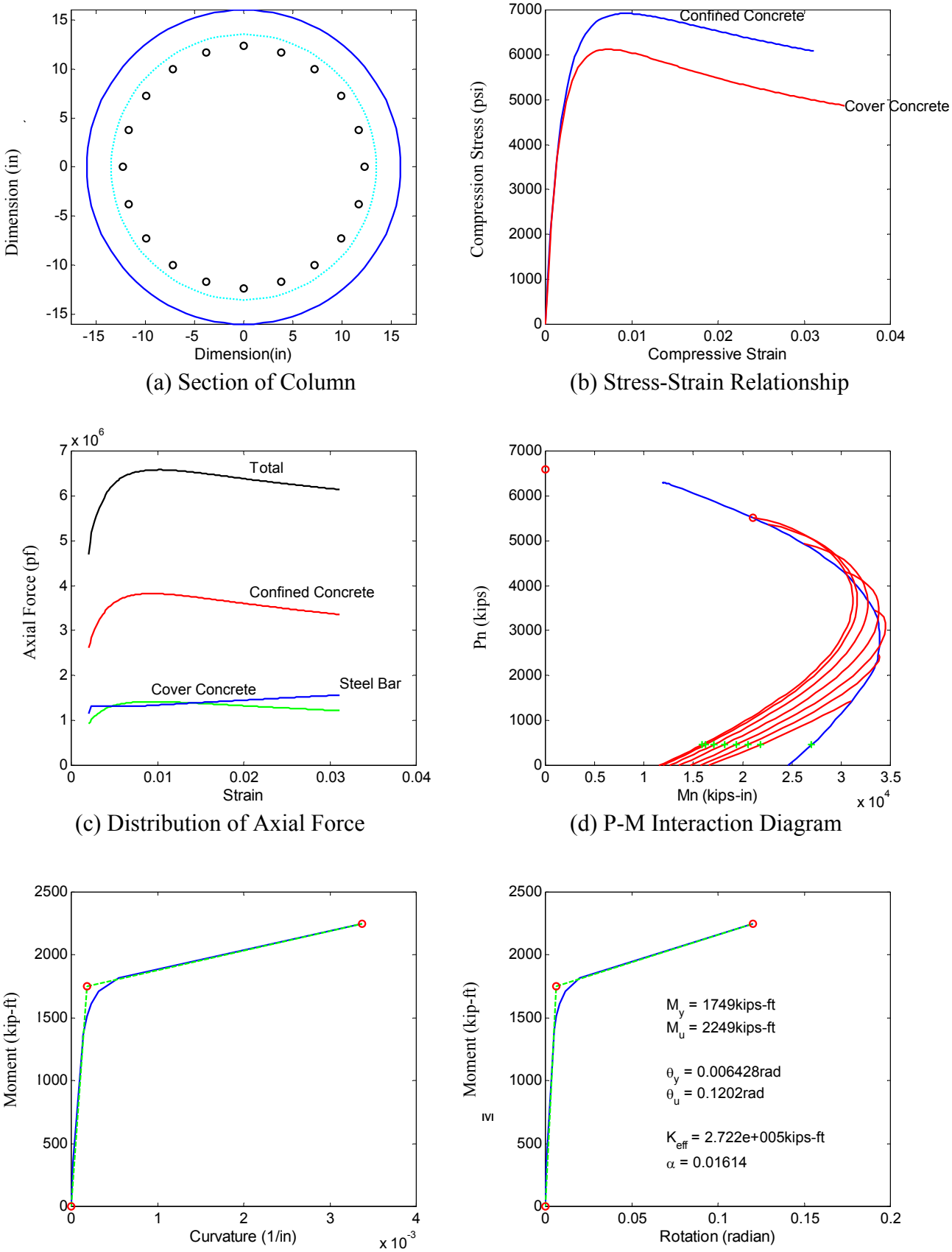

(a) Section of Column

(b) Stress-Strain Relationship

(c) Distribution of Axial Force

(d) P-M Interaction Diagram

(e) Moment-Curvature Curve

(f) Moment-Rotation Curve

Fig 2.5 Column 2 of Bridge 1 After Retrofit

2.5 Bridge Response Analysis

The *SAP2000/Nonlinear* finite element computer code (Computer and Structures, 2002) is utilized for the extensive two-dimensional response analysis of the bridge under sixty (60) Los Angeles earthquake time histories (http://nisee.berkeley.edu/data/strong_motion/sacsteel/ground_motions.html) listed in Table 2.2, to develop the fragility curves before and after column retrofit with steel jackets.

2.5.1 Input Ground Motions

These acceleration time histories were derived from historical records with some linear adjustments and consist of three (3) groups (each consisting of 20 time histories) having probabilities of exceedance of 10% in 50 years, 2% in 50 years and 50% in 50 years, respectively. A typical acceleration time history in each group is plotted in the same scale to compare the magnitude of the acceleration in Fig 2.6.

Table 2.2 Description of Los Angeles Ground Motions

10% Exceedence in 50 yr				2% Exceedence in 50 yr				50% Exceedence in 50 yr			
SAC Name	DT (sec)	Duration (sec)	PGA (cm/sec^2)	SAC Name	DT (sec)	Duration (sec)	PGA (cm/sec^2)	SAC Name	DT (sec)	Duration (sec)	PGA (cm/sec^2)
LA01	0.02	39.38	452.03	LA21	0.02	59.98	1258.00	LA41	0.01	39.38	578.34
LA02	0.02	39.38	662.88	LA22	0.02	59.98	902.75	LA42	0.01	39.38	326.81
LA03	0.01	39.38	386.04	LA23	0.01	24.99	409.95	LA43	0.01	39.08	140.67
LA04	0.01	39.38	478.65	LA24	0.01	24.99	463.76	LA44	0.01	39.08	109.45
LA05	0.01	39.38	295.69	LA25	0.005	14.945	851.62	LA45	0.02	78.60	141.49
LA06	0.01	39.38	230.08	LA26	0.005	14.945	925.29	LA46	0.02	78.60	156.02
LA07	0.02	79.98	412.98	LA27	0.02	59.98	908.70	LA47	0.02	79.98	331.22
LA08	0.02	79.98	417.49	LA28	0.02	59.98	1304.10	LA48	0.02	79.98	301.74
LA09	0.02	79.98	509.70	LA29	0.02	49.98	793.45	LA49	0.02	59.98	312.41
LA10	0.02	79.98	353.35	LA30	0.02	49.98	972.58	LA50	0.02	59.98	535.88
LA11	0.02	39.38	652.49	LA31	0.01	29.99	1271.20	LA51	0.02	43.92	765.65
LA12	0.02	39.38	950.93	LA32	0.01	29.99	1163.50	LA52	0.02	43.92	619.36
LA13	0.02	59.98	664.93	LA33	0.01	29.99	767.26	LA53	0.02	26.14	680.01
LA14	0.02	59.98	644.49	LA34	0.01	29.99	667.59	LA54	0.02	26.14	775.05
LA15	0.005	14.945	523.30	LA35	0.01	29.99	973.16	LA55	0.02	59.98	507.58
LA16	0.005	14.945	568.58	LA36	0.01	29.99	1079.30	LA56	0.02	59.98	371.66
LA17	0.02	59.98	558.43	LA37	0.02	59.98	697.84	LA57	0.02	79.46	248.14
LA18	0.02	59.98	801.44	LA38	0.02	59.98	761.31	LA58	0.02	79.46	226.54
LA19	0.02	59.98	999.43	LA39	0.02	59.98	490.58	LA59	0.02	39.98	753.70
LA20	0.02	59.98	967.61	LA40	0.02	59.98	613.28	LA60	0.02	39.98	469.07

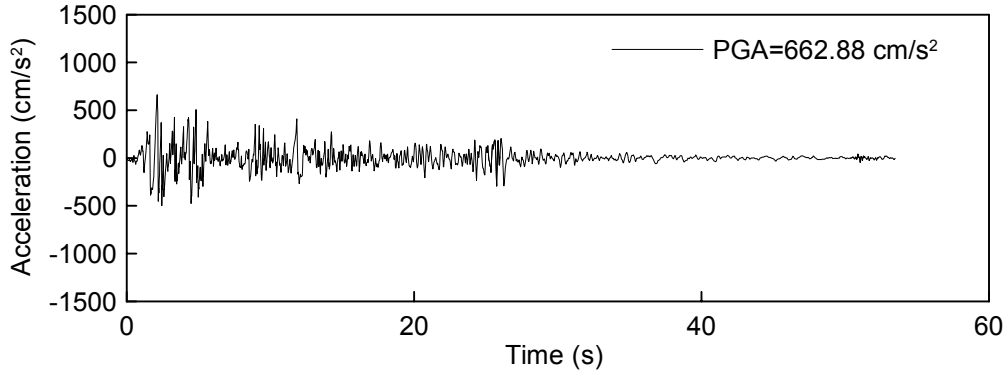

(a) 10% Probability of Exceedence in 50 Years

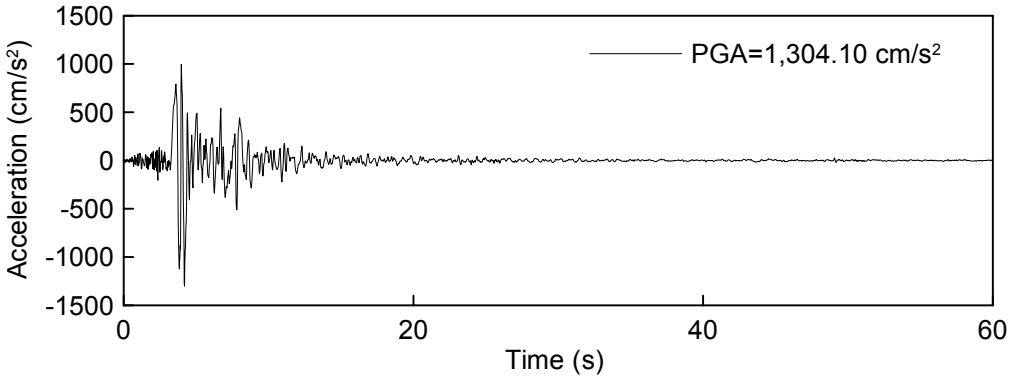

(b) 2% Probability of Exceedence in 50 Years

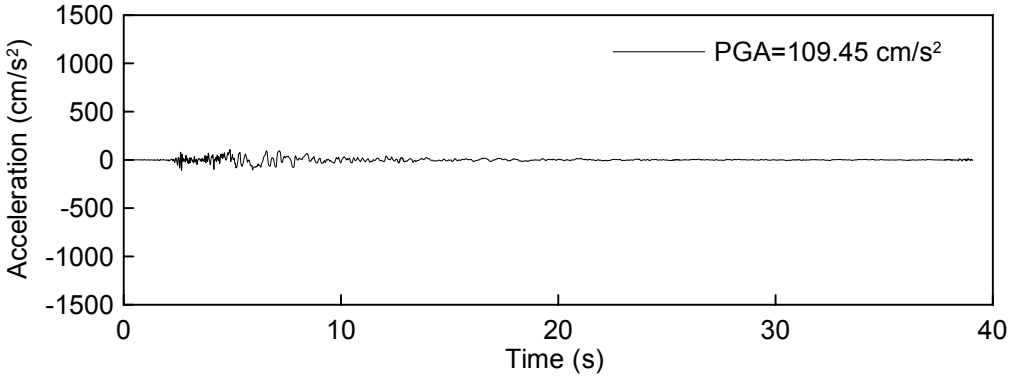

(c) 50% Probability of Exceedence in 50 Years

Fig 2.6 Acceleration Time Histories Generated for Los Angeles

2.5.2 Responses of Structures

Typical responses at column bottom end of Bridge 1 are plotted in Fig 2.7 with the acceleration time history in Fig 2.6a as input. It is reasonable to expect that the rotation after retrofit is generally smaller than before, while the accelerations do not necessarily behave that way and can be quite different each other. It is noted that some higher fluctuations in acceleration response appear after retrofit because the column becomes stiffer than before.

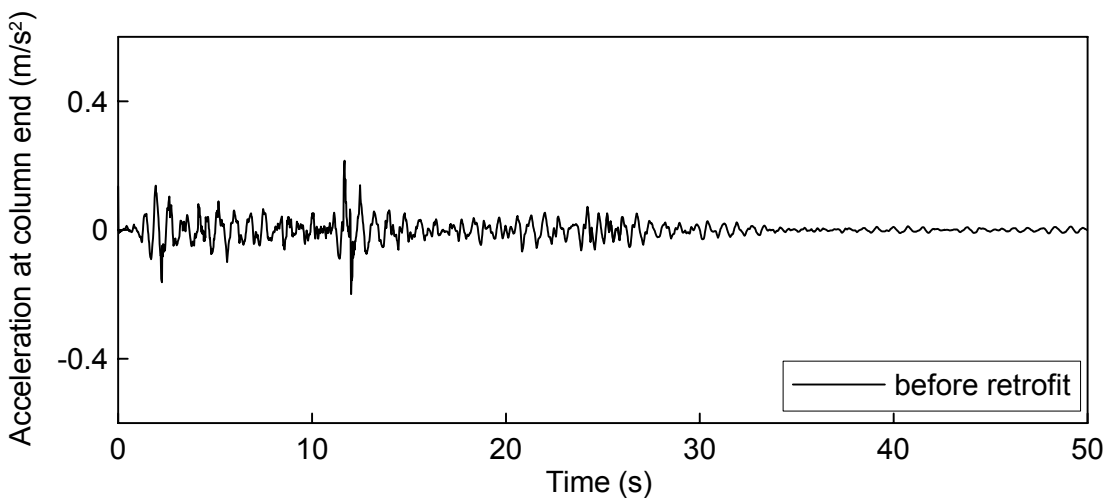

(a) Acceleration before retrofit

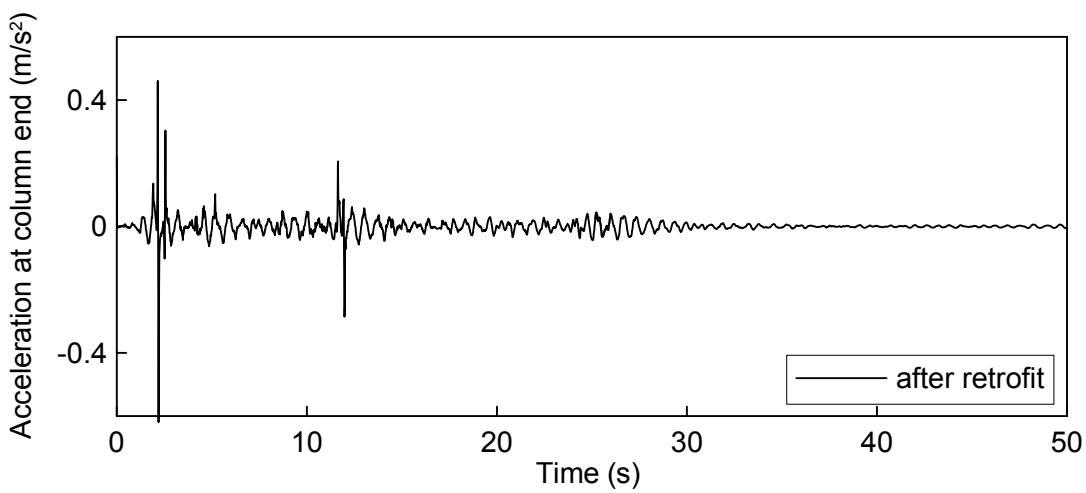

(b) Acceleration after retrofit

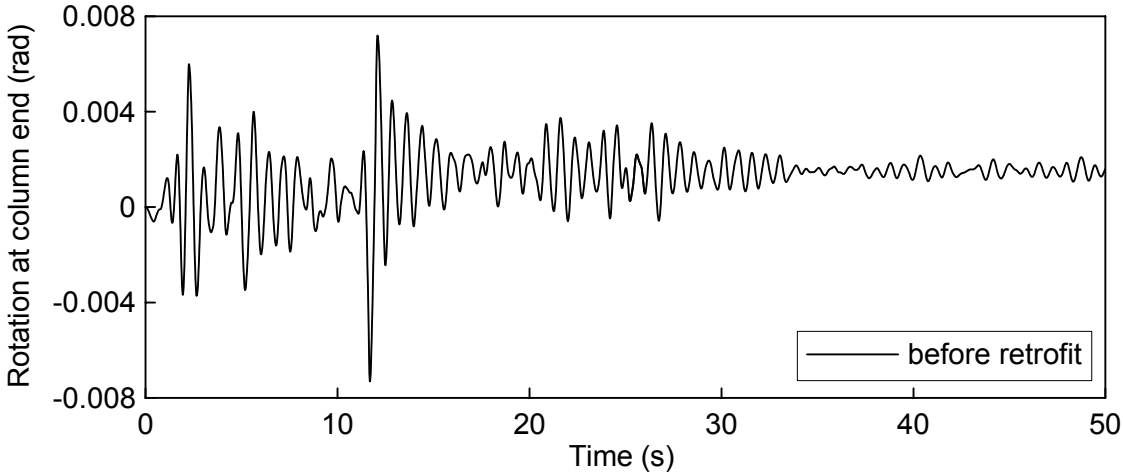

(c) Rotation before retrofit

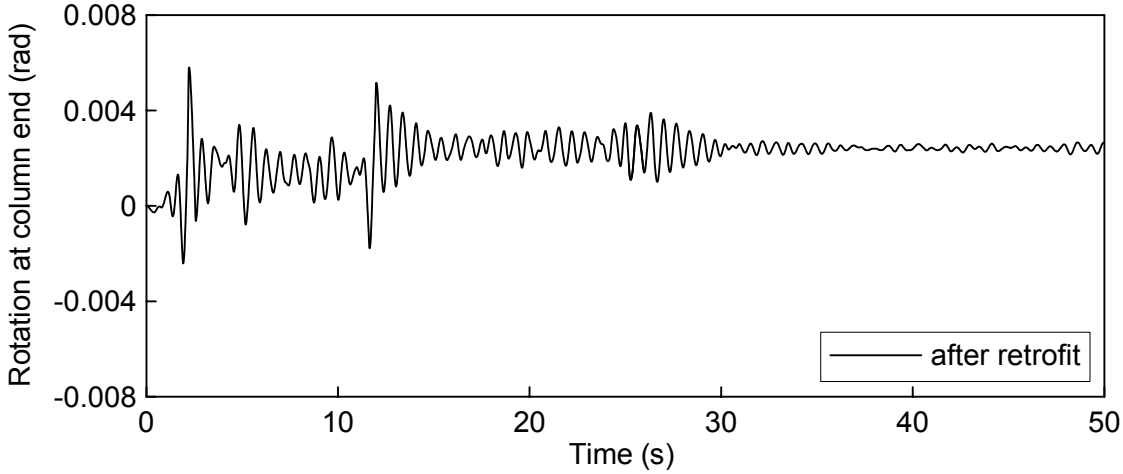

(d) Rotation after retrofit

Fig 2.7 Responses at Column End of Bridge 1

Typical responses at expansion joints of Bridge 1 are also plotted in Fig 2.8 to show the differences of the structural behaviors for the cases without and with considering gap and hook elements.

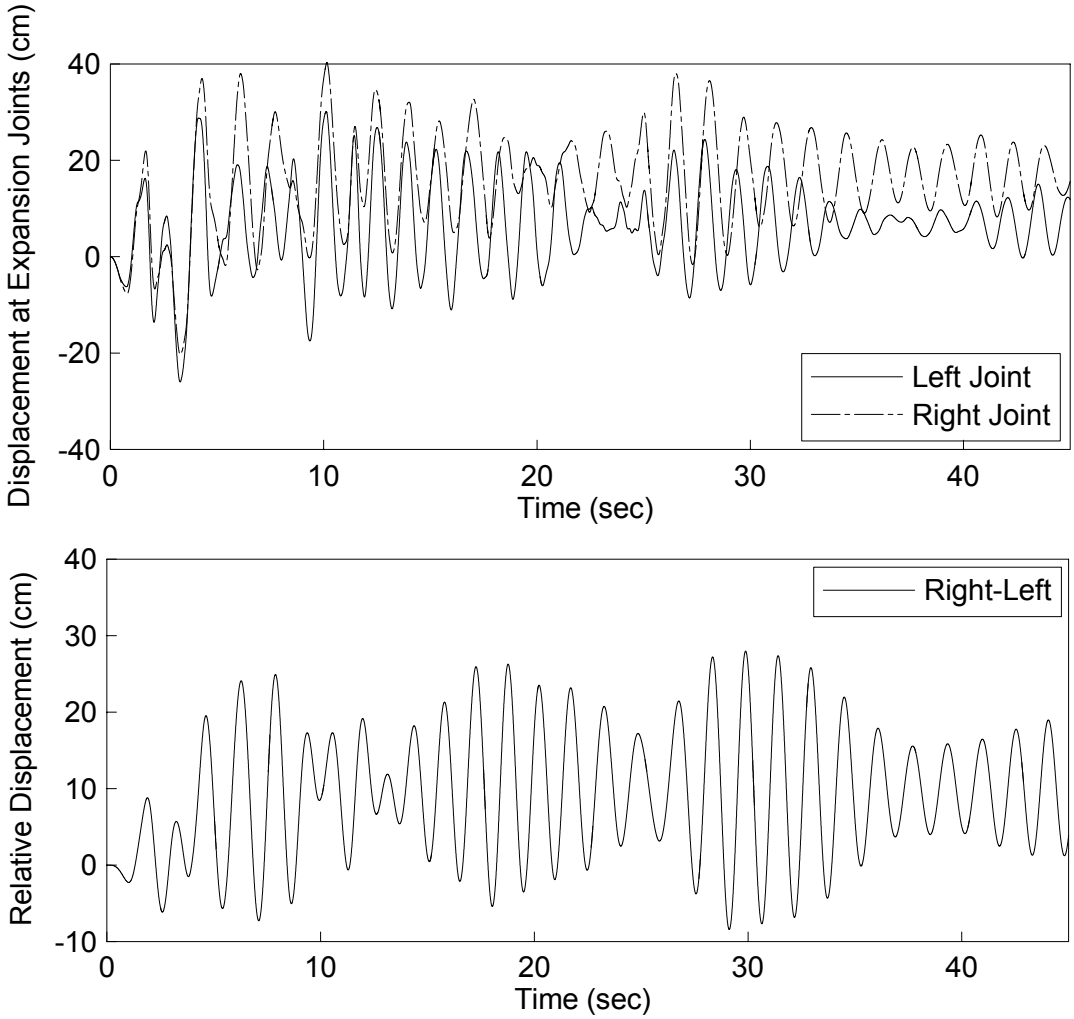

(a) Without Gap and Hook Elements

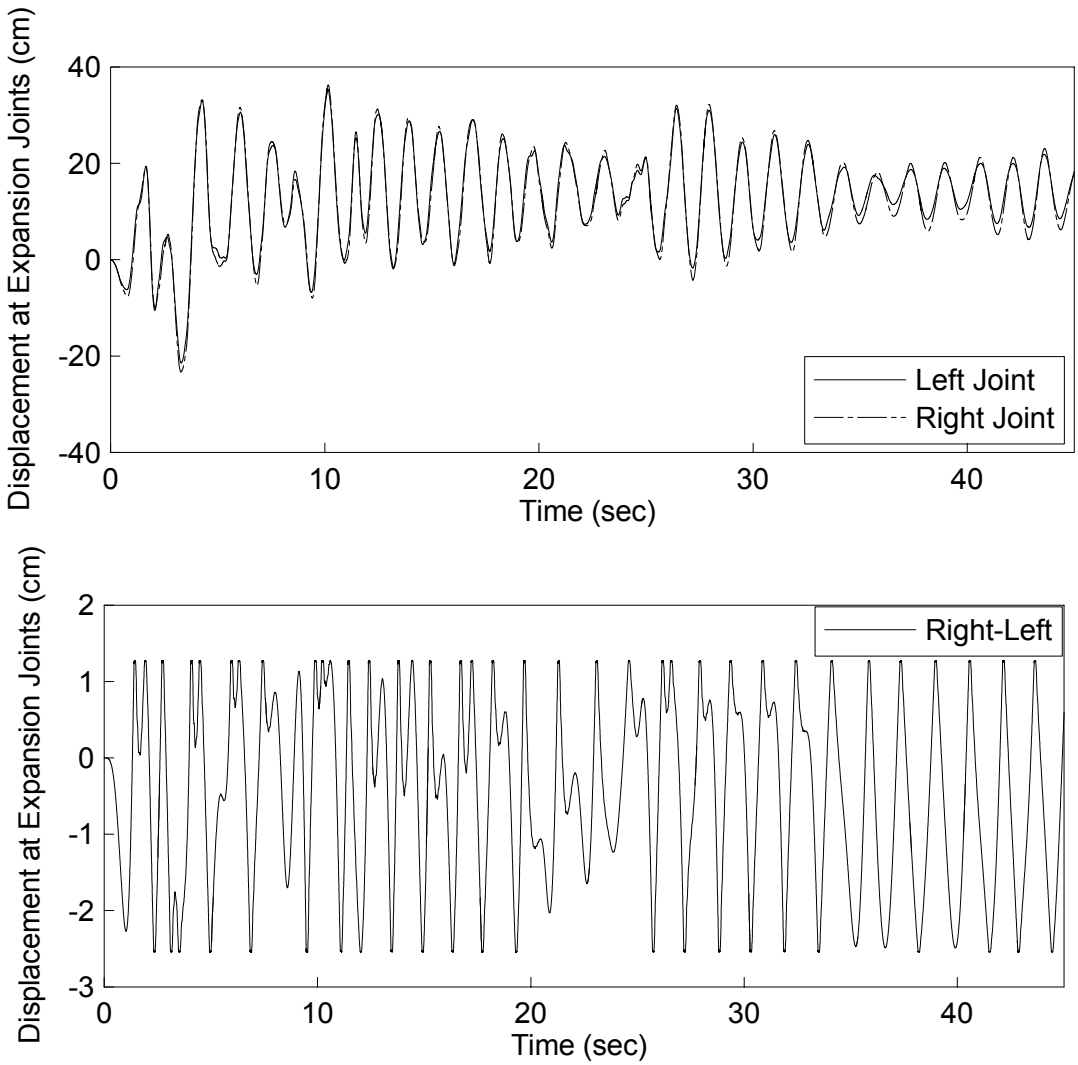

(b) with Gap and Hook Elements

Fig 2.8 Displacement at Expansion Joints of Bridge 1

2.6. Fragility Analysis of Bridges

2.6.1 Fragility Parameter Estimation

It is assumed that the fragility curves can be expressed in the form of two-parameter lognormal distribution functions, and the estimation of the two parameters (median and log-standard deviation) is performed with the aid of the maximum likelihood method. A common log-standard deviation, which forces the fragility curves not to intersect, can also be estimated. The following likelihood formulation described by Shinozuka et al. (2000) is introduced for the purpose of this method.

Although this method can be used for any number of damage states, it is assumed here for the ease of demonstration of analytical procedure that there are five states of damage including the state of (almost) no damage. A family of four (4) fragility curves exists in this case where events E_1, E_2, E_3, E_4 and E_5, respectively, indicate the state of (almost) no, (at least) slight, (at least) moderate, (at least) extensive damage and complete collapse. $P_{ik} = P(a_i, E_k)$ in turn indicates the probability that a bridge selected randomly from the sample will be in the damage state E_k when subjected to ground motion intensity expressed by PGA = a_i. All fragility curves are then represented

$$F_j(a_j; c_j, \varsigma_j) = \Phi\left[\frac{\ln(a_i / c_j)}{\varsigma_j}\right] \tag{2.2}$$

where $\Phi(\cdot)$ is the standard-normal distribution function, c_j and ς_j are the median and log-standard deviation of the fragility curves for the damage state of "(at least) slight", "(at least) moderate", "(at least) major" and "complete" identified by j = 1, 2, 3 and 4. From this definition of fragility curves, and under the assumption that the log-standard deviation is equal to ς common to all the fragility curves, one obtains;

$$P_{i1} = P(a_i, E_1) = 1 - F_1(a_i; c_1, \varsigma) \tag{2.3}$$

$$P_{i2} = P(a_i, E_2) = F_1(a_i; c_1, \varsigma) - F_2(a_i; c_2, \varsigma) \tag{2.4}$$

$$P_{i3} = P(a_i, E_3) = F_2(a_i; c_2, \varsigma) - F_3(a_i; c_3, \varsigma) \tag{2.5}$$

$$P_{i4} = P(a_i, E_4) = F_3(a_i; c_3, \varsigma) - F_4(a_i; c_4, \varsigma) \tag{2.6}$$

$$P_{i5} = P(a_i, E_5) = F_4(a_i; c_4, \varsigma) \tag{2.7}$$

The likelihood function can then be introduced as

$$L(c_1, c_2, c_3, c_4, \varsigma) = \prod_{i=1}^{n} \prod_{k=1}^{5} P_k(a_i; E_k)^{x_{ik}} \tag{2.8}$$

Where

$$x_{ik} = 1 \tag{2.9}$$

if the damage state E_k occurs in the bridge subjected to $a = a_i$, and

$$x_{ik} = 0 \tag{2.10}$$

otherwise. Then the maximum likelihood estimates c_{0j} for c_j and ς_0 for ς are obtained by solving the following equations,

$$\frac{\partial \ln L(c_1, c_2, c_3, c_4, \varsigma)}{\partial c_j} = \frac{\partial \ln L(c_1, c_2, c_3, c_4, \varsigma)}{\partial \varsigma} = 0 \; (j = 1, 2, 3, 4) \tag{2.11}$$

by implementing a straightforward optimization algorithm.

2.6.2 Definition of Damage States

A set of five (5) different damage states recommended by Dutta and Mander (1999) are introduced in Table 2.3 which displays the description of these five damage states and the corresponding drift limits for a typical column. For each limit state, the

drift limit can be transformed to peak ductility demand of the columns for the purpose of this study. Table 2.4 lists the values of these ductility demands for five (5) sample bridges.

Table 2.3 Description of Damaged States

Damage state	Description	Drift limits
Almost no	First yield	0.005
Slight	Cracking, spalling	0.007
Moderate	Loss of anchorage	0.015
Extensive	Incipient column collapse	0.025
Complete	Column collapse	0.050

Table 2.4 Peak Ductility Demand of First Left Column of Sample Bridges

Damage state	Bridge 1		Bridge 2		Bridge 3		Bridge 4		Bridge 5	
	before retrofit	after retrofit	before retrofit	After retrofit	before retrofit	after retrofit	before retrofit	after retrofit	before retrofit	after retrofit
Almost no	1.0	1.0	1.0	1.0	1.0	1.0	1.0	1.0	1.0	1.0
Slight	1.3	1.8	1.5	1.8	1.2	2.1	1.5	2.5	1.7	2.5
Moderate	2.6	4.9	3.5	5.2	2.2	6.4	3.5	8.2	4.3	8.3
Extensive	4.3	8.9	6.0	9.3	3.5	11.7	6.1	15.5	7.5	15.7
Complete	8.3	18.7	12.3	19.7	6.5	25.2	12.4	33.6	15.7	34.0

2.7 Pounding and Soil Effects on Fragility Curves

The section presents the fragility curves taking the effect of pounding at expansion joints on concrete bridge response to earthquake ground motions into consideration. The primary objective of this section is to develop fragility curves of the sample bridges and quantify the effect of pounding at expansion joints of the bridges. The effect of pounding at expansion joints on the seismic response is systematically examined and the resulting fragility curves are compared with those for the cases without pounding.

2.7.1 Pounding at Expansion Joint

Pounding at expansion joints (hinges) might have been another source of extensive damage during past earthquakes. In fact, the collapse of the 483 m (1610 ft) long bridge at the Interstate 5 and State Road 14 Interchange located approximately 12 km (7.5 mile) from the epicenter during the 1994 Northridge earthquake is an example suggesting that the effect of pounding at expansion joint might have caused the significant failure investigating damage states (Buckle 1994).

A preliminary investigation was performed by Shinozuka et al. (2002b) on impact phenomena as well as effects of seismically induced pounding at expansion joints of typical California bridges, through which it was found that pounding has significant effects on the acceleration and velocity responses, but little effects on the displacement responses. Although pounding effect is found to have negligible effect on the ductility demand, a need is felt to quantify the effect of pounding at the expansion joints by developing fragility curves of highway bridges, particularly for multi-span long bridges with expansion joints.

In order to investigate the effect of pounding of bridges, four (4) sample bridge models are considered for the nonlinear time history analysis. As described earlier in the Section 2.3, two (2) of them have mid overall lengths, but one hinge with same column height and two hinges with different column height. The other two have long overall lengths, but one hinge with same column height and four hinges with different column height.

It is typical for a California highway bridge with more than four spans to have expansion joints located nearly at inflection points (i.e., 1/4 to 1/5th of spans). The bridge superstructure consists of reinforced or prestressed concrete box girders. For

example, the material and cross-sectional properties of Bridge 2 as follows: Young's modulus=27.793 Gpa (4.03×10^6 ksi), mass density=2.401 Mg/m^3 (62.428 kip/ft^3), cross-section area and moment of inertia are respectively 6.701 m^2 (72.13 ft^2) and 4.625 m^4 (535.86 ft^4) for box girders, while they are 4.670 m^2 (50.27 ft^2)and 0.620 m^4 (71.83 ft^4) for columns.

Perhaps one of the most difficult-to-analyze nonlinear behaviors that occur in bridge systems idealized to include gap elements is the closing of a gap between different segments of the bridge. The usual gap element shown as Fig 2.9 has the following physical properties: 1) The element cannot develop a force until the opening d_0 is closed; and 2) the element can only develop a compression force. Note that the numerical convergence of the response analysis particularly at the gap element can be very slow if a large elastic stiffness k is used. In order to minimize the difficulty associated with this problem, the stiffness k should not be over 1,000 times the stiffness of the elements adjacent to the gap according to the authors' experience. This kind of dynamic contact problem involving two adjacent structural segments usually does not have a simple, unique solution. In fact, it is impractical to use continuum mechanics analysis in the vicinity of the contact area for local stress and strain evaluation and at the same time to pursue structural dynamic analysis to evaluate the bridge response as a system including, for example, ductility demand at the column ends. A viable alternative appears to be the deployment of the finite element analysis with gap elements having the stiffness value k selected from sensitivity analysis of gap element stiffness (Shinozuka et al., 2003c).

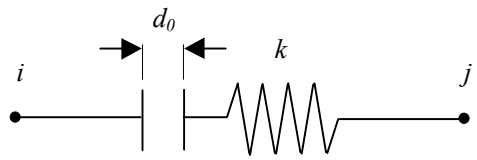

Fig 2.9 Gap Element

2.7.2 Numerical Simulation for Pounding

Numerical simulation were performed for the four (4) sample bridges under sixty (60) Los Angeles earthquakes for the cases without pounding and with pounding by considering gap element at expansion joints. The computer code *SAP2000/Nonlinear* was utilized in order to calculate the state of damage of the structure under ground acceleration time histories.

The structural responses with pounding were compared to those without pounding, in order to highlight how pounding affects the structural response behaviors. Numerical simulations were carried out under LA01 earthquake as shown Fig 2.10. Pounding force time history was also presented as shown Fig 2.11. Time histories of acceleration and displacement at the expansion joint, and rotation of the column end are plotted as shown Fig 2.12 and Fig 2.13 for the cases without and with pounding, respectively.

From these results, it is observed that (1) the pounding takes place twenty three (23) times during the duration of the earthquake, (2) the acceleration is affected much more by pounding than displacement and rotation are; (3) the peak value of the rotation at column end can be reduced by pounding. It is indicated that the pounding are not usually capable of causing large deformation to bridge structures while it may cause significantly

high axial compressive stress locally leading to a possible local damage at the contact area at the expansion joint.

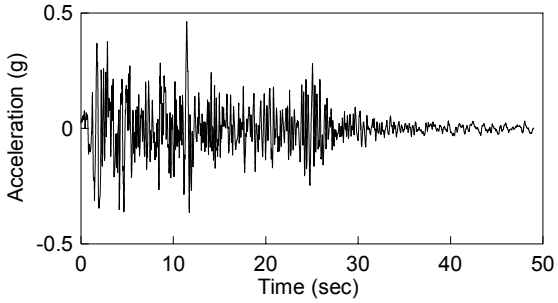

Fig 2.10 Ground Motion Time History for LA01

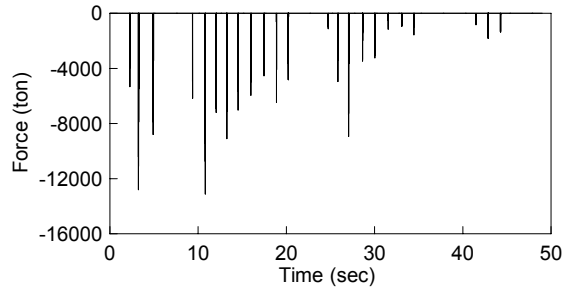

Fig 2.11 Pounding Force at Expansion Joint

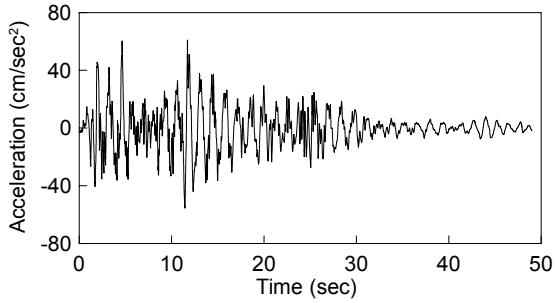

(a) Acceleration at Expansion Joint

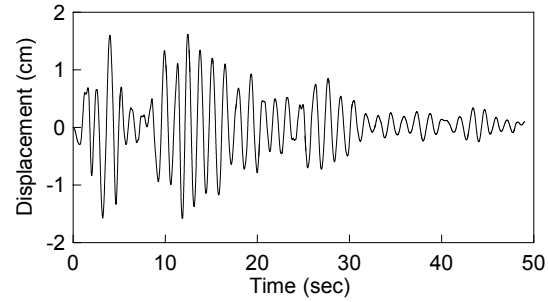

(b) Displacement at Expansion Joint

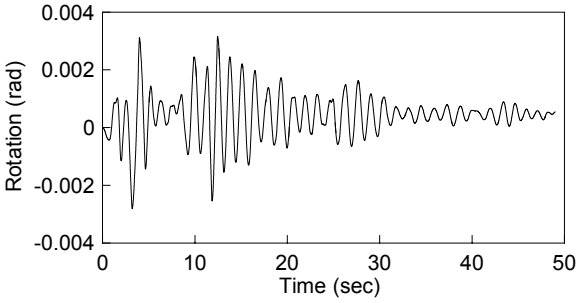

(c) Rotation at Column Bottom

Fig 2.12 Structural Responses without Pounding

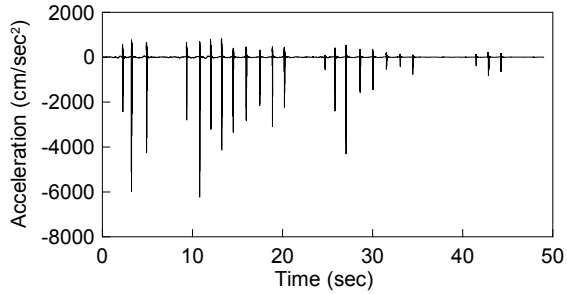

(a) Acceleration at Expansion Joint

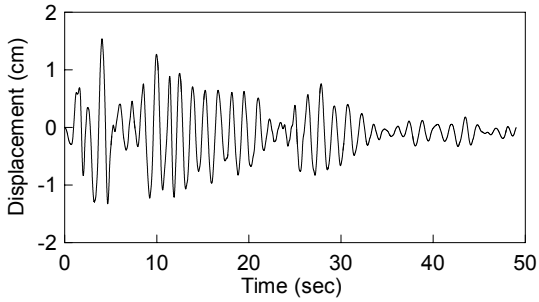

(b) Displacement at Expansion Joint

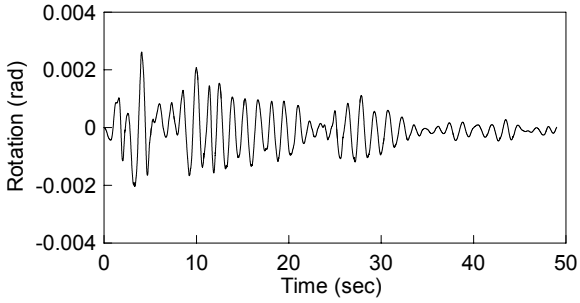

(c) Rotation at Column Bottom

Fig 2.13 Structural Responses with Pounding

2.7.3 Pounding Effects on Fragility Curves

The fragility curves for the four (4) sample bridges associated with the states of damage mentioned in the previous section were plotted as a function of peak ground acceleration in Figs 2.14-2.17, while the number of damaged bridges is listed in Tables 2.5-2.8, respectively. Each Fig has two curves for the cases without pounding and with pounding to compare how much the curves are shifted to left or right (more or less fragile). It is noted here that the log-standard deviation in each of Figs 2.14-2.17 was obtained by taking the whole events involving the cases without and with pounding using Equation 2.11 for these fragility curves. This is for the reason that the pair of fragility curves in each Fig is not theoretically expected to intersect each other.

The fragility curves in pairs produced mixed results in such a way that the pounding effect is even beneficial for some damage states, while it appears detrimental for some cases. In particular, if the number of bridges at a certain state of damage counted, it can be clearly seen that the pounding does not increase the number of damaged bridges (or the ductility factor) in general.

It is noted that bridge characteristics, such as overall length, number of spans, number of expansion joints and height of columns, might not a major factor to change the trend of the fragility curves by increasing or decreasing ductility demand. High response amplifications due to pounding might result only if the colliding bridge segments separated by an expansion joint are significantly different in natural period, however this condition does not usually exist in the bridge structure.

Table 2.5 Number of Damaged Bridges: Pounding Effect in Bridge 2

sample size=60

Damage States	without Pounding	with Pounding
No	8	9
Almost No	8	9
Slight	8	9
Moderate	8	4
Extensive	14	16
Complete	14	13

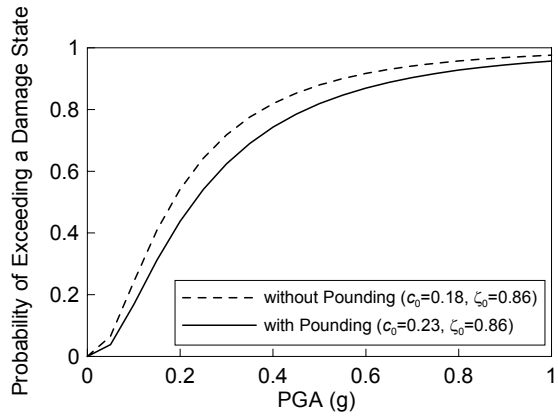

(a) Almost No Damage

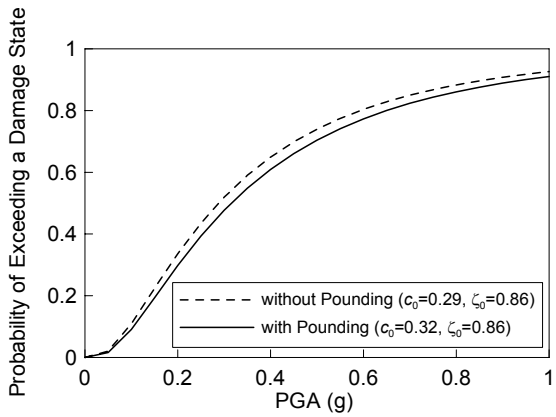

(b) Slight Damage

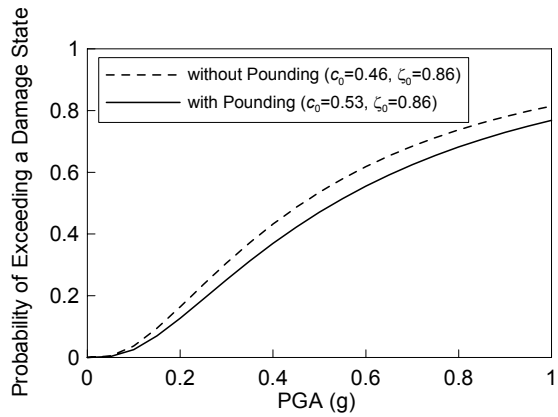

(c) Moderate Damage

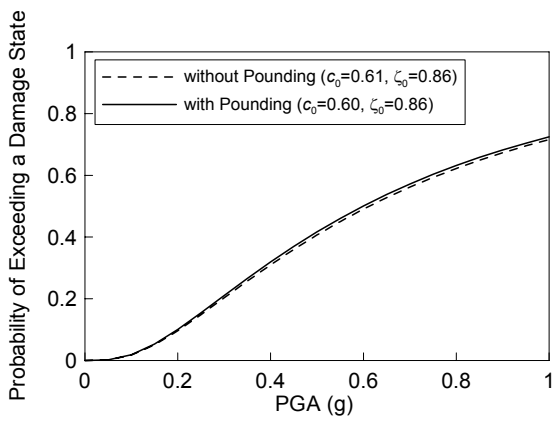

(d) Extensive Damage

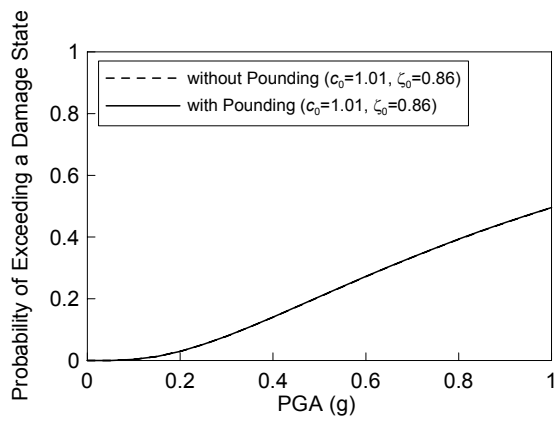

(e) Complete Collapse

Fig 2.14 Pounding Effect on Fragility Curves of Bridge 2

Table 2.6 Number of Damaged Bridges: Pounding Effect in Bridge Model 3

sample size=60

Damage States	without Pounding	with Pounding
No	1	1
Almost No	2	3
Slight	13	13
Moderate	4	2
Extensive	14	20
Complete	26	21

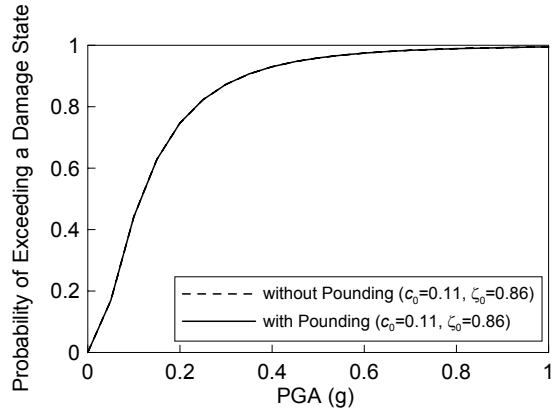

(a) Almost No Damage

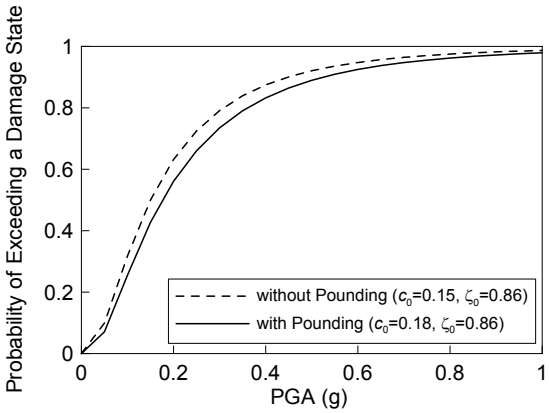

(b) Slight Damage

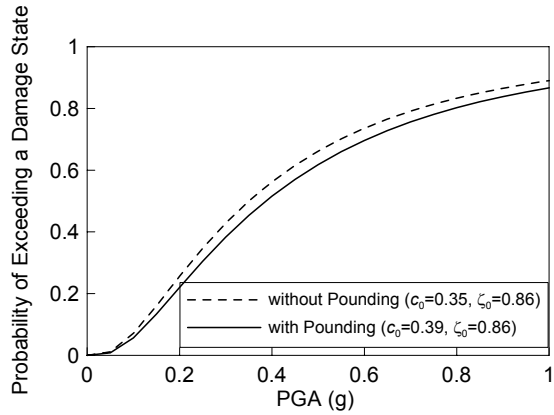

(c) Moderate Damage

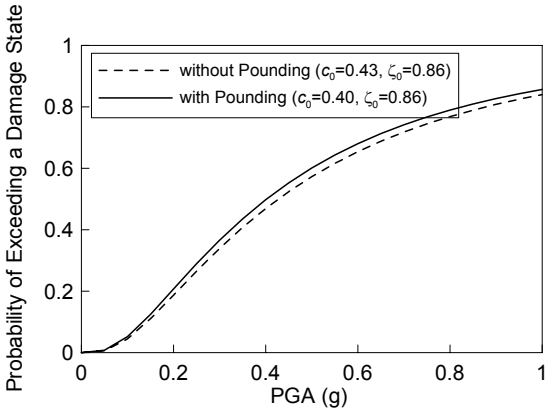

(d) Extensive Damage

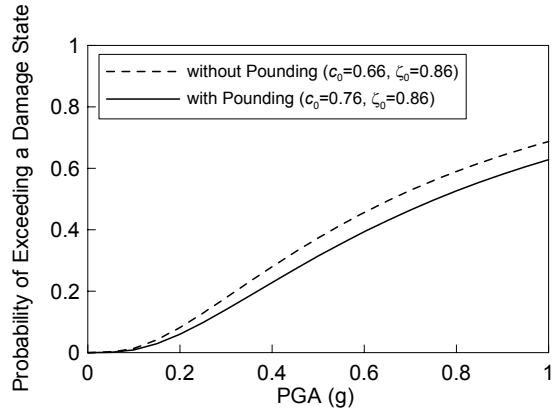

(e) Complete Collapse

Fig 2.15 Pounding Effect on Fragility Curves of Bridge 3

Table 2.7 Number of Damaged Bridges: Pounding Effect in Bridge 4

sample size=60

Damage States	without Pounding	with Pounding
No	1	1
Almost No	2	2
Slight	6	7
Moderate	7	6
Extensive	9	7
Complete	35	37

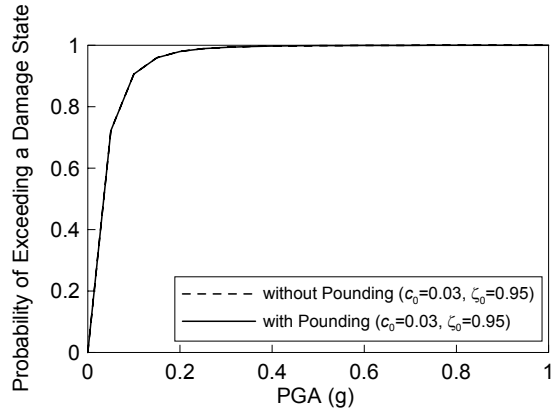

(a) Almost No Damage

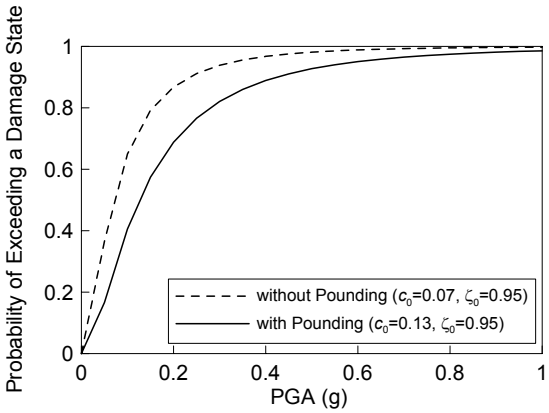

(b) Slight Damage

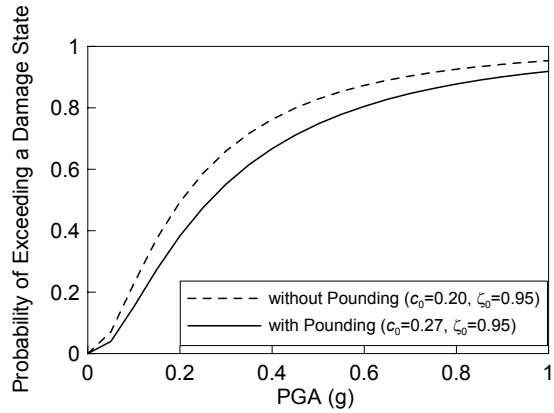

(c) Moderate Damage

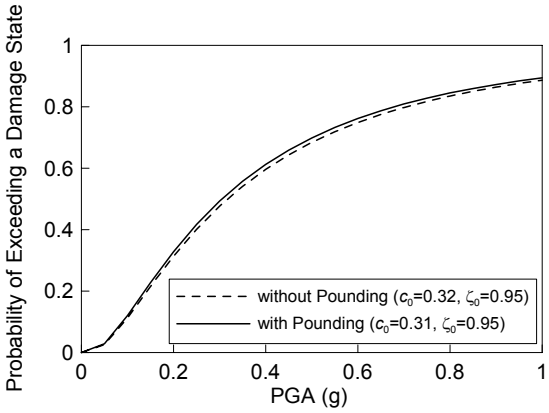

(d) Extensive Damage

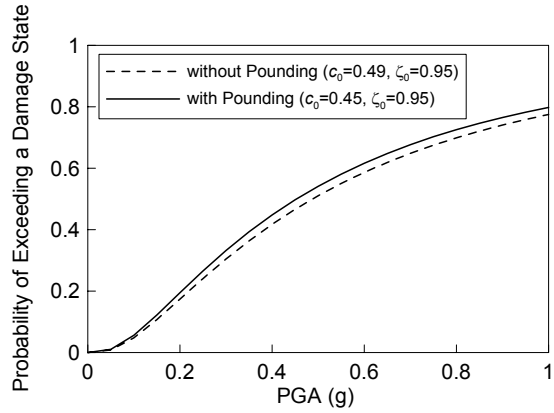

(e) Complete Collapse

Fig 2.16 Pounding Effect on Fragility Curves of Bridge 4

Table 2.8 Number of Damaged Bridges: Pounding Effect in Bridge 5

sample size=60

Damage States	without Pounding	with Pounding
No	8	7
Almost No	1	3
Slight	18	17
Moderate	9	9
Extensive	14	14
Complete	10	10

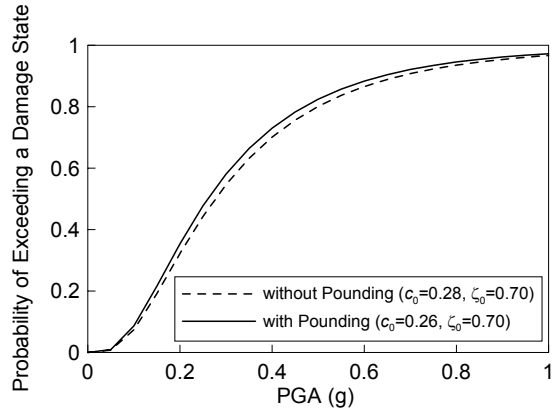

(a) Almost No Damage

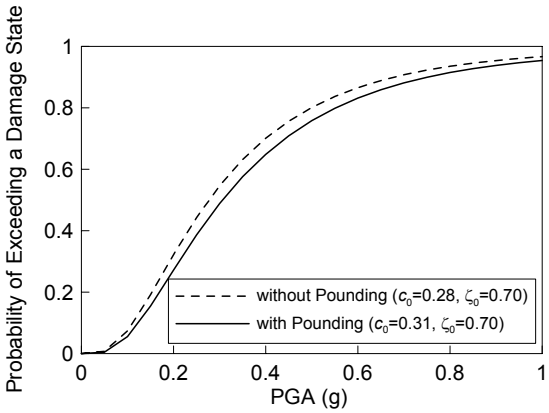

(b) Slight Damage

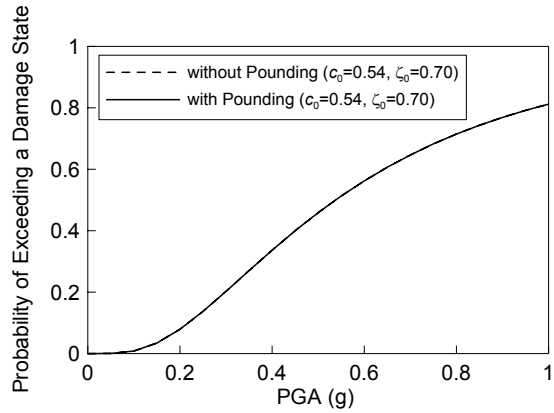

(c) Moderate Damage

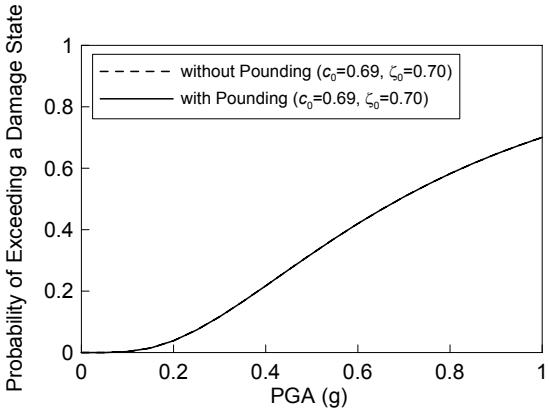

(d) Extensive Damage

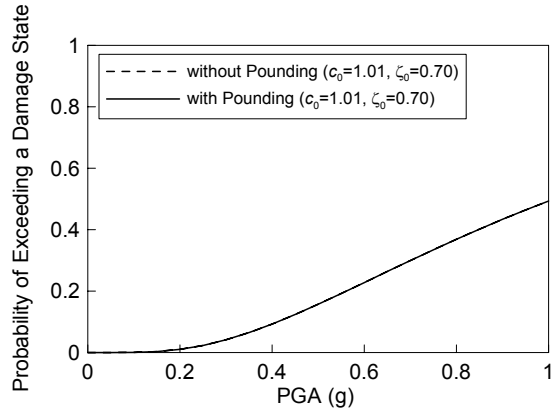

(e) Complete Collapse

Fig 2.17 Pounding Effect on Fragility Curves of Bridge 5

2.7.4 Pounding and Soil Effects on Fragility Curves

The fragility curves for the four (4) sample bridges associated with the states of damage mentioned in the previous section were plotted as a function of peak ground acceleration in Figs 2.18, 2.19, 2.20 and 2.21, while the number of damaged bridges is listed in Tables 2.9, 2.10, 2.11 and 2.12, respectively. Each Fig has four (4) curves for the following four (4) cases:

CASE 1: without pounding effects and without soil effects

CASE 2: with pounding effects and without soil effects

CASE 3: without pounding effects and with soil effects

CASE 4: with pounding effects and with soil effects

In order to compare how much the curves are shifted to left or right (more or less fragile) due to the effects of pounding and/or soil, the four (4) curves were put into one Figure. It is noted that the log-standard deviation in each of Figs 2.18, 2.19, 2.20 and 2.21 was obtained by taking the whole events involving the four (4) cases using equation 2.11 for these fragility curves. This is for the reason that the pair of fragility curves in each Fig is not theoretically expected to intersect each other.

The fragility curves produced mixed results in such a way that the pounding and/or soil effects are even beneficial for some damage states, while it appears detrimental for some cases. In particular, if the number of bridges at a certain state of damage counted, there is a definite effect but it is hard to say any trend.

Table 2.9 Number of Damaged Bridges: Pounding and Soil Effects in Bridge 2

sample size=60

Damage States	Case1	Case2	Case3	Case4
No	8	10	8	8
Almost No	9	5	12	9
Slight	8	11	7	8
Moderate	10	9	7	12
Extensive	15	14	16	13
Complete	10	11	10	10

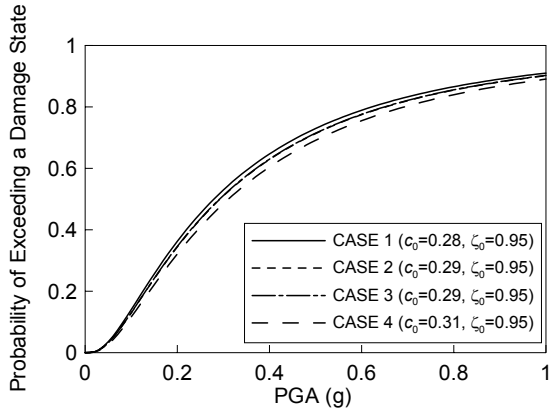

(a) Almost No Damage

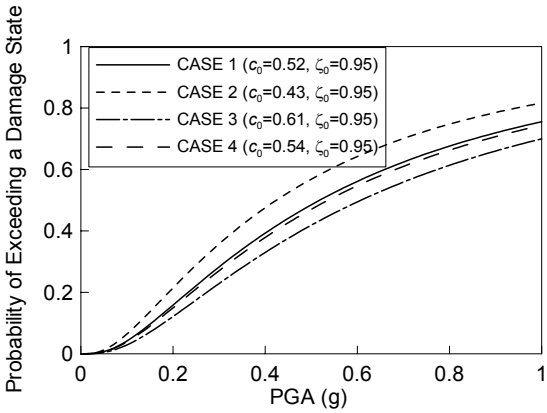

(b) Slight Damage

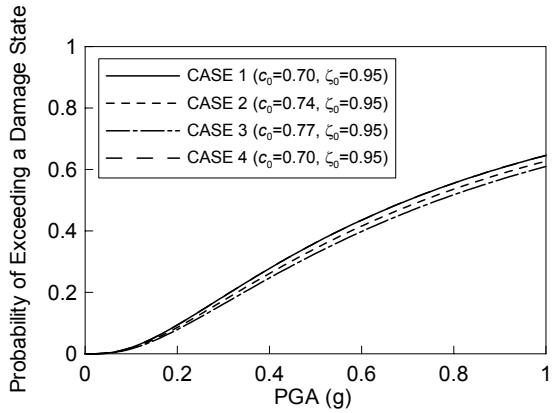

(c) Moderate Damage

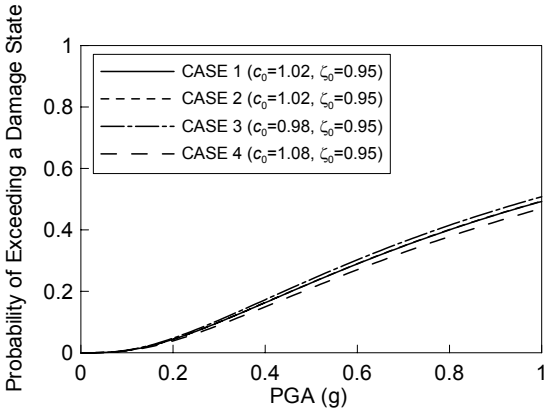

(d) Extensive Damage

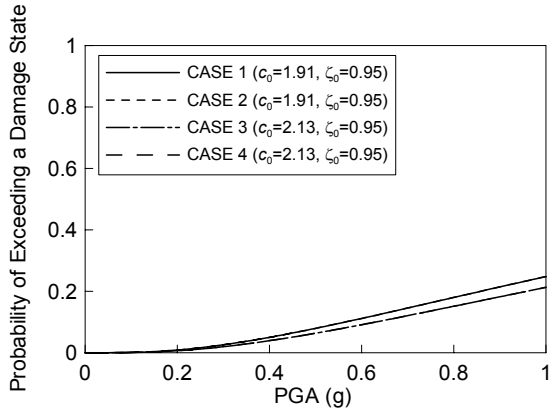

(e) Complete Collapse

Fig 2.18 Pounding and Soil Effects on Fragility Curves of Bridge 2

Table 2.10 Number of Damaged Bridges: Pounding and Soil Effects in Bridge 3

sample size=60

Damage States	Case1	Case2	Case3	Case4
No	2	2	2	10
Almost No	2	2	10	5
Slight	10	10	7	5
Moderate	8	5	5	3
Extensive	12	13	12	11
Complete	26	28	24	26

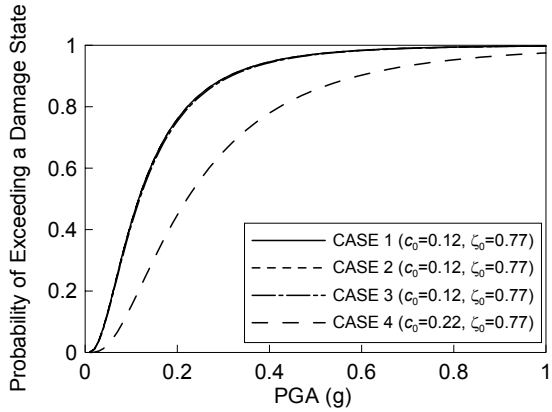

(a) Almost No Damage

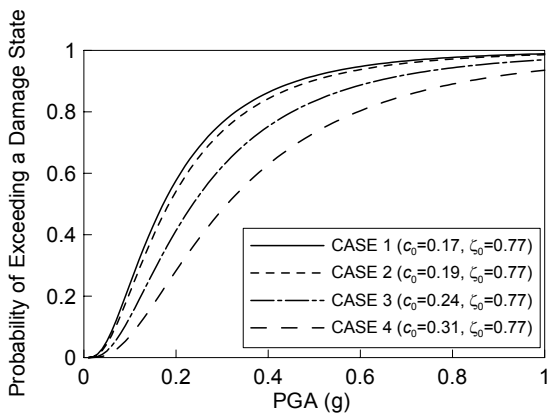

(b) Slight Damage

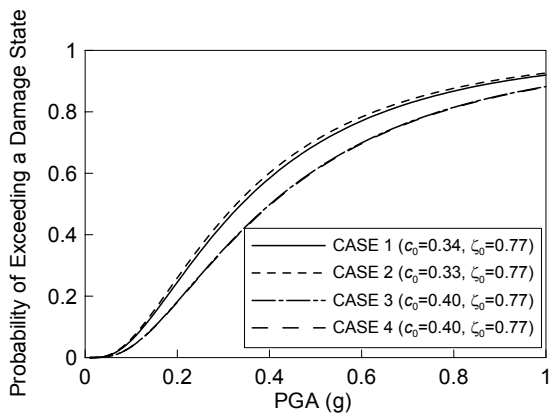

(c) Moderate Damage

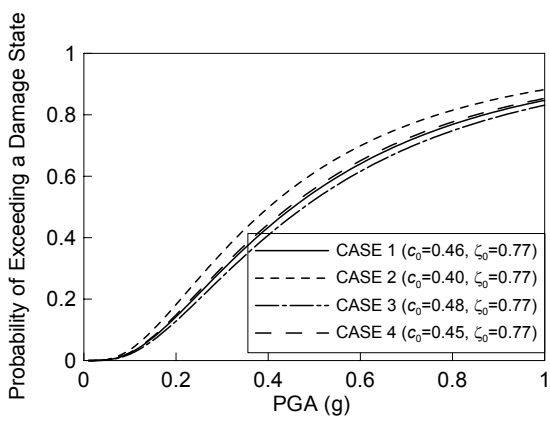

(d) Extensive Damage

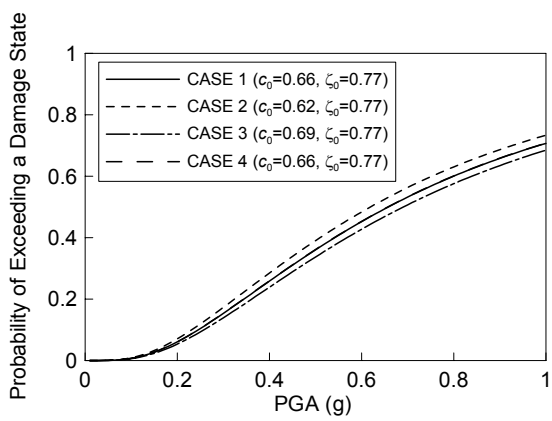

(e) Complete Collapse

Fig 2.19 Pounding and Soil Effects on Fragility Curves of Bridge 3

Table 2.11 Number of Damaged Bridges: Pounding and Soil Effects in Bridge 4

sample size=60

Damage States	Case1	Case2	Case3	Case4
No	5	3	9	7
Almost No	5	5	6	5
Slight	15	11	13	10
Moderate	11	7	9	8
Extensive	15	18	14	16
Complete	9	16	9	14

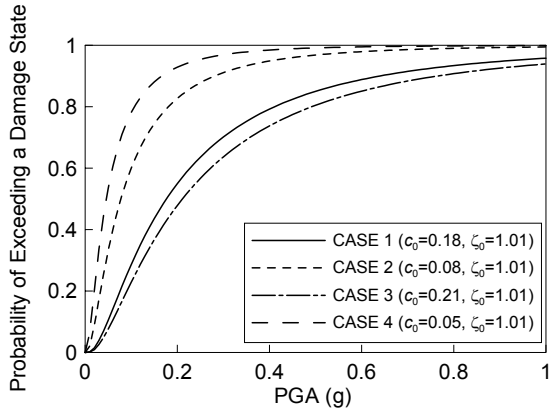

(a) Almost No Damage

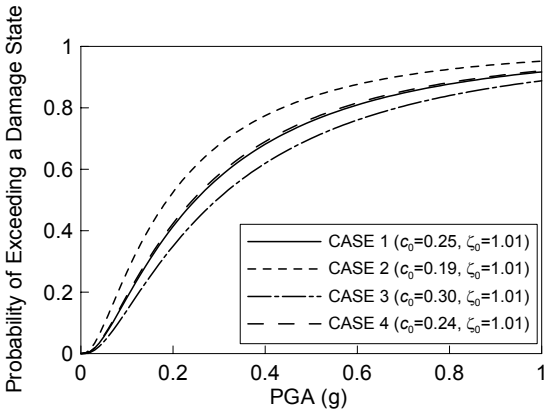

(b) Slight Damage

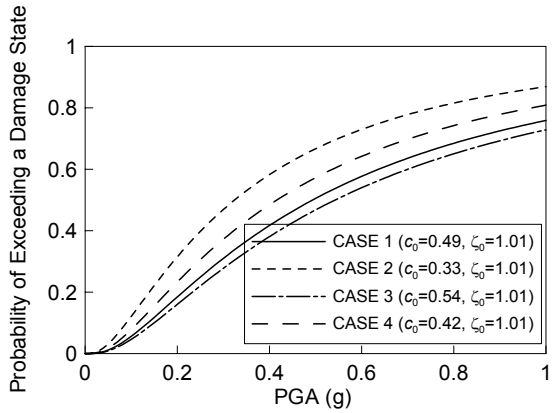

(c) Moderate Damage

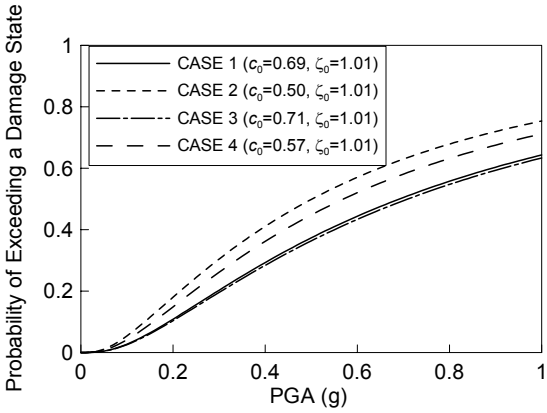

(d) Extensive Damage

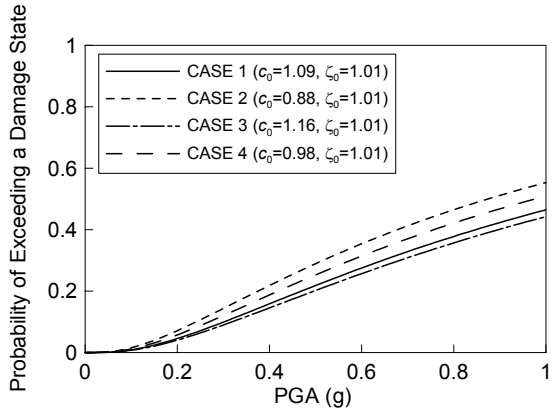

(e) Complete Collapse

Fig 2.20 Pounding and Soil Effects on Fragility Curves of Bridge 4

Table 2.12Number of Damaged Bridges: Pounding and Soil Effects in Bridge 5

sample size=60

Damage States	Case1	Case2	Case3	Case4
No	9	9	11	10
Almost No	7	6	4	4
Slight	14	15	12	13
Moderate	11	11	14	14
Extensive	13	13	12	12
Complete	6	6	7	7

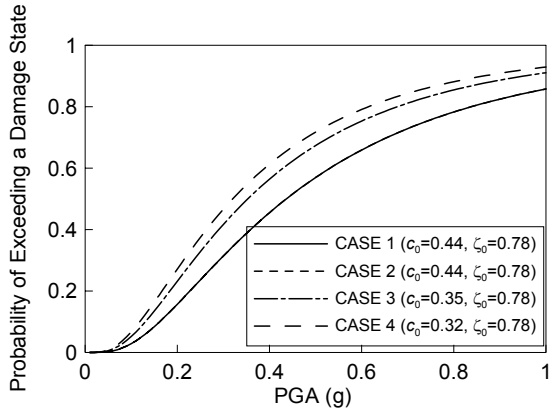

(a) Almost No Damage

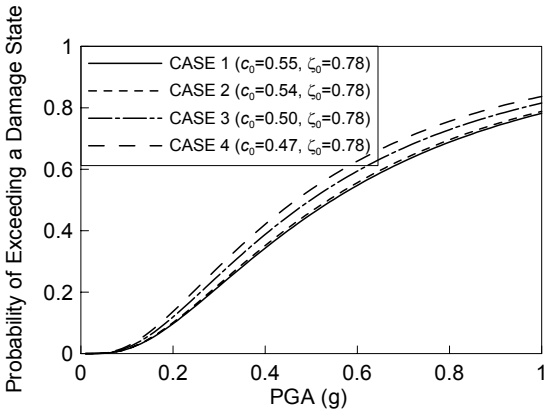

(b) Slight Damage

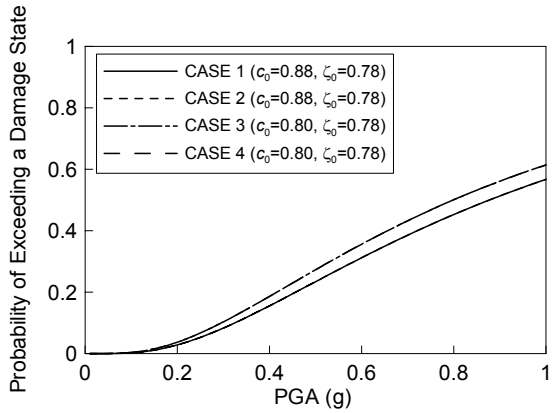

(c) Moderate Damage

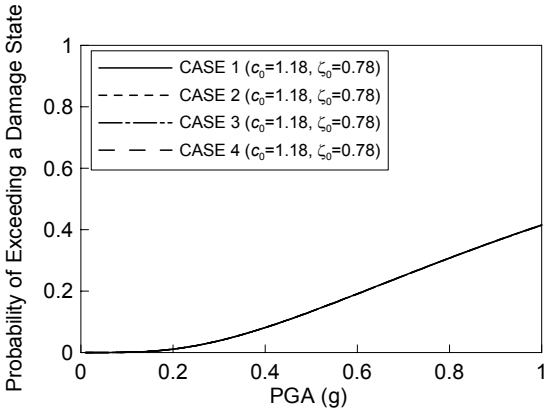

(d) Extensive Damage

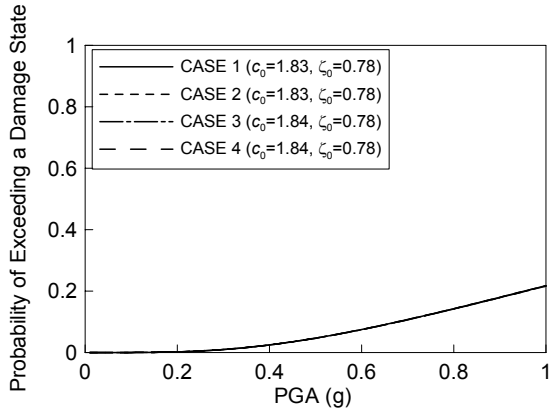

(e) Complete Collapse

Fig 2.21 Pounding and Soil Effects on Fragility Curves of Bridge 5

2.7.5 Jacketing and Restrainer Effects on Fragility Curves

The fragility curves for the four (4) sample bridges associated with the states of damage mentioned in the previous section were plotted as a function of peak ground acceleration in Figs 2.23, 2.24, 2.25 and 2.26, while the number of damaged bridges is listed in Tables 2.14, 2.15, 2.16 and 2.17, respectively. Each Fig has four (4) curves for the following four (4) cases:

CASE 1: without jacketing and without restrainer

CASE 2: with jacketing and without restrainer

CASE 3: without jacketing and with restrainer

CASE 4: with jacketing and with restrainer

In order to compare how much the curves are shifted to left or right (more or less fragile) due to the effects of jacketing and/or restrainer, the four (4) curves were put into one Fig. It is noted that the log-standard deviation in each of Figs 2.23, 2.24, 2.25 and 2.26 was obtained by taking the whole events involving the four (4) cases using equation 2.11 for these fragility curves. This is for the reason that the pair of fragility curves in each figure is not theoretically expected to intersect each other.

The damage state of a bridge is defined in terms of the maximum value of the peak ductility demands sustained by all the column ends. In this context, comparison between fragility curves in Figs 2.23-2.26 indicates that the bridge is less susceptible for damage to the ground motion after column retrofit than before, while the effect of restrainers at expansion joints is found to be negligible or even adversely affects on the column responses.

Table 2.13 Number of Damaged Bridges: Jacketing and Restrainer Effects on Bridge 2

sample size=60

Damage States	Case1	Case2	Case3	Case4
No	10	14	10	15
Almost No	4	8	6	7
Slight	11	18	11	18
Moderate	11	11	9	13
Extensive	13	8	15	6
Complete	11	1	9	1

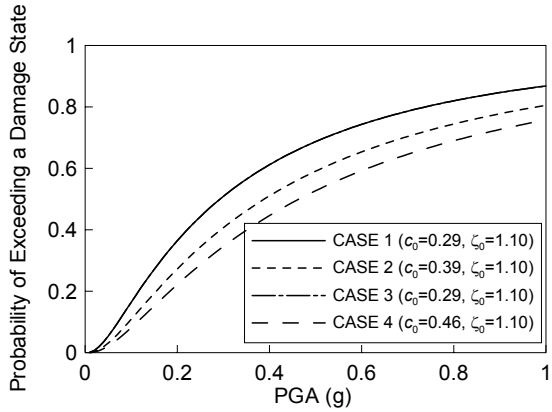

(a) Almost No Damage

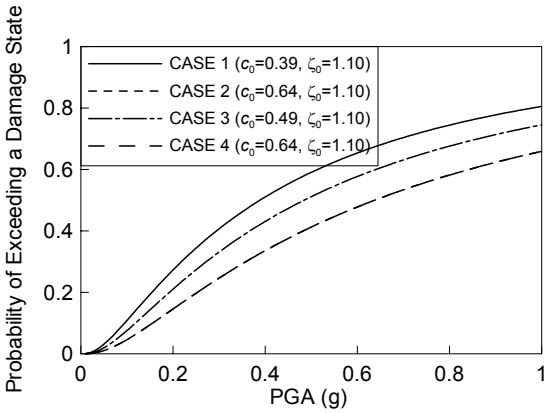

(b) Slight Damage

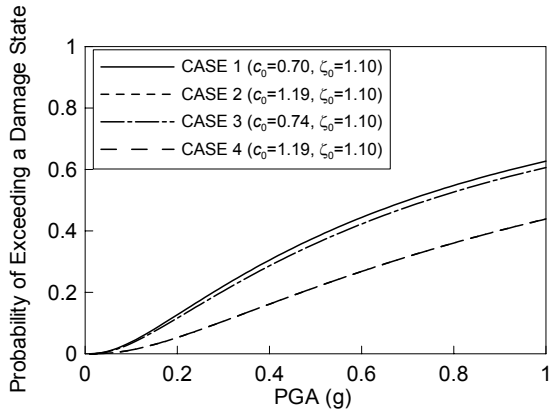

(c) Moderate Damage

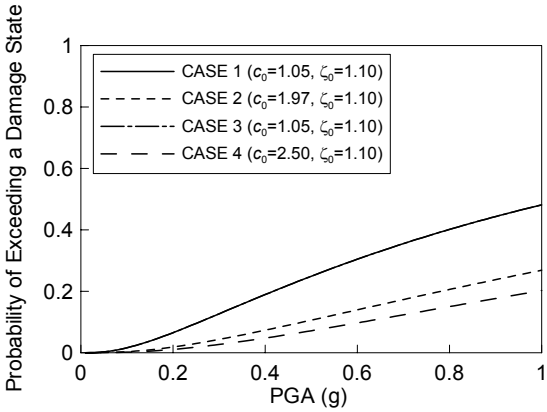

(d) Extensive Damage

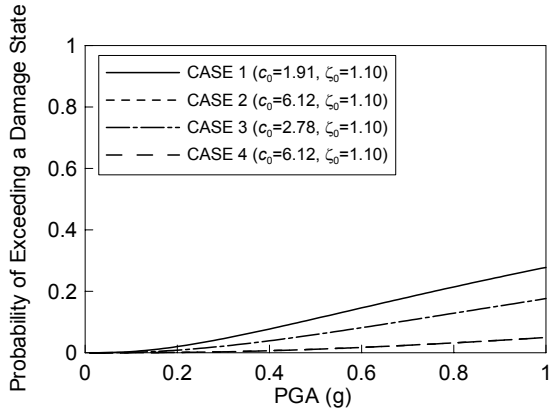

(e) Complete Collapse

Fig 2.22 Jacketing and Restrainer Effects on Fragility Curves of Bridge 2

Table 2.14 Number of Damaged Bridges: Jacketing and Restrainer Effects on Bridge 3

sample size=60

Damage States	Case1	Case2	Case3	Case4
No	1	3	2	5
Almost No	3	13	3	4
Slight	9	16	4	15
Moderate	6	11	9	14
Extensive	13	13	6	14
Complete	28	4	36	8

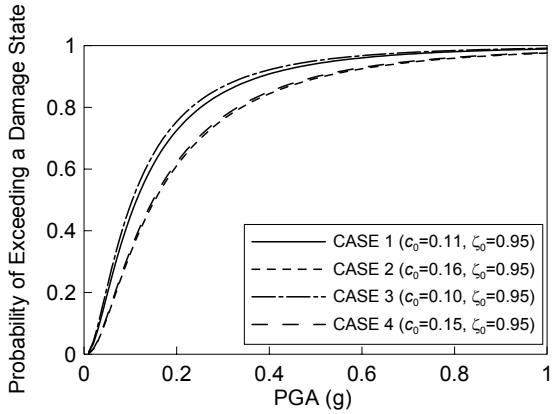

(a) Almost No Damage

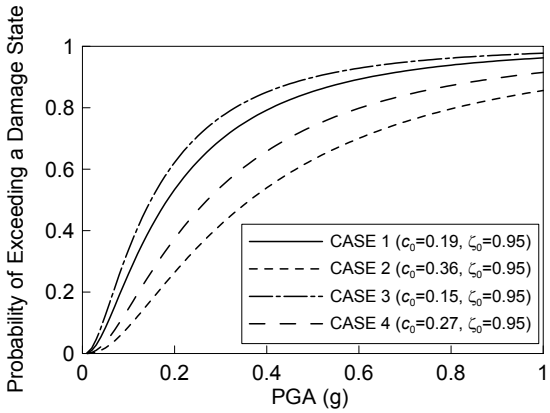

(b) Slight Damage

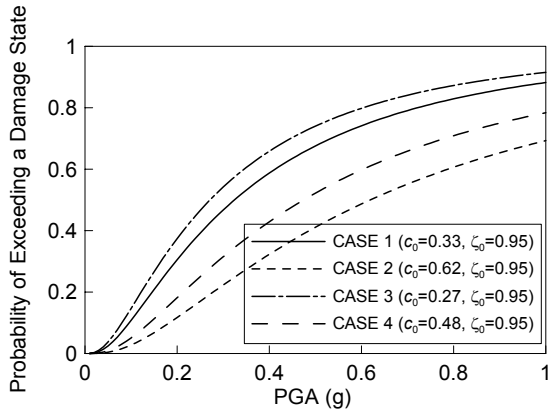

(c) Moderate Damage

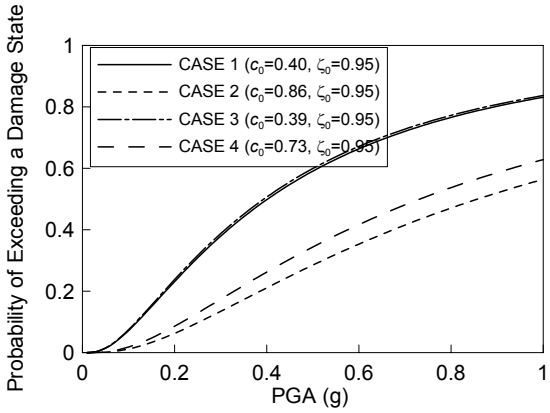

(d) Extensive Damage

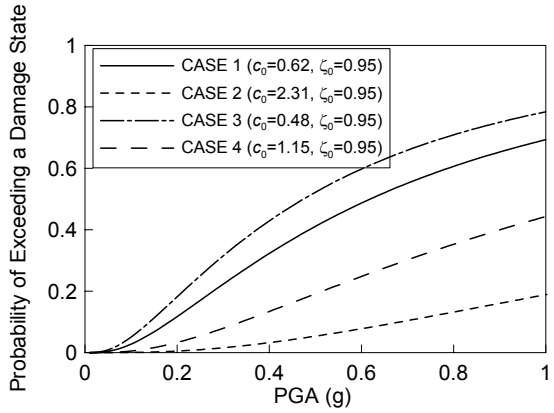

(e) Complete Collapse

Fig 2.23 Jacketing and Restrainer Effects on Fragility Curves of Bridge 3

Table 2.15 Number of Damaged Bridges: Jacketing and Restrainer Effects on Bridge 4

sample size=60

Damage States	Case1	Case2	Case3	Case4
No	3	8	3	8
Almost No	5	13	4	10
Slight	11	15	14	14
Moderate	7	12	5	9
Extensive	18	9	12	15
Complete	16	3	22	4

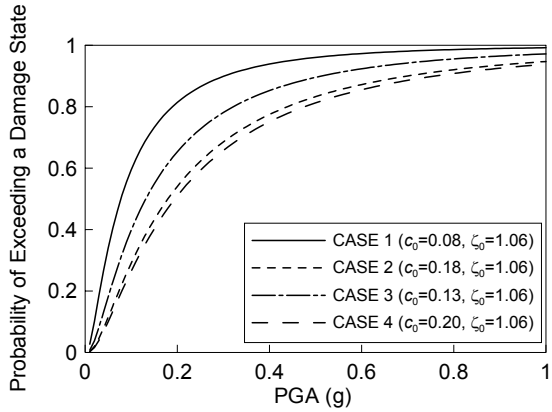

(a) Almost No Damage

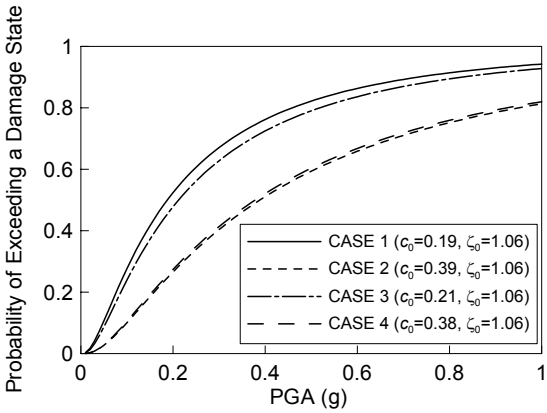

(b) Slight Damage

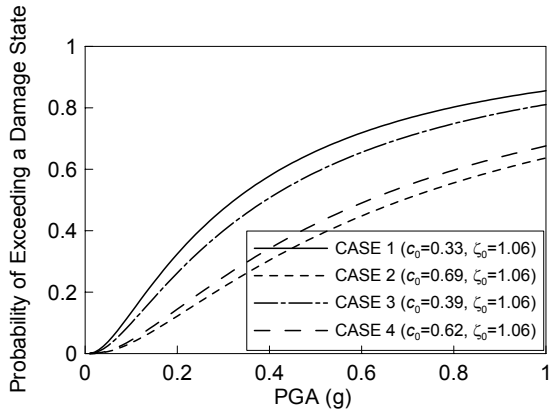

(c) Moderate Damage

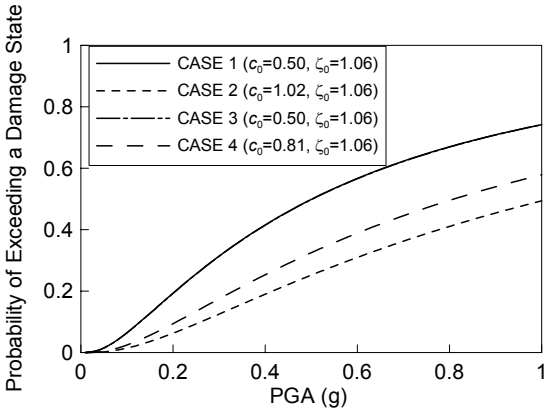

(d) Extensive Damage

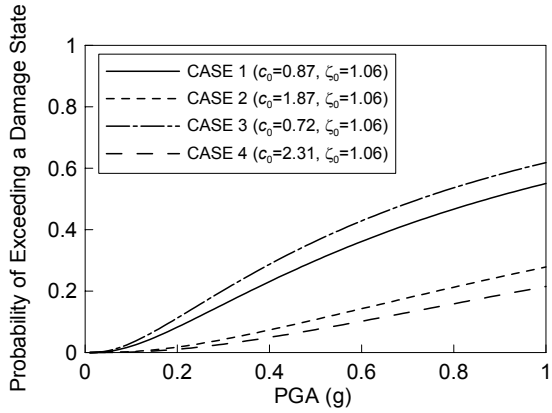

(e) Complete Collapse

Fig 2.24 Jacketing and Restrainer Effects on Fragility Curves of Bridge 4

Table 2.16 Number of Damaged Bridges: Jacketing and Restrainer Effects on Bridge 5

sample size=60

Damage States	Case1	Case2	Case3	Case4
No	4	6	3	5
Almost No	5	9	6	11
Slight	12	20	12	19
Moderate	10	11	11	13
Extensive	14	14	15	12
Complete	15	0	13	0

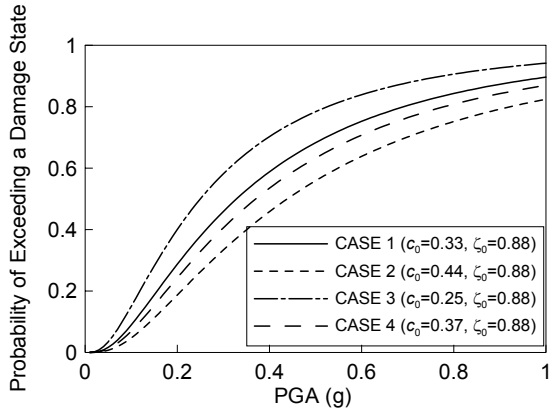

(a) Almost No Damage

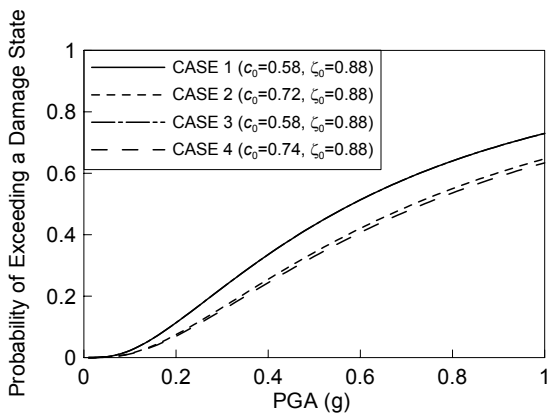

(b) Slight Damage

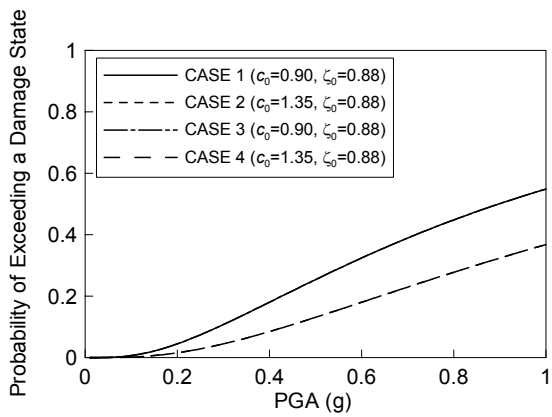

(c) Moderate Damage

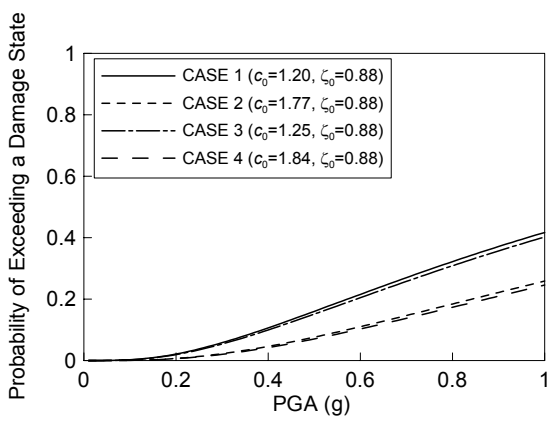

(d) Extensive Damage

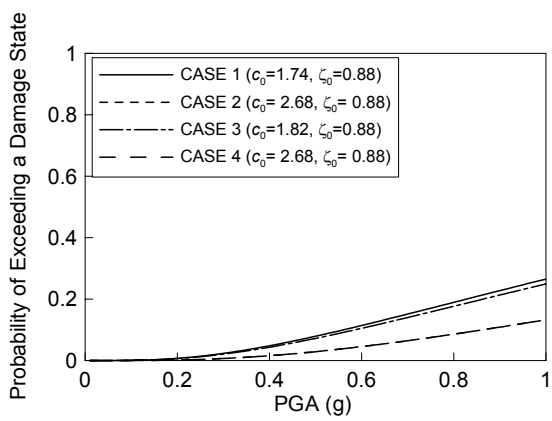

(e) Complete Collapse

Fig 2.25 Jacketing and Restrainer Effects on Fragility Curves of Bridge 5

2.8 Fragility Enhancement After Column Retrofit

2.8.1 Fragility Curves After Retrofit for Longitudinal Direction

The fragility curves for five (5) sample bridges associated with those damage states are plotted in Figs 2.26, 2.27, 2.28, 2.29 and 2.30, while the number of damaged bridges is listed in Tables 2.17, 2.18, 2.19, 2.20 and 2.21, respectively, for the cases before retrofit and after retrofit as a function of peak ground acceleration. It is noted here that the log-standard deviation for the pair of fragility curves in each of Figs is obtained by considering both two cases (before and after retrofit) together and calculating the optimal values from equation 2.11 for these fragility curves. This is for the reason that the bridge with jacketed columns is expected to be less vulnerable to ground motion than the bridge with the columns not jacketed and therefore we expect that the pair of these fragility curves should not theoretically intersect.

The damage state of a bridge in this case is defined in terms of the maximum value of the peak ductility demands sustained by all the column ends. In this context, comparison between the two curves in each of Figs 2.26-2.30 indicates that the bridge is less susceptible to damage from the ground motion after retrofit than before. The simulated fragility curves in this case demonstrate that, for all levels of damage states, the median fragility values after retrofit are larger than the corresponding values before retrofit. This implies the following: if the number of Type 1 bridges suffering from a certain state of damage is counted, on average, the damage is smaller when the bridge is subjected to these sixty (60) earthquakes after retrofit than before retrofit. The number is listed in Tables 2.17-2.21 for before and after retrofit to Bridge 1~5. The result in Tables 2.17-2.21 is consistent with the observation that the fragility enhancement is found to be

more significant for more severe state of damage in general. This is not unexpected because the ductility demands for more severe states of damage increase after retrofit by much larger multiples than those that occurred before retrofit.

Table 2.17 Number of Damaged Bridges: Retrofit Effect in Bridge 1

sample size=60

Damage States	before Retrofit	after Retrofit
No	4	7
Almost No	5	9
Slight	10	16
Moderate	7	13
Extensive	17	13
Complete	17	2

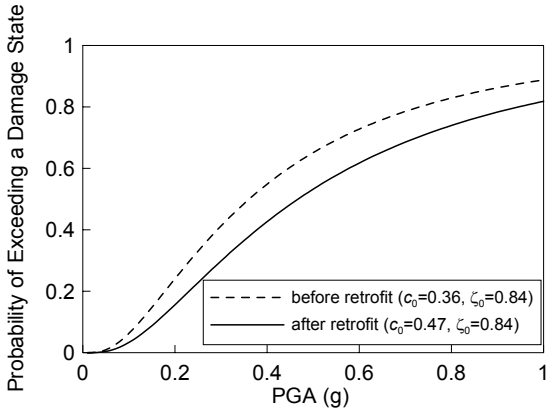

(a) Almost No Damage

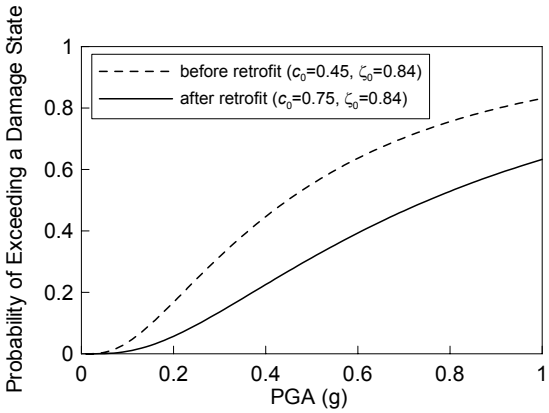

(b) Slight Damage

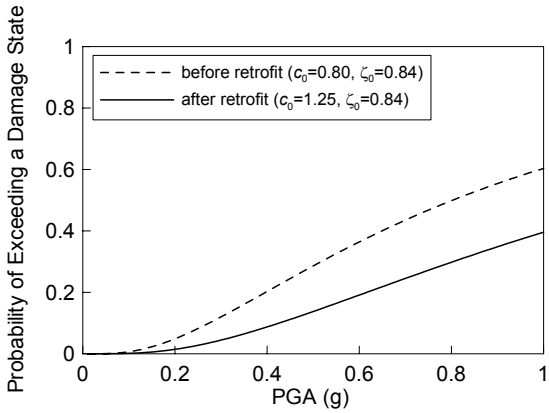

(c) Moderate Damage

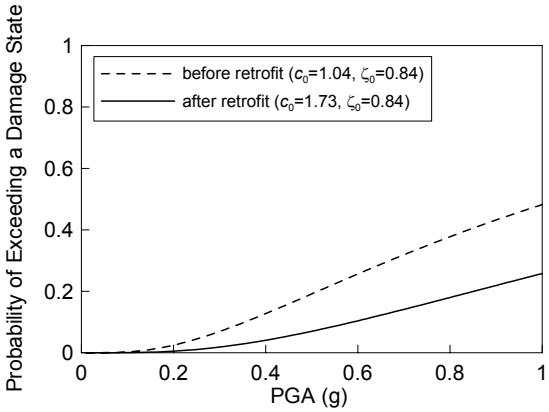

(d) Extensive Damage

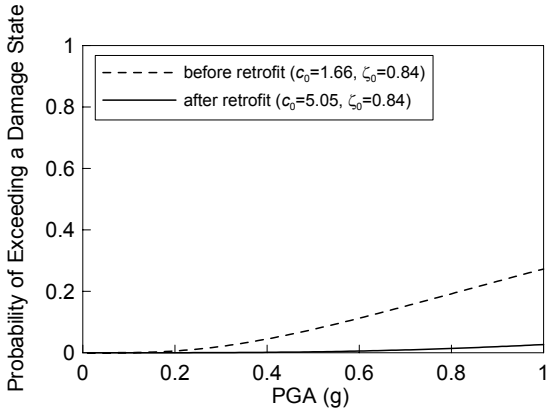

(e) Complete Collapse

Fig 2.26 Retrofit Effect on Fragility Curves of Bridge 1 (Longitudinal)

Table 2.18 Number of Damaged Bridges: Retrofit Effect in Bridge 2

sample size=60

Damage States	before Retrofit	after Retrofit
No	9	10
Almost No	4	9
Slight	10	19
Moderate	7	12
Extensive	16	6
Complete	14	4

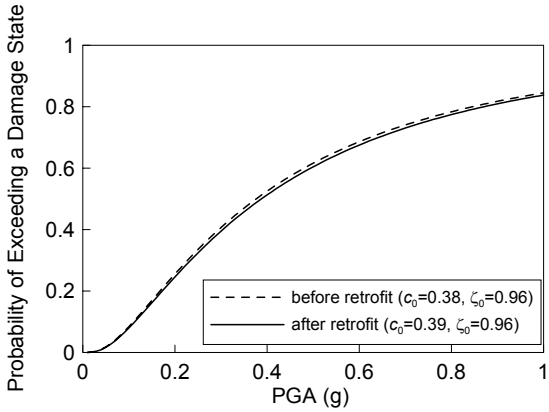

(a) Almost No Damage

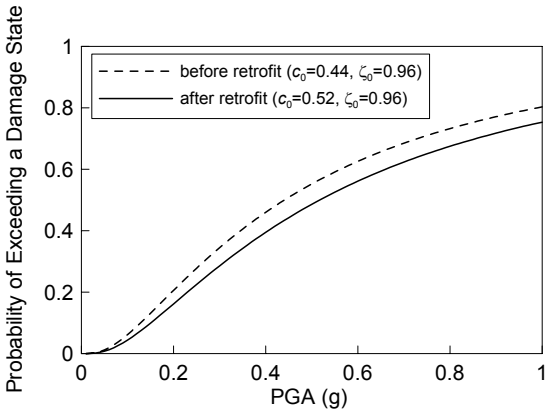

(b) Slight Damage

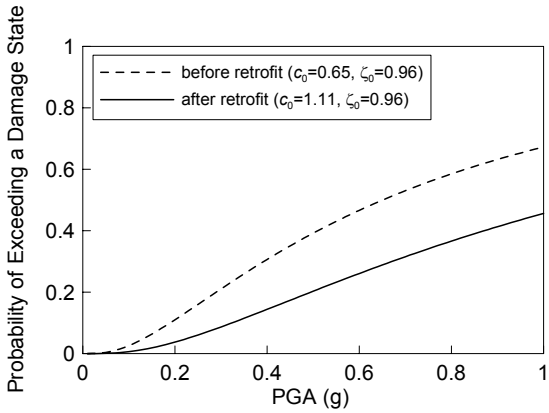

(c) Moderate Damage

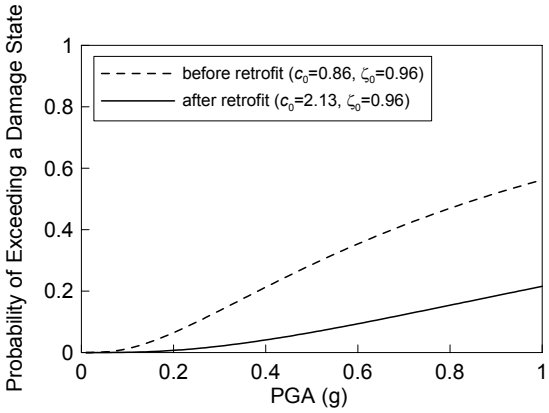

(d) Extensive Damage

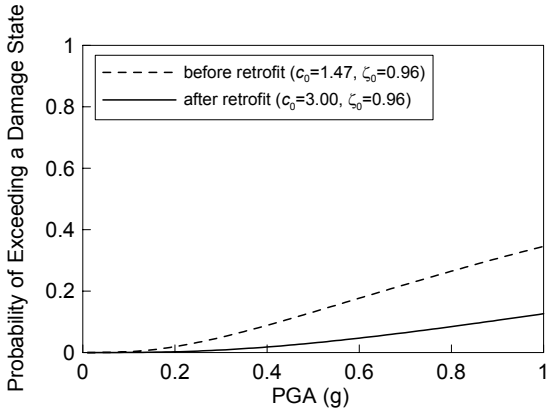

(e) Complete Collapse

Fig 2.27 Retrofit Effect on Fragility Curves of Bridge 2 (Longitudinal)

Table 2.19 Number of Damaged Bridges: Retrofit Effect in Bridge 3

sample size=60

Damage States	before Retrofit	after Retrofit
No	2	3
Almost No	2	13
Slight	9	16
Moderate	6	11
Extensive	13	13
Complete	28	4

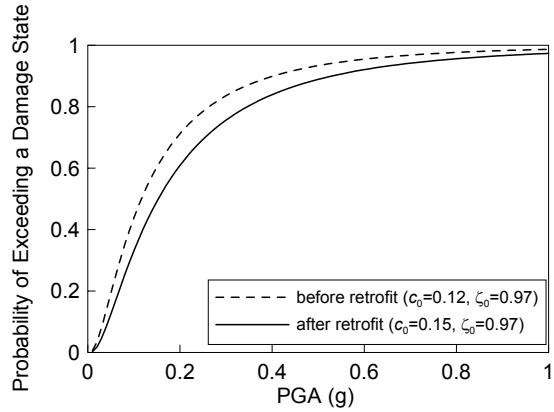

(a) Almost No Damage

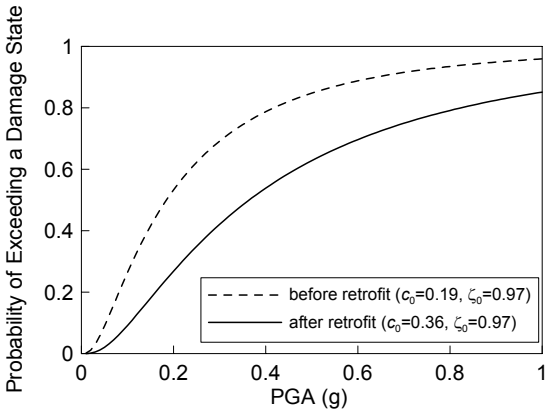

(b) Slight Damage

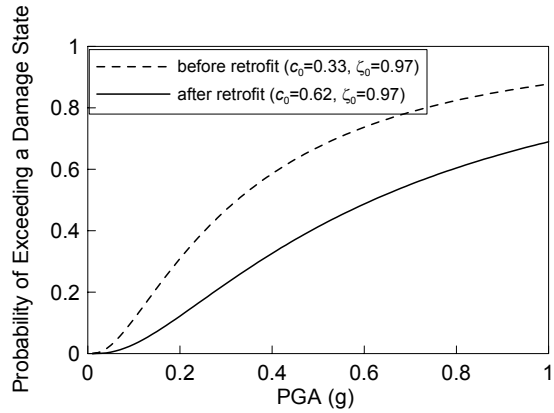

(c) Moderate Damage

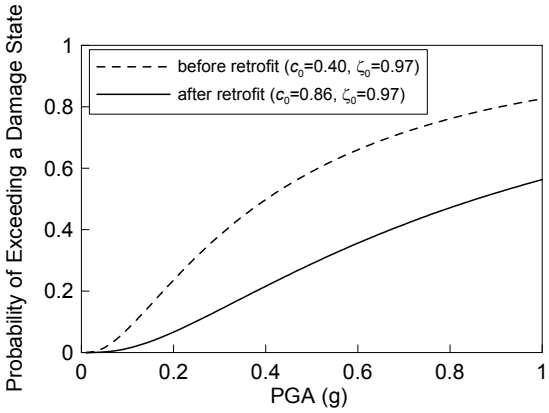

(d) Extensive Damage

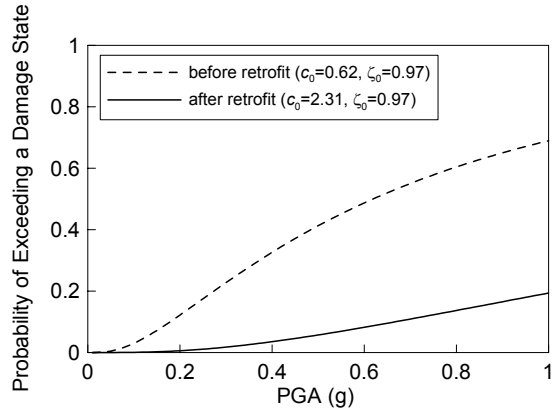

(e) Complete Collapse

Fig 2.28 Retrofit Effect on Fragility Curves of Bridge 3 (Longitudinal)

Table 2.20 Number of Damaged Bridges: Retrofit Effect in Bridge 4

sample size=60

Damage States	before Retrofit	after Retrofit
No	2	4
Almost No	5	17
Slight	12	14
Moderate	7	13
Extensive	18	9
Complete	16	3

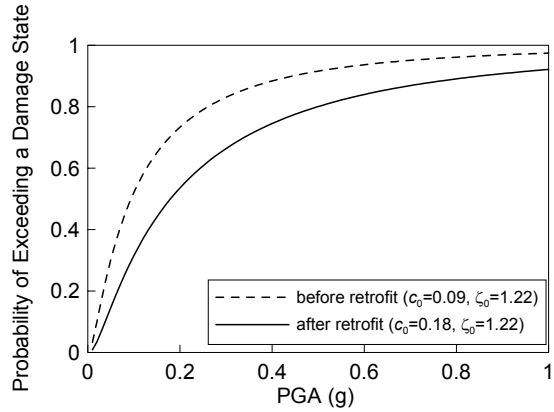

(a) Almost No Damage

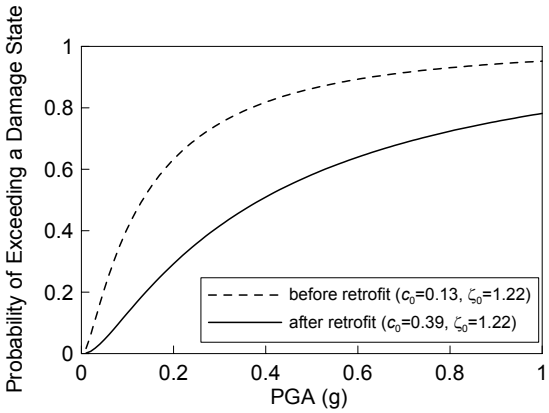

(b) Slight Damage

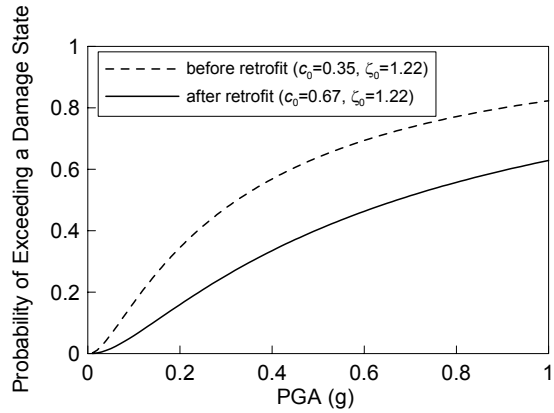

(c) Moderate Damage

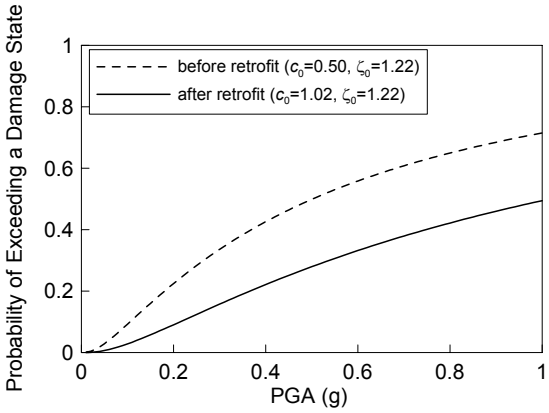

(d) Extensive Damage

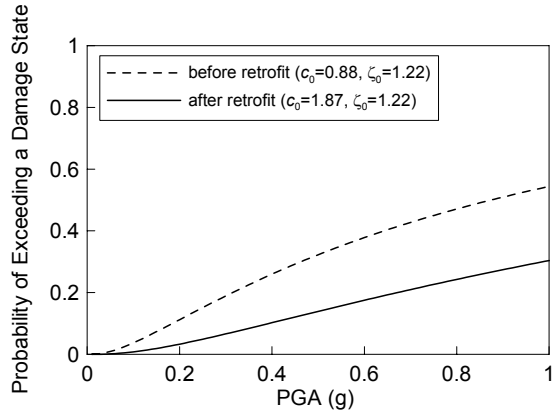

(e) Complete Collapse

Fig 2.29 Retrofit Effect on Fragility Curves of Bridge 4 (Longitudinal)

Table 2.21 Number of Damaged Bridges: Retrofit Effect in Bridge 5

sample size=60

Damage States	before Retrofit	after Retrofit
No	9	9
Almost No	7	12
Slight	14	24
Moderate	11	12
Extensive	13	2
Complete	6	1

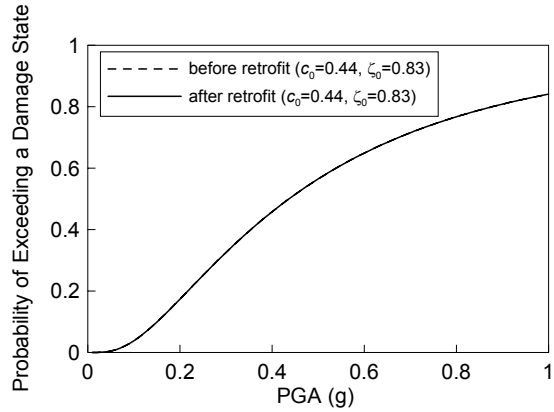

(a) Almost No Damage

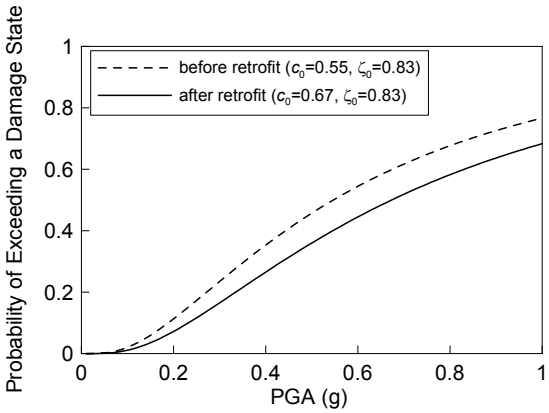

(b) Slight Damage

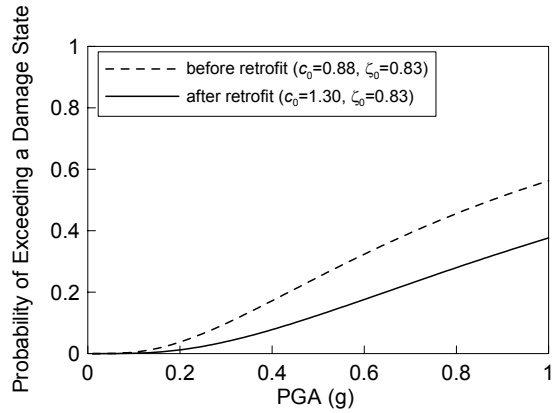

(c) Moderate Damage

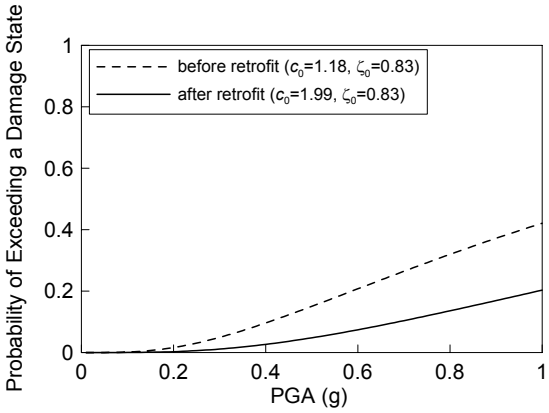

(d) Extensive Damage

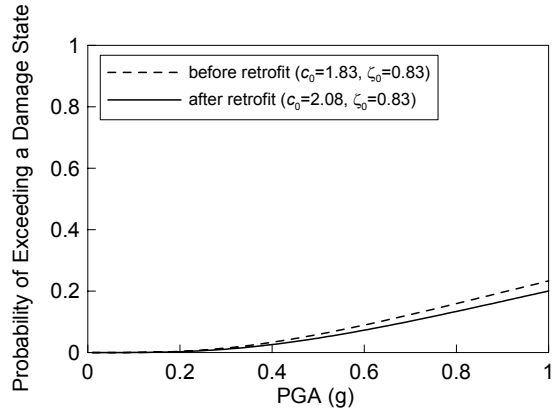

(e) Complete Collapse

Fig 2.30 Retrofit Effect on Fragility Curves of Bridge 5 (Longitudinal)

The result shows, for example, that the effect of column retrofit on the seismic performance is excellent in explaining that the bridges are up to three times less fragile for Bridge 1 (complete damage) and two for Bridge 2 (complete damage) after retrofit compared to the case before retrofit in terms of the median values.

2.8.1.1 Enhancement after Retrofit for Circular Column

Considering Bridge 1 and 2 which have circular columns and corresponding sets of fragility curves before and after retrofit, the average fragility enhancement over these two (2) bridges at each state of damage is computed and plotted as a function of the state of damage. An analytical function is interpolated and the "enhancement curve" is plotted through curve fitting as shown in Fig 2.31. This curve shows 20%, 34%, 58%, 98% and 167% improvement for each damage state described on the *x* axis in Fig 2.31.

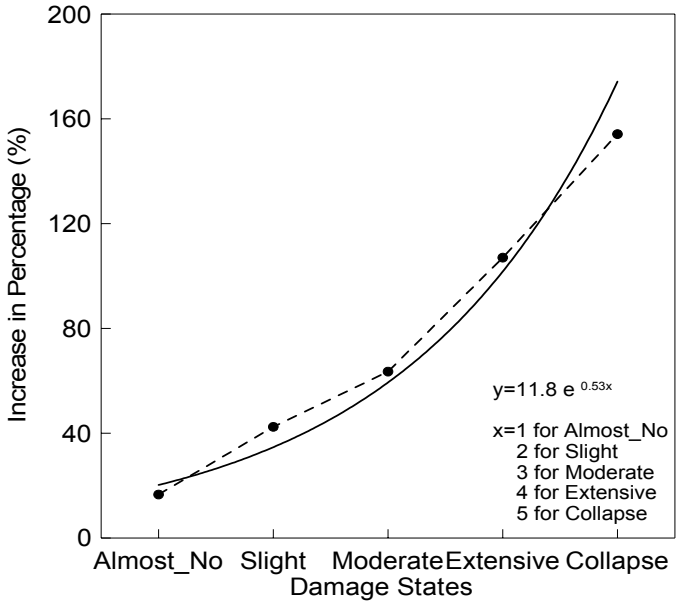

Fig 2.31 Enhancement Curve for Circular Columns with Steel Jacketing

2.8.1.2 Enhancement after Retrofit for Oblong Shape Column

For Bridge 3 and 5 with oblong columns, the fragility enhancement is developed in Fig 2.28 and 2.30.

Considering these two (2) sample bridges with oblong columns and corresponding sets of fragility curves before and after retrofit, the average fragility enhancement over these two (2) sample bridges at each state of damage is computed and plotted as a function of the state of damage. An analytical function is interpolated and the "enhancement curve" is plotted through curve fitting as shown in Fig 2.38. This curve shows 20%, 34%, 58%, 99% and 170% improvement for each damage state described on the *x* axis in Fig 32.

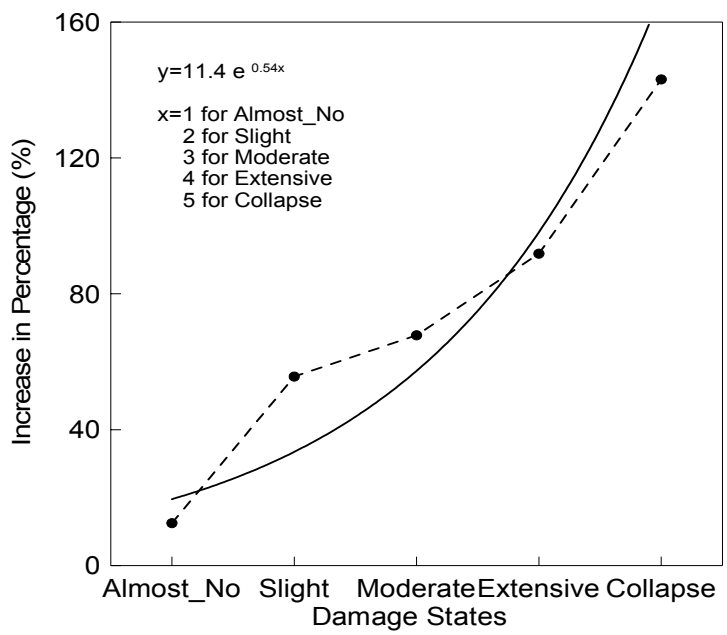

Fig 2.32 Enhancement Curve for Oblong Columns with Steel Jacketing

2.8.1.3 Enhancement after Retrofit for Rectangular Column

For Bridge 4 with rectangular columns, the fragility enhancement is developed in Fig 2.30.

Considering the sample bridge with rectangular columns and corresponding sets of fragility curves before and after retrofit at each state of damage is computed and plotted as a function of the state of damage. An analytical function is interpolated and the "enhancement curve" is plotted through curve fitting as shown in Fig 2.33. It is noted that the effect of retrofit is not good for Bridge 4 because the geometric shape after retrofit [Fig C4 (b1)~(b9)] is not efficient for steel jacketing to produce confinement effect.

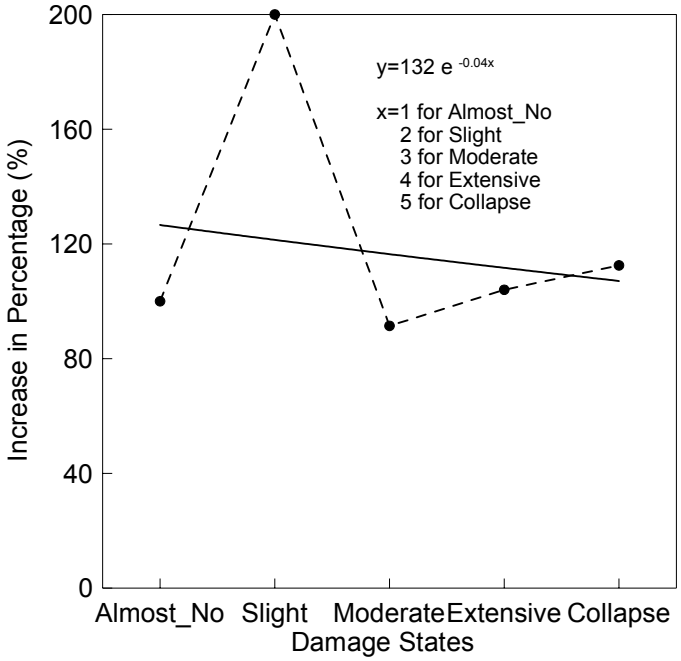

Fig 2.33 Enhancement Curve for Rectangular Columns with Steel Jacketing

2.8.1.4 Enhancement after Retrofit for All Types of Column

Considering all the sample bridges and corresponding sets of fragility curves before and after retrofit at each state of damage is computed and plotted as a function of the state of damage. An analytical function is interpolated and the "enhancement curve"

is plotted through curve fitting as shown in Fig 2.34. This curve shows 40%, 55%, 75%, 104% and 143% improvement for each damage state described on the *x* axis in Fig 2.34

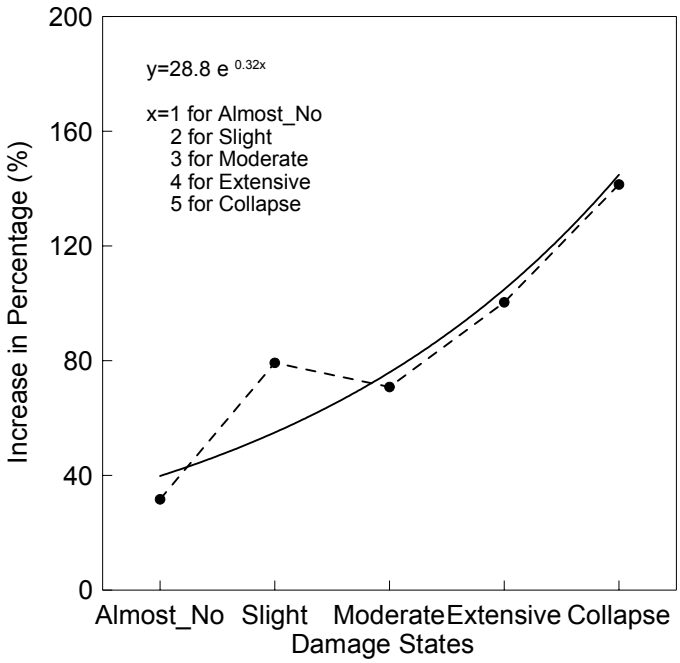

Fig 2.34 Enhancement Curve for Five Sample Bridges with Steel Jacketing

2.8.2 Enhancement after Calibrating the Analytical Fragility Curves

As described in the earlier part, analytical fragility curves are obtained using the damage state definitions given by Dutta and Mander (Table 2.4). To compare these analytically obtained fragility curves with past earthquake bridge damage data, empirical fragility curves for a third level subset (considering 'multiple span' and 'soil type C') have been developed (Shinozuka et al. 2003a) (see Chapter 3). Results indicate that the analytical curves are more probable to exceed a damage state than empirical ones (Shinozuka and Banerjee, 2004). They have defined the damage states of bridges for slight, moderate and extensive damage levels in terms of threshold ductility capacities,

for what, the analytical fragility curves will be consistent with empirical curves. These new definitions of threshold ductility capacities have extended to develop the fragility curves after retrofit. Fig 2.35 shows the empirical fragility curves and simulated fragility curves for three already stated damage states of Bridge 2. Obtained threshold ductility capacities at each damage states for bridge 2, 4, and 5 before and after retrofit are tabulated in Table 2.22 .

Table 2.22 Simulated Ductility Capacities of Sample Bridges

Damage state	Bridge 2		Bridge 4		Bridge 5	
	before retrofit	before retrofit	after retrofit	after retrofit	before retrofit	after retrofit
Slight	4.5	5.4	6.9	11.5	4.5	6.62
Moderate	6.5	9.66	7.31	17.13	8.4	16.21
Extensive	16.8	26.04	14.5	36.84	12.8	26.8

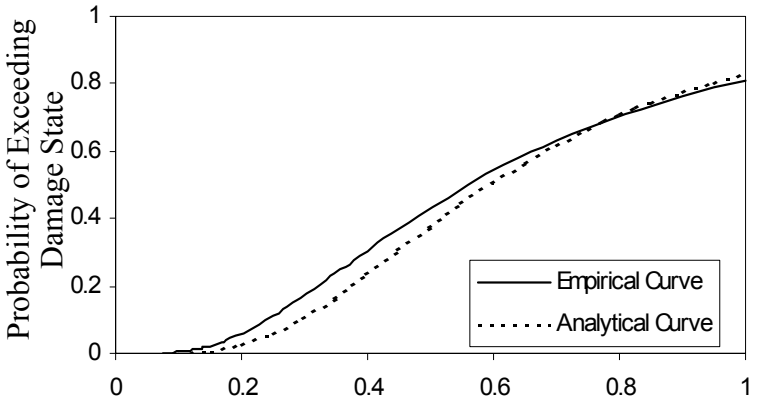

Slight Damage

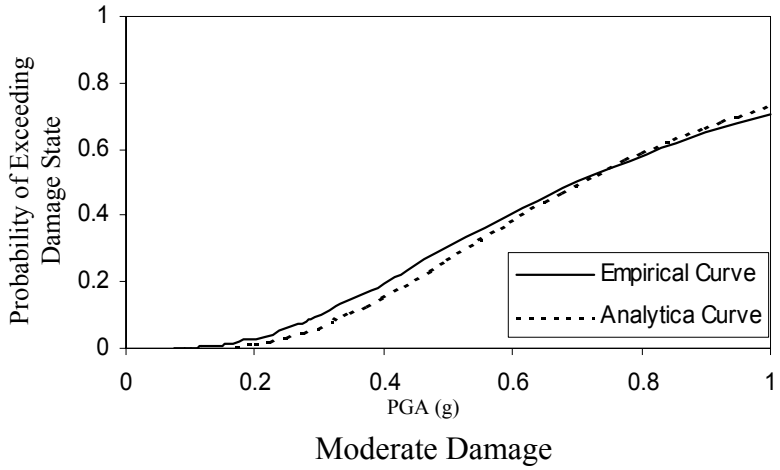

Moderate Damage

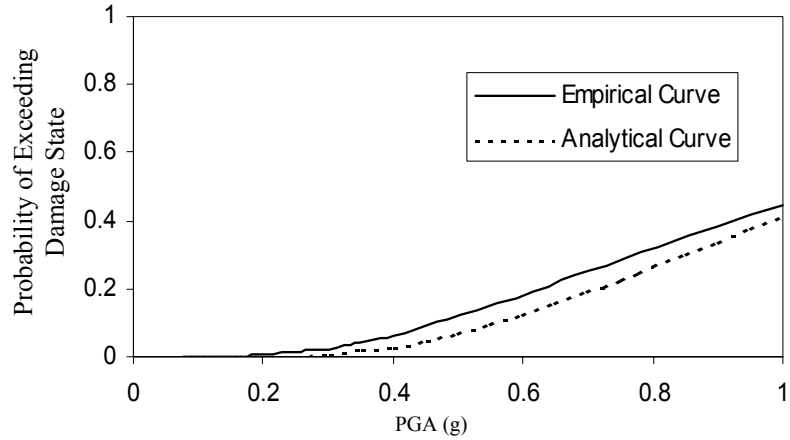

Extensive Damage

Fig 2.35 Empirical Fragility Curves and Calibrated Analytical Fragility Curves of Bridge 2

Based on the new definitions of damage states, the fragility curves of bridge 2(Circular Column), 4 (Rectangular Column) and 5 (Oblong Column) before and after retrofit are estimated again. Table 2.23 give the fragility parameters, and the enhancement ratios based on the 2 set of definitions of damage states are provided in Table 2.24.

Table 2.23 Fragility Curves based on Adjusted Damage States Definitions

Damage State	Bridge 2			Bridge 4			Bridge 5		
	c_0 (g)	$c_0^{'}$ (g)	ζ_0	c_0 (g)	$c_0^{'}$ (g)	ζ_0	c_0 (g)	$c_0^{'}$ (g)	ζ_0
At least minor	0.59	0.76	0.56	0.56	0.83	0.52	0.51	0.74	0.42
At least moderate	0.71	1.48	0.67	0.62	1.08	0.64	0.66	1.33	0.44
At least extensive	1.13	6.12	1.27	1.08	2.53	0.71	/	/	/

Table 2.24 Enhancement Ratios Comparison

Damage State	Bridge 2		Bridge 4		Bridge 5	
	Mander's	Calibrated	Mander's	Calibrated	Mander's	Calibrated
At least minor	18%	28%	200%	48%	22%	46%
At least moderate	71%	109%	91%	74%	48%	102%
At least extensive	148%	440%	104%	134%	69%	/

2.8.3 Fragility Curves for Transverse Direction

The fragility curves for five (5) sample bridges associated with those damage states are plotted in Figs 2.36, 2.37, 2.38, 2.39 and 2.40, while the number of damaged bridges is listed in tables 2.25, 2.26, 2.27, 2.28 and 2.29, respectively, for the cases before retrofit and after retrofit as a function of peak ground acceleration.

Table 2.25 Number of Damaged Bridges: Retrofit Effect in Bridge 1

sample size=60

Damage States	before Retrofit	after Retrofit
No	5	8
Almost No	3	8
Slight	10	17
Moderate	9	13
Extensive	18	13
Collapse	15	1

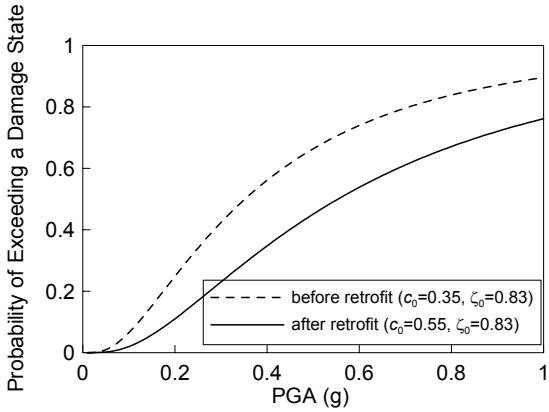

(a) Almost No Damage

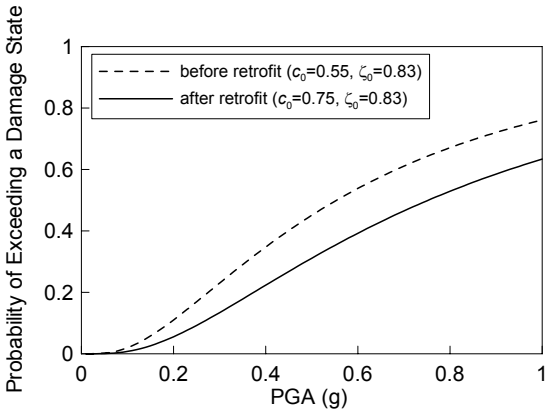

(b) Slight Damage

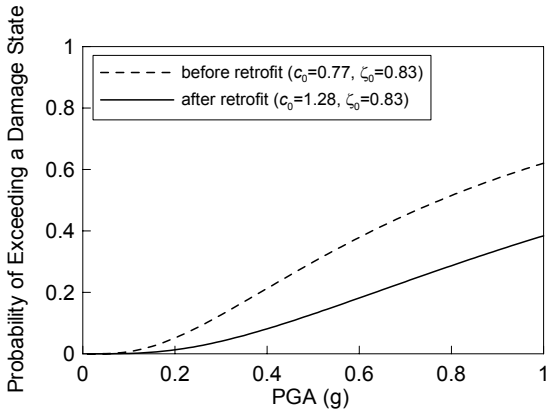

© Moderate Damage

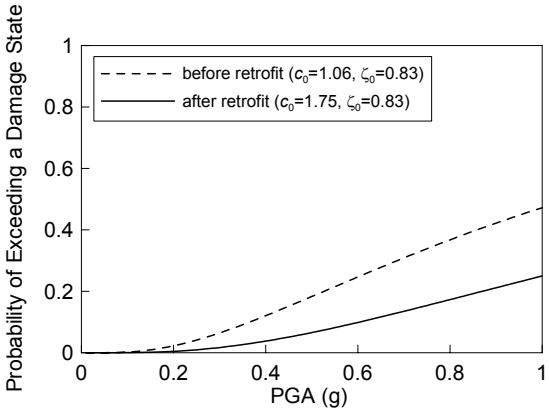

(d) Extensive Damage

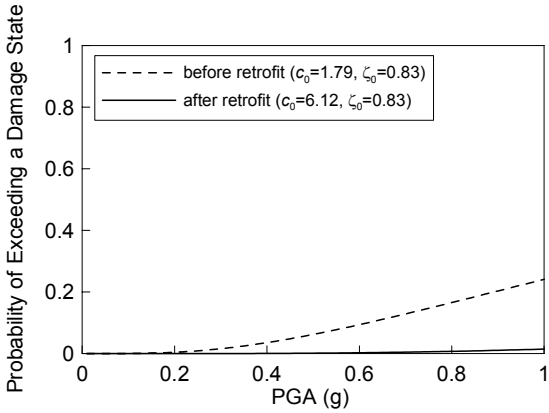

(e) Complete Collapse

Fig 2.36 Retrofit Effect on Fragility Curves of Bridge 1 (Transverse)

Table 2.27 Number of Damaged Bridges: Retrofit Effect in Bridge 2

sample size=60

Damage States	before Retrofit	after Retrofit
No	4	4
Almost No	4	16
Slight	16	18
Moderate	6	11
Extensive	18	9
Collapse	12	2

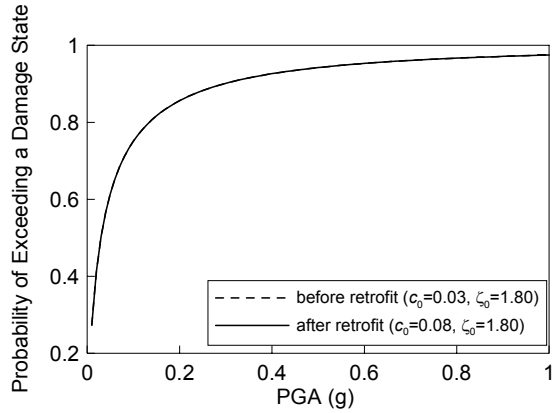

(a) Almost No Damage

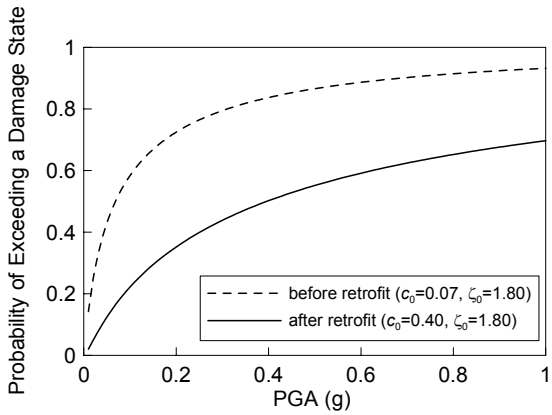

(b) Slight Damage

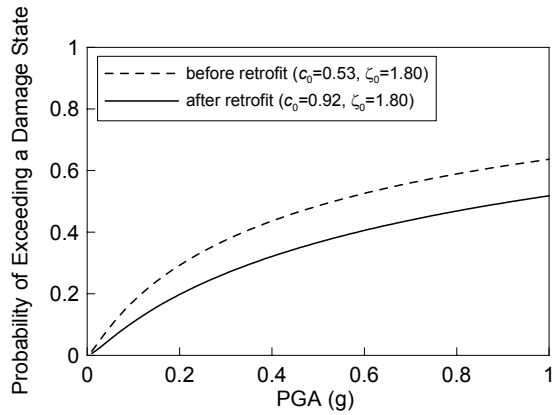

© Moderate Damage

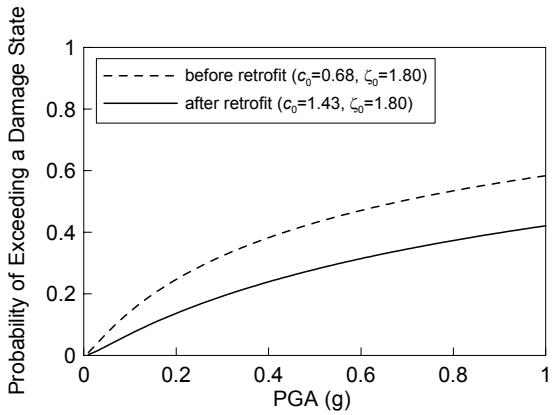

(d) Extensive Damage

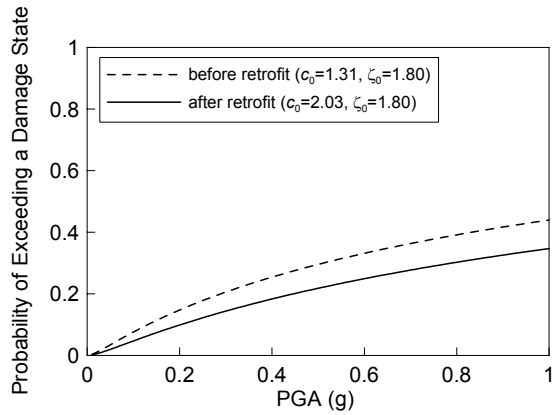

(e) Complete Collapse

Fig 2.37 Retrofit Effect on Fragility Curves of Bridge 2 (Transverse)

Table 2.28 Number of Damaged Bridges: Retrofit Effect in Bridge 3

sample size=60

Damage States	before Retrofit	after Retrofit
No	5	8
Almost No	5	8
Slight	4	22
Moderate	8	14
Extensive	14	7
Collapse	24	1

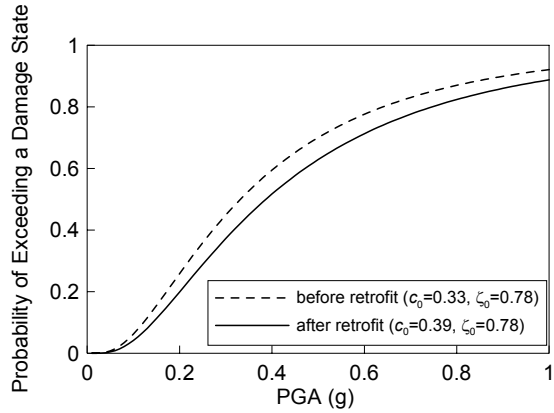

(a) Almost No Damage

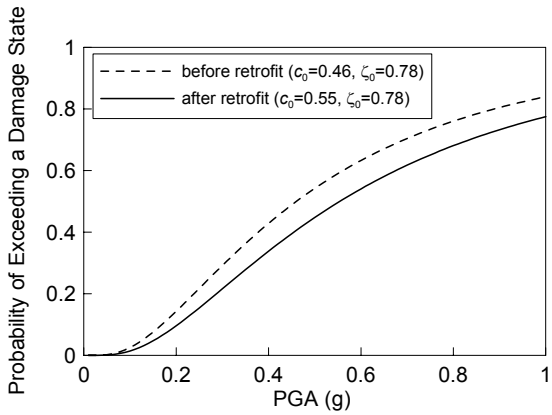

(b) Slight Damage

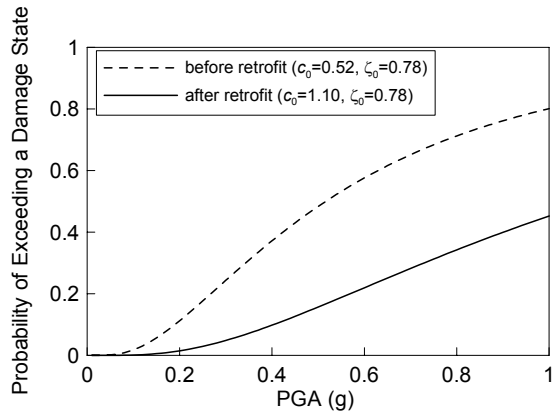

© Moderate Damage

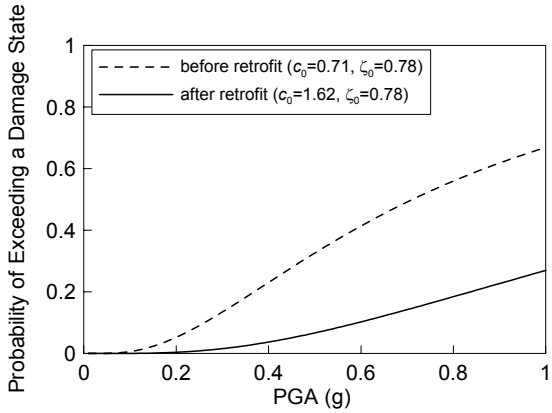

(d) Extensive Damage

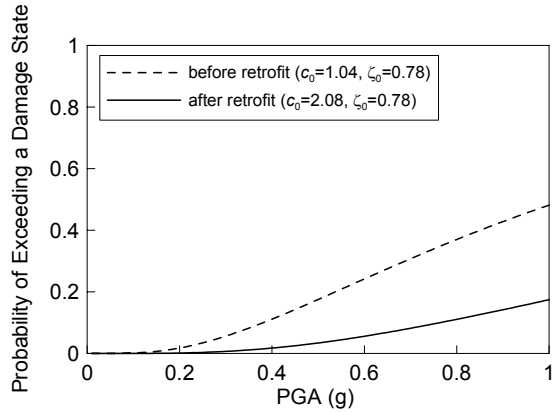

(e) Complete Collapse

Fig 2.38 Retrofit Effect on Fragility Curves of Bridge 3 (Transverse)

Table 2.29 Number of Damaged Bridges: Retrofit Effect in Bridge 4

sample size=60

Damage States	before Retrofit	after Retrofit
No	1	3
Almost No	3	11
Slight	12	17
Moderate	12	12
Extensive	15	14
Collapse	17	2

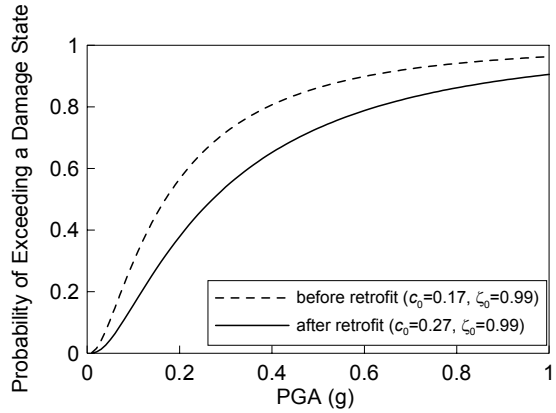

(a) Almost No Damage

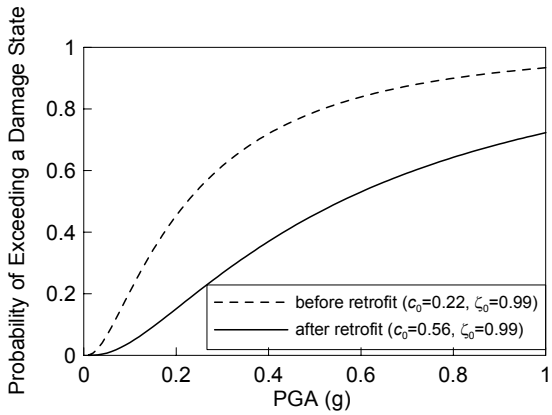

(b) Slight Damage

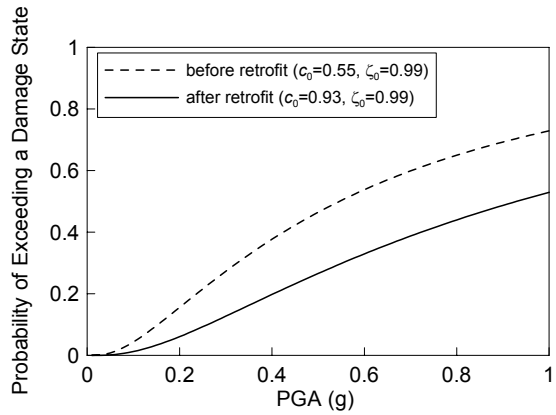

© Moderate Damage

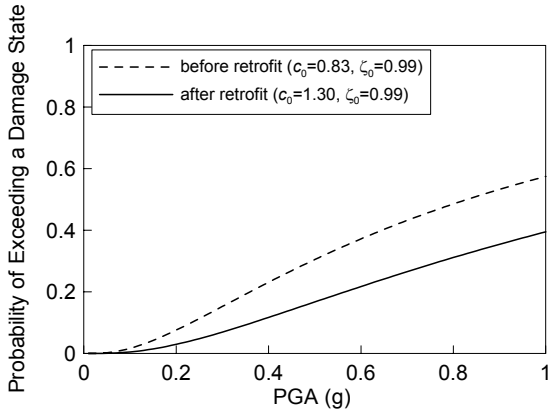

(d) Extensive Damage

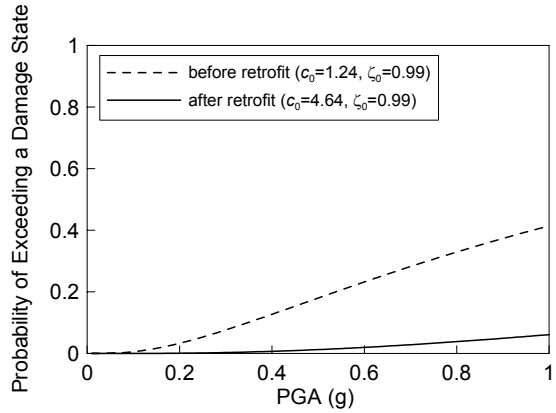

(e) Complete Collapse

Fig 2.39 Retrofit Effect on Fragility Curves of Bridge 4 (Transverse)

Table 2.30 Number of Damaged Bridges: Retrofit Effect in Bridge 5

sample size=60

Damage States	before Retrofit	after Retrofit
No	7	9
Almost No	2	6
Slight	10	16
Moderate	10	13
Extensive	14	13
Collapse	17	3

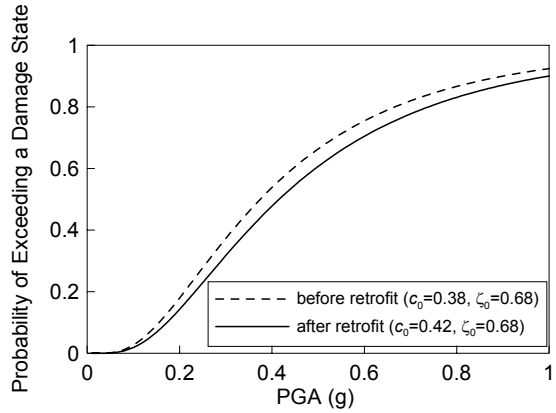

(a) Almost No Damage

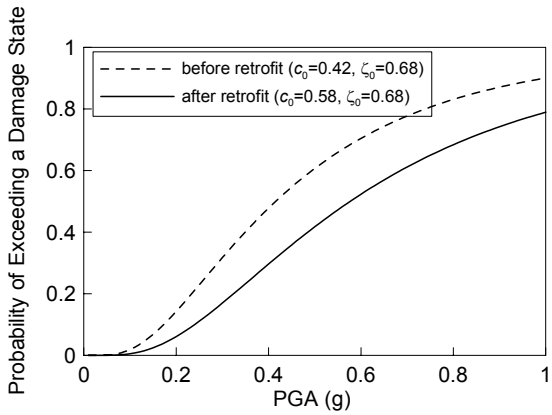

(b) Slight Damage

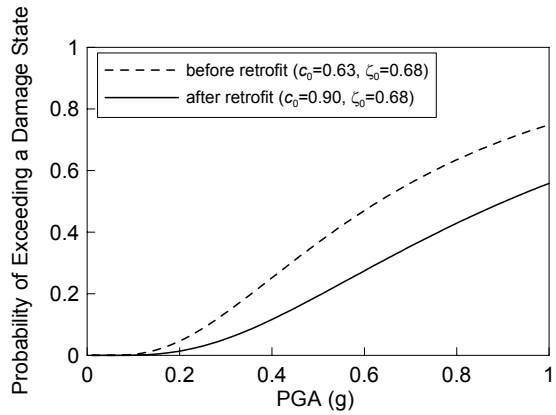

(c) Moderate Damage

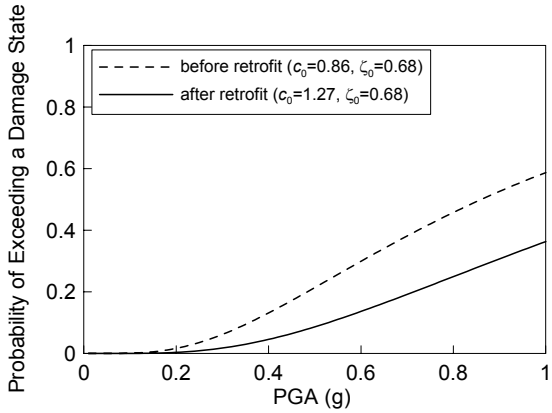

(d) Extensive Damage

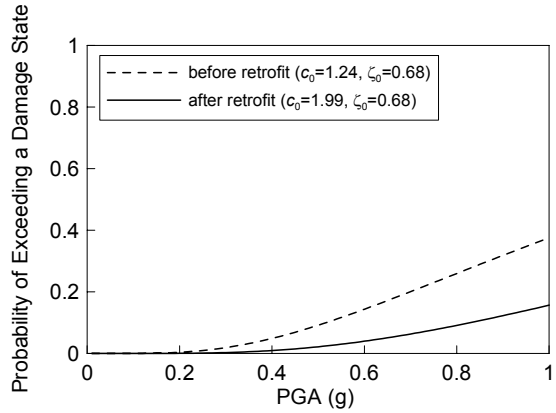

(e) Complete Collapse

Fig 2.40 Retrofit Effect on Fragility Curves of Bridge 5 (Transverse)

Chapter 3 Development of Empirical Fragility Curves for Bridges

3.1 Empirical Bridge Damage Data

The 1994 Northridge Earthquake caused tremendous damages to the human building environment. However, the damage investigation after the event provided valuable data basis for developing empirical fragility curves. After the event, 2209 highway bridges around Los Angeles Area were investigated and the damage of each bridge was classified as one of the five states: No, Minor, Moderate, Major or Collapse. Table 3.1 provides the summary of the bridge damage condition.

The site ground motion of each bridge structure can be derived from any ground motion spatial distribution (contour) map. Figs. 3.1 and 3.2 show PGA and PGV distribution in the 1994 Northridge Earthquake, which are acquired from the TriNet Shakemap (http://www.trinet.org/trinet.html). Table 3.2 lists part of the bridge damage table including bridge site ground motion determined from these two maps.

Table 3.1 Summary of Bridge Damage Status in the 1994 Northridge Earthquake

Damage State	No Damage	Minor Damage	Moderate Damage	Major Damage	Collapse Damage	Total
Number	1978	84	94	47	6	2209

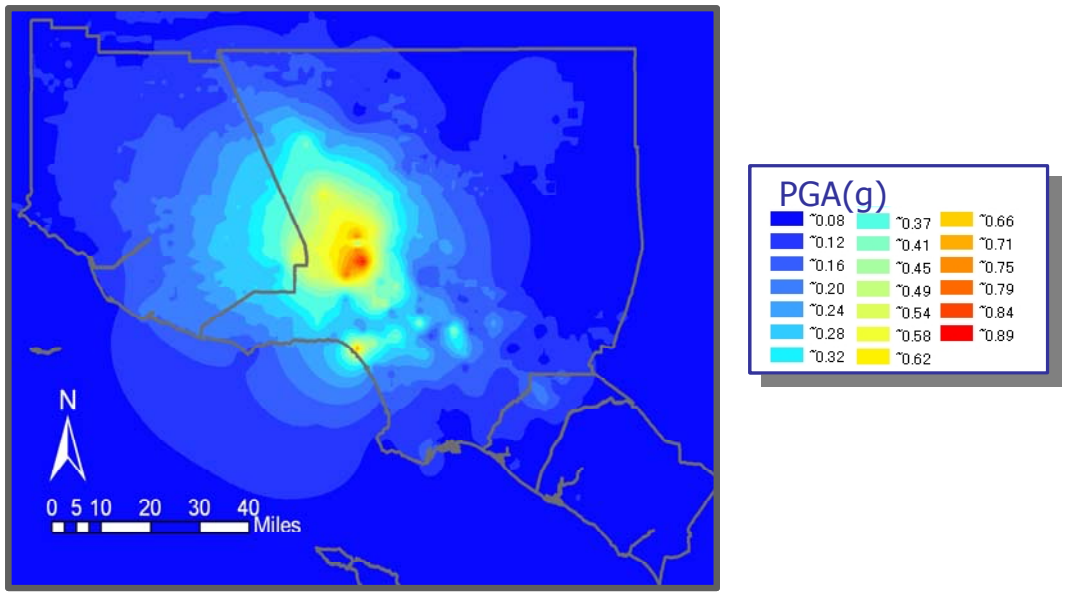

Fig 3.1 1994 Northridge Earthquake: PGA Distribution

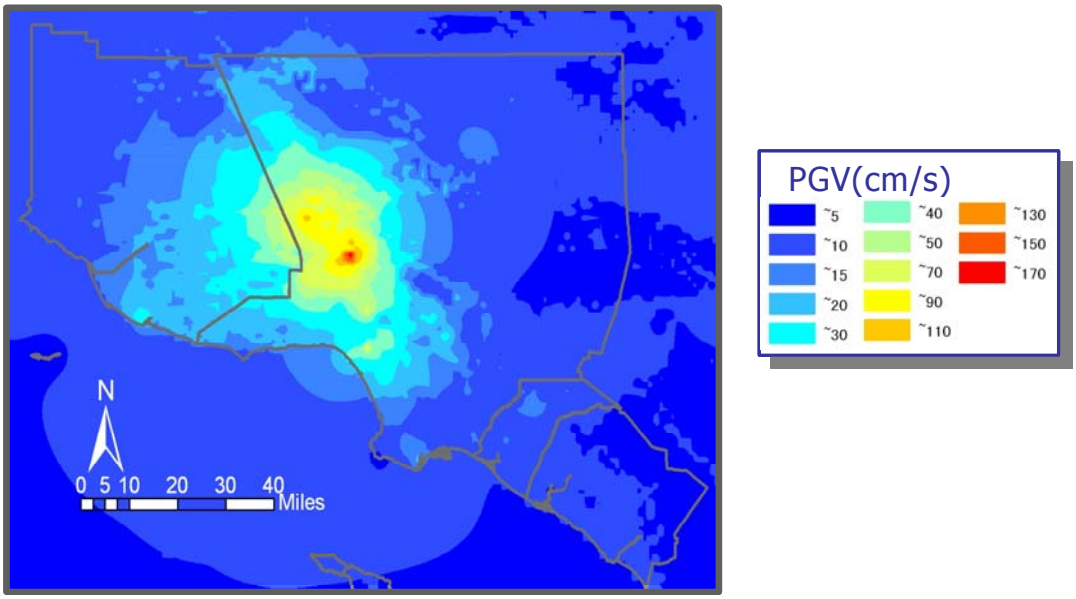

Fig 3.2 1994 Northridge Earthquake: PGV Distribution

Table 3.2 Seismic Damages of Bridges in the 1994 Northridge Earthquake

ID	BRIDGE_NO	Damage States	ShakeMap PGA (g)	ShakeMap PGV (cm/s)	LAT	LONG
1	53 1301	MOD*	0.2	16	34.0227	-118.2500
2	53 1471		0.12	12	33.7500	-118.2687
3	53 2618		0.08	6	33.7667	-118.2353
4	53 2216G	MAJ*	0.76	114	34.2667	-118.4697
5	53 1907G	MOD	0.24	20	34.1383	-118.2333
6	53 0595		0.28	16	34.0353	-118.2187
7	53 1851	MOD	0.28	28	33.9863	-118.4000
8	53 2549H		0.12	10	33.8687	-118.2843
9	53 1637F	MOD	0.4	42	34.0257	-118.4237
10	53 1790H	MOD	0.24	20	34.1520	-118.2747
11	53 1717H	MIN*	0.28	14	34.0353	-118.1677
12	53 1627G	MAJ	0.4	50	34.0257	-118.4343
13	53 2673		0.28	18	34.0520	-118.2227
14	53 1424	MOD	0.24	16	34.0757	-118.2217
15	53 2142F		0.12	10	33.8697	-118.1863
16	53 0707F		0.2	14	34.0393	-118.2697
17	53 2700G		0.12	10	33.9080	-118.1010
18	53 1714G	MOD	0.28	14	34.0353	-118.1677
19	53 0845		0.2	22	33.9353	-118.3903
20	53 2731		0.08	10	33.8373	-118.2040
21	52 0331R		0.28	22	34.2859	-118.8650
22	53 2143F		0.12	10	33.8697	-118.1843
23	53 2318G		0.16	14	34.1500	-118.1530
24	53 2327F	MAJ	0.6	72	34.2667	-118.4383
25	53 2329G	MAJ	0.6	72	34.2667	-118.4383
26	53 2102G	MAJ	0.4	46	34.2863	-118.4030
27	53 0405		0.28	18	34.0520	-118.2227
28	52 0118	MOD	0.24	20	34.3917	-118.9150
29	53 1960F	COL*	0.6	76	34.3350	-118.5083
30	53 1238G		0.2	18	33.9167	-118.3667
31	53 2104F	MOD	0.4	44	34.2853	-118.4020
32	52 0413		0.2	18	34.2011	-118.9758
33	53 2627		0.08	10	33.7843	-118.2217
34	53 1964F	COL	0.6	76	34.3353	-118.5056
35	53 1962F	MOD	0.64	76	34.3343	-118.5040
36	53 2200S	MOD	0.48	48	34.4010	-118.4540
37	53 1790	MIN	0.24	18	34.1510	-118.2717
....						

*MIN: Minor Damage MOD: Moderate Damage
MAJ: Major Damage COL: Collapse

3.2 Bridge Classification

In this research, the bridges are classified into different subsets according to the following three distinct attributes; (A) It is either single span (S) or multiple span (M), (B) it is built on either hard soil (S_A), medium soil (S_B) or soft soil (S_C) in the definition of UBC94, and (C) it has a skew angle θ_1 (less than 20°), θ_2 (between 20° and 60°) or θ_3 (larger than 60°).

To begin with, one might consider the first level hypothesis that the entire sample is taken from a statistically homogeneous population of bridges. The second level subsets are created by dividing the sample either (A) into two groups of bridges, one with single spans and the other with multiple spans, (B) into three groups, the first with soil condition SA, the second with SB and the third with SC, or (C) into three groups depending on the skew angles θ_1, θ_2 and θ_3. The third and fourth level sub-groupings were also considered for the development of corresponding fragility curves under PGA and PGV as ground motion intensity index (Shinozuka et al, 2003a).

3.3 Parameter Estimation

It is assumed that the curves can be expressed in the form of two parameter lognormal distribution functions, and the estimation of the two parameters (median and log-standard deviation) is performed with the aid of the maximum likelihood method. For this purpose, PGA and PGV values are used to represent the intensity of the seismic ground motion. The likelihood method for fragility parameter estimation was described in Chapter 2.

The median values and log-standard deviations of all levels of attribute combinations are listed in Table 3.3-3.6. Note that, if an element of a matrix in these

tables shows N/A, it indicates that no sub-sample was found for the particular combination of bridge attributes the element signifies. The family of fragility curves corresponding to the first level is plotted in Fig3.3 and 3.4. The curve with a "minor" designation represents, at each PGA or PGV value a, the probability that "at least a minor" state of damage will be sustained by a bridge (arbitrarily chosen from the sample of bridges) when it is subjected to PGA or PGV a. The same meaning applies to other curves with their respective damage state designations. All the other fragility curves in PGA are plotted in Figs 3.5-3.44

Table 3.3 First Level (Composite) Fragility Curve

Damage State	PGA (g)		PGV (cm/s)	
	c	ς	c	ς
Min	0.64	0.70	76	0.98
Mod	0.80	0.70	106	0.98
Maj	1.25	0.70	200	0.98
Col	2.55	0.70	555	0.98

Table 3.4 Second Level Fragility Curve

(a) Number of Span

Span	Damage State	PGA (g)		PGV (cm/s)	
		c	ς	c	ς
Single	Min	0.89	0.66	129	0.98
	Mod	1.15	0.66	188	0.98
	Maj	1.76	0.66	357	0.98
	Col	N/A	0.66	N/A	0.98
Multiple	Min	0.56	0.66	63	0.92
	Mod	0.70	0.66	87	0.92
	Maj	1.09	0.66	163	0.92
	Col	2.16	0.66	428	0.92

(b) Skew Angle

Skew	Damage State	PGA (g)		PGV (cm/s)	
		c	ς	c	ς
0^0-20^0	Min	0.82	0.76	108	1.07
	Mod	1.10	0.76	164	1.07
	Maj	1.86	0.76	343	1.07
	Col	3.49	0.76	833	1.07

20^0-60^0	Min	0.60	0.71	70	0.98
	Mod	0.72	0.71	90	0.98
	Maj	1.15	0.71	173	0.98
	Col	3.18	0.71	769	0.98
$>60^0$	Min	0.42	0.52	42	0.75
	Mod	0.52	0.52	56	0.75
	Maj	0.74	0.52	96	0.75
	Col	1.26	0.52	212	0.75

(c) Soil Type

Soil	Damage State	PGA (g)		PGV (cm/s)	
		c	ς	c	ς
A	Min	0.87	0.75	110	1.03
	Mod	1.10	0.75	151	1.03
	Maj	1.51	0.75	234	1.03
	Col	N/A	0.75	N/A	1.03
B	Min	0.64	0.71	65	0.81
	Mod	0.84	0.71	91	0.81
	Maj	1.24	0.71	145	0.81
	Col	N/A	0.71	N/A	0.81
C	Min	0.61	0.69	74	0.98
	Mod	0.76	0.69	102	0.98
	Maj	1.22	0.69	199	0.98
	Col	2.35	0.69	523	0.98

Table 3.5 Third Level Fragility Curve

(a) Span/Skew

Span	Skew	Damage State	PGA (g)		PGV (cm/s)	
			c	ς	c	ς
Single	0^0-20^0	Minor	1.37	0.82	276	1.28
		Moderate	2.04	0.82	502	1.28
		Major	3.56	0.82	1179	1.28
		Collapse	N/A	N/A	N/A	N/A
	20^0-60^0	Minor	0.63	0.43	82	0.7
		Moderate	0.70	0.43	98	0.7
		Major	0.96	0.43	164	0.7
		Collapse	N/A	N/A	N/A	N/A
	$>60^0$	Minor	0.62	0.13	86	0.10
		Moderate	N/A	N/A	N/A	N/A
		Major	N/A	N/A	N/A	N/A
		Collapse	N/A	N/A	N/A	N/A
Multiple	0^0-20^0	Minor	0.68	0.71	82	0.98
		Moderate	0.91	0.71	122	0.98
		Major	1.52	0.71	251	0.98
		Collapse	2.76	0.71	574	0.98

	20^0-60^0	Minor	0.56	0.74	63	0.99
		Moderate	0.69	0.74	84	0.99
		Major	1.11	0.74	162	0.99
		Collapse	3.14	0.74	716	0.99
	$>60^0$	Minor	0.38	0.38	37	0.58
		Moderate	0.42	0.38	43	0.58
		Major	0.56	0.38	68	0.58
		Collapse	0.67	0.38	92	0.58

(b) Span/Soil

Span	Soil	Damage State	PGA (g)		PGV (cm/s)	
			c	ς	c	ς
Single	A	Minor	0.90	0.40	116	0.50
		Moderate	N/A	N/A	N/A	N/A
		Major	N/A	N/A	N/A	N/A
		Collapse	N/A	N/A	N/A	N/A
	B	Minor	0.68	0.50	68	0.50
		Moderate	N/A	N/A	N/A	N/A
		Major	N/A	N/A	N/A	N/A
		Collapse	N/A	N/A	N/A	N/A
	C	Minor	0.74	0.57	106	0.90
		Moderate	0.91	0.57	144	0.90
		Major	1.37	0.57	274	0.90
		Collapse	N/A	N/A	N/A	N/A
Multiple	A	Minor	0.64	0.64	66	0.81
		Moderate	0.77	0.64	83	0.81
		Major	1.05	0.64	125	0.81
		Collapse	N/A	N/A	N/A	N/A
	B	Minor	0.47	0.45	44	0.53
		Moderate	0.56	0.45	57	0.53
		Major	0.76	0.45	86	0.53
		Collapse	N/A	N/A	N/A	N/A
	C	Minor	0.56	0.67	65	0.96
		Moderate	0.7	0.67	89	0.96
		Major	1.11	0.67	173	0.96
		Collapse	2.11	0.67	435	0.96

(c) Skew/Soil

Skew	Soil	Damage State	PGA (g)		PGV (cm/s)	
			c	ς	c	ς
0^0-20^0	A	Minor	0.70	0.50	61	0.50
		Moderate	0.98	0.50	90	0.50
		Major	N/A	N/A	N/A	N/A
		Collapse	N/A	N/A	N/A	N/A
	B	Minor	0.80	0.50	75	0.5
		Moderate	N/A	N/A	N/A	N/A

		Major	N/A	N/A	N/A	N/A
		Collapse	N/A	N/A	N/A	N/A
	C	Minor	0.74	0.72	98	1.04
		Moderate	0.97	0.72	144	1.04
		Major	1.61	0.72	299	1.04
		Collapse	2.99	0.72	728	1.04
20^0-60^0	A	Minor	0.73	0.48	79	0.50
		Moderate	0.73	0.48	79	0.50
		Major	0.83	0.48	88	0.50
		Collapse	N/A	N/A	N/A	N/A
	B	Minor	0.49	0.38	48	0.48
		Moderate	0.57	0.38	68	0.48
		Major	0.57	0.38	68	0.48
		Collapse	N/A	N/A	N/A	N/A
	C	Minor	0.57	0.72	66	0.57
		Moderate	0.69	0.72	86	0.69
		Major	1.19	0.72	187	1.19
		Collapse	3.07	0.72	759	3.07
$>60^0$	A	Minor	0.26	0.11	21	0.10
		Moderate	N/A	N/A	N/A	N/A
		Major	N/A	N/A	N/A	N/A
		Collapse	N/A	N/A	N/A	N/A
	B	Minor	N/A	N/A	N/A	N/A
		Moderate	N/A	N/A	N/A	N/A
		Major	N/A	N/A	N/A	N/A
		Collapse	N/A	N/A	N/A	N/A
	C	Minor	0.48	0.48	57	0.74
		Moderate	0.59	0.48	76	0.74
		Major	0.74	0.48	107	0.74
		Collapse	0.87	0.48	137	0.74

Table 3.6 Fourth Level Fragility Curve (Span/Skew/Soil)

Span	Skew	Soil	Damage State	PGA (g)		PGV (cm/s)	
				c	ς	c	ς
Single	0^0-20^0	A	Minor	0.63	0.22	81	0.40
			Moderate	N/A	N/A	N/A	N/A
			Major	N/A	N/A	N/A	N/A
			Collapse	N/A	N/A	N/A	N/A
		B	Minor	0.63	0.50	63	0.5
			Moderate	N/A	N/A	N/A	N/A
			Major	N/A	N/A	N/A	N/A
			Collapse	N/A	N/A	N/A	N/A
		C	Minor	0.98	0.57	239	1.16
			Moderate	1.19	0.57	340	1.16
			Major	1.85	0.57	780	1.16
			Collapse	N/A	N/A	N/A	N/A
	20^0-60^0	A	Minor	N/A	N/A	N/A	N/A
			Moderate	N/A	N/A	N/A	N/A
			Major	N/A	N/A	N/A	N/A
			Collapse	N/A	N/A	N/A	N/A
		B	Minor	N/A	N/A	N/A	N/A
			Moderate	N/A	N/A	N/A	N/A
			Major	N/A	N/A	N/A	N/A
			Collapse	N/A	N/A	N/A	N/A
		C	Minor	0.53	0.39	64	0.64
			Moderate	0.60	0.39	78	0.64
			Major	0.84	0.39	134	0.64
			Collapse	N/A	N/A	N/A	N/A
	$>60^0$	A	Minor	N/A	N/A	N/A	N/A
			Moderate	N/A	N/A	N/A	N/A
			Major	N/A	N/A	N/A	N/A
			Collapse	N/A	N/A	N/A	N/A
		B	Minor	N/A	N/A	N/A	N/A
			Moderate	N/A	N/A	N/A	N/A
			Major	N/A	N/A	N/A	N/A
			Collapse	N/A	N/A	N/A	N/A
		C	Minor	0.62	0.125	86	0.10
			Moderate	N/A	N/A	N/A	N/A
			Major	N/A	N/A	N/A	N/A
			Collapse	N/A	N/A	N/A	N/A

Table 3.6 Fourth Level Fragility Curve (Span/Skew/Soil) (cont.)

Span	Skew	Soil	Damage State	PGA (g)		PGV (cm/s)	
				c	ς	c	ς
Multiple	0^0-20^0	A	Minor	0.65	0.50	53	0.50
			Moderate	0.86	0.50	73	0.50
			Major	N/A	N/A	N/A	N/A
			Collapse	N/A	N/A	N/A	N/A
		B	Minor	N/A	N/A	N/A	N/A
			Moderate	N/A	N/A	N/A	N/A
			Major	N/A	N/A	N/A	N/A
			Collapse	N/A	N/A	N/A	N/A
		C	Minor	0.63	0.68	76	0.96
			Moderate	0.83	0.68	113	0.96
			Major	1.37	0.68	232	0.96
			Collapse	2.48	0.68	533	0.96
	20^0-60^0	A	Minor	0.50	0.33	55	0.49
			Moderate	0.50	0.33	55	0.49
			Major	0.59	0.33	63	0.49
			Collapse	N/A	N/A	N/A	N/A
		B	Minor	0.42	0.61	39	0.50
			Moderate	0.55	0.61	62	0.50
			Major	0.55	0.61	62	0.50
			Collapse	N/A	N/A	N/A	N/A
		C	Minor	0.57	0.79	66	1.08
			Moderate	0.71	0.79	89	1.08
			Major	1.28	0.79	202	1.08
			Collapse	3.40	0.79	830	1.08
	$>60^0$	A	Minor	0.26	0.32	21	0.10
			Moderate	N/A	N/A	N/A	N/A
			Major	N/A	N/A	N/A	N/A
			Collapse	N/A	N/A	N/A	N/A
		B	Minor	N/A	N/A	N/A	N/A
			Moderate	N/A	N/A	N/A	N/A
			Major	N/A	N/A	N/A	N/A
			Collapse	N/A	N/A	N/A	N/A
		C	Minor	0.68	0.37	74	0.37
			Moderate	0.68	0.37	74	0.37
			Major	0.69	0.37	97	0.37
			Collapse	N/A	N/A	N/A	N/A

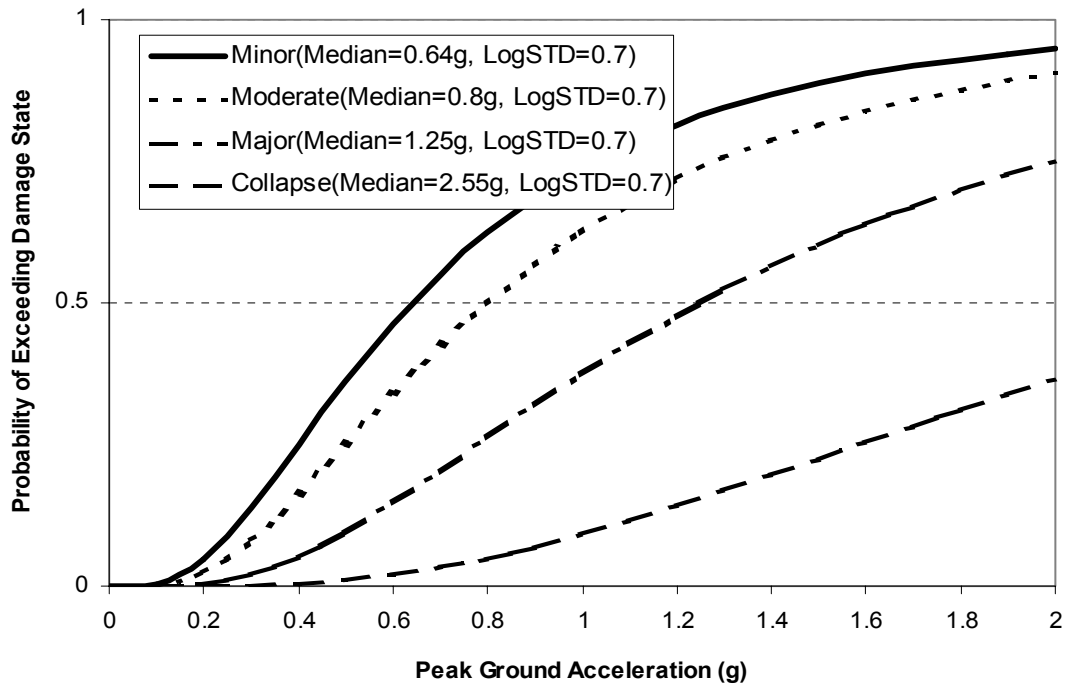

Fig 3.3 Fragility Curve in PGA (Composite)

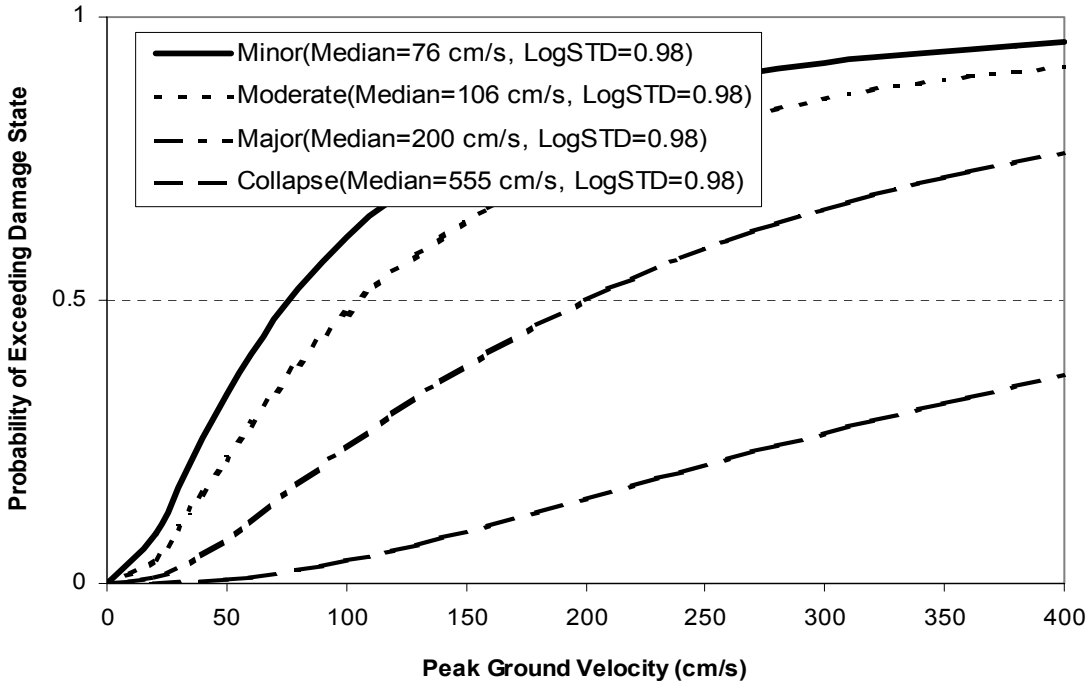

Fig 3.4 Fragility Curve in PGV (Composite)

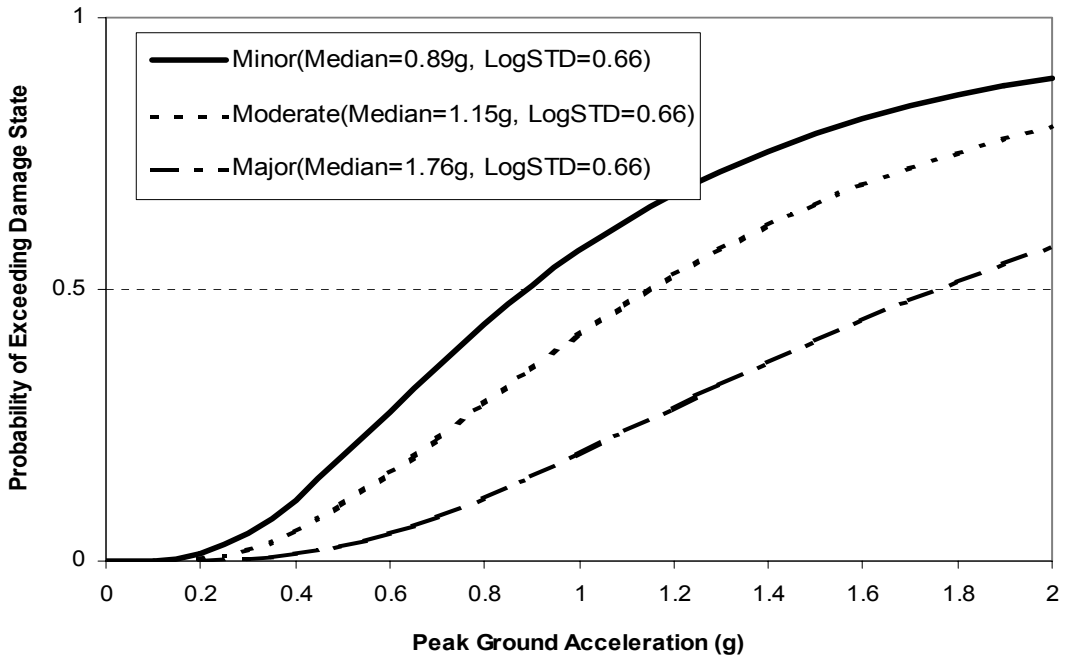

Fig 3.5 Fragility Curve in PGA (Single Span)

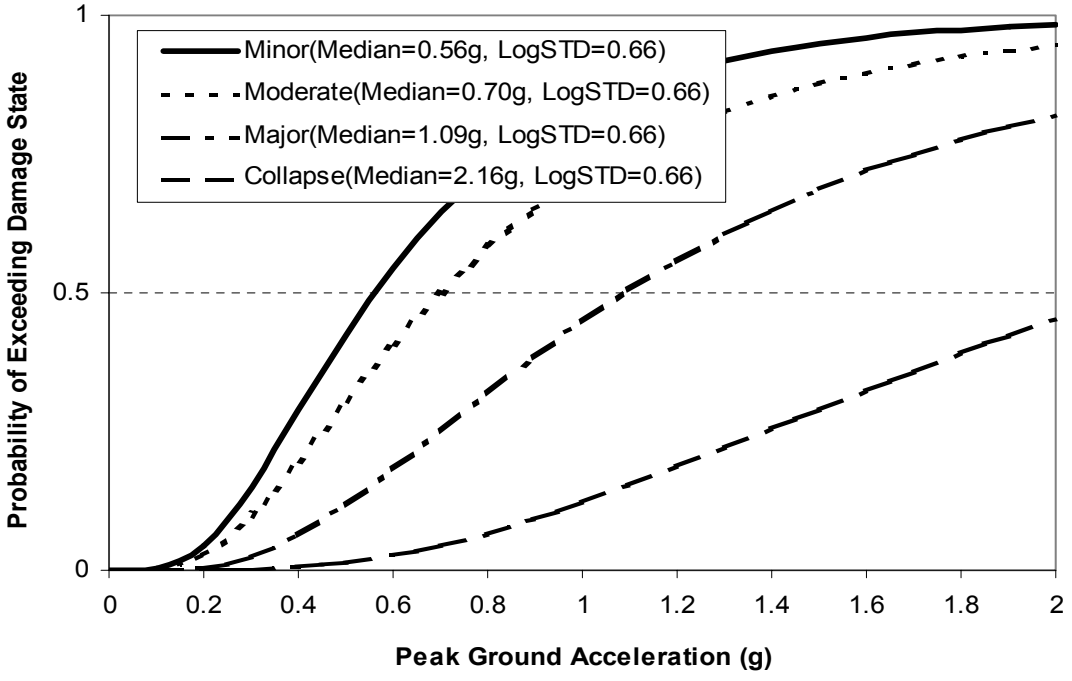

Fig 3.6 Fragility Curve in PGA (Multiple Span)

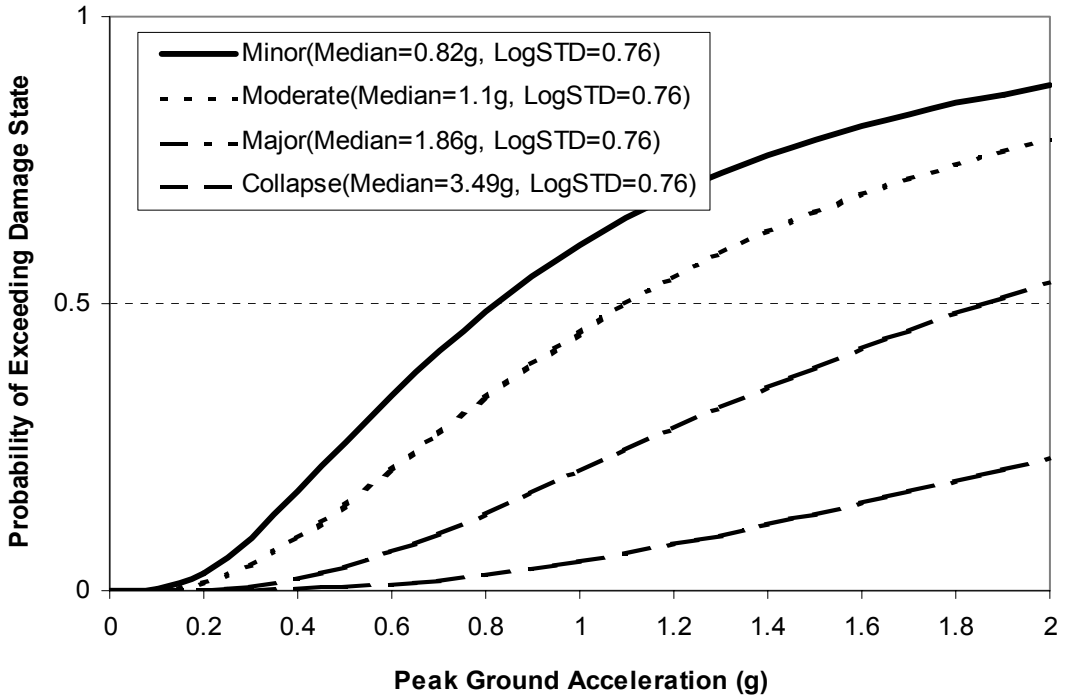

Fig 3.7 Fragility Curve in PGA (Skew 0^0-20^0)

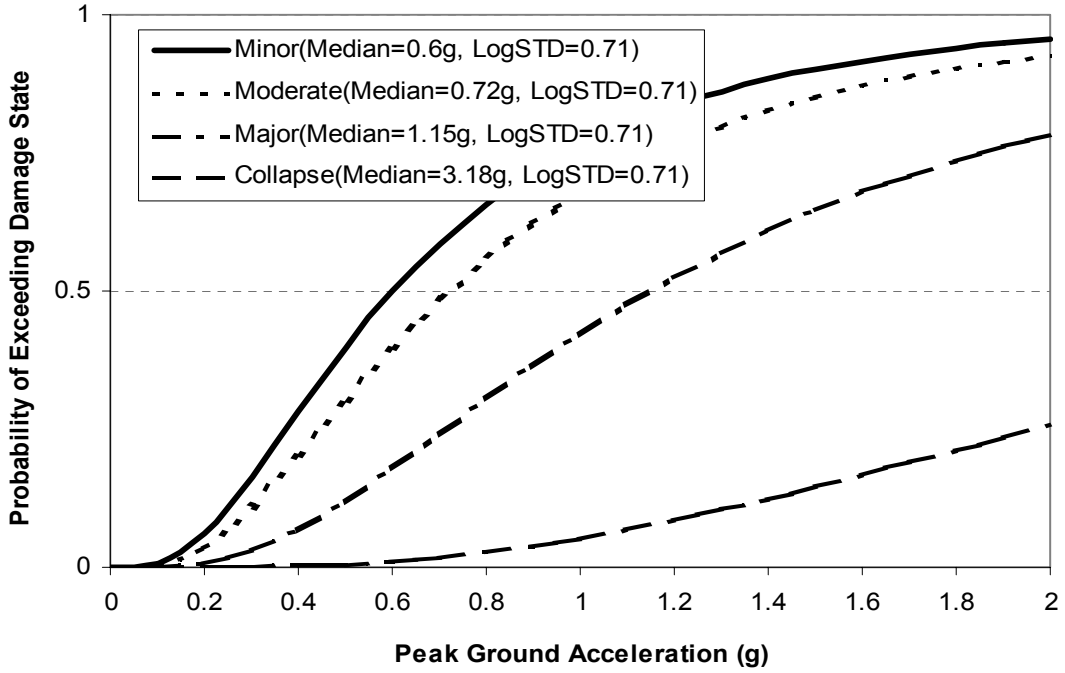

Fig 3.8 Fragility Curve in PGA (Skew 20^0-60^0)

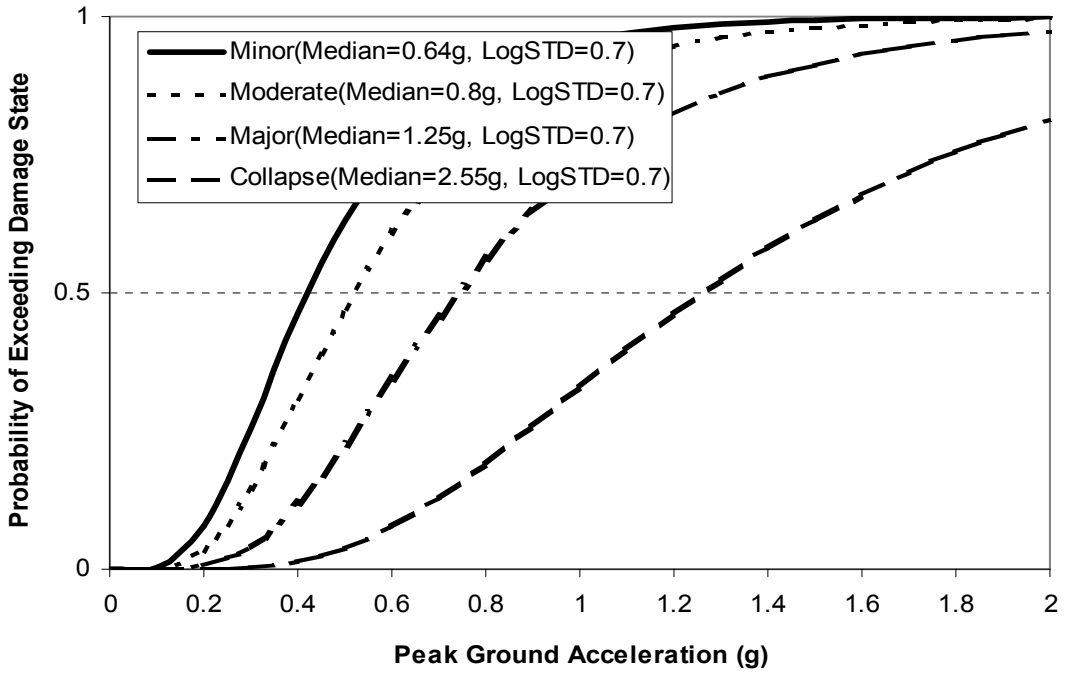

Fig 3.9 Fragility Curve in PGA (Skew >60^0)

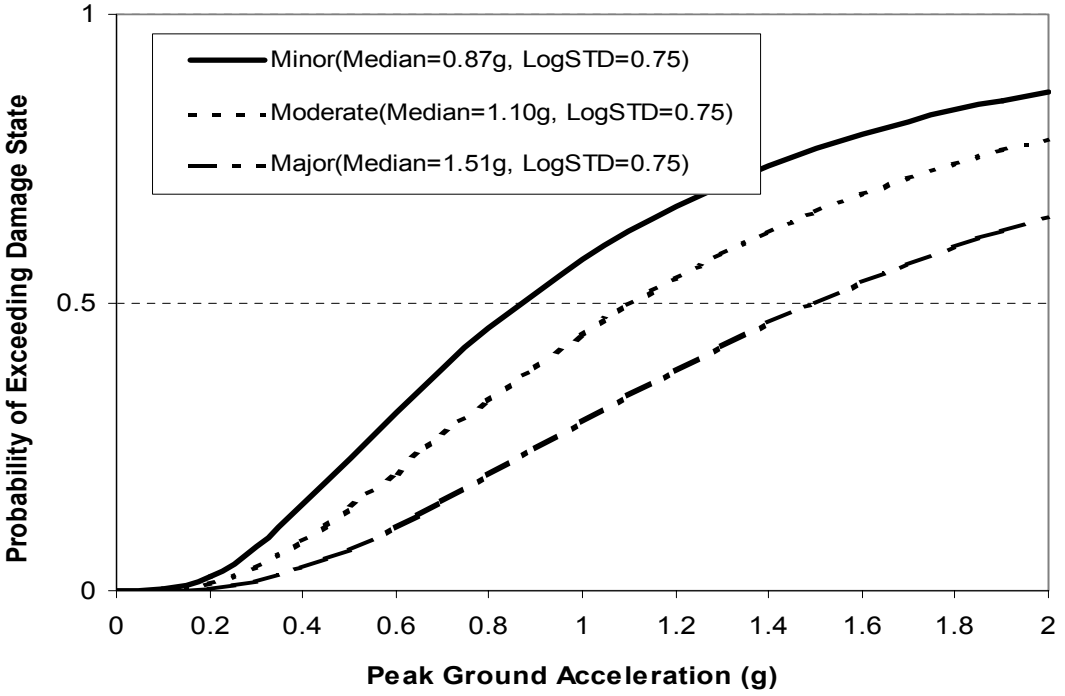

Fig 3.10 Fragility Curve in PGA (Soil A)

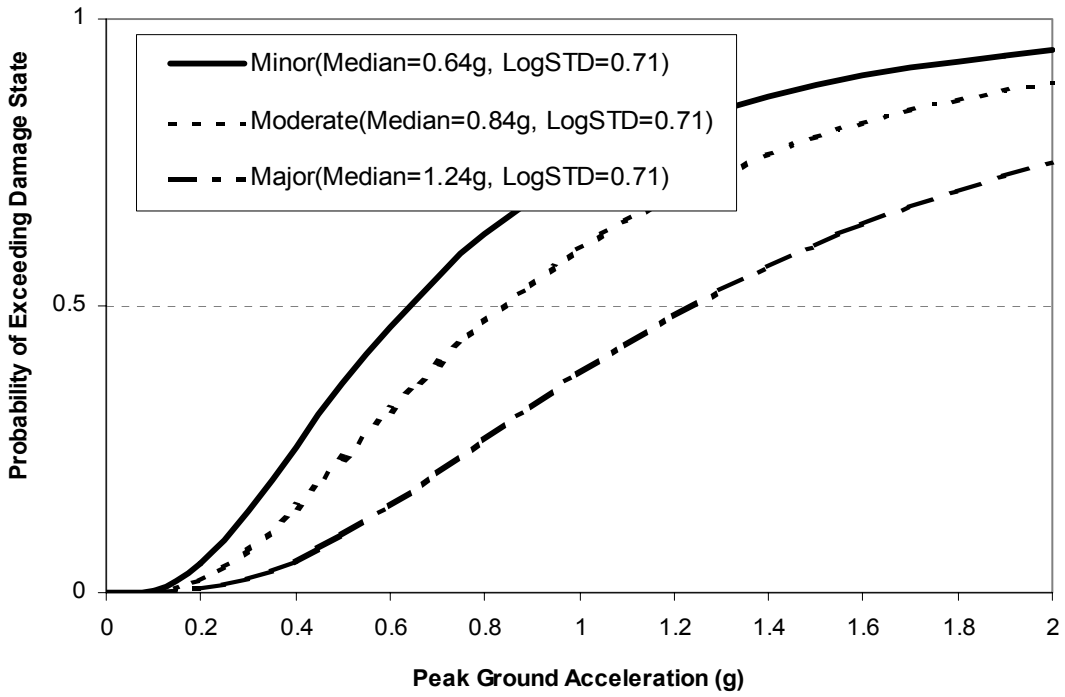

Fig 3.11 Fragility Curve in PGA (Soil B)

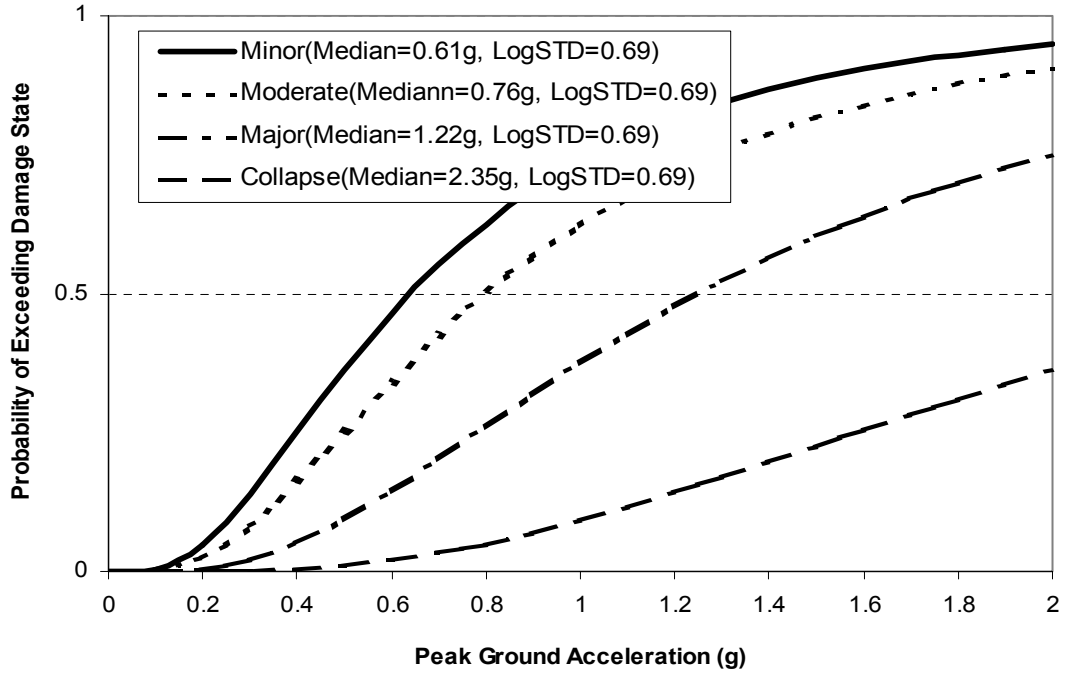

Fig 3.12 Fragility Curve in PGA (Soil C)

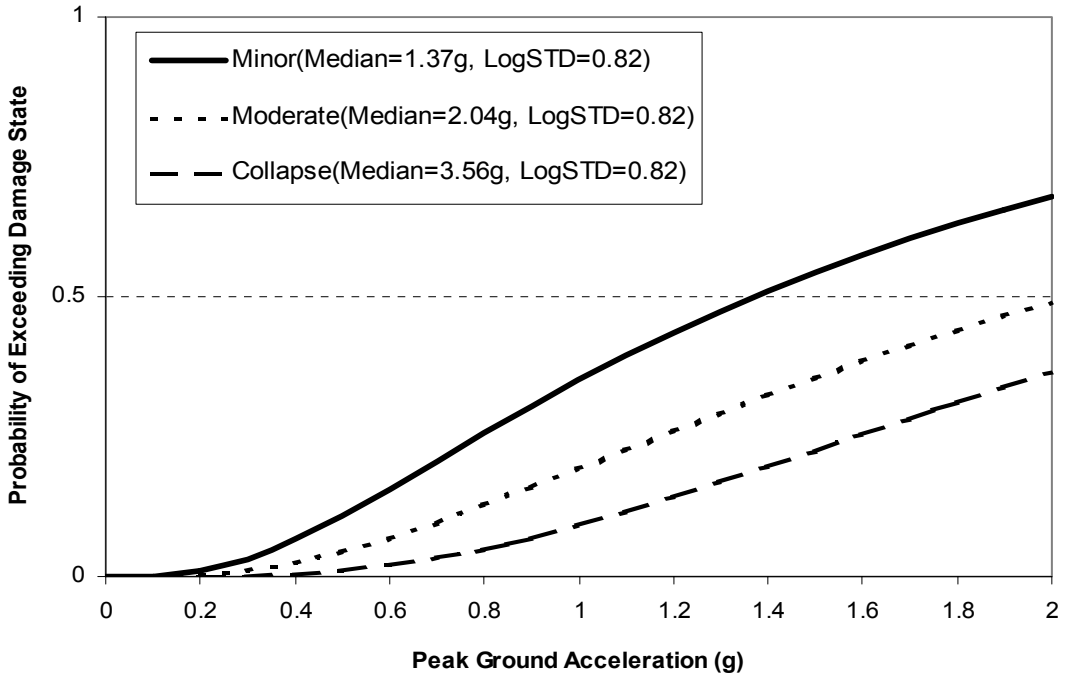

Fig 3.13 Fragility Curve in PGA (Single Span /Skew 0^0-20^0)

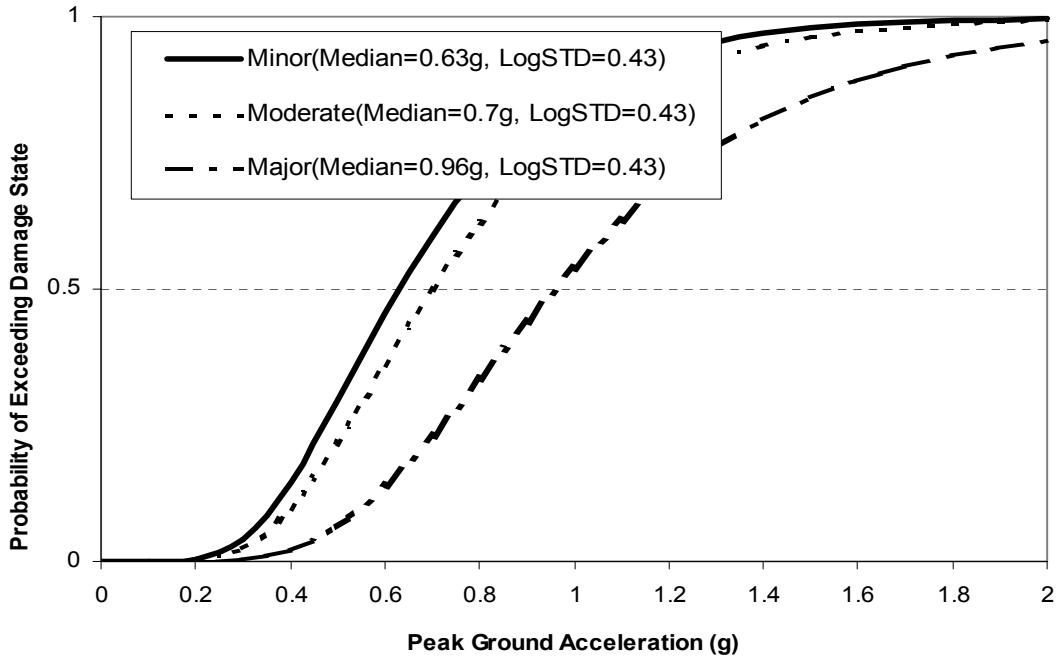

Fig 3.14 Fragility Curve in PGA (Single Span/Skew 20^0-60^0)

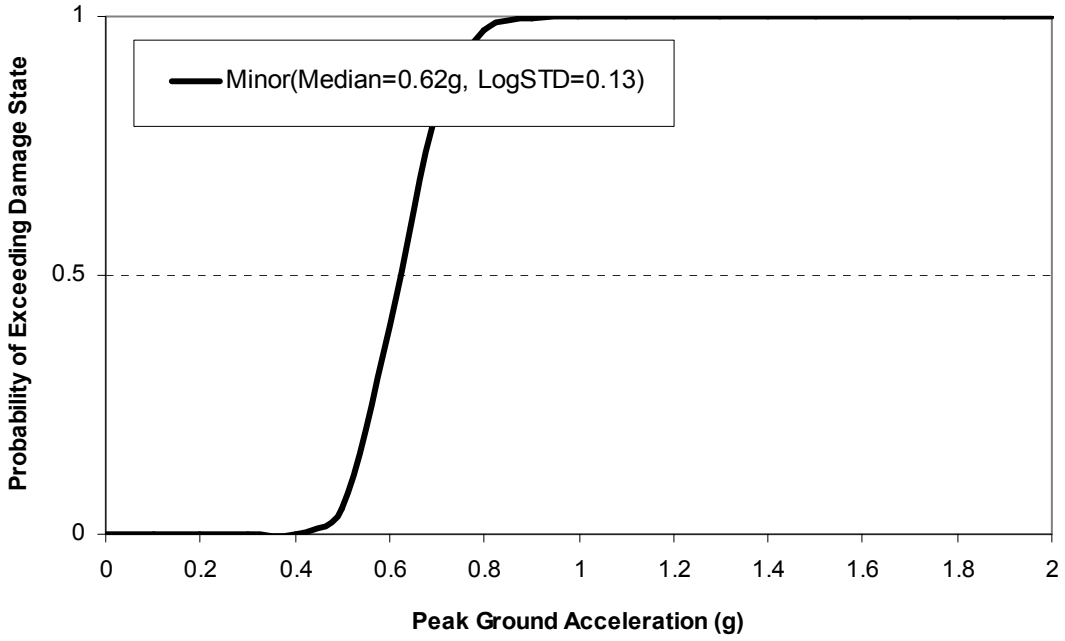

Fig 3.15 Fragility Curve in PGA (Single Span/Skew >60^0)

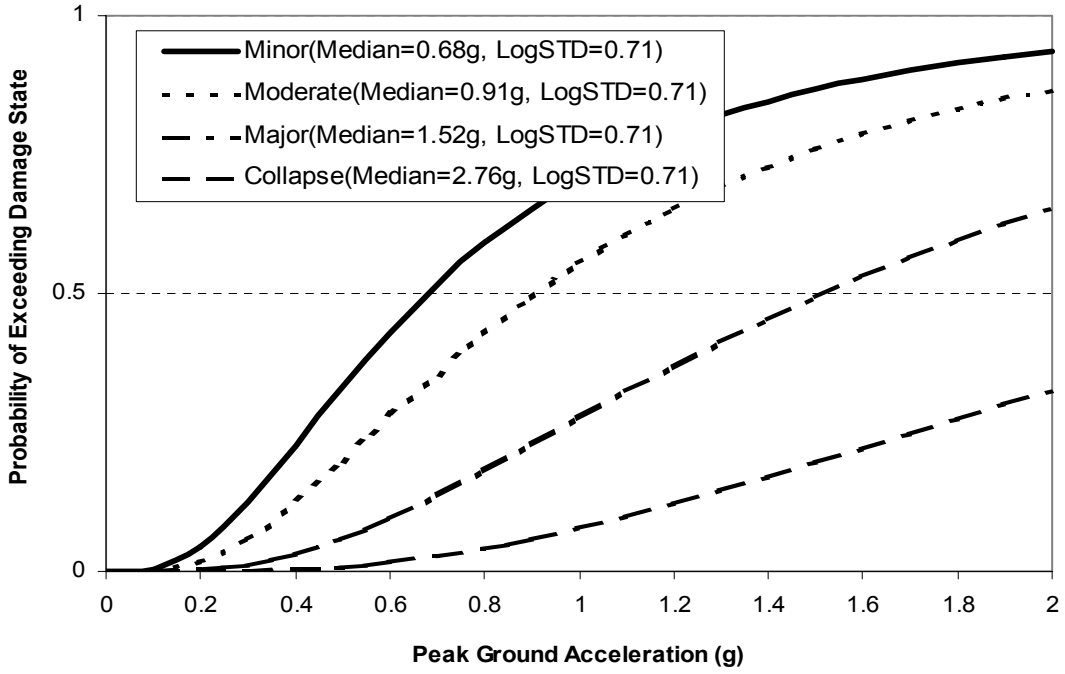

Fig 3.16 Fragility Curve in PGA (Multiple Span/ Skew 0^0-20^0)

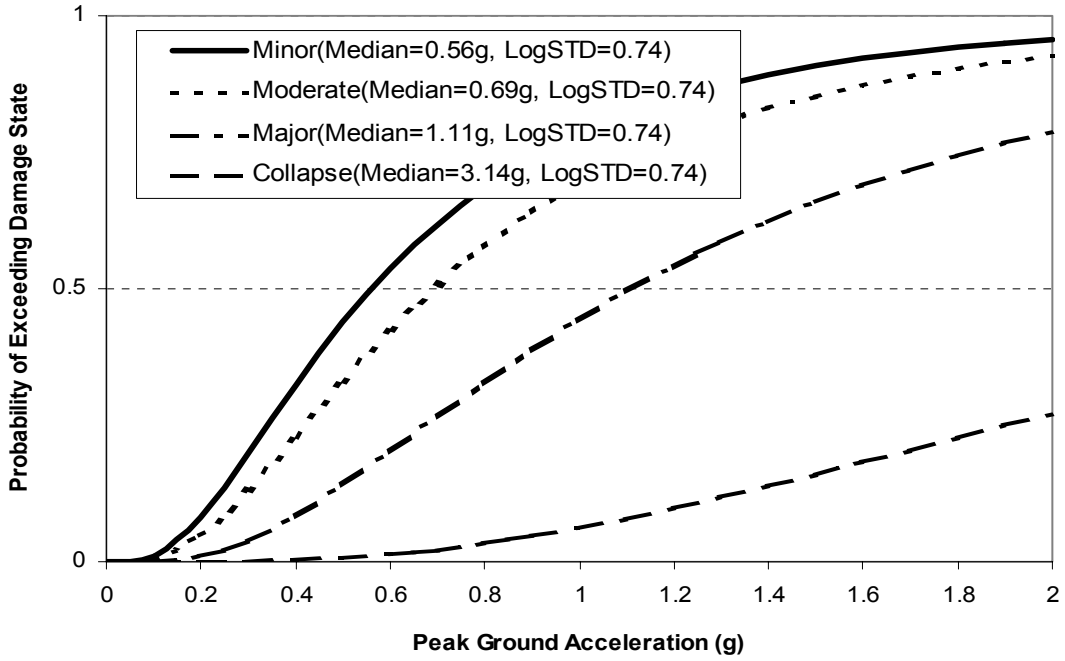

Fig 3.17 Fragility Curve in PGA (Multiple Span/Skew 20^0-60^0)

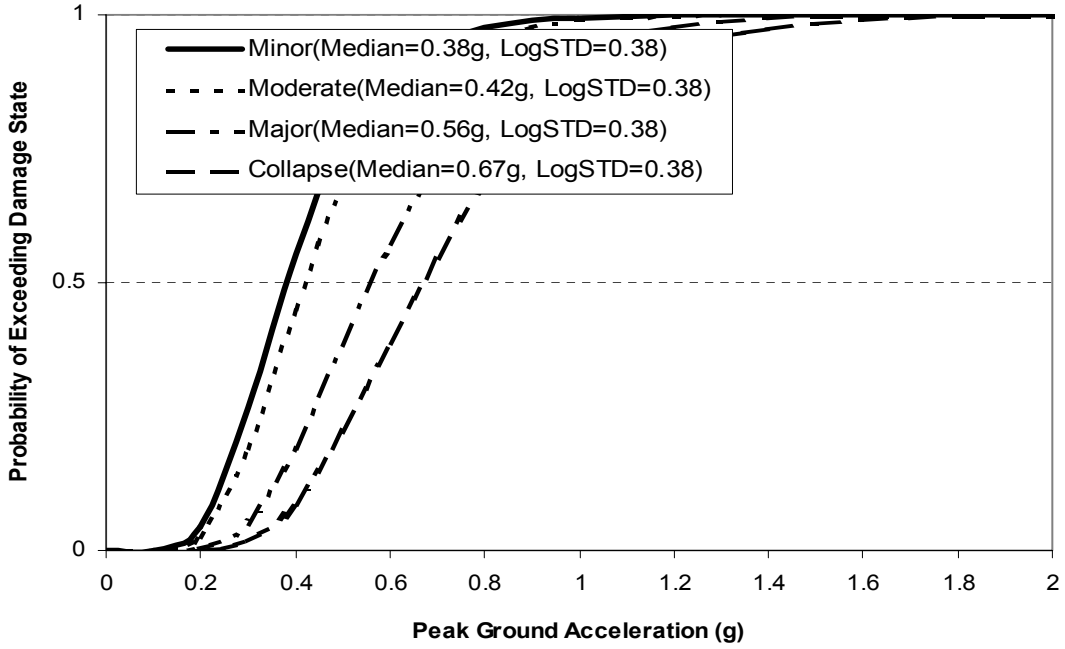

Fig 3.18 Fragility Curve in PGA (Multiple Span/Skew >60^0)

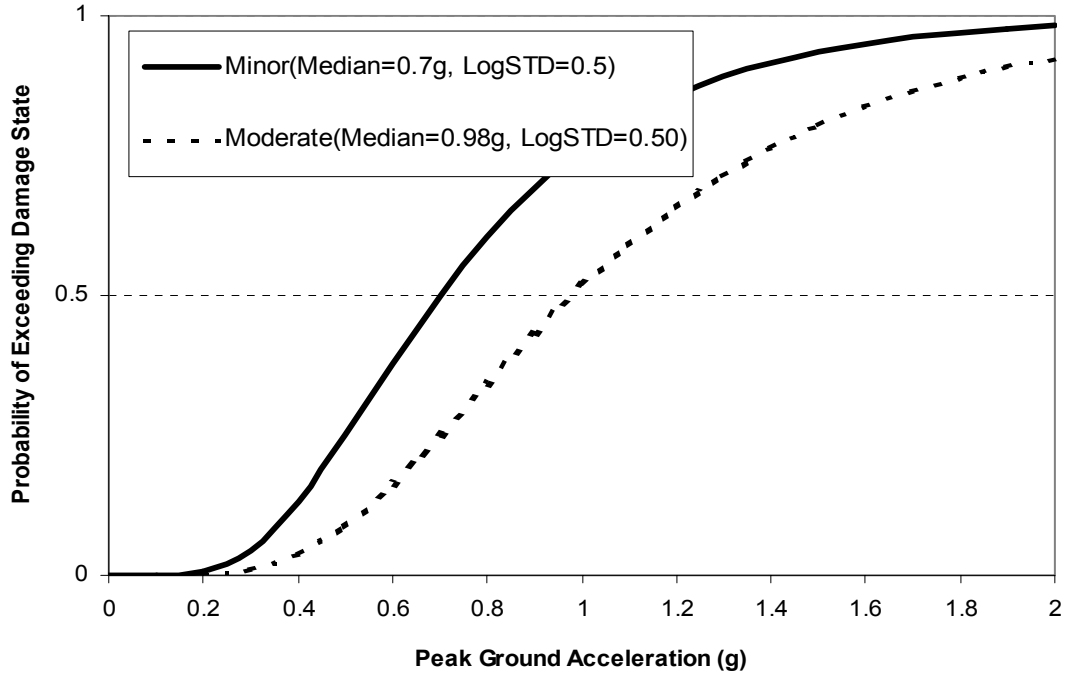

Fig 3.19 Fragility Curve in PGA (Skew 0^0-20^0/Soil A)

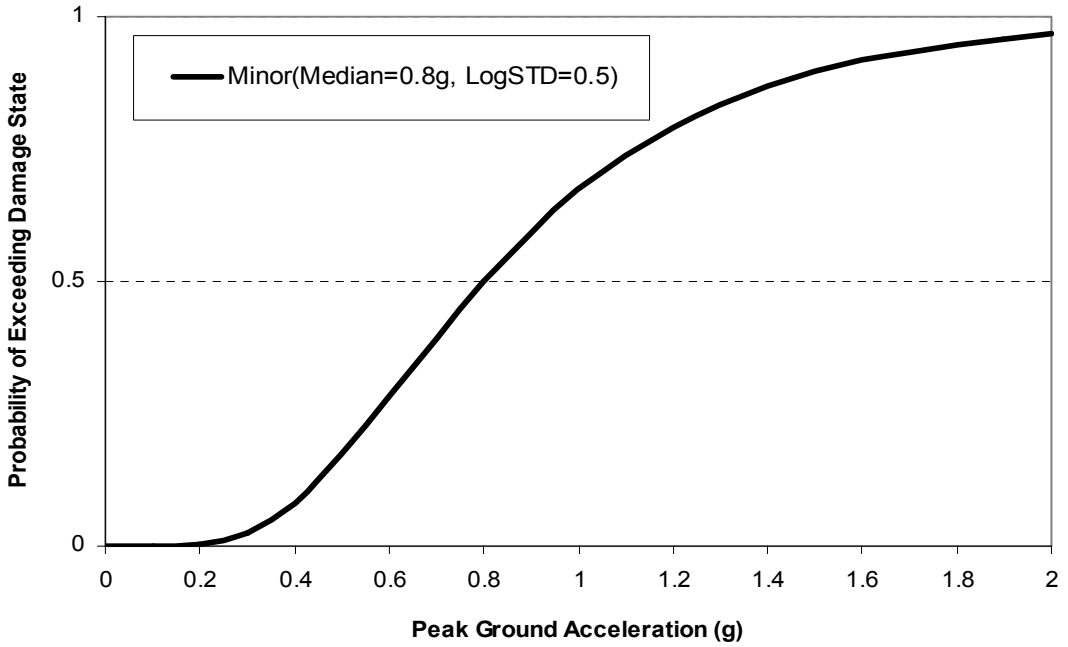

Fig 3.20 Fragility Curve in PGA (Skew 0^0-20^0 /Soil B)

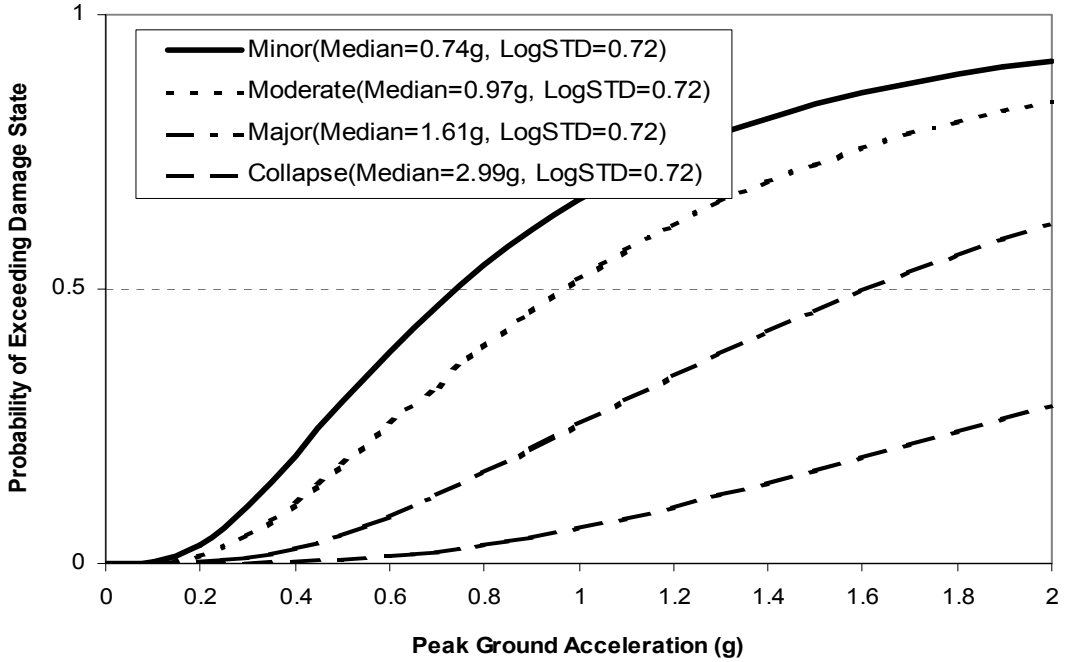

Fig 3.21 Fragility Curve in PGA (Skew 0^0-20^0 /Soil C)

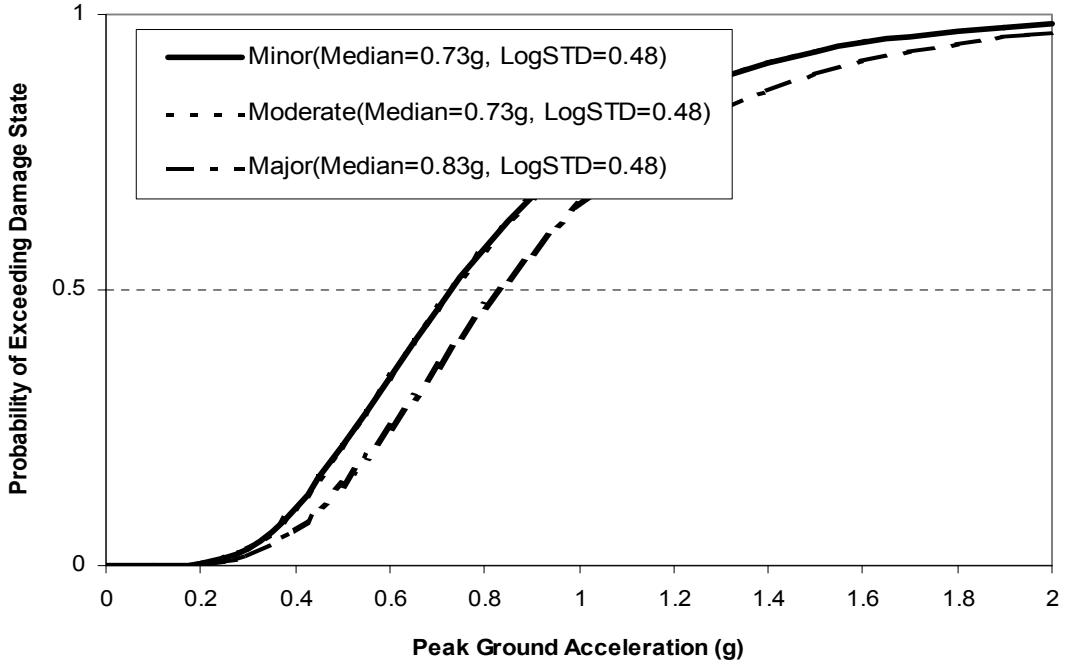

Fig 3.22 Fragility Curve in PGA (Skew 20^0-60^0 / Soil A)

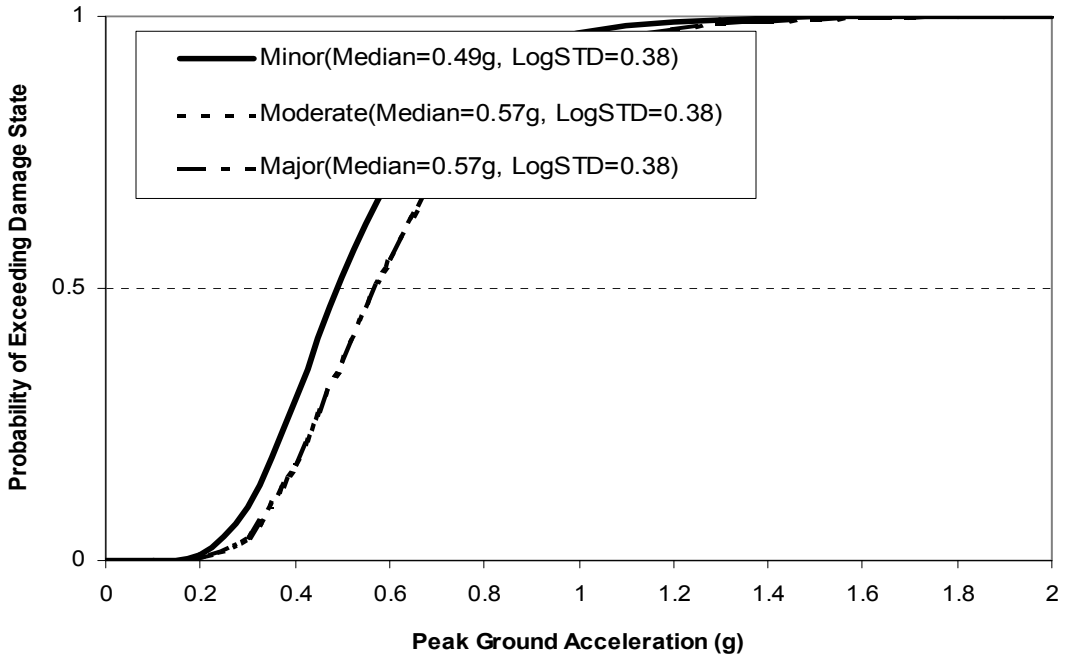

Fig 3.23 Fragility Curve in PGA (Skew 20^0-60^0 /Soil B)

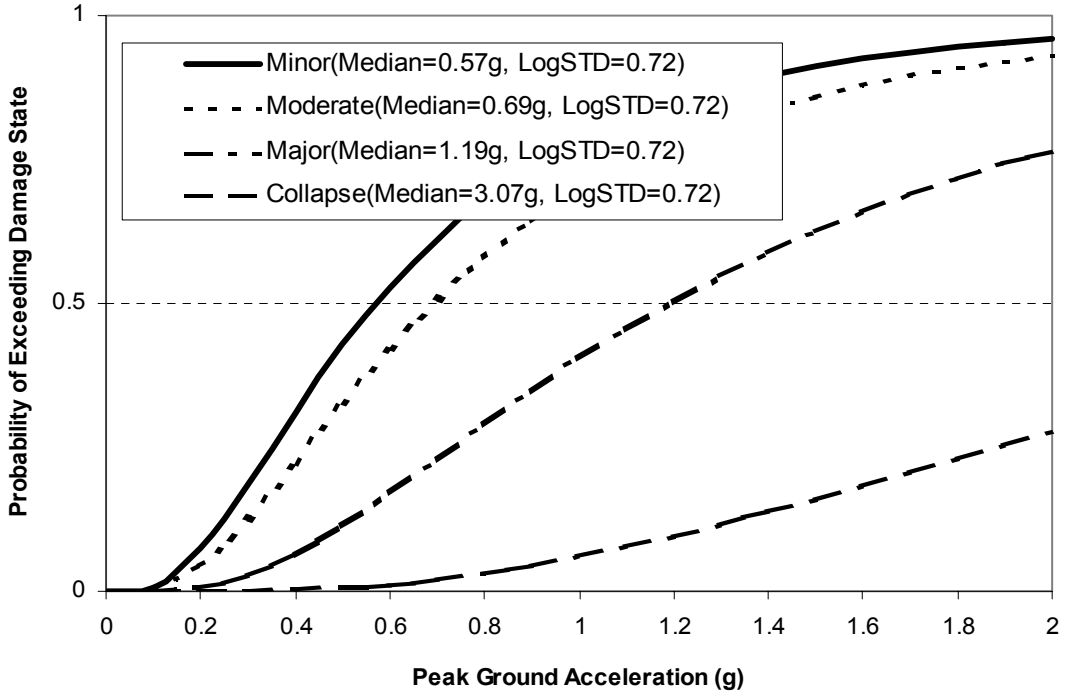

Fig 3.24 Fragility Curve in PGA (Skew 20^0-60^0 /Soil C)

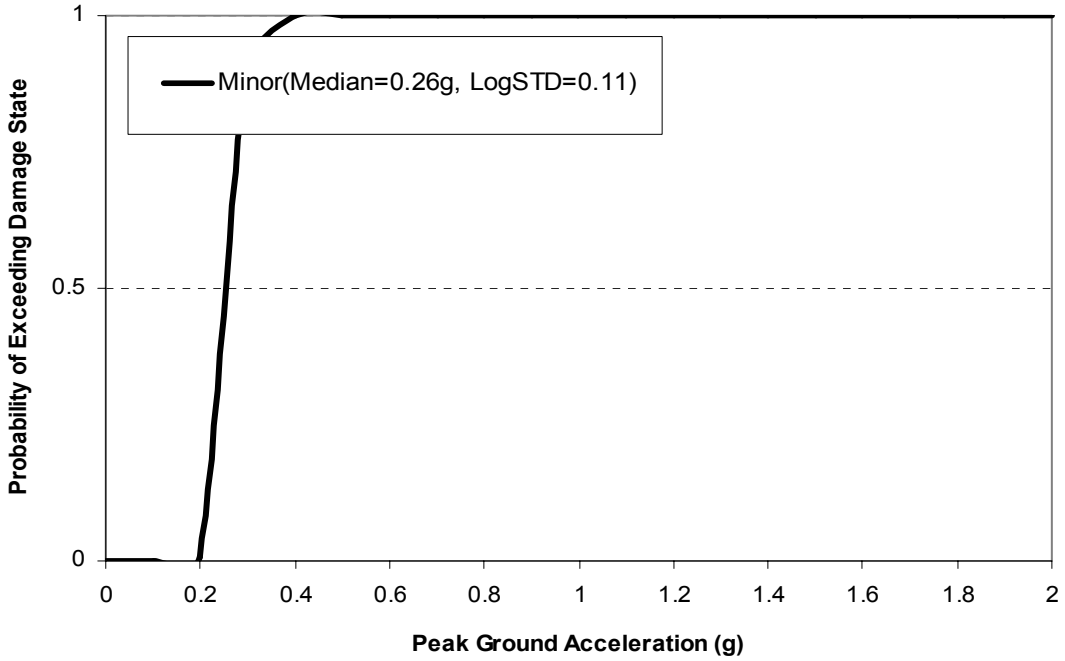

Fig 3.25 Fragility Curve in PGA (Skew >60^0 /Soil A)

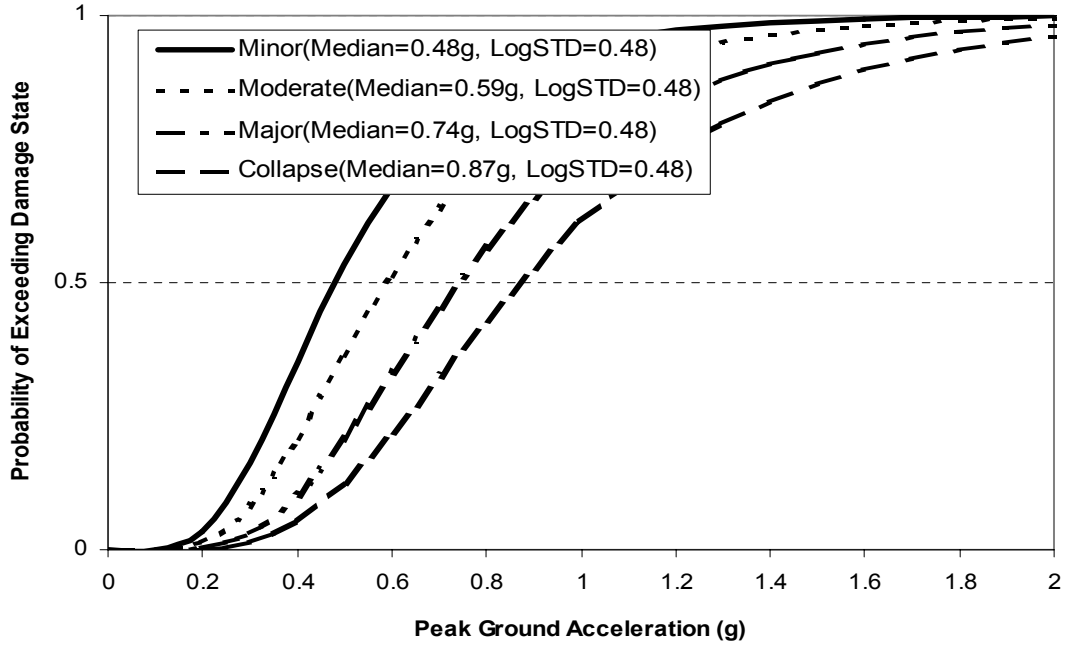

Fig 3.26 Fragility Curve in PGA (Skew >60^0 /Soil C)

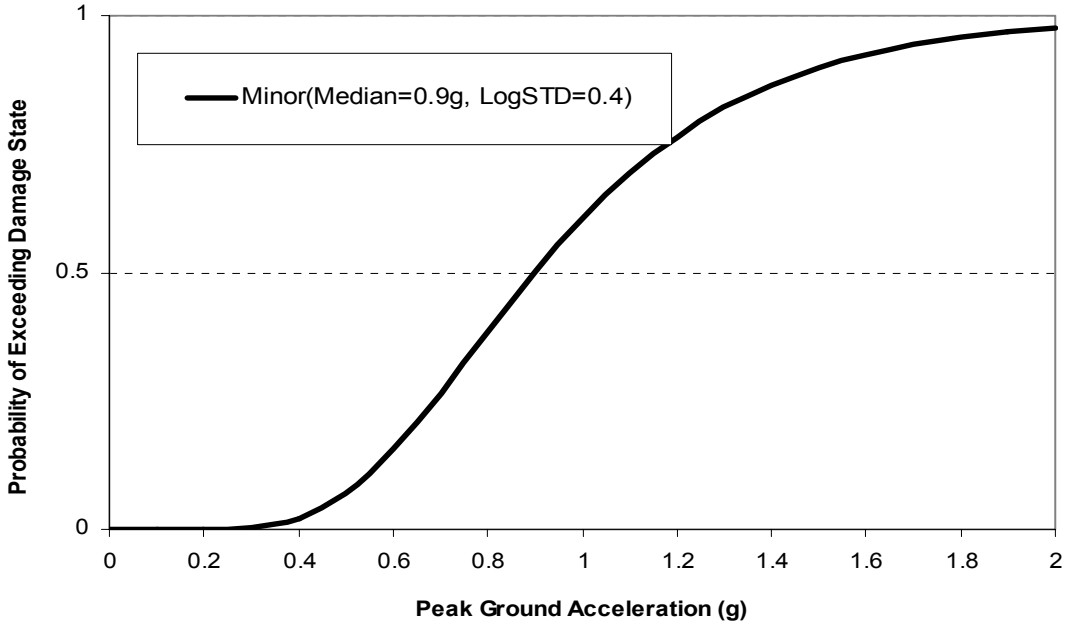

Fig 3.27 Fragility Curve in PGA (Single Span / Soil A)

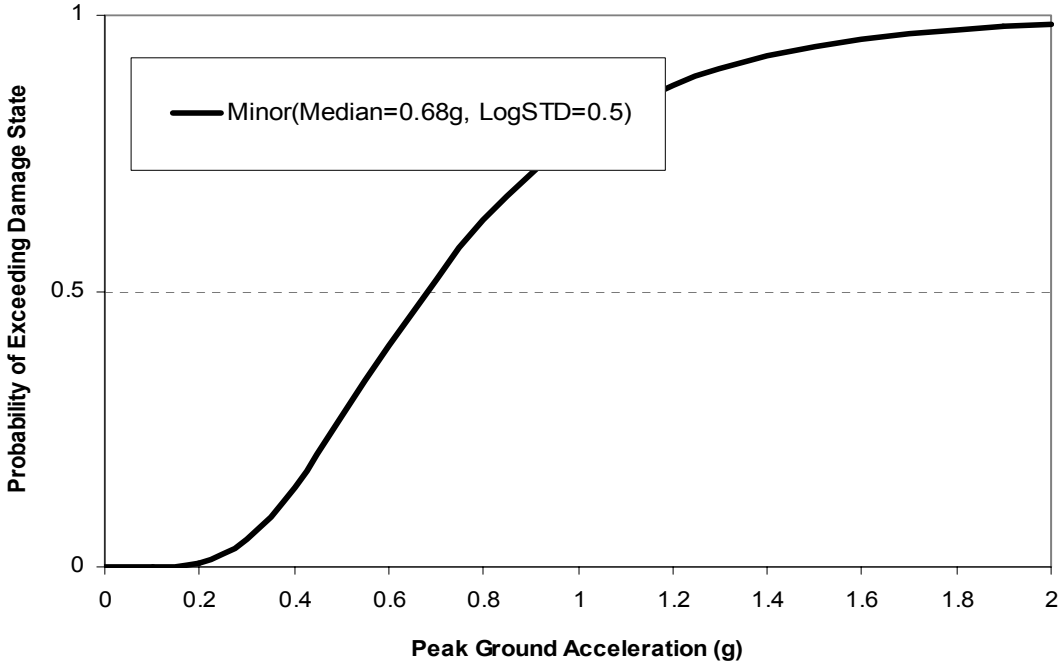

Fig 3.28 Fragility Curve in PGA (Single Span / Soil B)

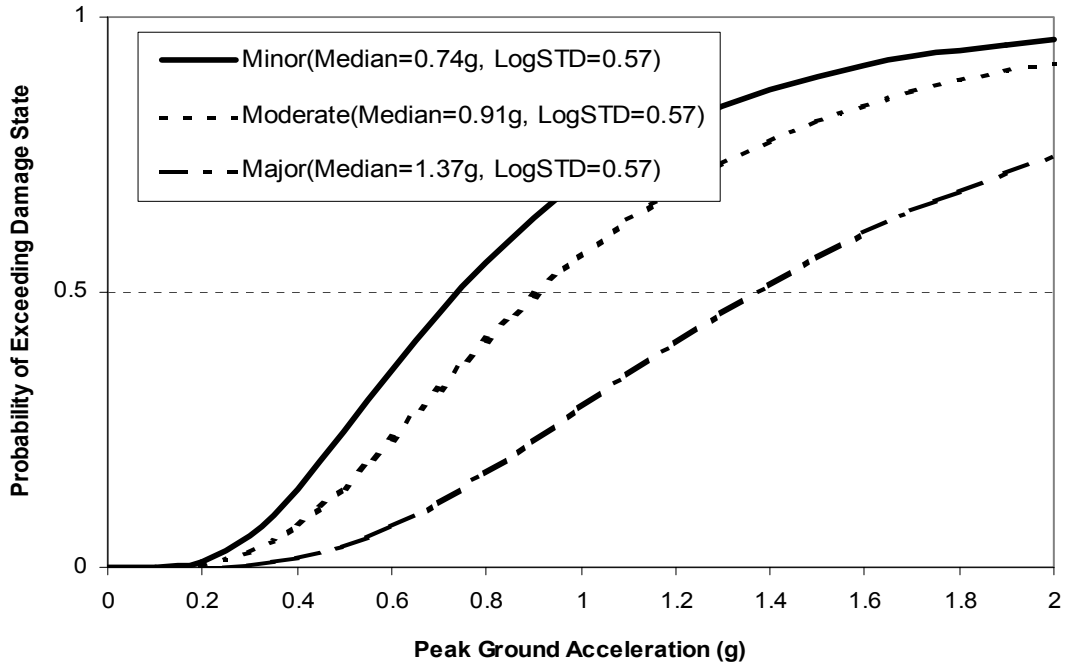

Fig 3.29 Fragility Curve in PGA (Single Span / Soil C)

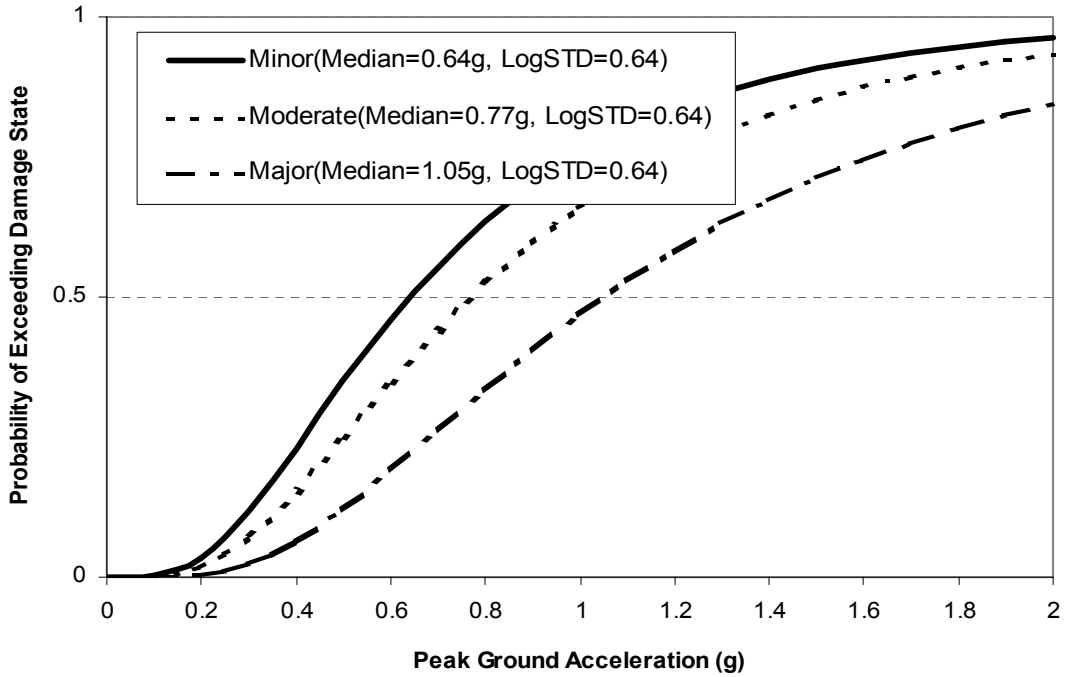

Fig 3.30 Fragility Curve in PGA (Multiple Span / Soil A)

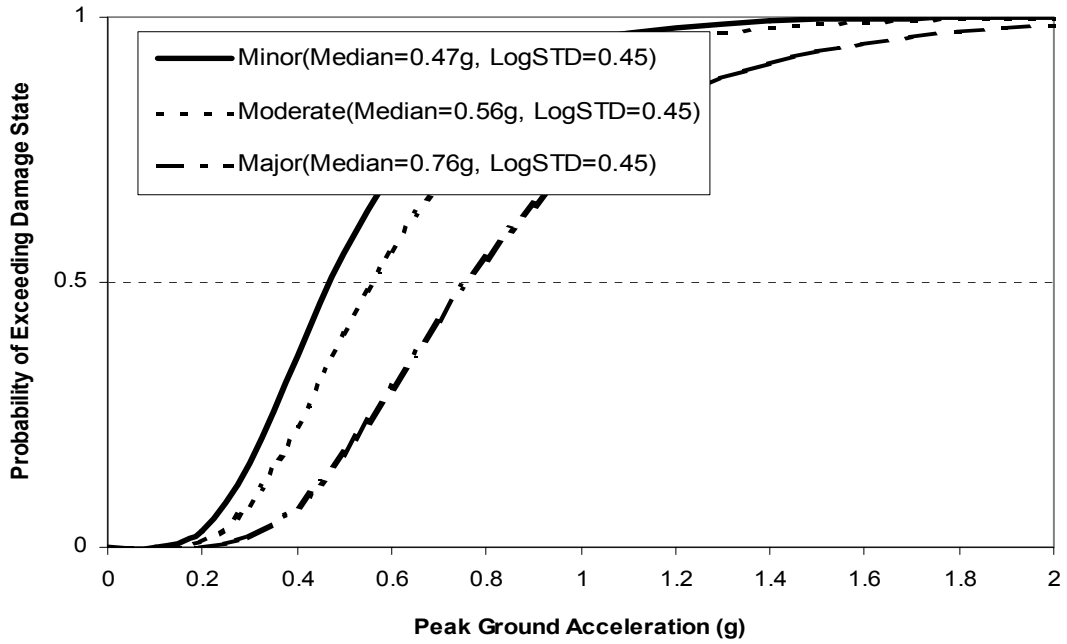

Fig 3.31 Fragility Curve in PGA (Multiple Span / Soil B)

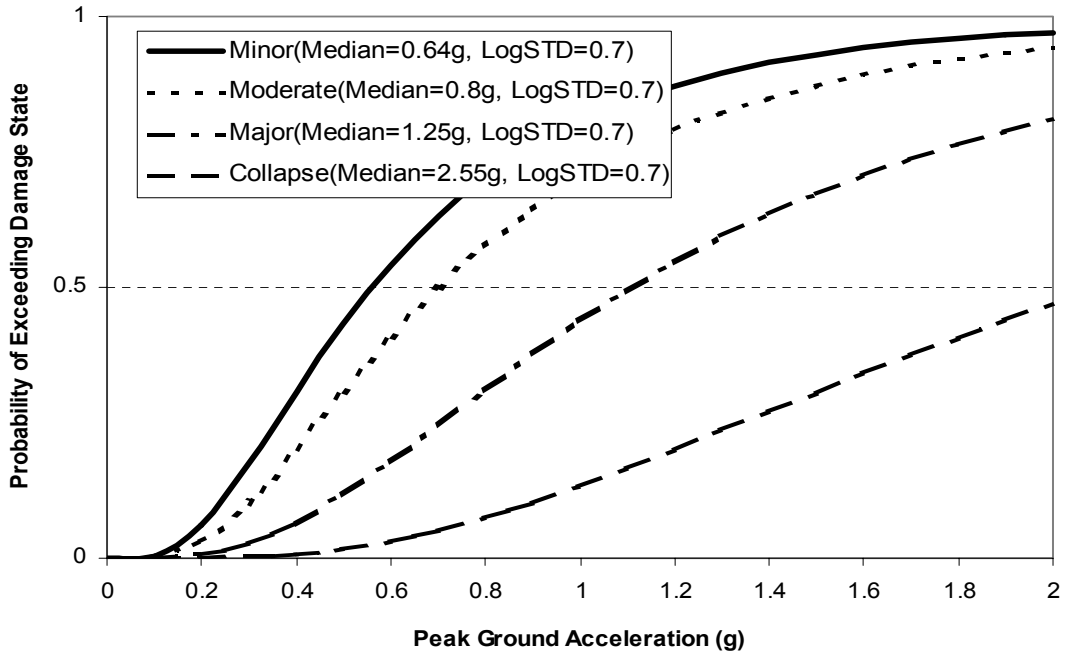

Fig 3.32 Fragility Curve in PGA (Multiple Span / Soil C)

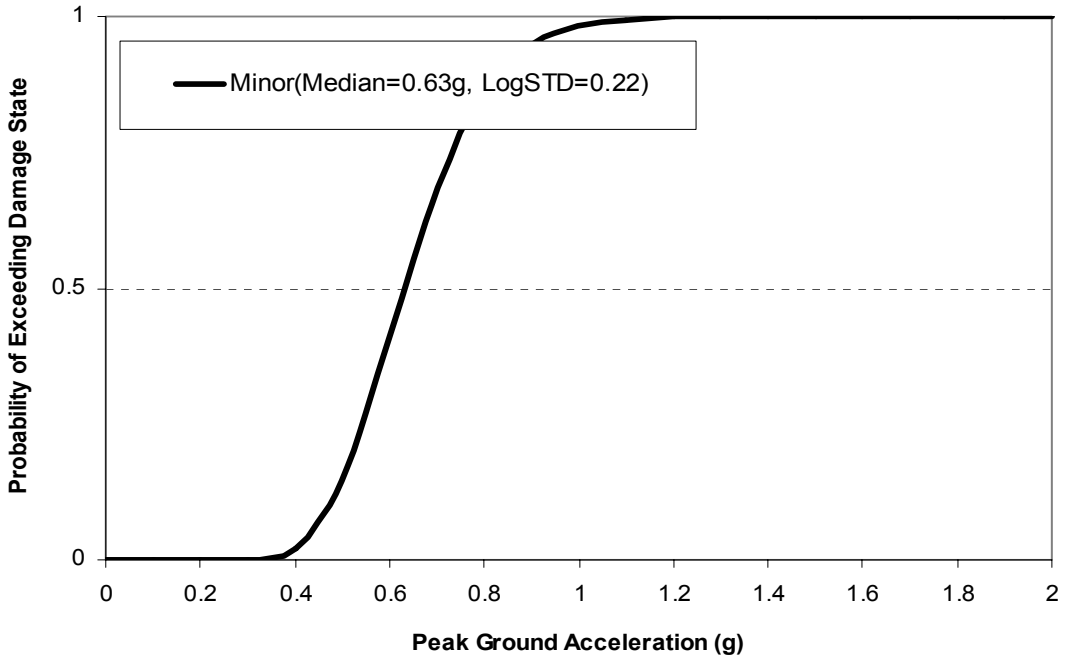

Fig 3.33 Fragility Curve in PGA (Single Span /Skew 0^0-20^0 / Soil A)

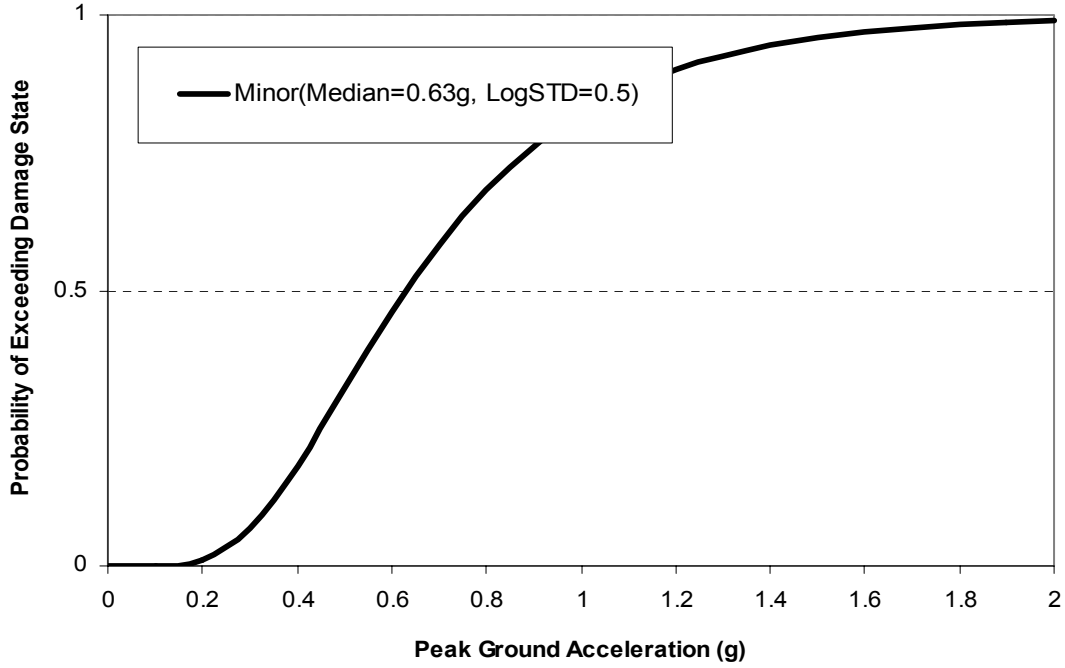

Fig 3.34 Fragility Curve in PGA (Single Span /Skew 0^0-20^0 / Soil B)

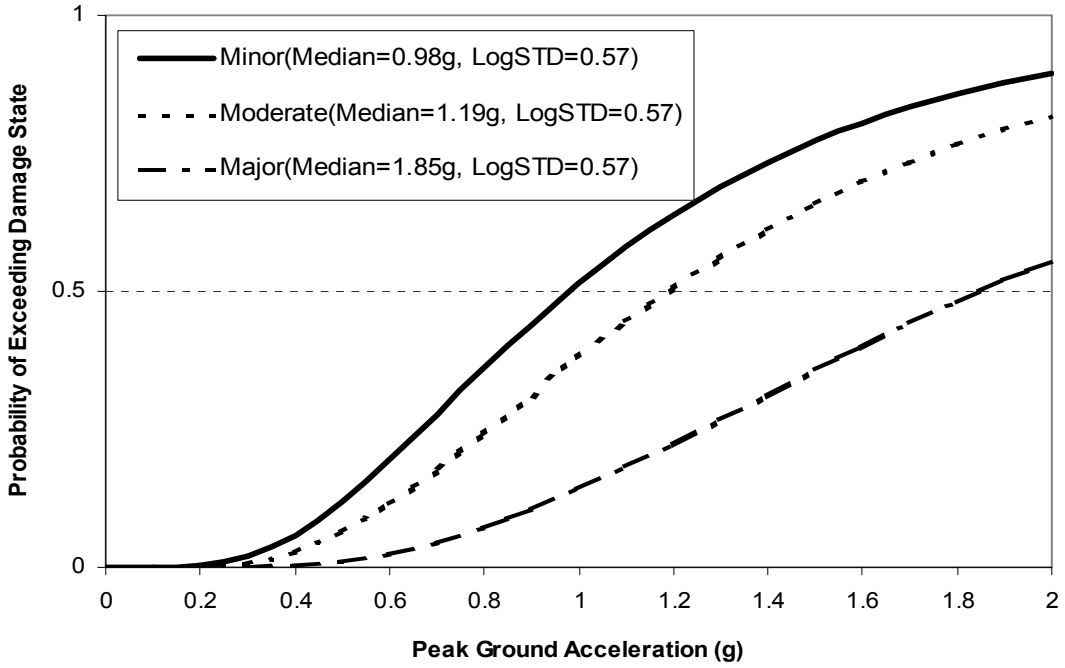

Fig 3.35 Fragility Curve in PGA (Single Span /Skew 0^0-20^0 / Soil C)

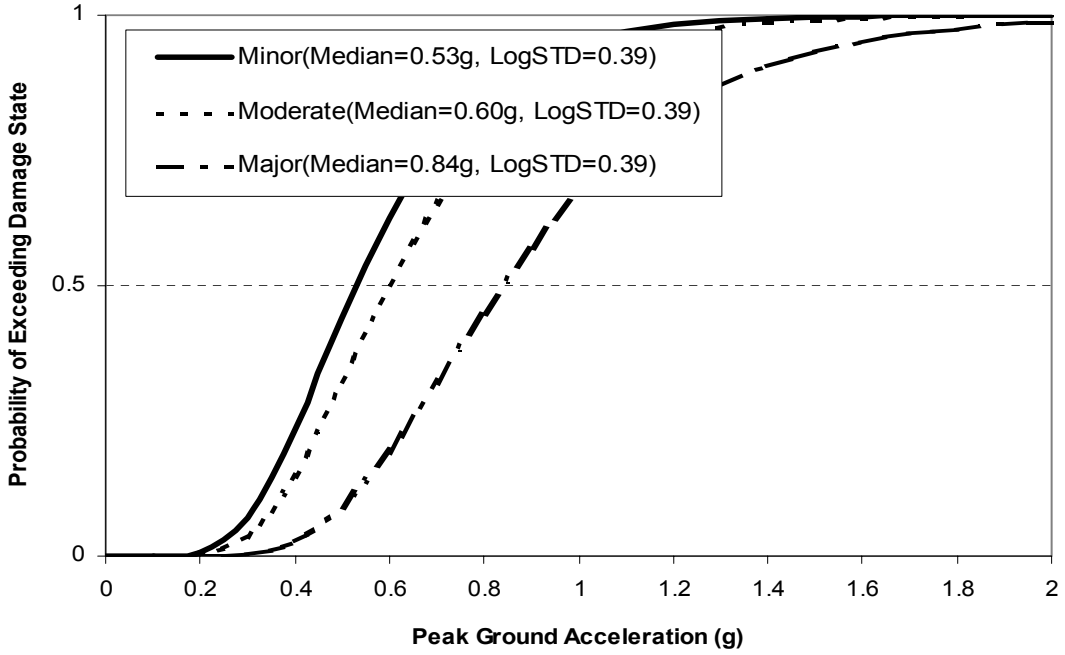

Fig 3.36 Fragility Curve in PGA (Single Span /Skew 20^0-60^0 / Soil C)

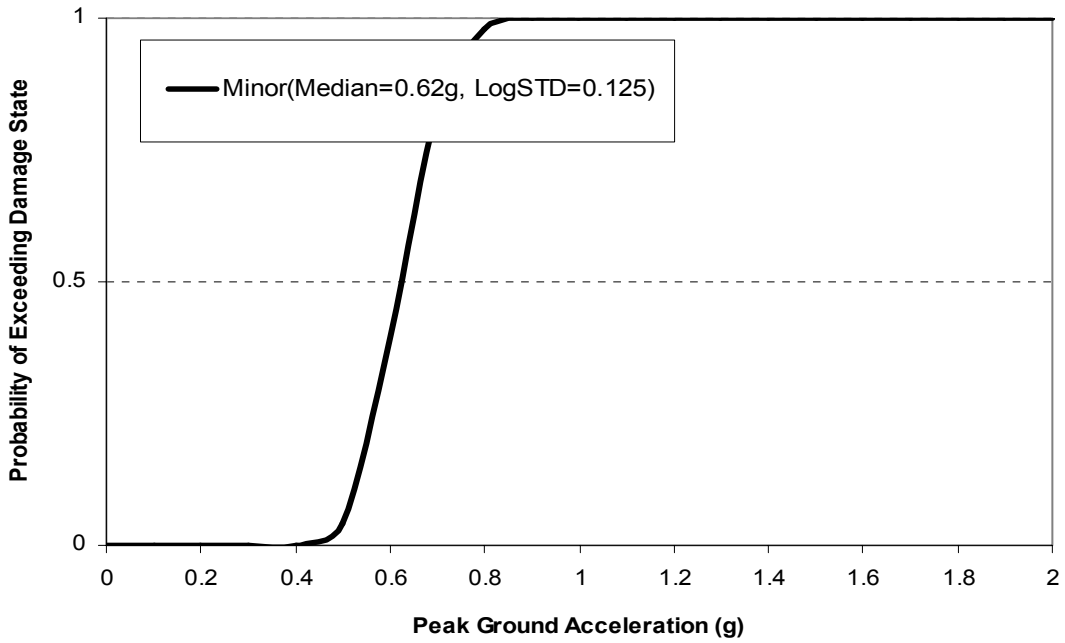

Fig 3.37 Fragility Curve in PGA (Single Span /Skew >60^0 / Soil C)

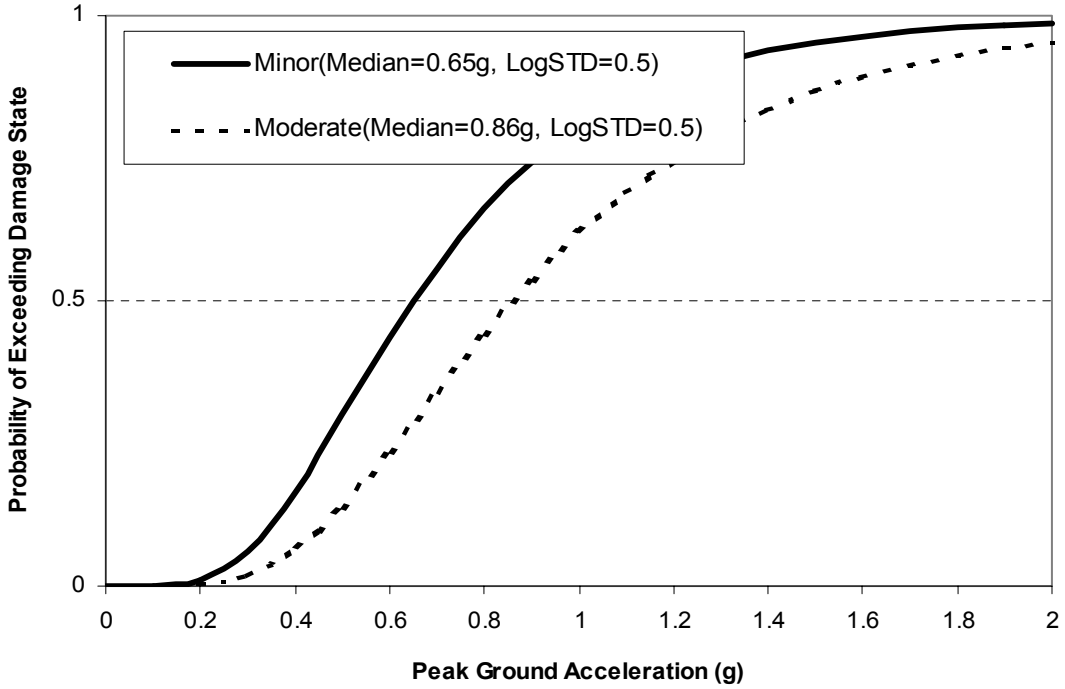

Fig 3.38 Fragility Curve in PGA (Multiple Span /Skew 0^0-20^0 / Soil A)

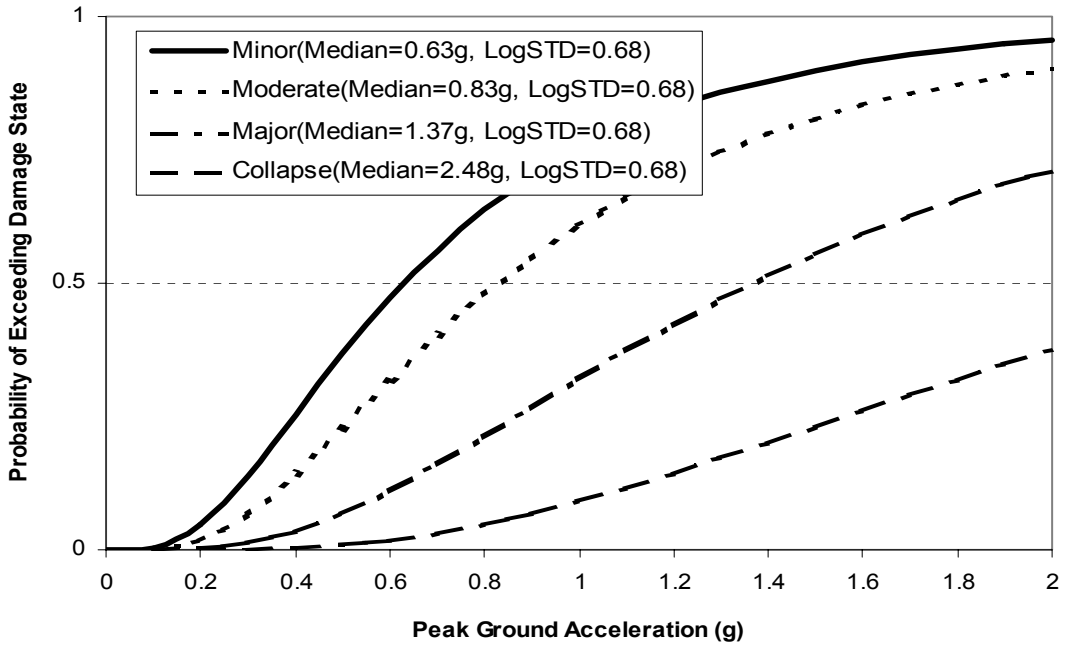

Fig 3.39 Fragility Curve in PGA (Multiple Span /Skew 0^0-20^0 / Soil C)

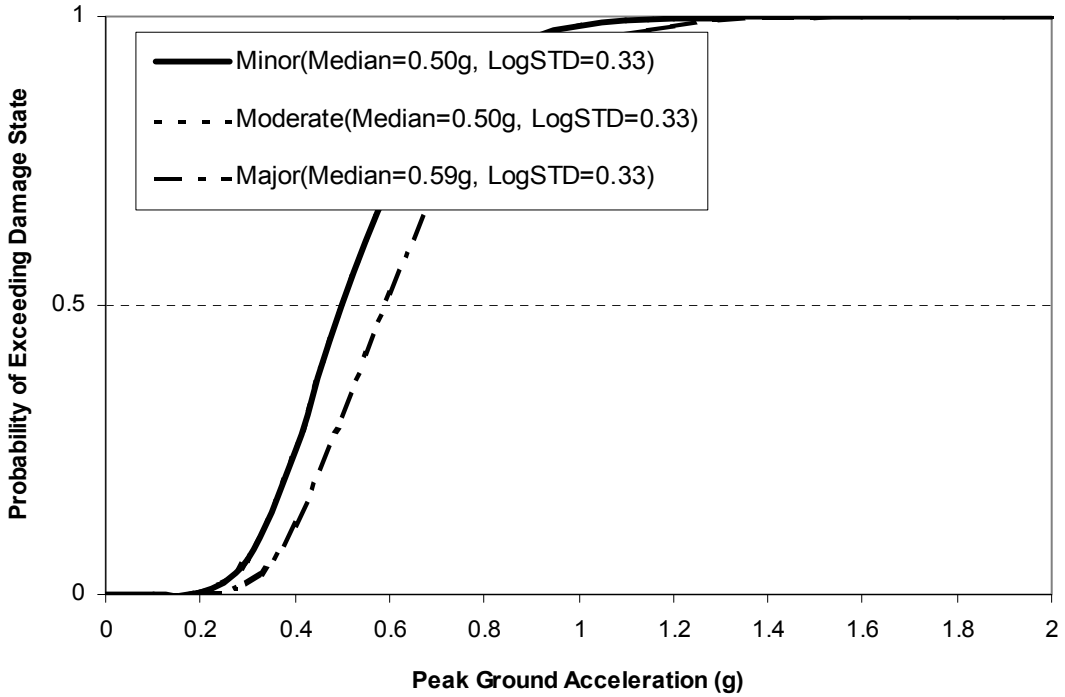

Fig 3.40 Fragility Curve in PGA (Multiple Span /Skew 20^0-60^0 / Soil A)

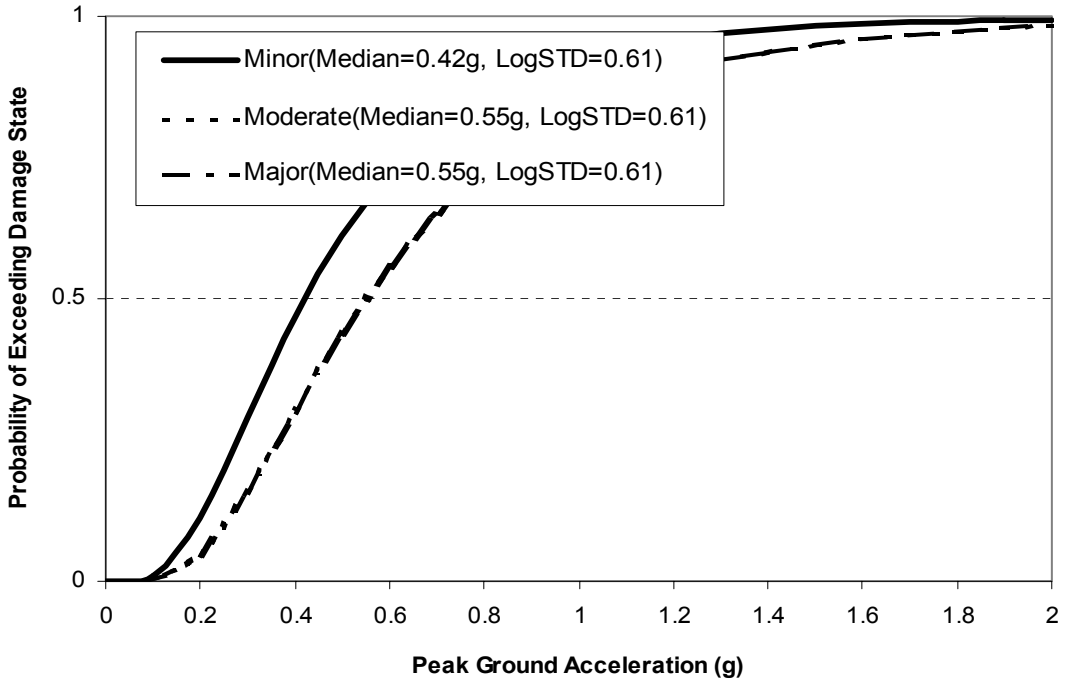

Fig 3.41 Fragility Curve in PGA (Multiple Span /Skew 20^0-60^0 / Soil B)

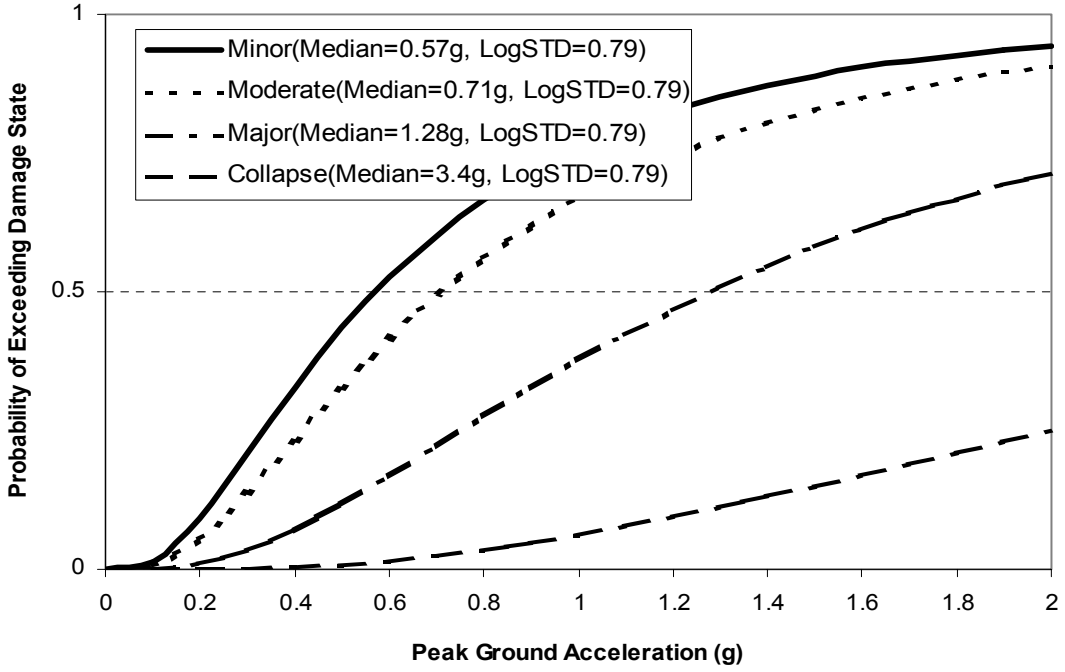

Fig 3.42 Fragility Curve in PGA (Multiple Span /Skew 20^0-60^0 / Soil C)

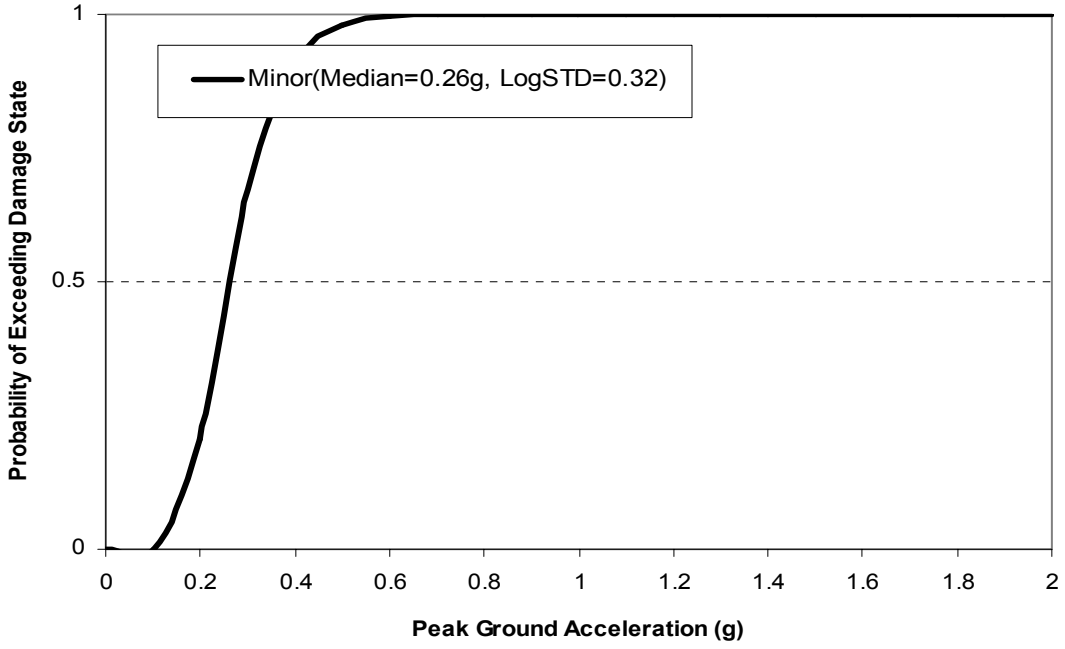

Fig 3.43 Fragility Curve in PGA (Multiple Span /Skew >60^0 / Soil A)

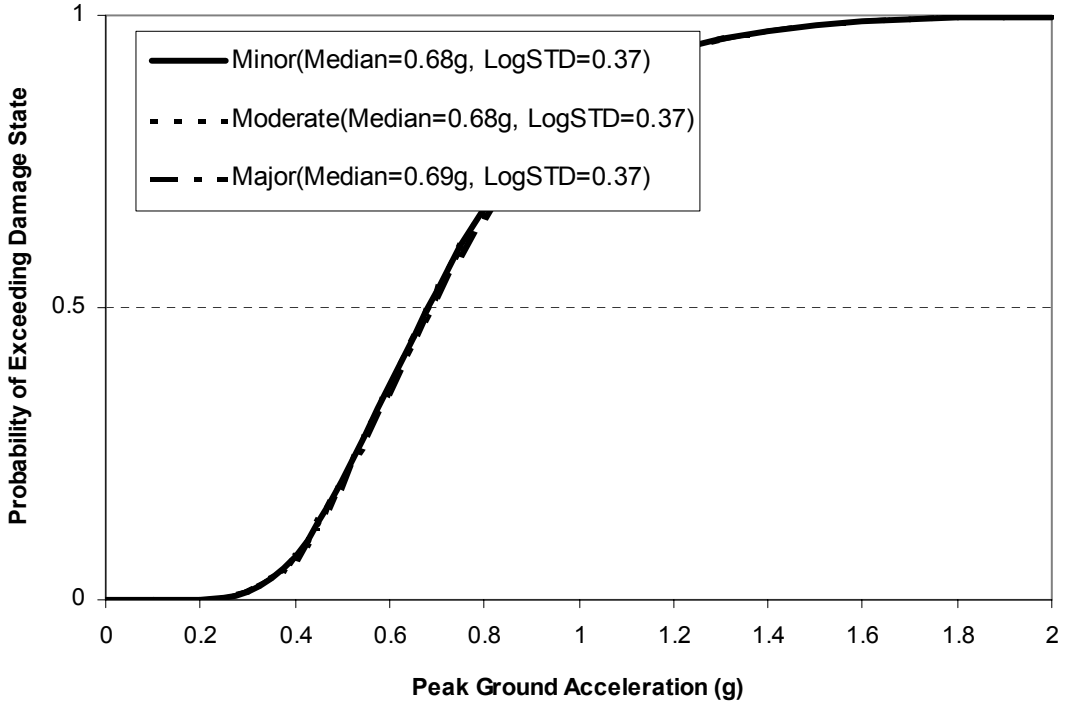

Fig 3.44 Fragility Curve in PGA (Multiple Span /Skew >60^0 / Soil C)

3.4 Enhancement of Empirical Fragility Curves

In Chapter 2, the fragility enhancement of bridges retrofitted by steel jacketing has already developed for the representative bridges. It is assumed that the enhancement ratios also apply to the enhancement of the empirical fragility curves developed in this Chapter. The enhancement ratios for medians are 40%, 55%, 75%, 104% and 145% for damage states of almost no damage, at least slight damage, at least moderate damage, at least extensive damage, complete damage, respectively. Under the assumption that Dutta and Mander's damage states (1999) are interchangeable with the Caltrans definitions so that "slight=minor", "moderate=moderate", "extensive=major" and "complete=collapse", two enhanced empirical fragility curves after retrofit for at least minor, at least moderate, at least major, and collapse damage are plotted in Figs 3.45-48, to be used in ensuing expressway network performance analysis introduced later on in this report.

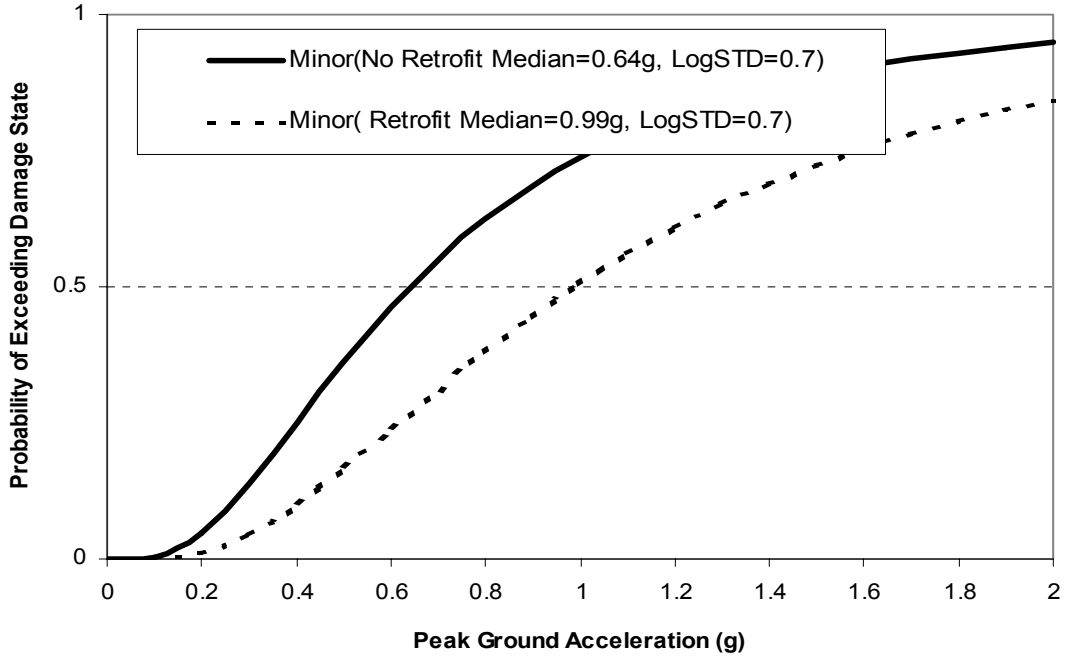

Fig 3.45 Enhanced Fragility Curve (Minor)

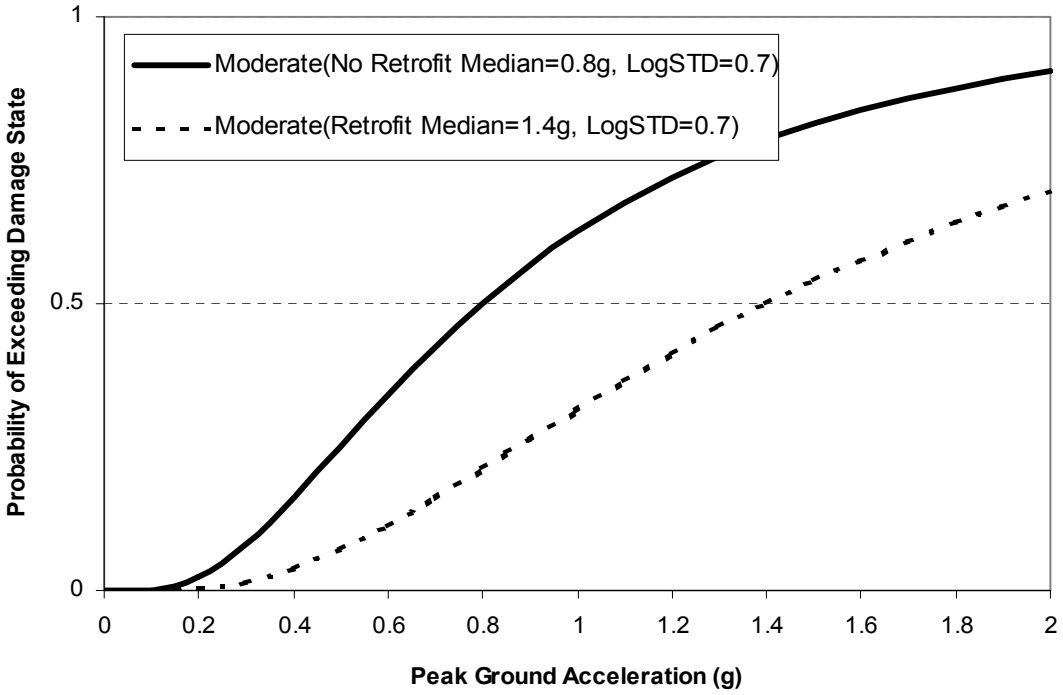

Fig 3.46 Enhanced Fragility Curve (Moderate)

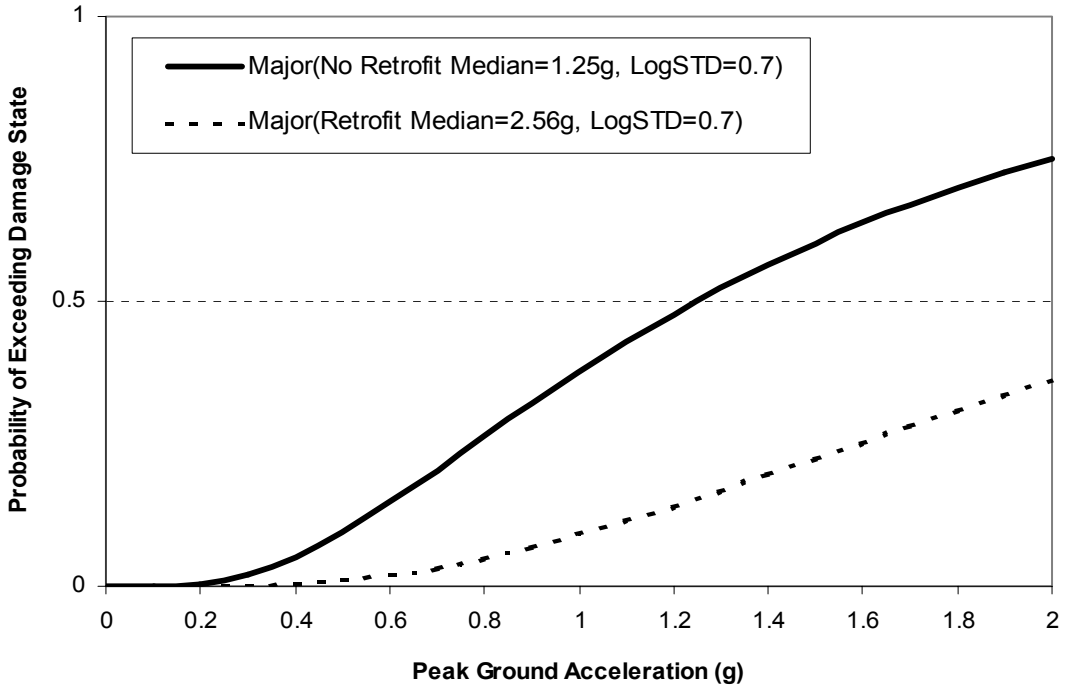

Fig 3.47 Enhanced Fragility Curve (Major)

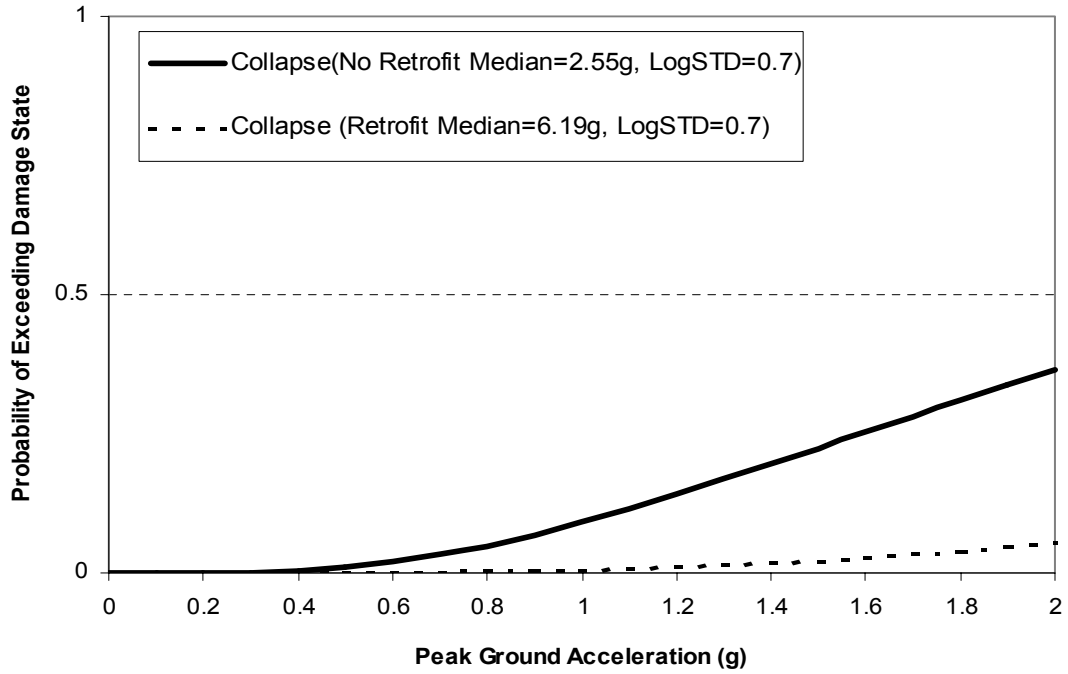

Fig 3.48 Enhanced Fragility Curve (Collapse)

Chapter 4 Seismic Hazard Modeling for Spatially Distributed Highway Network

4.1 Highway Network: Spatially Distributed System

Highway network is a typical spatially distributed system whose components are located in a relatively wide geographical region but functionally interconnected to fulfill the supposed functionality of the system. Bridges, Roadways, Tunnels and some other structural components are linking and working together to transport vehicles (passengers and cargo) from one place to another, and the location of the components, are scattered. For an example, bridges in a network may be many miles away from each other. Regarding seismic risk analysis of a spatially distributed system, three points should be stressed:

1) Firstly, the system's seismic performance depends on of a given set of states of all its components. Their relationship between the system performance and the states of the components may be very complex and cannot be expressed explicitly in a mathematical equation. The system performance may be below its normal level even out of operation due to the seismic damage of its components.

2) Secondly, the prediction/simulation of the states of its component and further the system performance evaluation should be scenario-based to reflect the spatial distribution of ground motion and be meaningful in the evaluation of the system performance.

3) Thirdly, the total loss resulting from any scenario earthquake will consist of two parts: repair cost of the damaged components and loss due to system/component performance degradation.

In this report, all these three topics will be covered in the following chapters. Before performing system analysis, however, the modeling of seismic hazard will be introduced to generate scenario-based input for either deterministic or probabilistic analysis. The methodology for evaluating the system performance of the highway network is then described, in which, bridge fragility Model, Network Model, Link Performance Model and Traffic Assignment Model are combined. Seismically-induced social cost, including travel time delay and opportunity cost, is used to measure the system post-event performance (see Chapter 5). When the fragility curves of bridges with or without retrofit are used in this methodology, the system performance improvement is expressed by the reduced social cost.

4.2 Deterministic Seismic Hazard

An earthquake can actually originate from rupture of any known or unknown faults and is not predictable in time, location and magnitude before it occurs. However, to have an idea about how the system will behave and what the consequence will be, it is important to evaluate the system performance under a given earthquake scenario which could generate ground motion as input. This earthquake scenario is called "given" in the meaning that information including the magnitude, location, faulting type and etc. is available and can be used to provide the spatial distribution of the ground motion in the study region. Since it is given, it is called determinist seismic hazard, which can be any specified earthquake scenario, either postulated or historical.

It should be noted that a deterministic seismic hazard does not mean that the ground motion at each site can be exactly determined. Actually, even for a historical earthquake occurred in a region densely instrumented with ground motion recording devices, the ground motion at sites differing from the recording stations can only be derived. For any postulated scenario, the spatial distribution of the ground motion can only be predicted by empirical attenuation functions developed statistically from historical ground motion records. Rather than a deterministic value, a empirical attenuation function usually provides both a best estimate, such as, median value, and its deviation which is used to describe the uncertainty of the site ground motion.

4.2 Probabilistic Seismic Hazard

In a region with high seismicity and a number of active seismic faults, such as Los Angeles Area, there are numerous possible earthquakes in the future. To perform a probabilistic seismic risk analysis, the probability of these events should also be quantified. To consider the effect of all these possible events, the most straightforward method is to generate them by simulation based on the magnitude –frequency relationship of each seismic source. Then each of them is used as input for system performance evaluation. The expected annual risk (loss) can then expressed as

$$R_{Annual} = \sum_{i=1}^{N} L(S \mid Q_i) p_i \tag{4.1}$$

In which

N = the total number of possible earthquakes;

Q_i = the ith possible earthquake;

p_i = the corresponding annual rate of occurrence of the ith possible earthquake;

S = the system's seismic performance and

$L(S|Q_i)$ = the loss resulting from the ith earthquake.

Considering that even one simulation for system performance evaluation under a scenario is tedious, and N is actually very large, it is very difficult to directly evaluate Equation (4-1) due to the tremendous calculation effort involved.

To overcome this barrier, the intuitive way is to reduce the number of earthquakes considered in the risk analysis. Chang and Shinozuka (2000) proposed the concept of probabilistic scenario earthquakes, in which a small set of scenario earthquakes with properly "assigned" annual occurrence probabilities are selected to approximate represent the regional probabilistic seismic hazard and used for probabilistic risk estimation of spatially distributed systems. This concept could be expressed as

$$\sum_{i=1}^{N} S(Q_i)p_i = \sum_{j=1}^{M} \overline{S}(\overline{Q}_j)\overline{p}_j \qquad (M << N) \tag{4.2}$$

In which

M = number of probabilistic scenario earthquakes

$\overline{Q}_j$ = jth probabilistic scenario earthquake;

$\overline{p}_j$ = annual rate of occurrence of jth probabilistic scenario earthquake;

$\overline{S}(\overline{Q}_j)$ = system performance due to jth probabilistic scenario earthquake.

Particularly, 47 scenario earthquakes consisting of 13 maximum credible events (MCE) and 34 user-defined events (U/D) (Table 4.1) are developed to represent the regional seismic hazard in Los Angles and Orange County (Chang, Shinozuka and etc., 2000). In this study, this set of probabilistic scenario earthquakes will be used as hazard

input in evaluating the probabilistic seismic risk of highway network in Los Angles and Orange County.

Table 4.1 Probabilistic Scenario Earthquake Set

Event No.	Scenario EQ	Type	Moment Magnitude	Annual PB	Lat.	Long.
1	Elysian Park	MCE	7.1	0.000728	34.1650	-117.8330
2	Malibu Coast	MCE	7.3	0.000068	34.0070	-118.6150
3	Newport-Inglewood(N.)	MCE	7.0	0.000495	33.9750	-118.3590
4	Newport-Inglewood(S.)	MCE	7.0	0.000495	33.6600	-117.9970
5	Palos Verdes	MCE	7.2	0.00154	33.6180	-118.1700
6	Raymond	MCE	6.7	0.00065	34.1270	-118.1200
7	San Andreas	MCE	8.0	0.00485	34.2780	-117.4770
8	San Jacinto	MCE	7.5	0.0008	33.8820	-117.0870
9	Santa Susana	MCE	6.9	0.004362	34.3180	-118.5990
10	Sierra Madre	MCE	7.4	0.00208	34.1430	-117.9360
11	Simi Santa Rosa	MCE	7.5	0.000214	34.2820	-118.8220
12	Verdugo	MCE	6.8	0.00062	34.1840	-118.2730
13	Whittier	MCE	7.5	0.000312	33.6430	-117.3480
14	Malibu Coast	U/D	6.0	0.0003	34.1395	-118.0422
15	Malibu Coast	U/D	6.0	0.0005	34.1161	-118.1578
16	Malibu Coast	U/D	6.0	0.0003	34.0944	-118.3717
17	Newport-Inglewood	U/D	6.0	0.001	33.8961	-118.2691
18	Newport-Inglewood	U/D	6.0	0.001	34.0079	-118.3739
19	Newport-Inglewood	U/D	6.0	0.001	33.8168	-118.1971
20	Newport-Inglewood	U/D	6.0	0.001	33.7369	-118.0793
21	Newport-Inglewood	U/D	6.0	0.001	33.6448	-117.9549
22	Palos Verdes	U/D	6.0	0.0016	33.7782	-118.3149
23	San Andreas	U/D	6.0	0.02	34.4306	-117.8153
24	San Andreas	U/D	6.0	0.02	34.6266	-118.3192
25	San Jacinto	U/D	6.0	0.01	34.2631	-117.4990
26	Santa Susana	U/D	6.0	0.01	34.3279	-118.6072
27	San Fernando	U/D	6.0	0.005	34.2937	-118.4676
28	Sierra Madre	U/D	6.0	0.01	34.2559	-118.2538
29	Sierra Madre	U/D	6.0	0.01	34.1605	-117.9200
30	Whittier	U/D	6.0	0.0015	33.9571	-117.9069
31	Malibu Coast	U/D	6.5	0.00015	34.1431	-118.1218
32	Malibu Coast	U/D	6.5	0.00015	34.1092	-118.0727
33	Malibu Coast	U/D	6.5	0.0001	34.0916	-118.3802
34	Newport-Inglewood	U/D	6.5	0.0005	33.9399	-118.3186
35	Newport-Inglewood	U/D	6.5	0.0005	33.7901	-118.1462
36	Newport-Inglewood	U/D	6.5	0.0005	33.6557	-117.9585

37	San Andreas	U/D	6.5	0.008	34.5936	-118.2052
38	San Andreas	U/D	6.5	0.008	34.4388	-117.8385
39	San Jacinto	U/D	6.5	0.005	34.2301	-117.4543
40	Santa Susana	U/D	6.5	0.0011	34.2966	-118.4232
41	Whittier	U/D	6.5	0.001	33.9242	-117.8406
42	Malibu Coast	U/D	7.0	0.00005	34.0652	-118.4560
43	Malibu Coast	U/D	7.0	0.00005	34.1232	-118.1570
44	San Jacinto	U/D	7.0	0.0015	34.2372	-117.4630
45	San Andreas	U/D	7.0	0.003	34.5726	-118.1789
46	San Andreas	U/D	7.0	0.003	34.4032	-117.7315
47	Whittier	U/D	7.0	0.0005	33.9401	-117.8843

Chapter 5 System Performance Evaluation of Highway Network

5.1 Overview

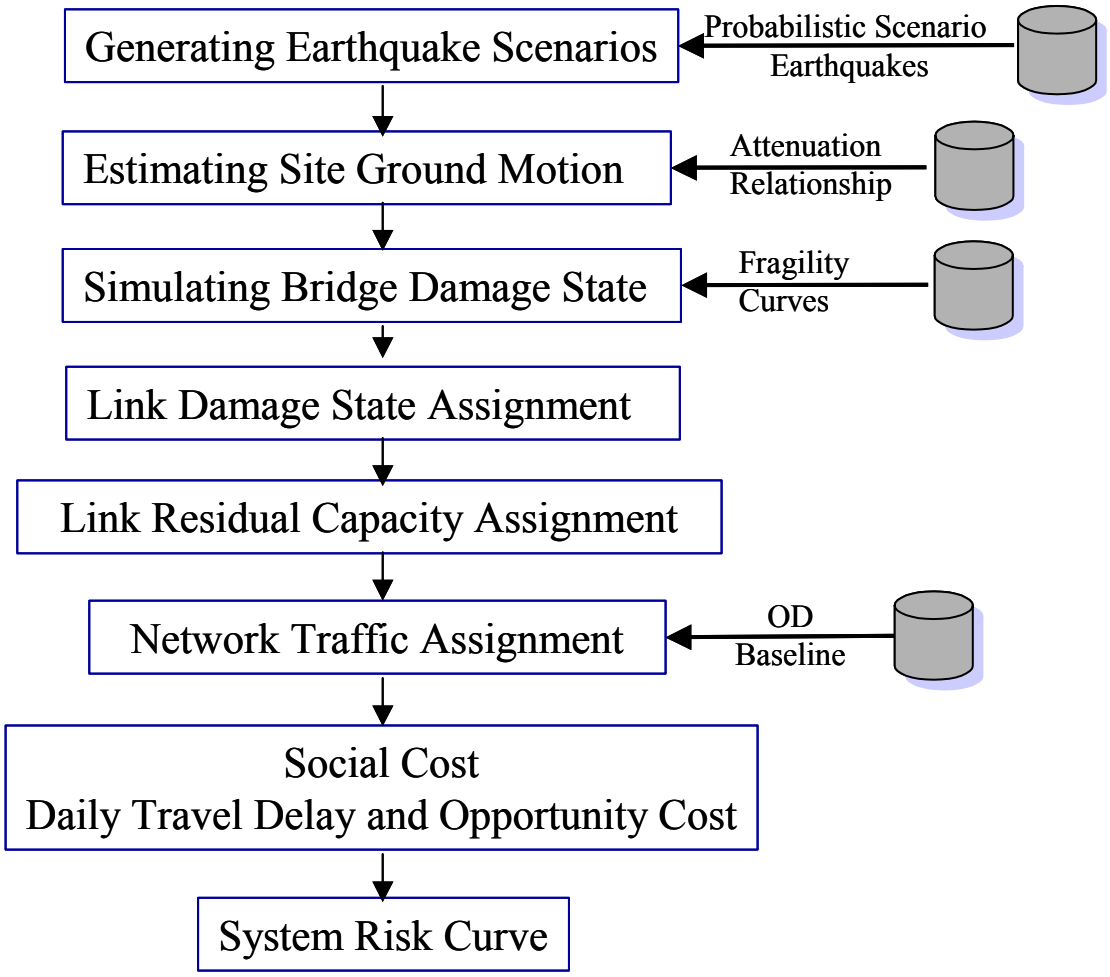

Fig 5.1 Flow Chart for System Risk Evaluation

It is intuitive to estimate consequence of a seismic event in a highway transportation system by comparing the pre-event and post-event system performance or

functionality. Therefore, it is essential to establish a methodology to for the evaluation of the network performance. In this study, a methodology combining various models is developed, in which an index called social cost, including travel delay time and opportunity cost, is used to quantify the negative consequence due to the seismic degradation of the system functionality. Fig 5.1 shows the flow chart of this methodology. The models involved are described in the following sections.

5.2 Site Ground Motion

With given information of seismic source, magnitude, site-source distance and the local soil condition, the ground motion intensity at each bridge site can be predicted by empirical attenuation relationship for a postulated scenario. The spatial distribution of ground motion from a well-recorded historical earthquake may be available in the form of contour map and the site ground motion could be obtained by spatial correlation.

For each of the 47 scenario earthquakes mentioned above, Campbell and etc. (1997) attenuation relationship is used to estimate site peak ground acceleration (PGA) for all the bridges of the system. Other ground motion indexes may be used if the fragility curves are expressed as the function of the corresponding index. Actually the system risk curve is not sensitive to the choice of the type of ground motion index used in the fragility curve, if the index is used consistently in the system risk estimation procedure (Shinozuka et al., 2003e).

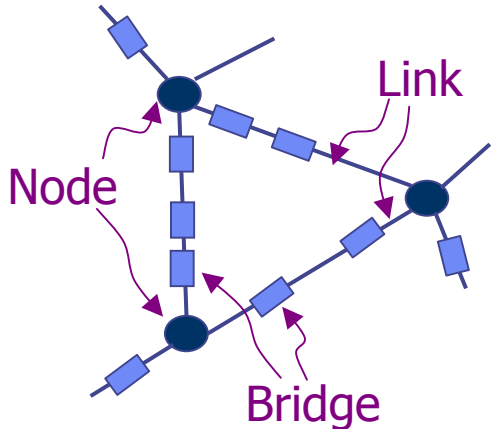

Fig 5.2 Highway Network: Link, Node and Bridge Component

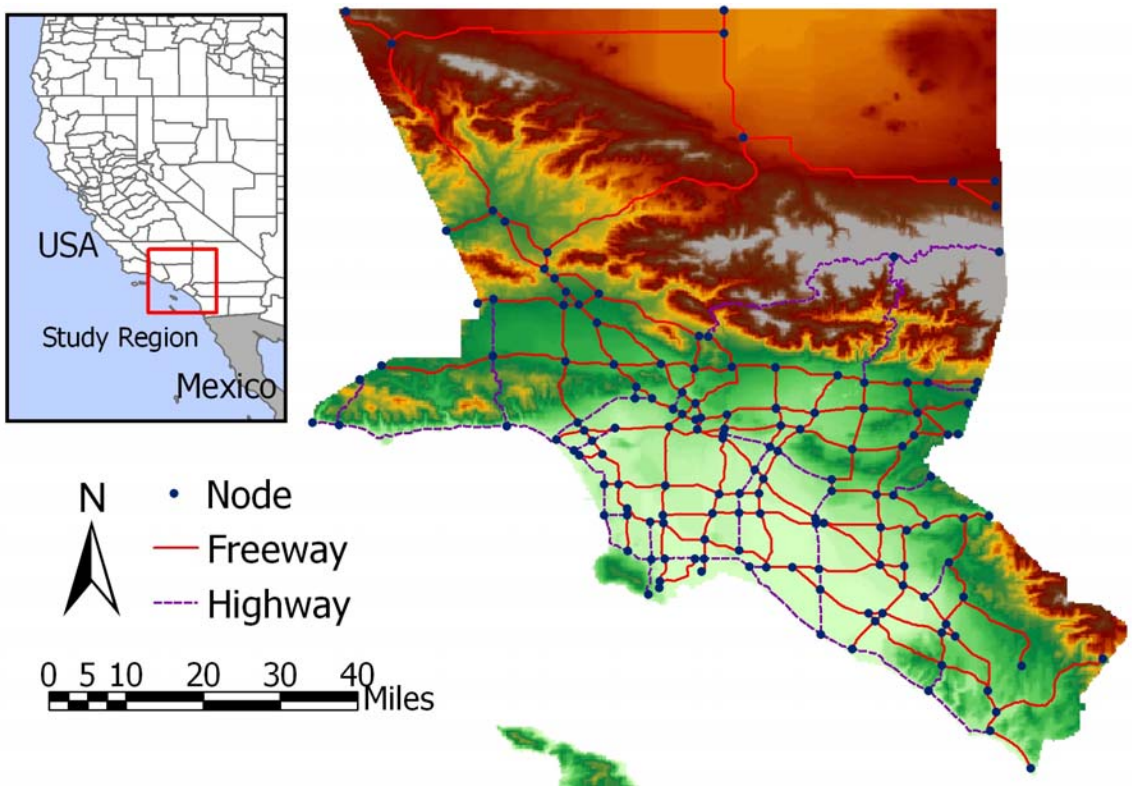

Fig 5.3 Network Model: Los Angeles and Orange County

5.3 Network Modeling

Like any highway system, the Caltrans' Highway transportation system in Los Angeles and Orange County is modeled as network which combines a series of nodes and links (Fig 5.2). Each link represents a roadway segment which connects to any other segment at a point called node. In each link, there may have 0 to several bridge components. A link could be a freeway segment (without traffic signal) or a highway segment (with traffic signal). Fig 5.3 shows all the nodes and links in the modeled Highway Network located in Los Angeles and Orange County. There are total 148 nodes and 231 links in the network.

If the link is a freeway segment without traffic signal, its speed limit is assumed to be 65 mph and each lane has a capacity of 2500 PCU (Passenger Car Unit) or a highway segment with traffic signal, the speed limit. If the link is a highway segment with traffic signal, the speed limit is 35 mph and each lane has a capacity of 1000 PCU. Together with the number of lanes and other information of each link obtained from the network database, these parameters are used to determine traffic capacity of each link (Table 5.1).

5.4 Bridge Damage State Simulation

In each link, only bridge component is assumed to be seismically vulnerable. Therefore, The damage states or performances of the bridges in one link directly relate to the link's post-event performance. In previous chapter, the seismic vulnerability is expressed in the form of fragility curve, which is actually a probabilistic expression of which damage state that a bridge may sustain, even given the ground motion that it is subjected to. Though it is known that the bridge may experience one of the defined damage states, which damage state it will sustain is not exactly know or random.

However, the damage states of the bridges should be determined in order to evaluate the link residual capacity and further the system performance.

Therefore, BDS_{lj}, the damage state of the jth bridge in link l, is best assigned by Monte Carlo simulation. In each simulation, a random number RN_{lj} satisfying uniform 0-1 distribution is generated for each bridge. Based on the ground motion intensity a_{lj} predicted by empirical attenuation relationships, and the fragility curves, $F_1(.)$, $F_2(.), F_3(.)$ and $F_4(.)$ corresponding to damage states of at least minor, at least moderate, at least major and collapse of a bridge, the damage state of this bridge can be assigned based on the following criteria:

$$
\begin{array}{lll}
BDS_{lj} = 0 & RN_{lj} > F_1(a_{lj}) & \text{No Damage} \\
BDS_{lj} = 1 & F_2(a_{lj}) < RN_{lj} <= F_1(a_{lj}) & \text{Minor Damage} \\
BDS_{lj} = 2 & F_3(a_{lj}) < RN_{lj} <= F_2(a_{lj}) & \text{Moderate Damage} \\
BDS_{lj} = 3 & F_4(a_{lj}) < RN_{lj} <= F_3(a_{lj}) & \text{Major Damage} \\
BDS_{lj} = 4 & RN_{lj} > F_4(a_{lj}) & \text{Collapse}
\end{array}
\tag{5.1}
$$

5.5 Assignment of Link Damage State and Residual Capacity

Link damage is represented by the worst state of damage of the bridges on that link (this is a bottle-neck hypothesis; if, for example, one of the bridges on a link suffers from major damage, and if that is the worst state of damage, the link is assumed to have major damage). Following the 1994 Northridge earthquake, the Freeway transportation system in the Los Angeles metropolitan area demonstrated a degree of system resiliency that was activated by enlisting and integrating some seismically unaffected secondary highways and artillery streets into the expressway network after it had suffered from the loss of several bridges (Fig. 5.4). For this reason, in this analysis, alternate routes are considered to exist, although they have less traffic capabilities in terms of both free flow

speed and capacity compared with the segment or the link of the expressway they replaced. This study quantifies the changes in these capacities as shown in Table 5.1, in terms of percent relative to the values under intact conditions, depending on the degree of the link damage. These percentage values also account for the changes resulting from the repair work. In Table 5.1, the values are given in three different sets of criteria to investigate the sensitivity of the system performance to the choice of the residual link capacity. These criteria are hypothetical and future research is needed to develop more reliable values.

The link performance is determined by:

$$t_a = t_a^0 \left[1 + \alpha \left(\frac{x_a}{C_a} \right)^\beta \right] \tag{5.2}$$

where

t_a : the travel time at flow x_a on link a

x_a : the flow on link a

t_a^0 : the travel time at free flow on link a

C_a : the "practical capacity" of link a

α and β : parameters(α =0.15 and β =4.0 are typically used)

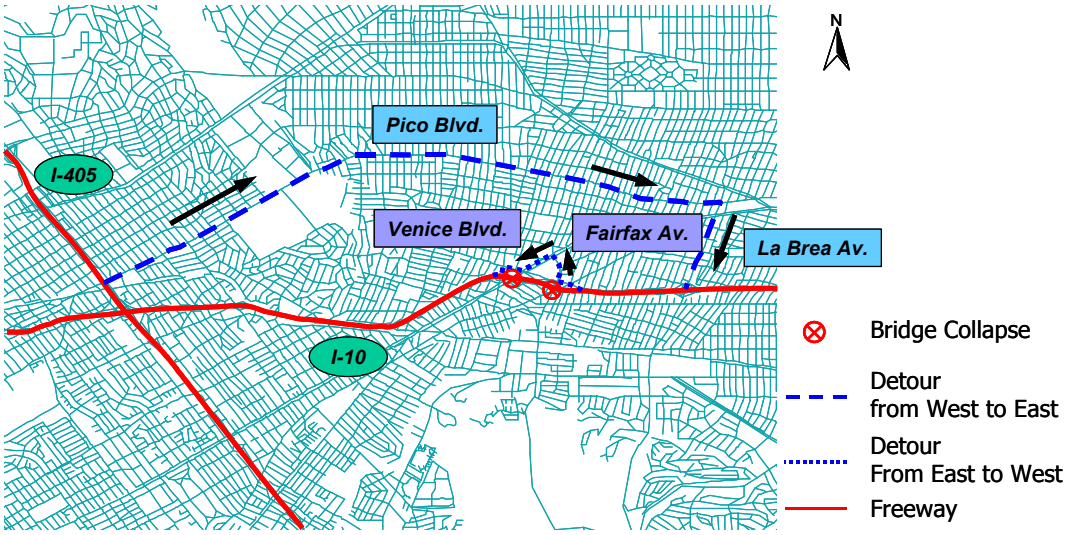

Fig. 5.4 Detour after Northridge Earthquake (January 20th 1994)

Table 5.1 Assumptions for Link Residual Capacity

State of Link Damage	Link Residual Capacity		
	High (Assumption 1)	**Moderate (Assumption 2)**	**Low (Assumption 3)**
No Damage	100%	100%	100%
Minor Damage	100%	100%	100%
Moderate Damage	75%	50%	25%
Major Damage	50%	25%	10%
Collapse	50%*	25%*	10%*

- *Local Detour Route Considered*

This equation shows travel time for each link depending on flow rate of the link which will be incorporated into the traffic assignment analysis described below.

5.6 Traffic Demand: Origin-Destination Data

5.6.1 1996 SCAG Origin-Destination Data

The origin-destination (OD) data used in this paper consist of 1996 southern California origin-destination survey data for 3217 traffic analysis zones (TAZ). Fig 5.5 shows traffic analysis zone and representative point of each traffic analysis zone. These traffic analysis zones are different from census tracts. The OD data covers a five-county area (Los Angeles County and Orange County, Ventura County and part of Riverside

County and San Bernardino County). The OD data consist of 6 types of OD matrices classified by trip purpose. SCAG (Southern California Association of Governments) (1997) defines 6 trip purposes which were based on a trip's origin and/or destination. The classes are home-work, home-other, other-other, other-work, home-shop, as defined below.

Home-work: Any trip where the origin (destination) is home or working at home, and the corresponding destination (origin) is work or work-related. Six

Home-other: Any trip where the origin (destination) is home or working at home, and the corresponding destination (origin) is neither work, work-related, nor shopping.

Other-other: any trip where the origin (destination) and corresponding destination (origin) is pick-up, school, shopping, social, recreation, eat out, personal, or other.

Other-work: any trip where the origin (destination) is work or work-related and the corresponding destination (origin) is neither home nor work at home.

Home-shop: any trip where the origin (destination) is home or working at home and the corresponding destination (origin) is shopping.

Truck Trip: Truck Trip between any two locations.

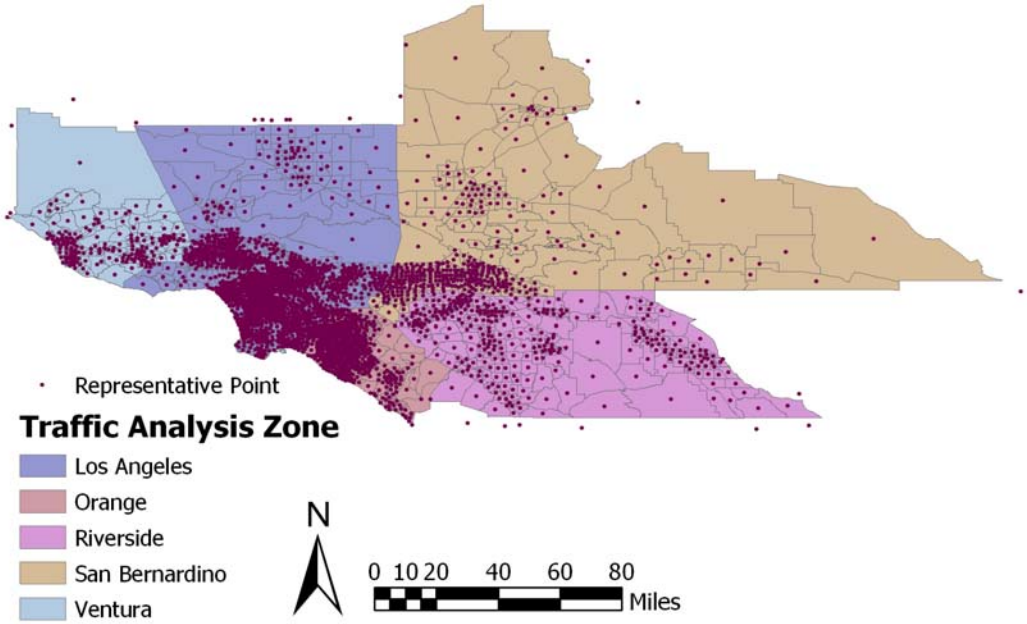

Fig 5.5 1996 Southern California Origin-Destination Data

Each matrix has 3217 rows and 3217 columns. However, the home-work matrix contains data on both home-to-work and work-to-home trips and Similarly, the home-shop trip.

Table 5.2 Trip Ratios of Each Directional Trip for 4 Time Span

Time	Time Span	Hour	Home-Work		Other-Work		Home-Non-Work		Other-Other
			H-W	W-H	O-W	W-O	H-N	N-H	
AM Peak	6am-9am	3	0.3403	0.0152	0.1492	0.0166	0.1178	0.0158	0.1336
Mid Day	9am-3pm	6	0.0786	0.0594	0.2199	0.2199	0.2665	0.1060	0.3725
PM Peak	3pm-7pm	4	0.0196	0.3215	0.0343	0.3089	0.1643	0.1476	0.3119
Night	7pm-6am	9	0.0944	0.0710	0.0256	0.0256	0.0698	0.1122	0.1820
Sum			0.5329	0.4671	0.4290	0.5710	0.6184	0.3816	1.0000

Table 5.3 3 Hours Average of AM Peak and Midday Applied Peak Ratio and Car Occupancy Rates

	Home-work	Other-work	Home-shop	Home-other	Other-other	Work-home	Work-other	Shop-home	Other-home
3HR	0.262	0.287	0.207	0.207	0.207	0.169	0.050	0.106	0.106
COR	1.10	1.25	1.46	1.70	1.72	1.10	1.25	1.46	1.70

3HR:3 Hour Ratio COR: Car Occupancy Rates

These data from the 1996 southern California origin-destination survey include the trip data for passengers through whole day. Table 5.2 (Shiraki 2000)shows trip ratios of each directional trip (home-to-work, work-to-home, other-to-work, work-to-other, home-to-non-work, non-work-to-home and other-to-other) for 4 time spans (6am-9am, 9am-3pm, 3pm-7pm and 7pm-6am). 3 hour average of AM peak and midday applied peak ratio are evaluated from table 3.3 by developing 6am-3pm (9hours) peak ratios to whole day and multiplying the sum by 1/3 (3hours/9hours). Table 5.3 shows 3 hours average of am and midday applied peak ratio and car occupancy rates. Origin-Destination data during 3 hours for 3217 traffic analysis zones are developed by multiplying 3 hours average ratio and dividing car occupancy rates for each and summing up.

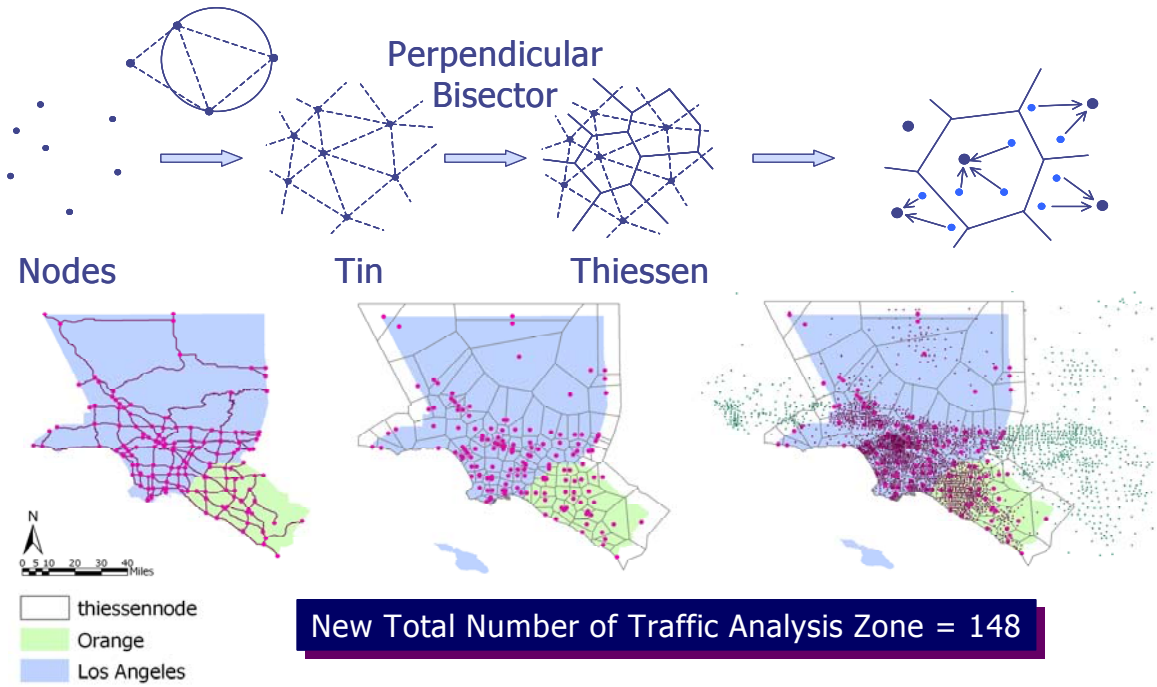

Fig 5.6 OD Data Condensation: Thiessen Polygon

5.6.2 Origin-Destination Data Condensation

The study area and the network data used in this research are different from those of the 1996 Southern California origin-destination survey data. The present study area is limited to Los Angeles County and Orange County. Furthermore, data from the 1996 southern California origin-destination survey data are converted to node OD data and used for the study network. To do this, the Thiessen function within the Arc/Info geographic information system (GIS) software package is utilized. To create Thiessen polygons, first, a TIN structure (Triangulated Irregular Network) is developed. The TIN data structure is based on two basic elements: points with x, y, z values, and a series of edges joining these points to form triangles. The TIN triangulation method satisfies the Delaunay criterion. Delaunay triangulation is a proximal method that satisfies the requirement that a circle drawn through the three nodes of a triangle will contain no other nodes. In other words, this means that all sample nodes are connected with their two nearest neighbors to form triangles. Thiessen polygons are developed by the perpendicular bisector lines for the TIN lines between all nodes. This means the point on the boundary of each polygon between two nodes should be same distance from those two nodes. Additionally, the nearest node from the point inside the polygon should be the node in that same polygon. Highway network nodes are used to develop the Thiessen polygons (Figure 5.6).

The Thiessen polygons were then modified to fit the Los Angeles County and Orange County study area. The OD distribution area used in this study consists of Los Angeles County and Orange County and the five miles zone from the edges of the two

counties (Figure 5.6). Outside of this area, the green points (Figure 5.6) were removed and each representative point of traffic analysis zone is overlaid with Thiessen polygons and is assigned to a Thiessen number same as a node number. The representative points of traffic analysis zone inside each Thiessen polygon were gathered and their OD data were summed. In this way, the OD data were converted from traffic analysis zones to nodes on the network. The new OD data consist of a 148 by 148 matrix. Also, trip attraction and generation of each of six trip types at these 148 nodes are also summarized for the later use to consider the trip reduction after an earthquake.

5.6.3 Origin-Destination Data Change After Earthquake

The usability of individual buildings and associated activity would be changed after earthquake. For example, the damages of building will cause the reduction of usable floor area, as the damage of transportation links and bridges would cause the reduction of capacity volume and the morphs of network configuration. Since seismically damaged buildings have less capacity than usual, trips to the building would also be reduced or reallocated to buildings in other place. The trip reduction/reallocation model based on the useable floor area of buildings, network configurations, and the reduction of associated activity aggregated from the statistics of zone boundaries.

Estimated post-earthquake trip production/attraction vectors should be converted to a demand matrix to ensure compatibility with transportation network model. Travel demand is ideally presented as a 2-dimensional matrix, where a cell in the i-th row and j-column portrays the number of travelers (or cars) generated from zone i, destined for zone j. However, the reduction model produces trip production and destination statistics in the form of vectors, since the model only considers zonal damage to buildings and

associated activity reduction, without counting where the activity is originated or destine to.

From various balancing algorithms that populate matrices from vectors, the gravity model fits the most for into the proposed model, because it allocates travel demand over 2-D space according to the inverse of travel time (impedance). In the gravity model, a trip interchange between origin and destination zones is proportional to (1) amount of trips originated from the origin zone; (2) amount of trips destined to the destination zone; and (3) the inverse of travel time or travel impedance between the two zones.

On the other hand, the travel time, which is estimated by the traffic assignment model, is based on travel demand. In short, while the Origin-Destination matrix is created according to travel time, the travel time also is a function of travel demand, which is the Origin-Destination matrix represents. To estimate the unknowns – Origin-Destination and travel time, the traffic assignment model (user equilibrium model) is integrated with the trip distribution model (gravity model), and iterative searches are performed by the model to achieve optimal solution. Figure 5.7 depicts the estimation flow within the assignment-distribution combined model. Rigorous description about the model is provided in the next section.

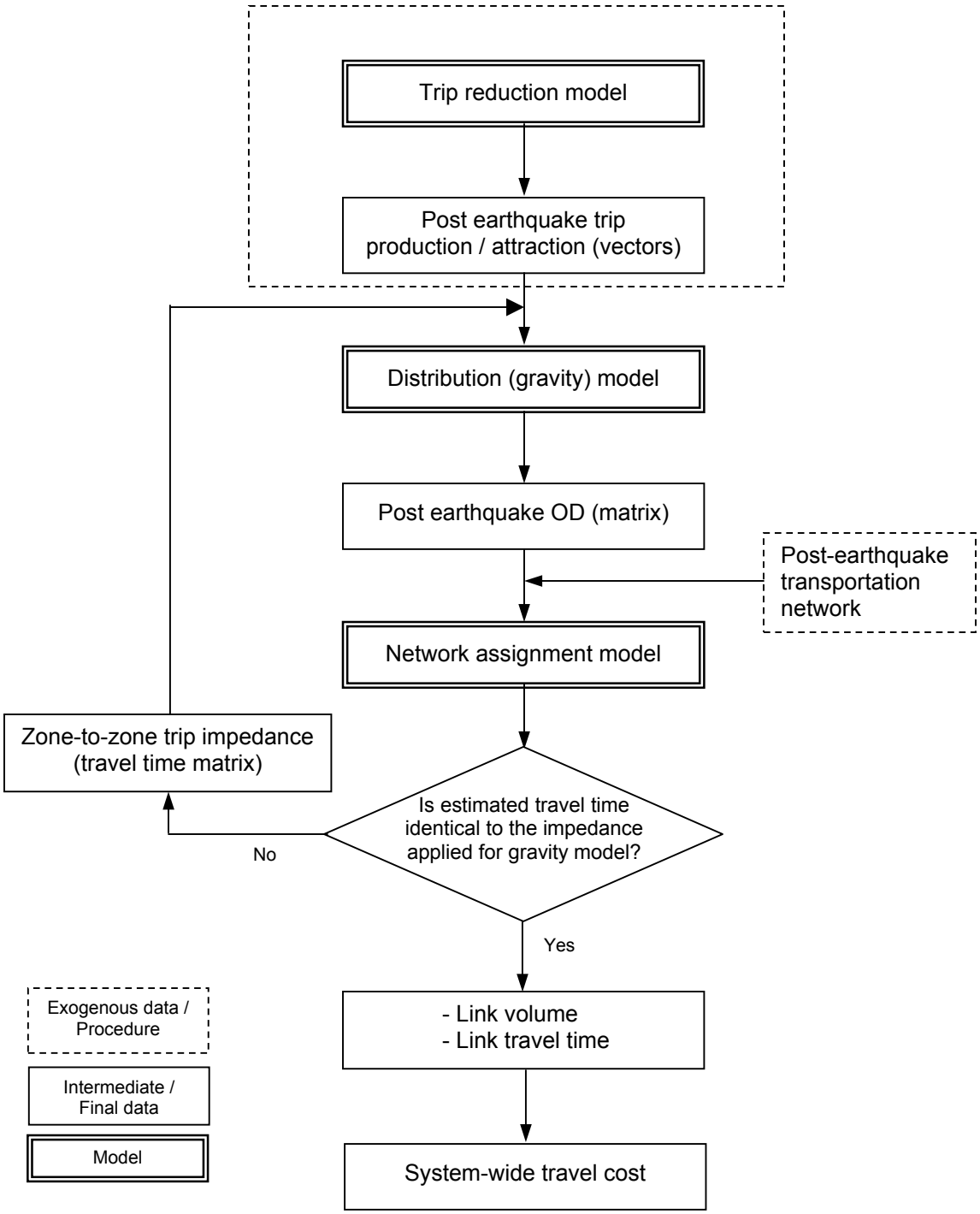

Fig 5.7 Integrated Trip Reduction and Network Models

5.7 The Integrated Model

The integrated model follows Evans (1976) formulation for the combined model of network assignment and distribution. The first term of the right-hand-side in Equation 5.3 presents travel cost associated with user equilibrium assignment. The second term estimates costs associated with the travel distribution. Minimizing these cost terms corroborates the generation of link traffic volume x_a (and thus the travel cost by Equation 5.7), and OD, t_{ij}^p.

Trip reduction model and gravity model are included in the integrated model as constraints. VEquations of (5.9a and 5.9b) discount baseline trip production and attraction according to estimated reduction rates for each TAZ and trip purpose. Equation (5.4) depicts the gravity model.

$$Z = \min Z(\mathbf{x},\mathbf{t}) = \sum_a \int_0^{x_a} c_a(w) \quad dw + \sum_p \left(\frac{1}{\beta^p} \sum_i \sum_j t_{ij}^p \cdot \ln\left(t_{ij}^p\right) \right) \quad \text{.....(5.3)}$$

subject to

$$f_{ij}^{pk} \geq 0 \qquad \forall\, p, k, i, j \quad \text{.....(5.4)}$$

$$t_{ij}^p \geq 0 \qquad \forall p, i, j \quad \text{.....(5.5)}$$

$$\sum_k f_{ij}^{pk} = t_{ij}^p \qquad \forall\, p, i, j \quad \text{.....(5.6)}$$

$$x_a = \sum_p \sum_{i,j} \sum_k f_{ij}^{pk} \cdot \delta_{ij}^{a,k} \qquad \forall\, a \quad \text{.....(5.7a)}$$

$$c_{ij} = \sum_a c_a\left(x_a\right) \cdot \delta_{ij}^{a,k} \qquad \forall\, a \quad \text{.....(5.7b)}$$

$$t_{ij}^p = O_i^p \cdot D_j^p \cdot \mathrm{K}_{ij}^p \cdot \exp\left(\alpha^p + \beta^p \cdot c_{ij}\right) \qquad \forall p, i, j \quad \text{.....(5.8)}$$

$$O_i^p = \mathbf{O}_i^p \cdot \left(1 - \xi_i^p\right) \quad \text{(5.9a)}$$

$$D_j^p = \mathbf{D}_s^n \cdot \left(1 - \zeta_j^p\right) \quad \text{(5.9b)}$$

where

x_a = Flow on link *a*.

t_{ij}^p = Trip rate of type *p* between OD pair *i-j*.

f_{ij}^{pk} = Flow of trip type *p* on path *k* connecting OD pair *i-j*.

c_{ij} = Travel time between OD pair *i-j*.

c_a = Link performance function of link *a*.

$\delta_{ij}^{a,k}$ = 1 if link *a* is on path *k* between OD pair *i-j*, 0 other-wise.

O_i^p = Trip generated from zone *i* for purpose *p*.

D_s^n = Trip destined to zone *j* for purpose *p*.

$\mathbf{O}_i^p$ = Baseline (pre-earthquake) trip generation from zone *i* for purpose *p*.

$\mathbf{D}_j^p$ = Baseline (pre-earthquake) trip destination to zone *j* for purpose *p*.

ξ_i^p = Trip reduction rate at zone *i* for production of purpose *p*.

ζ_j^p = Trip reduction rate at zone *j* for attraction of purpose *p*.

α^p, β^p = Calibrated distance-decay coefficients for purpose *p*.

K_{ij}^p = Calibrated balancing coefficients for purpose *p* ($\mathrm{K}_{ij}^p = A_i \cdot B_j$)

p= Trip purposes

With successive average schemes, an iterative secant method is able to solve the system of equations from Equations 5.3 through 5.9. Step 0 is to initialize variables. OD

and link volume are set 0, while c_{ij} is set to the travel time on minimum paths between zone-pairs estimated based on free flow speed. The trip reduction model calculates post-earthquake trip production and attraction. Step-1 checks if the algorithm is running too many times, relative to M. If it is, the algorithm stops at this moment. Step-2 estimates OD using calibrated gravity model with travel time. The estimated OD only reflects travel time that was calculated in Step-0, or Step-4, and combined with that previously estimated by weighted average. The new OD is used in Step-3 to generate link volume. Link volume is also combined with that generated by the previous iteration. Step-4 updates travel time. If travel times estimated from two consecutive iterations are not significantly different, the algorithm stops at this moment. Otherwise, Step 1 to Step 4 is repeated again.

5.8 Drivers' Delay

Total Travel Time can be expressed as:

$$\sum_a x_a t_a(x_a)$$

(5.10)

where

x_a=flow of link a

t_a=travel time of link a

The analysis applies a comprehensive index of total transportation cost (drivers' delay), λ, based on post-earthquake network topology relative to pre-earthquake intact conditions. Drivers' delay is:

$$\lambda = \sum_a x'_a \, t'_a \, (x'_a) - \sum_a x_a t_a (x_a)$$

(5.11)

where

x_a = flow on link a in intact network (pre-earthquake)

t_a = travel time on link a in intact network (pre-earthquake)

x'_a = flow on link a in damaged network (post-earthquake)

t'_a = travel time on link a in damaged network (post-earthquake)

5.9 Opportunity Cost

Reduced travel demand is an impact from the earthquake, assumed in this analysis via building damage, and it implies another type of social cost. Trip is derived from various activities, such as working, and shopping. If drivers cannot make trip in any reason, they also cannot achieve the purpose of activity that used to cause the trips. If the activities they used to perform have any economic value, they lose the value by not making the trips. And the value of this loss, called as opportunity cost, should be included in total cost, along with the cost from drivers' delay.

Opportunity cost of trip type p, ϕ^p is calculated as:

$$\phi^p = \sum_i \sum_j \left(\frac{\left(q_{ij}^p - q_{ij}'^p\right) \cdot \left(c'_{ij} - c_{ij}\right)}{2} \right)$$

(5.12)

where

q_{ij}^p = trips of type p from zone i to zone j in intact network (pre-earthquake)

c_{ij} = travel time zone i to zone j in intact network (pre-earthquake)

q'^{p}_{ij} = trips of type p from zone i to zone j in damaged network (post-earthquake)

c'_{ij} = travel time zone i to zone j in damaged network (post-earthquake)

Different from the drivers' delay calculation, the opportunity cost is calculated by trip purposes, p. In theory, link volume cannot be purpose-specific in node-based (or link-based) user equilibrium model. This is why there would be only one delay cost per model application. However, according to the systems of equations, in Equations 5.3 through 5.9, demand (or Origin-Destination) is estimated for individual trip types. Then Equation 5.12 can be applied to each O-D matrix, along with a common travel time matrix, c_{ij}. Consequently, the equation allows disaggregating a part of social cost into different activity types. For example, if an earthquake hits an area with concentrate industrial facilities, the disaggregated economic loss estimated by the proposed model might imply that work related trips (home-to-work, work-to-other) would have more impact than other recreational trips, and so force. From lump sum estimation, the economic impact is now distinguished by activity types according to locality, and urban structure.

Chapter 6 Direct Economic Loss

6.2 Number of Damaged Bridges from Earthquake

Due to inherent randomness in the fragility curve**,** the states of bridge damage suffered from an earthquake can only be determined by Monte Carlo simulation, as introduced in Chapter 5. Figure 6.1 and 6.2 graphically show the damage states of bridges and links when the network is subjected to an MCE event Elysian Park M7.1 based on one simulation given no bridge is retrofitted. The ruptured fault is just below the Los Angeles Downtown Area and many bridges are damaged: 179 with minor damage, 204 with moderate damage, 90 with major damage and 19 with collapse. For comparison, two other retrofit cases are also considered. One corresponds to the real retrofit status of the bridges in the freeway network of the Los Angeles and Orange County, that is, 712 out of 3133, or almost 23% are retrofitted. Another case is assumed that the bridges in the system are all retrofitted. For the latter two cases, the damaged bridges and links are shown in Figs 6.3-6.6. The comparisons graphically demonstrate that the less number of bridges are damaged in these cases as more bridges in the network are retrofitted.

Being more quantitative, Table 6.1 further provides average number of bridges sustaining different damage states in 100 simulations. It can be seen that as the number of the damaged bridges in the retrofitted network is dramatically reduced: bridges with minor damage by 4.9% and 30.9%, moderate damage by 21.4.% and 77.9%, major damage by 26.3 % and 26.7%, and collapse by 26.7% and 100% It can also be concluded that the retrofit measures' effect in improving the bridge seismic performance is more significant in preventing more severe damages, which actually is consistent with

the result for enhancement ratios of the median values of the fragility curves associated with different damage states, as shown in Chapter 2. The average number of bridges with collapse damage in case of 100% retrofit mean do not mean that no bridge will collapse in a real case, but suggests that the probability of a bridge experiencing collapse in such a scenario earthquake is extremely low. This is indeed a great benefit from the retrofit, not only because of less expected bridge restoration (repair/replacement) cost, but also less traffic interruption and associated opportunity cost which be introduced in the next chapter.

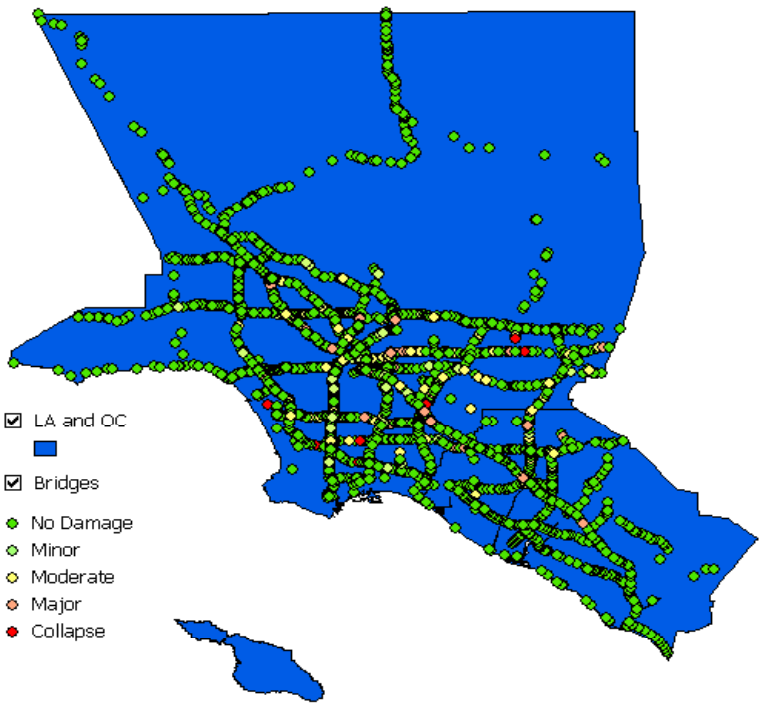

Fig 6.1 Bridge Damage in Elysian Park 7.1 (Without Retrofit)

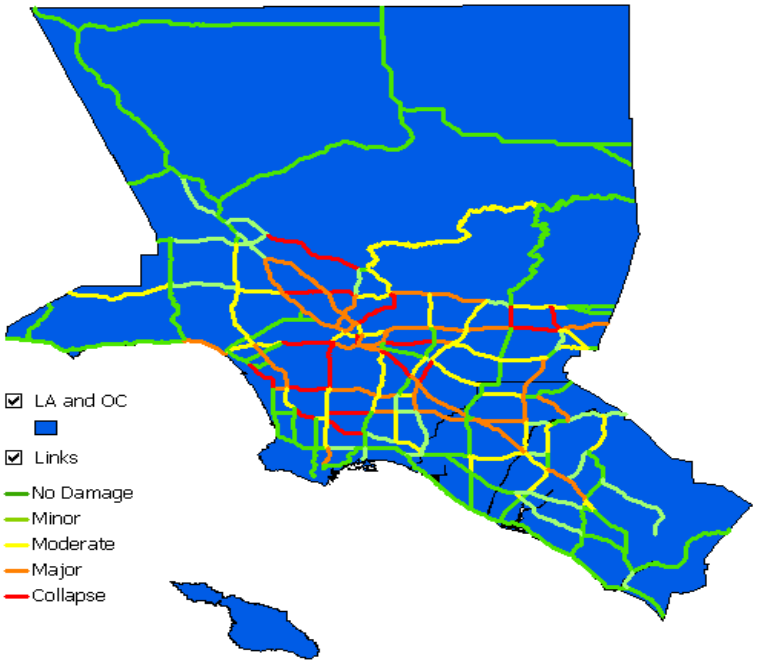

Fig 6.2 Link Damage in Elysian Park 7.1 (Without Retrofit)

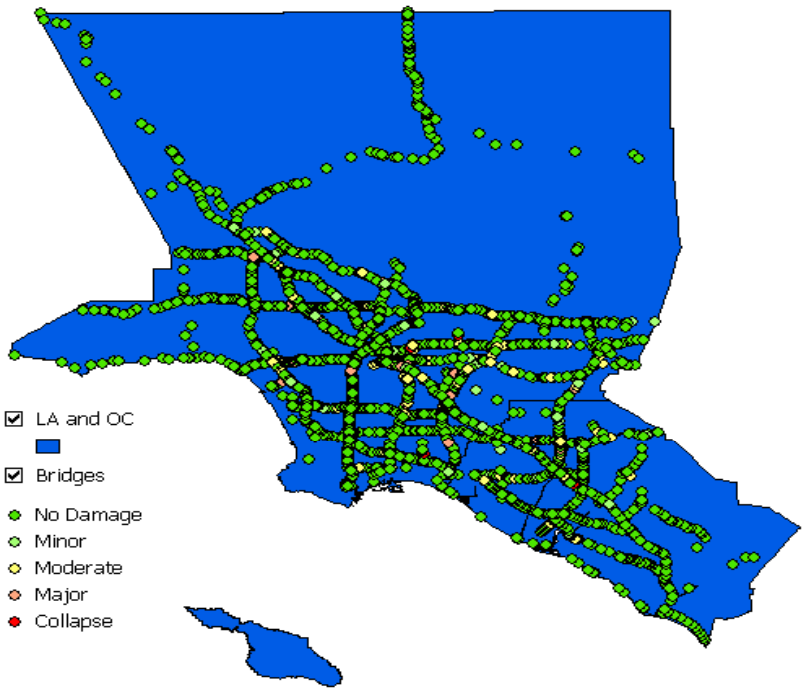

Fig 6.3 Bridge Damage in Elysian Park 7.1 (23% Retrofit)

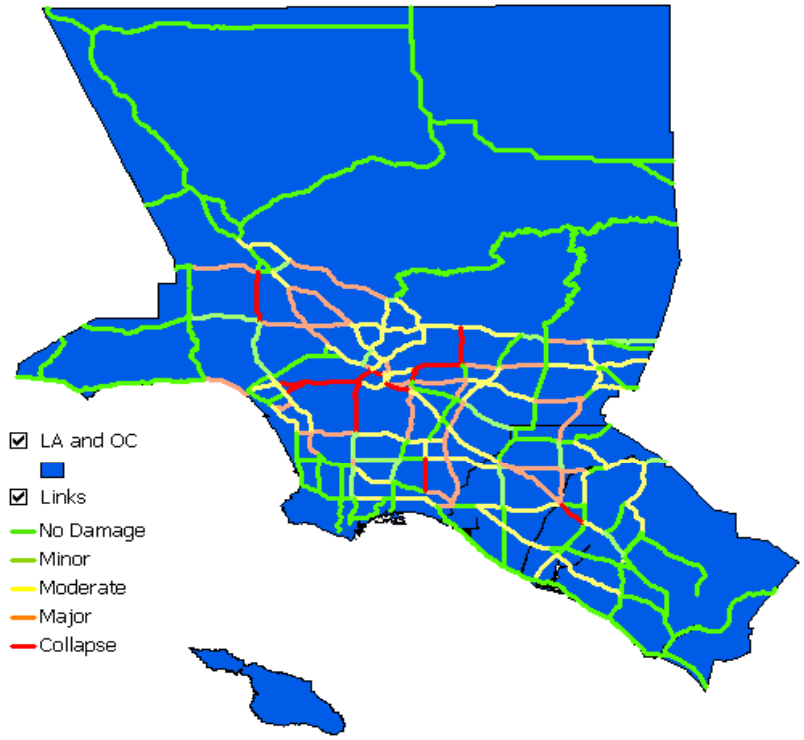

Fig 6.4 Link Damage in Elysian Park 7.1 (23% Retrofit)

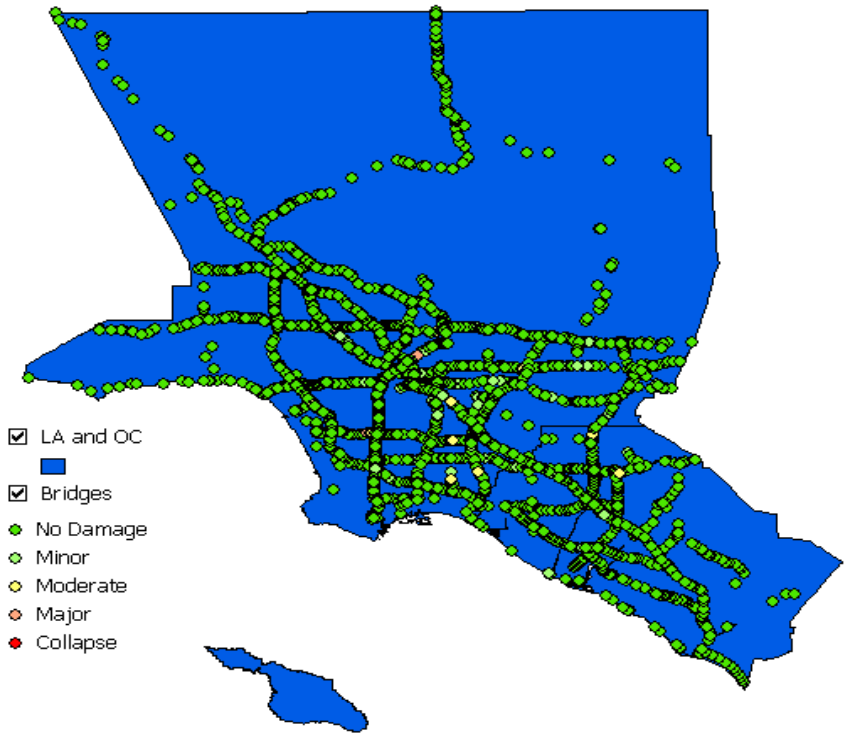

Fig 6.5 Bridge Damage in Elysian Park 7.1 (100% Retrofit)

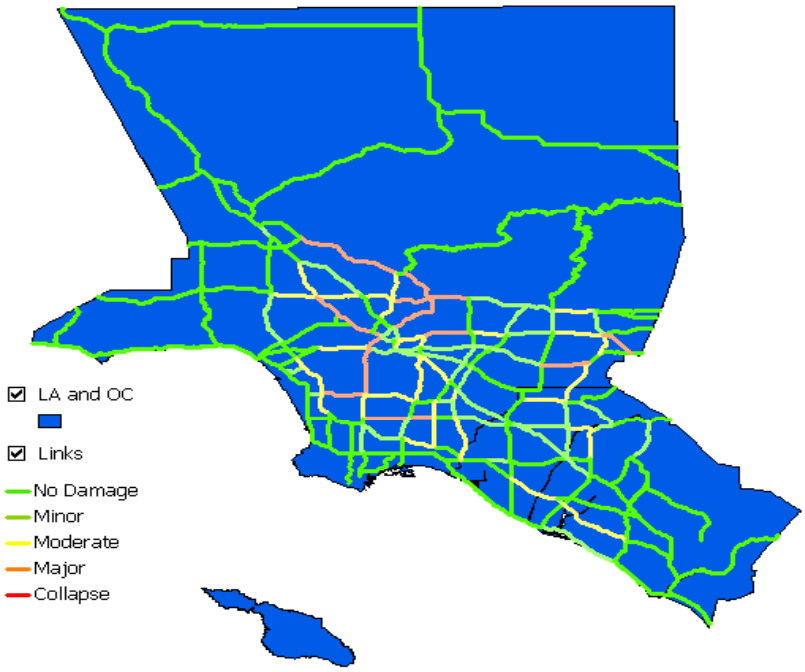

Fig 6.6 Link Damage in Elysian Park 7.1 (100% Retrofit)

Table 6.1 Damaged Bridges in Elysian Park M7.1
(Total 3133 Bridges)

Damage State	Number of Damaged Bridges			Reduction Percentage	
	No Retrofit	23% Retrofit	100% Retrofit	23% Retrofit	100% Retrofit
Minor	197	188	136	5	31
Moderate	256	201	56	21	78
Major	87	64	8	26	91
Collapse	9	6	0	27	100

This benefit in reducing the number of damaged bridges due to seismic retrofit can also be observed when the network is attacked by other earthquake events. For each of the other 46 scenario earthquakes described in Chapter 4, the simulation process is carried out for the same three cases. Table 6.2 lists the average number of bridges sustaining four different damage states based on 100 simulations. The results again show that as more bridges are retrofitted, less number of bridges will be expected to sustain any of the four damage states. However, the number of damaged bridges and associated

number reduction rates (Table 6.3) are not the same in different scenario earthquakes, because these scenarios are distinct in either location, magnitude, or their spatial relationship with the bridges distributed in the network.

Table 6.2 Comparison: Number of Damaged Bridges

Event No.	No Retrofit				23% Retrofit				100% Retrofit			
	Min	Mod	Maj	Col	Min	Mod	Maj	Col	Min	Mod	Maj	Col
1	195	256	87	8	188	201	64	6	136	56	8	0
2	172	236	139	18	170	200	104	12	147	99	17	1
3	144	176	69	7	130	143	55	6	102	45	7	0
4	102	118	41	4	96	99	31	3	63	28	4	0
5	81	85	28	2	71	71	22	2	43	18	2	0
6	134	181	110	13	131	151	77	10	112	79	13	1
7	72	66	24	2	63	56	20	2	33	16	2	0
8	10	6	2	0	8	5	1	0	3	1	0	0
9	49	63	37	6	46	56	30	3	40	27	5	0
10	186	252	154	18	179	214	115	14	155	109	17	1
11	100	119	65	8	92	100	53	6	71	46	7	0
12	149	209	126	16	146	171	93	11	129	90	14	1
13	170	194	68	6	156	158	54	5	102	44	6	0
14	44	52	22	3	40	40	17	2	29	16	3	0
15	77	98	49	6	72	74	35	4	58	34	5	0
16	63	75	33	3	57	59	22	3	41	22	3	0
17	42	47	14	1	39	39	12	1	23	10	1	0
18	37	41	13	1	35	35	10	1	20	8	1	0
19	32	36	11	1	30	28	8	1	18	7	1	0
20	18	16	4	0	14	11	3	0	7	3	0	0
21	12	11	3	0	12	10	3	0	5	2	0	0
22	14	11	4	0	12	10	3	0	6	2	0	0
23	1	0	0	0	1	0	0	0	0	0	0	0
24	1	1	0	0	1	1	0	0	0	0	0	0
25	0	0	0	0	0	0	0	0	0	0	0	0
26	20	22	10	1	19	19	8	1	14	6	1	0
27	35	48	32	4	34	43	25	3	29	24	3	0
28	37	37	17	2	31	28	11	1	19	12	2	0
28	28	33	17	2	27	28	13	1	19	11	2	0
29	18	14	4	0	14	12	3	0	7	2	0	0
30	110	155	85	11	106	123	62	7	96	60	10	0
31	107	143	78	9	100	115	56	7	85	54	8	0
32	112	143	77	9	106	116	55	7	86	55	9	0
33	83	97	34	4	72	85	29	3	53	22	4	0
34	59	64	23	2	54	52	17	2	34	14	2	0
35	31	33	11	1	29	27	8	0	17	6	1	0
36	8	9	3	0	7	8	3	0	5	2	0	0
37	2	2	1	0	2	1	0	0	1	0	0	0

38	1	0	0	0	0	0	0	0	0	0	0	0
39	61	78	49	6	55	67	38	5	48	36	6	0
40	41	36	11	1	33	29	8	1	18	7	1	0
41	155	215	128	17	154	180	94	12	133	92	16	1
42	179	249	160	20	178	215	114	15	158	114	19	1
43	4	168	0	0	3	2	0	0	1	0	0	0
44	14	14	6	1	13	13	4	0	8	4	1	0
45	7	5	1	0	6	4	1	0	3	1	0	0
46	136	149	52	5	121	121	39	4	78	34	5	0
47	195	256	87	8	188	201	64	6	136	56	8	0

Table 6.3 Reduction Rates in Number of Damaged Bridges

Event No.	23% Retrofit (%)				100% Retrofit (%)			
	Min	Mod	Maj	Col	Min	Mod	Maj	Col
1	3.90	21.36	26.42	25.74	30.15	77.95	90.65	100.00
2	1.39	15.28	25.46	29.87	14.53	57.98	88.10	96.25
3	9.62	18.84	20.45	21.34	29.52	74.61	90.52	96.17
4	5.34	16.21	24.29	17.45	37.58	76.54	91.41	96.95
5	11.55	15.59	22.14	14.05	46.52	78.59	91.12	98.35
6	2.37	16.89	29.84	24.87	16.54	56.51	87.97	95.83
7	12.02	15.69	16.05	3.70	53.96	75.82	92.12	95.37
8	16.88	13.49	39.39	0.00	68.23	87.18	94.55	99.99
9	5.14	11.22	19.66	39.97	17.85	56.67	86.11	94.98
10	3.67	15.03	24.99	21.36	16.64	56.54	88.80	95.60
11	7.98	15.58	18.32	22.41	29.35	61.58	88.80	95.77
12	1.65	18.19	25.75	31.92	13.13	56.88	88.52	96.40
13	7.84	18.77	21.21	16.23	39.68	77.32	91.09	97.21
14	9.52	22.09	25.48	38.97	34.38	69.76	88.74	96.90
15	6.29	24.15	28.42	26.63	24.27	64.82	89.77	95.65
16	8.28	21.51	31.15	3.01	34.62	70.33	91.07	97.32
17	8.95	15.59	13.37	14.29	45.41	79.43	91.50	99.99
18	6.08	14.32	23.03	43.88	47.39	79.88	91.71	99.99
19	7.88	20.60	30.28	48.98	45.33	79.18	91.02	99.99
20	18.80	30.38	35.94	50.00	59.89	80.57	95.39	99.99
21	6.27	8.63	8.17	26.09	61.73	81.82	94.44	99.99
22	17.01	12.11	29.82	14.29	54.52	81.45	91.00	99.99
23	6.94	9.09	52.94	50.00	77.78	93.18	99.99	99.99
24	12.33	7.95	14.29	/	71.92	93.18	95.24	/
25	33.33	99.99	/	/	99.99	99.99	/	/
26	3.46	16.25	21.14	39.84	30.86	71.53	90.46	99.99
27	2.85	10.86	21.18	21.82	17.87	50.47	89.25	96.10
28	14.78	24.13	33.12	28.07	48.18	67.93	88.59	95.32
29	5.83	14.37	24.84	21.86	33.26	65.05	89.17	93.99
30	22.05	19.23	28.21	48.28	63.15	82.53	92.31	96.55

31	3.10	20.13	27.46	36.00	12.80	60.95	87.75	96.50
32	6.53	19.68	28.32	25.17	20.04	61.88	89.19	96.69
33	5.61	19.19	28.71	28.85	23.87	61.81	88.44	95.59
34	12.85	12.54	14.49	22.61	35.73	77.81	89.40	99.99
35	8.37	19.23	25.41	28.81	41.59	78.36	90.55	99.99
36	7.32	19.71	23.46	47.87	45.65	81.49	91.39	99.99
37	6.19	14.74	14.72	5.88	39.79	78.99	91.30	99.99
38	7.14	28.90	46.27	83.33	63.87	80.92	89.55	99.99
39	21.05	8.33	/	/	89.47	99.99	/	/
40	9.37	14.32	22.05	25.08	21.92	54.40	87.87	96.59
41	18.51	17.55	25.84	29.13	56.68	79.08	91.59	99.99
42	0.99	16.24	25.96	30.39	14.39	57.37	87.59	96.46
43	0.49	13.78	28.39	24.61	11.40	54.37	88.11	96.39
44	23.56	99.07	18.75	99.99	83.89	99.90	99.99	99.99
45	10.74	6.15	21.65	50.00	44.01	71.94	88.91	92.42
46	17.80	19.25	4.59	84.62	62.31	88.97	91.74	99.99
47	11.12	18.95	24.48	24.95	42.90	77.18	91.03	99.99

6.2 Bridge Repair Cost Estimation in an Earthquake

After retrofit, less number of bridges will be damaged in an earthquake event. It also means that the less restoration effort will be required to recover the functionality of the damaged bridges and therefore, less associated cost. The exact estimation of bridge repair cost could be very complex and require much input. However, in this research, bridge repair costs are assumed to be proportional to the bridge's replacement value and the proportionality factor is directly related to its damage state. This proportionality factor is called damage ratio in HAZUS99-2 (NIBS, 1999) and the recommend values are provided in Table 6.4. The replacement value of each bridge is estimated to be the product of the deck area and a unit area replacement value. Unit area replacement values will vary depending on the bridge's structural type, material and other factors. Based on Caltrans' data, \$120/ft^2 is a reasonable estimate and is actually used for all the bridges as a preliminary estimate in this study.

Therefore, the evaluation of bridge repair cost resulting from event j can be expressed as

$$RP_j = \sum_{i=1}^{N} \sum_{k=1}^{4} p_i(DS = k \mid a_{ij}) \bullet C_i \bullet r_k \tag{6.1}$$

Where

RP_j = expected bridge restoration (repair or replacement) cost due to earthquake event j

N = total number of bridges

k = damage state of bridge (1:minor damage, 2: moderate damage, 3: major damage, 4: collapse)

a_{ij} = ground motion at the site of bridge i due to event j

$p_i(DS = k \mid a_{ij})$ = probability of bridge i sustaining damage state k under ground motion a_{ij}; this is a fragility curve of bridge i for damage state k evaluated at a_{ij}

C_i = replacement value of bridge i

r_k = damage ratio corresponding to damage state k

In equation 6.1, C_i can be estimated by unit area replacement value (\$120/ft^2) and deck area obtained from bridge inventory database, and r_k can be taken from Table 6.4. $p_i(DS = k \mid a_{ij})$ can be evaluated based on the fragility information of bridge i. Table 6.5 lists the expected repair cost of bridges in Los Angeles and Orange Counties resulting from the 48 scenarios in three retrofit cases. The Event No. 48 is the 1994 Northridge Earthquake and its ground motion distribution obtained from TriNet ShakeMap.

Table 6.4 Damage Ratios for Highway Bridge Components (from HAZUS 99)

Damage State	Best Estimate Damage Ratio	Range of Damage Ratios
Slight	0.03	0.01-0.03
Moderate	0.08	0.02-0.15
Extensive	0.25	0.10-0.40
Complete	1.00*	0.30-1.00

* If the number of spans is greater than 2, then the best estimate damage ratio for complete damage is [2/(number of spans)]

Table 6.5 Expected Bridge Repair Cost (in $ Million)

Event No.	No Retrofit	23% Retrofit	100% Retrofit	Event No.	No Retrofit	23% Retrofit	100% Retrofit
1	186.892	144.102	38.17	25	0.008	0.008	0
2	235.57	177.937	57.59	26	15.943	12.533	3.377
3	162.322	134.602	35.02	27	46.704	38.01	11.802
4	104.21	88.553	20.933	28	34.927	24.007	7.619
5	76.39	65.453	14.616	29	28.585	19.228	6.67
6	183.212	129.402	45.293	30	9.475	7.526	1.487
7	37.834	29.593	6.275	31	146.219	101.976	35.566
8	3.427	2.587	0.37	32	131.956	91.098	31.441
9	58.111	45.898	14.414	33	137.298	101.304	32.836
10	240.408	176.988	58.901	34	92.946	80.732	19.152
11	104.126	81.035	23.99	35	57.154	45.822	11.138
12	207.043	149.764	51.643	36	25.67	21.722	4.578
13	144.749	115.265	28.728	37	2.621	2.218	0.529
14	39.841	26.695	8.593	38	0.521	0.42	0.067
15	87.192	60.253	20.446	39	0.067	0.05	0.008
16	62.328	45.293	13.591	40	76.541	60.152	18.9
17	46.259	42.193	8.988	41	24.503	19.79	4.192
18	34.264	29.383	6.342	42	216.166	161.566	53.491
19	31.198	25.099	5.863	43	260.215	190.361	65.386
20	11.357	7.501	1.907	44	0.874	0.655	0.084
21	8.459	7.392	1.42	45	5.124	4.259	0.932
22	9.702	8.434	1.596	46	2.108	1.596	0.26
23	0.101	0.092	0.017	47	109.301	86.075	21.277
24	0.244	0.227	0.025	**48***	113.954	88.267	25.763

Event No.48: the 1994 Northridge Earthquake

6.3 Expected Annual Repair Cost of a Site-Specific Bridge

To estimate the expected annual repair cost for each bridge and further the expected annual repair cost for all the bridges in a study region, it is necessary to consider both the site seismic hazard at the bridge site and the bridge's fragility.

6.3.1 Annual Probability of Damage

The probability of being damaged for a bridge at a site is related with both the site seismic hazard and its seismic fragility. The site seismic hazard, or hazard curve, is often expressed as

$$y = F(x) \tag{6.2}$$

where

y =annual probability of exceedance

x =ground motion intensity (PGA, SA and etc.)

Since hazard curve is a cumulative distribution function in nature, its derivative or hazard density function rather than itself should be used to calculate annual probability of sustaining a specified damage state. The annual probability of suffering damage state i for a bridge could be expressed as

$$P_i = \int_0^\infty (-\frac{dy}{dx}) p_i(x) dx \tag{6.3}$$

where

P_i = the annual probability of suffering damage state i (1:minor damage; 2: moderate damage; 3 major damage; 4 collapse)

$-\frac{dy}{dx}$ = site seismic hazard density function

$p_i(x)$ = probability of suffering damage State i under PGA x

The $p_i(x)$ is determined by the fragility curves corresponding to the four damage states:

$$p_1 = p(DS = 1 \mid x) = \Phi[\frac{\ln(x/c_1)}{\zeta}] - \Phi[\frac{\ln(x/c_2)}{\zeta}]$$

$$p_2 = p(DS = 2 \mid x) = \Phi[\frac{\ln(x/c_2)}{\zeta}] - \Phi[\frac{\ln(x/c_3)}{\zeta}]$$

$$p_3 = p(DS = 3 \mid x) = \Phi[\frac{\ln(x/c_3)}{\zeta}] - \Phi[\frac{\ln(x/c_4)}{\zeta}]$$

$$p_4 = p(DS = 4 \mid x) = \Phi[\frac{\ln(x/c_4)}{\zeta}] \tag{6.4}$$

c_1, c_2, c_3 and c_4 are median values of fragility curves corresponding to exceeding damage state minor, moderate, major and collapse. ζ is the common log-standard deviation of the four fragility curves.

6.3.2 Expected Annual Repair Cost before Retrofit

The expected annual repair cost of a bridge before retrofit $\overline{C}^0_{RP}$ can be evaluated by

$$\overline{C}^0_{RP} = \sum_{i=1}^{4} P_i^0 r_i C_C \tag{6.5}$$

Where

P_i^0 = annual probability of sustaining damage state i based on bridge fragility curve before retrofit

r_i = repair cost ratio depending on damage state i (chosen from Table 6.4)

C_C = bridge replacement value or construction cost

6.3.3 Expected Annual Restoration Cost after Retrofit

The expected annual restoration cost of a bridge after retrofit $\overline{C}_{RP}^{1}$ can be evaluated by

$$\overline{C}_{RP}^{1} = \sum_{i=1}^{4} P_i^1 r_i C_C^{'} \tag{6.6}$$

Where

P_i^1 = annual probability of sustaining damage state i based on bridge fragility curve after retrofit

r_i = restoration cost ratio depending on damage state i (chosen from Table 6.4)

$C_C^{'}$ = bridge replacement value or construction cost after retrofit.

Since it is assumed that after restoration the bridge will possess its pre-event seismic performance, the bridge construction value considered here will include its initial bridge construction cost and the retrofit cost involved.

6.3.4 Expected Annual Bridges Restoration Cost

Assuming the hazard curve at a bridge site can be fit in the form of $y = e^{-ax^b}$ as a function of PGA in g with a=6.85 and b=0.471, PGA values corresponding to 10% and 2 % probability of exceedance in 50 years will be 0.81 g and 1.33g, respectively. If the fragility curves of the bridge are $c1 = 0.64g$, $c2 = 0.80g$, $c3 = 1.25g$, $c4 = 2.55g$ and $\zeta = 0.7$ before retrofit, and $c1 = 0.99g$, $c2 = 1.40g$, $c3 = 2.56g$, $c4 = 6.19g$ and $\zeta = 0.7$ after retrofit (composite empirical fragility curves as described in Chapter 3), the annual probabilities of sustaining each of four damage states can be calculated using the equations 6.2-6.4 and the results are listed in Table 6.6. The annual probability reduction

rates demonstrate that the effect of retrofit is more evident in reducing the more severe damages.

Table 6.6 Annual Probability of Sustaining Damage for a Bridge before and after Retrofit

Damage State	Minor	Moderate	Major	Collapse
Annual Probability (Before Retrofit)	0.327%	0.387%	0.212%	0.044%
Annual Probability (After Retrofit)	0.224%	0.155%	0.041%	0.0028%
Annual Probability Reduction Rate	33%	60%	81%	94%

To estimate the annual restoration cost, we assume that bridge initial construction cost is one million dollars and the retrofit cost is 20% of the initial construction cost. Again, the restoration cost ratios are selected as 0.03, 0.15, 0.3 and 1.0, corresponding to damage state of minor, moderate, major and collapse, respectively. Using Equations 6.5, the annual repair cost for the bridge before retrofit will be 1,758 dollars. Using Equations 6.6, the annual restoration cost for the bridge after retrofit will be only 538 dollar, about 70% less than that before retrofit. However, the annual restoration cost will change depending on the site seismic hazard curve and the bridge's seismic fragility.

For all the bridges (total 3133) in Caltrans' highway network located in Los Angeles and Orange Counties, the above restoration cost estimation procedure is carried out by considering site-specific seismic hazard curve of each bridge. Using the bridge inventory, the construction cost is estimated by the deck area multiplied by construction cost unit deck area (120 dollars/ft^2). The retrofit cost is also assumed uniformly to be 20% of the initial construction cost. Restoration cost ratios are the same as those used in the above example. The expected annual restoration cost in the three retrofit cases are separately estimated and the results are shown in Table 6.7. The annual bridge restoration cost in the system is reduced by 72% if all the bridges are retrofitted, from 4.7

million dollars to 1.33 million dollars. The reduction rate is lower (20%) if only some of the bridges (23%) are retrofitted.

Table 6.7 Annual Bridge Restoration Cost in the Network

Retrofit Case	No Retrofit	23% Retrofit	100% Retrofit
Expected Annual Restoration Cost (Million $)	4.70	3.76	1.33
Restoration Cost Reduction Rate	/	20%	72%

However, whether the seismic retrofit measure is cost-effective should be evaluated by considering the other benefits obtained from the bridge retrofit and the cost spent on the retrofit work, which will be discussed in the following two chapters.

Chapter 7 Social Cost Estimation

7.1 Daily Social Cost

7.1.1 Daily Social Cost under no Retrofit Condition

Based on the methodology introduced in Chapter 5, the daily social cost associated with the dysfunction of the highway transportation network due to an earthquake event can be estimated based on simulation of bridge damage states and traffic assignment in the damaged network. The intrinsic randomness in the nature of the bridge fragility curve requires multiple simulations in evaluating the post-event network performance to obtain reliable expected or average daily social cost. Two types of social cost are considered: drivers' delay cost and opportunity cost. Table 7.1 provides the average daily drivers' delay cost and opportunity cost soon after the occurrence of each of the 48 scenarios described earlier in this report, according to three different assumptions of defining link residual capacity (Table 5.1). The fragility curves of bridges without retrofit were used to obtain these simulation results.

From Table 7.1, it can be seen the assignment of lower link residual capacity to damaged link causes higher drivers' delay and opportunity cost. It can be also observed that the opportunity cost is more sensitive to the change of the link residual capacity than the drivers' delay. For example, in scenario Event No.1, as the criteria changes from high (assumption 1) to low link residual capacity (assumption 3), daily drivers' delay increases by about 2 times, while the opportunity increases by more than 16 times. This trend is observed for all other scenario earthquakes, although the increase ratios are

different in other scenarios. This confirms the significance of the seismic resilience of highway network in the social activity.

The system risk curves in terms of daily social cost are constructed based on the values in Table 7.1 and the annual probabilities of the 47 scenarios. Figures 7.1-7.3 show the system risk curve in term of daily drivers' delay time, daily opportunity cost time and daily social cost time (the sum of travel delay and opportunity cost), respectively.

Table 7.1 Daily Drivers' Delay and Opportunity Cost (without Retrofit)

Event No.	Daily Drivers' Delay (hour)			Daily Opportunity Cost (hour)		
	High	Moderate	Low	High	Moderate	Low
1	5.87E+05	1.20E+06	1.77E+06	3.24E+05	1.65E+06	5.89E+06
2	5.48E+05	1.15E+06	1.82E+06	3.09E+05	1.49E+06	5.46E+06
3	4.38E+05	8.89E+05	1.58E+06	2.62E+05	1.25E+06	4.33E+06
4	2.90E+05	5.42E+05	8.13E+05	1.43E+05	6.44E+05	2.14E+06
5	2.52E+05	5.34E+05	7.77E+05	1.16E+05	4.97E+05	1.56E+06
6	4.14E+05	7.73E+05	1.05E+06	2.18E+05	9.42E+05	2.93E+06
7	1.78E+05	4.72E+05	8.39E+05	4.87E+04	2.94E+05	9.09E+05
8	3.92E+04	1.18E+05	1.58E+05	9.39E+03	4.42E+04	1.39E+05
9	1.54E+05	3.66E+05	6.28E+05	5.09E+04	2.58E+05	9.64E+05
10	5.60E+05	1.08E+06	1.48E+06	2.82E+05	1.31E+06	4.30E+06
11	3.01E+05	6.45E+05	1.03E+06	1.30E+05	6.00E+05	2.19E+06
12	4.34E+05	9.54E+05	1.35E+06	2.17E+05	1.02E+06	3.46E+06
13	4.16E+05	8.85E+05	1.29E+06	2.52E+05	1.18E+06	4.50E+06
14	1.33E+05	2.69E+05	3.98E+05	5.17E+04	1.87E+05	4.93E+05
15	2.18E+05	4.72E+05	5.77E+05	9.59E+04	4.06E+05	1.08E+06
16	3.03E+05	6.53E+05	1.05E+06	1.23E+05	5.97E+05	1.84E+06
17	1.19E+05	2.70E+05	3.14E+05	5.86E+04	2.91E+05	8.73E+05
18	1.63E+05	3.66E+05	6.46E+05	6.49E+04	3.06E+05	9.23E+05
19	7.19E+04	1.55E+05	2.52E+05	4.23E+04	1.81E+05	5.23E+05
20	3.73E+04	1.01E+05	1.42E+05	2.08E+04	9.11E+04	2.34E+05
21	4.21E+04	9.03E+04	1.65E+05	1.15E+04	4.92E+04	2.00E+05
22	2.38E+04	6.87E+04	1.61E+05	8.97E+03	4.25E+04	1.83E+05
23	5.70E+01	5.05E+02	7.95E+03	2.47E+01	2.29E+02	2.11E+03
24	1.91E+03	6.86E+03	2.19E+04	1.24E+03	6.83E+03	1.89E+04
25	0.00E+00	0.00E+00	0.00E+00	0.00E+00	0.00E+00	0.00E+00
26	5.60E+04	1.43E+05	3.52E+05	1.38E+04	8.43E+04	3.47E+05
27	1.18E+05	3.00E+05	5.39E+05	3.42E+04	1.85E+05	7.09E+05
28	1.23E+05	2.64E+05	3.85E+05	2.96E+04	1.24E+05	3.18E+05
29	1.57E+05	2.26E+05	2.98E+05	4.54E+04	1.61E+05	4.56E+05

30	6.15E+04	1.30E+05	1.65E+05	2.16E+04	9.34E+04	2.19E+05
31	3.42E+05	6.82E+05	9.16E+05	1.74E+05	7.15E+05	2.09E+06
32	3.06E+05	6.54E+05	8.15E+05	1.57E+05	6.64E+05	1.88E+06
33	3.94E+05	8.89E+05	1.53E+06	2.00E+05	1.01E+06	3.59E+06
34	2.66E+05	5.47E+05	8.13E+05	1.46E+05	7.01E+05	2.22E+06
35	1.73E+05	3.21E+05	4.71E+05	8.90E+04	3.89E+05	1.13E+06
36	9.23E+04	2.05E+05	2.97E+05	3.63E+04	1.67E+05	5.15E+05
37	1.35E+04	2.99E+04	5.61E+04	4.44E+03	1.97E+04	6.91E+04
38	3.10E+03	2.71E+04	2.26E+04	6.33E+02	6.95E+03	1.93E+04
39	2.77E+03	2.35E+04	8.48E+03	5.02E+02	0.00E+00	7.90E+03
40	1.78E+05	4.72E+05	6.90E+05	6.24E+04	3.13E+05	1.17E+06
41	9.65E+04	2.28E+05	4.05E+05	4.61E+04	1.89E+05	6.18E+05
42	5.05E+05	1.06E+06	1.73E+06	2.77E+05	1.37E+06	4.93E+06
43	6.02E+05	1.15E+06	1.76E+06	3.34E+05	1.57E+06	5.51E+06
44	1.74E+04	4.52E+04	5.11E+04	3.12E+03	8.37E+03	5.37E+04
45	3.25E+04	6.33E+04	1.17E+05	6.67E+03	3.71E+04	1.18E+05
46	1.64E+04	6.37E+04	9.38E+04	3.09E+03	2.20E+04	6.46E+04
47	3.44E+05	6.78E+05	9.73E+05	1.88E+05	8.95E+05	3.16E+06
48	3.31E+05	7.70E+05	1.17E+06	1.55E+05	7.50E+05	2.73E+06

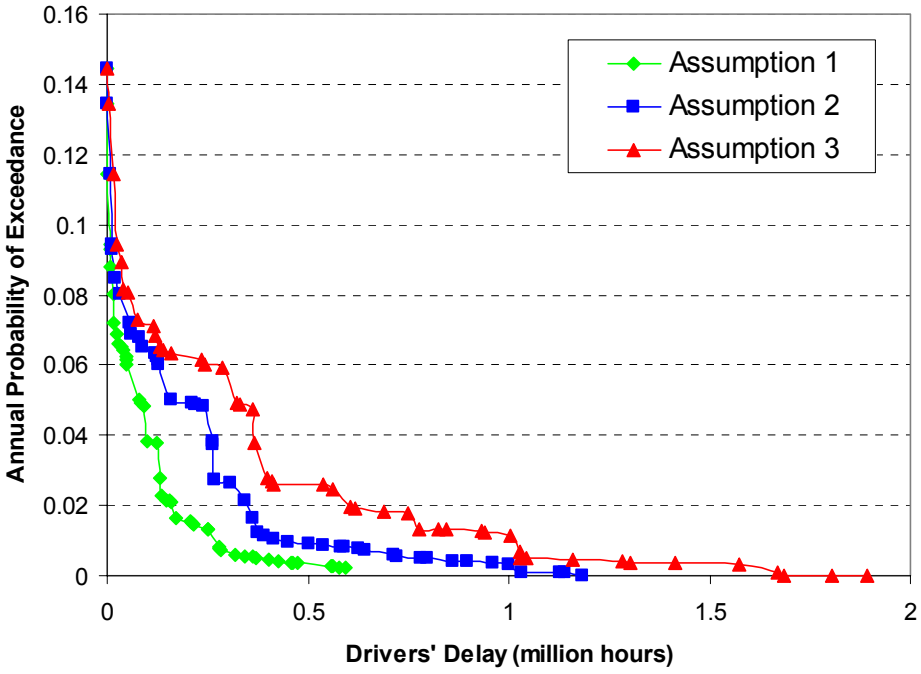

Fig. 7.1 System Risk Curve in terms of Daily Drivers' Delay (without Retrofit)

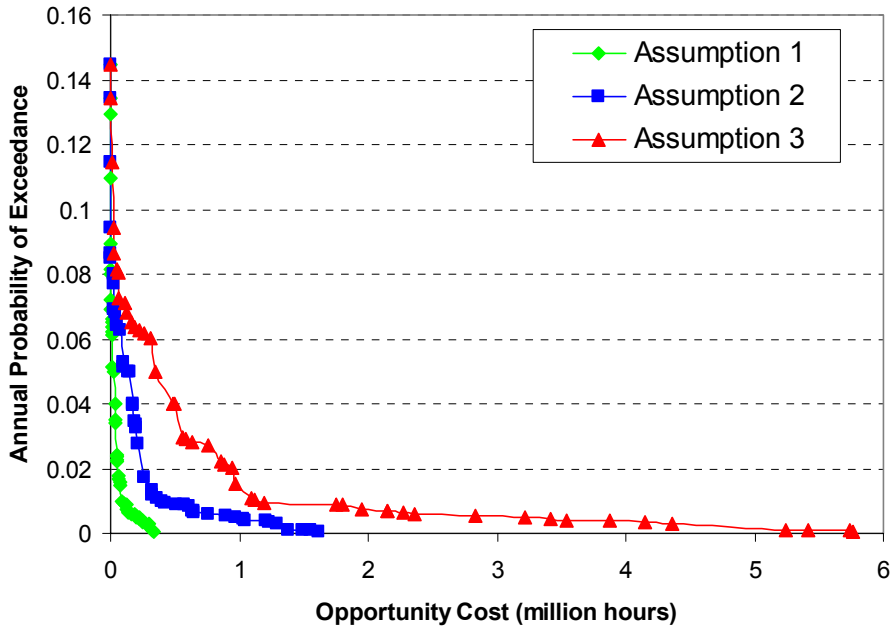

Fig. 7.2 System Risk Curve in terms of Daily Opportunity Cost Time (without Retrofit)

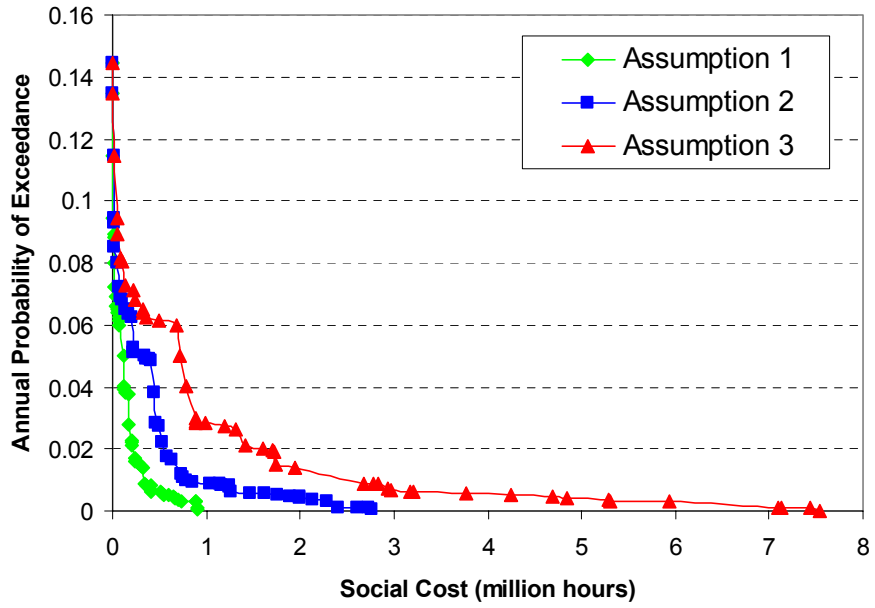

Fig. 7.3 System Risk Curve in terms of Daily Social Cost Time (without Retrofit)

7.1.2 Retrofit effect on Daily Social Cost

To consider the effect of bridge retrofit, two cases: 23% (Case 2) and 100% (Case 3) of the bridges retrofitted, are investigated. In the system performance evaluation, it can be done by using the fragility curves corresponding to retrofit status of each bridge. In Table 7.2 and Table 7.3, the daily travel delay time and opportunity cost resulting from the same set of 48 scenarios are listed. In Both cases, either daily travel time delay or opportunity cost time is smaller than that in no retrofit case (Table 7.1). Much less daily travel time and opportunity cost time in Case 3 than in Case 2, which indicate an obvious benefit from the bridge retrofit measure. The effect of bridge retrofit is further demonstrated in Figure 7.4-6 in plotting the system risk curves of 3 Cases in the same figure.

Table 7.2 Daily Drivers' Delay and Opportunity Cost (23% retrofit)

Event No.	Daily Drivers' Delay (hour)			Daily Opportunity Cost (hour)		
	High	Moderate	Low	High	Moderate	Low
1	5.13E+05	1.07E+06	1.59E+06	2.59E+05	1.32E+06	4.77E+06
2	4.82E+05	1.03E+06	1.76E+06	2.73E+05	1.32E+06	4.78E+06
3	4.02E+05	8.15E+05	1.24E+06	2.17E+05	1.04E+06	3.43E+06
4	2.45E+05	5.17E+05	6.45E+05	1.07E+05	5.48E+05	1.64E+06
5	2.17E+05	5.15E+05	7.48E+05	9.91E+04	4.95E+05	1.49E+06
6	3.45E+05	7.05E+05	1.01E+06	1.85E+05	7.95E+05	2.35E+06
7	1.72E+05	4.26E+05	6.03E+05	4.79E+04	2.40E+05	6.60E+05
8	2.54E+04	8.96E+04	1.35E+05	6.54E+03	3.46E+04	1.22E+05
9	1.26E+05	3.12E+05	5.62E+05	4.25E+04	2.29E+05	8.51E+05
10	5.07E+05	9.62E+05	1.41E+06	2.40E+05	1.12E+06	3.67E+06
11	2.68E+05	5.97E+05	9.48E+05	1.14E+05	5.34E+05	1.90E+06
12	3.79E+05	8.06E+05	1.27E+06	1.77E+05	8.37E+05	2.86E+06
13	3.59E+05	7.16E+05	1.20E+06	1.94E+05	9.21E+05	4.24E+06
14	9.91E+04	2.09E+05	3.03E+05	3.59E+04	1.32E+05	3.54E+05
15	1.77E+05	3.69E+05	4.78E+05	7.41E+04	3.12E+05	8.57E+05
16	2.41E+05	5.72E+05	9.00E+05	1.00E+05	4.74E+05	1.53E+06
17	1.01E+05	2.12E+05	3.05E+05	5.39E+04	2.53E+05	7.48E+05
18	1.41E+05	3.11E+05	5.85E+05	5.66E+04	2.41E+05	7.56E+05
19	6.10E+04	1.42E+05	2.40E+05	3.48E+04	1.52E+05	4.75E+05

20	3.29E+04	7.87E+04	1.26E+05	1.42E+04	5.75E+04	1.68E+05
21	4.06E+04	7.64E+04	1.34E+05	1.06E+04	3.74E+04	1.36E+05
22	1.84E+04	7.61E+04	1.54E+05	8.38E+03	4.25E+04	1.31E+05
23	0.00E+00	6.49E+02	1.96E+03	8.08E+00	1.64E+02	4.81E+02
24	1.48E+03	5.66E+03	1.73E+04	8.13E+02	4.35E+03	1.64E+04
25	0.00E+00	0.00E+00	0.00E+00	0.00E+00	0.00E+00	0.00E+00
26	4.78E+04	1.14E+05	3.19E+05	1.26E+04	6.71E+04	2.80E+05
27	1.07E+05	2.49E+05	5.13E+05	3.05E+04	1.62E+05	6.70E+05
28	8.39E+04	2.18E+05	3.36E+05	2.03E+04	8.52E+04	2.85E+05
29	1.47E+05	2.14E+05	2.55E+05	4.00E+04	1.60E+05	3.92E+05
30	3.60E+04	1.06E+05	1.62E+05	2.02E+04	8.90E+04	2.03E+05
31	2.98E+05	6.03E+05	7.63E+05	1.44E+05	5.91E+05	1.62E+06
32	2.88E+05	5.78E+05	7.08E+05	1.27E+05	5.42E+05	1.57E+06
33	3.56E+05	8.35E+05	1.36E+06	1.77E+05	8.59E+05	3.11E+06
34	2.17E+05	4.82E+05	7.73E+05	1.22E+05	5.89E+05	1.84E+06
35	1.34E+05	2.62E+05	3.85E+05	7.35E+04	3.03E+05	9.46E+05
36	8.80E+04	1.75E+05	2.63E+05	3.04E+04	1.29E+05	4.04E+05
37	1.18E+04	2.90E+04	5.39E+04	4.02E+03	1.79E+04	6.84E+04
38	2.60E+02	5.29E+03	2.01E+04	2.27E+02	1.62E+03	1.68E+04
39	4.54E+03	1.17E+04	4.09E+03	2.86E+02	0.00E+00	3.07E+03
40	1.56E+05	3.66E+05	6.56E+05	5.03E+04	2.80E+05	1.10E+06
41	7.62E+04	2.23E+05	3.62E+05	3.89E+04	1.65E+05	4.86E+05
42	4.41E+05	9.75E+05	1.68E+06	2.54E+05	1.19E+06	4.32E+06
43	4.92E+05	1.07E+06	1.72E+06	2.85E+05	1.36E+06	5.06E+06
44	1.02E+04	2.72E+04	4.62E+04	2.28E+03	1.36E+03	4.45E+04
45	2.80E+04	4.75E+04	1.18E+05	6.24E+03	2.98E+04	1.16E+05
46	1.27E+04	4.24E+04	7.85E+04	2.99E+03	1.81E+04	6.28E+04
47	2.79E+05	5.79E+05	7.91E+05	1.52E+05	6.82E+05	2.33E+06
48	2.93E+05	6.23E+05	1.05E+06	1.25E+05	5.87E+05	2.14E+06

Table 7.3 Daily Drivers' Delay and Opportunity Cost (100% Retrofit)

Event No.	Daily Drivers' Delay (hour)			Daily Opportunity Cost (hour)		
	High	Moderate	Low	High	Moderate	Low
1	1.09E+05	3.59E+05	6.24E+05	4.09E+04	2.38E+05	7.28E+05
2	1.88E+05	4.82E+05	8.99E+05	8.09E+04	4.91E+05	1.40E+06
3	9.84E+04	2.90E+05	5.15E+05	5.30E+04	2.67E+05	9.67E+05
4	2.64E+04	1.68E+05	3.04E+05	1.51E+04	1.14E+05	4.07E+05
5	1.65E+04	5.74E+04	2.77E+05	1.93E+04	4.58E+04	3.04E+05
6	1.40E+05	2.76E+05	5.18E+05	6.84E+04	2.16E+05	6.83E+05
7	1.97E+04	4.87E+04	1.63E+05	1.14E+04	2.44E+04	1.66E+05
8	0.00E+00	3.73E+03	1.53E+04	2.06E+02	3.59E+03	0.00E+00
9	4.18E+04	1.40E+05	3.07E+05	1.34E+04	7.02E+04	3.46E+05
10	2.00E+05	4.89E+05	9.11E+05	8.59E+04	3.47E+05	1.25E+06
11	8.55E+04	2.27E+05	3.54E+05	3.22E+04	1.59E+05	4.19E+05
12	1.62E+05	4.23E+05	5.96E+05	6.81E+04	2.80E+05	7.22E+05

13	1.21E+04	1.14E+05	4.36E+05	3.01E+04	1.09E+05	7.20E+05
14	2.72E+04	6.57E+04	1.32E+05	8.90E+03	3.11E+04	9.43E+04
15	7.65E+04	1.83E+05	2.84E+05	2.78E+04	1.13E+05	3.12E+05
16	9.30E+04	2.92E+05	7.24E+05	3.84E+04	1.48E+05	4.04E+05
17	3.12E+04	3.86E+04	1.30E+05	1.54E+04	2.89E+04	1.47E+05
18	2.64E+04	5.72E+04	2.14E+05	1.03E+04	3.45E+04	2.13E+05
19	3.11E+03	2.21E+04	4.39E+04	5.85E+03	1.99E+04	6.42E+04
20	8.62E+03	1.10E+04	2.14E+04	1.37E+03	2.00E+04	3.36E+04
21	4.76E+03	7.35E+03	2.74E+04	4.62E+02	6.09E+03	2.41E+04
22	5.48E+02	2.46E+03	5.03E+03	1.16E+03	7.92E+03	8.30E+03
23	0.00E+00	0.00E+00	0.00E+00	3.00E+00	3.00E+00	3.00E+00
24	0.00E+00	0.00E+00	0.00E+00	2.40E+01	3.35E+02	3.00E+00
25	0.00E+00	0.00E+00	0.00E+00	0.00E+00	0.00E+00	0.00E+00
26	1.32E+04	3.21E+04	1.43E+05	3.17E+03	1.21E+04	1.09E+05
27	4.66E+04	1.20E+05	3.42E+05	1.18E+04	5.48E+04	3.25E+05
28	2.65E+04	6.85E+04	1.15E+05	5.93E+03	2.04E+04	6.20E+04
29	1.83E+04	1.00E+05	1.22E+05	7.63E+03	4.65E+04	1.32E+05
30	2.64E+03	7.66E+03	4.11E+04	6.72E+03	1.05E+04	3.88E+04
31	1.34E+05	2.71E+05	3.89E+05	5.21E+04	1.60E+05	5.64E+05
32	1.18E+05	1.99E+05	3.58E+05	4.22E+04	1.30E+05	4.57E+05
33	1.34E+05	3.76E+05	5.71E+05	5.77E+04	2.55E+05	1.06E+06
34	3.40E+04	1.51E+05	4.33E+05	2.80E+04	1.32E+05	4.74E+05
35	1.24E+04	7.23E+04	1.54E+05	1.31E+04	5.49E+04	1.67E+05
36	1.07E+04	2.78E+04	6.41E+04	5.64E+03	2.56E+04	6.29E+04
37	4.33E+03	1.06E+04	2.71E+04	1.28E+03	4.84E+03	2.85E+04
38	8.78E+02	1.17E+03	3.30E+03	3.98E+01	2.51E+01	1.59E+01
39	0.00E+00	0.00E+00	0.00E+00	0.00E+00	0.00E+00	0.00E+00
40	4.16E+04	1.57E+05	4.25E+05	1.34E+04	8.85E+04	3.86E+05
41	9.91E+03	5.22E+04	4.37E+04	6.16E+03	3.51E+04	5.20E+04
42	2.03E+05	4.85E+05	8.11E+05	9.94E+04	4.17E+05	1.59E+06
43	1.88E+05	4.79E+05	9.01E+05	1.07E+05	5.03E+05	1.70E+06
44	1.44E+03	2.34E+03	3.35E+03	0.00E+00	0.00E+00	0.00E+00
45	5.20E+03	1.28E+04	4.14E+04	1.96E+03	6.03E+03	3.85E+04
46	7.30E+03	1.32E+04	1.82E+03	3.90E+02	4.21E+03	6.95E+03
47	5.86E+04	1.98E+05	3.75E+05	3.38E+04	1.49E+05	4.55E+05
48	7.81E+04	2.79E+05	5.36E+05	3.69E+04	1.99E+05	7.32E+05

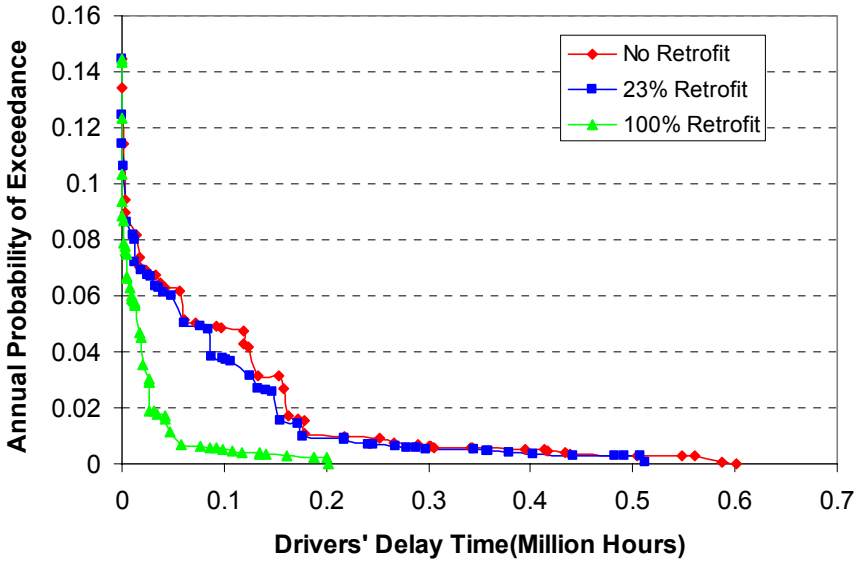

a) Daily Drivers' Delay

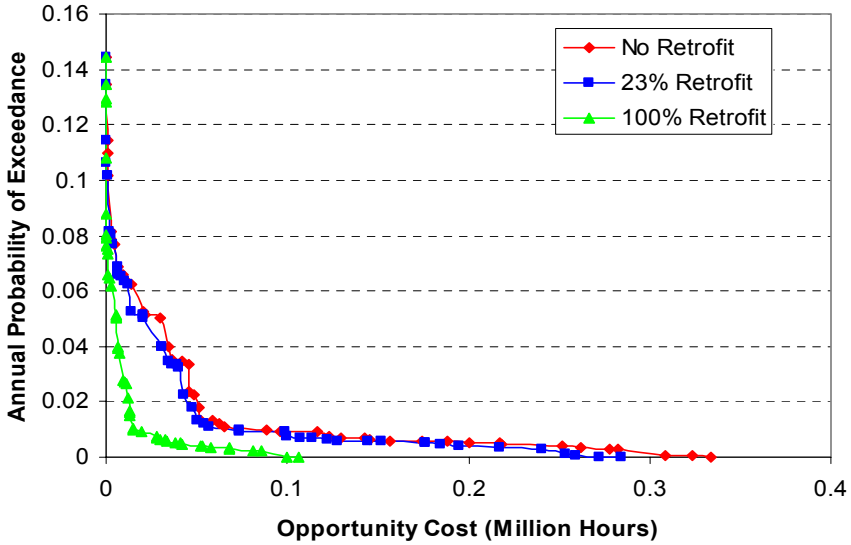

b) Daily Opportunity Cost

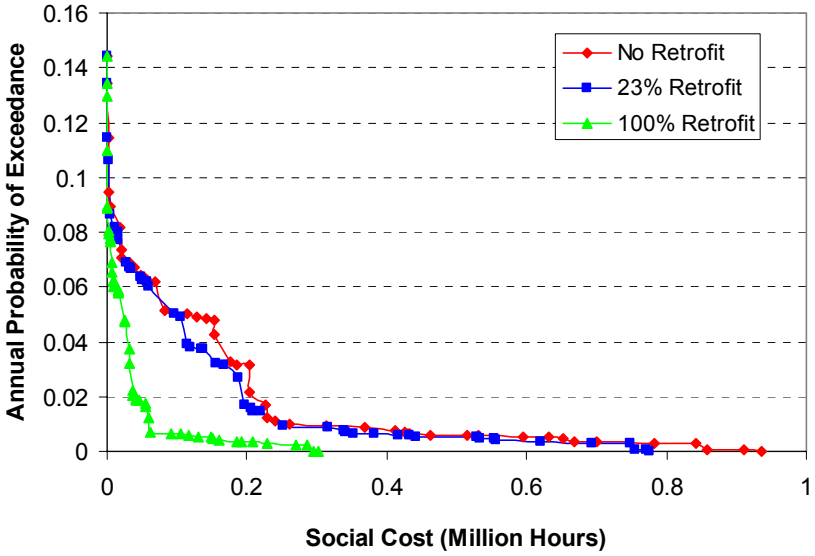

c) Daily Social Cost

Fig. 7.4 Effect of Retrofit on System Risk Curve (High Link Residual Capacity)

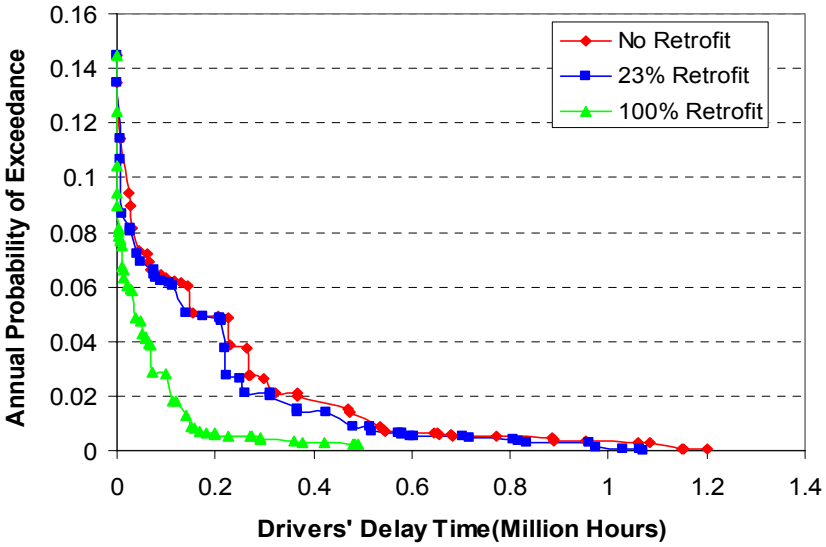

a) Daily Drivers' Delay

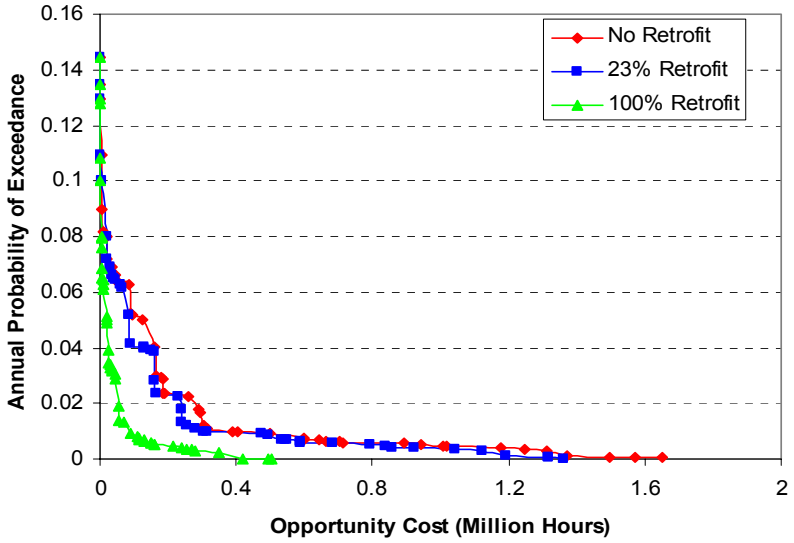

b) Daily Opportunity Cost

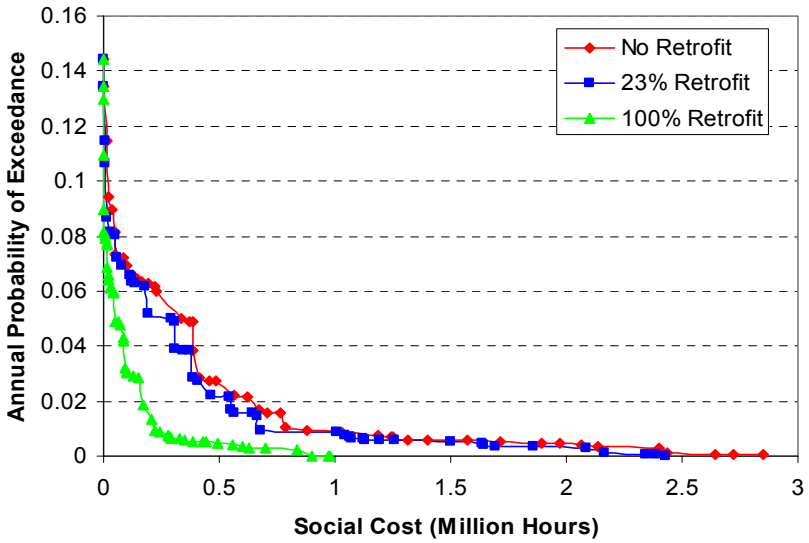

c) Daily Social Cost

Fig. 7.5 Effect of Retrofit on System Risk Curve (Moderate Link Residual Capacity)

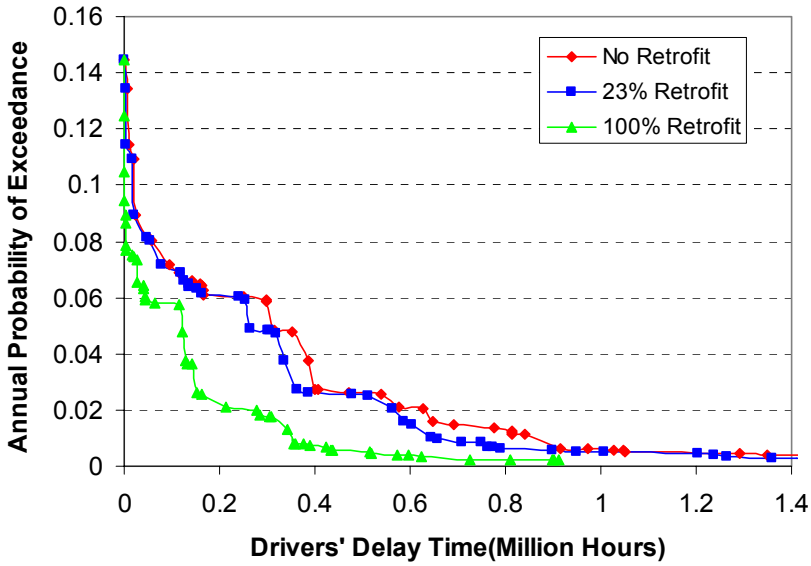

a) Daily Drivers' Delay

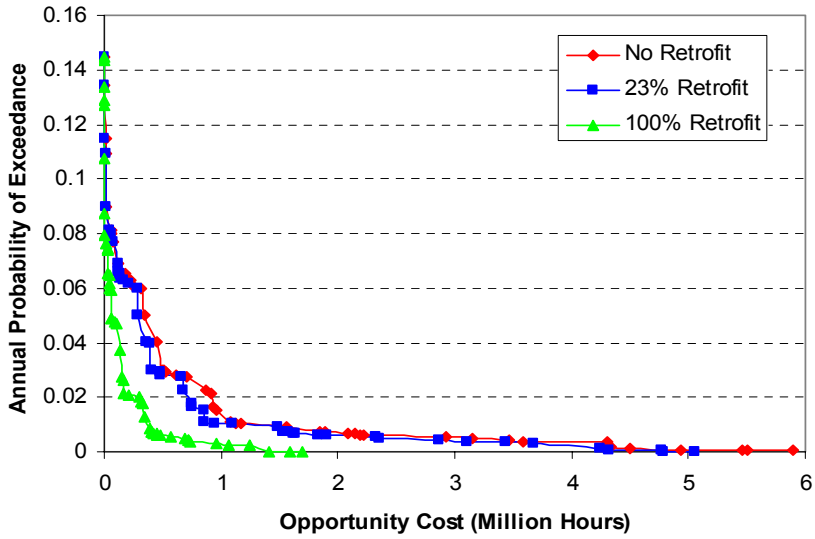

b) Daily Opportunity Cost

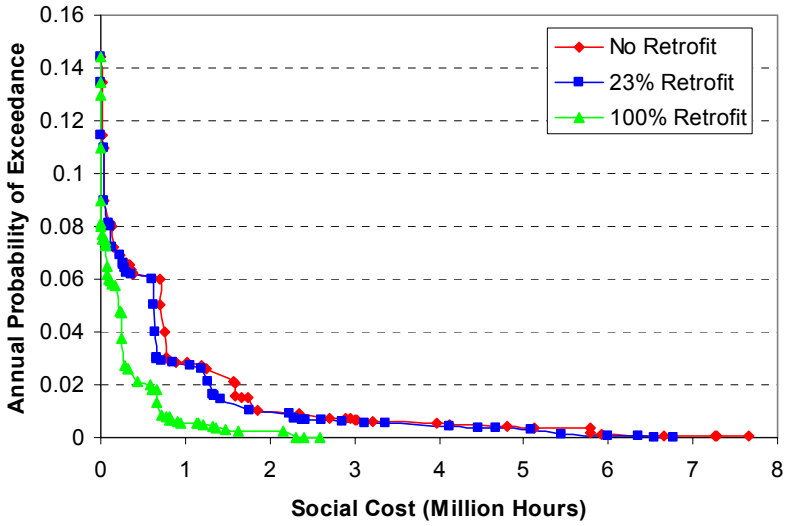

c) Daily Social Cost

Fig. 7.6 Effect of Retrofit on System Risk Curve (Low Link Residual Capacity)

7.2 System Restoration

7.2.1 System Restoration based on Bridge Repair Process

In section 7.1, the social cost at Day 0 (The day following the occurrence of an earthquake) is estimated. However, the social cost will continue to exist till the network and the social activity restore to its pre-event level. It would be necessary to integrate the daily social cost (over the time over which it persists) in order to evaluate the total social cost. Notably, the drivers' delay is not constant over the time it persists. Repair efforts improve the state of damage of the network, thus decreasing drivers' delay with time if the trip demand does not change. In this connection, this research accounts for bridge repair process. Unfortunately, this is quite difficult, because, it seems there exist little consistent and systematic processes according to which repair is conducted, and little

documentation is available on the priorities selected for repair. Highway repair is conducted by and large using the best judgment of the engineers and management involved, and hence this process cannot be easily modeled. Nonetheless, a model is developed for this simulation to provide some numerical insight to the problem.

In this research, the repair process is modeled as below. The time to completion of repair for travels ($t_{i,\min}$ and $t_{i,\max}$) in which i = 1, 2, 3 and 4 represent minor, moderate, major and collapse state of damage, respectively. For example, we postulate that $t_{i,\min}$=10 days and $t_{i,\max}$=150 days for a bridge that sustained a state of minor damage requires most optimistically 10 days and most pessimistically 150 days to complete repair and in between those two values, (see Fig.7.7). Also, it is postulated that chances are uniformly distributed for completion. Values of $t_{i,\min}$ and $t_{i,\max}$ given for i=2,3,4 are:

i=2	$t_{i,\min}$ = 20 days	$t_{i,\max}$=200 days
i=3	$t_{i,\min}$ = 60 days	$t_{i,\max}$=250 days
i=4	$t_{i,\min}$=75 days	$t_{i,\max}$=300 days

It is noted that the size and importance of bridges are not factored in this simplistic analysis, which are subject of future study.

Note that the functions do not necessarily assume that all bridges have the potential to start being repaired on Day 0, nor do they assume that the slopes (daily probabilities of repair), are the same. The choice of the parameters of the optimistic and pessimistic repair scenarios, (essentially, the earliest and latest days a bridge of a given damage state can be repaired), are left to the best judgment of those developing the model. It is important to note that there exist numerous different ways that the repair of

the system could have been probabilistically modeled. For instance, link flow data could have been used to estimate the priorities for bridge repair. The method used here is chosen for a pair of reasons: first, because there seems to exist a set of data to support the assumed correlation model between the damage state of a bridge and the amount of time of completion, and second, for simplicity of the model that provides the ease for Monte Carlo simulation analysis (Shinozuka et al., 2003a).

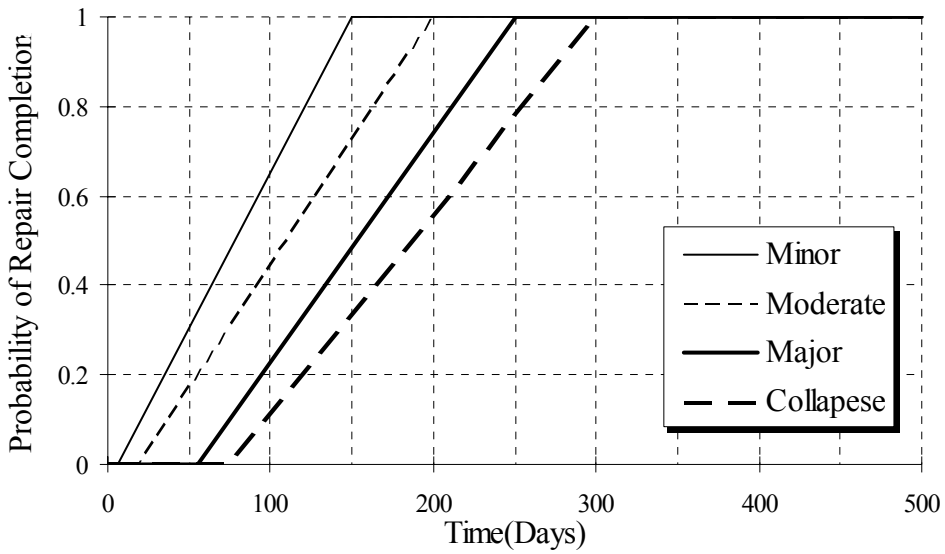

Fig.7.7 Probability Distribution Functions of Repair Completion Date

The repair process is simulated by Monte Carlo technique. Day 0 represents the day of the earthquake – when the system has the greatest extent of damage. The data available includes the damage state of each bridge, as well as the damage state of link and the Drivers' Delay. The bridge damage data is the relevant information for performing the repair simulation. This is done by considering each bridge one at a time. Based on the bridge's damage state, one can use a random number generator to decide when the

bridge repair is completed. As of this date, a repaired bridge shifts from its previous damage state directly to the no damage state, and its record is modified to reflect that change. This process is the repeated for every bridge in this study region. The result shows daily progress of bridge repair completion and corresponding improvement of network function.

7.2.2 System Restoration based on Bridge Functionality Restoration Process

In HAZUS99 (FEMA 1999), the bridge functionality restoration process is modeled by a normal cumulative distribution function for each of the four bridge damage states: minor, moderate, extensive (major) and complete (collapse). Table 7.4 provides the mean and standard deviation values of the four restoration functions corresponding to the four damage states of bridge, and the four restoration curves are plotted in Figure 7.8. Obviously, more severely damaged bridges need more time (long mean recovery time) to recover. In this research, this model will be also used to simulate the highway network system restoration. Different from the method introduced in 7.2.1, the restoration begins day 1 for all damaged bridges and each bridge improves its functionally continuously. In addition, all the bridges with the same initial damage state follow the same functionality restoration process. Assuming that the link residual capacity ratio is determined by the bridge in the link with the lowest percentage of functionality determined by this process at each day, we run integrated traffic assignment model in the network with updated link capacities to obtain the daily drivers' delay and opportunity cost.

Table 7.4 Restoration Function for Highway Bridges (after ATC-13, 1985)

Damage State	Mean (Days)	Sigma (Days)
Minor	0.6	0.6
Moderate	2.5	2.7
Extensive	75.0	42.0
Complete	230	110.0

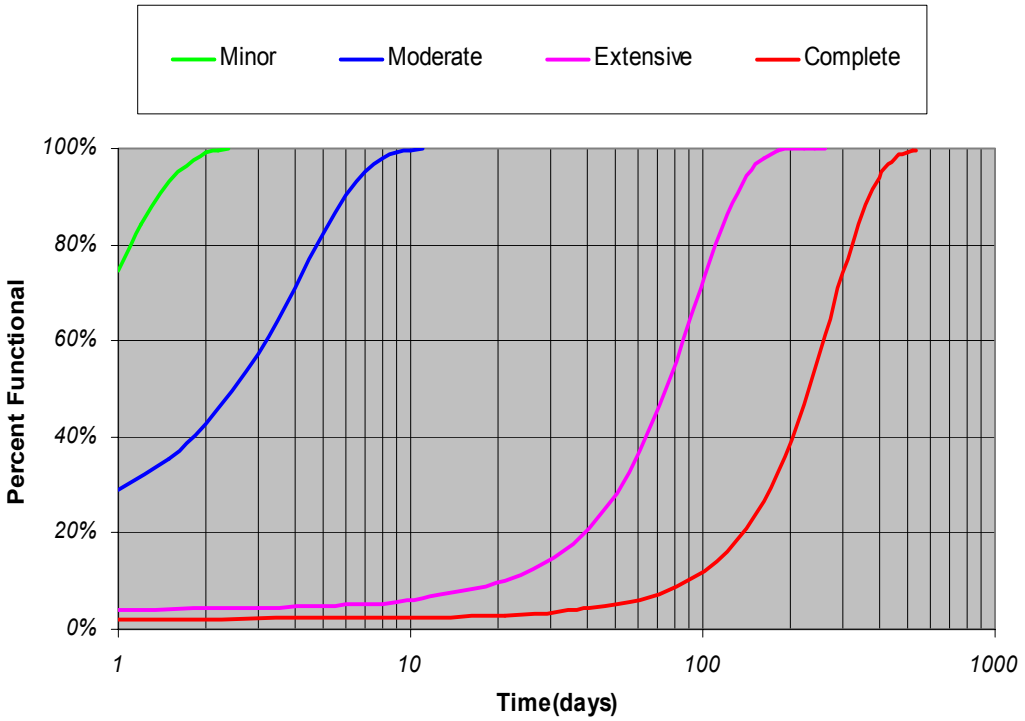

Fig 7.8 Restoration Curves for Highway Bridges (after ATC-13, 1985)

7.2.3 OD Recovery

As described in Chapter 5, the integrated traffic assignment model also considers the trip reduction due to the building damages resulting from an earthquake. This OD change due to trip reduction has its maximum value soon after the earthquake (Day 0). This change, however, is not permanent. As the post-event reconstruction actions (for example, repair work of the damaged buildings, bridges, and etc.) proceed, more people

will be willing to travel (going back to work, going to school, shopping and etc.) as before. How the OD of each trip type will gradually recover to its pre-earthquake level over time is very complicated. Though it seems that the recovery rate relates to both the initial damage status of buildings and the functionality recovery of the damaged buildings and facilities, its modeling is very difficult. However, each of the six trips is assumed in this study to be linearly going back to its pre-earthquake level depending on MMI value of the zone (Appendix B) for simplicity.

7.2.4 System Restoration Curves

Based on the simulated "improved" bridge damage status and new trip demand considering OD recovery, the integrated traffic assignment analysis is performed again to obtain both daily drivers' delay and opportunity cost at any specific time point after an event. When this analysis is repeated for a series of time points after the earthquake, a system restoration curve could be constructed to reflect the daily social cost change over the restoration period.

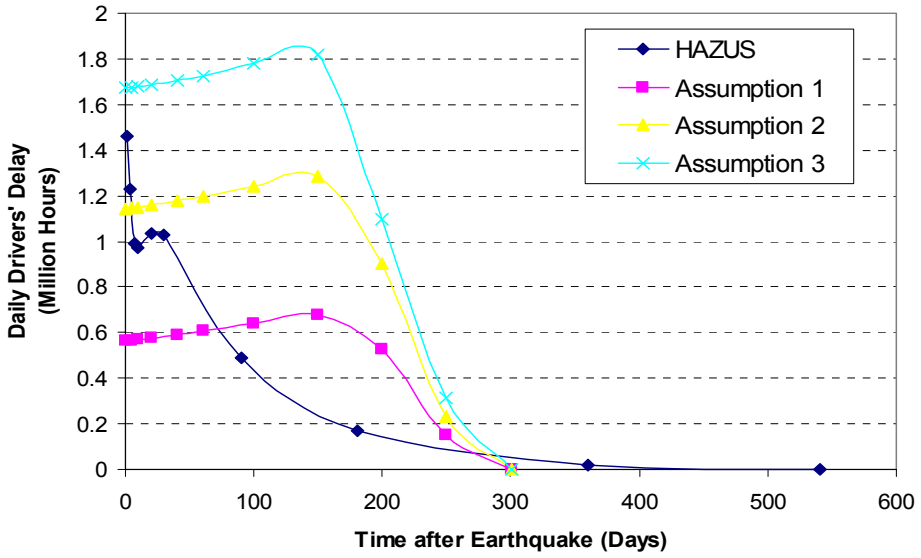

Fig. 7.9 System Restoration Curves After Elysian Park M7.1 (no Retrofit)

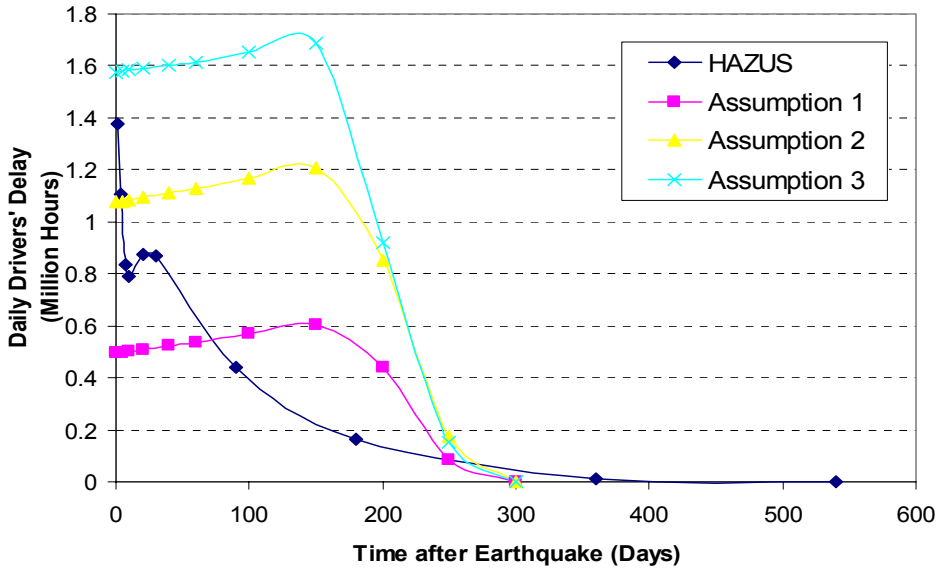

Fig. 7.10 System Recovery Curves After Elysian Park M7.1 (23% Retrofit)

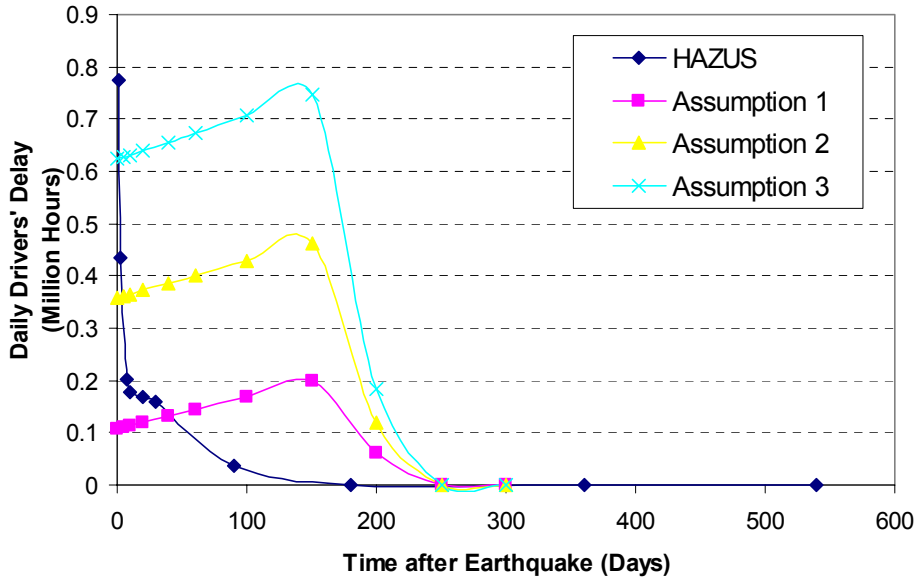

Fig. 7.11 System Recovery Curves After Elysian Park M7.1 (100% Retrofit)

Figures 7.9-7.11 give system recovery curves after the study highway network (no, 23% and 100% retrofit) is struck by scenario No. 1: Elysian Park M7.1. Though the daily opportunity cost is decreasing over the whole recovery period, the daily drivers' delay increase somewhat in the first 150 days and then gradually decreases to 0 regardless of the assumption made for link residual capacity. This is not surprising, since in the early days after the earthquake, the effect of bridge repair work on the improvement of the system performance cannot catch up with that of the gradually increasing trip demand in the network due to OD recovery. Again, the influence of the link residual capacity assumption is quite insignificant on the system restoration. It is noted the HAZUS restoration assumption results in considerably different restoration pattern.

The integration of daily time cost over the whole restoration period will give the total drivers' delay and opportunity cost time. Similarly, the recovery curves could be constructed for all the other scenario earthquakes (developed in computational scheme for ensuing benefit analysis, but not shown here).

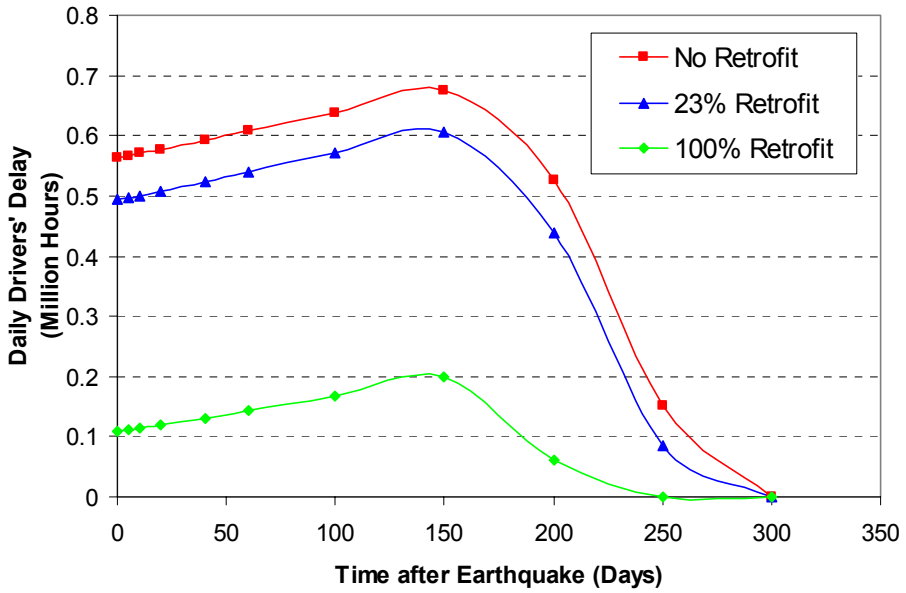

Fig. 7.12 Retrofit Effect on System Restoration Curve (Elysian Park 7.1, High Link Residual Capacity)

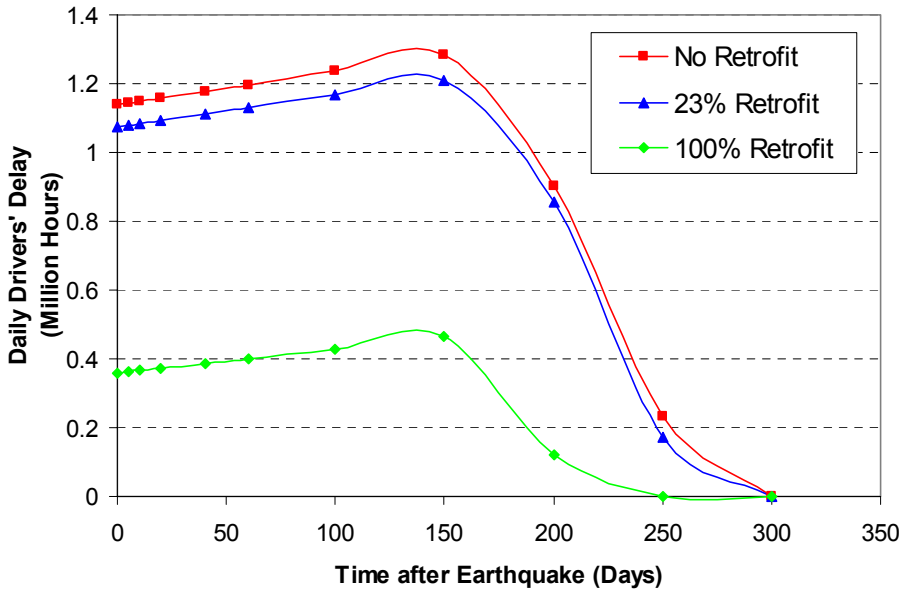

Fig. 7.13 Retrofit Effect on System Restoration Curve (Elysian Park 7.1 Moderate Link Residual Capacity)

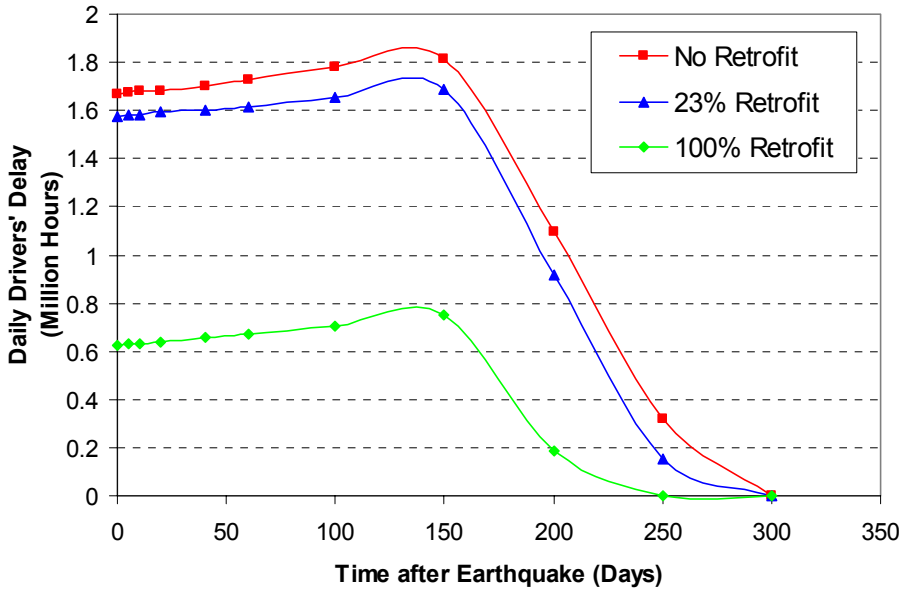

Fig. 7.14 Retrofit Effect on System Recovery Curve (Elysian Park 7.1, Low Link Residual Capacity)

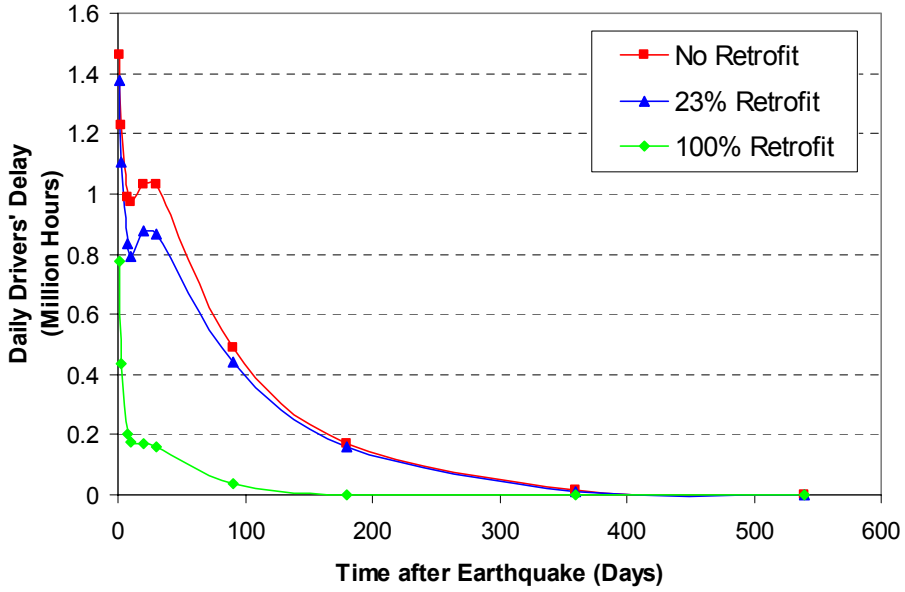

Fig. 7.15 Retrofit Effect on System Restoration Curve (Elysian Park 7.1, HAZUS)

Figs 7.11-7.15 demonstrate the retrofit effect on the system restoration curves under different assumptions for link residual capacity (Table 5.1). The benefit from the retrofit is obvious: the enclosed area (total cost) decreases as more bridges are retrofitted before the event.

Table 7.5-7.8 list the total drivers' delay and opportunity cost for all the 48 scenario earthquakes in three retrofit cases.

Table 7.5 Total Drivers' Delay and Opportunity Cost (no retrofit)

Event No.	Drivers' Delay (hour)				Opportunity Cost (hour)			
	High	Moderate	Low	HAZUS	High	Moderate	Low	HAZUS
1	1.44E+08	2.71E+08	3.78E+08	1.26E+08	7.34E+07	3.42E+08	1.18E+09	2.84E+08
2	1.55E+08	2.99E+08	4.39E+08	1.68E+08	6.98E+07	3.44E+08	1.25E+09	4.28E+08
3	1.09E+08	2.09E+08	3.49E+08	1.04E+08	5.29E+07	2.66E+08	8.10E+08	1.96E+08
4	6.72E+07	1.34E+08	1.55E+08	4.94E+07	2.80E+07	1.35E+08	4.52E+08	9.38E+07
5	7.32E+07	1.48E+08	2.36E+08	4.79E+07	2.54E+07	1.27E+08	3.58E+08	7.49E+07
6	9.78E+07	1.98E+08	2.27E+08	1.03E+08	4.87E+07	2.12E+08	6.02E+08	2.07E+08
7	6.27E+07	9.63E+07	2.15E+08	3.19E+07	1.55E+07	4.65E+07	1.93E+08	8.46E+07
8	8.82E+06	2.46E+07	3.45E+07	3.44E+06	1.65E+06	9.33E+06	7.44E+06	8.57E+06
9	4.05E+07	8.77E+07	1.88E+08	4.93E+07	1.07E+07	5.82E+07	2.15E+08	9.19E+07
10	1.63E+08	2.56E+08	3.86E+08	1.48E+08	6.30E+07	2.77E+08	9.45E+08	4.44E+08
11	7.24E+07	1.62E+08	2.42E+08	7.96E+07	2.68E+07	1.35E+08	4.61E+08	1.75E+08
12	1.20E+08	2.38E+08	3.13E+08	1.17E+08	4.69E+07	2.23E+08	7.37E+08	2.29E+08
13	1.14E+08	1.85E+08	2.61E+08	8.67E+07	5.11E+07	2.50E+08	8.40E+08	2.03E+08
14	3.44E+07	4.63E+07	8.91E+07	2.34E+07	1.04E+07	2.84E+07	9.52E+07	1.65E+07
15	5.31E+07	1.06E+08	1.43E+08	4.78E+07	2.08E+07	8.32E+07	2.25E+08	5.26E+07
16	7.25E+07	1.22E+08	2.20E+08	6.71E+07	2.49E+07	1.07E+08	3.63E+08	8.90E+07
17	3.36E+07	6.15E+07	7.17E+07	2.19E+07	1.48E+07	6.75E+07	1.74E+08	3.09E+07
18	4.48E+07	9.48E+07	1.22E+08	3.35E+07	1.40E+07	7.95E+07	1.76E+08	3.25E+07
19	2.15E+07	3.70E+07	5.34E+07	1.29E+07	8.71E+06	3.74E+07	1.24E+08	1.65E+07
20	9.88E+06	2.75E+07	2.80E+07	5.87E+06	3.51E+06	2.04E+07	4.62E+07	7.17E+06
21	1.15E+07	1.77E+07	3.18E+07	5.85E+06	2.73E+06	9.38E+06	3.44E+07	5.14E+06
22	1.20E+07	2.27E+07	3.70E+07	6.25E+06	2.51E+06	1.16E+07	3.34E+07	7.14E+06
23	7.48E+04	2.15E+05	6.03E+05	3.63E+04	6.51E+03	9.90E+04	1.10E+05	3.16E+04
24	9.74E+05	1.60E+06	3.02E+06	5.84E+05	3.66E+05	8.72E+05	1.99E+06	5.19E+05
25	0.00E+00	3.09E+06	8.57E+06	1.19E+04	0.00E+00	5.32E+05	0.00E+00	6.31E+03
26	1.17E+07	2.98E+07	8.73E+07	2.06E+07	2.70E+06	1.63E+07	7.68E+07	3.23E+07
27	3.20E+07	7.45E+07	1.37E+08	4.32E+07	7.72E+06	4.40E+07	1.70E+08	8.01E+07
28	2.13E+07	5.83E+07	7.67E+07	1.80E+07	4.62E+06	2.96E+07	6.35E+07	1.19E+07
29	3.90E+07	5.55E+07	6.80E+07	2.11E+07	8.78E+06	4.48E+07	1.07E+08	1.08E+08

30	1.23E+07	2.74E+07	4.86E+07	7.86E+06	3.14E+06	1.84E+07	5.05E+07	8.94E+06
31	9.20E+07	1.71E+08	1.85E+08	7.12E+07	4.01E+07	1.64E+08	4.60E+08	1.09E+08
32	8.45E+07	1.35E+08	1.90E+08	6.92E+07	3.53E+07	1.21E+08	4.07E+08	1.03E+08
33	1.24E+08	2.13E+08	3.08E+08	1.10E+08	4.44E+07	2.31E+08	7.66E+08	2.49E+08
34	6.58E+07	1.47E+08	2.00E+08	5.77E+07	2.78E+07	1.49E+08	4.92E+08	9.88E+07
35	3.79E+07	8.54E+07	9.26E+07	2.82E+07	1.76E+07	8.75E+07	2.38E+08	4.16E+07
36	2.46E+07	4.86E+07	6.84E+07	1.36E+07	9.05E+06	3.44E+07	1.08E+08	1.75E+07
37	4.22E+06	7.70E+06	1.45E+07	4.78E+06	7.86E+05	4.31E+06	1.22E+07	5.64E+06
38	1.90E+06	1.02E+07	6.61E+06	2.71E+05	1.77E+05	1.90E+06	3.97E+06	1.96E+05
39	0.00E+00	3.50E+06	4.10E+06	6.69E+04	0.00E+00	5.96E+05	4.22E+06	2.88E+04
40	5.36E+07	1.01E+08	1.75E+08	5.77E+07	1.40E+07	7.03E+07	2.46E+08	1.12E+08
41	3.37E+07	6.01E+07	8.89E+07	1.75E+07	1.07E+07	3.93E+07	1.12E+08	2.71E+07
42	1.25E+08	2.60E+08	4.56E+08	1.37E+08	5.96E+07	3.09E+08	1.16E+09	3.81E+08
43	1.53E+08	2.90E+08	4.14E+08	1.61E+08	7.13E+07	3.29E+08	1.18E+09	4.53E+08
44	4.57E+06	3.04E+06	1.56E+07	1.16E+06	5.34E+05	5.89E+05	1.32E+07	4.09E+06
45	6.53E+06	1.65E+07	2.53E+07	5.38E+06	1.11E+06	6.88E+06	2.49E+07	6.87E+06
46	5.55E+06	1.26E+07	2.46E+07	1.82E+06	8.55E+05	3.77E+06	2.23E+07	4.14E+06
47	8.54E+07	1.70E+08	2.35E+08	6.69E+07	4.32E+07	1.84E+08	6.48E+08	1.37E+08
48	8.77E+07	1.96E+08	3.18E+08	9.37E+07	3.28E+07	1.60E+08	5.74E+08	1.72E+08

Table 7.6 Total Drivers' Delay and Opportunity Cost (23% retrofit)

Event No.	Drivers' Delay (hour)				Opportunity Cost (hour)			
	High	Moderate	Low	HAZUS	High	Moderate	Low	HAZUS
1	1.24E+08	2.53E+08	3.40E+08	1.11E+08	5.47E+07	2.76E+08	8.74E+08	2.21E+08
2	1.21E+08	2.54E+08	4.19E+08	1.44E+08	5.36E+07	2.88E+08	1.05E+09	3.25E+08
3	9.17E+07	2.06E+08	3.29E+08	9.25E+07	4.61E+07	2.35E+08	6.94E+08	1.65E+08
4	5.75E+07	1.02E+08	1.50E+08	3.86E+07	2.41E+07	1.01E+08	3.60E+08	5.65E+07
5	5.63E+07	1.14E+08	1.65E+08	3.98E+07	2.22E+07	1.09E+08	2.92E+08	5.26E+07
6	9.70E+07	1.57E+08	2.12E+08	7.90E+07	4.00E+07	1.82E+08	5.48E+08	1.40E+08
7	4.59E+07	7.34E+07	1.10E+08	2.84E+07	9.51E+06	3.47E+07	1.14E+08	4.26E+07
8	8.45E+06	1.24E+07	8.82E+06	2.44E+06	1.17E+06	4.71E+06	2.58E+07	6.18E+06
9	3.82E+07	7.76E+07	1.41E+08	4.33E+07	1.05E+07	4.59E+07	1.93E+08	8.03E+07
10	1.39E+08	2.52E+08	3.21E+08	1.22E+08	4.90E+07	2.38E+08	6.97E+08	3.67E+08
11	6.41E+07	1.51E+08	2.40E+08	6.65E+07	2.18E+07	1.22E+08	4.05E+08	1.26E+08
12	1.13E+08	1.98E+08	2.93E+08	1.04E+08	4.04E+07	1.90E+08	5.98E+08	1.83E+08
13	1.05E+08	1.73E+08	2.59E+08	7.00E+07	4.11E+07	2.04E+08	6.28E+08	1.40E+08
14	2.54E+07	4.49E+07	4.70E+07	1.80E+07	7.66E+06	2.47E+07	5.11E+07	1.41E+07
15	4.61E+07	9.48E+07	1.35E+08	3.24E+07	1.54E+07	6.97E+07	2.07E+08	3.26E+07
16	6.36E+07	1.10E+08	2.18E+08	5.94E+07	2.20E+07	9.67E+07	3.12E+08	6.32E+07
17	2.20E+07	5.02E+07	5.73E+07	2.09E+07	1.02E+07	5.23E+07	1.46E+08	2.59E+07
18	3.44E+07	7.30E+07	1.22E+08	3.23E+07	1.23E+07	4.74E+07	1.25E+08	3.00E+07
19	1.78E+07	3.60E+07	3.13E+07	1.13E+07	7.67E+06	2.88E+07	6.56E+07	1.49E+07

20	7.86E+06	2.36E+07	1.30E+07	3.73E+06	3.51E+06	1.47E+07	2.66E+07	4.49E+06
21	9.74E+06	1.33E+07	2.83E+07	5.58E+06	1.76E+06	4.47E+06	3.13E+07	4.52E+06
22	7.63E+06	2.14E+07	2.38E+07	5.98E+06	2.42E+06	1.10E+07	1.98E+07	6.76E+06
23	0.00E+00	3.90E+04	5.17E+05	9.33E+03	1.25E+03	3.86E+03	1.53E+05	1.06E+04
24	1.78E+05	1.50E+06	9.06E+05	4.43E+05	1.00E+05	3.64E+05	7.21E+05	4.22E+05
25	0.00E+00	1.12E+04	5.47E+05	1.05E+03	0.00E+00	0.00E+00	0.00E+00	2.46E+02
26	1.12E+07	2.87E+07	7.26E+07	1.64E+07	1.98E+06	1.11E+07	6.05E+07	2.22E+07
27	3.05E+07	6.12E+07	1.26E+08	3.96E+07	7.50E+06	3.70E+07	1.25E+08	7.16E+07
28	2.06E+07	4.72E+07	6.66E+07	1.67E+07	4.46E+06	2.20E+07	4.50E+07	1.13E+07
29	2.89E+07	5.10E+07	6.34E+07	1.90E+07	8.27E+06	3.94E+07	8.47E+07	5.48E+07
30	1.17E+07	2.29E+07	3.39E+07	6.31E+06	2.41E+06	1.60E+07	4.29E+07	7.91E+06
31	8.59E+07	1.26E+08	1.50E+08	6.40E+07	2.94E+07	1.03E+08	3.33E+08	8.02E+07
32	7.23E+07	1.25E+08	1.52E+08	6.39E+07	2.76E+07	9.18E+07	2.53E+08	8.56E+07
33	1.21E+08	1.95E+08	3.05E+08	9.55E+07	3.88E+07	1.77E+08	7.22E+08	1.83E+08
34	5.66E+07	1.19E+08	1.98E+08	4.12E+07	2.58E+07	1.35E+08	3.75E+08	7.25E+07
35	3.40E+07	7.24E+07	8.51E+07	2.02E+07	1.60E+07	5.86E+07	1.64E+08	2.63E+07
36	2.21E+07	4.33E+07	5.91E+07	1.36E+07	6.20E+06	2.51E+07	8.21E+07	1.43E+07
37	2.49E+06	7.50E+06	1.18E+07	3.30E+06	7.73E+05	4.20E+06	1.60E+07	4.11E+06
38	2.27E+05	2.74E+06	1.29E+06	2.52E+05	3.04E+04	6.26E+05	5.86E+05	1.77E+05
39	0.00E+00	6.38E+04	0.00E+00	4.72E+04	0.00E+00	0.00E+00	0.00E+00	2.15E+04
40	4.49E+07	9.12E+07	1.49E+08	5.15E+07	1.26E+07	6.46E+07	2.12E+08	9.57E+07
41	2.22E+07	3.22E+07	6.48E+07	1.65E+07	9.30E+06	2.12E+07	8.08E+07	2.68E+07
42	1.20E+08	2.57E+08	3.90E+08	1.23E+08	5.32E+07	2.71E+08	8.99E+08	2.88E+08
43	1.35E+08	2.79E+08	4.13E+08	1.43E+08	5.92E+07	2.97E+08	1.01E+09	3.56E+08
44	2.06E+06	1.21E+06	3.93E+06	6.90E+05	2.92E+05	2.73E+05	3.08E+06	3.34E+06
45	4.52E+06	1.47E+07	2.50E+07	5.30E+06	9.76E+05	6.06E+06	2.07E+07	6.41E+06
46	2.40E+06	1.20E+07	1.30E+07	1.39E+06	5.34E+05	3.34E+06	1.04E+07	1.56E+06
47	8.51E+07	1.37E+08	1.83E+08	5.30E+07	3.20E+07	1.49E+08	4.85E+08	8.89E+07
48	6.55E+07	1.50E+08	2.55E+08	7.91E+07	2.32E+07	1.21E+08	4.58E+08	1.40E+08

Table 7.7 Total Drivers' Delay and Opportunity Cost (100% retrofit)

Event No.	Drivers' Delay (hour)				Opportunity Cost (hour)			
	High	Moderate	Low	HAZUS	High	Moderate	Low	HAZUS
1	3.09E+07	7.91E+07	1.23E+08	1.50E+07	8.07E+06	4.36E+07	1.30E+08	1.36E+07
2	5.03E+07	1.13E+08	1.99E+08	3.54E+07	1.54E+07	9.83E+07	2.58E+08	4.32E+07
3	2.93E+07	6.81E+07	1.12E+08	1.06E+07	1.04E+07	5.19E+07	1.80E+08	1.31E+07
4	1.03E+07	3.77E+07	6.29E+07	3.85E+06	2.79E+06	2.19E+07	7.53E+07	5.01E+06
5	1.26E+07	1.87E+07	6.08E+07	1.16E+06	3.79E+06	8.01E+06	5.60E+07	3.79E+06
6	3.95E+07	6.16E+07	1.19E+08	1.81E+07	1.33E+07	3.95E+07	1.27E+08	1.75E+07
7	9.95E+06	1.42E+07	3.79E+07	1.14E+06	2.13E+06	4.19E+06	3.27E+07	4.63E+06
8	2.07E+05	2.66E+06	8.69E+05	0.00E+00	3.74E+04	6.26E+05	0.00E+00	9.26E+05
9	1.22E+07	3.38E+07	7.32E+07	1.07E+07	2.52E+06	1.38E+07	7.15E+07	1.72E+07
10	5.80E+07	1.14E+08	2.09E+08	2.71E+07	1.70E+07	6.80E+07	2.47E+08	6.29E+07

11	2.50E+07	5.46E+07	8.16E+07	1.27E+07	6.13E+06	3.16E+07	7.99E+07	2.00E+07
12	4.21E+07	9.60E+07	1.22E+08	2.83E+07	1.33E+07	5.47E+07	1.32E+08	2.99E+07
13	1.61E+07	3.40E+07	1.01E+08	2.90E+06	5.56E+06	1.92E+07	1.38E+08	9.43E+06
14	6.74E+06	1.44E+07	2.74E+07	2.79E+06	1.60E+06	5.71E+06	1.78E+07	1.24E+06
15	2.02E+07	4.17E+07	6.07E+07	5.78E+06	5.33E+06	2.21E+07	5.96E+07	4.02E+06
16	2.82E+07	7.13E+07	1.63E+08	1.37E+07	7.81E+06	2.85E+07	7.46E+07	7.36E+06
17	9.06E+06	9.37E+06	2.90E+07	1.24E+06	3.02E+06	4.92E+06	2.74E+07	1.19E+06
18	1.03E+07	1.56E+07	4.74E+07	4.18E+06	1.87E+06	6.03E+06	3.97E+07	2.68E+06
19	2.29E+06	7.42E+06	1.07E+07	3.65E+05	1.11E+06	3.77E+06	1.15E+07	1.32E+06
20	8.19E+05	4.55E+06	6.33E+06	0.00E+00	2.41E+05	4.06E+06	6.37E+06	6.98E+05
21	1.56E+05	2.80E+06	6.32E+06	0.00E+00	7.99E+04	1.14E+06	4.23E+06	4.04E+05
22	8.69E+05	3.12E+06	3.25E+06	0.00E+00	2.21E+05	1.47E+06	1.42E+06	7.51E+05
23	0.00E+00	6.87E+03	2.70E+04	0.00E+00	4.50E+01	4.50E+01	4.50E+01	2.76E+02
24	4.98E+03	7.23E+04	4.99E+05	0.00E+00	3.17E+03	5.49E+04	4.50E+01	5.37E+03
25	0.00E+00	0.00E+00	0.00E+00	0.00E+00	0.00E+00	0.00E+00	0.00E+00	0.00E+00
26	3.51E+06	7.16E+06	3.36E+07	3.40E+06	6.09E+05	2.31E+06	2.27E+07	3.81E+06
27	1.06E+07	2.63E+07	7.75E+07	1.06E+07	2.33E+06	1.09E+07	6.80E+07	1.30E+07
28	7.24E+06	1.46E+07	2.38E+07	3.16E+06	1.11E+06	3.72E+06	1.15E+07	1.81E+06
29	5.76E+06	2.17E+07	2.56E+07	2.75E+06	1.42E+06	9.21E+06	2.42E+07	7.81E+06
30	2.13E+06	3.89E+06	1.01E+07	0.00E+00	1.47E+06	1.92E+06	6.92E+06	5.10E+05
31	3.44E+07	5.80E+07	8.39E+07	1.11E+07	1.01E+07	2.88E+07	1.07E+08	9.76E+06
32	2.95E+07	4.27E+07	7.43E+07	1.24E+07	8.07E+06	2.32E+07	8.46E+07	7.75E+06
33	3.87E+07	8.86E+07	1.21E+08	1.54E+07	1.12E+07	4.84E+07	2.00E+08	2.05E+07
34	1.65E+07	3.86E+07	1.03E+08	6.22E+06	5.30E+06	2.45E+07	8.68E+07	7.86E+06
35	6.63E+06	1.77E+07	3.33E+07	6.26E+05	2.39E+06	1.00E+07	3.15E+07	2.37E+06
36	5.20E+06	8.41E+06	1.50E+07	3.72E+05	1.07E+06	5.01E+06	1.15E+07	1.78E+06
37	1.45E+06	2.60E+06	6.42E+06	1.78E+05	2.17E+05	8.42E+05	5.92E+06	4.25E+05
38	3.10E+04	2.19E+04	0.00E+00	0.00E+00	6.75E+03	3.98E+03	2.26E+03	4.30E+03
39	0.00E+00	3.76E+03	0.00E+00	0.00E+00	0.00E+00	0.00E+00	0.00E+00	1.57E+02
40	1.19E+07	3.61E+07	9.83E+07	1.41E+07	2.46E+06	1.74E+07	8.04E+07	1.87E+07
41	2.89E+06	1.49E+07	1.27E+07	0.00E+00	1.18E+06	6.40E+06	9.17E+06	1.99E+06
42	5.63E+07	1.13E+08	1.74E+08	2.56E+07	1.96E+07	8.12E+07	3.09E+08	3.74E+07
43	5.53E+07	1.14E+08	1.93E+08	2.34E+07	2.09E+07	9.87E+07	3.22E+08	3.39E+07
44	2.78E+05	2.81E+05	9.79E+05	0.00E+00	0.00E+00	2.60E+02	1.14E+05	7.12E+03
45	1.87E+06	3.28E+06	9.13E+06	6.02E+05	3.54E+05	1.06E+06	7.96E+06	9.56E+05
46	2.94E+05	3.56E+05	1.44E+06	0.00E+00	6.73E+04	7.62E+05	1.29E+06	8.35E+04
47	2.33E+07	5.01E+07	8.13E+07	3.37E+06	6.54E+06	2.80E+07	8.25E+07	6.04E+06
48	2.57E+07	6.47E+07	1.24E+08	1.46E+07	7.18E+06	3.89E+07	1.44E+08	2.45E+07

7.3 Economic Loss Estimation Related to System Social Cost Time

The cost rate assigned to drivers' delay (the value of time) is very controversial. Some agencies adopt their own rates based on regional economic data and other agencies

have used nationally published data. Also, the cost rate usually varies depending on the vehicle type (e.g. Automobile, Single Unit Trucks or Combination Unit Trucks). In this study, the cost rate is taken as the most current average time value in the great Los Angles area obtained from RAND California Traffic Congestion Statistics (2004) with source data originally from the Texas Transportation Institute, The Texas A&M University System. Based on this statistics, the value of time is $13.45 per hour in 2002 value and it will be $14.39 per hour in 2005 value if taking the inflation factor into account. The economic loss due to travel delay resulting from an earthquake event is therefore calculated by multiplying total travel delay time by this local unit time value.

The economic loss due to opportunity cost time, however, is estimated by considering the local average hourly wage. According to Department of Labor, the average hourly wage is $ 19.32 in the May of 2003 in the area of Los Angeles – Long Beach. Table 7.8-7.10 provides the average total economic loss due to system social cost in time for all the 48 scenario earthquakes in the 3 retrofit cases.

Table 7.8 Economic Loss due to Network Dysfunction (No Retrofit) (Million Dollars)

Event No.	High	Moderate	Low	HAZUS	Event No...	High	Moderate	Low	HAZUS
1	3483.9	10501.9	28264.0	7297.6	25	0.0	54.8	123.3	0.3
2	3577.2	10945.9	30438.7	10684.8	26	220.5	742.6	2739.4	920.9
3	2584.2	8149.9	20675.2	5291.4	27	609.3	1922.0	5258.9	2168.9
4	1509.0	4532.0	10963.0	2522.7	28	395.5	1409.7	2331.2	489.8
5	1543.9	4594.8	10304.4	2136.3	29	730.7	1663.7	3037.6	2398.8
6	2348.9	6947.6	14899.2	5472.3	30	238.2	749.2	1675.8	285.9
7	1200.9	2285.1	6814.8	2093.2	31	2097.4	5614.7	11557.1	3127.1
8	158.8	533.9	639.9	215.0	32	1898.6	4277.9	10600.5	2993.2
9	790.2	2387.0	6865.1	2486.1	33	2641.5	7525.3	19227.4	6397.8
10	3566.6	9039.4	23808.5	10705.1	34	1484.2	4983.8	12379.7	2739.5
11	1559.6	4946.6	12387.9	4522.9	35	885.7	2920.7	5924.8	1211.0
12	2633.6	7734.8	18745.2	6121.0	36	528.3	1364.8	3080.4	533.4
13	2632.7	7496.0	19985.2	5161.7	37	75.8	194.0	443.9	177.8
14	696.8	1214.6	3122.5	656.0	38	30.7	183.2	171.8	7.7

15	1166.3	3127.1	6396.3	1703.9	39	0.0	61.8	140.5	1.5
16	1524.9	3818.6	10181.4	2685.0	40	1042.0	2810.1	7263.9	2989.2
17	770.5	2189.3	4398.5	911.8	41	692.2	1624.0	3451.8	775.6
18	915.1	2900.5	5158.2	1109.5	42	2952.0	9715.1	28890.2	9340.4
19	477.9	1254.8	3168.6	503.7	43	3578.3	10527.7	28718.6	11070.6
20	210.0	789.8	1295.1	223.0	44	76.1	55.1	477.9	95.7
21	218.8	435.6	1121.1	183.5	45	115.3	370.5	845.3	210.2
22	221.4	551.7	1177.6	227.9	46	96.3	254.5	785.8	106.2
23	1.2	5.0	10.8	1.1	47	2062.3	6004.5	15900.2	3599.2
24	21.1	39.9	81.8	18.4	48	1896.0	5919.1	15674.5	4679.3

Table 7.9 Economic Loss due to Network Dysfunction (23% Retrofit) (Million Dollars)

Event No.	High	Moderate	Low	HAZUS	Event No.	High	Moderate	Low	HAZUS
1	2840.3	8981.4	21780.4	5874.5	25	0.0	0.2	7.9	0.0
2	2782.8	9218.2	26398.1	8362.0	26	200.1	628.4	2213.6	665.1
3	2210.3	7490.1	18145.5	4518.4	27	584.1	1594.5	4233.5	1952.3
4	1293.4	3404.6	9112.3	1647.7	28	382.6	1105.6	1829.0	458.6
5	1238.8	3736.9	8015.2	1588.2	29	575.9	1496.1	2548.0	1331.9
6	2167.7	5769.8	13630.0	3840.2	30	215.3	638.2	1315.9	243.7
7	843.5	1726.9	3785.7	1232.1	31	1803.6	3800.5	8590.7	2470.9
8	144.3	269.7	626.3	154.5	32	1573.5	3576.4	7073.7	2572.6
9	752.2	2003.4	5747.8	2175.2	33	2491.6	6222.5	18334.0	4917.3
10	2944.2	8219.9	18078.1	8838.2	34	1313.9	4322.7	10101.7	1992.9
11	1344.0	4518.7	11286.0	3382.2	35	799.2	2173.8	4393.8	799.7
12	2412.9	6506.3	15764.0	5033.9	36	438.3	1108.7	2437.1	472.3
13	2301.2	6434.7	15862.0	3706.9	37	50.8	189.1	477.5	126.9
14	513.5	1123.3	1662.5	531.0	38	3.9	51.6	29.8	7.0
15	961.4	2710.5	5937.7	1096.6	39	0.0	0.0	0.9	1.1
16	1339.9	3452.8	9158.6	2076.4	40	888.7	2559.3	6240.2	2590.4
17	514.6	1733.5	3640.6	800.8	41	499.2	872.9	2494.7	754.8
18	731.4	1966.2	4168.7	1043.9	42	2758.1	8923.2	22987.0	7333.6
19	404.9	1073.9	1717.1	449.8	43	3093.5	9761.5	25542.5	8943.8
20	180.9	623.6	700.3	140.3	44	35.3	22.7	116.1	74.5
21	174.2	277.7	1011.8	167.7	45	83.8	329.2	758.7	200.0
22	156.5	520.2	725.7	216.6	46	44.8	237.1	388.7	50.1
23	0.0	0.6	10.4	0.3	47	1842.6	4848.4	12004.8	2481.1
24	4.5	28.6	27.0	14.5	48	1390.8	4506.0	12506.5	3848.8

Table 7.10 Economic Loss due to System Dysfunction (100% Retrofit)
(Million Dollars)

Event. No.	High	Moderate	Low	HAZUS	Event No.	High	Moderate	Low	HAZUS
1	600.6	1981.6	4286.5	477.4	25	0.0	0.0	0.0	0.0
2	1021.4	3523.9	7847.2	1343.4	26	62.3	147.7	921.8	122.7
3	622.9	1982.5	5096.0	405.4	27	197.8	588.4	2427.6	404.1
4	202.7	966.8	2359.8	152.1	28	125.6	282.7	563.4	80.5
5	253.8	424.0	1957.0	90.0	29	110.2	490.1	837.3	190.5
6	826.2	1649.7	4173.9	598.7	30	59.1	93.0	278.6	9.9
7	184.3	285.1	1178.2	105.9	31	689.9	1391.6	3274.2	348.9
8	3.7	50.4	12.5	17.9	32	580.5	1063.1	2704.3	328.5
9	224.7	752.5	2435.0	487.7	33	772.2	2211.0	5601.0	617.6
10	1163.5	2953.1	7777.3	1604.1	34	340.3	1029.8	3164.4	241.3
11	478.6	1395.2	2718.9	569.5	35	141.7	448.5	1086.6	54.8
12	862.8	2437.9	4303.3	983.4	36	95.6	217.8	439.3	39.7
13	339.0	859.6	4126.0	223.8	37	25.1	53.6	206.7	10.8
14	127.9	317.7	737.2	64.1	38	0.0	0.0	0.4	0.1
15	394.0	1028.5	2024.8	160.9	39	0.0	0.0	0.1	0.0
16	556.2	1577.1	3790.3	339.3	40	219.3	857.0	2967.5	564.4
17	188.8	230.0	946.5	41.0	41	64.3	337.9	360.6	38.4
18	184.7	341.3	1449.6	111.9	42	1189.9	3191.3	8476.0	1091.4
19	54.4	179.6	376.3	30.7	43	1198.6	3546.3	9002.6	990.5
20	16.4	143.9	214.1	13.5	44	4.0	4.0	16.3	0.1
21	3.8	62.3	172.7	7.8	45	33.8	67.7	285.2	27.1
22	16.8	73.4	74.1	14.5	46	5.5	19.8	45.7	1.6
23	0.0	0.1	0.4	0.0	47	461.8	1262.2	2763.4	165.3
24	0.1	2.1	7.2	0.1	48	509.0	1682.8	4565.8	683.2

Chapter 8 Cost-Benefit Analysis

8.1 Introduction

Engineering significance of the seismically retrofitted bridges in the highway network is obvious, as demonstrated in Chapter 2. After retrofit, the number of damaged bridges is significantly reduced, and hence the bridge repair cost is much lower than before retrofit is implemented (Chapter 6). The social cost, consisting of the sum of travel delay time and opportunity cost resulting from the network dysfunction, also decreases substantially due to the enhanced seismic resilience of the highway transportation network after the retrofit.

These benefits from the retrofit measures, however, are achieved at the expense of the "investment" involved in retrofitting the bridges. Whether the retrofit measures applied in the bridges of the highway network is cost-effective, therefore, should be evaluated quantitatively on the basis of a cost-benefit analysis taking these cost and benefit factors into consideration.

8.2 Retrofit Cost

The bridge retrofit cost varies from one bridge to another, and involves many factors including structural type, material used, importance, location, design code followed and retrofit measures implemented. Lack of solid statistical data, the retrofit cost of each bridge is assumed to be proportional to its replacement value is expressed as

$$C_R = \sum_{i=1}^{N} C_i * r_i = \sum_{i=1}^{N} C_{Ri} \tag{8.1}$$

Where

C_R = total retrofit cost (in current value)

C_i = replacement value of $i-th$ retrofitted bridge

r_i = retrofit cost ratio

C_{Ri} = retrofit cost of $i-th$ retrofitted bridge

N = total number of retrofitted bridges

Once a bridge is retrofitted, it is assumed that it will possess enhanced seismic performance throughout its residual service period T under normal maintenance. Though the design service time for a highway bridge is normally 75 years, the actual total length of service time is not necessarily equal to this value. In fact, Caltrans bridge inventory in Los Angles and Orange Counties shows that many bridges older than 75 years are still sound and in service. However, for simplicity, T is taken as a constant for all retrofitted bridges and is assumed to be 50 years. At this moment, no accurate model for estimating the remaining service time T of a bridge is available and development of such a model is a subject of future study. T will be used later when we evaluate the total benefit from the bridge retrofit measures over the remaining service life.

8.3 Benefit from Retrofit

8.3.1 Annual Benefit

The annual benefit from retrofit is the sum of annual social cost avoided (consisting of drivers' delay and opportunity cost avoided), and restoration cost avoided for damaged bridges. In Chapter 6, the annual bridge restoration cost in the three retrofit cases are estimated. The annual restoration cost avoided in case 2 (23% retrofit) and case 3 (100% retrofit) can be directly derived from the results in Table 6.6.

The expected annual benefit from retrofit measures in improved network performance, can then be expressed as (Chang, Shinozuka and etc., 2000)

$$\overline{B} = \sum_{i=1}^{N} (L(\overline{S}_0 \mid \overline{Q}_i) - L(\overline{S}_R \mid \overline{Q}_i)) \bullet \overline{p}_i \tag{8.2}$$

Where

N = number of all the scenario earthquakes;

L = social cost due to degradation of network performance;

$\overline{S}_0$ = network performance without retrofit ;

$\overline{S}_R$ = network performance with retrofit;

$\overline{Q}_i = i - th$ scenario earthquake;

$\overline{p}_i$ = annual occurrence probability of $i - th$ scenario earthquake.

The social cost avoided associated with the network performance is the difference between the social cost associated with the network not retrofitted (Case 1) and the cost associated with the network retrofitted (Case 2 and Case 3). These social costs are estimated in Chapter 7. The expected annual benefit is computed then by multiplying the social cost avoided by the annual probability of occurrence associated with each of the probabilistic scenario earthquakes. The set of 47 probabilistic scenario earthquakes again is used in this equation, since they represent the regional seismic hazard as described in Chapter 4. Table 8.1 provides the annual social cost avoided when the regional seismic hazard is approximated by these 47 probabilistic scenario earthquakes.

Table 8.1 Annual Avoided Social Cost (High Link Residual Capacity)

Event No.	Annual Probability	Social Cost Avoided ($)		Expected Annual Social Cost Avoided ($)	
		Case 2	Case 3	Case 2	Case 3
1	0.000728	6.44E+08	2.88E+09	4.69E+05	2.10E+06
2	0.000068	7.94E+08	2.56E+09	5.40E+04	1.74E+05
3	0.000495	3.74E+08	1.96E+09	1.85E+05	9.71E+05
4	0.000495	2.16E+08	1.31E+09	1.07E+05	6.47E+05
5	0.00154	3.05E+08	1.29E+09	4.70E+05	1.99E+06
6	0.00065	1.81E+08	1.52E+09	1.18E+05	9.90E+05
7	0.00485	3.57E+08	1.02E+09	1.73E+06	4.93E+06
8	0.0008	1.45E+07	1.55E+08	1.16E+04	1.24E+05
9	0.004362	3.80E+07	5.66E+08	1.66E+05	2.47E+06
10	0.00208	6.22E+08	2.40E+09	1.29E+06	5.00E+06
11	0.000214	2.16E+08	1.08E+09	4.61E+04	2.31E+05
12	0.00062	2.21E+08	1.77E+09	1.37E+05	1.10E+06
13	0.000312	3.32E+08	2.29E+09	1.03E+05	7.16E+05
14	0.0003	1.83E+08	5.69E+08	5.50E+04	1.71E+05
15	0.0005	2.05E+08	7.72E+08	1.02E+05	3.86E+05
16	0.0003	1.85E+08	9.69E+08	5.55E+04	2.91E+05
17	0.001	2.56E+08	5.82E+08	2.56E+05	5.82E+05
18	0.001	1.84E+08	7.30E+08	1.84E+05	7.30E+05
19	0.001	7.29E+07	4.24E+08	7.29E+04	4.24E+05
20	0.001	2.91E+07	1.94E+08	2.91E+04	1.94E+05
21	0.001	4.46E+07	2.15E+08	4.46E+04	2.15E+05
22	0.0016	6.49E+07	2.05E+08	1.04E+05	3.27E+05
23	0.02	1.18E+06	1.20E+06	2.36E+04	2.40E+04
24	0.02	1.66E+07	2.09E+07	3.32E+05	4.19E+05
25	0.01	0.00E+00	0.00E+00	0.00E+00	0.00E+00
26	0.01	2.04E+07	1.58E+08	2.04E+05	1.58E+06
27	0.005	2.52E+07	4.11E+08	1.26E+05	2.06E+06
28	0.01	1.29E+07	2.70E+08	1.29E+05	2.70E+06
29	0.01	1.55E+08	6.20E+08	1.55E+06	6.20E+06
30	0.0015	2.29E+07	1.79E+08	3.44E+04	2.69E+05
31	0.00015	2.94E+08	1.41E+09	4.41E+04	2.11E+05
32	0.00015	3.25E+08	1.32E+09	4.88E+04	1.98E+05
33	0.0001	1.50E+08	1.87E+09	1.50E+04	1.87E+05
34	0.0005	1.70E+08	1.14E+09	8.51E+04	5.72E+05
35	0.0005	8.65E+07	7.44E+08	4.33E+04	3.72E+05
36	0.0005	9.00E+07	4.33E+08	4.50E+04	2.16E+05
37	0.008	2.50E+07	5.07E+07	2.00E+05	4.06E+05
38	0.008	2.69E+07	3.01E+07	2.15E+05	2.41E+05
39	0.005	0.00E+00	0.00E+00	0.00E+00	0.00E+00

40	0.0011	1.53E+08	8.23E+08	1.69E+05	9.05E+05
41	0.001	1.93E+08	6.28E+08	1.93E+05	6.28E+05
42	0.00005	1.94E+08	1.76E+09	9.69E+03	8.81E+04
43	0.00005	4.85E+08	2.38E+09	2.42E+04	1.19E+05
44	0.0015	4.08E+07	7.21E+07	6.11E+04	1.08E+05
45	0.003	3.15E+07	8.15E+07	9.44E+04	2.45E+05
46	0.003	5.15E+07	9.08E+07	1.55E+05	2.72E+05
47	0.0005	2.20E+08	1.60E+09	1.10E+05	8.00E+05
Total Expected Annual Social Loss Avoided				9.71E+06	4.36E+07

Table 8.2 Annual Social Cost Avoided (Moderate Link Residual Capacity)

Event No.	Annual Probability	Social Cost Avoided ($)		Expected Annual Social Cost Avoided ($)	
		Case 2	Case 3	Case 2	Case 3
1	0.000728	1.52E+09	8.52E+09	1.11E+06	6.20E+06
2	0.000068	1.73E+09	7.42E+09	1.17E+05	5.05E+05
3	0.000495	6.60E+08	6.17E+09	3.27E+05	3.05E+06
4	0.000495	1.13E+09	3.57E+09	5.58E+05	1.76E+06
5	0.00154	8.58E+08	4.17E+09	1.32E+06	6.42E+06
6	0.00065	1.18E+09	5.30E+09	7.66E+05	3.44E+06
7	0.00485	5.58E+08	2.00E+09	2.71E+06	9.70E+06
8	0.0008	2.64E+08	4.83E+08	2.11E+05	3.87E+05
9	0.004362	3.84E+08	1.63E+09	1.67E+06	7.13E+06
10	0.00208	8.20E+08	6.09E+09	1.70E+06	1.27E+07
11	0.000214	4.28E+08	3.55E+09	9.16E+04	7.60E+05
12	0.00062	1.23E+09	5.30E+09	7.62E+05	3.28E+06
13	0.000312	1.06E+09	6.64E+09	3.31E+05	2.07E+06
14	0.0003	9.13E+07	8.97E+08	2.74E+04	2.69E+05
15	0.0005	4.17E+08	2.10E+09	2.08E+05	1.05E+06
16	0.0003	3.66E+08	2.24E+09	1.10E+05	6.72E+05
17	0.001	4.56E+08	1.96E+09	4.56E+05	1.96E+06
18	0.001	9.34E+08	2.56E+09	9.34E+05	2.56E+06
19	0.001	1.81E+08	1.08E+09	1.81E+05	1.08E+06
20	0.001	1.66E+08	6.46E+08	1.66E+05	6.46E+05
21	0.001	1.58E+08	3.73E+08	1.58E+05	3.73E+05
22	0.0016	3.15E+07	4.78E+08	5.03E+04	7.65E+05
23	0.02	4.37E+06	4.91E+06	8.74E+04	9.82E+04
24	0.02	1.13E+07	3.78E+07	2.25E+05	7.56E+05
25	0.01	5.46E+07	5.48E+07	5.46E+05	5.48E+05
26	0.01	1.14E+08	5.95E+08	1.14E+06	5.95E+06
27	0.005	3.27E+08	1.33E+09	1.64E+06	6.67E+06
28	0.01	3.04E+08	1.13E+09	3.04E+06	1.13E+07
29	0.01	1.68E+08	1.17E+09	1.68E+06	1.17E+07
30	0.0015	1.11E+08	6.56E+08	1.67E+05	9.84E+05

31	0.00015	1.81E+09	4.22E+09	2.72E+05	6.33E+05
32	0.00015	7.02E+08	3.21E+09	1.05E+05	4.82E+05
33	0.0001	1.30E+09	5.31E+09	1.30E+05	5.31E+05
34	0.0005	6.61E+08	3.95E+09	3.31E+05	1.98E+06
35	0.0005	7.47E+08	2.47E+09	3.73E+05	1.24E+06
36	0.0005	2.56E+08	1.15E+09	1.28E+05	5.73E+05
37	0.008	4.90E+06	1.40E+08	3.92E+04	1.12E+06
38	0.008	1.32E+08	1.83E+08	1.05E+06	1.46E+06
39	0.005	6.09E+07	6.18E+07	3.05E+05	3.09E+05
40	0.0011	2.51E+08	1.95E+09	2.76E+05	2.15E+06
41	0.001	7.51E+08	1.29E+09	7.51E+05	1.29E+06
42	0.00005	7.92E+08	6.52E+09	3.96E+04	3.26E+05
43	0.00005	7.66E+08	6.98E+09	3.83E+04	3.49E+05
44	0.0015	3.25E+07	5.11E+07	4.87E+04	7.67E+04
45	0.003	4.13E+07	3.03E+08	1.24E+05	9.08E+05
46	0.003	1.74E+07	2.35E+08	5.22E+04	7.04E+05
47	0.0005	1.16E+09	4.74E+09	5.78E+05	2.37E+06
Total Expected Annual Social Cost Avoided				2.71E+07	1.21E+08

Table 8.3 Annual Social Cost Avoided (Low Link Residual Capacity)

Event No.	Annual Probability	Social Cost Avoided ($)		Expected Annual Social Cost Avoided ($)	
		Case 2	Case 3	Case 2	Case 3
1	0.000728	6.48E+09	2.40E+10	4.72E+06	1.75E+07
2	0.000068	4.04E+09	2.26E+10	2.75E+05	1.54E+06
3	0.000495	2.53E+09	1.56E+10	1.25E+06	7.71E+06
4	0.000495	1.85E+09	8.60E+09	9.16E+05	4.26E+06
5	0.00154	2.29E+09	8.35E+09	3.53E+06	1.29E+07
6	0.00065	1.27E+09	1.07E+10	8.25E+05	6.97E+06
7	0.00485	3.03E+09	5.64E+09	1.47E+07	2.73E+07
8	0.0008	1.36E+07	6.27E+08	1.09E+04	5.02E+05
9	0.004362	1.12E+09	4.43E+09	4.87E+06	1.93E+07
10	0.00208	5.73E+09	1.60E+10	1.19E+07	3.33E+07
11	0.000214	1.10E+09	9.67E+09	2.36E+05	2.07E+06
12	0.00062	2.98E+09	1.44E+10	1.85E+06	8.95E+06
13	0.000312	4.12E+09	1.59E+10	1.29E+06	4.95E+06
14	0.0003	1.46E+09	2.39E+09	4.38E+05	7.16E+05
15	0.0005	4.59E+08	4.37E+09	2.29E+05	2.19E+06
16	0.0003	1.02E+09	6.39E+09	3.07E+05	1.92E+06
17	0.001	7.58E+08	3.45E+09	7.58E+05	3.45E+06
18	0.001	9.89E+08	3.71E+09	9.89E+05	3.71E+06
19	0.001	1.45E+09	2.79E+09	1.45E+06	2.79E+06
20	0.001	5.95E+08	1.08E+09	5.95E+05	1.08E+06

21	0.001	1.09E+08	9.48E+08	1.09E+05	9.48E+05
22	0.0016	4.52E+08	1.10E+09	7.23E+05	1.77E+06
23	0.02	3.89E+05	1.04E+07	7.79E+03	2.08E+05
24	0.02	5.49E+07	7.47E+07	1.10E+06	1.49E+06
25	0.01	1.15E+08	1.23E+08	1.15E+06	1.23E+06
26	0.01	5.26E+08	1.82E+09	5.26E+06	1.82E+07
27	0.005	1.03E+09	2.83E+09	5.13E+06	1.42E+07
28	0.01	5.02E+08	1.77E+09	5.02E+06	1.77E+07
29	0.01	4.90E+08	2.20E+09	4.90E+06	2.20E+07
30	0.0015	3.60E+08	1.40E+09	5.40E+05	2.10E+06
31	0.00015	2.97E+09	8.28E+09	4.45E+05	1.24E+06
32	0.00015	3.53E+09	7.90E+09	5.29E+05	1.18E+06
33	0.0001	8.93E+08	1.36E+10	8.93E+04	1.36E+06
34	0.0005	2.28E+09	9.22E+09	1.14E+06	4.61E+06
35	0.0005	1.53E+09	4.84E+09	7.66E+05	2.42E+06
36	0.0005	6.43E+08	2.64E+09	3.22E+05	1.32E+06
37	0.008	1.21E+08	3.14E+08	9.67E+05	2.52E+06
38	0.008	1.42E+08	1.72E+08	1.14E+06	1.37E+06
39	0.005	1.41E+08	1.41E+08	7.03E+05	7.03E+05
40	0.0011	1.02E+09	4.30E+09	1.13E+06	4.73E+06
41	0.001	9.57E+08	3.09E+09	9.57E+05	3.09E+06
42	0.00005	5.90E+09	2.04E+10	2.95E+05	1.02E+06
43	0.00005	3.18E+09	1.97E+10	1.59E+05	9.86E+05
44	0.0015	3.62E+08	4.62E+08	5.43E+05	6.92E+05
45	0.003	8.66E+07	5.60E+08	2.60E+05	1.68E+06
46	0.003	3.97E+08	7.40E+08	1.19E+06	2.22E+06
47	0.0005	3.90E+09	1.31E+10	1.95E+06	6.57E+06
Total Expected Annual Social Cost Avoided				8.77E+07	2.81E+08

Table 8.4 Annual Social Cost Avoided (HAZUS Model)

Event No.	Annual Probability	Social Cost Avoided ($)		Expected Annual Social Cost Avoided ($)	
		Case 2	Case 3	Case 2	Case 3
1	0.000728	1.42E+09	6.82E+09	1.04E+06	4.96E+06
2	0.000068	2.32E+09	9.34E+09	1.58E+05	6.35E+05
3	0.000495	7.73E+08	4.88E+09	3.83E+05	2.42E+06
4	0.000495	8.75E+08	2.37E+09	4.33E+05	1.17E+06
5	0.00154	5.48E+08	2.05E+09	8.44E+05	3.15E+06
6	0.00065	1.63E+09	4.87E+09	1.06E+06	3.17E+06
7	0.00485	8.61E+08	1.99E+09	4.17E+06	9.63E+06
8	0.0008	6.05E+07	1.97E+08	4.84E+04	1.58E+05
9	0.004362	3.11E+08	2.00E+09	1.36E+06	8.71E+06
10	0.00208	1.87E+09	9.10E+09	3.88E+06	1.89E+07
11	0.000214	1.14E+09	3.95E+09	2.44E+05	8.46E+05

12	0.00062	1.09E+09	5.14E+09	6.74E+05	3.18E+06
13	0.000312	1.45E+09	4.94E+09	4.54E+05	1.54E+06
14	0.0003	1.25E+08	5.92E+08	3.75E+04	1.78E+05
15	0.0005	6.07E+08	1.54E+09	3.04E+05	7.71E+05
16	0.0003	6.08E+08	2.34E+09	1.82E+05	7.03E+05
17	0.001	1.11E+08	8.71E+08	1.11E+05	8.71E+05
18	0.001	6.56E+07	9.97E+08	6.56E+04	9.97E+05
19	0.001	5.39E+07	4.73E+08	5.39E+04	4.73E+05
20	0.001	8.26E+07	2.09E+08	8.26E+04	2.09E+05
21	0.001	1.58E+07	1.76E+08	1.58E+04	1.76E+05
22	0.0016	1.13E+07	2.13E+08	1.81E+04	3.41E+05
23	0.02	7.94E+05	1.13E+06	1.59E+04	2.25E+04
24	0.02	3.91E+06	1.83E+07	7.83E+04	3.66E+05
25	0.01	2.73E+05	2.93E+05	2.73E+03	2.93E+03
26	0.01	2.56E+08	7.98E+08	2.56E+06	7.98E+06
27	0.005	2.16E+08	1.76E+09	1.08E+06	8.82E+06
28	0.01	3.12E+07	4.09E+08	3.12E+05	4.09E+06
29	0.01	1.07E+09	2.21E+09	1.07E+07	2.21E+07
30	0.0015	4.22E+07	2.76E+08	6.33E+04	4.14E+05
31	0.00015	6.56E+08	2.78E+09	9.84E+04	4.17E+05
32	0.00015	4.20E+08	2.66E+09	6.31E+04	4.00E+05
33	0.0001	1.48E+09	5.78E+09	1.48E+05	5.78E+05
34	0.0005	7.46E+08	2.50E+09	3.73E+05	1.25E+06
35	0.0005	4.11E+08	1.16E+09	2.06E+05	5.78E+05
36	0.0005	6.11E+07	4.94E+08	3.05E+04	2.47E+05
37	0.008	5.09E+07	1.67E+08	4.08E+05	1.34E+06
38	0.008	6.53E+05	7.61E+06	5.23E+03	6.09E+04
39	0.005	4.26E+05	1.52E+06	2.13E+03	7.58E+03
40	0.0011	3.99E+08	2.42E+09	4.39E+05	2.67E+06
41	0.001	2.08E+07	7.37E+08	2.08E+04	7.37E+05
42	0.00005	2.01E+09	8.25E+09	1.00E+05	4.12E+05
43	0.00005	2.13E+09	1.01E+10	1.06E+05	5.04E+05
44	0.0015	2.12E+07	9.55E+07	3.18E+04	1.43E+05
45	0.003	1.03E+07	1.83E+08	3.08E+04	5.49E+05
46	0.003	5.60E+07	1.05E+08	1.68E+05	3.14E+05
47	0.0005	1.12E+09	3.43E+09	5.59E+05	1.72E+06
Total Expected Annual Social Cost Avoided				3.32E+07	1.19E+08

8.3.2 Total Benefit

The total benefit is the sum of the discounted benefit over the bridge residual service time T. If we assume that the unit time value per hour ($/hour) for delay and

opportunity and unit repair cost ($/ft^2) do not change in the next T years, we will have uniform annual benefit each year as calculated above. The total benefit in present value, however, should take discount rate into account and can be computed by using the formula for uniform series to present value:

$$B = \sum_{n=1}^{N} \frac{\overline{B}}{(1+i)^n} = \overline{B} \bullet \frac{(1+i)^N - 1}{i(1+i)^N} = \overline{B} \bullet F \tag{8.3}$$

Where:

B = total benefit in present value;

$\overline{B}$ = annual benefit (Eq. 8.2);

i = discount rate;

N = time period under consideration

F = Factor for converting uniform series to present worth

Assuming $N = T = 50$ years, discount factor F is computed under different discount rates and given in Table 8.5. These values can be used to calculate the total benefit due to both social and bridge restoration cost avoided.

Table 8.5 Factor for Converting Uniform Series to Present Value

Discount Rate (%)	Discount Factor
3%	25.73
5%	18.26
7%	13.80

8.4 Cost-effectiveness Evaluation

The cost-effectiveness of the retrofit is expressed in terms of the ratio of the present value of the cost avoided to the retrofit cost. Obviously, the larger this ratio, the more cost-effective the retrofit. Table 8.6-8.8 list total retrofit, total social cost avoided

and total bridge restoration cost avoided and evaluate the cost-effectiveness ratios in retrofit Case 2 (current retrofit status with 23 % of all the bridge are retrofitted) and Case 3 (all bridges are retrofitted). We can observe:

(1) As expected, the cost-effectiveness ratio decreases as the discount rate increases, and the cost-effectiveness ratio is dominantly controlled by the selected discount rate.

(2) The cost-effectiveness ratio in terms of bridge restoration cost avoided in case 2 is bigger than in case 3, but the ratios in both cases are much lower than 1 (in fact, less than 0.1). It shows that the retrofit is not cost-effective if it is only for reducing bridge restoration cost.

(3) The cost-effectiveness ratios in both retrofit cases are significantly increased when the social cost avoided is considered. The contribution of social cost avoided to the total benefit is far more than that of bridge restoration cost avoided. This indicates that most of the benefit due to retrofit comes from the social cost avoided.

(4) Higher cost-effectiveness ratios are observed when lower link residual capacity ratios are assigned to the damaged links of the freeway network. In fact, the cost-effectiveness is very sensitive to the magnitude of the link residual capacity ratio. Since the link residual capacity relates to the traffic flow effectiveness through local detour routes, more accurate value of this ratio should be found by incorporating the local highway network into the freeway network analysis in future research.

(5) The cost-effectiveness ratio is different when different bridge repair process model is used. Though it seems that the cost-effectiveness ratio based on HAZUS model is approximately equal to that based on Shinozuka's model with link residual capacity under Assumption 2 (moderate link residual capacity), further study is required to examine both process models for possible integration taking advantage of their complementary temporal characteristics, for example, completely probabilistic (Shinozuka's model) vs totally deterministic (HAZUS model).

Table 8.6 Cost-effectiveness Analysis (Discount Rate =3%)
(a) Assumption 1: High Link Residual Capacity

Benefit-Cost	Case 2: 23% Retrofit	Case 3:100% Retrofit
Total Social Cost Avoided ($Million) (1)	250	1123
Total Restoration Cost Avoided ($Million) (2)	24.2	86.7
Total Retrofit Cost ($Million) (3)	393	1665
Cost-effectiveness in terms of Restoration Cost Avoided (4)=(2)/(3)	0.062	0.052
Cost-effectiveness in terms of Social Cost Avoided (5)=(1)/(3)	0.636	0.674
Total Cost-effectiveness Ratio (6)=(4)+(5)	0.697	0.726

(b) Assumption 2: Moderate Link Residual Capacity

Benefit-Cost	Case 2: 23% Retrofit	Case 3:100% Retrofit
Total Social Cost Avoided ($Million) (1)	697	3121
Total Restoration Cost Avoided ($Million) (2)	24.2	86.7
Total Retrofit Cost ($Million) (3)	393	1665
Cost-effectiveness in terms of Restoration Cost Avoided (4)=(2)/(3)	0.062	0.052
Cost-effectiveness in terms of Social Cost Avoided (5)=(1)/(3)	1.78	1.88
Total Cost-effectiveness Ratio (6)=(4)+(5)	1.84	1.93

(c) Assumption 3: Low Link Residual Capacity

Benefit-Cost	Case 2: 23% Retrofit	Case 3:100% Retrofit
Total Social Cost Avoided ($Million) (1)	2257	7220
Total Restoration Cost Avoided ($Million) (2)	24.2	86.7
Total Retrofit Cost ($Million) (3)	393	1665
Cost-effectiveness in terms of Restoration Cost Avoided (4)=(2)/(3)	0.062	0.052
Cost-effectiveness in terms of Social Cost Avoided (5)=(1)/(3)	5.75	4.34
Total Cost-effectiveness Ratio (6)=(4)+(5)	5.81	4.39

(d) HAZUS

Benefit-Cost	Case 2: 23% Retrofit	Case 3:100% Retrofit
Total Social Cost Avoided ($Million) (1)	854	3059
Total Restoration Cost Avoided ($Million) (2)	24.2	86.7
Total Retrofit Cost ($Million) (3)	393	1665
Cost-effectiveness in terms of Restoration Cost Avoided (4)=(2)/(3)	0.062	0.052
Cost-effectiveness in terms of Social Cost Avoided (5)=(1)/(3)	2.18	1.84
Total Cost-effectiveness Ratio (6)=(4)+(5)	2.24	1.89

Table 8.7 Cost-effectiveness Analysis (Discount Rate =5%)

(a) Assumption 1: High Link Residual Capacity

Benefit-Cost	Case 2: 23% Retrofit	Case 3:100% Retrofit
Total Social Cost Avoided ($Million) (1)	177	796
Total Restoration Cost Avoided ($Million) (2)	17.2	61.5
Total Retrofit Cost ($Million) (3)	393	1665
Cost-effectiveness in terms of Restoration Cost Avoided (4)=(2)/(3)	0.044	0.037
Cost-effectiveness in terms of Social Cost Avoided (5)=(1)/(3)	0.451	0.478
Total Cost-effectiveness Ratio (6)=(4)+(5)	0.495	0.515

(b) Assumption 2: Moderate Link Residual Capacity

Benefit-Cost	Case 2: 23% Retrofit	Case 3:100% Retrofit
Total Social Cost Avoided ($Million) (1)	495	2215
Total Restoration Cost Avoided ($Million) (2)	17.2	61.5
Total Retrofit Cost ($Million) (3)	393	1665
Cost-effectiveness in terms of Restoration Cost Avoided (4)=(2)/(3)	0.044	0.037
Cost-effectiveness in terms of Social Cost Avoided (5)=(1)/(3)	1.26	1.33
Total Cost-effectiveness Ratio (6)=(4)+(5)	1.30	1.37

(c) Assumption 3: Low Link Residual Capacity

Benefit-Cost	Case 2: 23% Retrofit	Case 3:100% Retrofit
Total Social Cost Avoided ($Million) (1)	1601	5124
Total Restoration Cost Avoided ($Million) (2)	17.2	61.5
Total Retrofit Cost ($Million) (3)	393	1665
Cost-effectiveness in terms of Restoration Cost Avoided (4)=(2)/(3)	0.044	0.037
Cost-effectiveness in terms of Social Cost Avoided (5)=(1)/(3)	4.08	3.08
Total Cost-effectiveness Ratio (6)=(4)+(5)	4.12	3.12

(d) HAZUS

Benefit-Cost	Case 2: 23% Retrofit	Case 3:100% Retrofit
Total Social Cost Avoided ($Million) (1)	606	2171
Total Restoration Cost Avoided ($Million) (2)	17.2	61.5
Total Retrofit Cost ($Million) (3)	393	1665
Cost-effectiveness in terms of Restoration Cost Avoided (4)=(2)/(3)	0.044	0.037
Cost-effectiveness in terms of Social Cost Avoided (5)=(1)/(3)	1.55	1.30
Total Cost-effectiveness Ratio (6)=(4)+(5)	1.59	1.34

Table 8.8 Cost-effectiveness Analysis (Discount Rate =7%)

(a) Assumption 1: High Link Residual Capacity

Benefit-Cost	Case 2: 23% Retrofit	Case 3:100% Retrofit
Total Social Cost Avoided ($Million) (1)	134	602
Total Restoration Cost Avoided ($Million) (2)	13.0	46.5
Total Retrofit Cost ($Million) (3)	393	1665
Cost-effectiveness in terms of Restoration Cost Avoided (4)=(2)/(3)	0.033	0.028
Cost-effectiveness in terms of Social Cost Avoided (5)=(1)/(3)	0.341	0.361
Total Cost-effectiveness Ratio (6)=(4)+(5)	0.374	0.389

(b) Assumption 2: Moderate Link Residual Capacity

Benefit-Cost	Case 2: 23% Retrofit	Case 3:100% Retrofit
Total Social Cost Avoided ($Million) (1)	374	1674
Total Restoration Cost Avoided ($Million) (2)	13.0	46.5
Total Retrofit Cost ($Million) (3)	393	1665
Cost-effectiveness in terms of Restoration Cost Avoided (4)=(2)/(3)	0.033	0.028
Cost-effectiveness in terms of Social Cost Avoided (5)=(1)/(3)	0.953	1.01
Total Cost-effectiveness Ratio (6)=(4)+(5)	0.986	1.04

(c) Assumption 3: Low Link Residual Capacity

Benefit-Cost	Case 2: 23% Retrofit	Case 3:100% Retrofit
Total Social Cost Avoided ($Million) (1)	1210	3872
Total Restoration Cost Avoided ($Million) (2)	13.0	46.5
Total Retrofit Cost ($Million) (3)	393	1665
Cost-effectiveness in terms of Restoration Cost Avoided (4)=(2)/(3)	0.033	0.028
Cost-effectiveness in terms of Social Cost Avoided (5)=(1)/(3)	3.08	2.33
Total Cost-effectiveness Ratio (6)=(4)+(5)	3.11	2.36

(d) HAZUS

Benefit-Cost	Case 2: 23% Retrofit	Case 3:100% Retrofit
Total Social Cost Avoided ($Million) (1)	458	1641
Total Restoration Cost Avoided ($Million) (2)	13.0	46.5
Total Retrofit Cost ($Million) (3)	393	1665
Cost-effectiveness in terms of Restoration Cost Avoided (4)=(2)/(3)	0.033	0.028
Cost-effectiveness in terms of Social Cost Avoided (5)=(1)/(3)	1.17	0.985
Total Cost-effectiveness Ratio (6)=(4)+(5)	1.20	1.01

Table 8.9 summarizes the cost-benefit analysis results based on Shinozuka's bridge repair process model (Fig 7.7). In this table, cost-effectiveness is defined as "No" if "benefit/cost" ratio $r < 1.5$, "Moderate" if $1.5 \le r < 2.5$, and "Yes" if $r \ge 2.5$. Again, the link residual capacity of traffic flow highly influence the cost-effectiveness and more objective method of evaluation of the capacity reduction appears to be important subject of future research.

Table 8.9 Cost-Benefit Analysis Summary

Discount Rate	Link Residual Capacity	23% Retrofit		100% Retrofit	
		Benefit/Cost Ratio	Cost-effectiveness	Benefit/Cost Ratio	Cost-effectiveness
3%	High	0.697	No	0.726	No
	Moderate	1.84	Moderate	1.93	Moderate
	Low	5.81	Yes	4.39	Yes
5%	High	0.495	No	0.515	No
	Moderate	1.30	No	1.37	No
	Low	4.12	Yes	3.12	Yes
7%	High	0.374	No	0.389	No
	Moderate	0.986	No	1.04	No
	Low	3.11	Yes	2.36	Moderate

Chapter 9 Conclusions

This study concentrates on the evaluation of the socio-economic impact resulting from the retrofit performed on the Caltrans' bridges on the Freeway network in the Los Angeles and Orange Counties by means of column jacketing with steel. A series of studies, including the development of analytical and empirical fragility curves for retrofitted and non-retrofitted bridges, freeway network seismic performance evaluation, post-event network restoration simulation, bridge repair cost, retrofit cost and social cost estimation, and cost-benefit analysis, are carried out to evaluate the cost-effectiveness of the retrofit.

The nonlinear time history analysis performed for the 5 representative bridges demonstrates that their seismic performance is significantly improved after column retrofit by steel jacketing. When the fragility curves are used to describe the bridges' seismic vulnerability, this improvement can be expressed quantitatively by "enhancement ratio". This is ratio is obtained by the ratio of the increase of median values (PGA) to the median value under no retrofit, which are 34%, 58%, 98% and 167%, corresponding to damage states of at least minor, at least moderate, at least major and collapse, respectively, for the 5 sample bridges. These results demonstrate that the retrofit is more effective in reduction of more severe damages (major or collapse) than lighter damages (minor or moderate).

The enhancement ratios are applied to the empirical fragility curves developed from bridge damage data collected from 1994 Northridge Earthquake. Based on the enhanced fragility curves, the damage states of retrofitted bridges are simulated. The

simulation shows that the number of damaged bridges in the network is greatly reduced under earthquake attack. The accompanying benefit is the reduced bridge repair cost required for the damaged bridges. As more bridges are retrofitted beforehand, this reduction is more obvious.

The evaluation of degradation of the network performance using a comprehensive traffic assignment analysis in the impaired freeway network demonstrates that two kinds of social cost in terms of time are associated with the dysfunction of the freeway network: travel delay and opportunity cost. Other than using fixed OD data, this traffic assignment algorithm considers the trip reduction after an earthquake and therefore more realistically models the expected post-event trip demand and traffic congestion in the network. The results show that even only 23 % of the bridges (the current retrofit status) in the network are retrofitted, the reduction rate in social cost are tremendously high.

The total social cost associated with the seismically impaired network was obtained by simulating the network performance as a function of elapsed time after the earthquake based on a time- and damage-dependent bridge restoration model. The simulation results show that the network performance restoration rates are much higher in the several days after the earthquakes than thereafter. When the bridges are retrofitted, the system recovery period is expected to be shorter and the total social cost, which is estimated by the integration of the daily time cost over the restoration period, is also smaller. The economic loss due to social cost is estimated by considering the local unit time value.

In the cost-benefit analysis related to the bridge retrofit scheme, the sum of social cost avoided and bridge restoration cost avoided is considered as the benefit, and retrofit

cost as the cost. The results show that either 23% (Case 2, current status) or 100% (Case 3, all) retrofit is cost-effective for the cases that the link residual capacity is reduced considerably. However, the bridge restoration cost avoided is only a small portion of the benefit obtained from the bridge retrofit. In fact, if only reduction in bridge restoration cost is considered, either retrofit condition (23% retrofit or 100% retrofit) proves to be not cost-effective. The dominant part of the benefit is provided by the social (drivers' delay and opportunity) cost avoided due to the enhanced network resilience resulting from the bridge retrofit. If we include the social cost avoided, the retrofit is more cost-effective when the network residual capacities are smaller, discount rate smaller, and percent of bridges retrofitted is larger.

Appendix A: Moment Rotation Curves With/Without Column Steel Jacketing

A.1 Moment-Curvature Curves for Longitudinal Direction of Bridges

In this appendix, the cross sections and moment rotation curves of the columns with or without steel jacketing of the five sample bridges are given in the following figures.

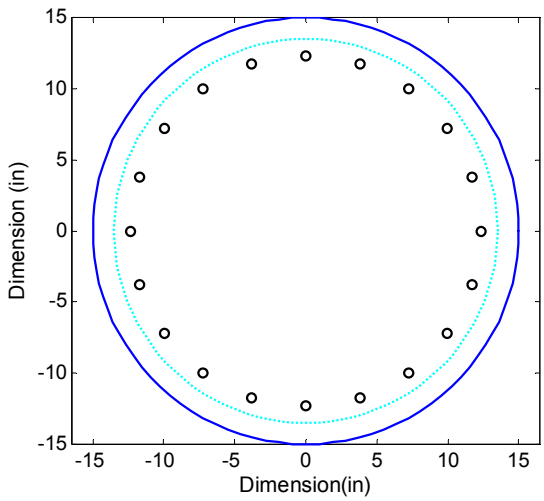

(a) Section of Column

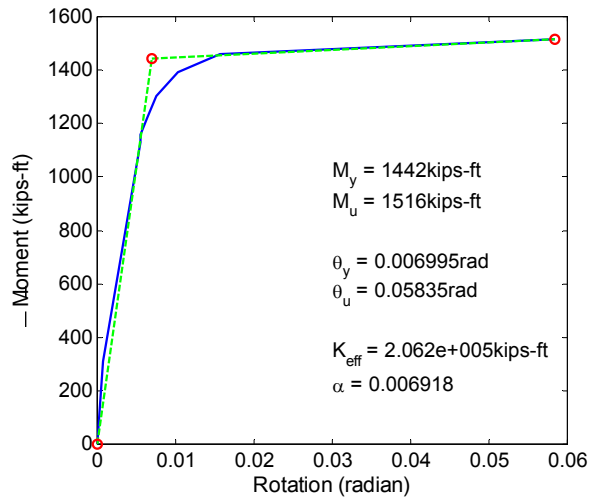

(b) Moment-Rotation Curve

(a1) Column 1 of Bridge 1 before retrofit

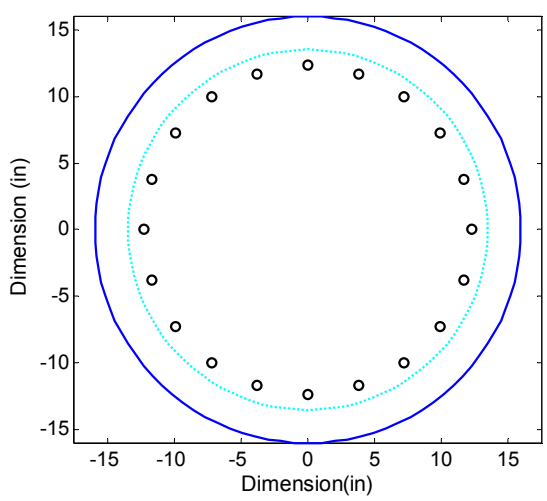

(a) Section of Column

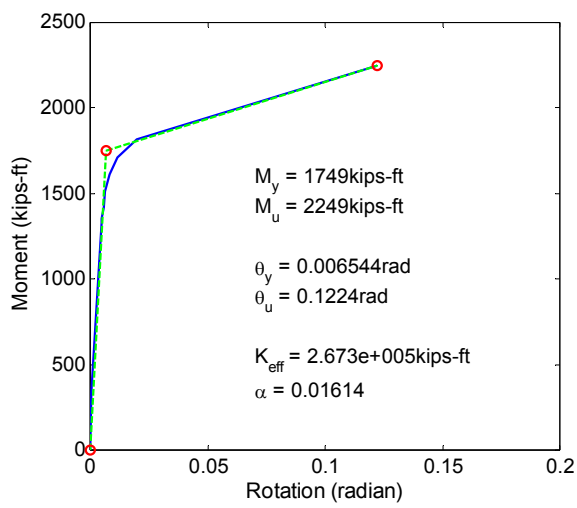

(b) Moment-Rotation Curve

(b1) Column 1 of Bridge 1 before Retrofit

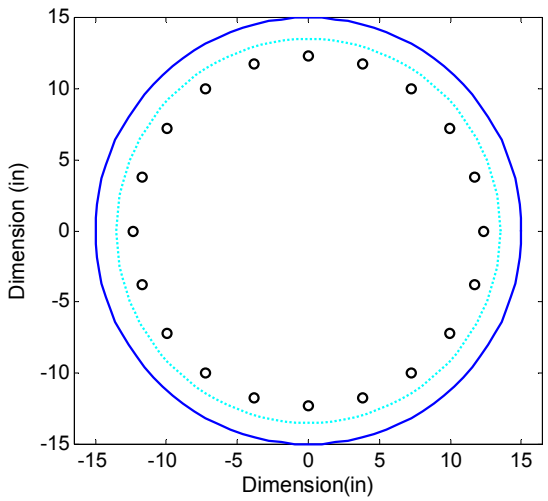

(a) Section of Column

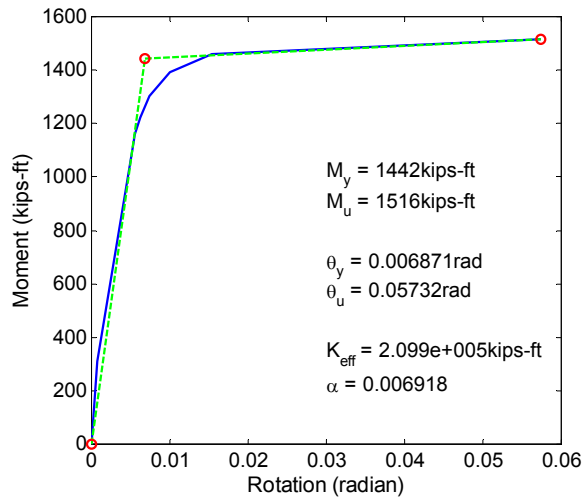

(b) Moment-Rotation Curve

(a2) Column 2 of Bridge 1 before retrofit

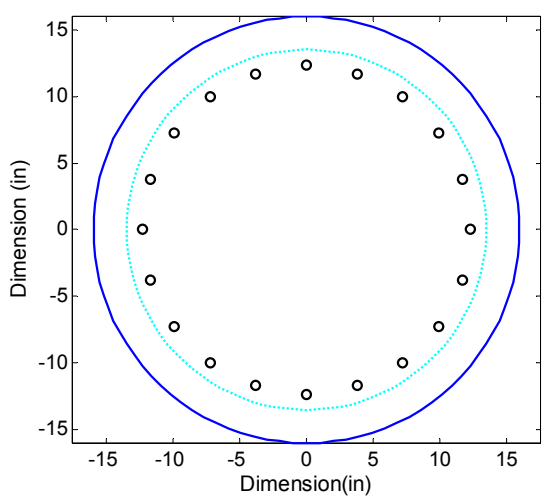

(a) Section of Column

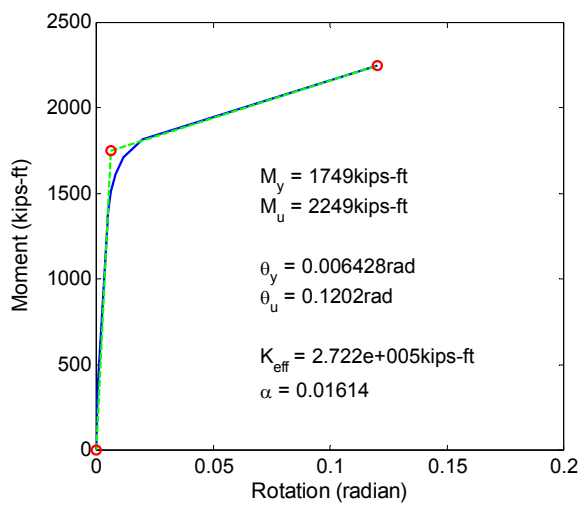

(b) Moment-Rotation Curve

(b2) Column 2 of Bridge 1 after retrofit

Fig. A.1 Moment-Curvature Analysis of Bridge 1

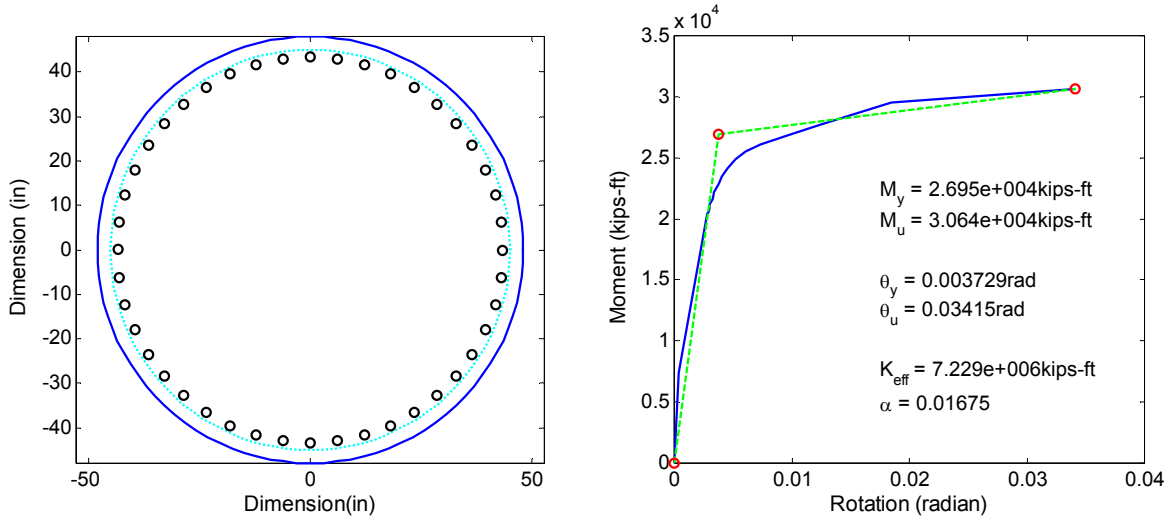

(a) Section of Column (b) Moment-Rotation Curve

(a1) Column 1 of Bridge 1 before retrofit

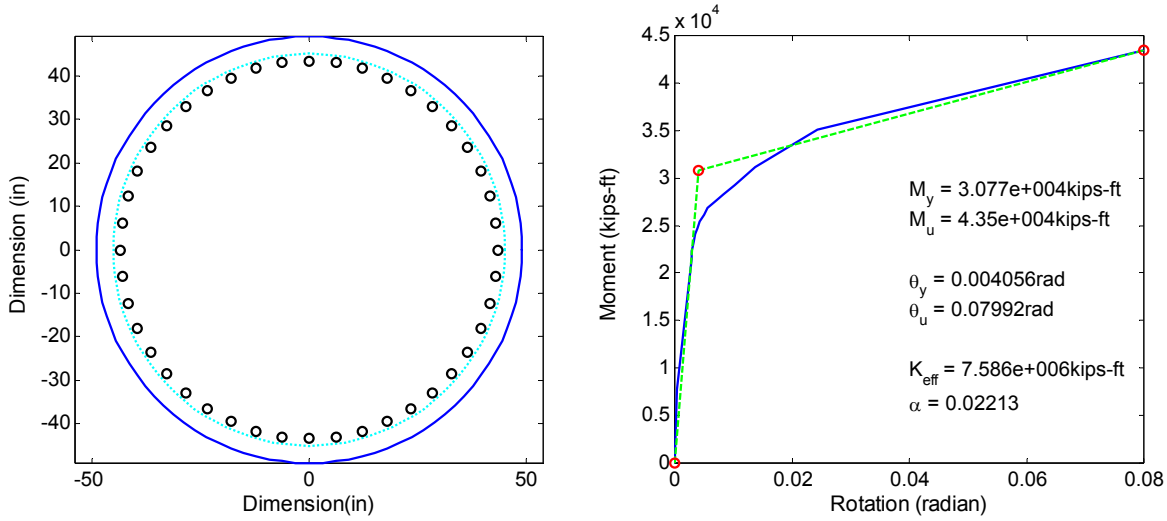

(a) Section of Column (b) Moment-Rotation Curve

(b1) Column 1 of Bridge 2 after retrofit

Fig. A.2 Moment-Curvature Analysis of Bridge 2

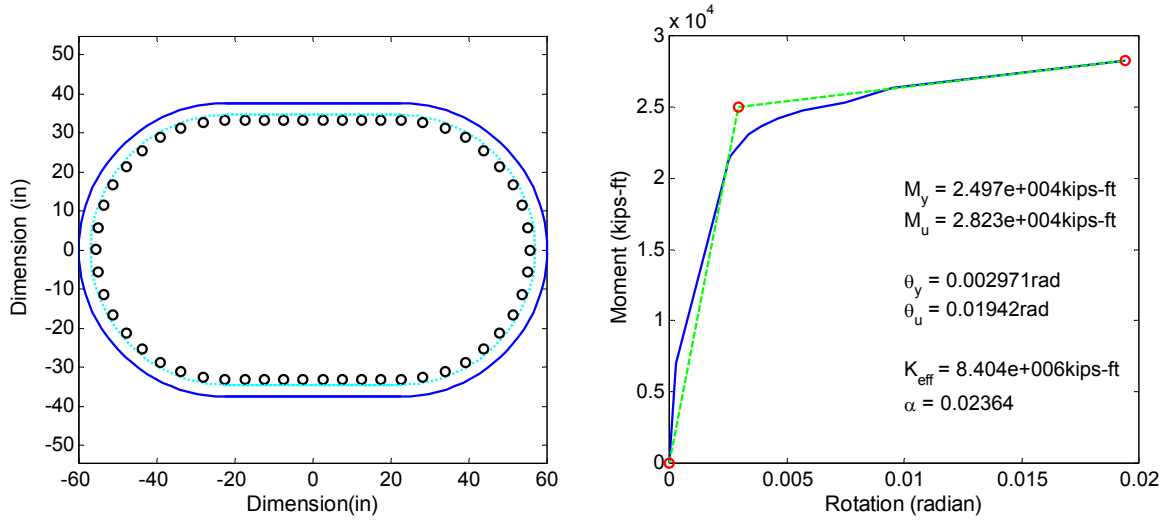

(a) Section of Column (b) Moment-Rotation Curve

(a1) Column 1 of Bridge 3 before retrofit

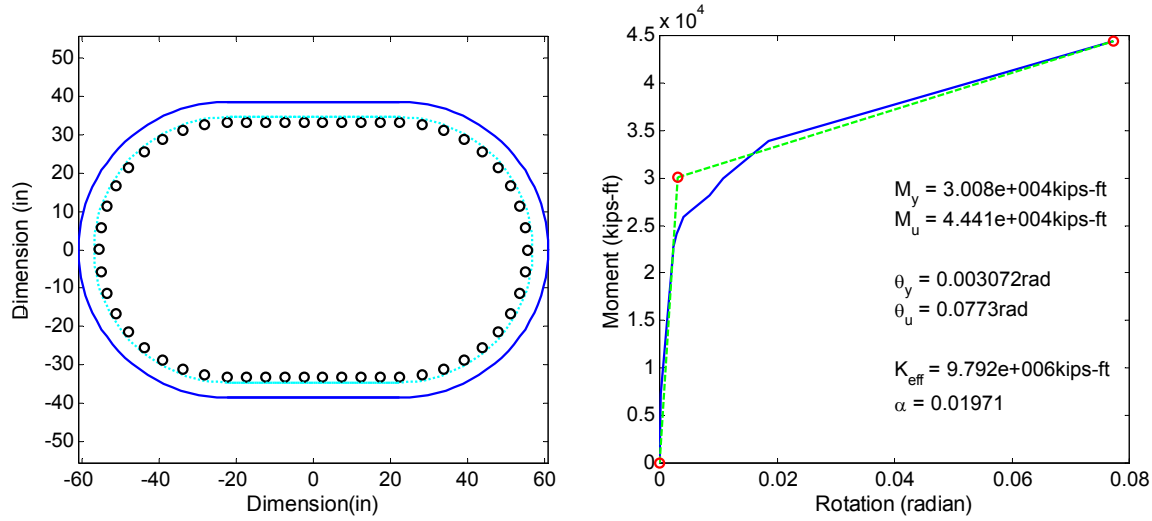

(a) Section of Column (b) Moment-Rotation Curve

(b1) Column 1 of Bridge 3 after retrofit

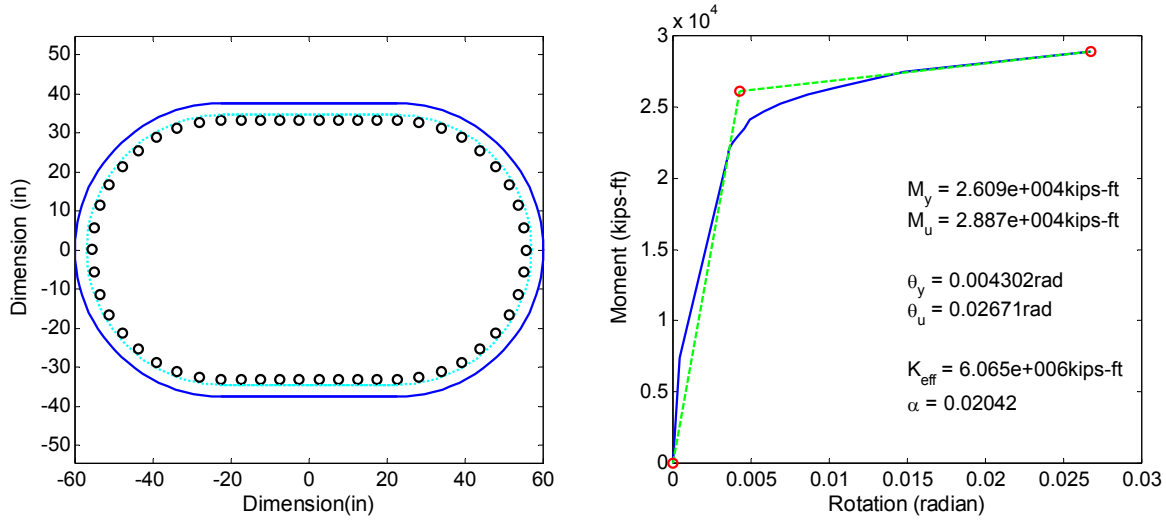

(a) Section of Column (b) Moment-Rotation Curve

(a2) Column 2 of Bridge 3 before retrofit

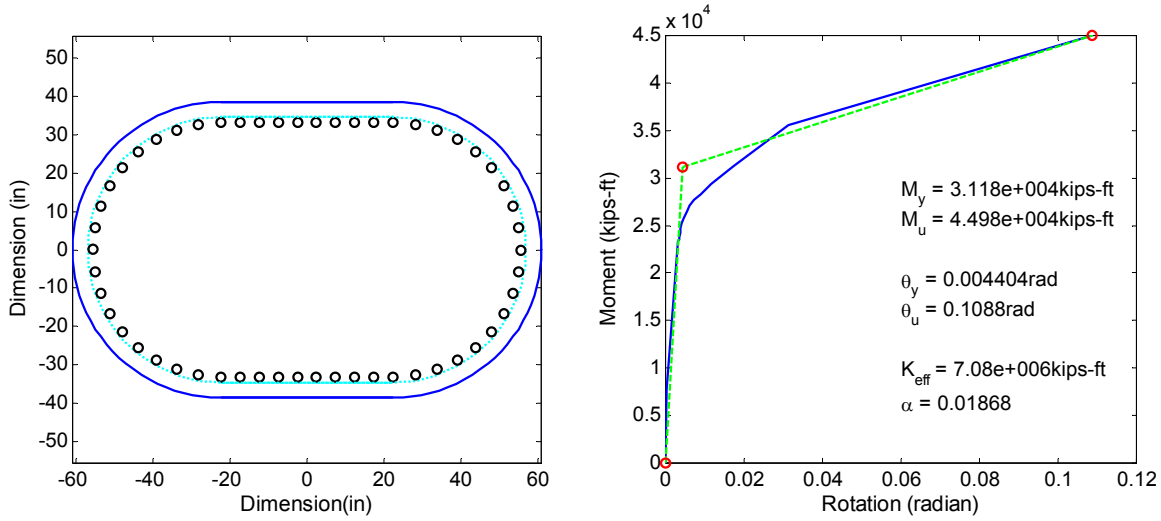

(a) Section of Column (b) Moment-Rotation Curve

(b2) Column 2 of Bridge 3 after retrofit

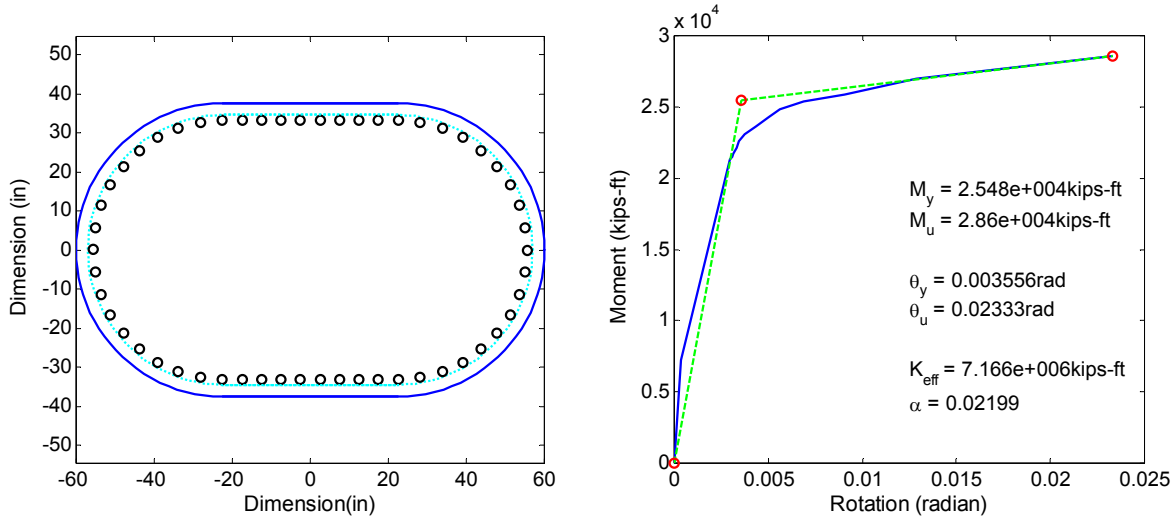

(a) Section of Column (b) Moment-Rotation Curve

(a3) Column 3 of Bridge 3 before retrofit

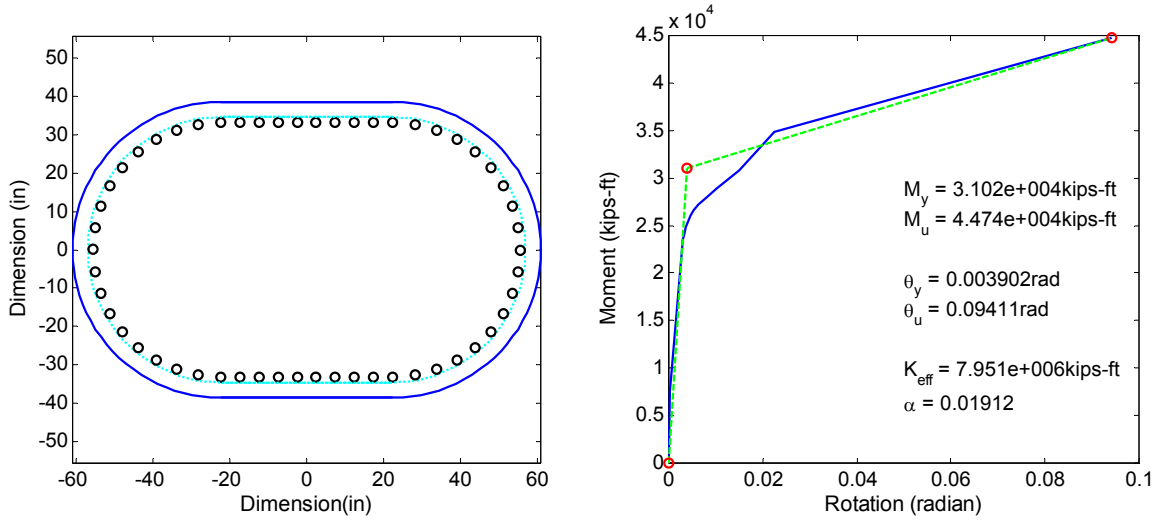

(a) Section of Column (b) Moment-Rotation Curve

(b3) Column 3 of Bridge 3 after retrofit

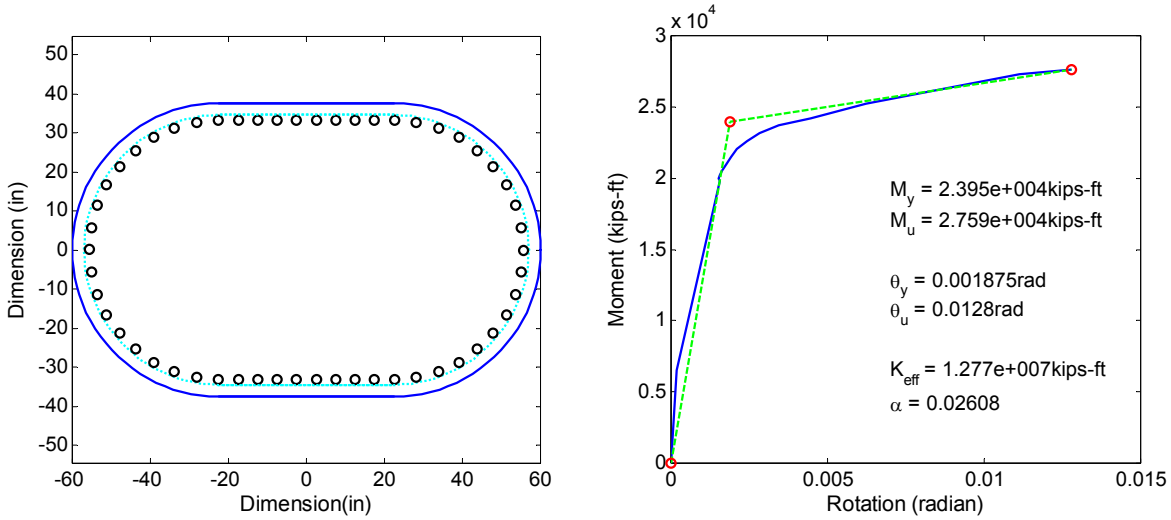

(a) Section of Column (b) Moment-Rotation Curve

(a4) Column 4 of Bridge 3 before retrofit

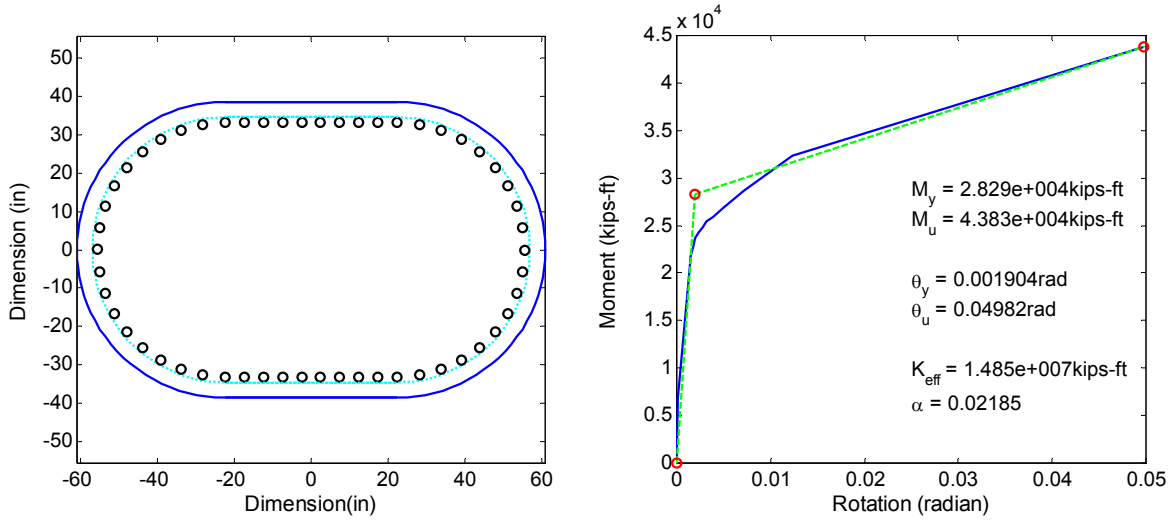

(a) Section of Column (b) Moment-Rotation Curve

(b4) Column 4 of Bridge 3 after retrofit

Fig. A.3 Moment-Curvature Analysis of Bridge 3

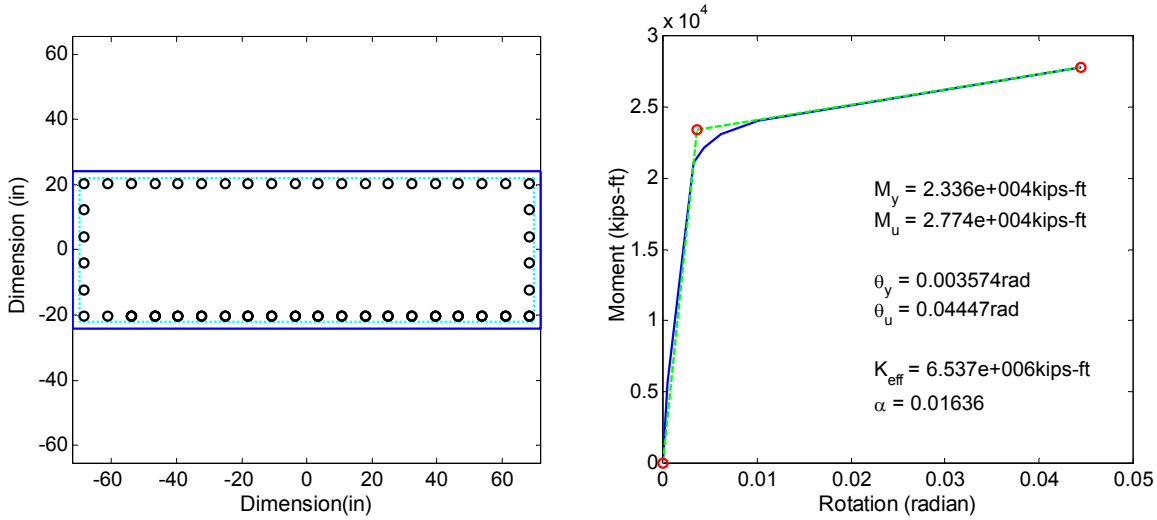

(a) Section of Column (b) Moment-Rotation Curve

(a1) Column 1 of Bridge 4 before retrofit

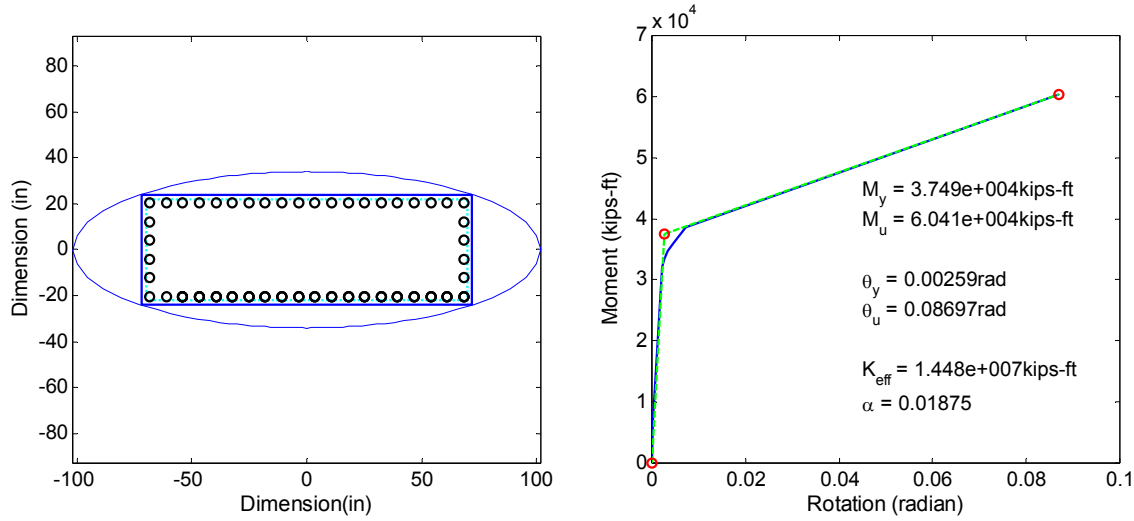

(a) Section of Column (b) Moment-Rotation Curve

(b1) Column 1 of Bridge 4 after retrofit

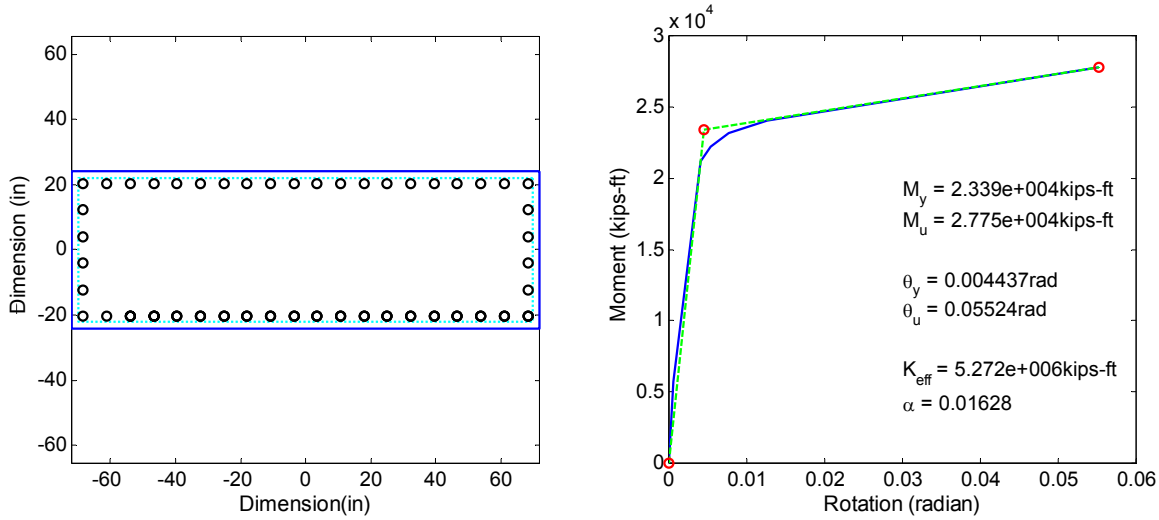

(a) Section of Column (b) Moment-Rotation Curve

(a2) Column 2 of Bridge 4 before retrofit

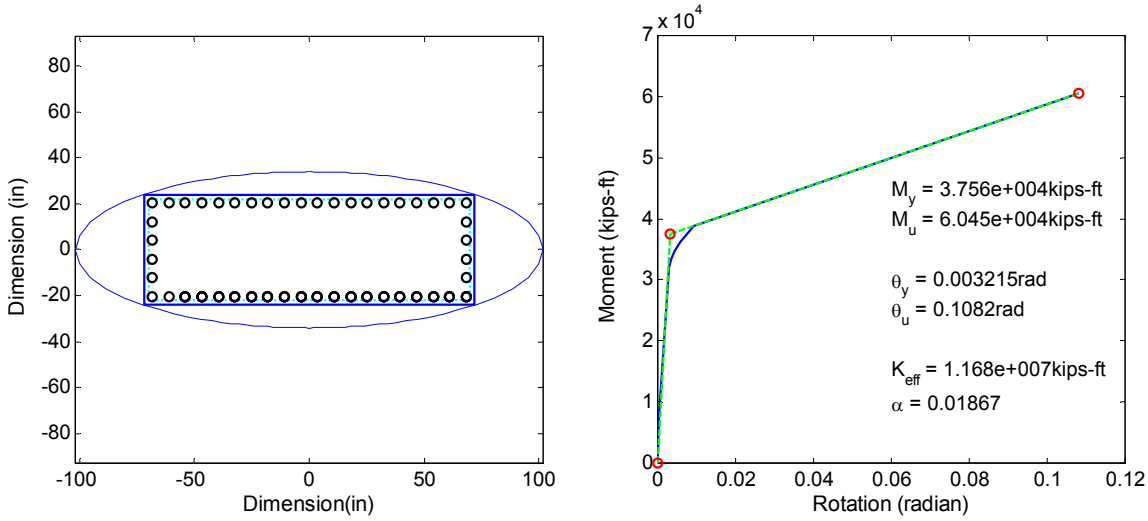

(a) Section of Column (b) Moment-Rotation Curve

(b2) Column 2 of Bridge 4 after retrofit

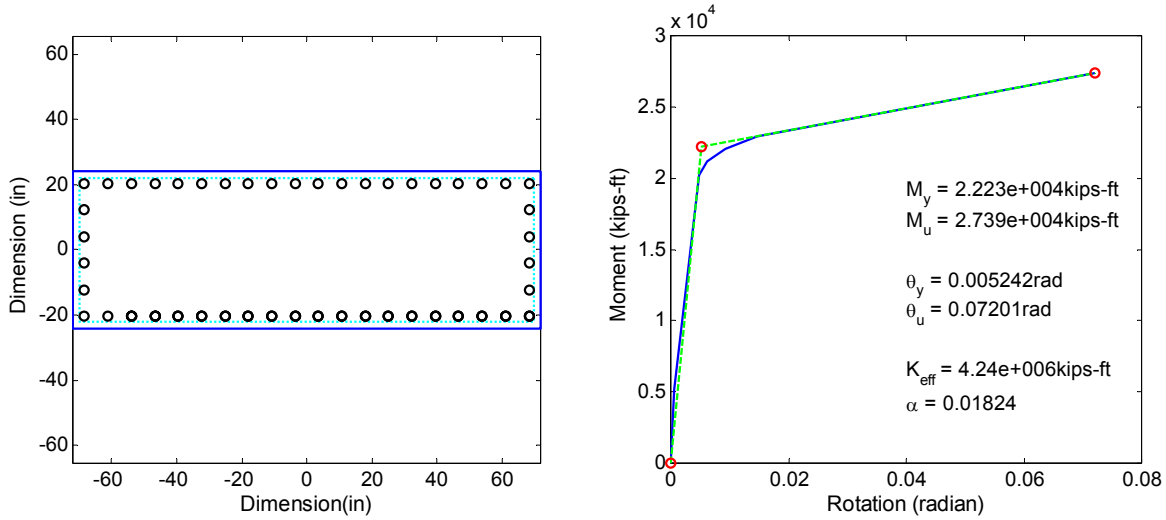

(a) Section of Column (b) Moment-Rotation Curve

(a3) Column 3 of Bridge 4 before retrofit

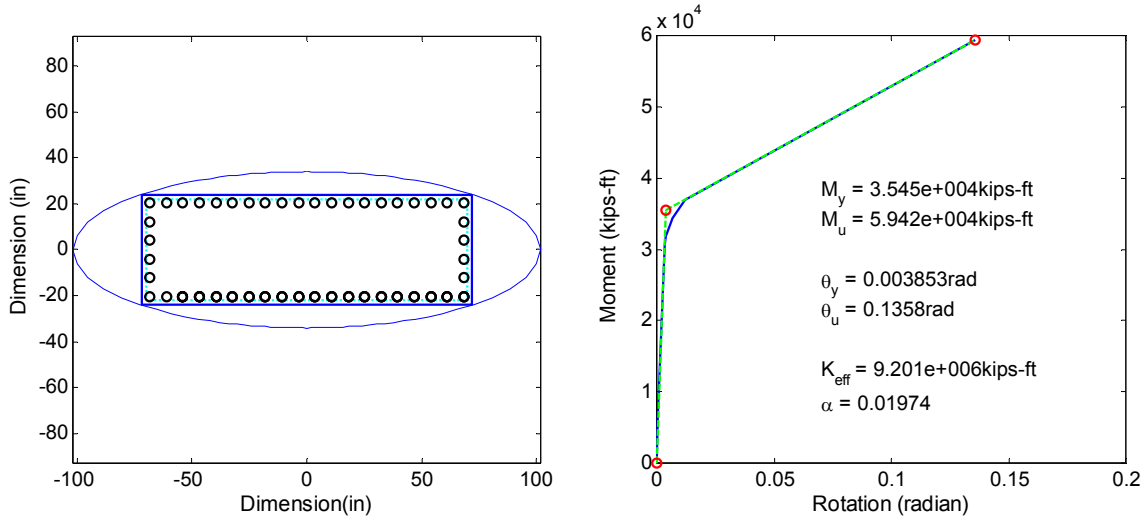

(a) Section of Column (b) Moment-Rotation Curve

(b3) Column 3 of Bridge 4 after retrofit

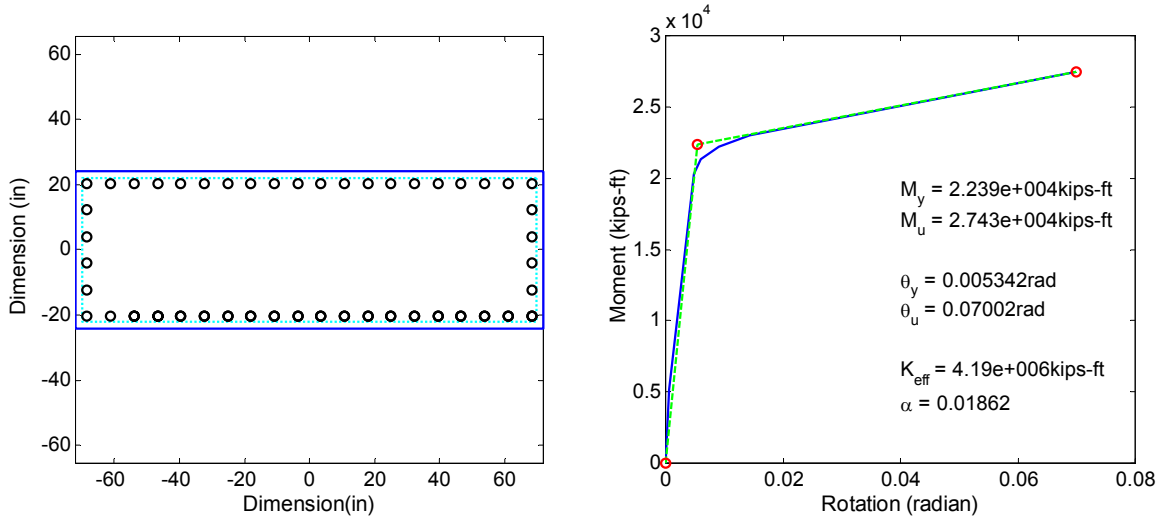

(a) Section of Column (b) Moment-Rotation Curve

(a4) Column 4 of Bridge 4 before retrofit

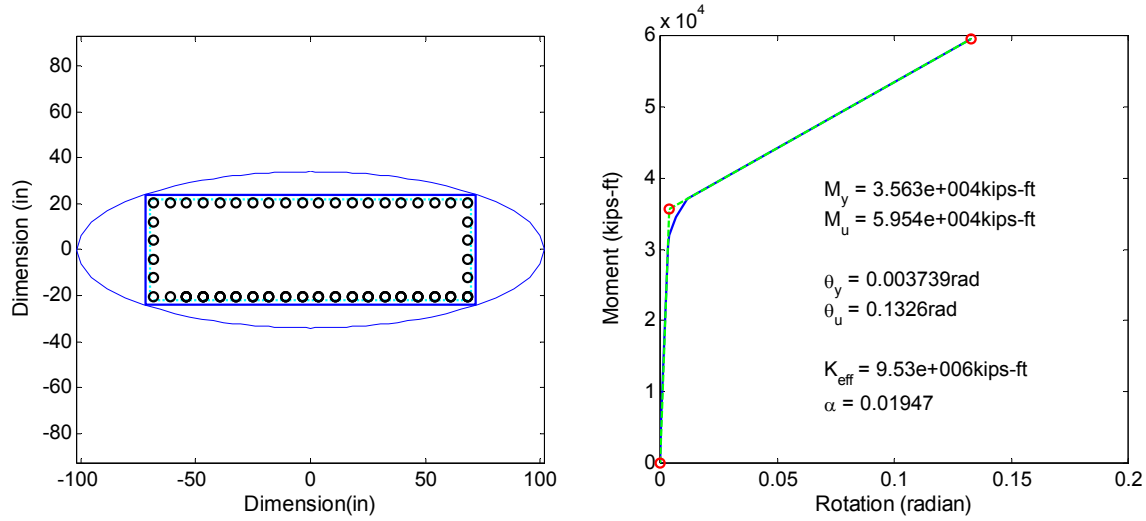

(a) Section of Column (b) Moment-Rotation Curve

(b4) Column 4 of Bridge 4 after retrofit

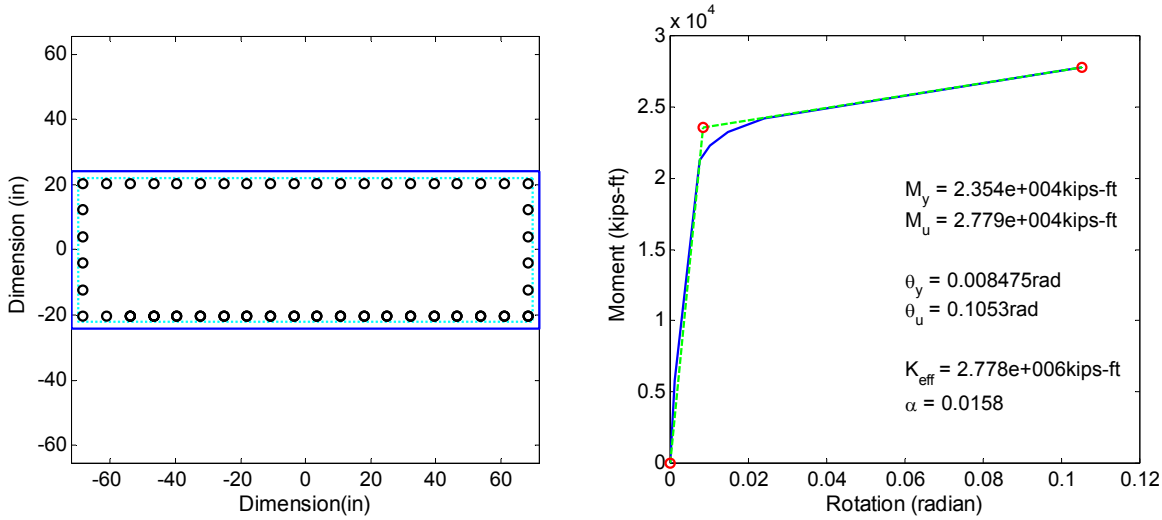

(a) Section of Column (b) Moment-Rotation Curve

(a5) Column 5 of Bridge 4 before retrofit

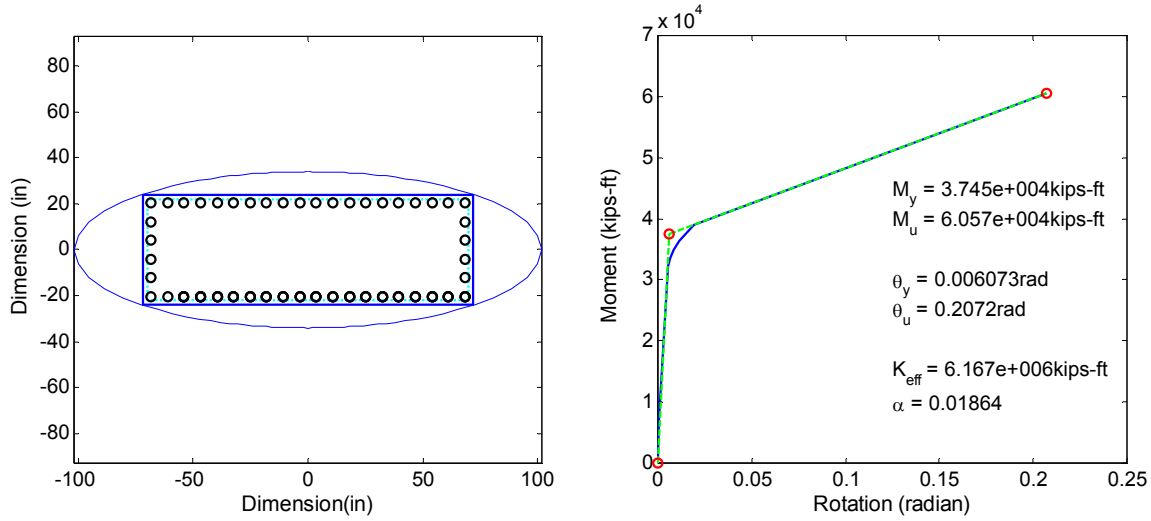

(a) Section of Column (b) Moment-Rotation Curve

(b5) Column 5 of Bridge 4 after retrofit

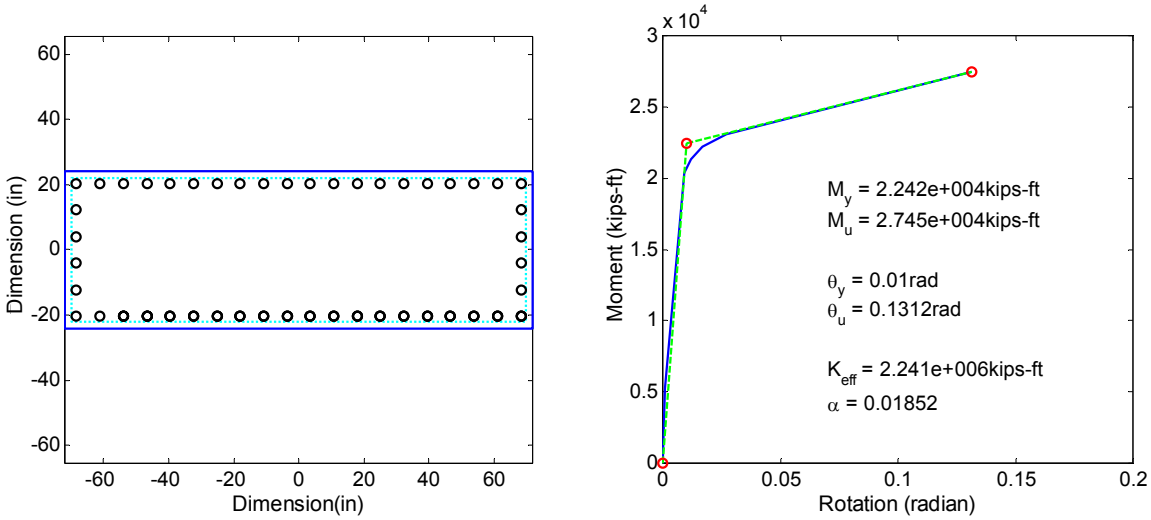

(a) Section of Column (b) Moment-Rotation Curve

(a6) Column 6 of Bridge 4 before retrofit

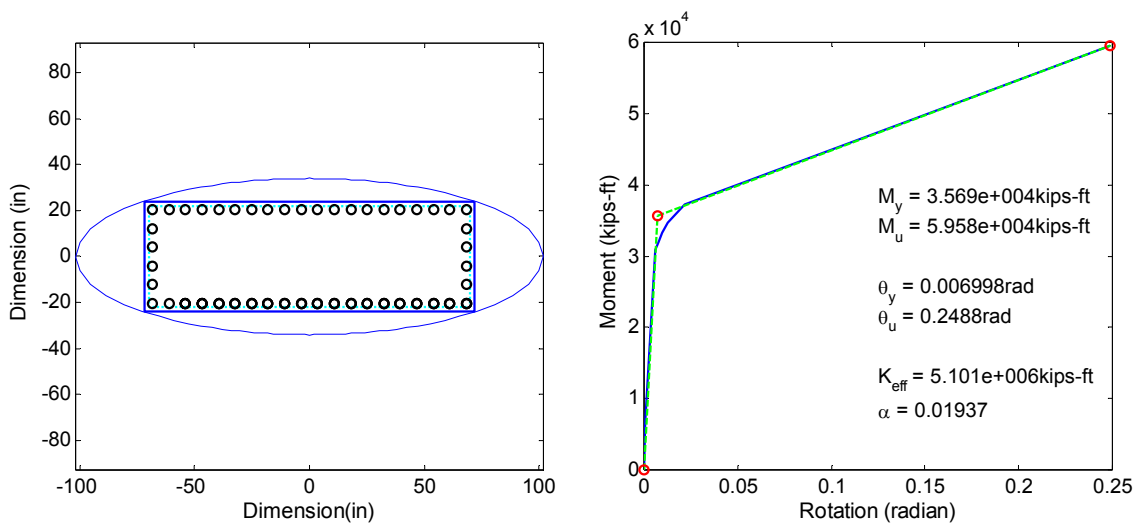

(a) Section of Column (b) Moment-Rotation Curve

(b6) Column 6 of Bridge 4 after retrofit

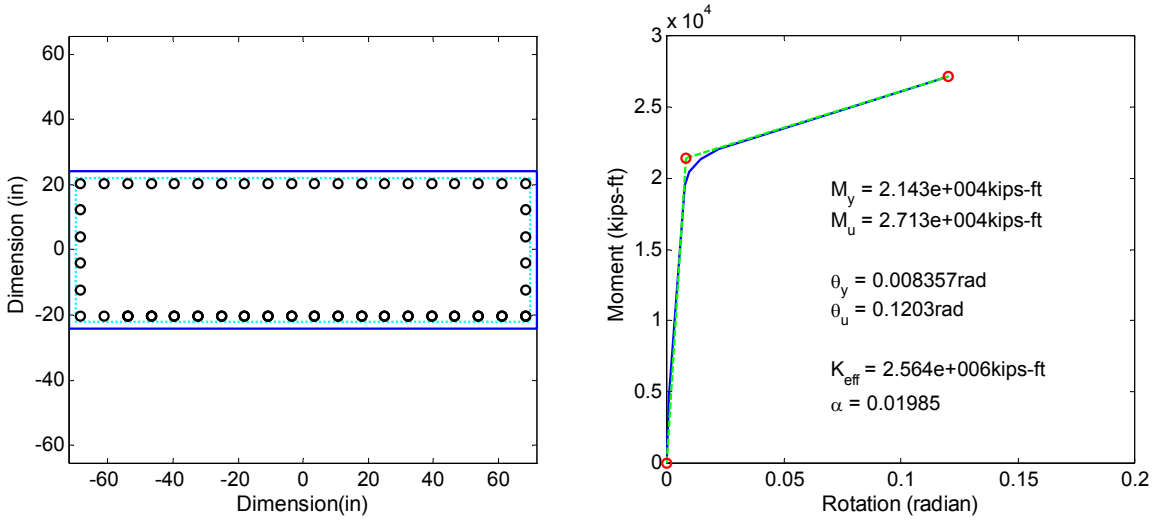

(a) Section of Column (b) Moment-Rotation Curve

(a7) Column 7 of Bridge 4 before retrofit

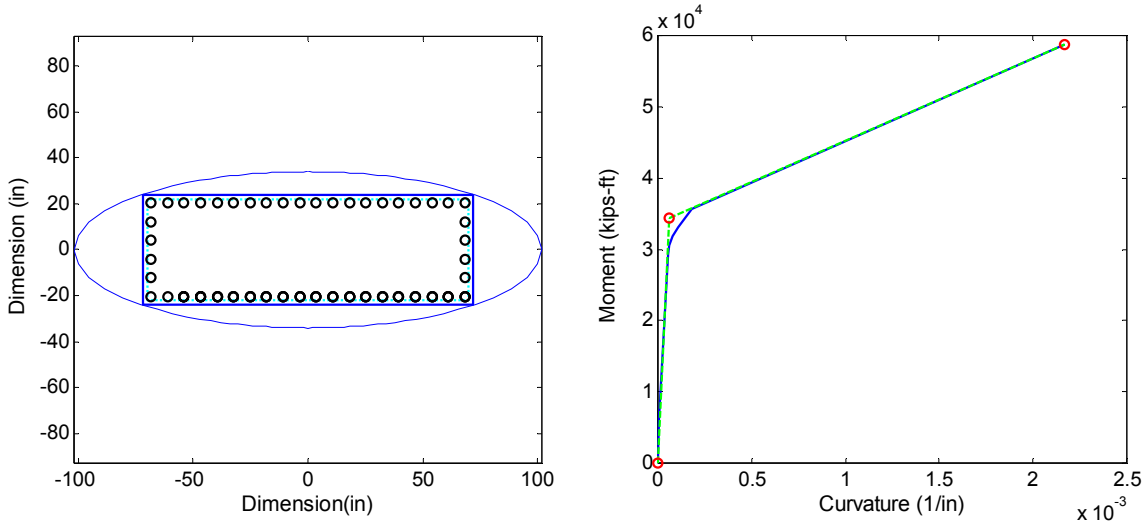

(a) Section of Column (b) Moment-Rotation Curve

(b7) Column 7 of Bridge 4 after retrofit

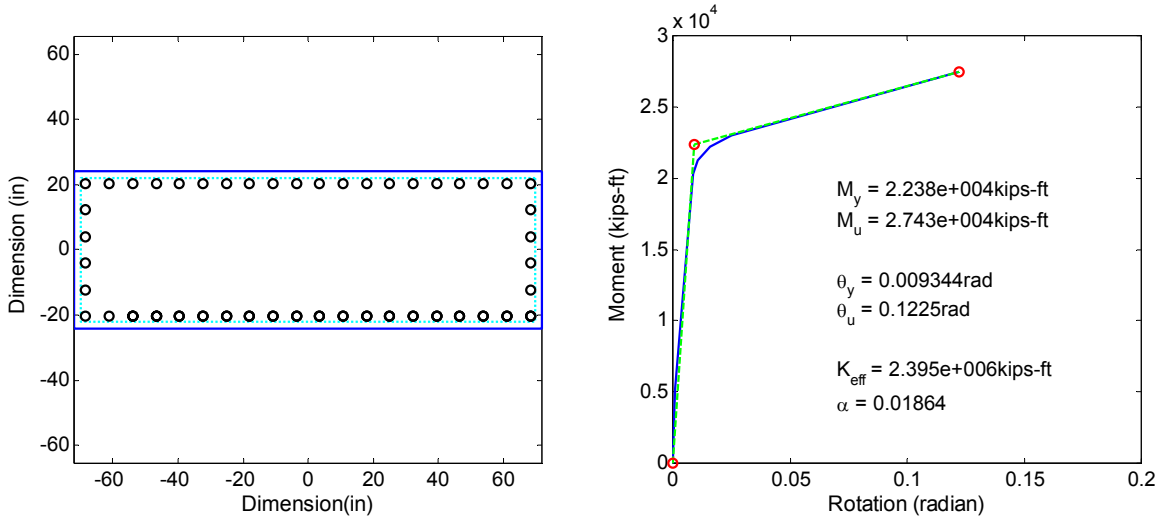

(a) Section of Column (b) Moment-Rotation Curve

(a8) Column 8 of Bridge 4 before retrofit

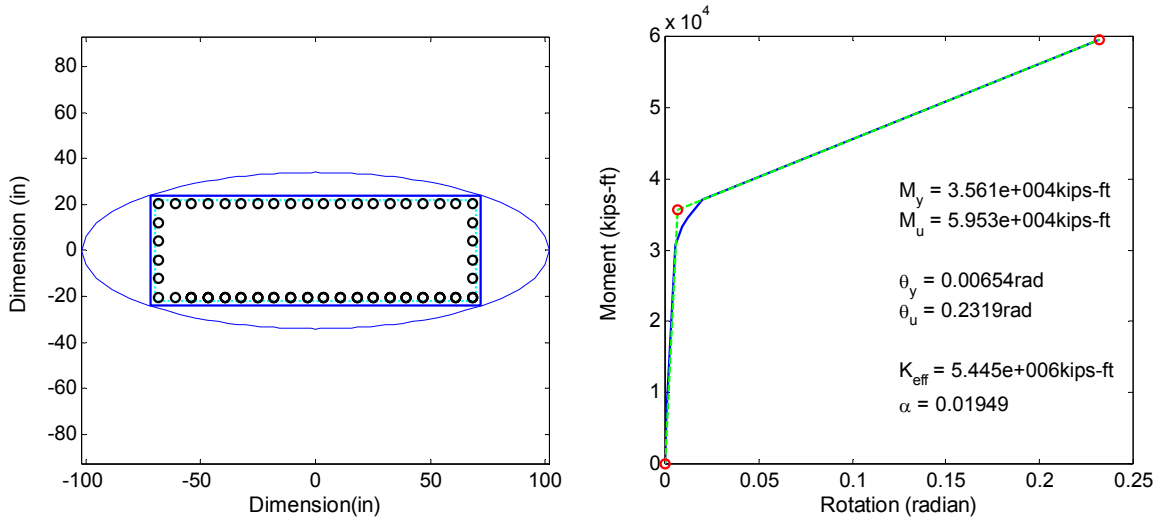

(a) Section of Column (b) Moment-Rotation Curve

(b8) Column 8 of Bridge 4 after retrofit

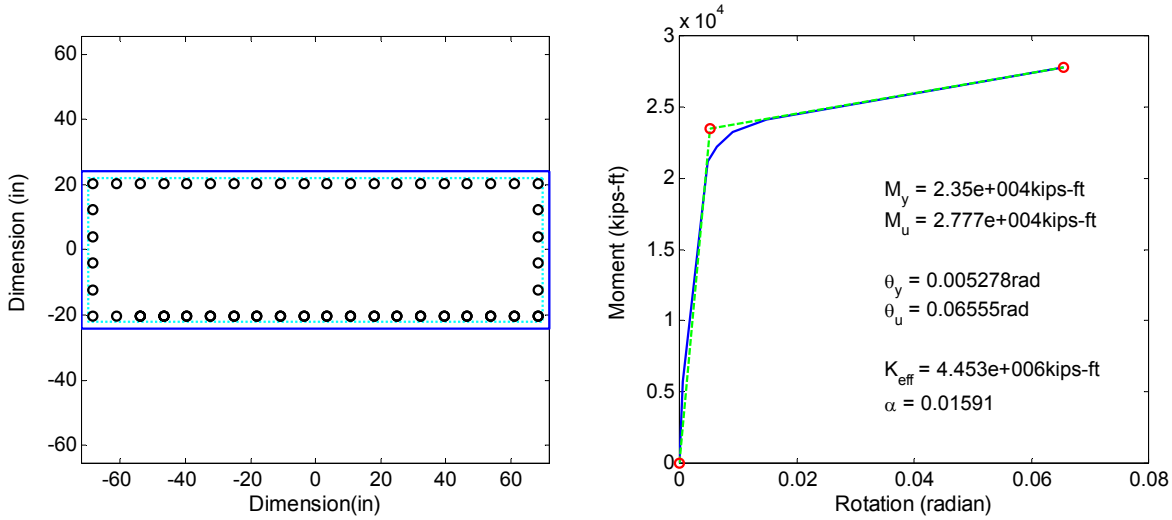

(a) Section of Column (b) Moment-Rotation Curve

(a9) Column 9 of Bridge 4 before retrofit

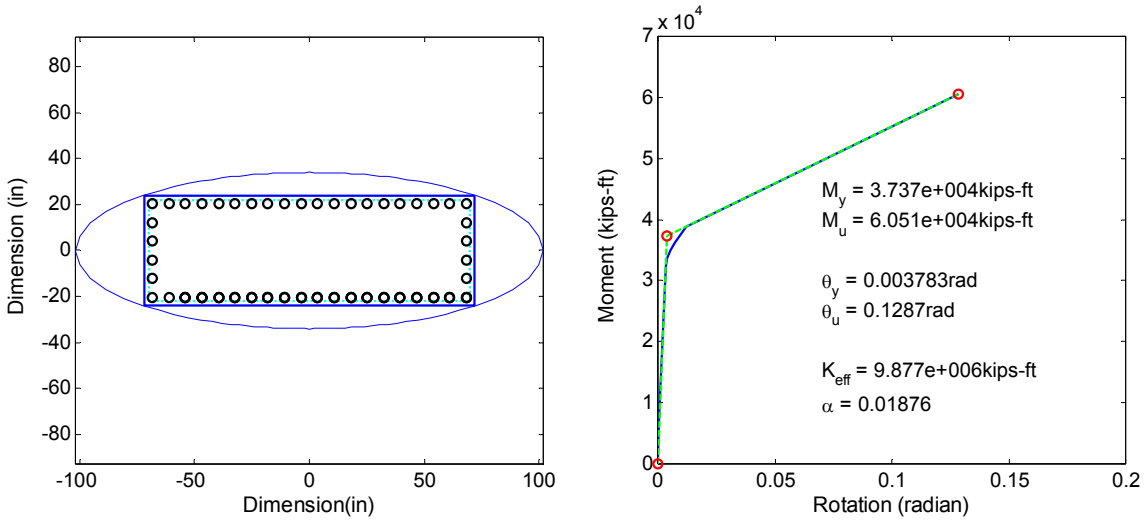

(a) Section of Column (b) Moment-Rotation Curve

(b9) Column 9 of Bridge 4 after retrofit

Fig. A.4 Moment-Curvature Analysis of Bridge 4

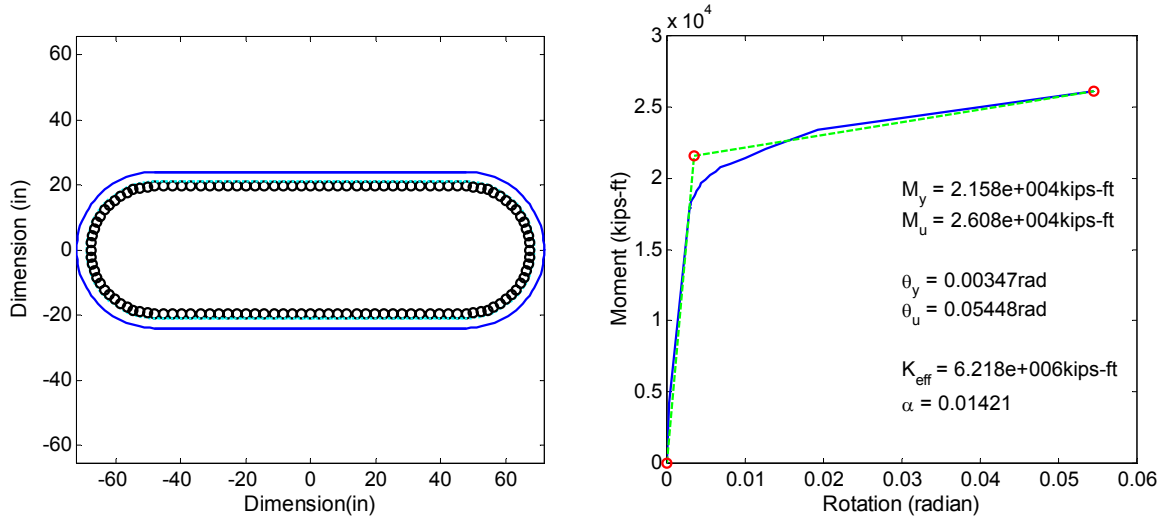

(a) Section of Column (b) Moment-Rotation Curve

(a1) Column 1 of Bridge 5 before retrofit

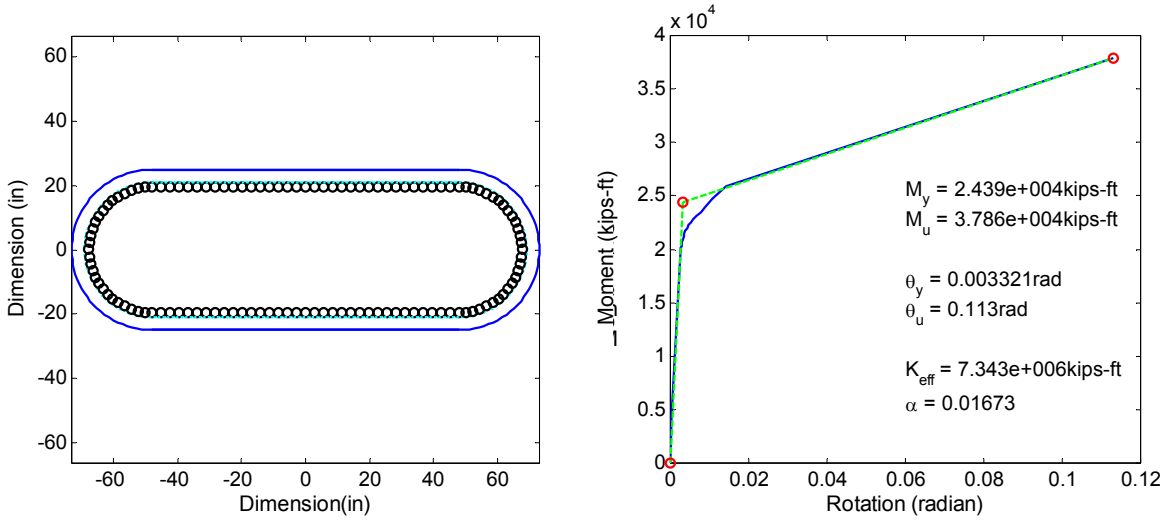

(a) Section of Column (b) Moment-Rotation Curve

(b1) Column 1 of Bridge 5 after retrofit

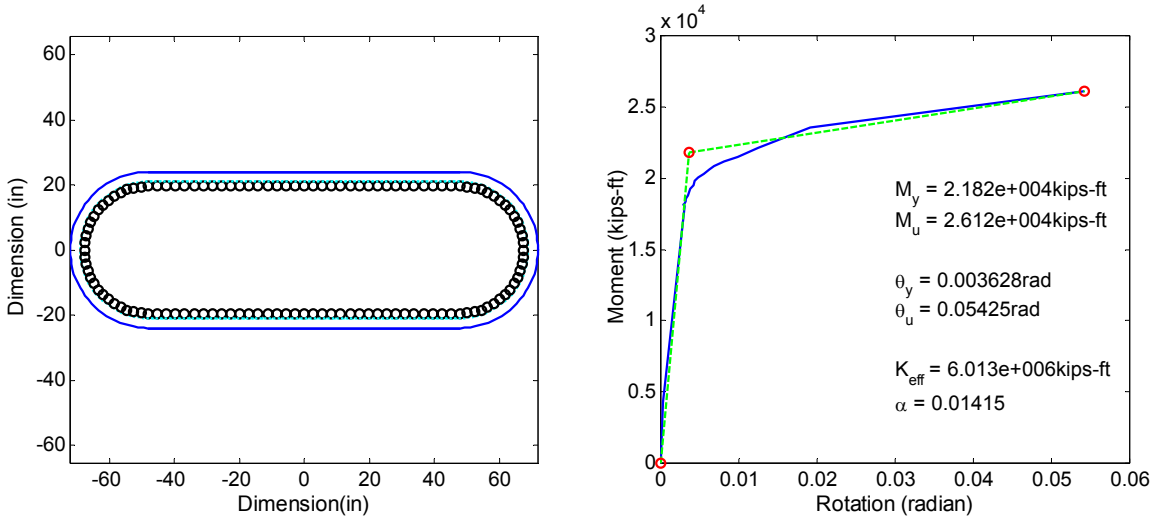

(a) Section of Column (b) Moment-Rotation Curve

(a2) Column 2 of Bridge 5 before retrofit

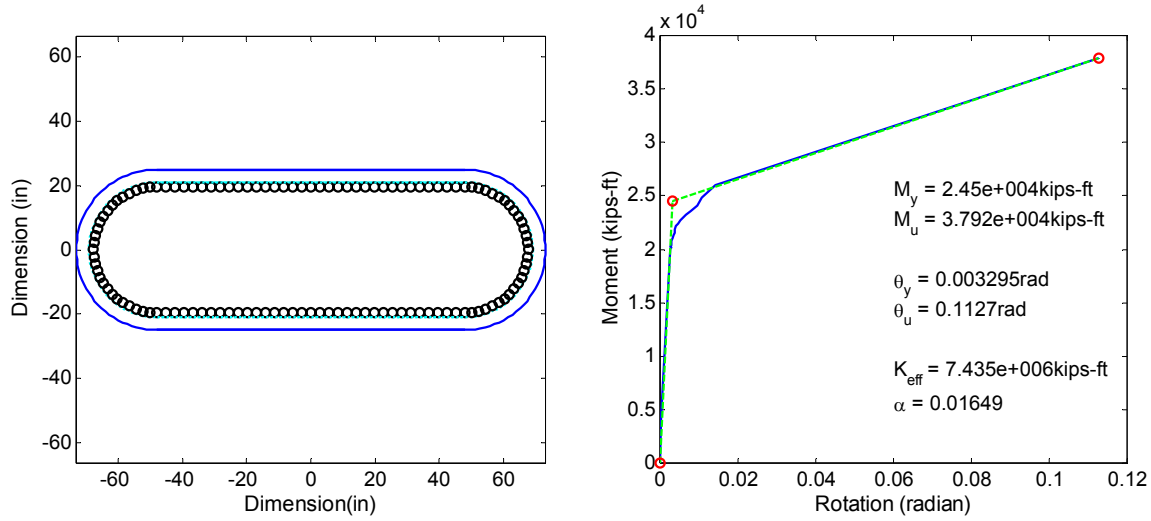

(a) Section of Column (b) Moment-Rotation Curve

(b2) Column 2 of Bridge 5 after retrofit

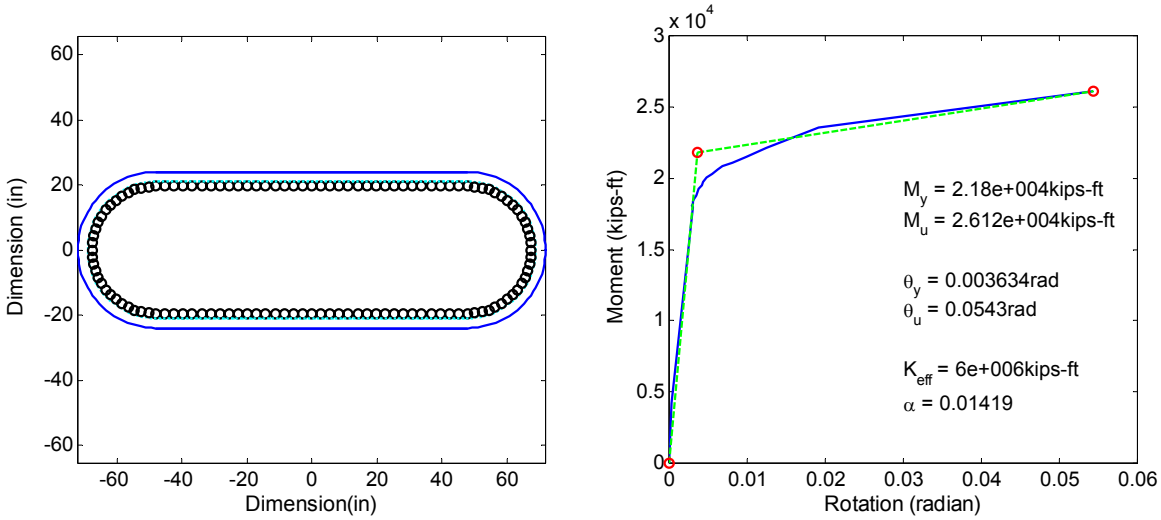

(a) Section of Column (b) Moment-Rotation Curve

(a3) Column 3 of Bridge 5 before retrofit

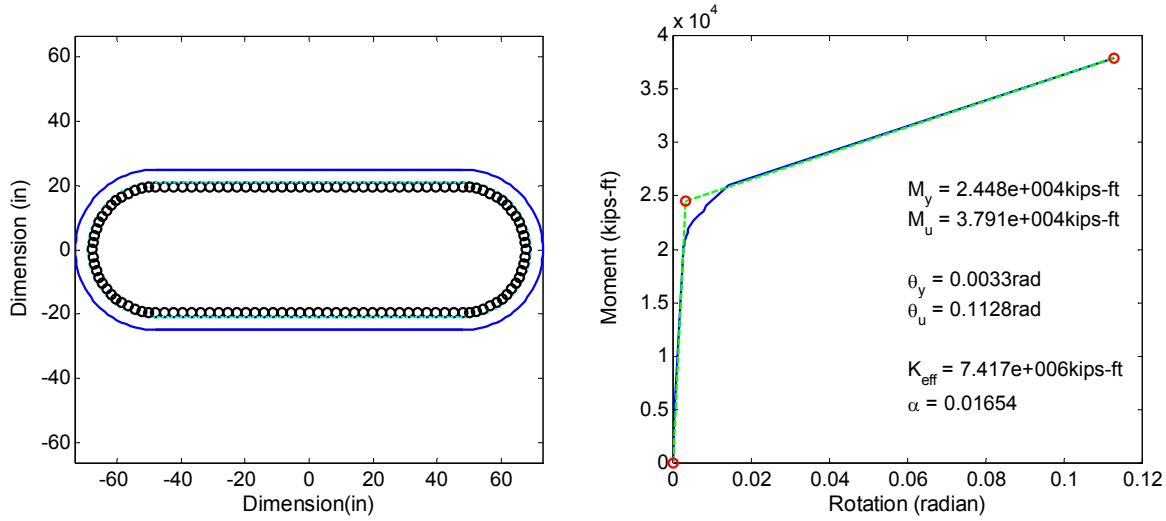

(a) Section of Column (b) Moment-Rotation Curve

(b3) Column 3 of Bridge 5 after retrofit

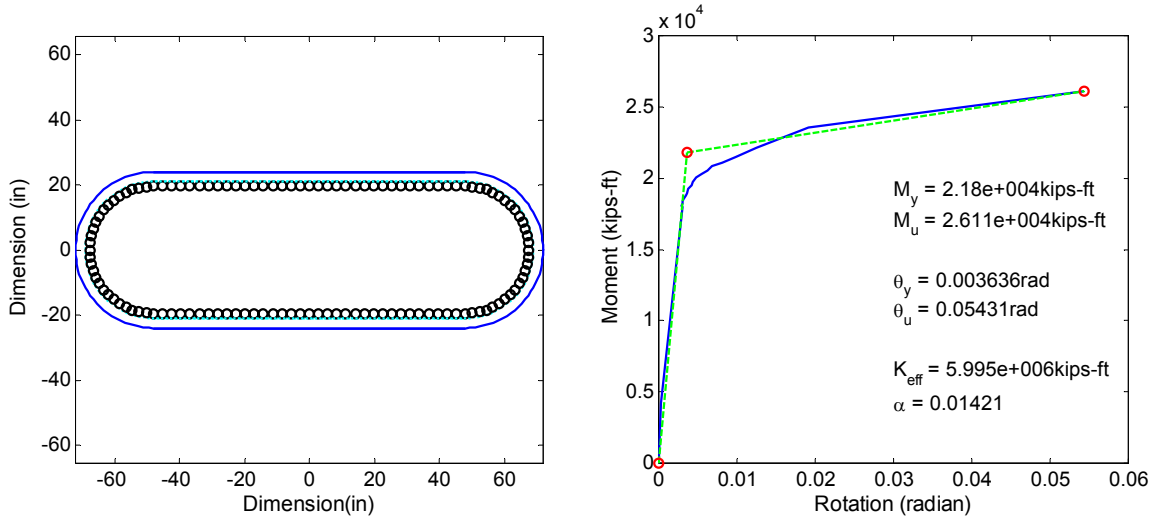

(a) Section of Column (b) Moment-Rotation Curve

(a4) Column 4 of Bridge 5 before retrofit

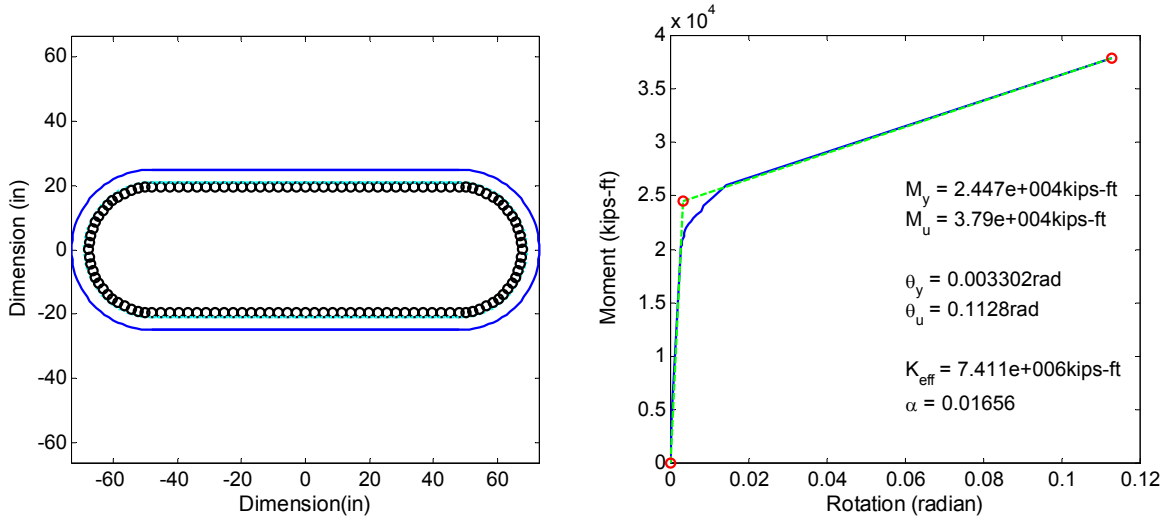

(a) Section of Column (b) Moment-Rotation Curve

(b4) Column 4 of Bridge 5 after retrofit

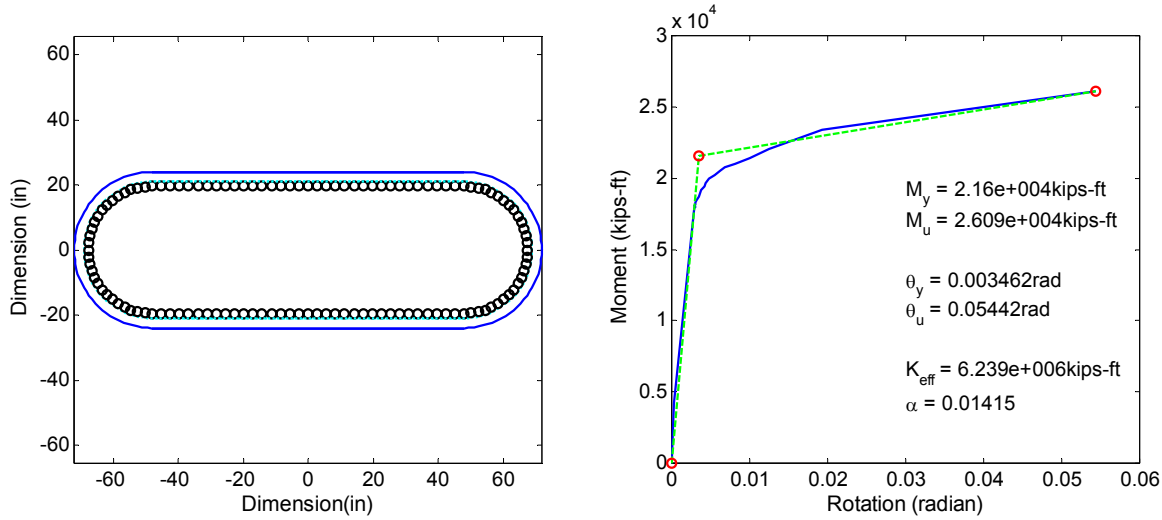

(a) Section of Column (b) Moment-Rotation Curve

(a5) Column 5 of Bridge 5 before retrofit

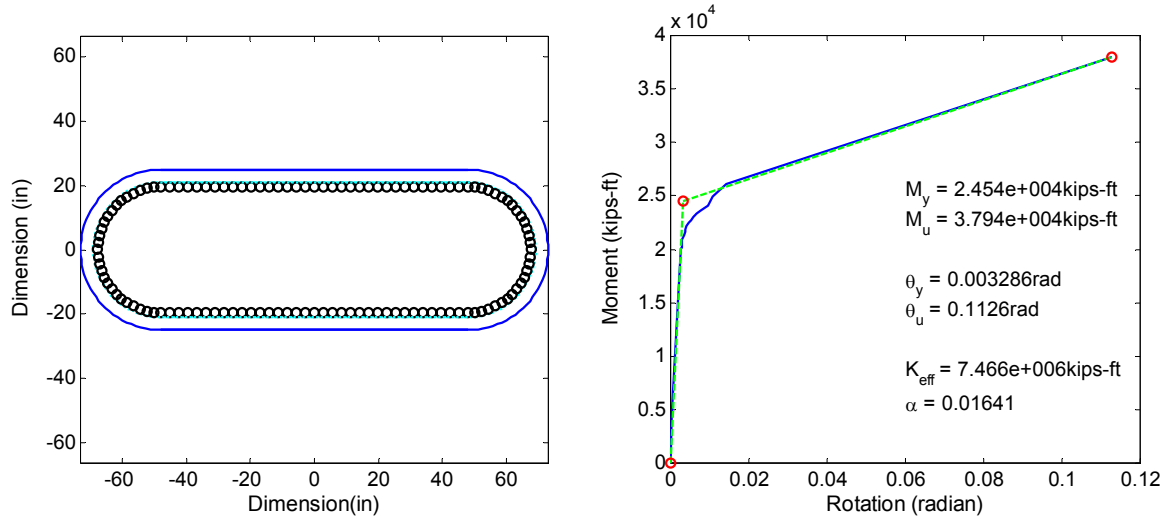

(a) Section of Column (b) Moment-Rotation Curve

(b5) Column 5 of Bridge 5 after retrofit

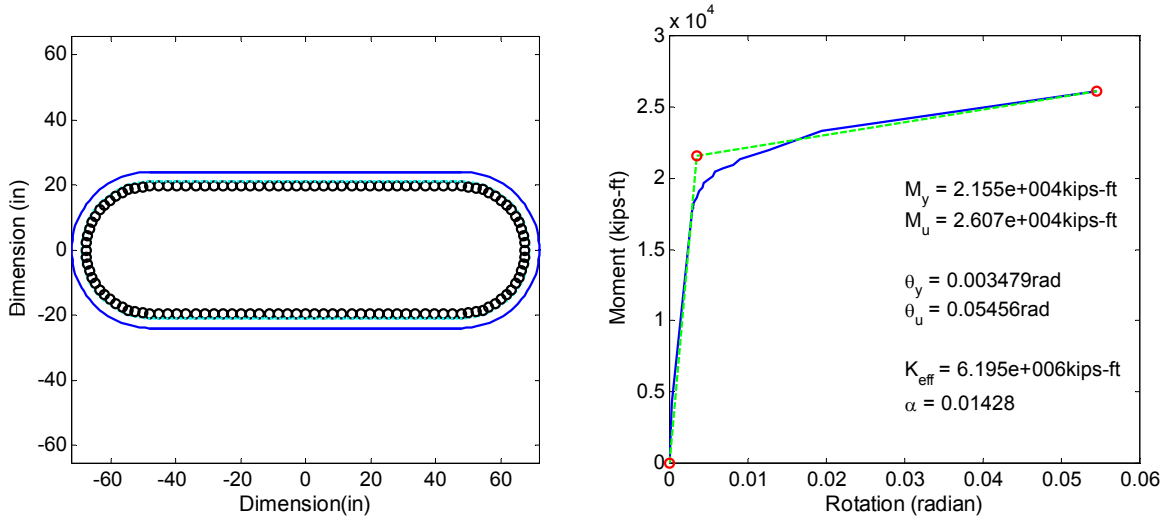

(a) Section of Column (b) Moment-Rotation Curve

(a6) Column 6 of Bridge 5 before retrofit

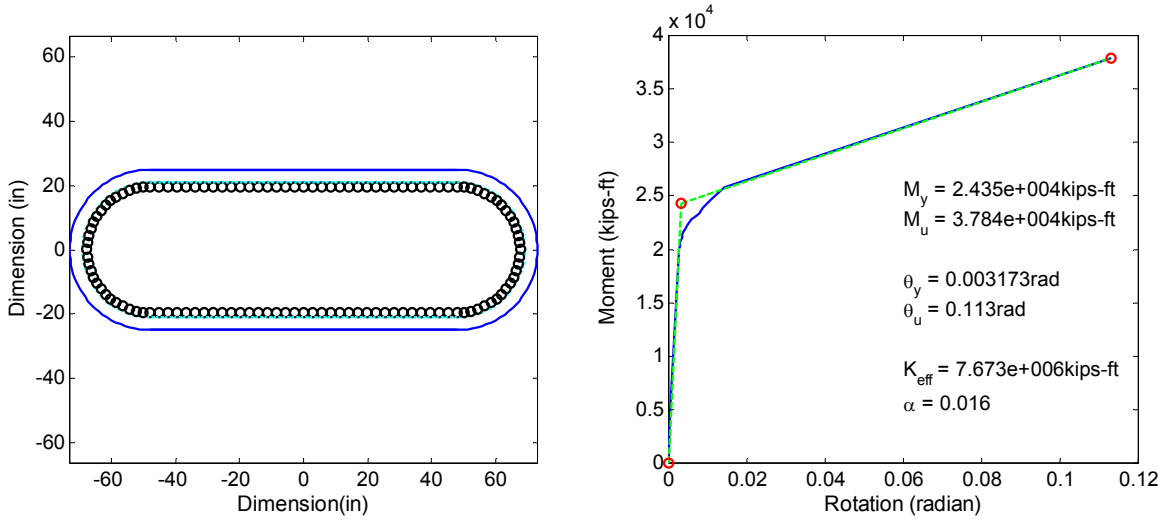

(a) Section of Column (b) Moment-Rotation Curve

(b6) Column 6 of Bridge 5 after retrofit

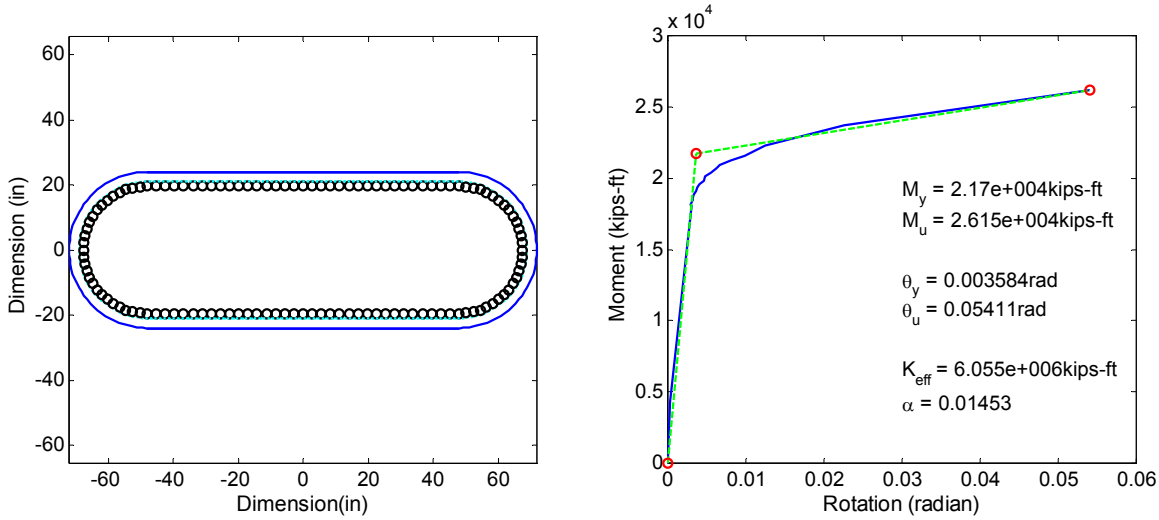

(a) Section of Column (b) Moment-Rotation Curve

(a7) Column 7 of Bridge 5 before retrofit

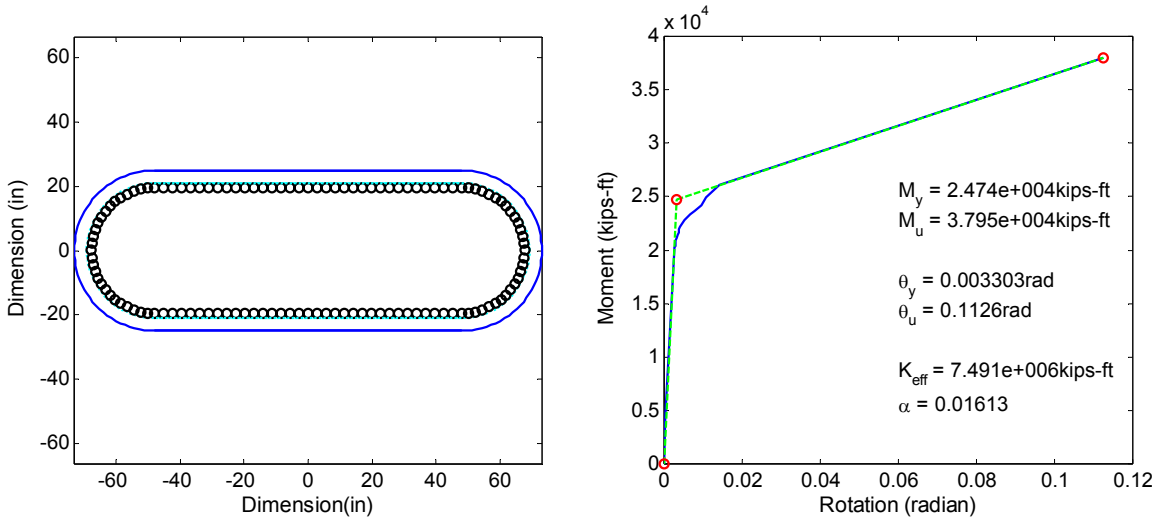

(a) Section of Column (b) Moment-Rotation Curve

(b7) Column 7 of Bridge 5 after retrofit

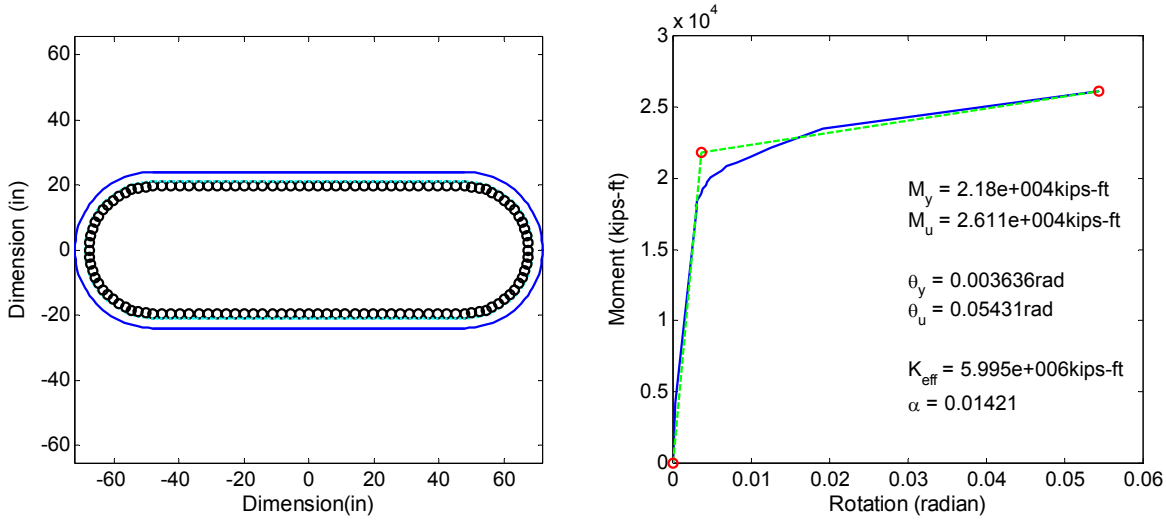

(a) Section of Column (b) Moment-Rotation Curve

(a8) Column 8 of Bridge 5 before retrofit

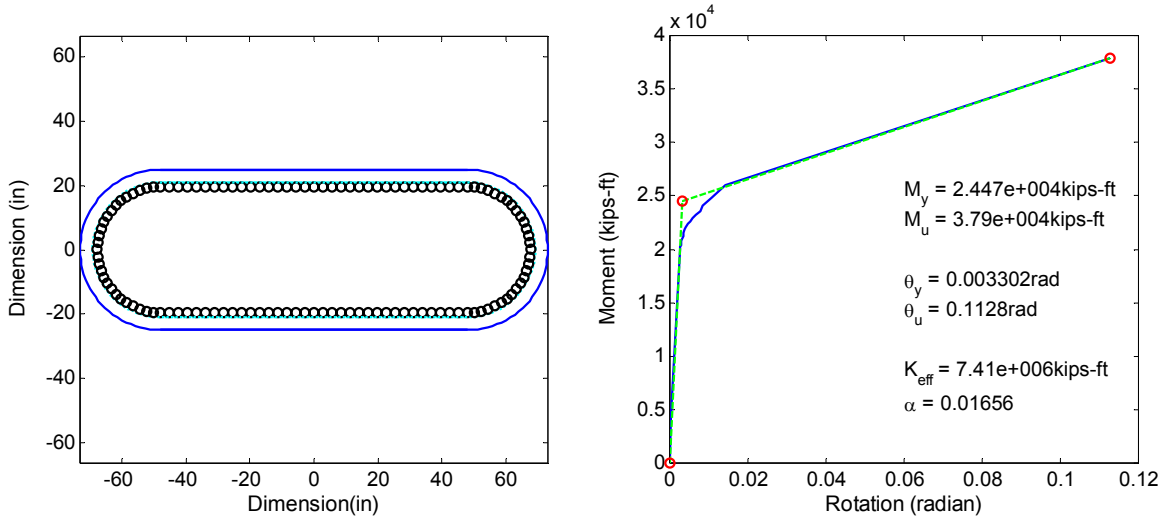

(a) Section of Column (b) Moment-Rotation Curve

(b8) Column 8 of Bridge 5 after retrofit

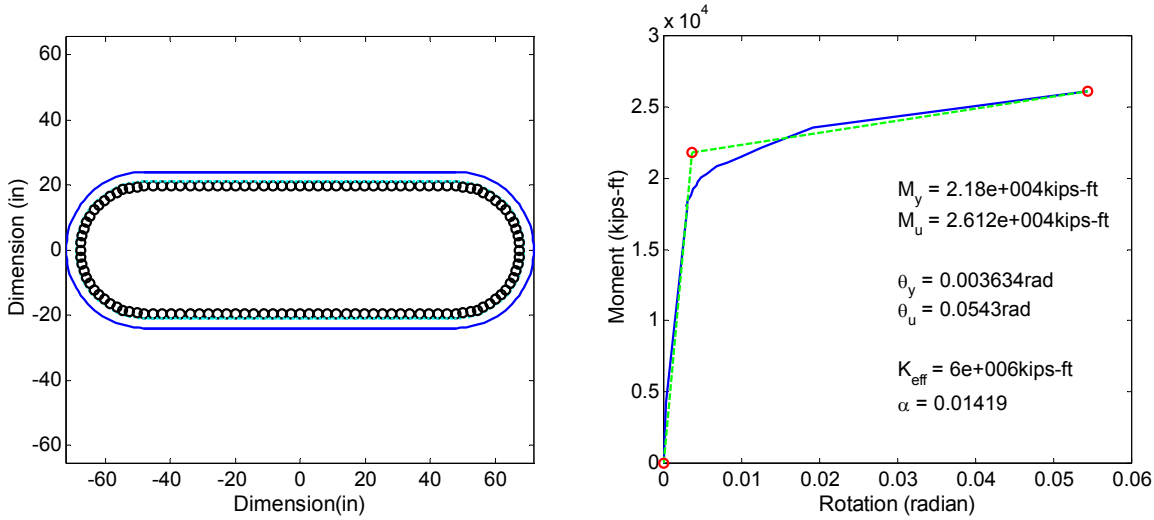

(a) Section of Column (b) Moment-Rotation Curve

(a9) Column 9 of Bridge 5 before retrofit

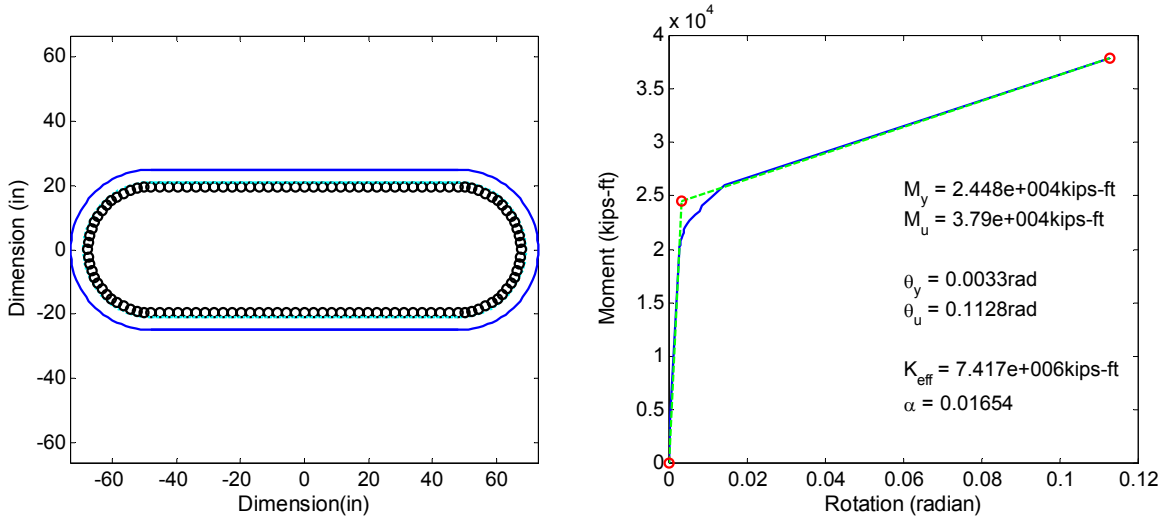

(a) Section of Column (b) Moment-Rotation Curve

(b9) Column 9 of Bridge 5 after retrofit

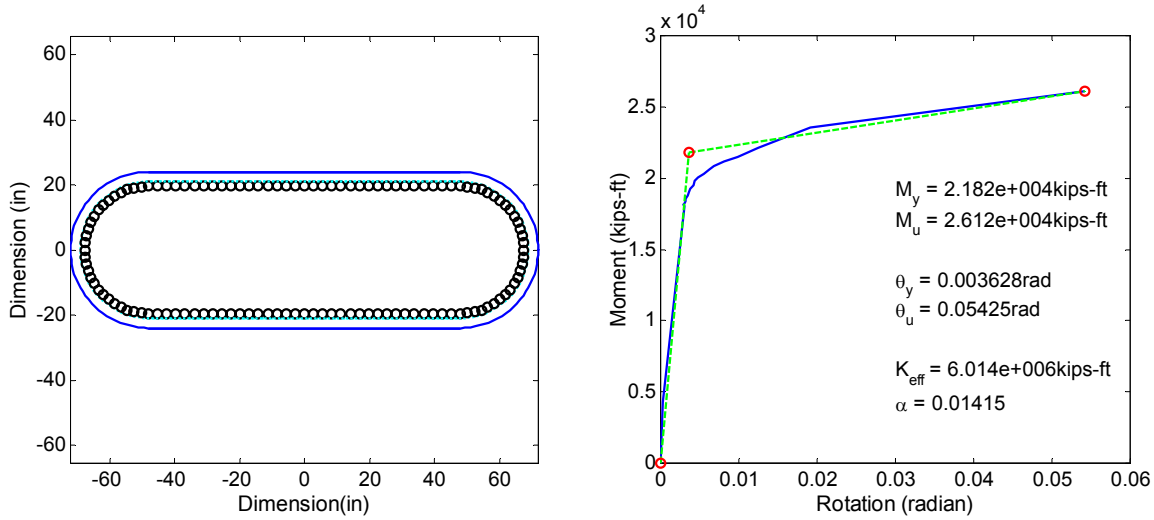

(a) Section of Column (b) Moment-Rotation Curve

(a10) Column 10 of Bridge 5 before retrofit

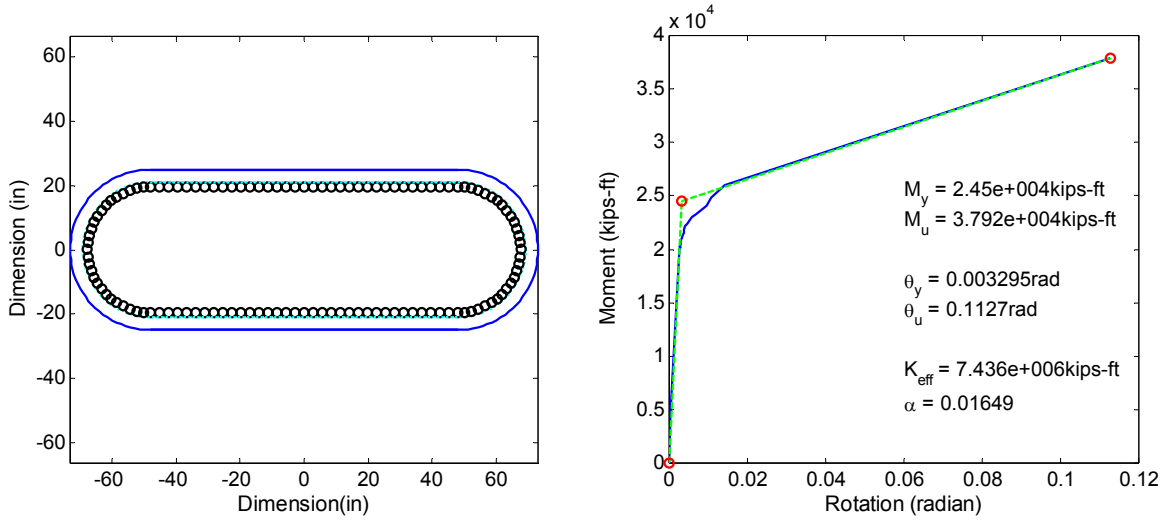

(a) Section of Column (b) Moment-Rotation Curve

(b10) Column 10 of Bridge 5 after retrofit

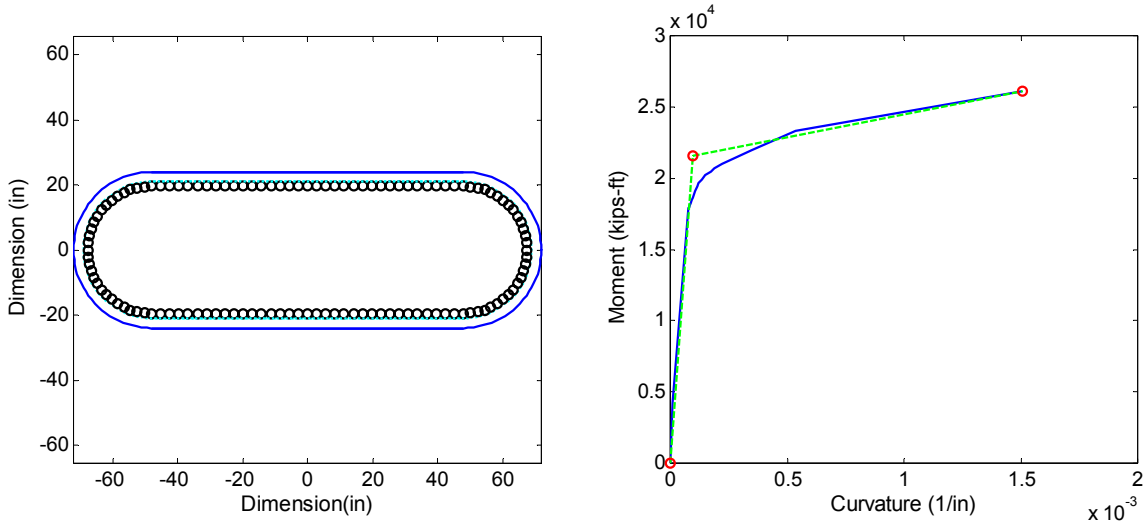

(a) Section of Column (b) Moment-Rotation Curve

(a11) Column 11 of Bridge 5 before retrofit

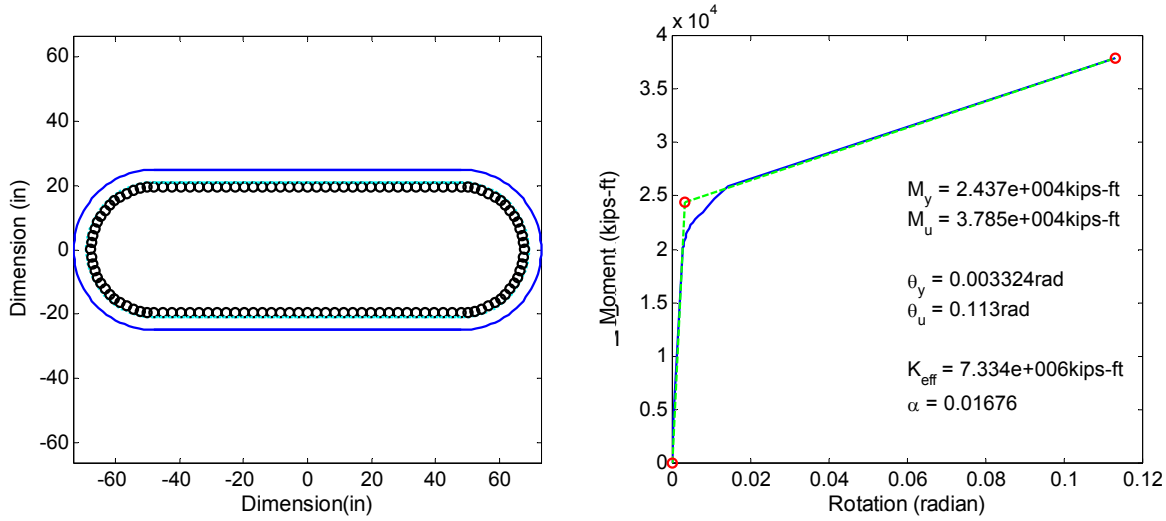

(a) Section of Column (b) Moment-Rotation Curve

(b11) Column 11 of Bridge 5 after retrofit

Fig. A.5 Moment-Curvature Analysis of Bridge 5

A.2 Moment-Curvature Curves for Transverse Direction of Bridges

Section of the column, stress-strain relationship, distribution of axial force, P-M interaction diagram, moment-curvature curve and moment-rotation curve for columns of Bridge 3~5 before and after retrofit are plotted in the following figures.

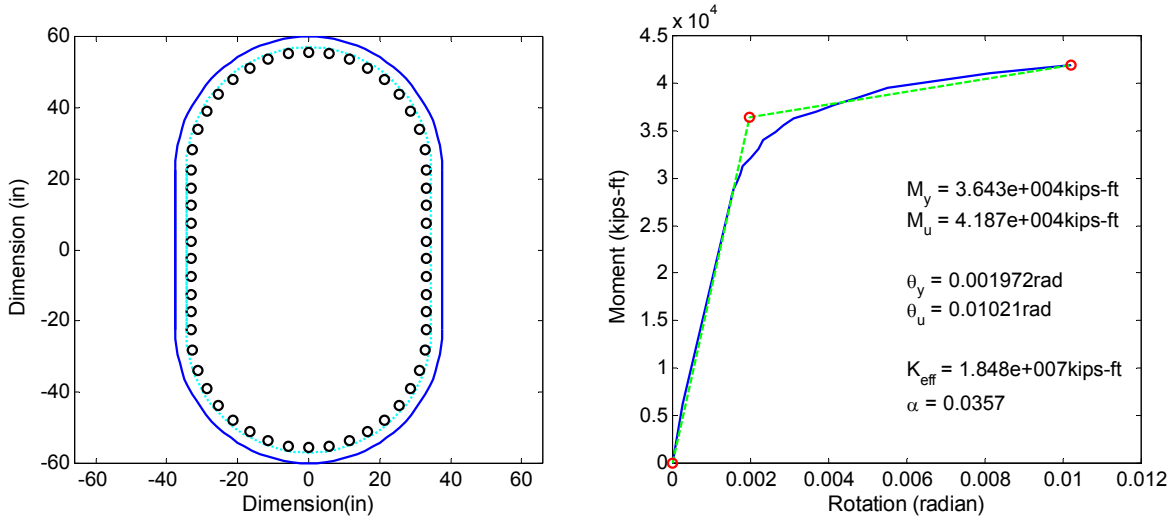

(a) Section of Column (b) Moment-Rotation Curve

(a1) Column 1 of Bridge 3 before retrofit

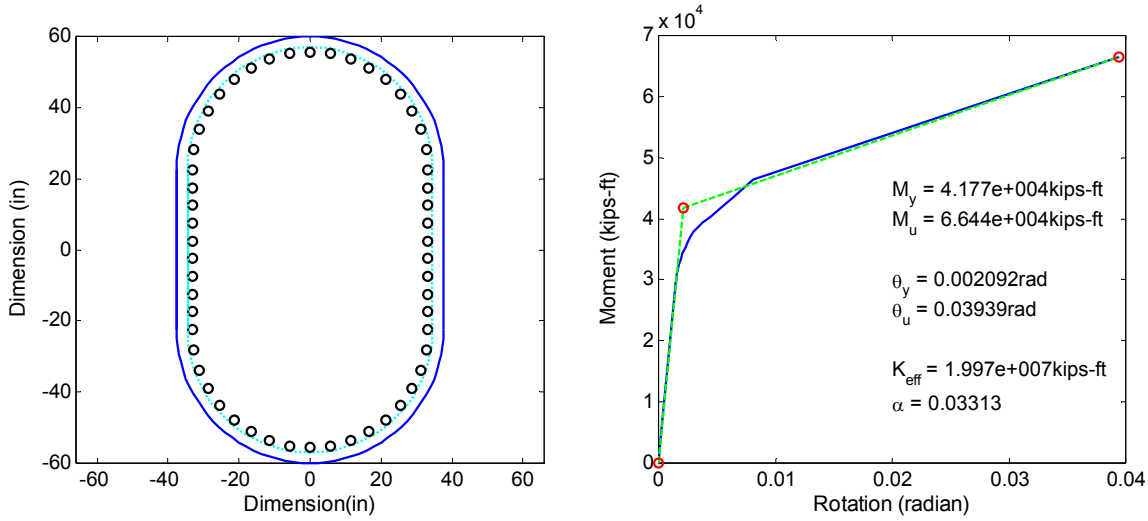

(a) Section of Column (b) Moment-Rotation Curve

(b1) Column 1 of Bridge 3 after retrofit

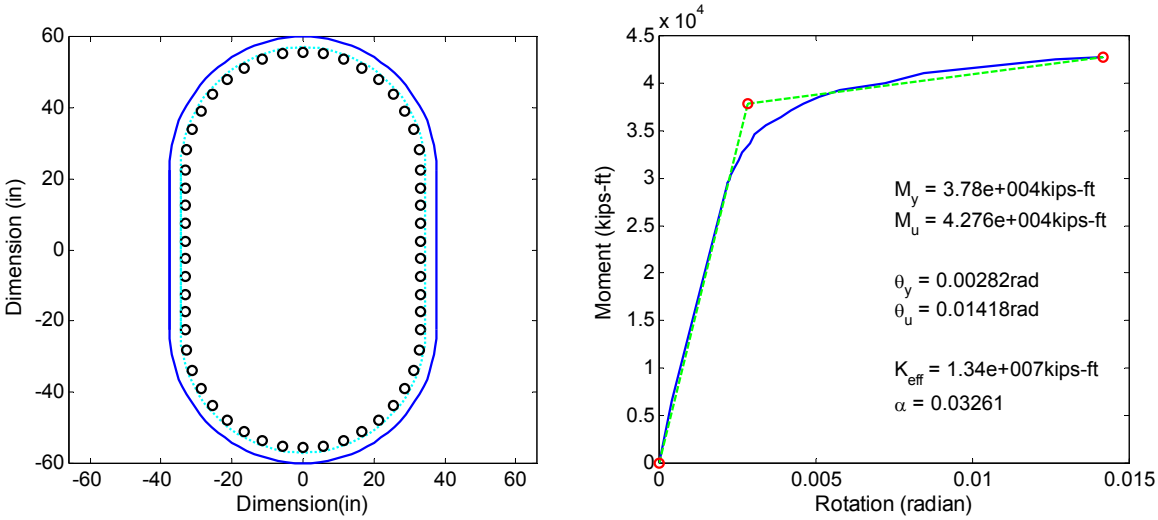

(a) Section of Column (b) Moment-Rotation Curve

(a2) Column 2 of Bridge 3 before retrofit

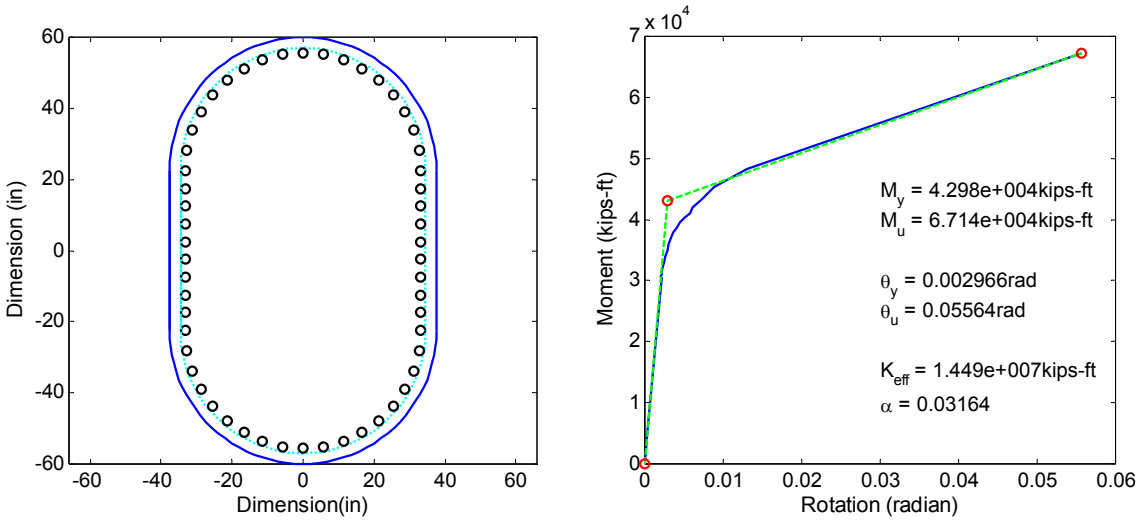

(a) Section of Column (b) Moment-Rotation Curve

(b2) Column 2 of Bridge 3 after retrofit

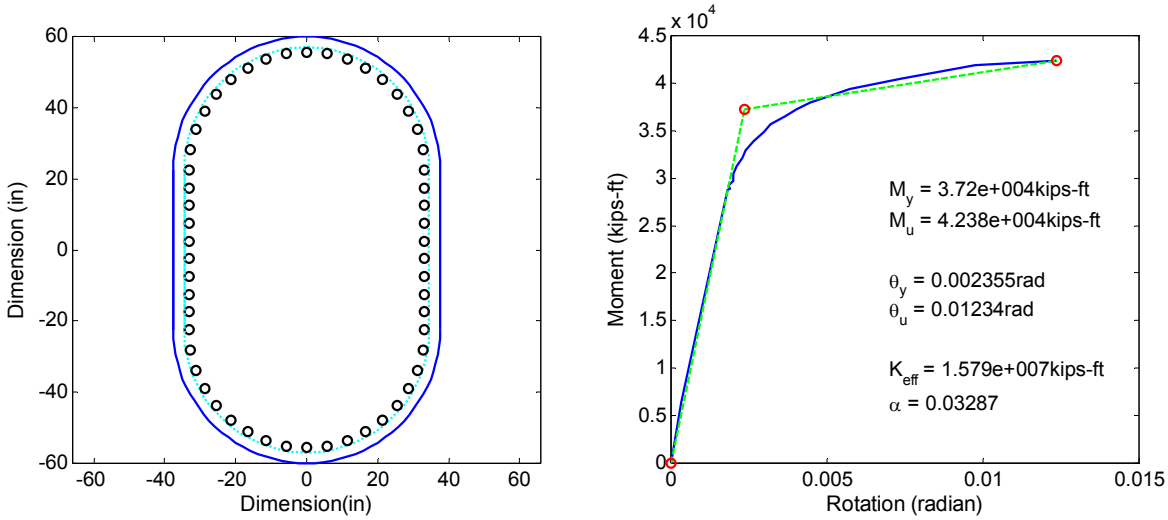

(a) Section of Column (b) Moment-Rotation Curve

(a3) Column 3 of Bridge 3 before retrofit

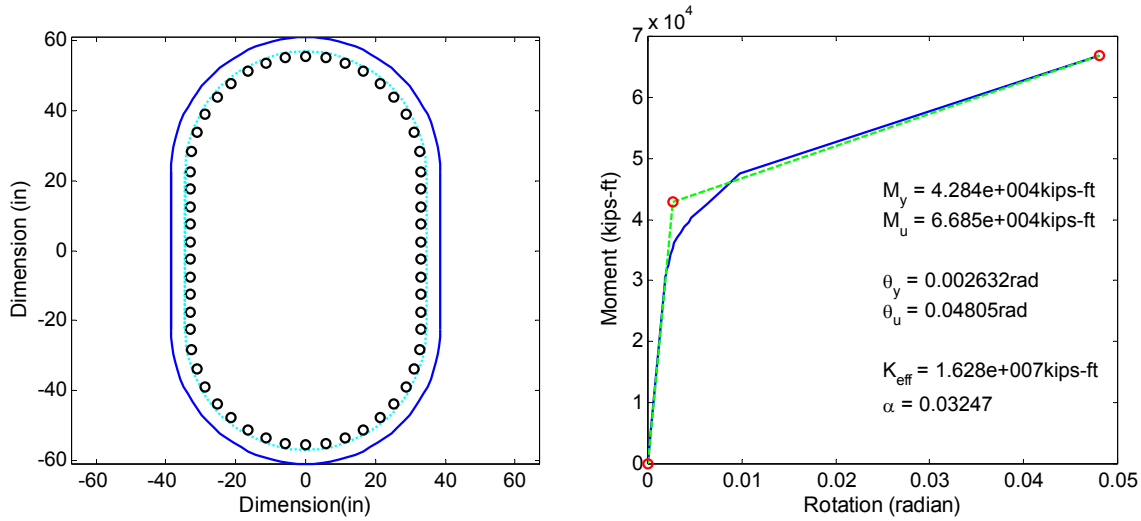

(a) Section of Column (b) Moment-Rotation Curve

(b3) Column 3 of Bridge 3 after retrofit

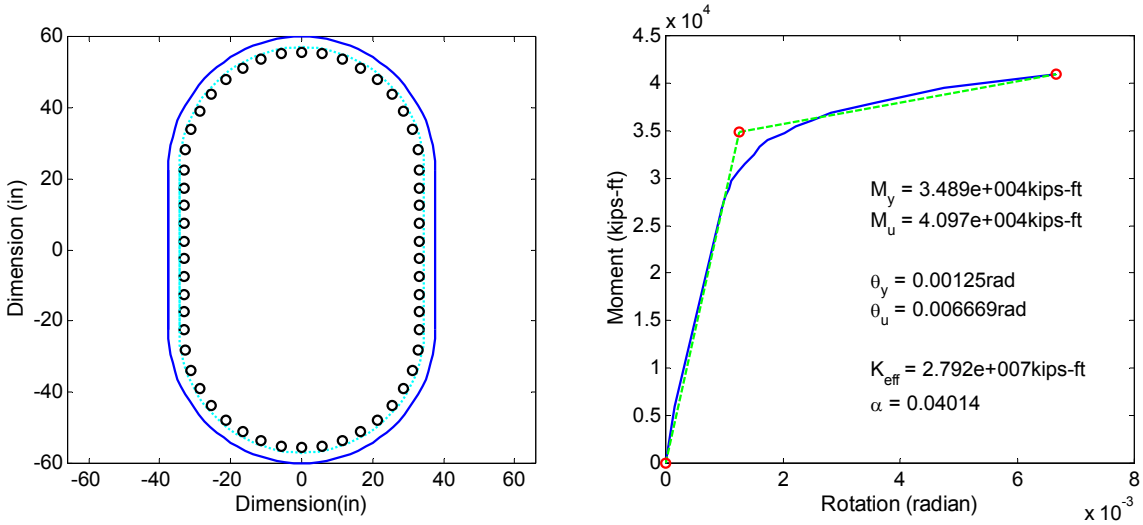

(a) Section of Column (b) Moment-Rotation Curve

(a4) Column 4 of Bridge 3 before retrofit

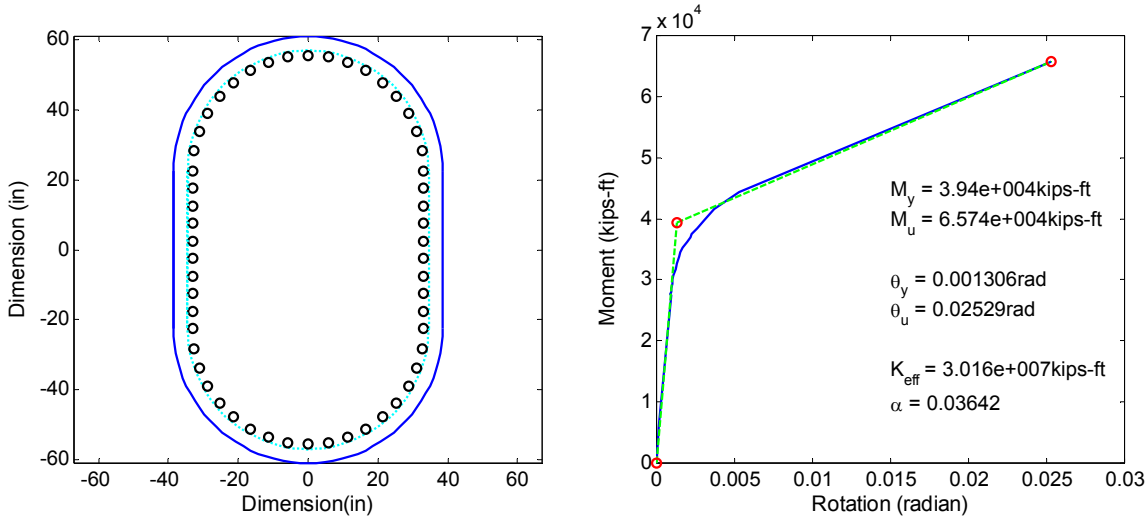

(a) Section of Column (b) Moment-Rotation Curve

(b4) Column 4 of Bridge 3 after retrofit

Fig. A.6 Moment-Curvature Analysis of Bridge 3

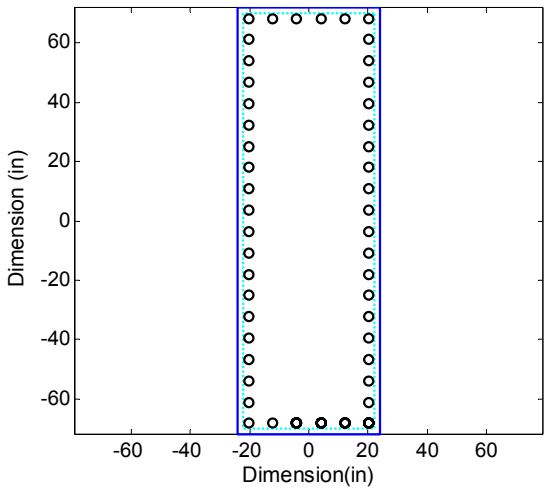

(a) Section of Column

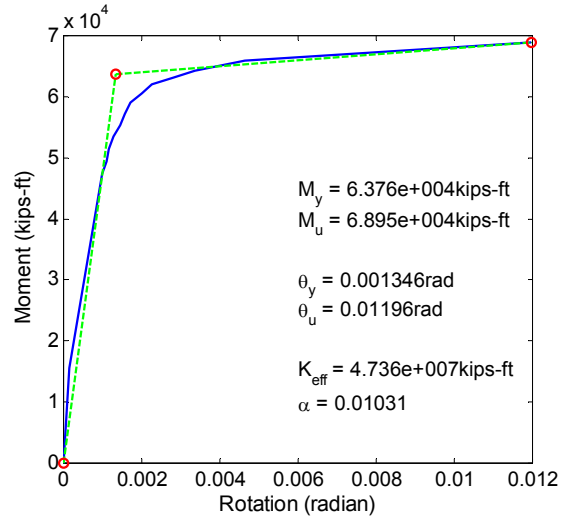

(b) Moment-Rotation Curve

(a1) Column 1 of Bridge 4 before retrofit

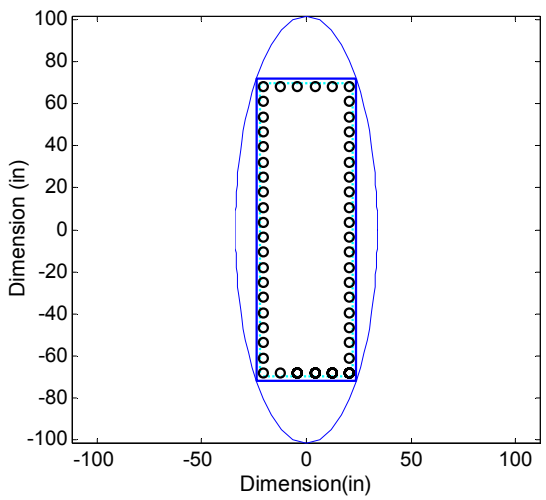

(a) Section of Column

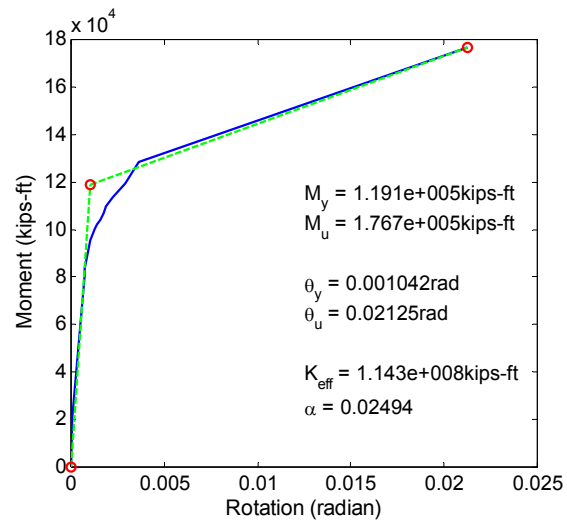

(b) Moment-Rotation Curve

(b1) Column 1 of Bridge 4 after retrofit

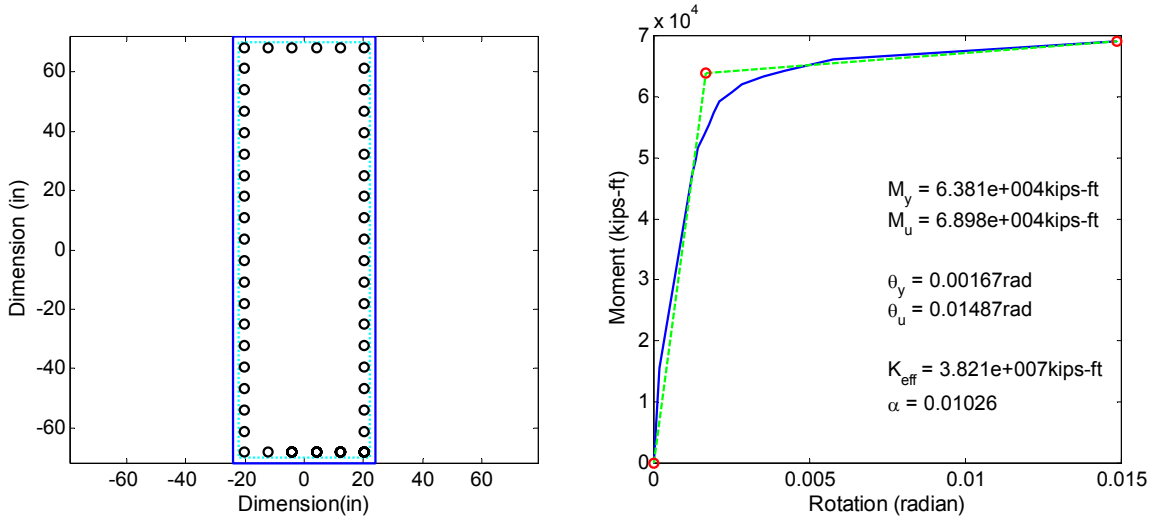

(a) Section of Column (b) Moment-Rotation Curve

(a2) Column 2 of Bridge 4 before retrofit

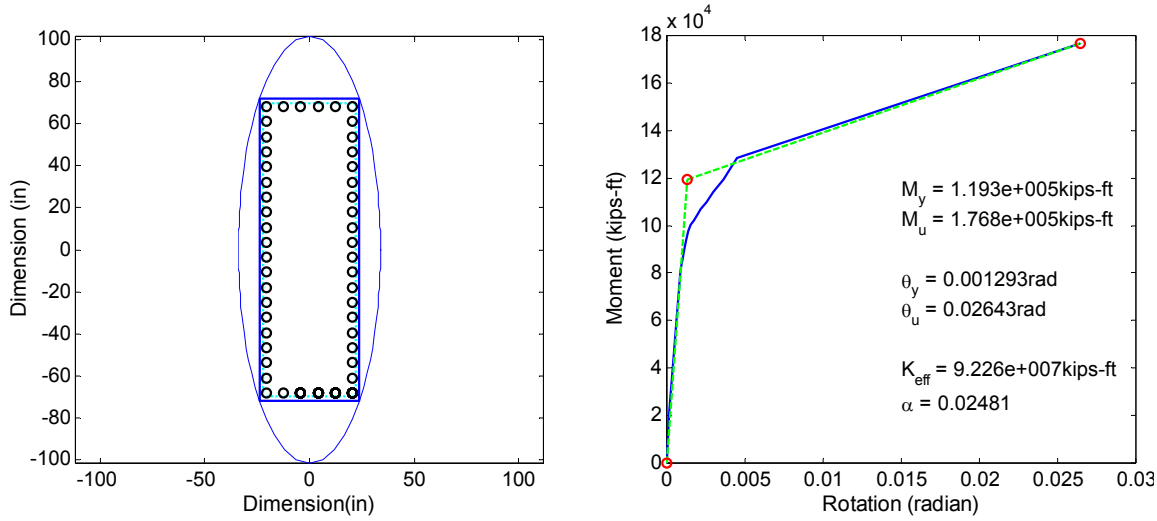

(a) Section of Column (b) Moment-Rotation Curve

(b2) Column 2 of Bridge 4 after retrofit

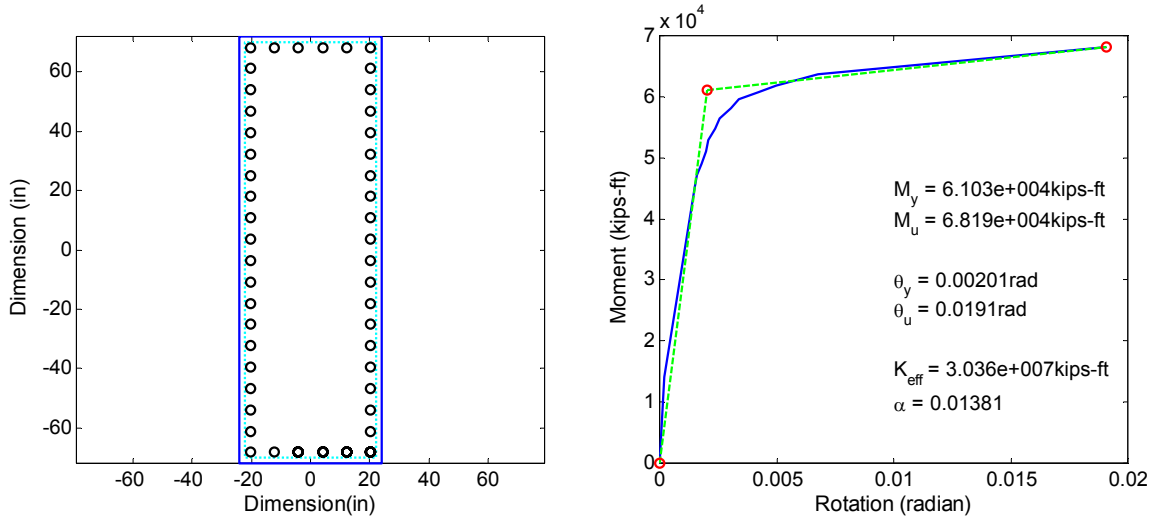

(a) Section of Column (b) Moment-Rotation Curve

(a3) Column 3 of Bridge 4 before retrofit

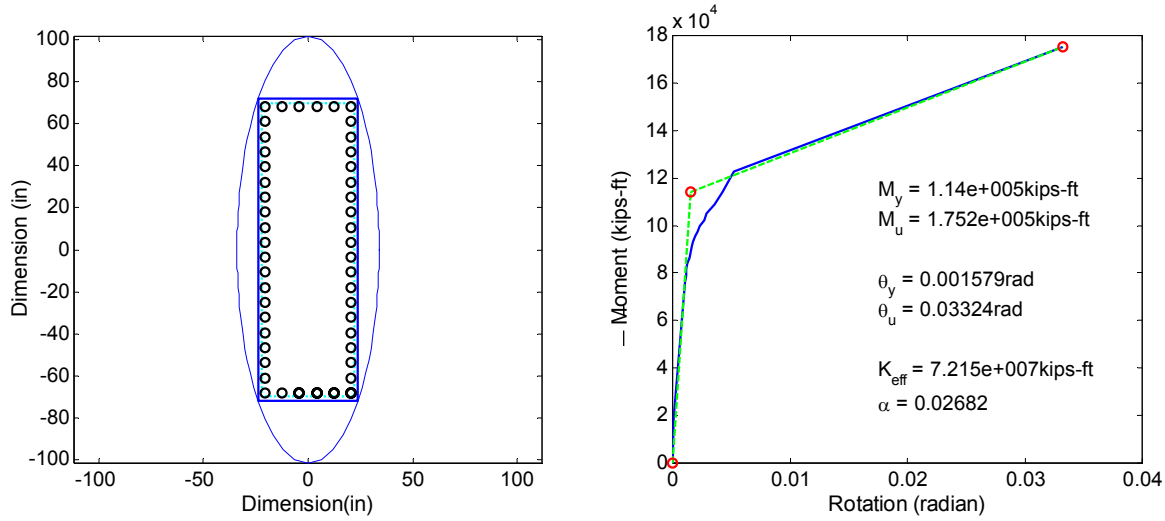

(a) Section of Column (b) Moment-Rotation Curve

(b3) Column 3 of Bridge 4 after retrofit

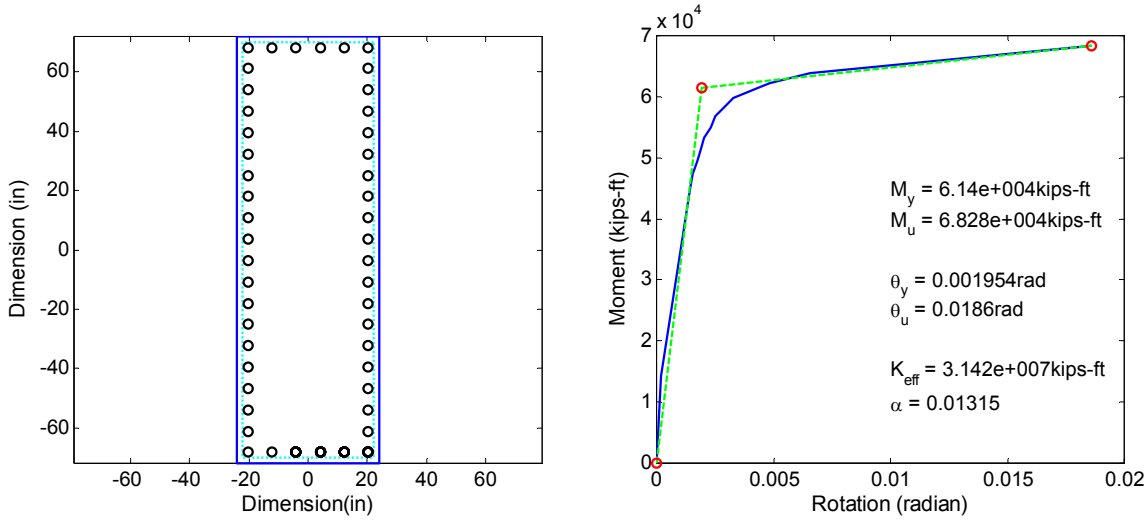

(a) Section of Column (b) Moment-Rotation Curve

(a4) Column 4 of Bridge 4 before retrofit

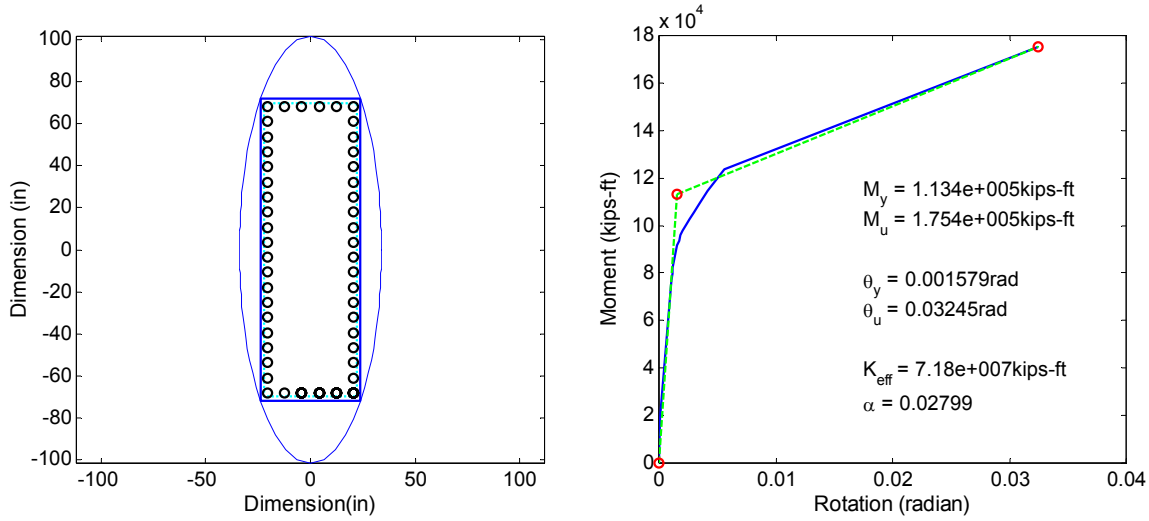

(a) Section of Column (b) Moment-Rotation Curve

(b4) Column 4 of Bridge 4 after retrofit

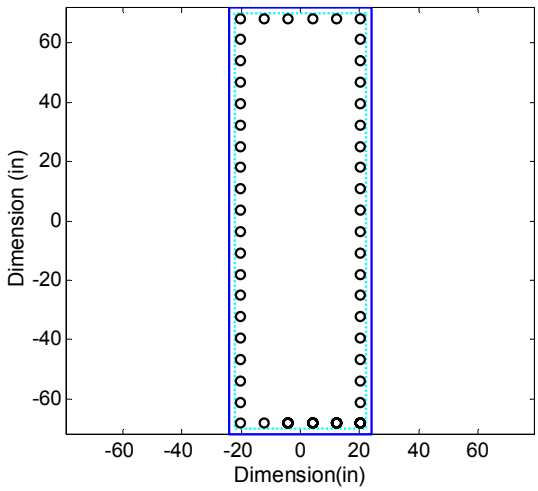

(a) Section of Column

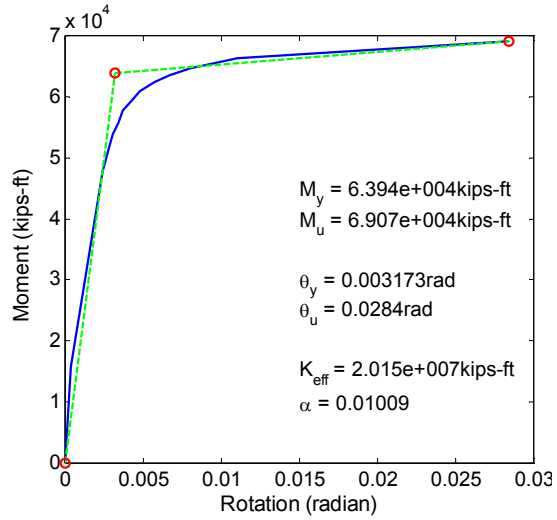

(b) Moment-Rotation Curve

(a5) Column 5 of Bridge 4 before retrofit

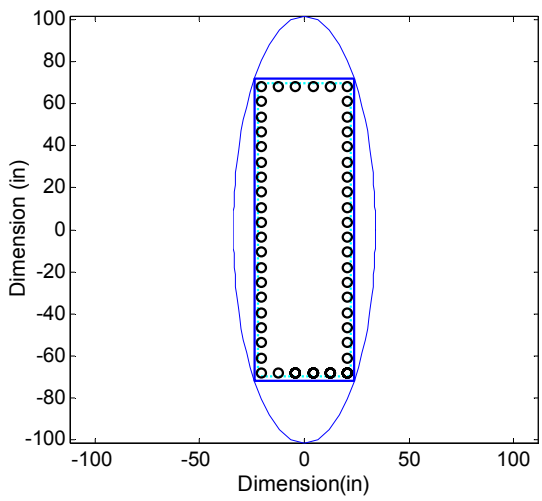

(a) Section of Column

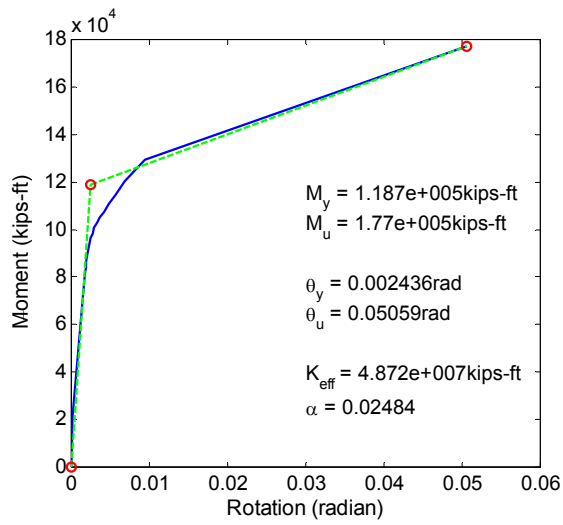

(b) Moment-Rotation Curve

(b5) Column 5 of Bridge 4 after retrofit

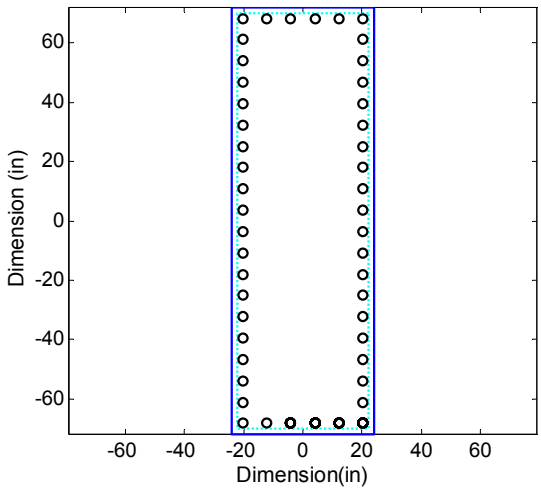

(a) Section of Column

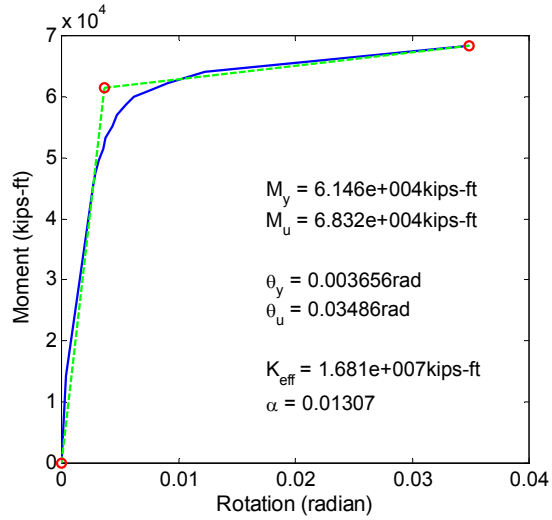

(b) Moment-Rotation Curve

(a6) Column 6 of Bridge 4 before retrofit

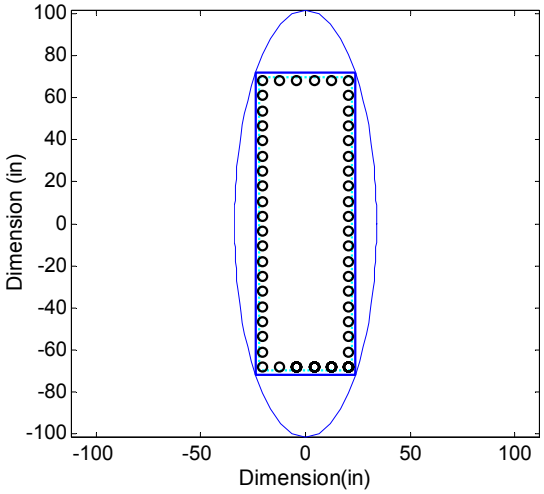

(a) Section of Column

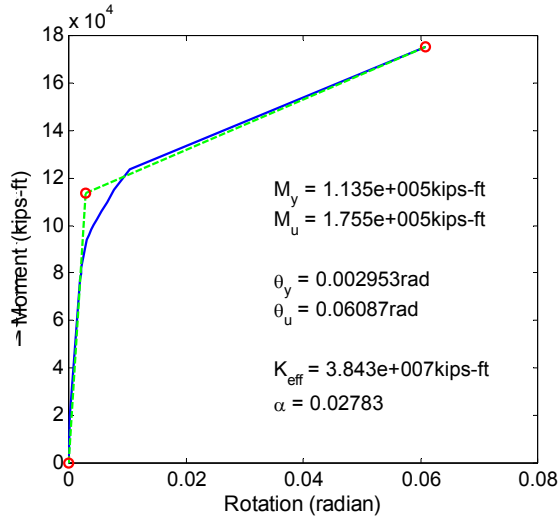

(b) Moment-Rotation Curve

(b6) Column 6 of Bridge 4 after retrofit

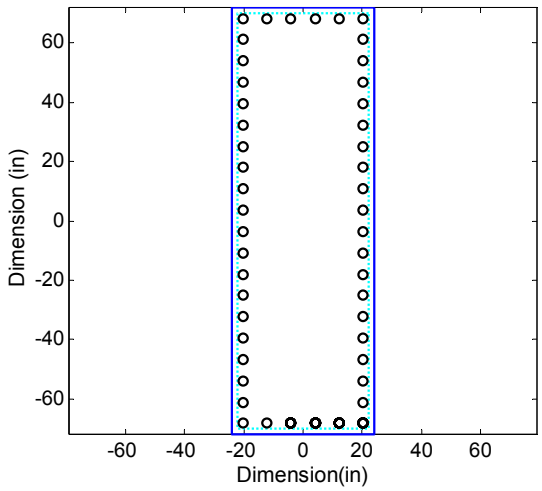

(a) Section of Column

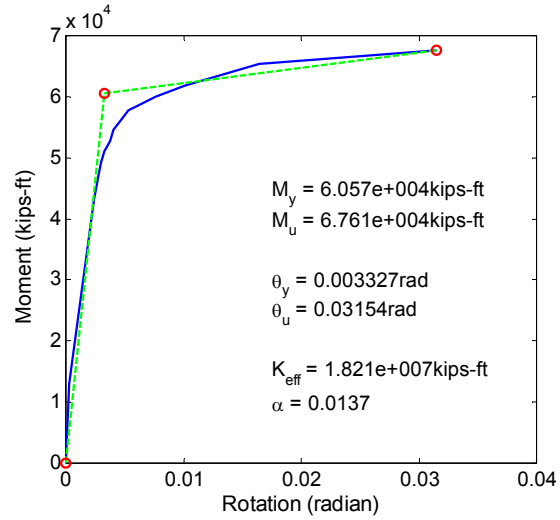

(b) Moment-Rotation Curve

(a7) Column 7 of Bridge 4 before retrofit

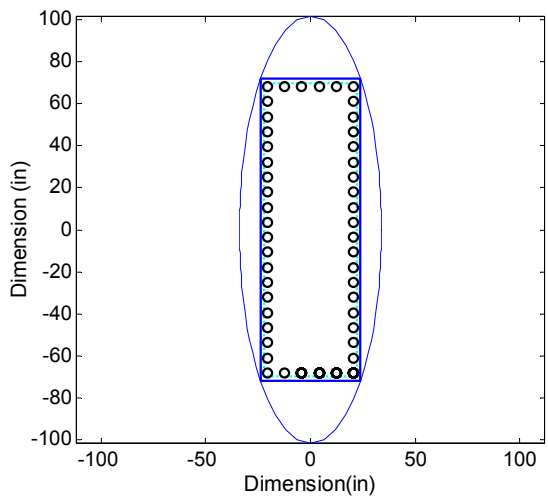

(a) Section of Column

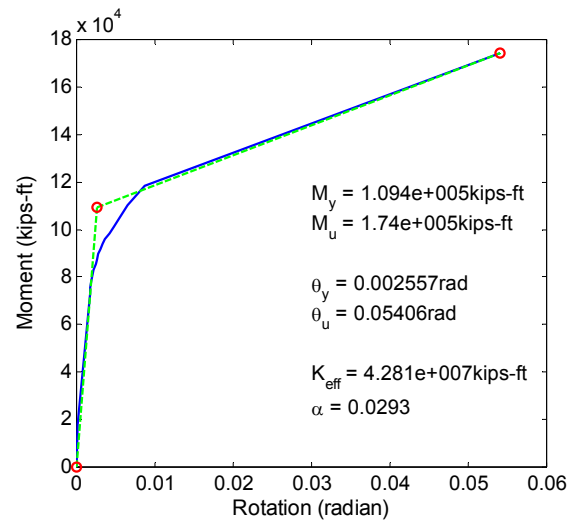

(b) Moment-Rotation Curve

(b7) Column 7 of Bridge 4 after retrofit

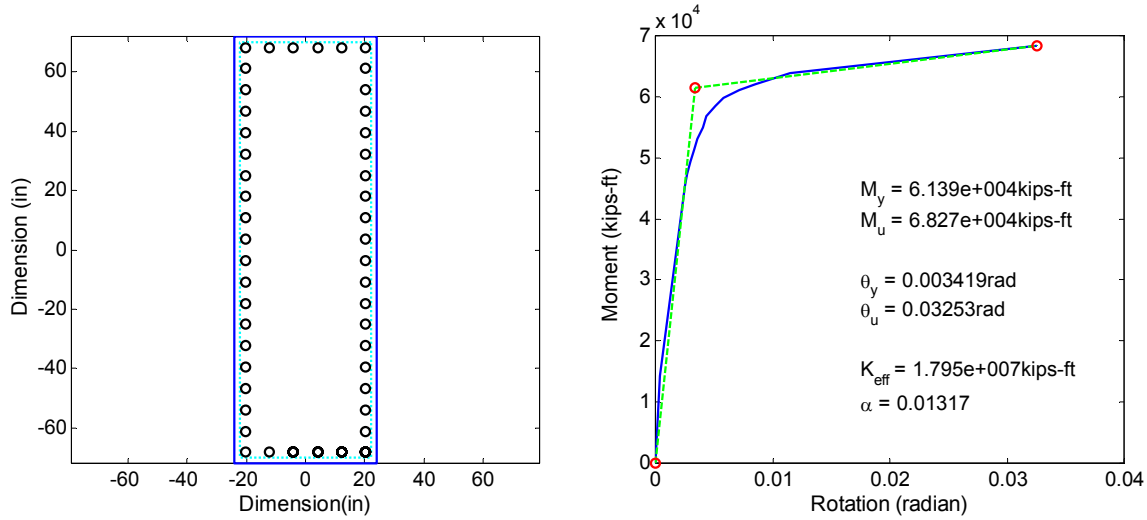

(a) Section of Column (b) Moment-Rotation Curve

(a8) Column 8 of Bridge 4 before retrofit

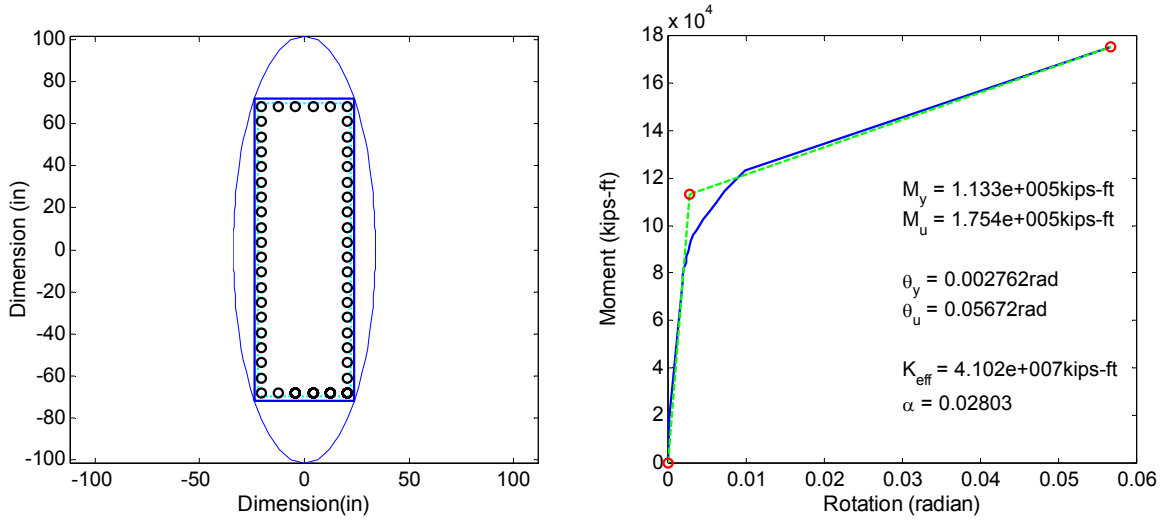

(a) Section of Column (b) Moment-Rotation Curve

(b8) Column 8 of Bridge 4 after retrofit

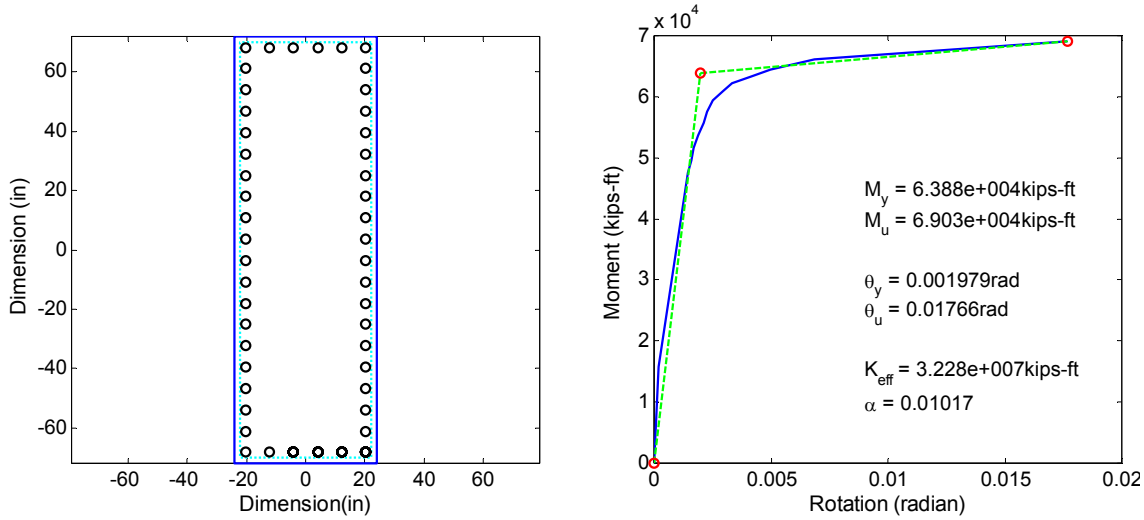

(a) Section of Column (b) Moment-Rotation Curve

(a9) Column 9 of Bridge 4 before retrofit

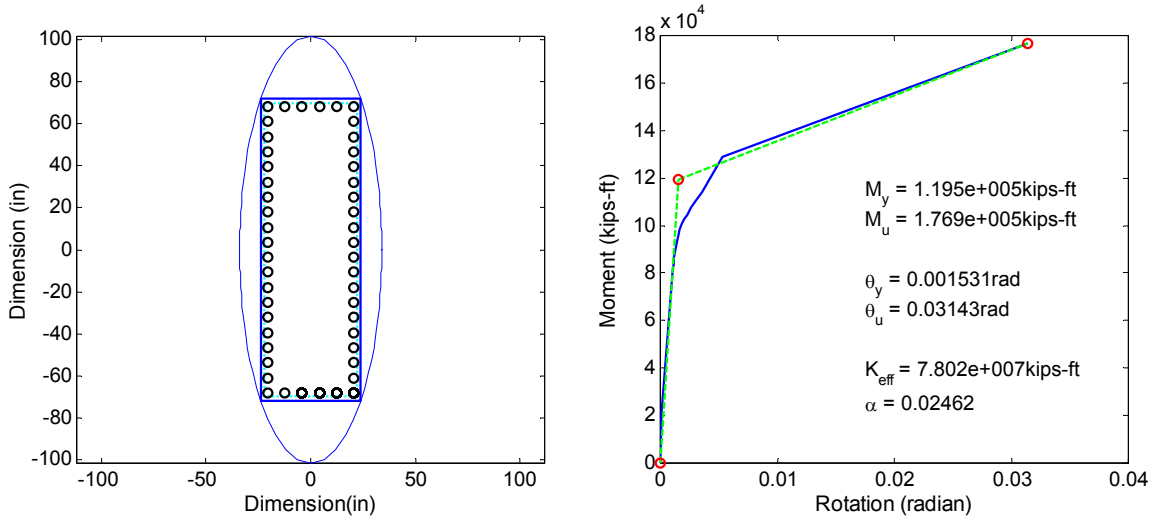

(a) Section of Column (b) Moment-Rotation Curve

(b9) Column 9 of Bridge 4 after retrofit

Fig. A.7 Moment-Curvature Analysis of Bridge 4

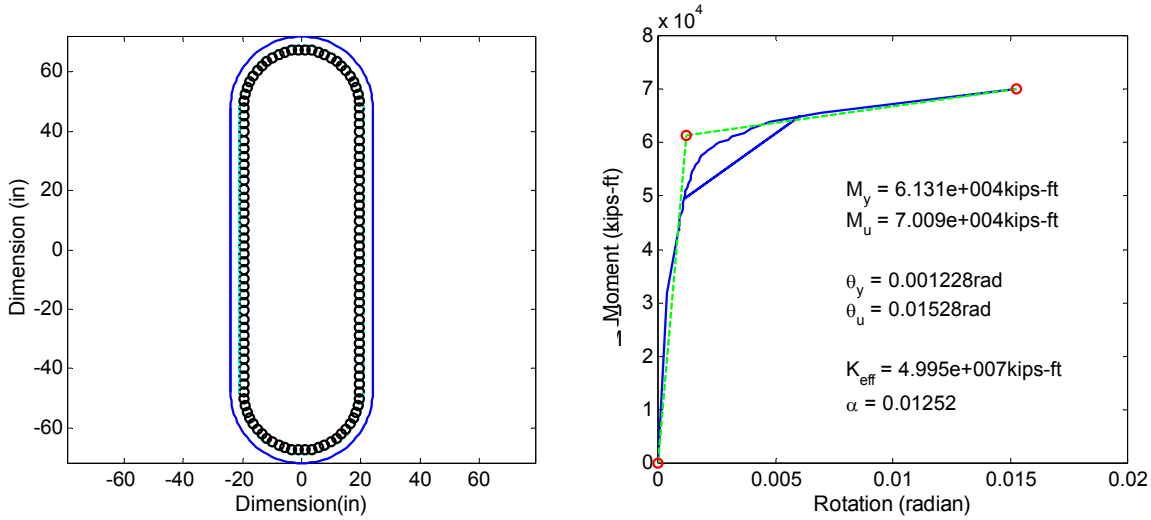

(a) Section of Column (b) Moment-Rotation Curve

(a1) Column 1 of Bridge 5 before retrofit

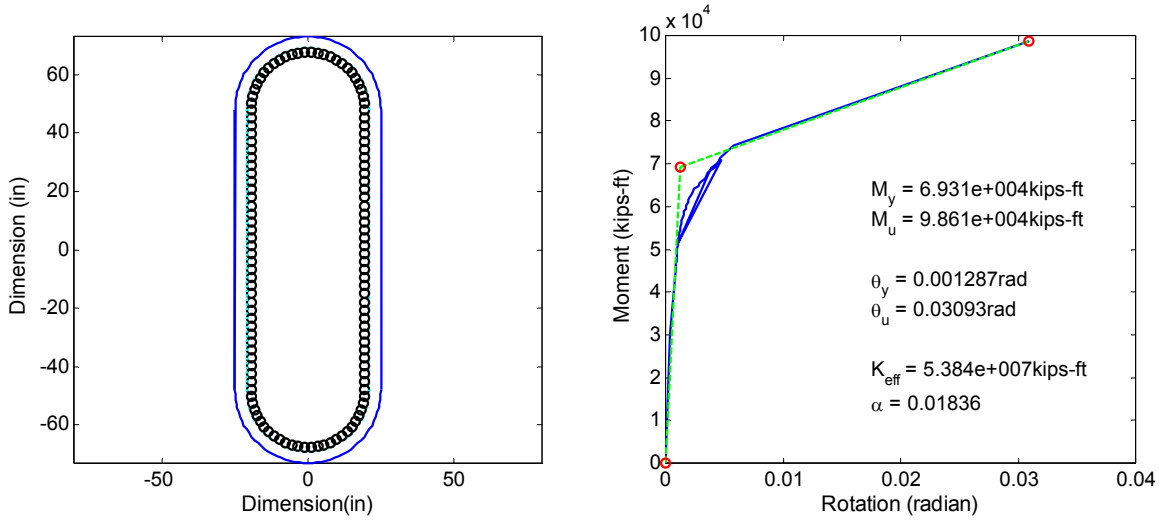

(a) Section of Column (b) Moment-Rotation Curve

(b1) Column 1 of Bridge 5 after retrofit

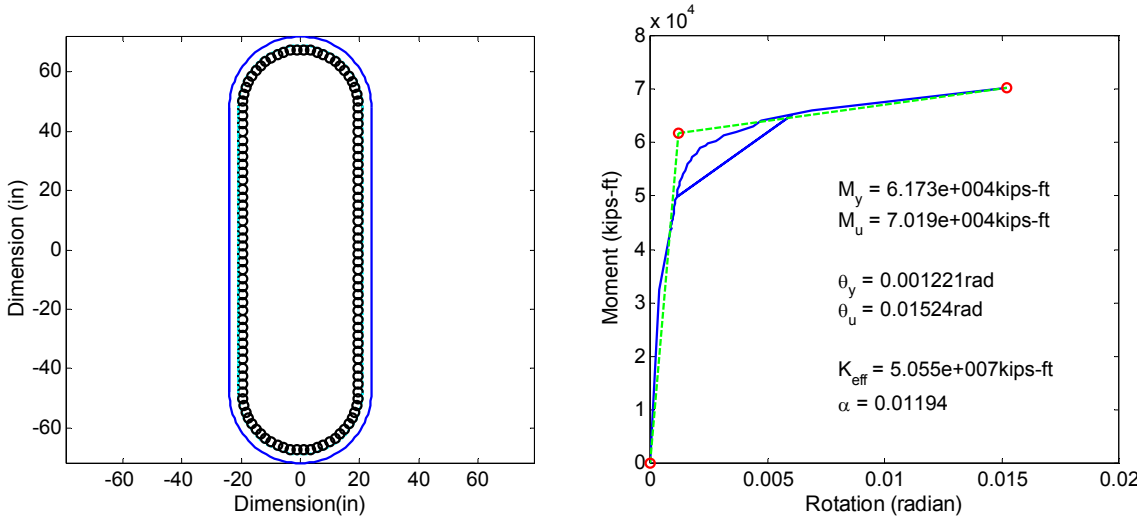

(a) Section of Column (b) Moment-Rotation Curve

(a2) Column 2 of Bridge 5 before retrofit

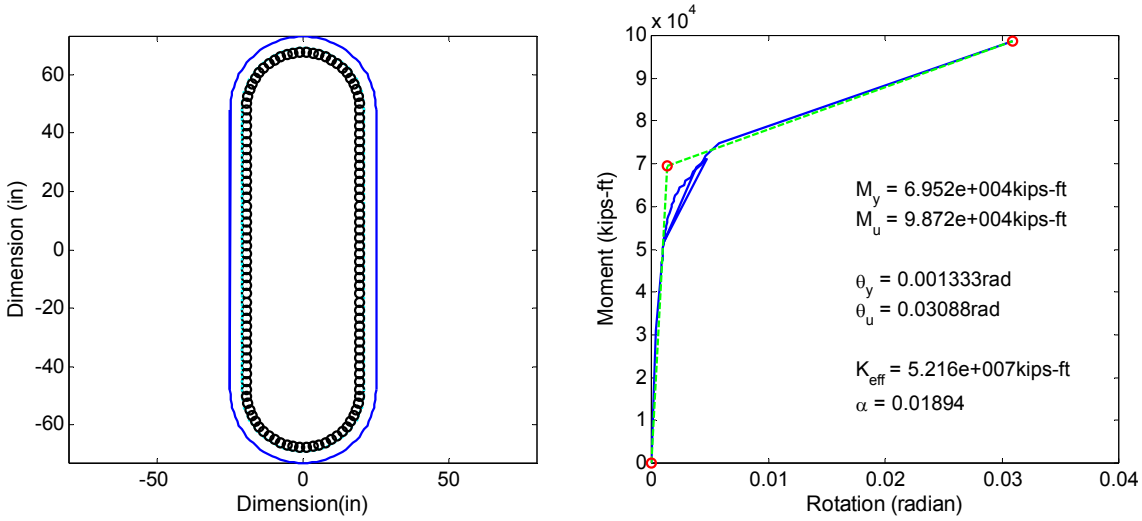

(a) Section of Column (b) Moment-Rotation Curve

(b2) Column 2 of Bridge 5 after retrofit

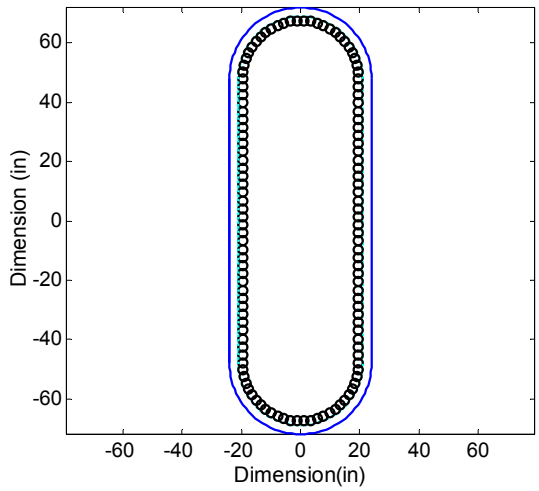

(a) Section of Column

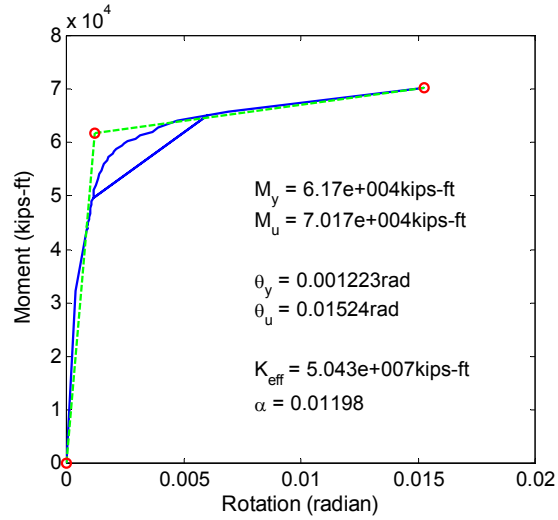

(b) Moment-Rotation Curve

(a3) Column 3 of Bridge 5 before retrofit

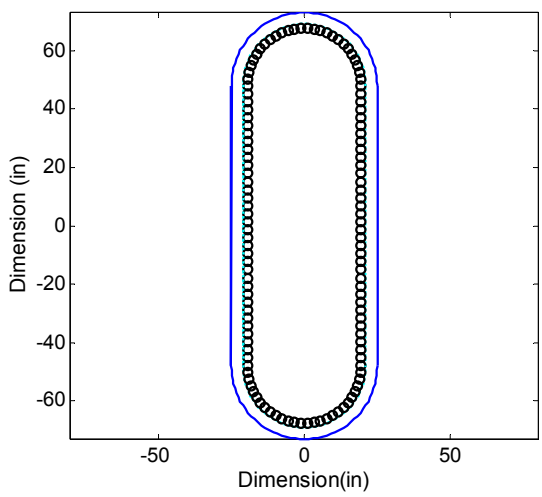

(a) Section of Column

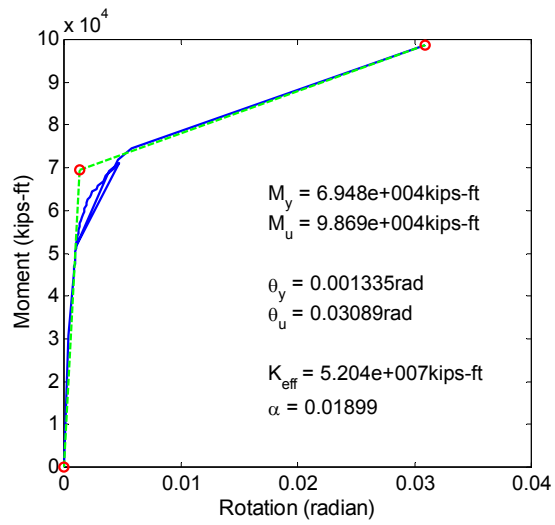

(b) Moment-Rotation Curve

(b3) Column 3 of Bridge 5 after retrofit

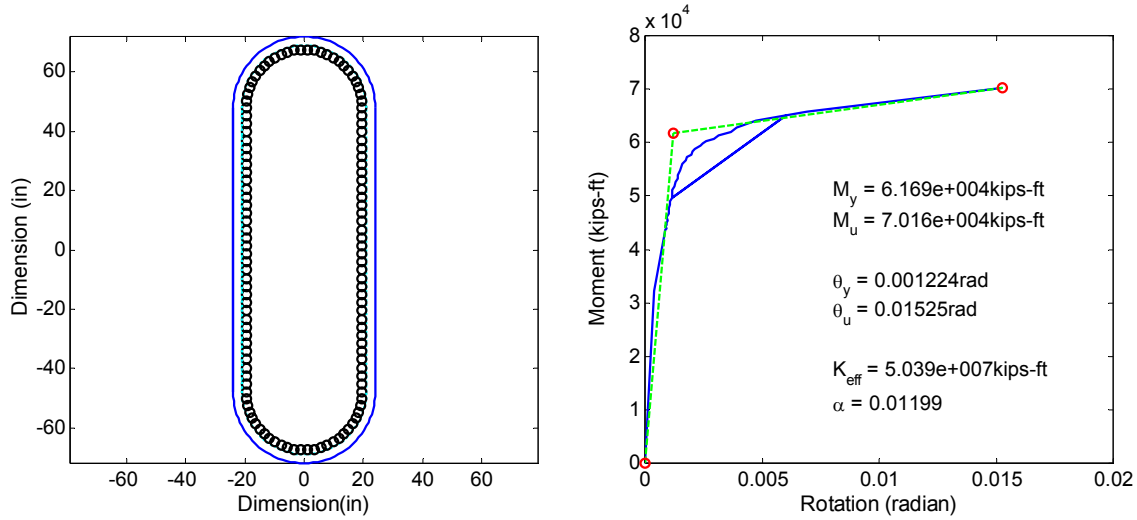

(a) Section of Column (b) Moment-Rotation Curve

(a4) Column 4 of Bridge 5 before retrofit

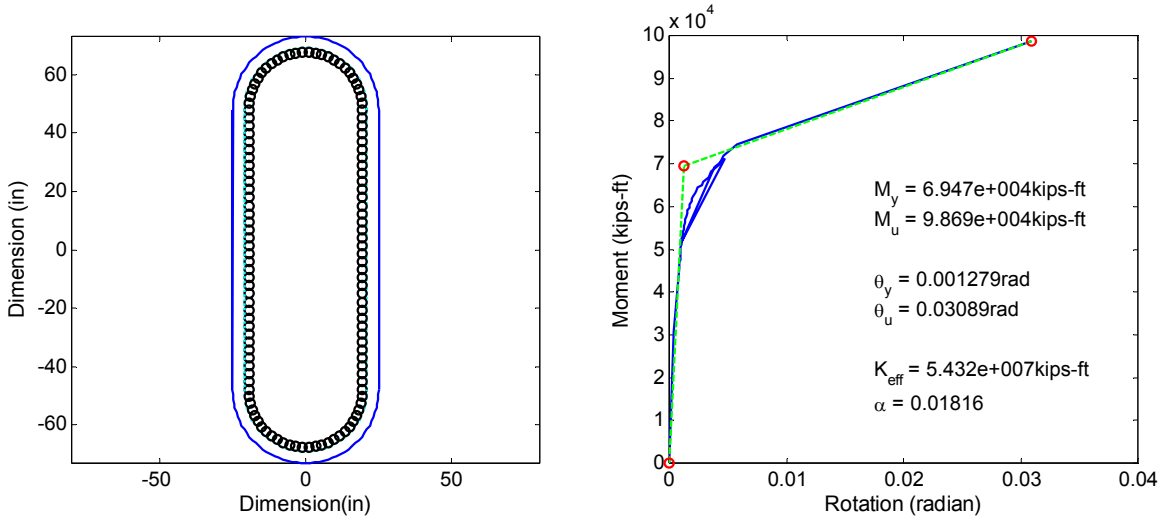

(a) Section of Column (b) Moment-Rotation Curve

(b4) Column 4 of Bridge 5 after retrofit

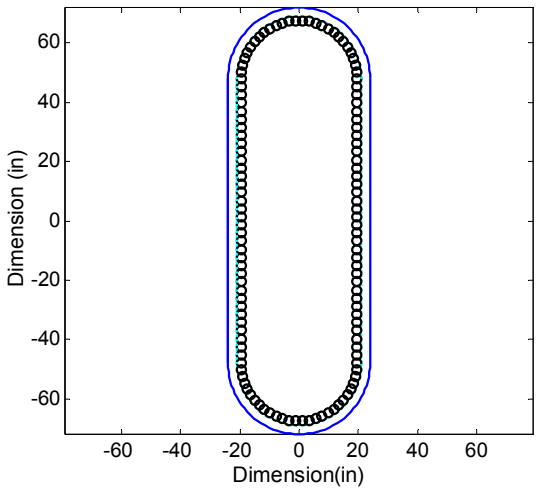

(a) Section of Column

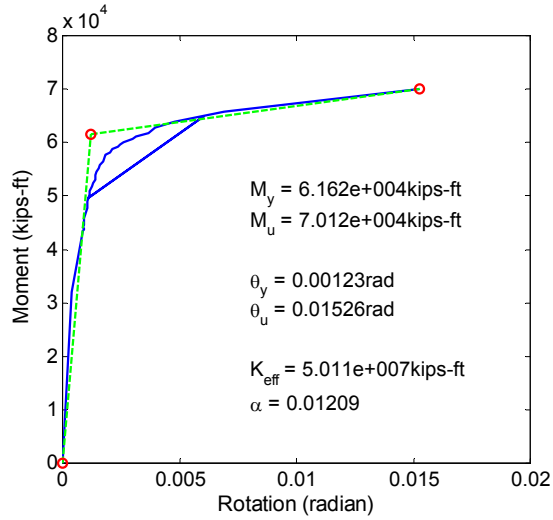

(b) Moment-Rotation Curve

(a5) Column 5 of Bridge 5 before retrofit

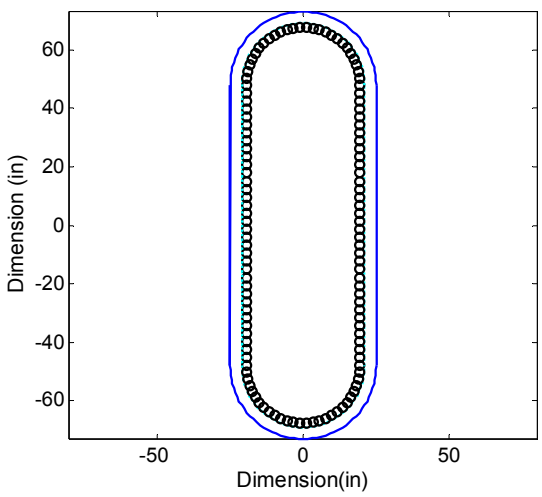

(a) Section of Column

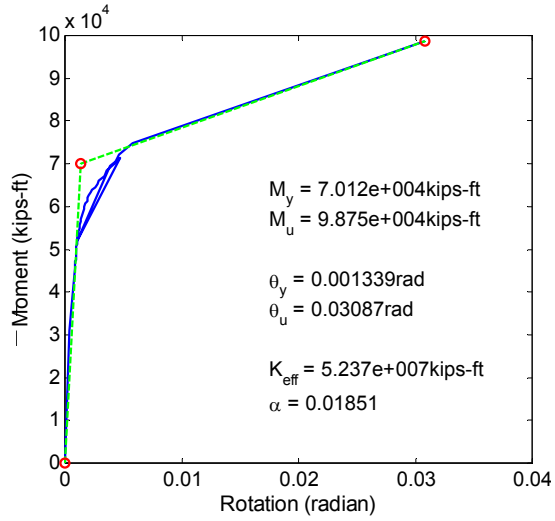

(b)) Moment-Rotation Curve

(b5) Column 5 of Bridge 5 after retrofit

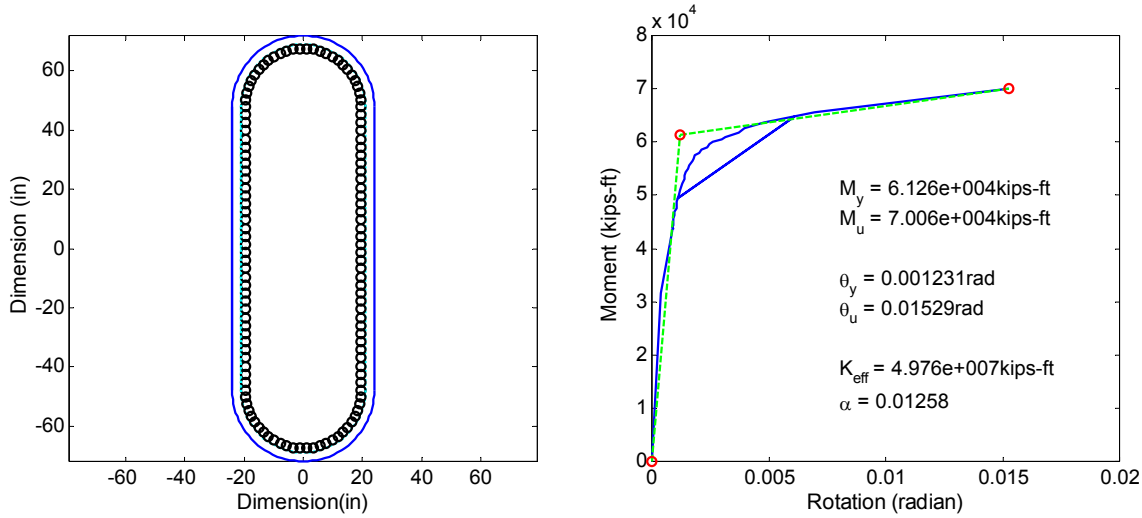

(a) Section of Column (b) Moment-Rotation Curve

(a6) Column 6 of Bridge 5 before retrofit

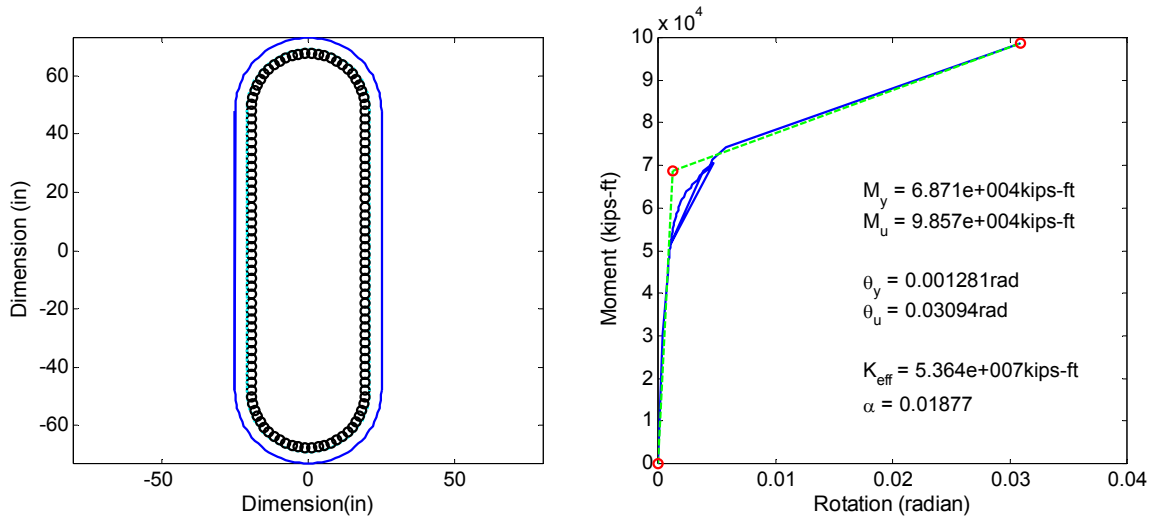

(a) Section of Column (b) Moment-Rotation Curve

(b6) Column 6 of Bridge 5 after retrofit

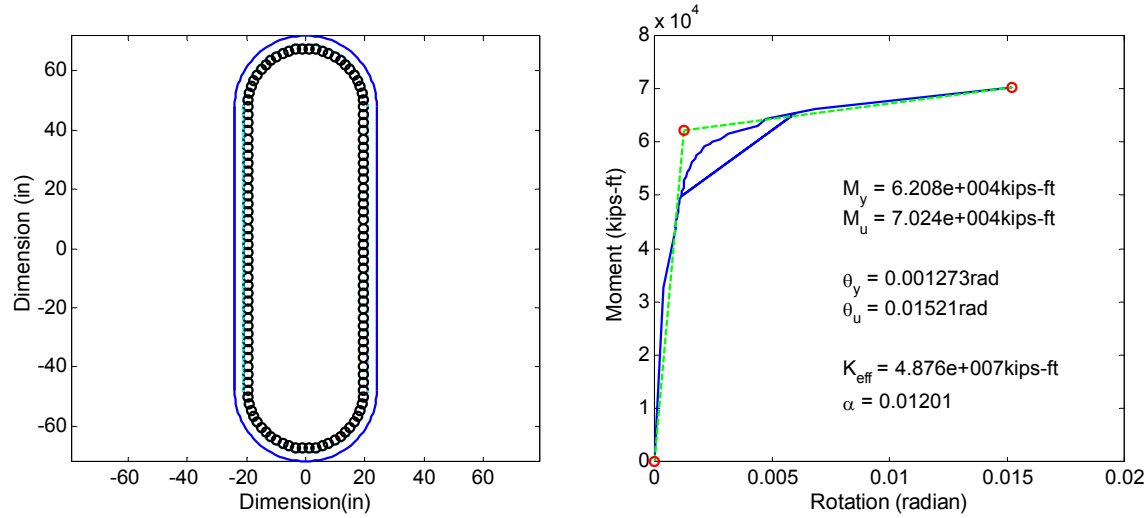

(a) Section of Column (b) Moment-Rotation Curve

(a7) Column 7 of Bridge 5 before retrofit

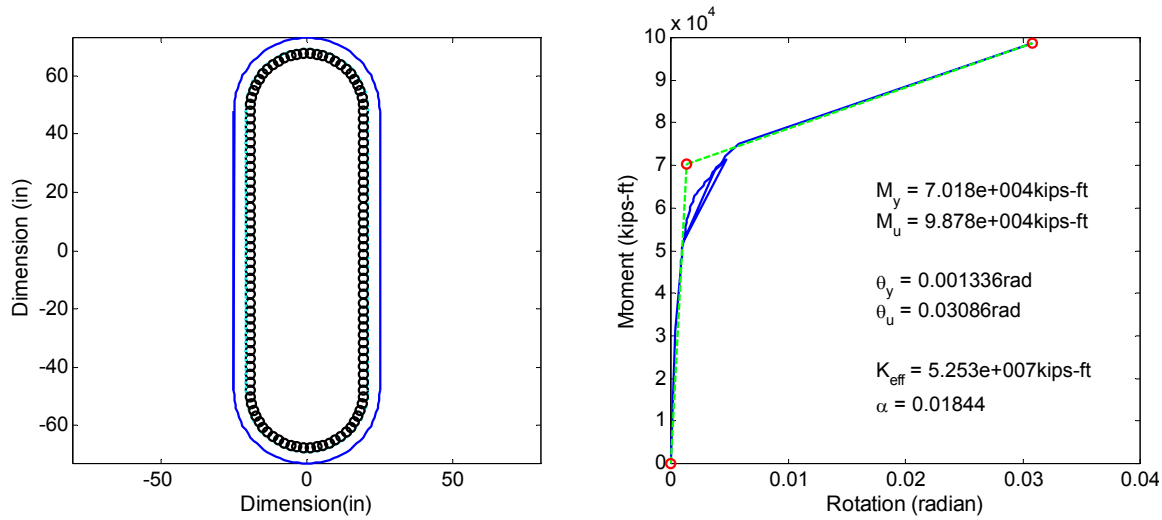

(a) Section of Column (b) Moment-Rotation Curve

(b7) Column 7 of Bridge 5 after retrofit

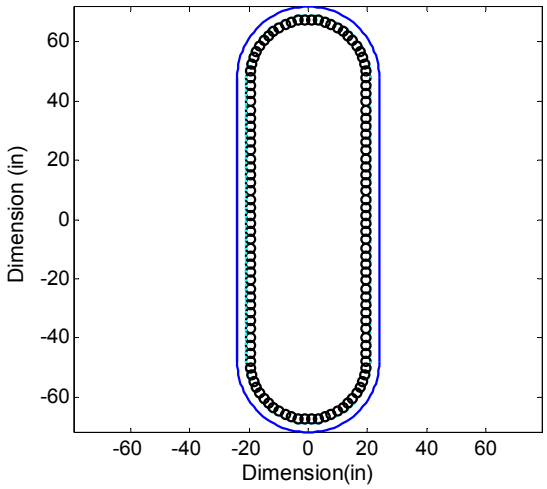

(a) Section of Column

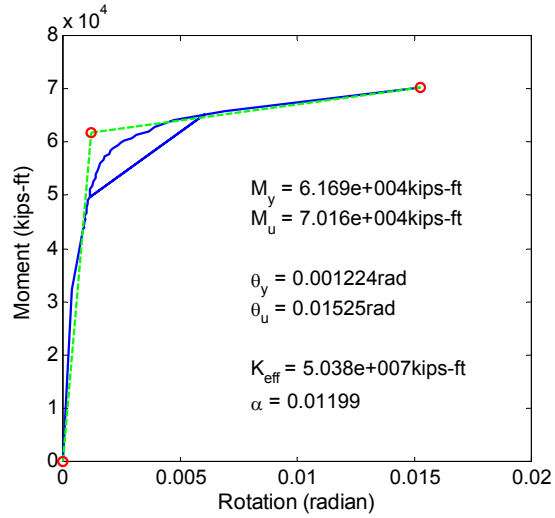

(b) Moment-Rotation Curve

(a8) Column 8 of Bridge 5 before retrofit

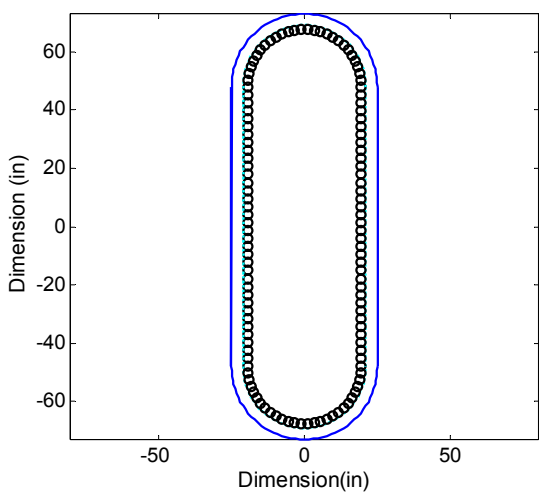

(a) Section of Column

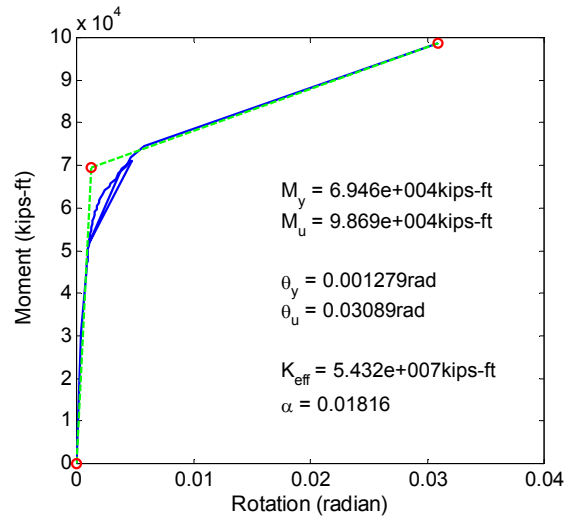

(b) Moment-Rotation Curve

(b8) Column 8 of Bridge 5 after retrofit

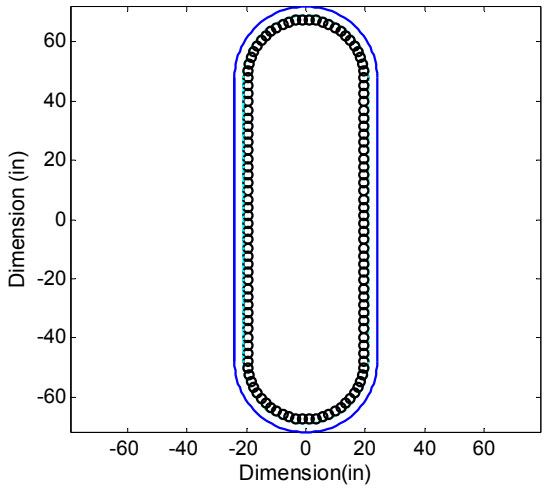

(a) Section of Column

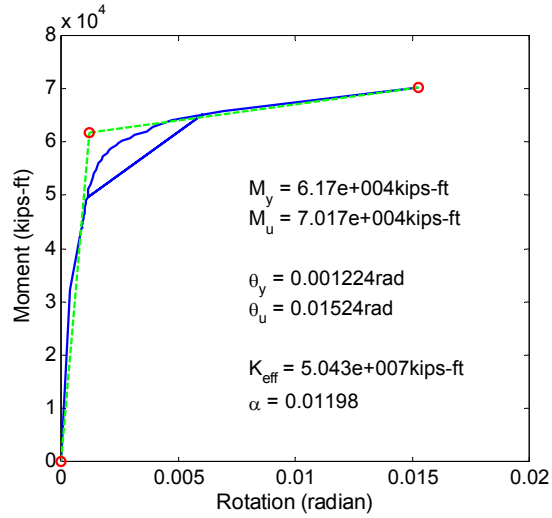

(b) Moment-Rotation Curve

(a9) Column 9 of Bridge 5 before retrofit

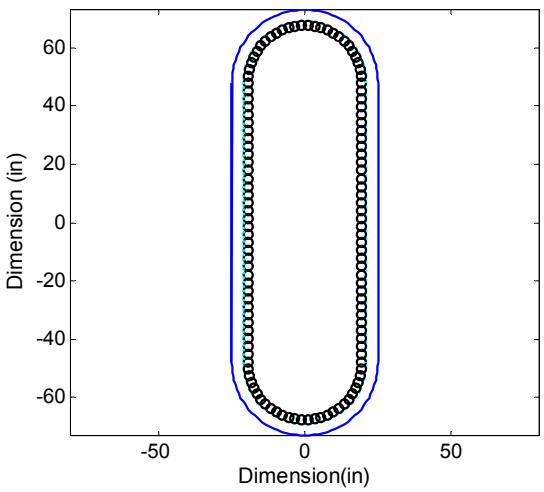

(a) Section of Column

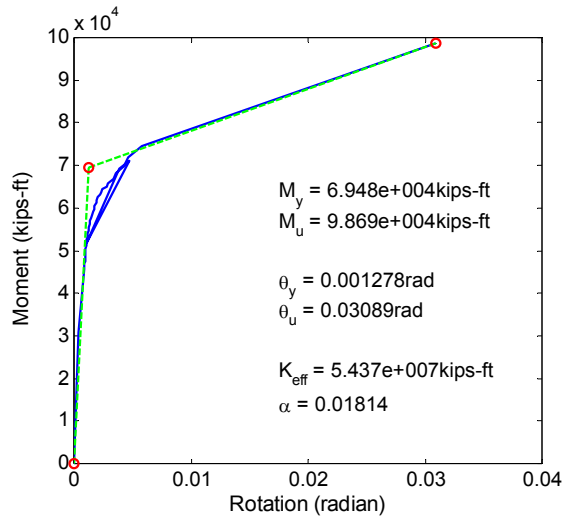

(b) Moment-Rotation Curve

(b9) Column 9 of Bridge 5 after retrofit

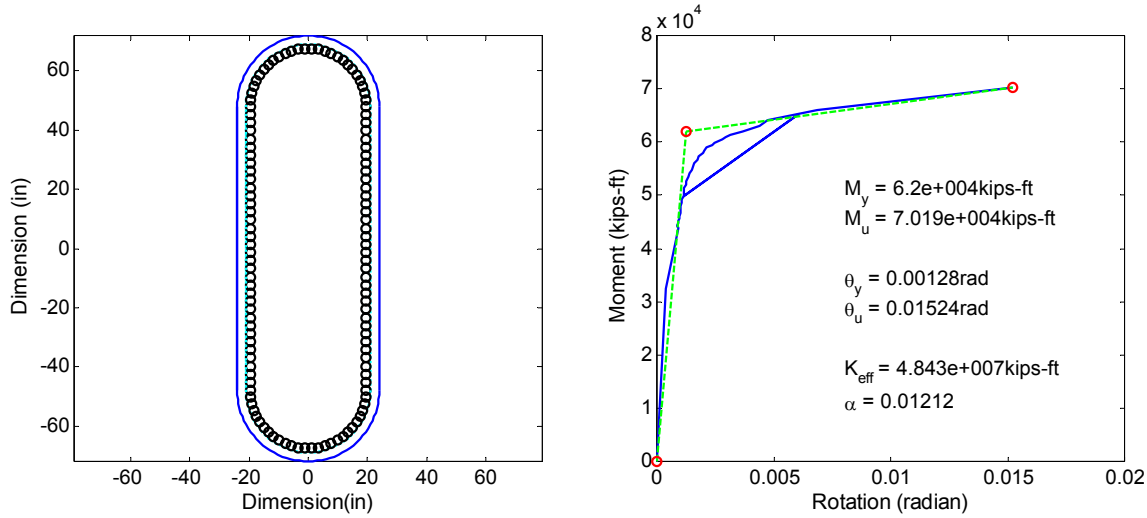

(a) Section of Column (b) Moment-Rotation Curve

(a10) Column 10 of Bridge 5 before retrofit

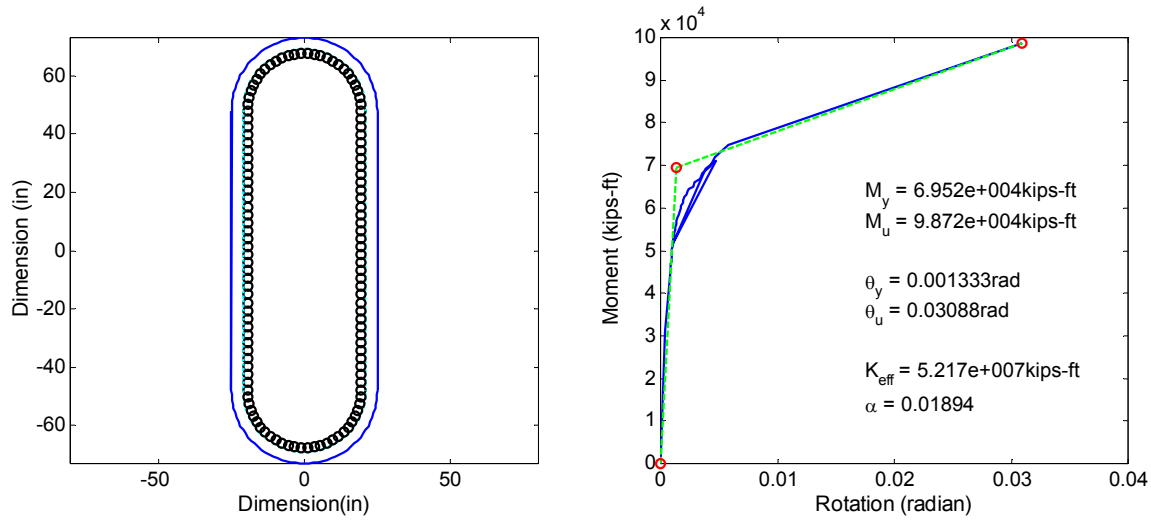

(a) Section of Column (b) Moment-Rotation Curve

(b10) Column 10 of Bridge 5 after retrofit

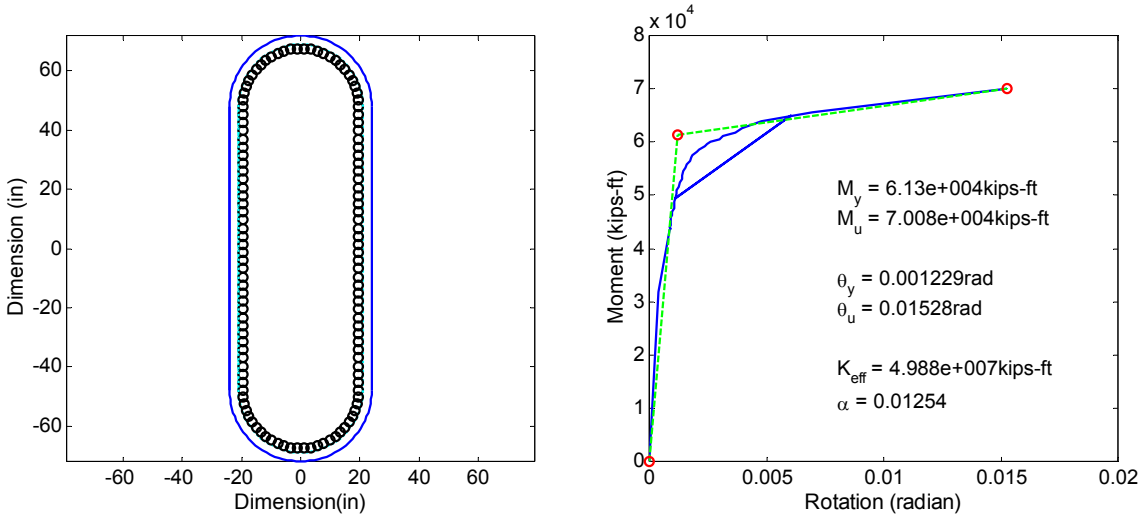

(a) Section of Column (b) Moment-Rotation Curve

(a11) Column 11 of Bridge 5 before retrofit

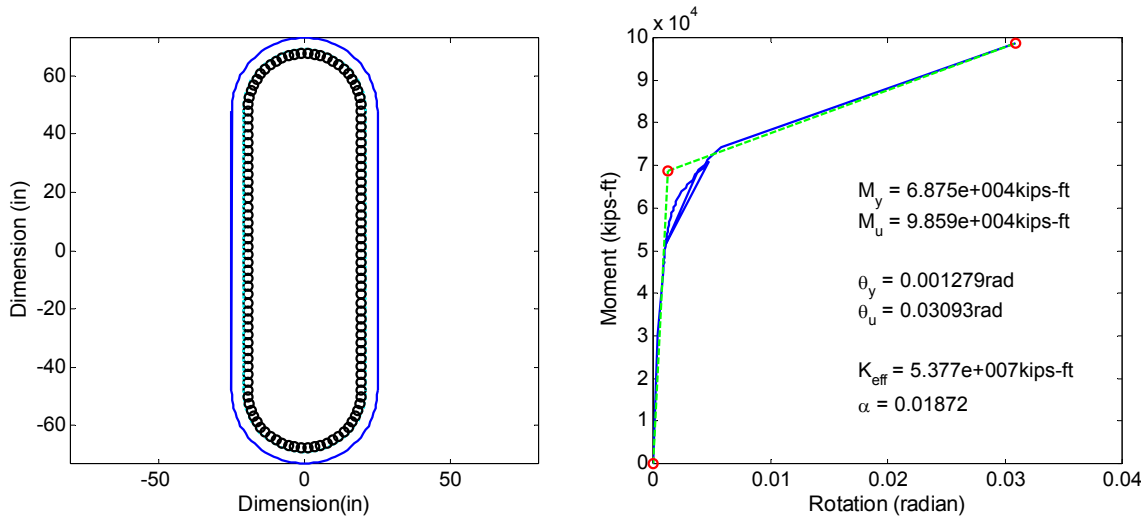

(a) Section of Column (b) Moment-Rotation Curve

(b11) Column 11 of Bridge 5 after retrofit

Fig. A.8 Moment-Curvature Analysis of Bridge 5

A.3 Source Code of Kushiyama's Program

```
% Drawing of M-P Interaction Curve
% see. Priestley et at. 1996
% Seible_MPinteraction.m   ; Final treatment of the section with steel jacket
%
t0 = clock;
global job_title bi_flag
global L AXN m Esec roht fy Ke fyj Kej rohtj fyh
global tc bra bar_A ra rDP
global Mn Pn idan
global neuax_m neuax  r_flag np
global beta1
global epy fy
global fc c eupper
global ra bra m nbar bar_A
global D DP b bp As Asp ias iasp d dp D_rect d_rect dp_rect
global dhoop dbl nbar nbarp alp bet
global Es Ec
global sby Y
global roht Ke
global fl flp fcc ecu ec0 ecc Esec r eup
global cov_flp cov_fcc cov_ecu cov_ecc cov_Esec cov_r
global e_compsteel a pc
global jacket_flag rect_flag tc rDP DP b bp fc esu cov_esp esh
global fcc r et_compsteel
global sforce1 sforce2 f_cent1 f_cent2
global sig area1 icwarn iwarning
global nbar_rect nbarp_rect rect_flag
global xeps Pn0 Pn1 Pn2 Pn3 e t_Asb ssig %temporaly
global T Csb Ccb1 Ccb2 s1 s2 Mom ep es fs is cforce1 cforce2 fsp %temporaly
global x y bx by angle b_ang %temp
global bxp byp
%global bx by bxp byp %temporaly

global LableSize LineWidth FontSize
LableSize=14;
LineWidth=2;
AxisFontSize=13;
FontSize=13;
%
% ******* notation ********
% epy: the yield strain for steel bar
% esp: the strain of compressive steel bar
% es:  the strain of tensile steel bar
% fsp: the stress of compressive steel
```

```
% c: the distance from the neutral axis to the extreme compressive fiber
% Cs: compressive force of steel bar
% Cc: compressive force of concrete
% T:  tensile force of steel bar
% Pn: axial force
% ep: the distance from applied point of Pn to the centroid of tensile steel bar
% Mn: the moment on M-P interaction curve
% Pn: the axial force on M-P interaction curve
% e:  the reciprocal of the eccentricity
% ------- the following notation are for the balanced point ------------
% cb: the distance from the neutral axis to the extreme compressive fiber
% Csb: compressive force of steel bar
% Ccb: compressive force of concrete
% Pnb: axial force
% epb: the distance from applied point of Pn to the centroid of tensile steel bar
% Mnb: the moment on M-P interaction curve
% Pnb: the axial force on M-P interaction curve
% eb:  the reciprocal of the eccentricity
%

close all
% Define the size and location of the figure
bdwidth=5;
topbdwidth=70;
bottomwidth=60;
set(0,'Units','pixels');
scnsize=get(0,'ScreenSize');
pos1=[bdwidth, scnsize(4)*0.42+bottomwidth, scnsize(3)-2*bdwidth,scnsize(4)*0.58-
(topbdwidth+bottomwidth)];
h1=figure('Position',pos1);
pos2=[bdwidth, scnsize(4)*0.42+bottomwidth, scnsize(3)-2*bdwidth,scnsize(4)*0.58-
(topbdwidth+bottomwidth)];
h2=figure('Position',pos2);
pos3=[bdwidth, scnsize(4)*0.42+bottomwidth, scnsize(3)-2*bdwidth,scnsize(4)*0.58-
(topbdwidth+bottomwidth)];
h3=figure('Position',pos3);

%
Input_TY1H_P1
%

ias=length(As);
iasp=length(Asp);
if rect_flag==1 & jacket_flag==1
   d=d+(2*bet-DP)/2;
   dp=dp+(2*bet-DP)/2;
```

```
else
   d=d+(D-DP)/2;
   dp=dp+(D-DP)/2;
end


% --------------------- common input data -------------------------------------
fl=0.5*roht*fyh; % fl: maximum effective lateral pressure
flj=0.5*rohtj*fyj; % for jacket
flp=Ke*fl+Kej*flj; % flp: effective lateral confining stress for confined concrete
fcc=fc*(2.254*sqrt(1+7.94*flp/fc)-2*flp/fc-1.254);
ecu=0.004+1.4*(roht*fyh+rohtj*fyj)*esu/fcc; % ecu: ultimate compressive strain of concrete
ec0=0.002;
ecc=ec0*(1+5*(fcc/fc-1)); % ecc: the strain at the maximum compressive strength
Esec=fcc/ecc;
r=Ec/(Ec-Esec);
if jacket_flag==0
   cov_flp=0; % flp: effective lateral confining stress, the flp is equal to zero for cover concrete.
   cov_fcc=fc*(2.254*sqrt(1+7.94*cov_flp/fc)-2*cov_flp/fc-1.254);
   cov_ecu=0.004+1.4*roht*fyh*esu/cov_fcc;
   cov_ecc=ec0*(1+5*(cov_fcc/fc-1));
   cov_Esec=cov_fcc/cov_ecc;
   cov_r=Ec/(Ec-cov_Esec);
else % jacket_flag==1 for the outerside confined concrete
   %if rect_flag==1
   %    cov_roht=2*tc/sqrt(alp*bet); % for ellipse
   %else
   %    cov_roht=4*tc/D; % for circle
   %end
   cov_roht=rohtj;
   cov_fl=0.5*cov_roht*fyj;
   cov_flp=Kej*cov_fl;
   cov_fcc=fc*(2.254*sqrt(1+7.94*cov_flp/fc)-2*cov_flp/fc-1.254);
   cov_ecu=0.004+1.4*(roht*fyh+rohtj*fyj)*esu/cov_fcc;
   cov_ecc=ec0*(1+5*(cov_fcc/fc-1));
   cov_Esec=cov_fcc/cov_ecc;
   cov_r=Ec/(Ec-cov_Esec);
end

%return

%%%
```

```
fignumb=1;
Conc_sig_eps_function(fc,fignumb)
fignumb=2;
St_sig_eps_function(Es,fy,fignumb)
%return

% --------------- pure axial loading -------------------------
% moment about the axis of the extreme tensile fiber
pure_axial_function(esh,fignumb)
maxPn0=max(Pn0);
%return

% ---------------- calculation of Mnb,Pnb & Maximum Mn,Pn -----------------------
% Pn,e and Mn at arbitrary point

divc=D/100; % incremental value of neutral axis location
if rect_flag==4
   divc=(D_rect+D)/100; % incremental value of neutral axis location
end
c0=d(1)*ecu/(ecu+epy) % the initial distance from the neutral axis to the extreme compressive
fiber
pnstate=1;
ic=Priestley_MPcalcu(pnstate,esu,c0,divc,pc,maxPn0,AXN);
Mnb=Mn(1);
Pnb=Pn(1);

% drawing M-P curve
%    fignumb=2;
%    figure(fignumb)
subplot(1,2,2)
plot(Mn(1:ic),Pn(1:ic),'LineWidth',LineWidth)

%    title('M-P Interaction Curve')
xlabel('Mn (kips-in)','FontSize',LableSize)
ylabel('Pn (kips)','FontSize',LableSize)
hold on
plot(Mnb,Pnb,'ro','LineWidth',LineWidth)
Mn0=0; maxPn0=maxPn0/1000;
plot(Mn0,maxPn0,'ro','LineWidth',LineWidth)
hold off
%return


pnstate=2;
ic=Priestley_MPcalcu(pnstate,esu,c0,divc,pc,maxPn0,AXN);
```

```
if icwarn==ic
  hold on
  plot(Mn(1:ic),Pn(1:ic),'LineWidth',LineWidth)
  hold off
else
  hold on
  plot(Mn(1:icwarn),Pn(1:icwarn),'LineWidth',LineWidth)
  plot(Mn(icwarn:ic),Pn(icwarn:ic),'c:','LineWidth',LineWidth)
  hold off
end
%return


% calculation of the intersection interaction curve and the axial force
% if AXN<=Pnb
for ii=1:ic
  if ii~=1 & (AXN-Pn(ii))*(AXN-Pn(ii-1))<0
    Mmax=(Mn(ii-1)-Mn(ii))*(AXN-Pn(ii))/(Pn(ii-1)-Pn(ii))+Mn(ii)
    neuax_max=(neuax_m(ii-1)-neuax_m(ii))*(AXN-Pn(ii))/(Pn(ii-1)-Pn(ii))+neuax_m(ii)
%eupper(ii)
    fai_max=ecu/neuax_max % fai: the curvature when the member is yield
  end
end

hold on
plot(Mmax,AXN,'g+','LineWidth',LineWidth)
XLimit=XLim;
YLimit=YLim;
axis([0.0 XLimit(2) 0.0 YLimit(2)])

hold off
%return

% ---------------- Calculation of yield surface ---------------------
icounty=0;
pnstate=3;
for idan=1:ias+iasp
  s=sprintf('idan= %d',idan);
  disp(s)
  ic=Priestley_MPcalcu(pnstate,esu,c0,divc,pc,maxPn0,AXN);
  % idan;icwarn;ic
  if icwarn==ic
    hold on
    plot(Mn(1:ic),Pn(1:ic),'r-','LineWidth',LineWidth)
    hold off
  else
```

```
    hold on
    plot(Mn(1:icwarn),Pn(1:icwarn),'r-','LineWidth',LineWidth)
    plot(Mn(icwarn:ic),Pn(icwarn:ic),'c:','LineWidth',LineWidth)
    hold off
  end
  %
  % calculation of the intersection interaction curve and
  %         the axial force by dead load
  ajdraw=0;
  for ii=ic:-1:1
    if ajdraw==1 % to avoid multipul intersections
      break
    end
    if ii~=1 & (AXN-Pn(ii))*(AXN-Pn(ii-1))<0
      ajdraw=1;
      icounty=icounty+1;
      s=sprintf('idan= %d',idan);
      disp(s)
      My(icounty)=(Mn(ii-1)-Mn(ii))*(AXN-Pn(ii))/(Pn(ii-1)-Pn(ii))+Mn(ii)
      neuax_y=(neuax(ii-1)-neuax(ii))*(AXN-Pn(ii))/(Pn(ii-1)-Pn(ii))+neuax(ii)
      %eupper(ii)
      fai(icounty)=eupper(ii)/neuax_y
      % fai: the curvature when the member yields
      NN(icounty)=AXN;
    end
  end
  if iwarning==1
    break
  end
end % idan

hold on
plot(My(1:icounty),NN(1:icounty),'g+','LineWidth',LineWidth)
hold off
%return


% ------------------- Calculation of cracking moment --------------------
ft=9.0*sqrt(fc);
ept=ft/Ec; % the tensile strain at cracking of concrete
if rect_flag==1
  if jacket_flag==0
    Ic=b*D^3/12;
  else
    Ic=pi*alp*bet^3/4;
    % inertia for ellipse shape around the strong axis or the weak axis
```

```
  end
elseif rect_flag==2 % circular shape
  Ic=pi*ra^4/4;
elseif rect_flag==3 % (rect+circle) shape around weak direction
  Ic=b*D^3/12+pi*ra^4/4;
else % rect_flag==4 % (rect+circle) shape around strong direction
  Ic=b*D_rect^3/12+pi*ra^4/4;
end
Isp=0;
for ii=1:iasp
  Isp=Isp+Asp(ii)*(Es/Ec-1)*(D/2-dp(ii))^2;
end
Ist=0;
for ii=1:ias
  Ist=Ist+As(ii)*(Es/Ec-1)*(d(ii)-D/2)^2;
end
Is=Isp+Ist;
if rect_flag==1 & jacket_flag==1
  Z=(Ic+Is)/(bet);
else
  Z=(Ic+Is)/(D/2);
end
if rect_flag==1 & jacket_flag==0
  Ac=b*D;
elseif rect_flag==1 & jacket_flag==1
  Ac=pi*bet*alp;
elseif rect_flag==2 % cicular shape
  Ac=pi*ra^2;
else % (rect+circle) shape
  Ac=b*D+pi*ra^2;
end
Mc=(ft+AXN*1000/(Ac+(Es/Ec-1)*(sum(Asp(:))+sum(As(:)))))*Z/1000


% ---------------- drawing M-fai graph ----------------------
EI=Ec*(Ic+Is); % the bending stiffness
precr_fai=(Mc/EI)*1000 % just before cracking occurs
curv(1)=0;
curv(2)=precr_fai;
for ii=1:icounty
  curv(2+ii)=fai(ii);
end
curv(icounty+3)=fai_max;
M(1)=0;
M(2)=Mc;
for ii=1:icounty
```

```
  M(2+ii)=My(ii);
end
M(icounty+3)=Mmax;
fignumb=3;
figure(fignumb)
subplot(1,2,1)
plot(curv(1:3+icounty),M(1:3+icounty) ./12,'LineWidth',LineWidth)

%    title('Moment-Curvature')
xlabel('Curvature (1/in)','FontSize',LableSize)
ylabel('Moment (kips-ft)','FontSize',LableSize)
%

alpha=((My(1)-Mc)/(fai(1)-precr_fai))*1000/EI
for ii=1:icounty-1
  beta(ii)=((My(ii+1)-My(ii))/(fai(ii+1)-fai(ii)))*1000/EI
end
if icounty~=0
  beta(icounty)=((Mmax-My(icounty))/(fai_max-fai(icounty)))*1000/EI
end
%
disp('-----------------------------------------')
s=sprintf('Mmax= %d',Mmax);
disp(s)
s=sprintf('fai_max= %d',fai_max);
disp(s)


if icounty>1
  My(icounty+1)=Mmax;
  fai(icounty+1)=fai_max;
  x1=precr_fai;x2=fai(1);
  y1=Mc;y2=My(1);
  for ii=1:icounty+1
    py(ii)=My(ii)-My(1);
    px(ii)=fai(ii)-fai(1);
  end
  s=0;
  for ii=1:icounty
    s=s+(py(ii)+py(ii+1))*(px(ii+1)-px(ii))/2; % area
  end
  if bi_flag==2 % approximation of bi_linear
    s=s+0.5*x1*y1+0.5*(y1+y2)*(x2-x1)+My(1)*px(icounty+1);
  end
  ic=1;
  dy=py(icounty+1)/100;
```

```
  while ic
    kmy=dy*ic;
    kmx=kmy/(y2/x2);
    as=0.5*(x2+kmx)*(y2+kmy)+((y2+kmy)+My(icounty+1))*(px(icounty+1)-kmx)/2;
    if as>s
      app_My=kmy+My(1)
      break
    end
    ic=ic+1;
  end
  app_faiy=app_My*(x2/y2)
  x0=0;
  y0=0;
  %
  hold on
  X1=[x0 app_faiy fai_max];
  Y1=[y0 app_My Mmax];
  plot(X1,Y1 ./12,'g--','LineWidth',LineWidth)
  plot(X1,Y1 ./12,'ro','LineWidth',LineWidth)
  hold off
  %
  app_fai_alpha=(app_My/app_faiy)/(Mc/precr_fai)
  app_fai_beta=((Mmax-app_My)/(fai_max-app_faiy))/(Mc/precr_fai)
end
s=sprintf('erapse_time= %d',etime(clock,t0));
disp(s)
%return

fye=fy/1000; %fye : ksi unit
Lp=0.08*L+0.15*fye*dbl;
Lp_min=0.3*fye*dbl;
if (Lp<Lp_min)
  Lp=Lp_min;
end

fignumb=3;
figure(fignumb)
subplot(1,2,2)
plot(curv(1:3+icounty)*Lp,M(1:3+icounty) ./12,'LineWidth',LineWidth)
%   title('M-R Relationship')
xlabel('Rotation (radian)','FontSize',LableSize)
ylabel('Moment (kips-ft)','FontSize',LableSize)
fignumb=fignumb+1;
%
%
%
```

```
hold on
X1=[x0 app_faiy fai_max]*Lp;
Y1=[y0 app_My Mmax];
Keff=Y1(2)/X1(2)/12.;
Kafter=(Y1(3)-Y1(2))/(X1(3)-X1(2))/12.;
alpha=Kafter/Keff;

plot(X1,Y1 ./12,'g--','LineWidth',LineWidth)
plot(X1,Y1 ./12,'ro','LineWidth',LineWidth)

%legend1=['M_y = ',num2str(Y1(1)./12,'%0.4g'),'kips-ft'];
legend2=['M_y = ',num2str(Y1(2)./12,'%0.4g'),'kips-ft'];
legend3=['M_u = ',num2str(Y1(3)./12,'%0.4g'),'kips-ft'];
%legend4=['\theta_y = ',num2str(X1(1),'%0.4g'),'rad'];
legend5=['\theta_y = ',num2str(X1(2),'%0.4g'),'rad'];
legend6=['\theta_u = ',num2str(X1(3),'%0.4g'),'rad'];
legend7=['K_e_f_f = ',num2str(Keff,'%0.4g'),'kips-ft'];
legend8=['\alpha = ',num2str(alpha,'%0.4g')];


XLimit=XLim;
YLimit=YLim;
FontSize=13;
%text(XLimit(2)*0.5,YLimit(2)*0.7*1.00,legend1,'FontSize',FontSize);
text(XLimit(2)*0.5,YLimit(2)*0.7*0.90,legend2,'FontSize',FontSize);
text(XLimit(2)*0.5,YLimit(2)*0.7*0.80,legend3,'FontSize',FontSize);
%text(XLimit(2)*0.5,YLimit(2)*0.7*0.70,legend4,'FontSize',FontSize);
text(XLimit(2)*0.5,YLimit(2)*0.7*0.60,legend5,'FontSize',FontSize);
text(XLimit(2)*0.5,YLimit(2)*0.7*0.50,legend6,'FontSize',FontSize);
text(XLimit(2)*0.5,YLimit(2)*0.7*0.30,legend7,'FontSize',FontSize);
text(XLimit(2)*0.5,YLimit(2)*0.7*0.20,legend8,'FontSize',FontSize);


hold off


figure(1)
subplot(1,2,1), set(gca,'FontSize',AxisFontSize)
subplot(1,2,2), set(gca,'FontSize',AxisFontSize)
figure(2)
subplot(1,2,1), set(gca,'FontSize',AxisFontSize)
subplot(1,2,2), set(gca,'FontSize',AxisFontSize)
figure(3)
subplot(1,2,1), set(gca,'FontSize',AxisFontSize)
subplot(1,2,2), set(gca,'FontSize',AxisFontSize)
```

%%%%%%%%%%%%%%% the end of calculation
%%%%%%%%%%%%%%%%%%%%%%%%
return

Appendix B: Trip Reduction Model using Dynamic OD for Post-Disaster Network Analysis

B.1. Overview

The concept of estimating trip reduction from seismic damaged buildings is illustrated in Fig. B.1. The process involves: 1) identifying relationships between earthquake intensity and building damage, and 2) converting building damage to change in activity and travel demand. Once established, this methodology will be integrated into an existing transportation network model.

The development of a variable travel demand model will require four basic steps: (1) develop the baseline of the demand function; (2) automate the calibration of distance decay coefficients; (3) identify the cost of trips forgone; and (4) long-term management of trip reduction data.

Building damage due to ground shaking is estimated using fragility models. Of the various publicly available sources, the present study employs the EPEDAT (Early Post Earthquake Damage Estimation Tool) [1] fragility model. This model estimates building damage by structure type and ground motion intensity, as the percentage of floor area that can no longer be used. It was calibrated based on the 1994 Northridge earthquake, in terms of the counted yellow and red tagged buildings per unit of ground motion intensity, for different building types such as wooden or steel frame buildings.

Estimated fragility is converted to a measure of activity system vulnerability. First, structural fragility is translated into the percent damage ratio by occupancy type (or usage). This assumes inherent consistency between building type and usage. Regional statistics on building occupancy are compiled from FEMA building stock databases

released with HAZUS [2]. Although EPEDAT includes a detailed building stock database, it only covers the counties of Los Angeles, and Orange. Selecting the HAZUS database renders the model more widely applicable. This approach may limit application of the model to other locations, because structure-to-occupancy statistics are unique to each region. Each of census tracks does not have same structure-to-occupancy ratio. Where other regions share similar construction practices, the same average ratio may apply.

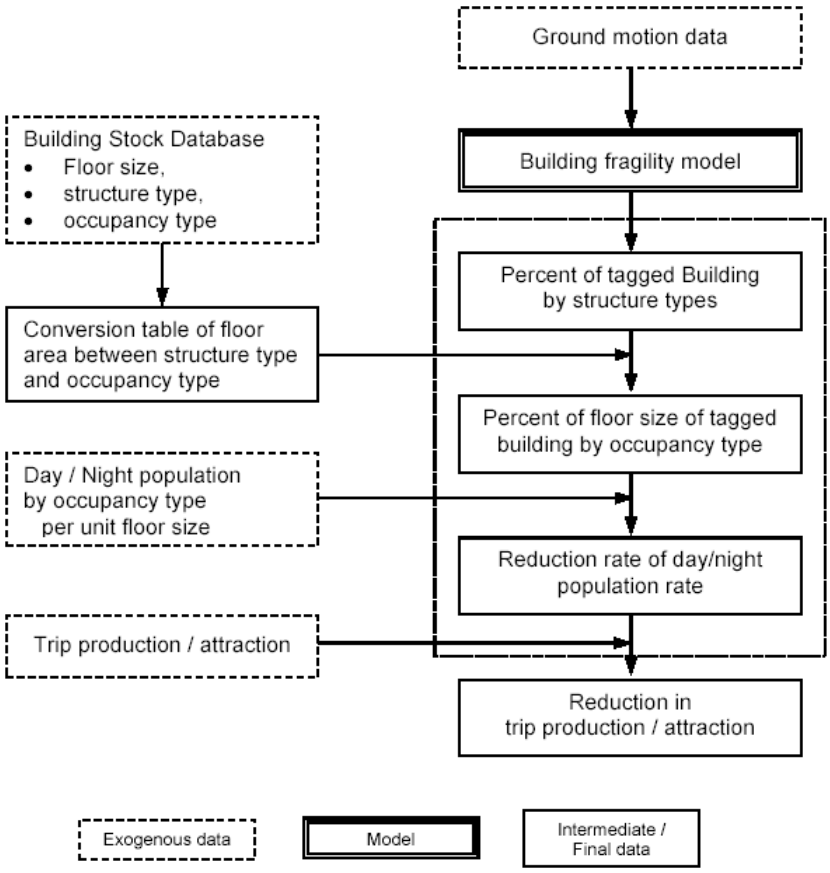

Fig. B.1. Framework of Trip Reduction Estimation

Once the distribution of fragility by ground motion intensity is associated with the building occupancy type, the damaged floor area is converted into a percent fall in daytime/nighttime population. This is achieved using the average population by occupancy type per unit floor area.

The conversion is based on the assumption that activity is proportional to floor area. However, usability of a building is arguably a stepwise rather than a continuous function. For example, a building with 5% damaged floor area would continue being used, whereas activity would cease within a structure with 60% of damage, due to safety concerns. In addition, with respect to usability, level of activity may not be linearly proportional to the percent of building damage, because, for example, 60% and 100% damage levels are not significantly different. Although this argument is valid for the usability of individual buildings, the percent reduction in usable floor size, and associated activity reduction employed here, are aggregated statistics based on zone boundaries. In a zonal context, these statistics can be presented as a continuous probability distribution for a region which consists of many zones.

The ratio of reduced day/night population to the baseline population will be used to modify trip origins from or destinations to a given zone. The reduction in trips for a given purpose will reflect occupancy levels, and the time of day. For example, the population of a residential area will be obtained from night time occupancy, while the number of daytime trips to work will be adjusted by damage to office buildings. The end product is vectors, representing the number of post earthquake trips generated from and destined to a particular zone.

Estimated trip reduction is then integrated into a transportation modeling framework. Given the post-earthquake network configuration (usually characterized with reduced capacity), and reduced travel demand (from building damage), the model produces post-earthquake traffic volumes (in passenger car unit, PCU), and estimates system-wide travel costs (hours) for economic loss estimation. The model uses an iterative process that: (1) searches for an optimal route between two zones, in terms of given travel time; (2) loads travel demand on the selected route(s) between the two zones; (3) updates congested travel time (or impedance) between zones; and (4) finds the new best route between zones based on updated travel time.

Estimated post-earthquake trip production/attraction vectors should be converted to a demand matrix to ensure compatibility with transportation network model. Travel demand is ideally presented as a 2-dimensional matrix, where a cell in the i-th row and j-column portrays the number of travelers (or car) generated from zone i, destined for zone j. Unfortunately, the reduction model produces trip production and destination statistics in the form of vectors, since the model only considers zonal damage to buildings and associated activity reduction, without counting where the activity origin or destination. To convert the estimated vectors into an OD matrix, a distribution model, such as the gravity model, will be incorporated. In theory, gravitational force is the interaction between two masses over in space, and is proportional to the multiplication of two masses, and inverse of square of distance. This notion may also be applied to trip interaction between zones. There will be more trips between the activity centers that are close together than demand between centers either located further apart, or with less activity.

By performing this redistribution process, travel demand generated from a given zone is assigned to its destination zones. The model repeats this process until all rows in the OD matrix are filled. The sum of destined demand to a zone in the OD matrix should be identical to the trip attraction vector that was estimated by the trip reduction model. The distance measure is then replaced by congested travel time, so that the distribution of demand is now expressed a cost.

The user equilibrium network model assigns the estimated post-earthquake travel demand, represented by the OD matrix, to the most efficient routes between zones. In a network system, there are many alternative routes to accommodate travel demand. The network model adjusts link volume and congested travel time to achieve the equilibrium condition where travel times are identical for all routes. Flow on any unused route, or route recording a lower travel time, will therefore be adjusted to reinstate the equilibrium. The total travel time spent by drivers at equilibrium represents the new system-wide travel cost, and its difference from original pre-earthquake baseline costs constitutes the seismically induced economic loss.

Travel times used in the distribution model and estimated by the equilibrium network model are unrelated. If such inconsistency in these datasets is allowed, trip production/attraction vectors and estimated OD matrix will not accurately represent estimated congestion patterns. Iteration between the distribution and network models will alleviate this discrepancy. A distribution model produces the OD matrix according to given travel impedance. This output is input to the network model. In turn, the network model results in congested zone-to-zone travel time, which can be fed back to the distribution model. Repeatedly running the models and adjusting intermediate

estimations like auxiliary link volume and trip rate, will reach a converged state with respect to the travel time matrix. For a simple demand (travel demand) - supply (network capacity) system such as this, convergence of price (travel cost) leads the system stability.

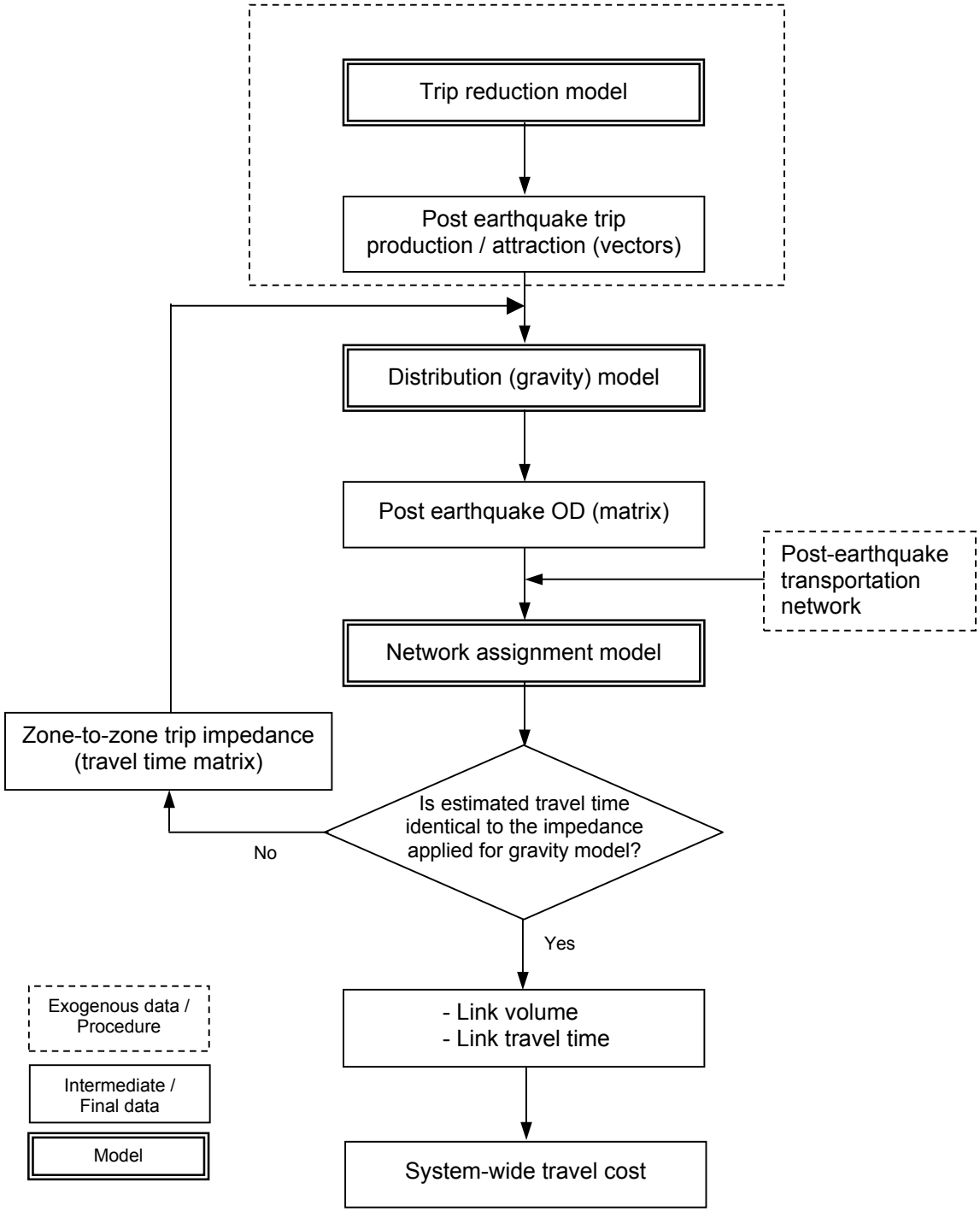

Fig. B.2 Integrated Analysis of Trip Reduction and Network Models

Fig. B.2 presents the framework for an integrated trip reduction model, which iterates between network and distribution models. In this study, the gravity (distribution) model is integrated with user equilibrium network model. The user equilibrium assignment model already requires iterations (inner iteration within the network model) to adjust link volumes so the results meet equilibrium principal. Using the iterative approach, the gravity model involves the inner iteration within user equilibrium model to adjust the OD matrix. With this approach, the distribution model is blended into the network model. This approach is clearly different from sequential, independent deployment of the two models. In this latter case, the two models are waiting until the other model finishes one complete run including all inner iterations. It is beneficial inasmuch that less inner iterations are required to achieve consistency.

B.2. Person Trip Reduction Model

Fig. B.3 illustrates the established methodology and intermediate data for estimating the reduction in personal trips following an earthquake event:

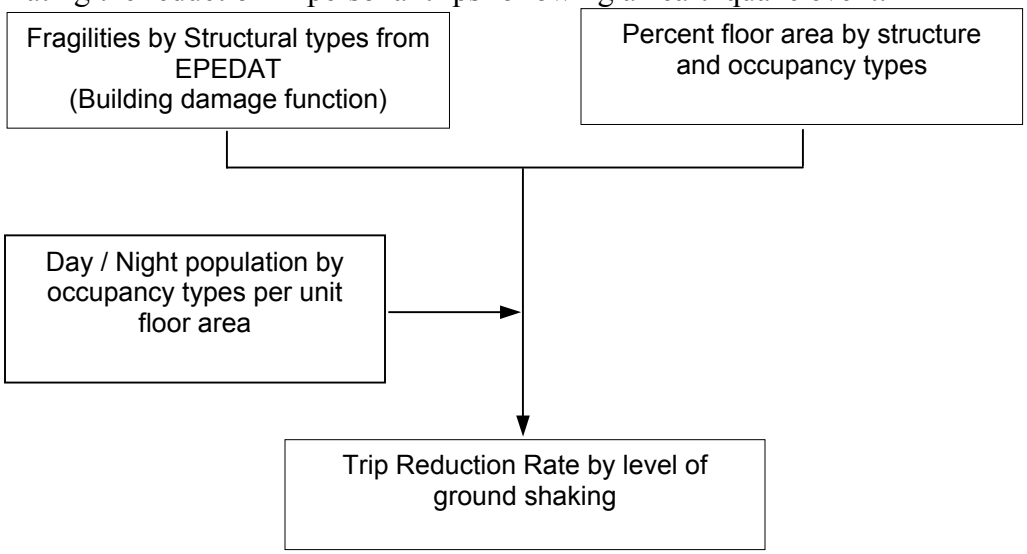

Fig. B.3.Personal Trip Reductions Caused by Regional Building Damage

B.2.1 Building Damage Functions

The trip reduction model is developed based on regional characteristics of buildings, and an existing building fragility model. We adopted the fragility model from EPEDAT (Early Post Earthquake Damage Estimation Tool) which is known that the model was calibrated for Southern California applications, based on experience from the 1994 Northridge earthquake. However, the available document does not include model parameters (such as dispersion factor for the lognormal distribution of fragility). Therefore, the fragility model was inferred according to the estimation result by EPEDAT, using the 20 Most Credible Earthquake (MCE) events.

Aggregated EPEDAT results are used to estimate the percent of severely damaged (red and yellow tagged) buildings in terms of floor area. Along with referencing a document on development of the tool[1], EPEDAT was applied to various combinatorial conditions of building types and levels of ground motion. The application results were averaged for each of ground motion level. MMI and PGA are both used for ground motion measurement.[2]

Table B.1 describes building fragility implemented in EPEDAT. It shows that wooden light frame buildings are most impervious to extreme ground shaking up to PGA 1.0g. On the other hand, mobile homes are extremely vulnerable so that more than half of buildings would be damaged by ground motion of MMI 10. In the next section, the percent of damaged buildings by structure types is converted to percentage by occupancy type (usage), according to the statistics on building usage by structural type.

---

[1] EQE International, 1994, Final Technical Report: Development of an early post-earthquake damage assessment tool for Southern California

[2] EPEDAT estimates ground motion in the center of each census tract in MMI and PGA

Table B.1. Building fragility by structure types

HAZUS Classification			Fragility (to total area of red and yellow tagged building)				
Code		Description	PGA=0.13	PGA=0.27	PGA=0.52	PGA=0.93	PGA=1.55
			MMI6	MMI7	MMI8	MMI9	MMI10
Wood	W1	Wood, Light Frame	0.0300	0.2500	0.7400	5.2500	13.0000
	W2	Wood, Commercial and Industrial	0.0375	0.3100	0.9250	6.5625	16.2500
Steel	S1L	Steel Moment Framd, Low	0.0375	0.3950	0.5700	5.2000	18.0500
	S2L	Steel Braced Frame, Low	0.0375	0.3950	0.5700	5.2000	18.0500
	S3	Steel Light Frame	0.0375	0.3950	0.5700	5.2000	18.0500
	S4L	Steel Frame with Cast-in-Place Concrete Shear Walls	0.0375	0.3100	0.9250	6.5625	16.2500
Concrete	C1L	Concret Moment Frame, Low	0.0285	0.2420	0.6005	5.7800	20.6850
	C2L	Concrete Shear Walls, Low	0.0285	0.2420	0.6005	5.7800	20.6850
	C3L	Concrete Frame with Unreinforced Masonry Infill Wall	0.0285	0.2420	0.6005	5.7800	20.6850
Precast	PC1	Precast Concrete Tilt-up walls	0.0550	0.2800	0.8000	11.6000	37.6000
	PC2L	Precast Concrete Frames with Concrete Shear Walls	0.0550	0.2800	0.8000	11.6000	37.6000
ML & Etc	RM1L	Reinforced Masonry Bearing Walls with wood or Metal Deck Diaphragms	0.0400	0.2900	0.6000	6.7500	23.2000
	RM2L	Reinforced Masonry Bearing Walls with precast concrete Diaphragms	0.0400	0.2900	0.6000	6.7500	23.2000
	MH	Mobile Homes	0.1550	1.0100	2.2500	20.8000	64.6000
	URML	Unreinforced Masonry Bearing Walls	0.0450	0.3000	0.6200	7.9000	28.7000

Source: 'Inferred' from technical report for EPEDAT and its application results.

B.2.2. Regional Building Stock

Building stock is classified based on occupancy types described in *HAZUS 99*.[3] The basic model building structure types are also based on *HAZUS 99* building classes. Tables B-2 and B-3 provide a listing of structural building types and building occupancy types, along with associated statistics. According to the HAZUS database, there are 36

[3] It is not clear when the building database was established by whom. Based on two facts that 1) the data was distributed by California OES; 2) number figure is slightly lower than that of EPEDAT database, which is compiled just after 1994 Northridge earthquake, Building database Southern California building stock database seems established before 1994 by state of California.

specific building structure types and 28 specific building occupancy types. For Southern California (5-county area that consists of Los Angeles, Orange, Riverside, San Bernardino, and Ventura), 15 building structure types and all of the 28 building occupancy types were observed. For this study, the types of structure and occupancy were re-aggregated into 5 structure types and 4 occupancy types.

According to the database, 3.6 million buildings are used in Southern California, with a total floor area of 9.7 billion square foot (Table B.2). Average building size is therefore ~2,700 sq-ft. Almost 90% of buildings are constructed with a wooden structure. However, the total floor area of wooden structures is only ~70%, and the average size relatively small at ~2,000 sq-ft. Based on these statistics, fragility models of wooden buildings, especially light frame structures will dominate the overall building damage estimation.

Table B.3 illustrates buildings in Southern California with respect to occupancy type (or main usage).[4] According to the database, more than 96% of buildings, including 6% of counted mobile home, are used for residential purposes. This accounts for ~70% of the total floor area. Besides residential purpose, 2.4 % of buildings, corresponding with 18% of floor area, are used for commercial activity. Industrial building are less than 1% in count, but the more than 6% of floor area.

Table B.4. summarizes further details of the building composition, with respect to floor area. This table, which is a cross-tab from Table B.2 and B-3, reveals the proportion of floor size by structure, for different building occupancies. For example, of the 72.7% of floor size used for residential purposes, 64.1% of building floor area is constructed in

[4] The difference of total figure between Table 2-1, and 2-2 is due to missing data in the database.

wooden structure. A minor proportion goes to other structural types, including mobile homess.

Building composition is assumed to be unique and identical throughout the region. As such, any transportation analysis zone is assumed to have a consistent composition, which can bye represented by a set of fragility curves and their associated "vulnerabilities". However, this composition should be used with caution, because characteristics of buildings might not be transferable to other regions.

Table B.2. Southern California Building Stock by Structure Types

HAZUS Classification			Number of Buidlings		Floor Area	
Code		Description	Count	%	1,000 sq ft	%
Wood	W1	Wood, Light Frame	3,206,272	88.9	6,284,854	64.6
	W2	Wood, Commercial and Industrial	21,680	0.6	472,206	4.9
	Subtotal		3,227,952	89.5	6,757,060	69.4
Steel	S1L	Steel Moment Framd, Low	11,714	0.3	239,425	2.5
	S2L	Steel Braced Frame, Low	5,757	0.2	153,624	1.6
	S3	Steel Light Frame	5,708	0.2	110,212	1.1
	S4L	Steel Frame with Cast-in-Place Concrete Shear Walls	7,699	0.2	155,516	1.6
	Subtotal		30,878	0.9	658,777	6.8
Concrete	C1L	Concret Moment Frame, Low	3,810	0.1	82,600	0.8
	C2L	Concrete Shear Walls, Low	23,981	0.7	500,949	5.1
	C3L	Concrete Frame with Unreinforced Masonry Infill Wall	1,322	0.0	23,153	0.2
	Subtotal		29,113	0.8	606,702	6.2
Precast	PC1	Precast Concrete Tilt-up walls	21,645	0.6	490,499	5.0
	PC2L	Precast Concrete Frames with Concrete Shear Walls	5,549	0.2	107,694	1.1
	Subtotal		27,194	0.8	598,194	6.1
ML & Etc	RM1L	Reinforced Masonry Bearing Walls with wood or Metal Deck Diaphragms	61,980	1.7	654,784	6.7
	RM2L	Reinforced Masonry Bearing Walls with precast concrete Diaphragms	2,379	0.1	53,696	0.6
	MH	Mobile Homes	217,955	6.0	225,586	2.3

	URML	Unreinforced Masonry Bearing Walls	9,318	0.3	175,880	1.8
	Subtotal		291,632	8.1	1,109,946	11.4
Total			3,606,769	100.0	9,730,680	100.0

Source : HAZUS 99 Default Building database for California application, FEMA, California OES

Table B.3. Southern California Building Stock by Occupancy Types

HAZUS Classification			Number of Buildings		Floor Area	
Code		Description	Count	%	1,000 sq ft	%
Residential	RES1	Single Family Dwelling	3,140,023	87.0	4,710,035	48.4
	RES2	Mobile Home	217,810	6.0	217,810	2.2
	RES3	Multi Family Dwelling	117,688	3.3	1,881,825	19.3
	RES4	Temporary Lodging	1,014	0.0	55,736	0.6
	RES5	Institutional Dormitory	6,356	0.2	192,016	2.0
	RES6	Nursing Home	303	0.0	15,129	0.2
	Subtotal		3,483,194	96.6	7,072,550	72.7
Commercial	COM1	Retail Trade	24,450	0.7	341,886	3.5
	COM2	Wholesale Trade	11,957	0.3	419,897	4.3
	COM3	Personal and Repair Service	16,092	0.4	192,998	2.0
	COM4	Professional / Technical Service	15,758	0.4	551,310	5.7
	COM5	Banks	1,275	0.0	30,251	0.3
	COM6	Hospital	407	0.0	41,250	0.4
	COM7	Medical Office / Clinic	7,249	0.2	87,791	0.9
	COM8	Entertainment & Recreation	8,014	0.2	104,476	1.1
	COM9	Theaters	99	0.0	2,793	0.0
	COM10	Parking	-	-	-	-
	Subtotal		85,301	2.4	1,772,650	18.2
Industrial	IND1	Heavy Industries	4,324	0.1	223,235	2.3
	IND2	Light Industries	11,719	0.3	236,167	2.4
	IND3	Food / Drugs / Chemicals	3,113	0.1	67,448	0.7
	IND4	Metals / Minerals Processing	1,296	0.0	21,730	0.2
	IND5	High Technology	623	0.0	11,035	0.1
	IND6	Construction	5,094	0.1	97,035	1.0
	Subtotal		26,169	0.7	656,650	6.7
Etc	AGR1	Agriculture	1,921	0.1	28,913	0.3
	REL1	Church / Non-Profit	5,399	0.1	81,181	0.8
	GOV1	General Services	861	0.0	29,063	0.3
	GOV2	Emergency Response	237	0.0	2,405	0.0

	EDU1	Grade Schools	3,399	0.1	66,585	0.7
	EDU2	Colleges / Universities	781	0.0	19,892	0.2
	Subtotal		12,598	0.3	228,039	2.3
Total			3,607,262		9,729,889	

Source : HAZUS 99 Default Building database for California application, FEMA, California OES

Table B.4. Summary of Southern California Buildings by structure and occupancy Types

(a) Floor Area (1,000 sq-ft)

		Structure Type					
		Wood	Steel	Concrete	Precast	ML & ETC	Sum
Occupancy Type	Residential	6,237,975	125,307	197,649	19,739	491,782	7,072,453
	Commercial	409,541	229,781	292,757	377,155	461,438	1,770,671
	Industrial	60,254	246,985	68,118	188,661	93,728	657,746
	ETC	49,289	56,705	48,178	12,639	62,999	229,810
	Sum	6,757,060	658,777	606,702	598,194	1,109,946	9,730,680

(b) Percent of Floor Area

		Structure Type					
		Wood	Steel	Concrete	Precast	ML & ETC	Sum
Occupancy Type	Residential	64.1	1.3	2.0	0.2	5.1	72.7
	Commercial	4.2	2.4	3.0	3.9	4.7	18.2
	Industrial	0.6	2.5	0.7	1.9	1.0	6.8
	ETC	0.5	0.6	0.5	0.1	0.6	2.4
	Sum	69.4	6.8	6.2	6.1	11.4	100.0

The composition of structure type in Table B.4 (b)[5] is applied as a weight to convert the fragility, which is given by structural type in Table B.1, into the "vulnerability" of building occupancy. Table B.5 shows detailed vulnerability of building occupancy from ground motion. According to the table, with the exception of mobile homes, buildings used for residential purposes have a lower chance of being damaged by

[5] Actually more detailed version of composition table is used, of which classifications are corresponding to Table 2-2 and 2-3.

earthquake events. Commercial and industrial buildings have almost identical probability distribution of building damage. The maximum proportion of floor damage from extremely high ground motion is ~ 26% of the total square footage within a transportation analysis zone.

EPEDAT also estimates percentage of building damage by occupancy type for aggregated in residential and commercial/industrial categories. It is obvious that the converted fragility (or vulnerability) of these occupancy types should be identical to the EPEDAT estimate. Any difference is due to discrepancies between the EPEDAT and HAZUS building databases. Fig. B.4 compares the two set of vulnerability curves, and shows that the difference is marginal.

Table B.5 Vulnerability of building occupancy

HAZUS Classification			Fragility (to total area of red and yellow tagged building)				
Code		Description	PGA=0.13	PGA=0.27	PGA=0.52	PGA=0.93	PGA=1.55
			MMI6	MMI7	MMI8	MMI9	MMI10
Residential	RES1	Single Family Dwelling	0.0301	0.2504	0.7386	5.2650	13.1020
	RES2	Mobile Home	0.0450	0.3000	0.6200	7.9000	28.7000
	RES3	Multi Family Dwelling	0.0349	0.2796	0.7699	5.9455	16.1425
	RES4	Temporary Lodging	0.0371	0.2953	0.7485	6.2690	18.5565
	RES5	Institutional Dormitory	0.0340	0.2772	0.6898	5.9762	18.4497
	RES6	Nursing Home	0.0346	0.2668	0.7209	6.1236	17.5700
	Mean		0.0320	0.2608	0.7420	5.5563	14.5891
Commercial	COM1	Retail Trade	0.0458	0.3338	0.8067	8.0210	25.2280
	COM2	Wholesale Trade	0.0502	0.3257	0.8072	9.3042	30.0079
	COM3	Personal and Repair Service	0.0495	0.3407	0.8175	8.7008	27.9671
	COM4	Professional / Technical Service	0.0441	0.3297	0.8263	7.6375	23.4262
	COM5	Banks	0.0441	0.3297	0.8263	7.6375	23.4262
	COM6	Hospital	0.0389	0.3049	0.7631	6.8778	20.9752
	COM7	Medical Office / Clinic	0.0409	0.3338	0.8178	6.8260	20.0405
	COM8	Entertainment & Recreation	0.0447	0.3595	0.7222	7.1615	23.8420
	COM9	Theaters	0.0425	0.3630	0.6762	6.6517	22.3622
	COM10	Parking	-	-	-	-	-
	Mean		0.0462	0.3322	0.8088	8.1345	25.6252
Industrial	IND1	Heavy Industries	0.0416	0.3527	0.6853	6.8173	22.4134
	IND2	Light Industries	0.0481	0.3330	0.7487	8.7633	28.6675
	IND3	Food / Drugs / Chemicals	0.0476	0.3420	0.7433	8.4187	27.7017
	IND4	Metals / Minerals Processing	0.0420	0.3489	0.6686	6.9605	23.2781
	IND5	High Technology	0.0450	0.3047	0.6967	8.4985	28.0725
	IND6	Construction	0.0460	0.3413	0.8022	7.9772	24.9313
	Mean		0.0453	0.3419	0.7309	7.8860	25.7017
Etc	AGR1	Agriculture	0.0415	0.3287	0.7383	6.8694	21.1481
	REL1	Church / Non-Profit	0.0406	0.3223	0.7361	6.8051	21.7071
	GOV1	General Services	0.0404	0.3282	0.7163	6.8071	22.4014
	GOV2	Emergency Response	0.0385	0.3060	0.7864	6.6076	19.0999
	EDU1	Grade Schools	0.0358	0.2918	0.6564	6.1827	19.7773
	EDU2	Colleges / Universities	0.0377	0.3020	0.6323	6.4547	21.6028
	Mean		0.0390	0.3130	0.7021	6.5991	21.1246

(a) Residential building

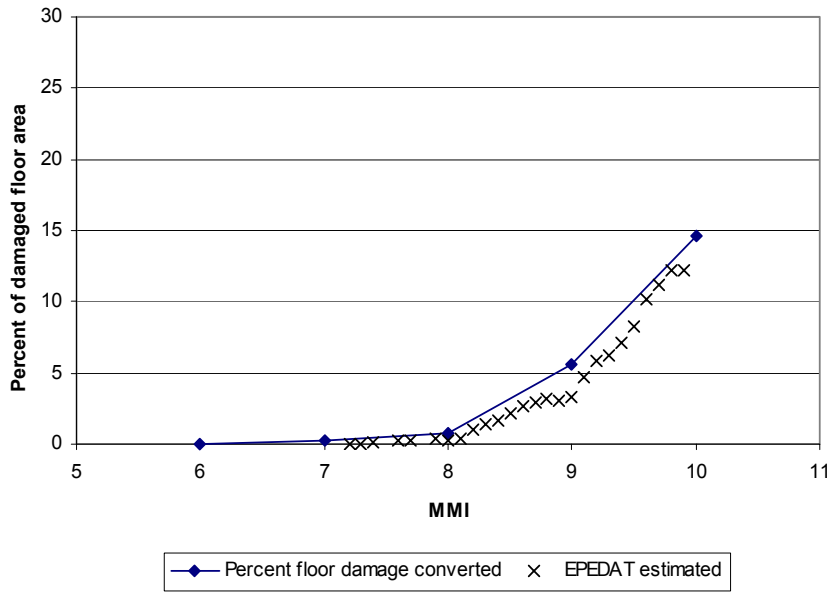

(b) Commercial/industrial buildings

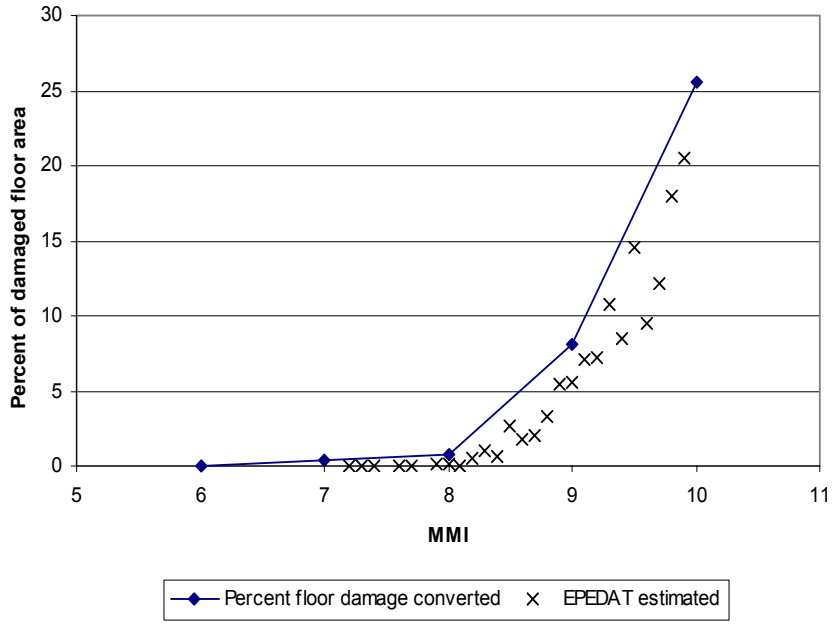

Fig. B.4.Comparison of EPEDAT Fragility and the Study Estimated Fragility for Selected Building Occupancy Yypes

B.2.3. Activity population

This section considers the number of people who perform activities within a building. The meaning of percentage of physical damage needs to be converted to a

tangible reduction in 'activity', since estimates of trip reduction are activity based. Average population per unit floor area (1,000 sq-ft) is used in both of HAZUS and EPEDAT for estimating fatalities from earthquake. Table B.6 portrays the population figures.

The total activity population may not be identical to the up-to-date statistics. However, this study applies activity population to adjust vulnerability of activity based on assumptions that: 1) the change of relative activity population between occupancy would be minor; and 2) average occupancy rate per unit floor area is applicable throughout the region.

B.2.4. Trip reduction rate

By incorporating the activity population by building occupancy types from Section B.2.3, the unit of structural vulnerability of buildings in Table B.5 (although it is sorted by occupancy type, the percentage still represents damage to building) is converted to the percent of people no longer doing a particular activity. The resulting table is not shown here, because weighting occupancy rate to the vulnerability is only effective when the percent of damage is aggregated to certain category, rather than to the detailed HAZUS classification.

The percentage of reduced activity population by occupancy types, can be directly interpreted as reduction rate of trips destined to, or originating from the buildings. This assumes that there is no significant changes of occupancy rate after the earthquake hits a region. It is true that people may not want to stay in an individual building, regardless of the damage severity. However, from a regional perspective, the measurement of usability, or willingness to use the building can be described with a probability distribution.

Therefore, a certain portion of people still travel to the subregions where buildings are damaged.

Reduction rates are associated with trip purpose, which in turn have important distinguishing characteristics. For example, the decision making for mandatory trips such as a working trip would be less sensitive even after earthquake. Thus, unless the office building is collapsed, employers and employees would continue to make the trip. However, the same analogy is not applicable to optional shopping trips. In this study, personal trips (travel made by people) are stratified into five purposes: Home-to-Work; Home-to-School; Home-to-Other; Work-to-Other; and Other-to-Other[6].

Occupancy type of a building, as the origin side of a trip, is different to the usage of a destination building. As an obvious example, a home-to-work trip starts from a residential building and terminates at a building constituting the work place. Therefore, to convert the reduction of activity[7] to trip reduction, building occupancy types need to be associated with the origin/destination of trip purposes. Table B.7 depicts the association between building occupancy types and trip purposes. This table was developed based on the assumption that most home-based trips will generate from residential buildings, while majority of commercial / industrial buildings will be destination or origin of work-related trips.

[6] Trip classification is after SCAG 1996 Transportation Model Validation.
[7] After applying occupancy rate to percent damage to floor area

Table B.6 Activity population by building occupancy types

HAZUS Classification			Occupancy rate		Floor are 1000 sq-ft	Activity Population	
Code		Description	Day	Night		Day pop	NT pop
Residential	RES1	Single Family Dwelling	1.2	3.1	4,710,035	5,652,041	14,601,107
	RES2	Mobile Home	1.2	3.1	217,810	261,372	675,211
	RES3	Multi Family Dwelling	1.2	3.1	1,881,825	2,258,190	5,833,658
	RES4	Temporary Lodging	0.6	2.5	55,736	33,441	139,340
	RES5	Institutional Dormitory	2.0	3.0	192,016	384,031	576,047
	RES6	Nursing Home	2.0	3.0	15,129	30,258	45,388
	Mean / Subtotal		1.2	3.1	7,072,550	8,619,334	21,870,749
Commercial	COM1	Retail Trade	10.0	0.0	341,886	3,418,855	0
	COM2	Wholesale Trade	1.0	0.0	419,897	419,897	0
	COM3	Personal and Repair Service	4.0	0.1	192,998	771,990	19,300
	COM4	Professional / Technical	4.0	0.0	551,310	2,205,238	0
	COM5	Banks	4.0	0.0	30,251	121,002	0
	COM6	Hospital	5.0	2.0	41,250	206,249	82,500
	COM7	Medical Office / Clinic	5.0	2.0	87,791	438,953	175,581
	COM8	Entertainment & Recreation	6.0	0.0	104,476	626,857	0
	COM9	Theaters	6.0	0.0	2,793	16,760	0
	COM10	Parking	0.2	0.0	0	0	0
	Mean / Subtotal		4.6	0.2	1,772,650	8,225,801	277,380
Industrial	IND1	Heavy Industries	3.0	0.3	223,235	669,704	66,970
	IND2	Light Industries	3.0	0.3	236,167	708,502	70,850
	IND3	Food / Drugs / Chemicals	4.0	0.0	67,448	269,792	0
	IND4	Metals / Minerals Processing	4.0	0.0	21,730	86,919	0
	IND5	High Technology	4.0	0.0	11,035	44,138	0
	IND6	Construction	4.0	0.0	97,035	388,141	0
	Mean / Subtotal		3.3	0.2	656,650	2,167,196	137,821
Etc	AGR1	Agriculture	0.2	0.0	28,913	5,783	0
	REL1	Church / Non-Profit	65.0	0.0	81,181	5,276,752	0
	GOV1	General Services	4.0	0.0	29,063	116,252	0
	GOV2	Emergency Response	3.0	0.4	2,405	7,215	962
	EDU1	Grade Schools	20.0	0.0	66,585	1,331,704	0
	EDU2	Colleges / Universities	20.0	0.0	19,892	397,844	0
	Mean / Subtotal		31.3	0.0	228,039	7,135,550	962
Mean / Total			2.7	2.3	9,729,889	26,147,881	22,286,912

Source: HAZUS 99 technical manual, HAZUS99 Building database for California

Table B.7 Trip types and building Occupancy types

HAZUS Code	Trip Purpose									
	Home-Work		Home-School		Home-Other		Work-Other		Other-Other	
	Origin	Destin	Origin	Destin	Origin	Destin	Origin	Destin	Origin	Destin
RES1	X		X		X					
RES2	X		X		X					
RES3	X		X		X					
RES4									X	X
RES5									X	X
RES6		X				X		X	X	X
COM1		X				X	X	X	X	X
COM2		X				X	X	X	X	X
COM3		X				X	X	X	X	X
COM4		X					X			
COM5		X				X	X	X	X	X
COM6		X				X	X	X	X	X
COM7		X				X	X	X	X	X
COM8						X		X	X	X
COM9						X		X	X	X
COM10						X		X	X	X
IND1		X					X			
IND2		X					X			
IND3		X					X			
IND4		X					X			
IND5		X					X			
IND6		X					X			
AGR1		X					X			
REL1						X		X	X	X
GOV1		X					X			
GOV2									X	X
EDU1				X						
EDU2										

Vulnerability of building occupancy in Table B.5 is weighted by activity population of Table B.6, and aggregated into each of trip purposes according to the associations in Table B.7. The result can be interpreted as the reduction rate of trips due to building damage from ground shaking. Table B.8 shows the rate, and Fig. B.4 depicts the reduction rate for trips over PGA scale.

There is no guarantee that the adjusted number of originated and destined trips will be identical to each other after applying the reduction rate. In fact, to be used with

network model, the sum of origin, and destination trips should be same. It is because the OD matrix represents travel demand, which is not volatile, and conservation rule is in effect -e.g. all generated trips should be destined. However, the reduction method applies different rates to trip origin and destination, and no OD matrix can be constructed from vectors where sums are inconsistent. To avoid this problem, reduced trip production (origin), and attraction (destination) vectors are compared, and the sum is readjusted to the least sum.

In summary, this chapter outlined the process of computing reduction rates for person trips due to earthquake damage and building damage from ground motion. The following chapter records application of the same technique to estimate the reduction rate for truck trips.

Table B.8. Person Trip reduction rates

Trip purposes		Level of ground motion				
		MMI6	MMI7	MMI8	MMI9	MMI10
		PGA=0.13g	PGA=0.27g	PGA=0.52g	PGA=0.93g	PGA=1.55g
Home-Work	Origin	0.032	0.260	0.743	5.537	14.441
	Destination	0.045	0.334	0.794	7.911	24.938
Home-Schl	Origin	0.032	0.260	0.743	5.537	14.441
	Destination	0.036	0.294	0.651	6.243	20.185
Home-Other	Origin	0.032	0.260	0.743	5.537	14.441
	Destination	0.043	0.329	0.769	7.422	23.548
Work-Other	Origin	0.045	0.334	0.794	7.911	24.938
	Destination	0.043	0.329	0.769	7.422	23.548
Other-Other	Origin	0.043	0.326	0.765	7.339	23.246
	Destination	0.043	0.326	0.765	7.339	23.246

B.3. Freight Trip Reduction Model

B.3.1. Freight trip reduction

An identical concept from the passenger trip reduction previously is applied to the freight trip reduction. In this case, reduction rates for person trips under seismic condition are estimated according to 1) percent damage to floor area by building occupancy; 2) occupancy rate (population per unit floor area); and 3) association of trip purposes to occupancy types. Instead of using activity population per floor area, freight reduction will be estimated based on 'truck generation rate per employment'.

The trip reduction measure will consider the number of trucks used for shipping products from the trip generation side, and the number of trucks traveling to the trip destination side. In this study, industries are aggregated into five sectors after the truck survey study performed for SCAG, including: 1) agriculture / mining / construction; 2) manufacturing; 3) retail; 4) wholesale; and 5) service. Employment of the industries will be estimated based on the activity population by building occupancy rate (see Table B.6).

(a) Home-to-Work

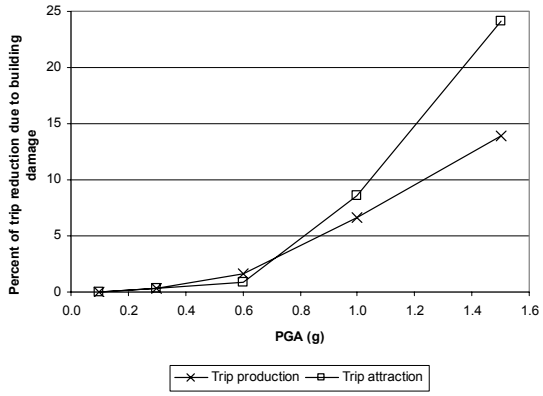

(b) Home-to-School

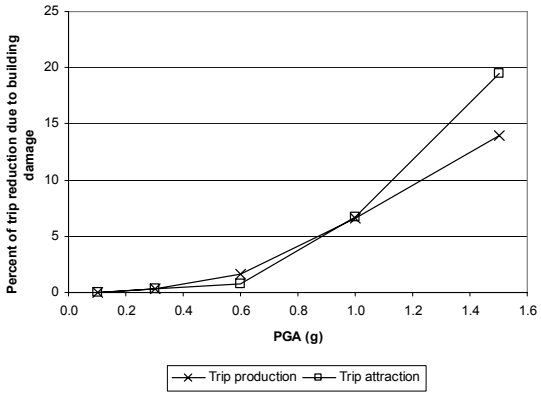

(c) Home-to-Other

(d) Work-to-Other

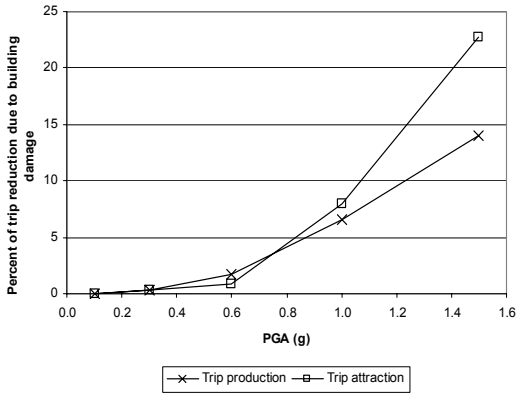

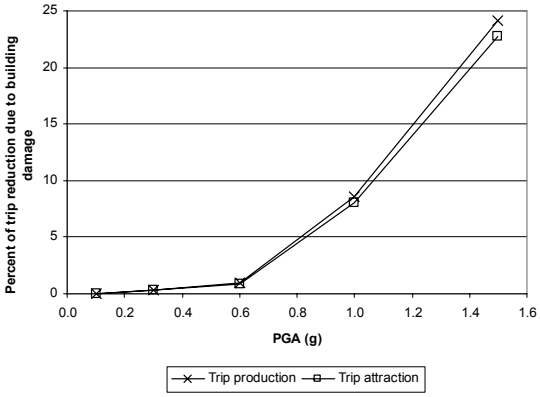

e) Other-to-Other

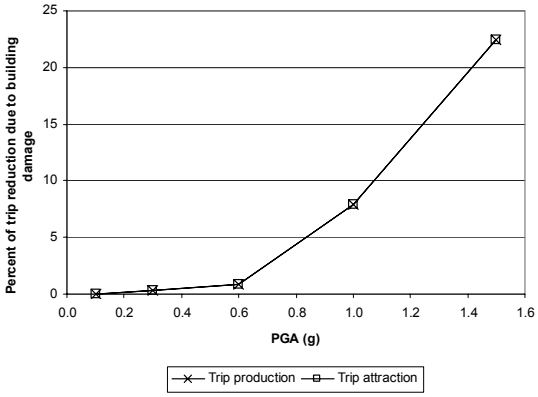

Fig. B.5 Trip reduction rate

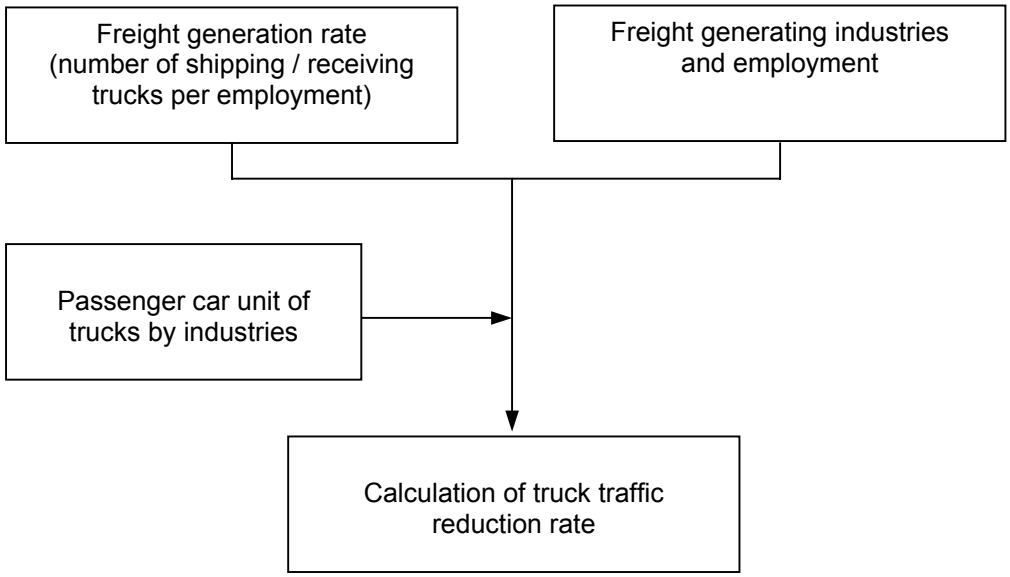

Fig. B.6 Estimation procedure of truck trip reduction

The measure 'number of trucks' will be modified to a unified unit of Passenger Car Equivalent (PCE). This study does not distinguish trucks by loaded goods, and all estimated trucks with their associate reduction, will be merged into one category of trip. Merging all trucks into one category might be problematic. Due to the size and acceleration / deceleration capability, a heavy duty truck contributes more congestion than small sized cars. Therefore the 'number' of cars and trucks can not model congestion correctly. FHWA suggests using PCE unit to implement the congestion effect of various vehicle types.[8] Depending on the characteristics of products, industries would use different types of vehicles for their deliveries, and thus, the effect of one vehicle generated from an industry is not identical to others. For example, the retail sector could use more small trucks than container trucks because delivery is more frequent and the quantity small. However, a wholesale business would deliver goods in a less frequent manner, using big trucks.

B.3.2. Shipping-Receiving rate per employee

This study uses the truck trip rate surveyed by Southern California Association of Governments (SCAG).[9] The shipping-and-receiving rates, as the number of trucks per employee, are used to determine the number of truck trips generated by different industries, or destined to other sectors given employment levels. According to the Table B.9, a business in the retail sector may generate 18.5 trucks per every 1000 employment per day, while it receives 76.1 trucks. In wholesale, a 1000-employment would generate more than 105 trucks.

[8] FHWA 1996, Highway Capacity Manual.
[9] Heavy-duty truck model and VMT estimation, SCAG 1998

Table B.9. Truck Generation Rate

	Industrial Sectors				
	Agriculture Mining Construction	Manufacture	Retail	Wholesale	Service
Shipping rate per employee (Production)	0.15119	0.07143	0.01853	0.10503	0.10508
Receiving rate per employee (Attraction)	0.04073	0.06044	0.07613	0.06261	0.01527

Source: Table 9, Heavy-duty truck model and VMT estimation, SCAG

The basis of using truck generation rate per 'employment' assumes that economic activity is stable, so that labor productivity and the composition of product to be shipped are stable across over the region. This assumption is valid for the urban transportation model, because similar industries located within close proximity operate with the same level of productivity and behavior. Otherwise, the industry with lower productivity would not survive.

B.3.3. Employment by building occupancy and freight generating industries

HAZUS 99 building usage is linked with freight trip generating industrial sectors listed in Table B.9. Linkage of HAZUS building occupancy to estimate employment is based on activity population by is applied with truck generation rates.

Out of 28 building occupancy types, 10 were identified as generating goods movement, and thus contributing to truck traffic demand. Among the commercial usages,

retail, wholesale, and personal/professional services might be related to truck traffics. Most industrial usages relate to freight shipping. The subset of building occupancies were associated with industries where truck generation rates were provided.

The ratio of employment to occupancy rate is assumed to estimate the number of employments within the activity population. The activity population in commercial facilities consists of shoppers and employees, while most of the population in industrial building can be employed. In this study, 30% of total population in retail building, and 40% of population in service building are assumed employed, and related to truck traffic generation.

The total number of employments is estimated from floor area by building occupancy types, occupancy rate, and ratio of employees. Employment estimation for building occupancy is summed for each industrial sector assigned with a freight generation rate. Retail employment was estimated at more than 1 million. Direct comparison to statistics such as census, may match employment estimates applied by this, because the estimation is rough and performed using limited data. However it is consistent to passenger trip reduction, since it relies on same database and rates.

Table B.10 Building usage and truck-trip generating industries

HAZUS classification		Floor Area 1000 sq-ft	Occupancy / 1000 sq-ft	Ratio of Employee to Occupancy	Estimated employees	Associated industry
Code	Description					
COM1	Retail Trade	341,886	10	0.3	1,025,657	Retail
COM2	Wholesale Trade	419,897	1	0.1	41,990	Wholesale
COM3	Personal and Repair Service	192,998	4	0.4	308,796	Service
COM4	Professional / Technical Service	551,310	4	0.4	882,095	Service
IND1	Heavy Industries	223,235	3	1.0	669,704	Manufact

IND2	Light Industries	236,167	3	1.0	708,502	Manufact
IND3	Food / Drugs / Chemicals	67,448	4	1.0	269,792	Manufact
IND4	Metals / Minerals Processing	21,730	4	1.0	86,919	Manufact
IND5	High Technology	11,035	4	1.0	44,138	Manufact
IND6	Construction	97,035	4	1.0	388,141	Agr / Mine & Const
ARG1	Agriculture	28,913	0.2	1.0	5,783	Agr / Mine & Const

Source: Floor Area and Occupancy per 1000 sq-ft, HAZUS99
Associated industry, and ratio of employment to occupancy are assumed

B.3.4. Calculation of Average Passenger Car Equivalent (PCE) for trucks

For this particular analysis, to estimate the total reduction of truck-trips in each TAZ within any region after an earthquake, the PCE for trucks is computed. The truck PCE varies with the percent mixture of truck vehicles in traffic flow, geometric grade of transportation network link, and link length.[10] The assumption for this study is 5-10% truck mixture, 0-2% grade, and link-length of less than 1mile. PCE by sectors are estimated by calculating weighted average of PCE with truck-trip generation rate.

According to the calculation shown in Table B.11, a truck generated from, or delivered to the service sector corresponds with 3.49 passenger cars, with respect to the effect on roadway congestion. A truck with wholesale product has a PCE of 4.25.

Table B.11 Estimated PCE by Industries

	Usage by trick size [1]			PCE by sectors [3]
	Light truck	Medium truck	Heavy truck	
Agriculture/Mining/Const	0.0513	0.0836	0.0569	4.01879
Manufacturing	0.0353	0.0575	0.0391	4.01801

[10] Highway Capacity Manual (HCM) 1996, defines parameters like Truck mixture, Geometric grade of transportation network link, and Link length as impedance to traffic flow

Retail	0.0605	0.0962	0.0359	3.70439
Wholesale	0.0393	0.0650	0.0633	4.24703
Service	0.0091	0.0141	0.0033	3.49347
PCE [2]	1.88	4.01	5.96	

Source: 1) Table 10 – Heavy-duty truck model and VMT estimation, SCAG
2) Table 18 - Heavy-duty truck model and VMT estimation, SCAG
3) PCE calculated

B.3.5. Travel demand reduction for freight trips

The reduction rate of truck traffic is calculated as an average of building vulnerability, weighted by truck generation rate, employment estimation, and PCE (see Equation B.1) Alternatively, the equation is able to be interpreted as a ratio of (1) the sum of affected truck traffic by building damage in PCE to (2) the sum of PCE of all truck trips.

Percent truck trip reduction for given ground motion=

$$\frac{\sum_i \sum_j \left[PCE_i \cdot rate_i \cdot Emp_j \cdot F_j \cdot D_{ij} \right]}{\sum_i \sum_j \left[PCE_i \cdot rate_i \cdot Emp_j \cdot D_{ij} \right]} \quad \text{.....}$$

(B.1)

where

i =index for industries (i=1...5)

j =index for building occupancy type (j=1...28)

PCE_i =PCE by industrial sectors i (Table B.11)

$rate_i$ = freight shipping rate of industry i for reduction in trip production

freight receiving rate of industry i for reduction in trip attraction

(Table B.9)

Emp_j= Estimated freight generating employment by building occupancy j (Table B.10)

F_j =Percent building damage for given ground motion by building occupancy j (Table B.5)

D_{ij} =1 if industry i has relationship with building occupancy j, 0 otherwise (Table B.11)

Estimated reduction rates of truck origin and destination are similar. For events with extreme ground motion, the transportation system would loose one quarter of its baseline truck traffic demand, with respect to both trip production and destination. Fig. B.6 depicts this reduction rate.

In summary, this chapter presents the procedure for computing trip reduction rates for truck traffic, due to building damage caused by earthquakes. The applied concept behind the calculation is same as that used in computing passenger trip reduction, where vulnerability of building occupancy is converted based on factors of (economic) activities. In following chapter, the truck reduction model will be integrated into a equilibrium user transportation model.

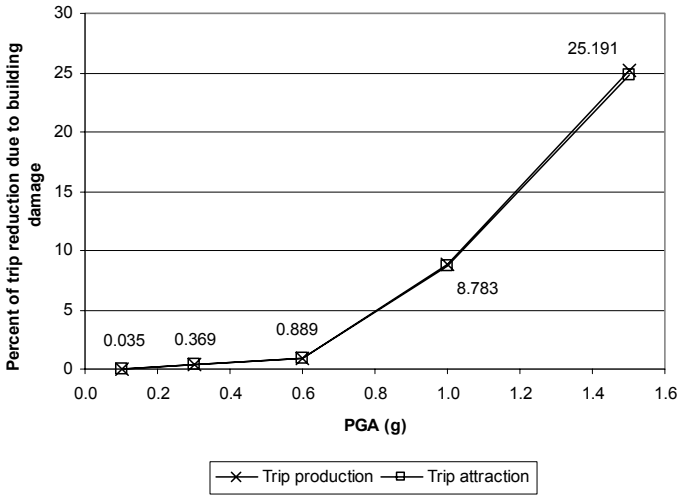

Fig. B.7 Truck trip reduction rate

B.4. POST-EARTHQUAKE OD

In this section, the passenger trip reduction models, developed in previous section, are incorporated into an integrated model for post-earthquake transportation system. The reduction models adjust pre-earthquake trip production and attraction according to building damage. A distribution model generates an OD matrix for post-earthquake travel demand based on adjusted trip production and attraction, and travel cost. A network assignment model then loads the travel demand in an OD matrix onto the seismically damaged network, and estimates post-earthquake traffic volume and congested travel time.

The distribution model will make a connection between the reduction model and assignment model. Production/attraction vectors are a type of disaggregated measurement for travel demand. The vectors explain "how many people depart from a zone", or "how many cars enter a zone". With respect to the network model, these two vectors should be combined to generate information about "how many cars depart from zone a to travel to

zone b". In other words, travel demand information needs to be disaggregated into associated origin and destination zones. Distribution models estimate travel demand in a matrix form in which rows represent origin zones, and columns destination. In this study, a doubly-constrained gravity model is applied, distributing post-earthquake travel demand based on two criteria:

(1) Travel demand between an origin-destination pair is proportional to the trips emanating from the origin zone and trips attracted to the destination zone. Estimated post-earthquake trip production – attraction vectors by reduction model, will be used according to this criterion.

(2) The lesser the travel time (cost) between a zone-pair, the more demand is allocated. This criterion is included in the model by means of a distance-decay function.

Integrating the three component models – reduction, distribution, and network models – involves arranging them in such a way that it yields stable solutions. With endogenous travel demand estimation, the integrated model is expected to generate post-earthquake traffic volume and congested time. As mentioned above, travel demand will be distributed over the zones according to the travel time, while congested travel time is calculated along with the travel time. This means that travel time is generated from the network model and used by gravity model, while OD matrix is generated by the gravity model using travel time. Thus, in the integrated model, trip distribution and network models should be deployed so that the intermediate input and output are consistent.

The present study suggests an iterative transportation planning model with successive average, rather than the traditional 4-step approach. The four-step approach

does not guarantee consistency between estimated OD and congested travel time, because the approach does not adjust OD in proper way. Following Evans (1976) [4], the suggested model will adjust OD matrix and link volume (and thereby congested travel time) simultaneously, with application of simplified updating mechanism between iterations. In the Evans model, results from two consecutive iterations are integrated through a secant line so that in every iteration, the new combined results are closer to the global solution of a non-linear optimization problem. Rather than implementing the detailed solution algorithm, the model uses pre-defined secant lines for each iteration step (see Fig. B.2).

B.4.1 Gravity Model as the Demand Model

The gravity model is a trip distribution model that estimates trip interchanges between zone i and j, t_{ij}, based on aggregated trip production and attraction from/to each zone. Equation (1) presents the gravity model. The equation shows that, according to the first criterion, travel demand is proportional to the production (O_i) and attraction (D_j). The conservation rule is applied to distributed travel demand, and the sum of the travel demand generated from a zone i over the all of its destination j, where $\sum_j t_{ij}$, should be equal to the O_i. Destined demand to a zone should also be equal to the sum of demand over the origin zones. Application of the conservation rule over the distribution process implies that the distribution model would not alter the (reduced) post-earthquake demand by the reduction model.

$$t_{ij} = O_i \cdot D_j \cdot A_i \cdot B_j \cdot f(c_{ij}) \tag{B.2}$$

where t_{ij} : travel demand between zone i and zone j

c_{ij} : endogenous travel time between zone i and zone j

$f(c_{ij})$: distance decay function, $f(c_{ij}) = \exp(\alpha + \beta \cdot c_{ij})$

O_i : before and after earthquake trip production from origin zone i ,

$$O_i = \sum_j t_{ij}, \forall i, j$$

D_j : before and after earthquake trip attraction to destination zone j.

$$D_j = \sum_i t_{ij}, \forall i, j$$

A_i : balancing factor associated with each origin i, $A_i = \dfrac{D_j}{\sum_j t_{ij} \cdot B_j}$

B_j : balancing factor associated with each destination j, $B_j = \dfrac{O_i}{\sum_i t_{ij} \cdot A_i}$

α, β : model parameters to be estimated.

Zones are distinguished by the travel time (more generally, cost) from an origin. Demand from the origin zone is distributed according to difficulty in traversing the network to the destination zone. Where a destination zone is closer to the origin, the difficulty associated with traveling between the origin and destination is low. Consequently, more demand would be allocated onto this zone-pair. Demand is thereby distributed according to the difficulty of travel. In the gravity model, a function, $f(c_{ij})$ termed the 'distance decay function', is used to explain this mechanism. In this study,

exponential function with a negative coefficient to travel time ($\beta < 0$) is used to represent decreasing rate travel demand over increasing travel time.

B.4.2 Calibration of the Demand Model

The 1996 SCAG [5] transportation data set, which comprises 3217 traffic analysis zones (TAZ), was used to calibrate the distance decay function. Travel demands are stratified by five purposes of passenger trips (Home-to-Work, Home-to-School, Home-to-Other, Work-to-Other, and Other-to-Other) , and one truck trips for freight movement. Table B.12 shows calibrated coefficients α, β, and R^2. The exponential function with travel time is able to explain the distance decay of home-based trips (to-work, to-trips, and to-other) with R^2 higher than 0.9. The R^2 for work-related trips and others were no lower than 0.85.

Table B.12 Calibration of Decay Function Parameter

Trip Purpose	Time of Day*	α	β	R^2
Home to Work	AM	3.151973	-0.06616	0.9903
	PM	3.170573	-0.06693	0.9917
	MD	3.469839	-0.10274	0.9822
	NT	3.539828	-0.13011	0.9771
Home to School	AM	4.288389	-0.12286	0.9311
	PM	4.544710	-0.14933	0.9513
	MD	5.568479	-0.27000	0.9775
	NT	5.856893	-0.33459	0.9853
Home to Other	AM	3.607120	-0.08362	0.9121
	PM	4.279050	-0.12497	0.9034
	MD	4.564984	-0.17333	0.9004
	NT	4.966864	-0.23647	0.9211
Work to Other	AM	4.580842	-0.14985	0.9547
	PM	3.620443	-0.08406	0.9143
	MD	3.970968	-0.12998	0.8586
	NT	4.446589	-0.18854	0.8999
Other to Other	AM	4.186721	-0.11903	0.9017
	PM	4.322647	-0.12511	0.9324
	MD	4.545936	-0.16752	0.9358
	NT	4.846849	-0.22063	0.9520
Truck	AM	1.458376	-0.02360	0.6302
	PM	1.566471	-0.02587	0.6684
	MD	1.531339	-0.03088	0.6168
	NT	1.349884	-0.03104	0.4556

* AM: Morning Peak; PM: Evening Peak; MD: Mid-day; NT: Night.

B.4.3. OD RECOVERY MODEL

A simplified travel demand recovery model is integrated. Demand reduction is a function of building damage from earthquakes. Demand would be recovered as damaged buildings are restored. In this study, we simply used linear time-demand reduction curve for OD recovery model (Fig. B.8). Recovery period for travel demand is simply enumerated by experience. As shown in Fig. B.8, we assume that travel demand reduction will be recovered continuously within a time. T_{max} is the period for full demand recovery. For the earthquake to cause ground motion of MMI 9, we assume one year is required for full structural recovery. Therefore T_{max} is 365 days. Comparatively, a less intensive ground motion will apply a shorter recovery period.

Based on the assumption predescribed, the recovery time, T_{max}, is modeled as a function of a zonal ground motion as:

$$T_{max} = \frac{365}{10 - g}$$

(B.3)

Where

g is the zonal ground motion in MMI scale, $g < 10$.

And the trip reduction rate, R_T, in an arbitrary time from the earthquake is given by,

$$R_T = R_0 \frac{T}{T_{max}}$$

(B.4)

where

R_0 is initial trip reduction rate estimated from the reduction model.

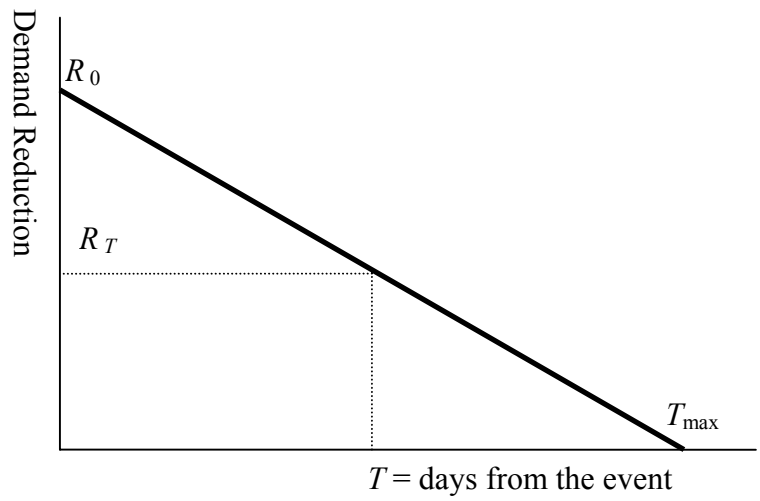

Fig. B.8 Conceptual OD recovery model

References

1. Eguchi, R.T., Goltz, J.D., Selingson, H.A., Flores, P.J., Blais, N.C., Heaton, T.H. and Bortugno, E., 1997, "Real-time Loss Estimation as an Emergency Response Decision Support System: the Early Post-Earthquake Response Tool (EPDAT)," Earthquake Spectra, Vol.13, 1997, pp.815-832.
2. National Institute of Building Sciences, 1999, "Earthquake Loss Estimation Methodology: HAZUS 99 (SR2) Technical Manual", Developed by Federal Emergency Management Agency, Washington DC, http://www.fema.gov/hazus.
3. Southern California Association of Governments, "1996 Origin-destination survey", Los Angeles, CA.
4. Shinozuka, M., Murachi, Y., Dong, X., Zhou, Y. and Orlikowski, M.J., 2003, "Effect of Seismic Retrofit of Bridges on Transportation Networks", Research Progress and Accomplishments 2001-2003, Multidisciplinary Center for Earthquake Engineering Research (MCEER), 2003, pp.35-49.
5. Chang, S.E., Shinozuka, M. and Moore, J., 2000, "Probabilistic Earthquake Scenarios: Extending Risk Analysis Methodologies to Spatially Distributed Systems", Earthquake Spectra, Vol.16, No.3, pp.-557-572.
6. Sheffi, Y., Urban Transportation Networks: Equilibrium Analysis with Mathematical Programming Methods, Prentice Hall, Englewood Cliffs, NJ, 1985.
7. Shiraki, N., 2000, "Performance of Highway Network Systems under Seismically Induced Traffic Delays", M.S. Thesis, Kyoto University, Kyoto, Japan.
8. ArcGIS 8.2, 1999, ESRI Inc., http://www.esri.com
9. Wardrop, J., (1952), "Some Theoretical Aspects of Road Traffic Research", Proceedings of Institute of Civil Engineers, Volume 1, No. 2, pp 325-378.

Appendix C: Manual for Software HighwaySRA

C.1 Introduction

Highway Seismic Risk Analysis (HighwaySRA) is a GIS-based software developed for the seismic risk analysis of highway transportation system in Los Angles and Orange County. It can be used to perform a complete seismic risk analysis for the highway transportation system. Its major capabilities include: earthquake scenario definition and ground motion generation, simulation of bridge and link damage state, assignment of residual link capacity, network traffic assignment analysis, simulation of system performance recovery, estimation of direct economic loss (bridge repair cost) and indirect economic loss (social loss).

C.2 Analysis Procedure

A complete seismic risk analysis include the following steps:

- Define an earthquake scenario. A scenario could be one of the imbedded scenarios, an event imported from a GIS ground motion map or a user-defined arbitrary event.
- Set up Analysis Parameters. These parameters include bridge fragility information, criteria for link residual performance and criteria for economic loss.
- Perform analysis: The software is able to perform both deterministic and probabilistic seismic risk analysis for the highway transportation system. In deterministic analysis, an earthquake scenario is first selected, which can be any of the embedded scenario earthquakes or any imported GIS ground motion map. From the given scenario, the ground motion (PGA) at the site of each component of the system will be obtained. The physical damage state of each component

(bridge) is then simulated based on its site-specific ground motion value and its fragility information that is previously developed (Shinozuka and etc., 2003) and imbedded in the software. The highway system is modeled as a network consisting of nodes and links. Each link consists of several roadway components and bridge components, and bridges are considered as the only components in a link to be vulnerable to earthquake. The damage state of each link is then determined based on the damage state of the bridge sustaining the most severe damage in this link, and its residual traffic capacity is assigned according to its damage states by scaling down its initial capacity. A deterministic equilibrium method is then performed to assign the traffic (Origin-destination) demand to the degraded system and the daily travel time can then be found. The difference between the total travel time needed in the damaged network and intact network, called the drivers' time delay, provided an comprehensive index measuring the system performance of the highway network in seismic condition. Finally, the loss resulting from the repair effort of the damaged components will be estimated and the drivers' time delay is also converted into related economic loss. The sum of these losses, therefore, provides the loss estimate or risk of the highway transportation system exposed to this given earthquake.

The probabilistic seismic risk analysis, however, is more complicated. The main reason is that all the possible scenario earthquakes, in or close to the region where the highway network is spatially distributed, and their probability of occurrence should be considered, which makes the calculation tedious and very expensive. To overcome this difficulty, a small, manageable set of scenario earthquakes carefully selected with

assigned "probabilities" are used to approximately represent the regional seismic hazard. To perform the probabilistic risk analysis, the risk resulting from each of these scenario earthquakes using the deterministic analysis described above is first estimated. Then, the expected risk of the highway network can be obtained by summing up all the products of the annual probability of occurrence of each scenario and its corresponding risk.

C.3 Interface Introduction

The main interface is a window-based visual program developed from Visual BASIC 6.0 (Fig. C.1). All the functionalities of the seismic risk analysis are implemented in the five main menus in the menu bar and 7 toolbar items. The use of these five menus, including Map, Inventory, Hazard, Analysis and Results, and the toolbar items will be introduced in the following sections.

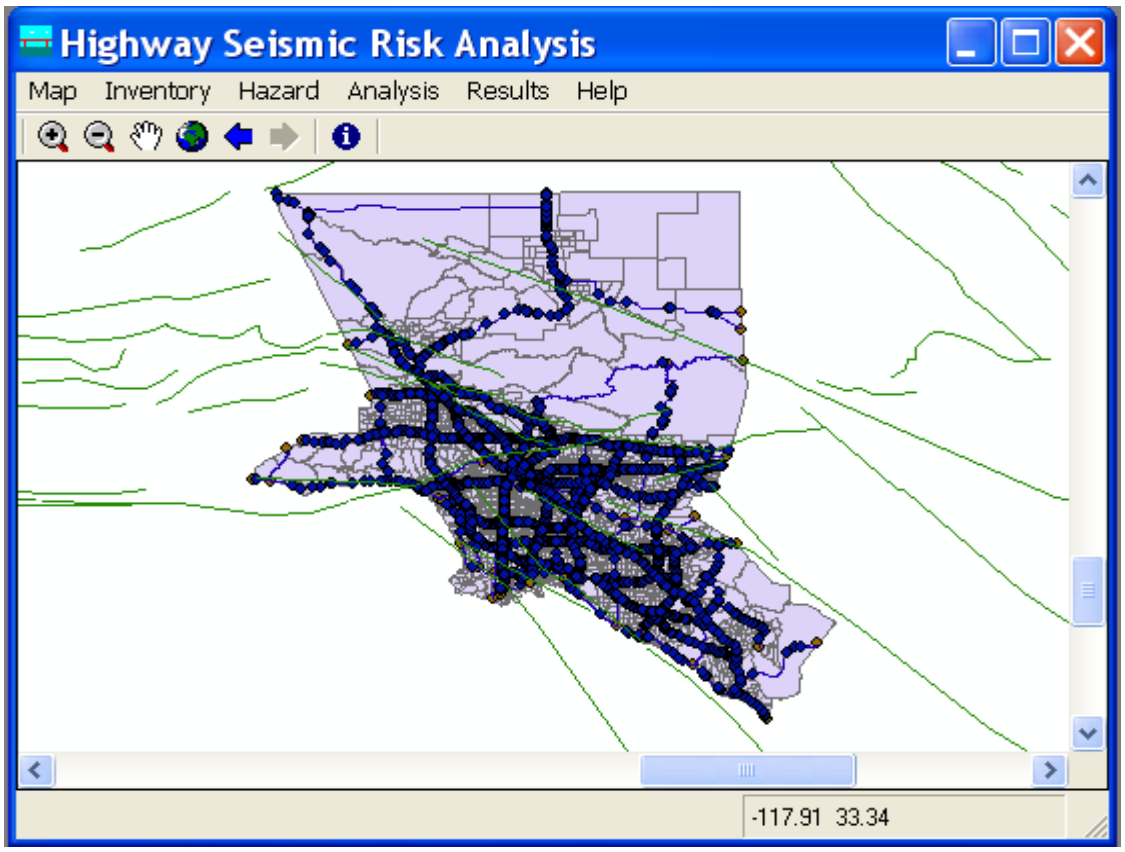

Fig. C.1 Main Interface

C3.1 Menu

Map

The menu Map (Fig.C.2) organizes the function of displaying the basic maps used for the seismic risk analysis of highway transportation system in Los Angles and Orange County. These maps are Study Region Map (Los Angles and Orange Counties) (Fig.C.3), Highway Network Link Map (Fig.C.4), Highway Network Node Map (Fig.C.5) and Bridge Location Map (Fig.C.6) . The study region map is set to be visible all the time, while the other three maps can be turned off as invisible in user's convenience.

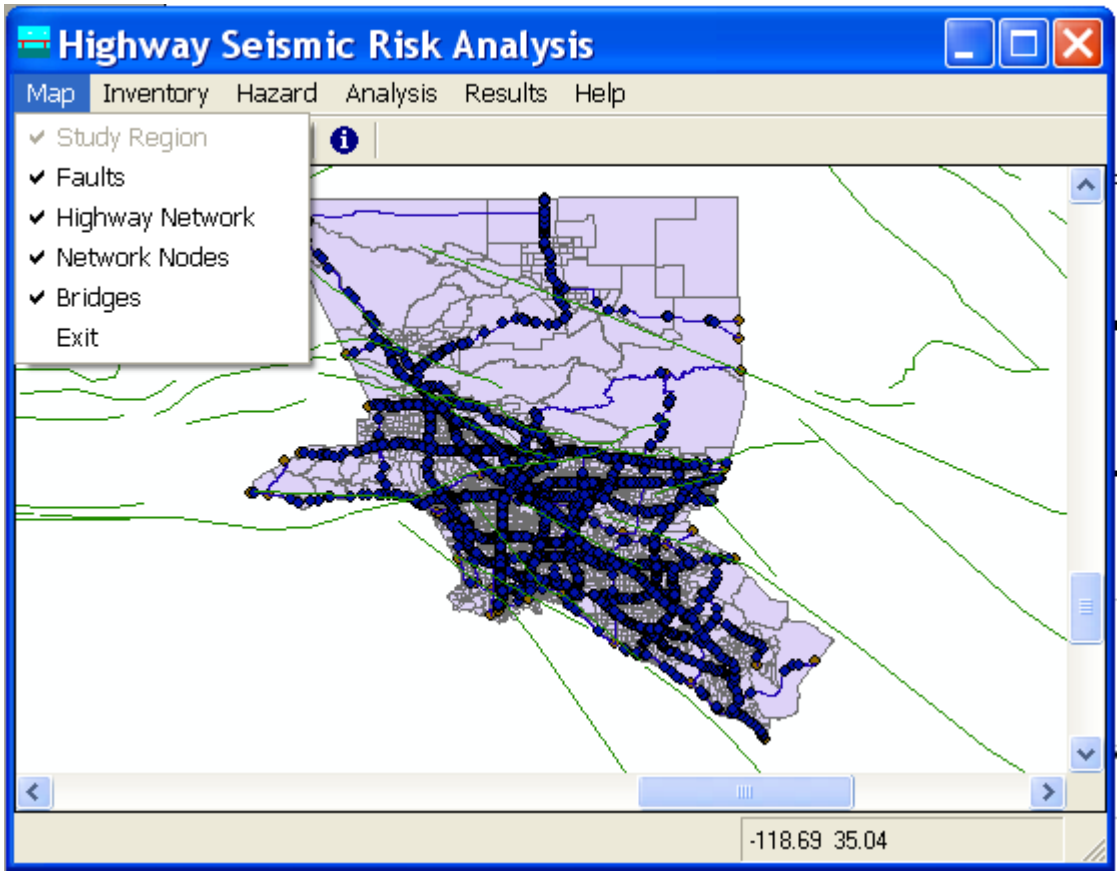

Fig. C.2 Menu "Map"

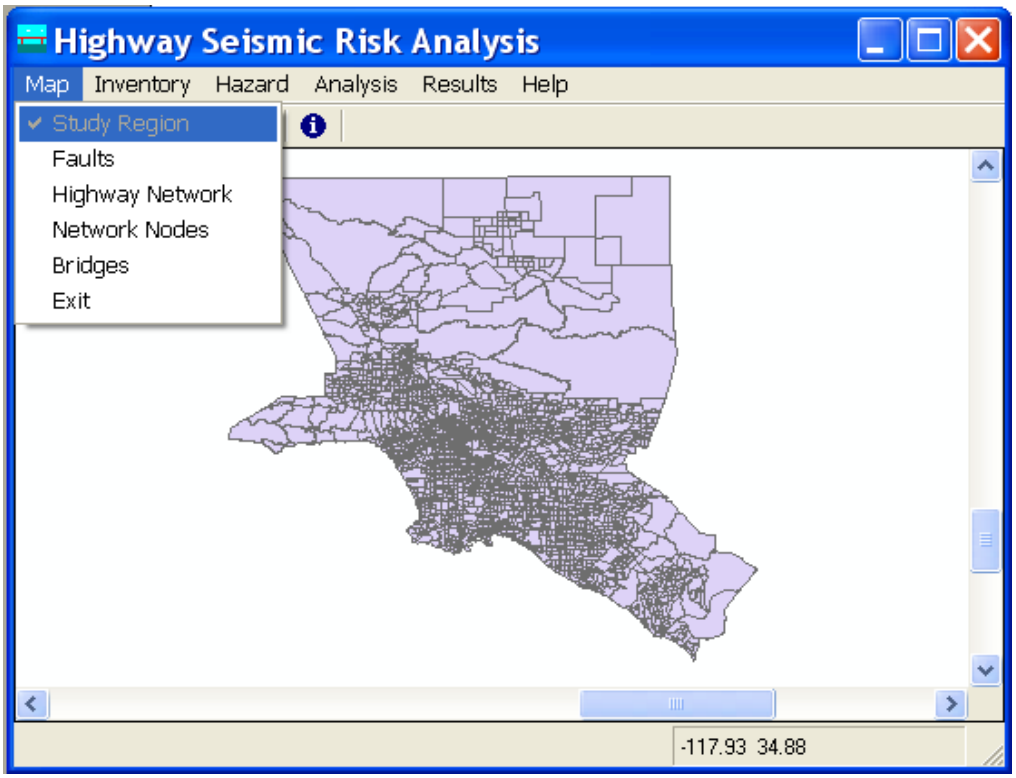

Fig. C.3 Map of Study Region

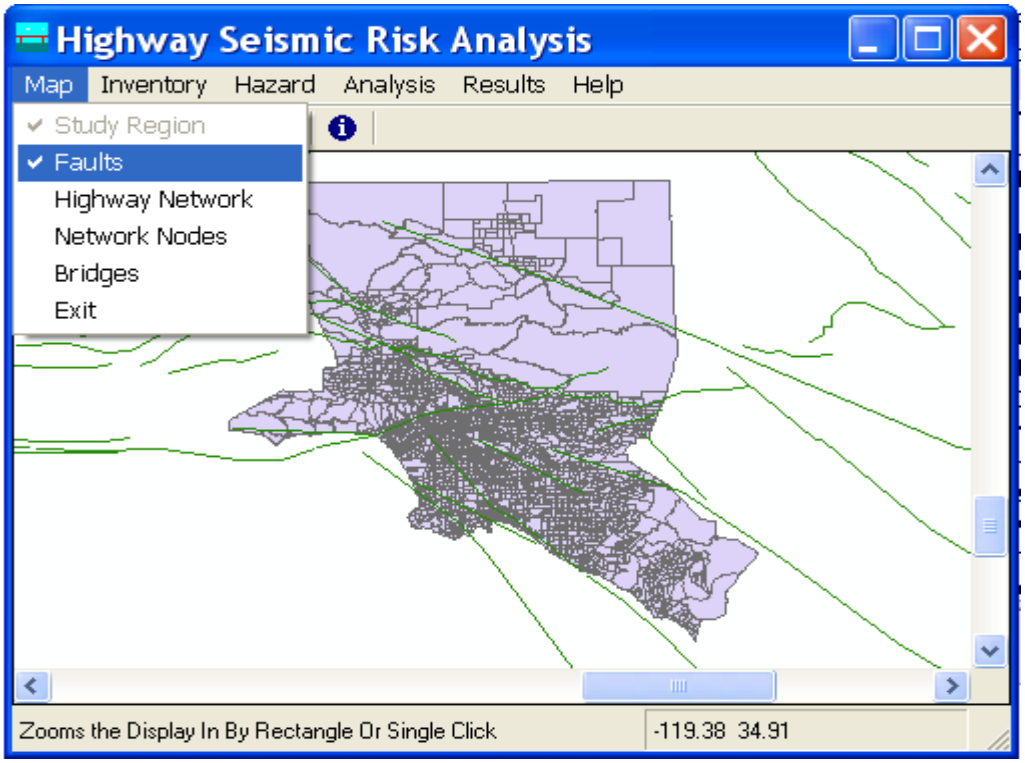

Fig. C.4 Map of Faults

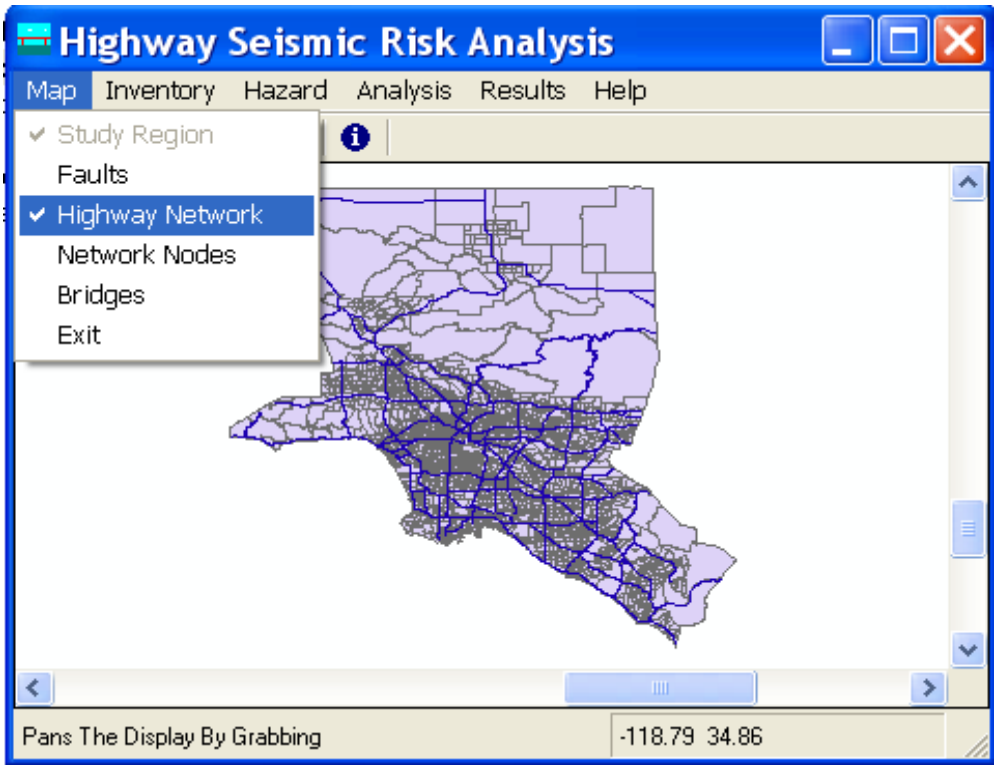

Fig. C.5 Map of Freeway Network

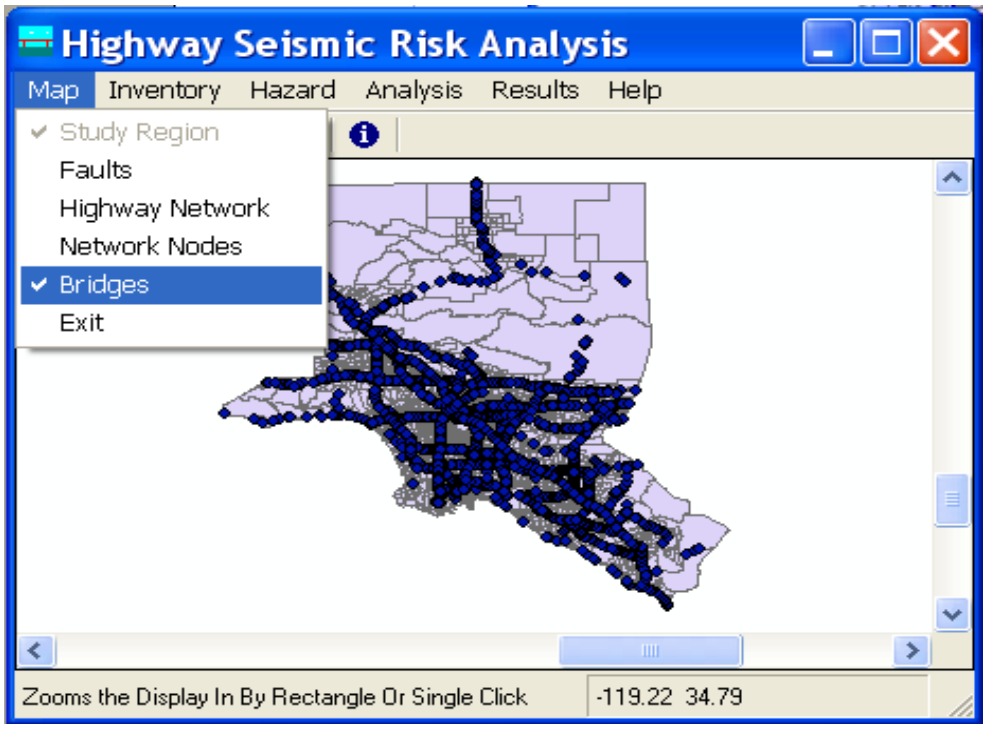

Fig. C.6 Map of Bridges

Inventory

The basic inventory data include the bridge attributes and network configuration (Fig. C.7). They can be viewed in tables but are not editable. Figs. C.7 and C.8 display the bridge attribute table and network attribute table, respectively.

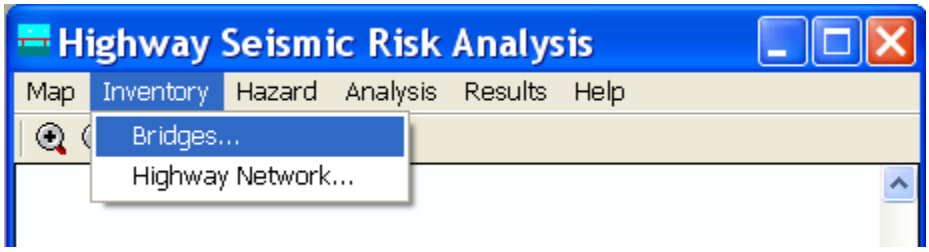

Fig. C.7 Menu "Inventory"

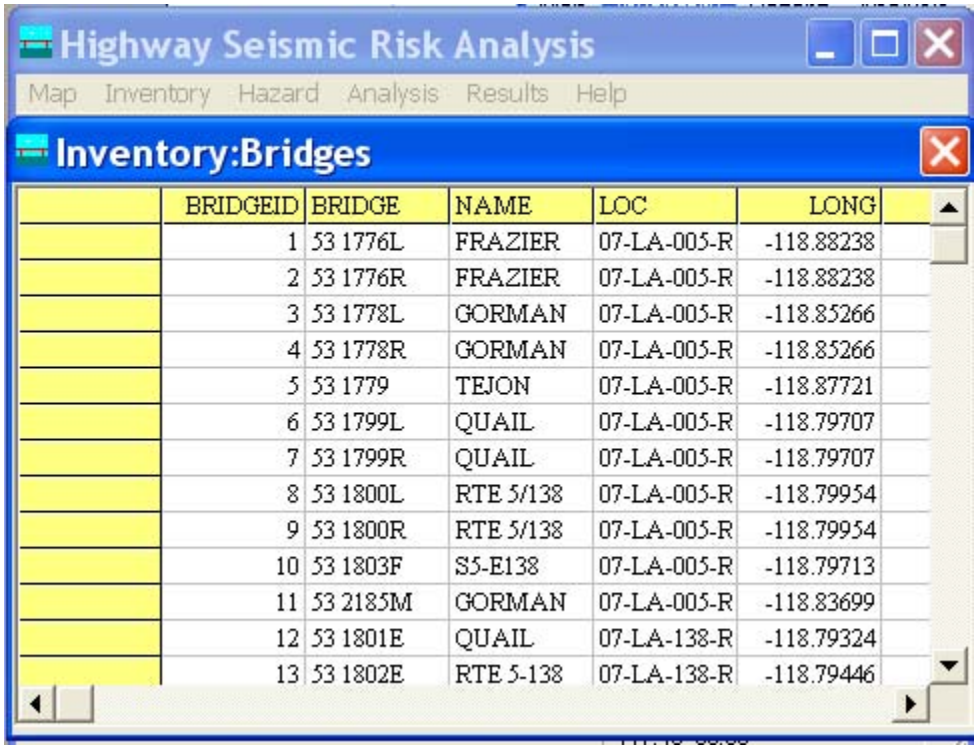

	BRIDGEID	BRIDGE	NAME	LOC	LONG
	1	53 1776L	FRAZIER	07-LA-005-R	-118.88238
	2	53 1776R	FRAZIER	07-LA-005-R	-118.88238
	3	53 1778L	GORMAN	07-LA-005-R	-118.85266
	4	53 1778R	GORMAN	07-LA-005-R	-118.85266
	5	53 1779	TEJON	07-LA-005-R	-118.87721
	6	53 1799L	QUAIL	07-LA-005-R	-118.79707
	7	53 1799R	QUAIL	07-LA-005-R	-118.79707
	8	53 1800L	RTE 5/138	07-LA-005-R	-118.79954
	9	53 1800R	RTE 5/138	07-LA-005-R	-118.79954
	10	53 1803F	S5-E138	07-LA-005-R	-118.79713
	11	53 2185M	GORMAN	07-LA-005-R	-118.83699
	12	53 1801E	QUAIL	07-LA-138-R	-118.79324
	13	53 1802E	RTE 5-138	07-LA-138-R	-118.79446

Fig. C.8 Inventory: Bridges

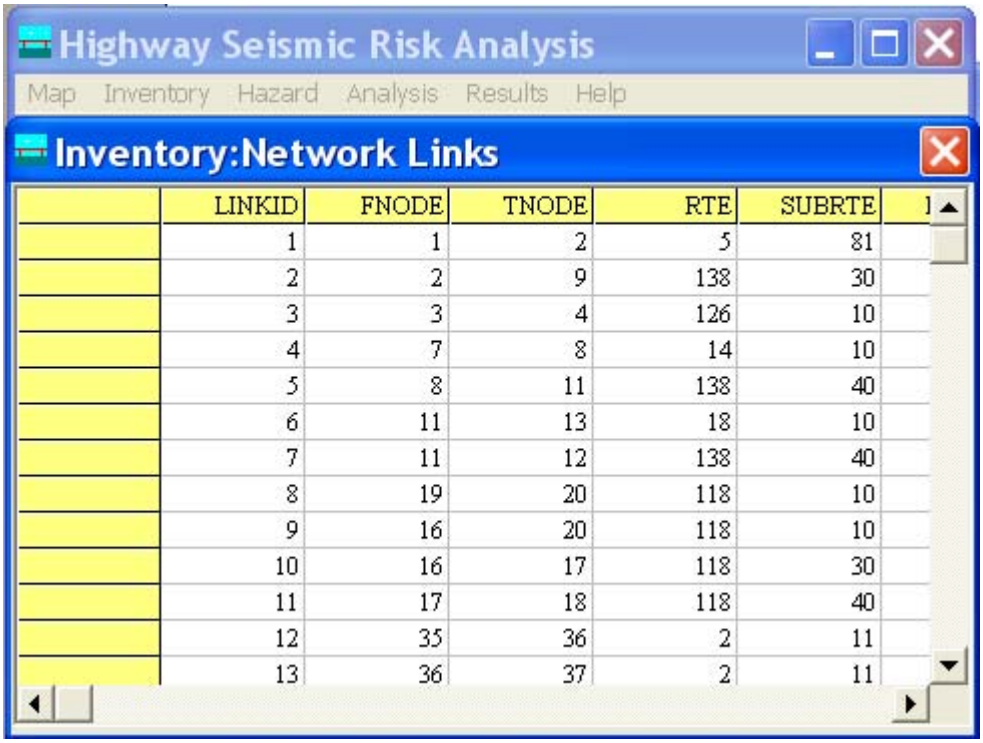

	LINKID	FNODE	TNODE	RTE	SUBRTE
	1	1	2	5	81
	2	2	9	138	30
	3	3	4	126	10
	4	7	8	14	10
	5	8	11	138	40
	6	11	13	18	10
	7	11	12	138	40
	8	19	20	118	10
	9	16	20	118	10
	10	16	17	118	30
	11	17	18	118	40
	12	35	36	2	11
	13	36	37	2	11

Fig. C.9 Inventory: Network Links

Hazard

Currently, the seismic hazard used for risk analysis can be defined in three ways (Fig. C.10). The first One (Fig. C.11) is chosen from 48 predefined events including 13 Maximum Credible Events, 34 smaller events and 1 historical event (1994 Northridge Earthquake). The second way (Fig. C.12) is to import ground motion contour map in the format of GIS shape files. The third way (Fig. C.12) is to define a scenario based on the user's input.

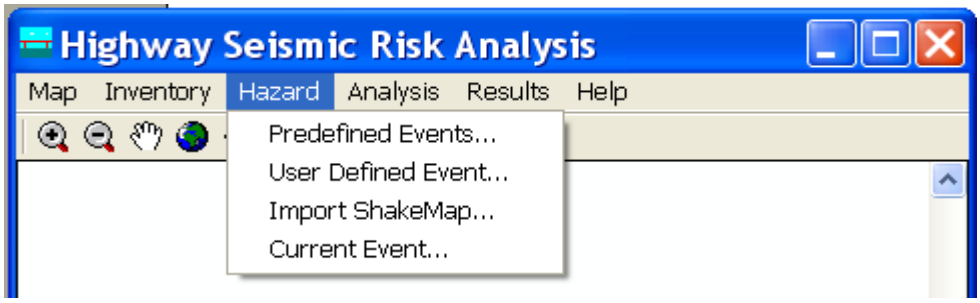

Fig. C.10 Menu "Hazard"

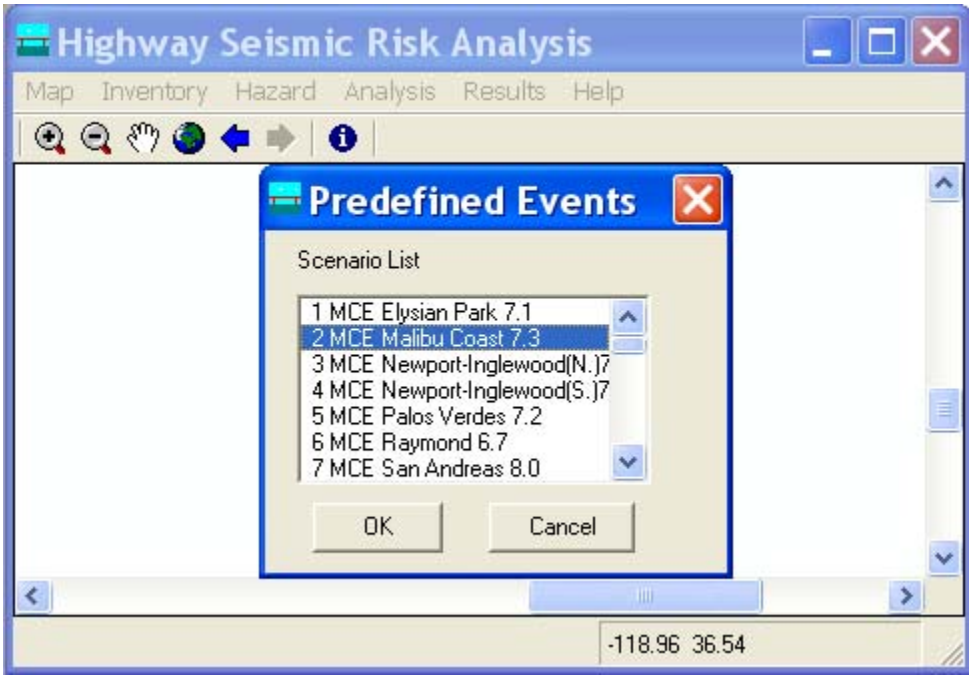

Fig. C.11 Predefined Events

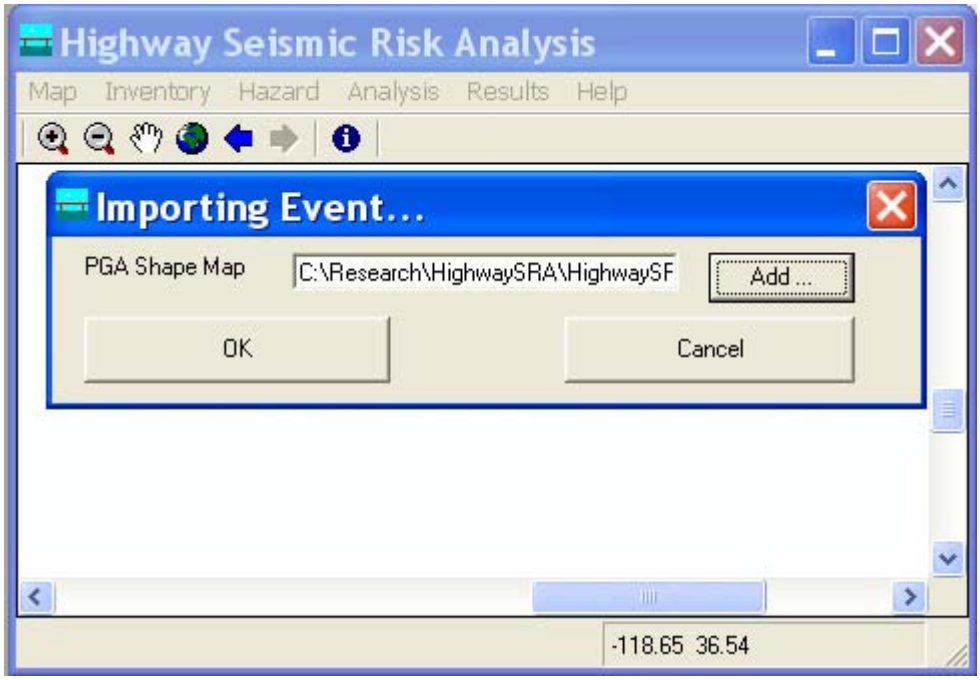

Fig. C.12 Importing PGA Shape Map

Fig. C.13 User Defined Event

User can define an arbitrary event by specifying empirical attenuation relation(, epicenter magnitude and fault angle (North to South)

Fig. C.14 User Defined Event

Analysis

Before performing the risk analysis, user can set up the parameters which are the assumptions necessary for the calculation. In Menu "Analysis-> Setting" (Fig. C.15), These Parameters are organized into three groups: Bridges Fragility Information, Criteria for Link Damage States and Traffic Capacity, and Loss Estimation Parameters (Figs. C.16-18).

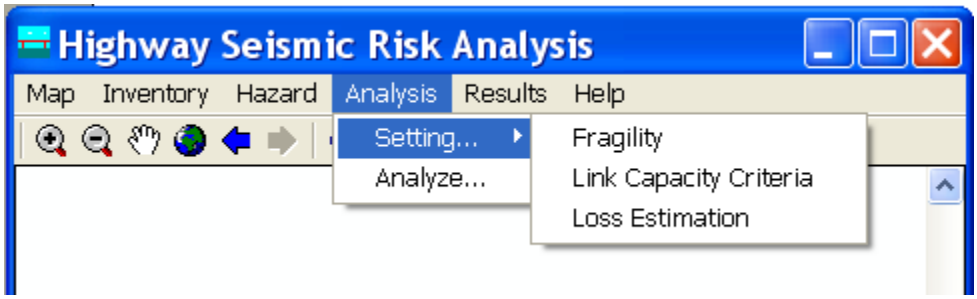

Fig. C.15 Analysis: Setting

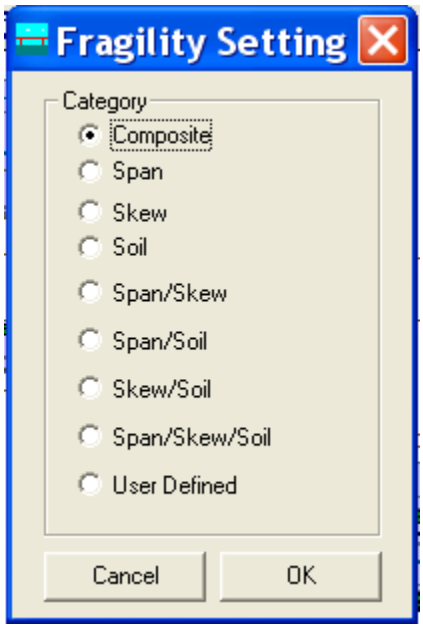

Fig. C.16 Bridge Fragility Setting

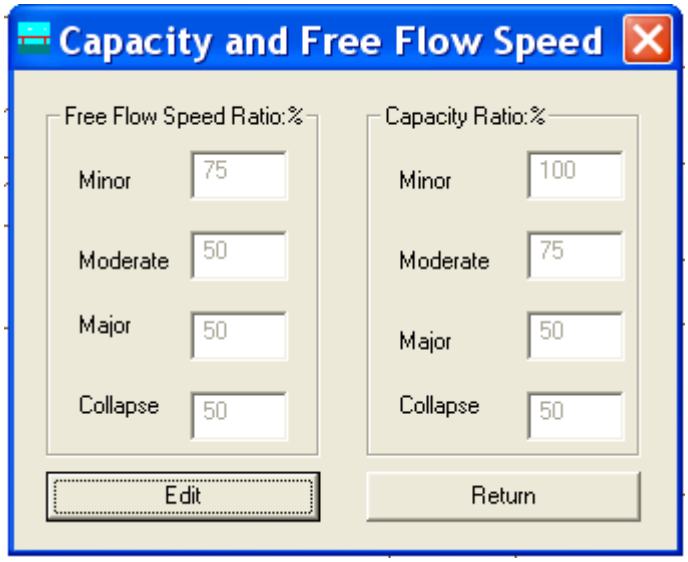

Fig. C.17 Residual Link Performance Setting

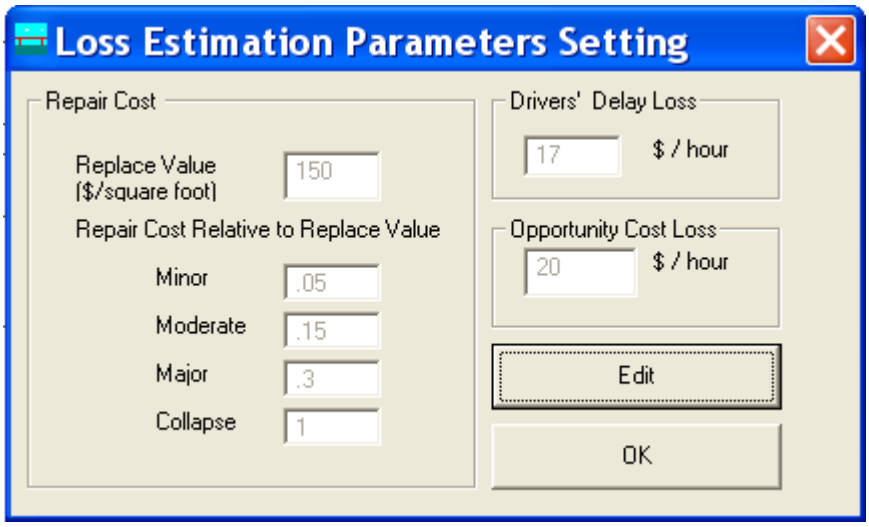

Fig. C.18 Economic Loss Estimation Parameter Setting

When click Menu "Analysis-> Analyze…" , Analysis Option Dialog will appear (Fig. C.19). There are 6 options: Ground Motion , Bridge Damage, Link Damage, System Performance(Day 0) , System Recovery and Loss Estimation. A complete analysis requires all these option checked and the analysis procedure will follow the above order.

When “system recovery” is checked, the analysis option with lower order (Ground motion, bridge damage, link damage, system performance) will also automatically checked.

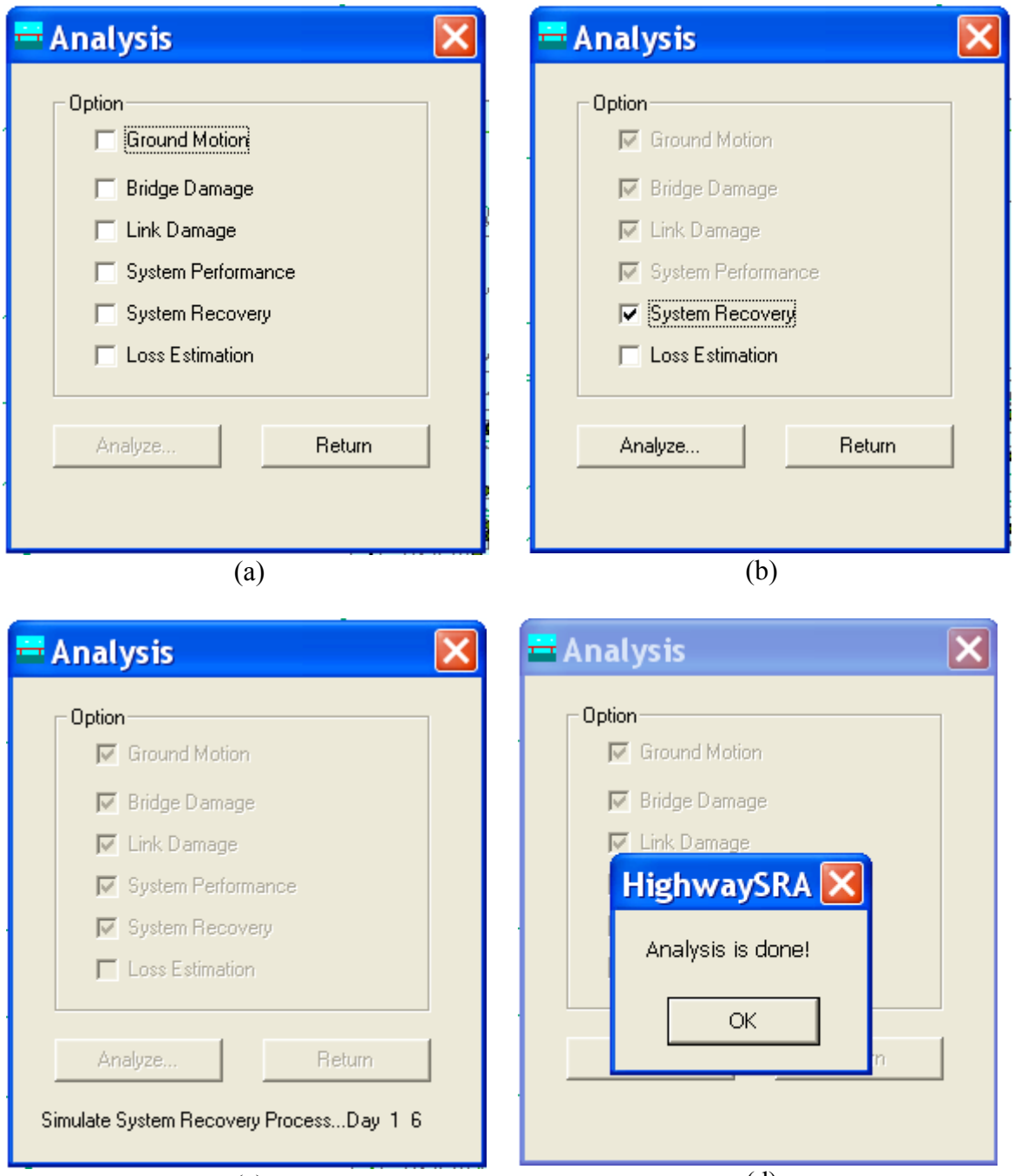

Fig. C.19 Risk Analysis Option

Results

In Menu "Results". User can view the analysis results (Fig. C.20) of each step: Ground Motion,Bridge Damage, Link Damage, System Performance and Economic Loss (Figs. C.21-25).

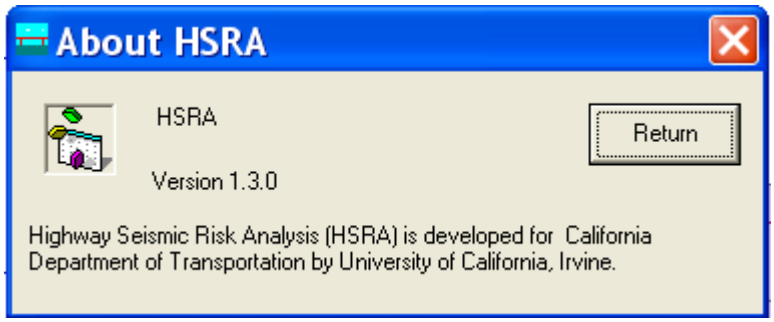

Fig. C.20 Menu "Results"

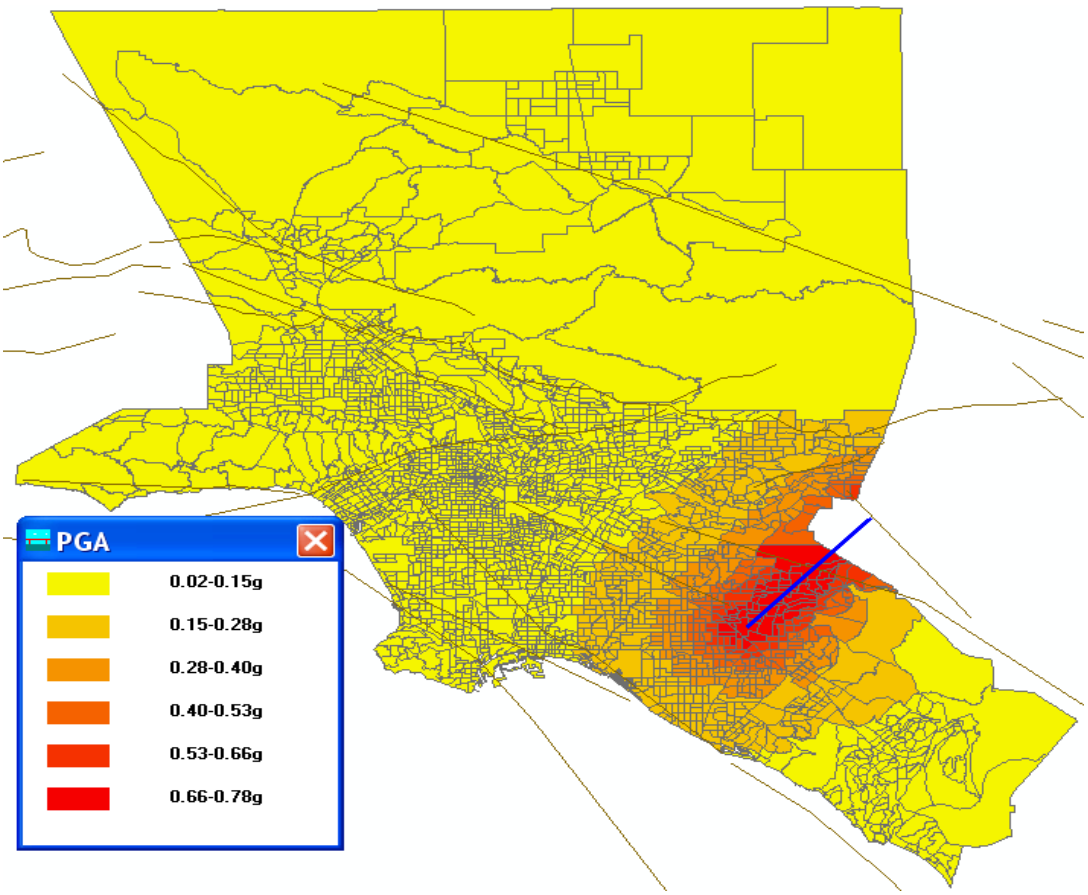

Fig. C.21 PGA distribution

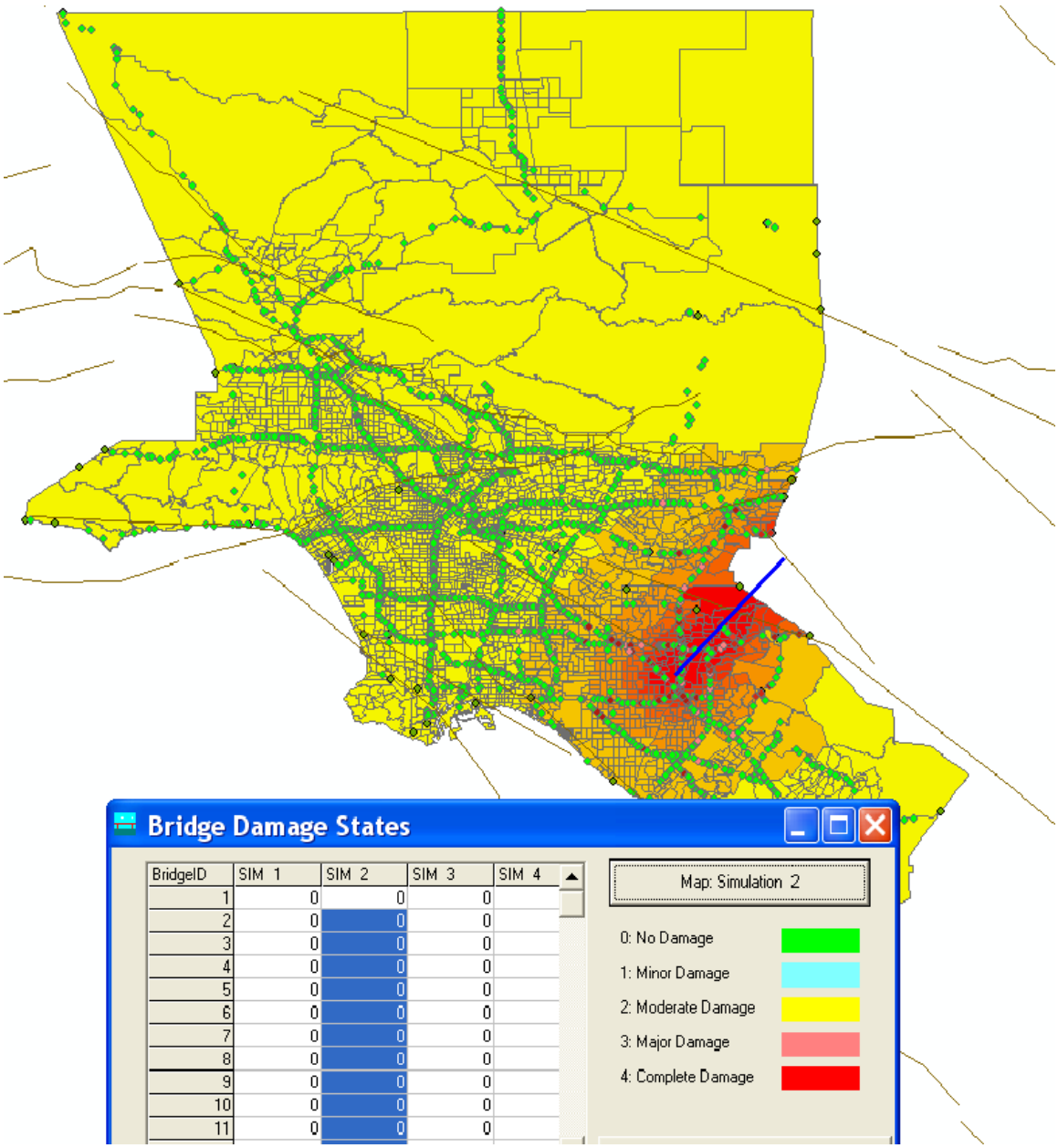

Fig. C.22 Display Bridge Damage States

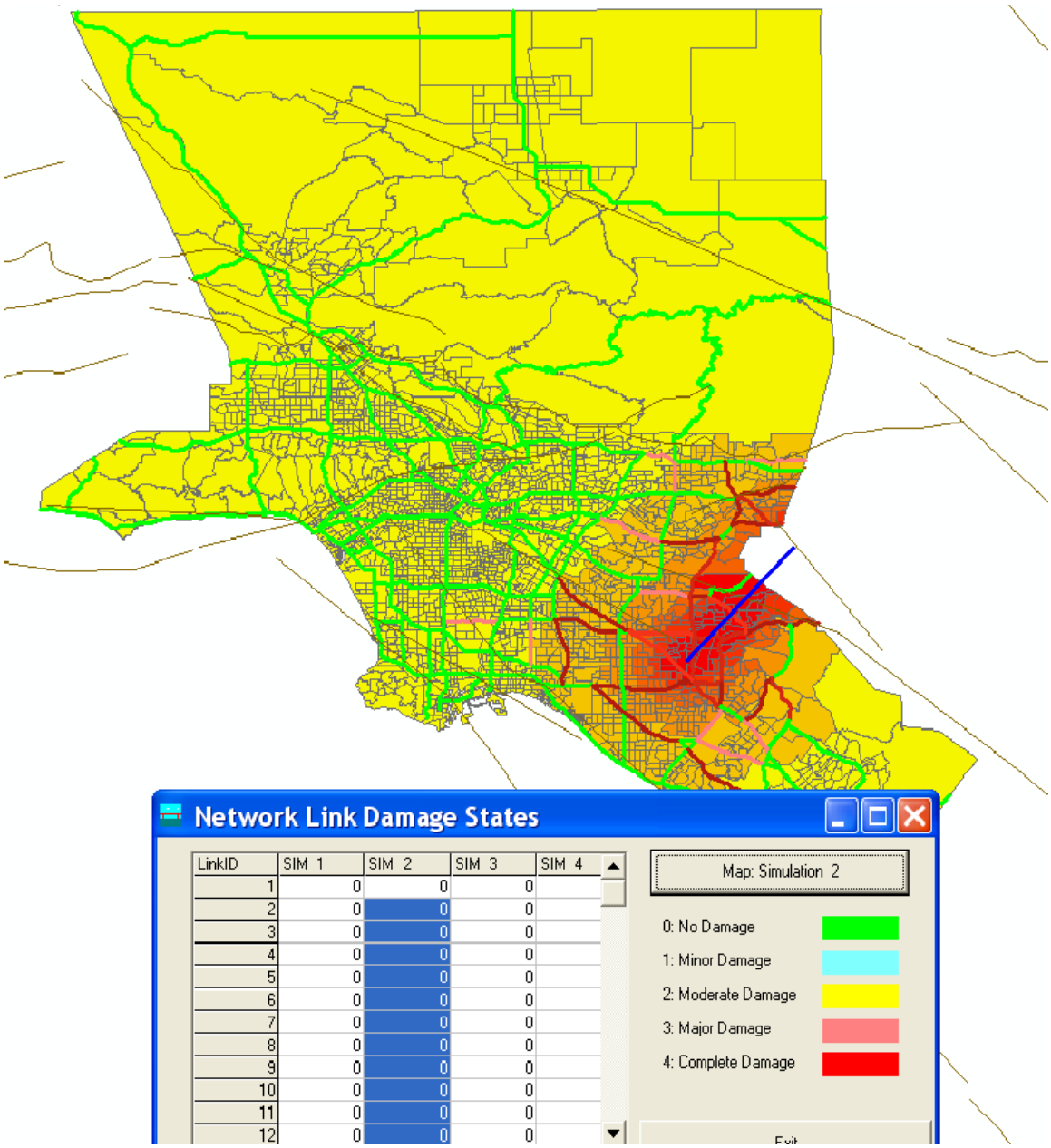

Fig. C.23 Display Link Damage States

SC_DAY0.txt - Notepad

File Edit Format View Help

Systme Social Cost (Drivers Delay and Opportunity Cost)

SIM NO.	D.D.(hrs)	O.C.(hrs)	
1	51528	60256	111784
2	100318	60054	160372
3	103610	59816	163426
4	86814	56268	143082
5	105857	77456	183313
6	45270	58277	103547
7	62897	69052	131949
8	89079	57966	147045
9	72331	62421	134752
10	132758	123017	255775
Average	85046	68458	

Ln 1, Col 1

(a) System Performance at Day 0

SC_Recovery.txt - Notepad

File Edit Format View Help

System Recovery Process after Earthquake

Drivers Delay (hrs)

Day	SIM1	SIM2	SIM3
0	51528	100318	103610
1	52040	100792	104174
3	52844	101869	104766
7	54930	103696	106899
10	56427	104775	108641
20	60954	110115	114471
30	65657	114466	119835
40	70238	118892	125373
60	80044	128238	136528
90	94097	142166	153600
120	106628	154846	167927
150	112921	161497	174863
180	117491	167950	179475
210	88255	92709	106783
240	92271	97130	110914
270	18069	21876	43725
300	0	0	0
360	0	0	0
420	0	0	0
480	0	0	0

Opportunity Cost (hrs)

Day	SIM1	SIM2	SIM3
0	60256	60054	59816
1	60232	60030	59799
3	60184	60016	59757
7	60098	59953	59642
10	60038	59793	59591

Ln 1, Col 1

(b)System Social Loss

Fig. C.24 Economic Loss

brepaircost.txt - Notepad

File Edit Format View Help

SIM NO.	Repair Cost(Dollars)
1	7090891
2	7333784
3	7949227
4	7349626
5	11607654
6	7861126
7	9034591
8	7939491
9	6829784
10	12133120
Average	8512929

Ln 1, Col 1

(a) Bridge Repair Cost

socialloss.txt - Notepad

File Edit Format View Help

SIM NO.	D.D.(Dollars)	O.C.(Dollars)
1	408580159	281547060
2	576831879	275245300
3	635088414	280026440
4	537943563	255161820
5	649176484	369055040
6	389824178	278513480
7	481186275	330688500
8	564380841	273226580
9	474530911	290965780
10	724682086	603011860
Average	544222479	323744180

Ln 1, Col 1

(b) System Social Loss

Fig. C.25 Economic Loss

Reference

Anagnostopoulos, S. A., and Spiliopoulos, K. V. (1992). "An investigation of earthquake induced pounding between adjacent buildings." *J. Earthquake Engrg, and Struct. Dyn.*, 21(4), 289-302.

Anagnostopoulos, S. A. (1988). "Pounding of buildings in series during earthquakes." *J. Earthquake Engrg, and Struct. Dyn.*, 16, 443-456.

ArcGIS 8.2, (1999), ESRI Inc., http://www.esri.com.

Applied Technology Council (1995), "Earthquake Damage Evaluation Data for California", ATC-13, Redwood City, CA, 1985

Basoz, N., and Kiremidjian, A. S. (1998). "Evaluation of bridge damage data from the Loma Prieta and Northridge, California earthquake." Technical Report MCEER-98-0004.

Buckle, I. G. (Editor) (1994). "The Northridge, California Earthquake of January 17, 1994: Performance of Highway Bridge." Technical Report, NCEER-94-0008, National Center for Earthquake Engineering Research, State University of New York, Buffalo.

California Department of Transportation. (1993), *COLx Users Manual*, Sacramento, CA.

Chai, Y.H., Priestley, M.J.N. & Seible F. 1991. Seismic Retrofit of Circular Bridge Columns for Enhanced Flexural Performance. ACI Structural Journal V. 88 (No. 5): 572-584.

Chang, E.S., Shinozuka, M., Moore, J., (2000), Probabilistic Earthquake Scenarios: Extending Risk Analysis Methodologies to Spatially Distributed Systems, Earthquake Spectra, Vol.16, No.3, pp-557-572.

Chopra, A. K. (1995). *Dynamics of structures: theory and application to earthquake engineering*, Prentice-Hall, Inc., Englewood Cliffs, N.J.

Computer and Structures, Inc. (2002). *SAP2000/Nonlinear Users Manual*, Berkeley, CA.

Cornell, C. A. (1996) "Calculating Buildings Seismic Performance Reliability: A Basis for Multi-Level Design Norms." *Proc. 11th WCEE*, Acapulco, Mexico.

Coburn, A.W. and Spence, R.J.S., (1992), "Factors Determining Human Casualty Levels in Earthquakes:Mortality Prediction in Building Collapse", Proceedings of the 10th WCEE, Madrid, Span: 5989-5994.

Desroches, R., and Fenves, G. L. (1997). "New design and analysis procedures for intermediate hinges in multiple-frame bridges." Report No. UCB/EERC-97/12, Earthquake Engineering Research Center, University of California, Berkeley, December.

Dutta, A. & Mander, J.B. (2002), "Rapid and Detailed Seismic Fragility Analysis of Highway Bridges", Technical Report at Multidisciplinary Center for Earthquake Engineering, NY, USA.

Durkin, M.E. and Thiel, C.C., (1991), "Integrating Earthquake Causalty and Loss Estimation," Proceeding of the Workshop on Modeling Earthquake Casualties for Planning and Response, Sacramento.

Eguchi, R.T., Goltz, J.D. Seligson, H.A. Flores, P.J. Blais, N.C. Heaton T.H. and Bortugno, E., (1997), "Real-time Loss Estimation as an Emergency Response Decision Support System: the Early Post-Earthquake Response Tool (EPEDAT)", Earthquake Spectra, Vol.13, 1997, pp.815-832.

FEMA, (1999) "HAZUS SR2 Technical Manual", Federal Emergency Management Administration, 1999.

Jankowski, R., Wilde, K., and Fujino, Y. (1998). "Pounding of superstructure segments in isolated elevated bridge during earthquakes." *J. Earthquake Engrg, and Struct. Dyn*., 27, 487-502.

Kushiyama, S. (2002), Calculation Moment-Rotation Relationship of Reinforced Concrete Member with/without Steel Jacket. Unpublished Report at University of Southern California, CA, USA.

Kushiyama, S. & Shinozuka, M. (2002). Development of Fragility Curve by PDF Interpolation Technique. Unpublished Report at University of Southern California, CA, USA.

Malhotra, P. K. (1998). "Dynamics of seismic pounding at expansion joints of concrete bridges." *J. Engrg. Mech*., ASCE, 124(7), 794-802.

Malhotra, P. K. (1997). "Dynamics of seismic impacts in base-isolated buildings." *J. Earthquake Engrg, and Struct. Dyn*., 26(8), 797-813.

Malhotra, P. K., Huang, M. J., and Shaksl, A. F. (1995). "Seismic interaction at separation joints of instrumented concrete bridge." *J. Earthquake Engrg, and Struct. Dyn*., 24(8), 1055-1067.

National Institute of Building Sciences, (1999), Earthquake Loss Estimation Methodology: HAZUS 99 (SR2) Technical Manual, Developed by Federal Emergency Management Agency, Washington D.C., http://www.fema.gov/hazus.

Priestley, M.J.N., Seible, F. & Calvi, G.M. (1996), "Seismic Design and Retrofit of Bridges". John Wiley & Sons, Inc.: 270-273.

Shinozuka, M. and Banerjee, S. (2004) “Dynamic Progressive Damage model for Bridges under Seismic Excitation”, Proceeding of International Conference in Commemoration of 5th Anniversary of the 1999 Chi-Chi Earthquake, Taiwan, Taipei, September

Shinozuka, M., Feng, M. Q., Kim, H.-K., and Kim, S.-H. (2000a). “Nonlinear static procedure for fragility curve development.” *J. Engrg. Mech* . ASCE, Vol. 126, No. 12, pp. 1287-1295.

Shinozuka, M., Feng, M. Q., Lee, J., and Nagaruma, T. (2000b). “Statistical analysis of fragility curves.” *J. Engrg. Mech*. ASCE, Vol. 126, No. 12, pp. 1224-1231.

Shinozuka, M., Feng, M.Q., Kim, H.-K., Uzawa, T., and Ueda, T., (2003a) "Statistical Analysis of Fragility Curves.", Technical Report at Multidisciplinary Center for Earthquake Engineering Research, MCEER-03-0002, 2003.

Shinozuka, M., Feng, Q.M., Dong, X.J, Chang, S., Cheng, T.C., Jin, X.H and Saadeghvaziri, M. A., (2003b) “Advances in Seismic Performance Evaluation of Power System”, Research Progress and Accomplishments, 2001-2003, MCEER-03-SP01, 2003.

Shinozuka, M., Grigoriu, M., Ingraffea, A. R., Billington, S.L., Feenstra, P., Soong, Tsu, T., Reinhorn, A.M., and Maragakis, E., (2000c) “Development of Fragility Information for Structures and Nonstructural Components ” Research Progress and Accomplishments, 1999-2000, MCEER-00-SP01, 2000.

Shinozuka, M., and Kim, S.-H. (2003c). “Effects of Seismically Induced Pounding at Expansion Joints of Concrete Bridges.” Accepted for Publication. *J. Engrg. Mech*. ASCE.

Shinozuka, M. Kim, S.H. Kushiyama, S. and Yi, J.H., (2002), Fragility Curves of Concrete Bridges Retrofitted by Column Jacketing, the Journal of Earthquake Engineering and Engineering Vibration, Vol.1, No.2, Dec. 2002.

Shinozuka, M., Murachi, Y., Dong, X.J., Zhou, Y.W., and Orlikowski, M. J., (2003d) “Effect of Seismic Retrofit of Bridges on Transportation Networks”, Research Progress and Accomplishments, 2001-2003, MCEER-03-SP01, 2003.

Shinozuka, M., Murachi, Y., Dong, X., Zhou, Y., and Orlikowski, M. J., (2003e), “Effect of Seismic Retrofit of Bridges on Transportation Networks,” Earthquake Engineering and Engineering Vibration, Vol. 2, No. 2, 2003, pp 169-180

Shinozuka, M. Shiraki, N. and Kameda H., (2000d), Performance of Highway Network Systems under Earthquake Damage, Proceedings of the Second International Workshop on Mitigation of Seismic Effects on Transportation Structures, Taiwan, Sep. 13-15, 2000, pp. 303-317.

Shiraki, N., (2000), “Performance of Highway Network Systems under Seismically Induced Traffic Delays”, M. S. Thesis, Kyoto University, Kyoto, Japan.

Southern California Association of Governments, (1997), 1997 Model Validation and Summary.

Texas Transportation Institute (1999), the 1999 Annual Mobility Report.

U.S. Nuclear Regulatory Commission (U.S. NRC), (1983), ‘‘PRA procedures guide.’’ Tech. Rep. NUREG/CR-2300, Vol. 2, Washington, D.C., pp11-46.